NASA/TP—2000-210031

DOT/FAA/AR-99/89

U.S. Department of Transportation
Federal Aviation Administration

Ice Accretions and Icing Effects for Modern Airfoils

Harold E. Addy, Jr.
Glenn Research Center, Cleveland, Ohio

April 2000

The NASA STI Program Office . . . in Profile

Since its founding, NASA has been dedicated to the advancement of aeronautics and space science. The NASA Scientific and Technical Information (STI) Program Office plays a key part in helping NASA maintain this important role.

The NASA STI Program Office is operated by Langley Research Center, the Lead Center for NASA's scientific and technical information. The NASA STI Program Office provides access to the NASA STI Database, the largest collection of aeronautical and space science STI in the world. The Program Office is also NASA's institutional mechanism for disseminating the results of its research and development activities. These results are published by NASA in the NASA STI Report Series, which includes the following report types:

- TECHNICAL PUBLICATION. Reports of completed research or a major significant phase of research that present the results of NASA programs and include extensive data or theoretical analysis. Includes compilations of significant scientific and technical data and information deemed to be of continuing reference value. NASA's counterpart of peer-reviewed formal professional papers but has less stringent limitations on manuscript length and extent of graphic presentations.

- TECHNICAL MEMORANDUM. Scientific and technical findings that are preliminary or of specialized interest, e.g., quick release reports, working papers, and bibliographies that contain minimal annotation. Does not contain extensive analysis.

- CONTRACTOR REPORT. Scientific and technical findings by NASA-sponsored contractors and grantees.

- CONFERENCE PUBLICATION. Collected papers from scientific and technical conferences, symposia, seminars, or other meetings sponsored or cosponsored by NASA.

- SPECIAL PUBLICATION. Scientific, technical, or historical information from NASA programs, projects, and missions, often concerned with subjects having substantial public interest.

- TECHNICAL TRANSLATION. English-language translations of foreign scientific and technical material pertinent to NASA's mission.

Specialized services that complement the STI Program Office's diverse offerings include creating custom thesauri, building customized data bases, organizing and publishing research results . . . even providing videos.

For more information about the NASA STI Program Office, see the following:

- Access the NASA STI Program Home Page at ***http://www.sti.nasa.gov***

- E-mail your question via the Internet to help@sti.nasa.gov

- Fax your question to the NASA Access Help Desk at (301) 621-0134

- Telephone the NASA Access Help Desk at (301) 621-0390

- Write to:
  NASA Access Help Desk
  NASA Center for AeroSpace Information
  7121 Standard Drive
  Hanover, MD 21076

NASA/TP—2000-210031

DOT/FAA/AR–99/89

U.S. Department of Transportation
Federal Aviation Administration

Ice Accretions and Icing Effects for Modern Airfoils

Harold E. Addy, Jr.
Glenn Research Center, Cleveland, Ohio

National Aeronautics and
Space Administration

Glenn Research Center

April 2000

Acknowledgments

I would like to thank Dave Sheldon, Bill Sexton, and the IRT staff for their great support in conducting the icing tunnel tests. I would like to thank Tom Ratvasky for conducting the first entry of the business jet model tests. I would also like to thank Debi Tomek and the staff of the LTPT for their terrific support during the dry tunnel tests of this project. Finally, special thanks to Tammy Langhals for digitizing the ice shapes included in this report and for assembling and organizing the data.

Available from

NASA Center for Aerospace Information
7121 Standard Drive
Hanover, MD 21076
Price Code: A13

National Technical Information Service
5285 Port Royal Road
Springfield, VA 22100
Price Code: A13

Ice Accretions and Icing Effects for Modern Airfoils

Harold E. Addy, Jr.
National Aeronautics and Space Administration
Glenn Research Center
Cleveland, Ohio 44135

Abstract

Icing tests were conducted to document ice shapes formed on three different two-dimensional airfoils and to study the effects of the accreted ice on aerodynamic performance. The models tested were representative of airfoil designs in current use for commercial transport, business jet, and general aviation aircraft. The models were subjected to a range of icing conditions in an icing wind tunnel. The conditions were selected primarily from the Federal Aviation Administration's Federal Aviation Regulations 25 Appendix C atmospheric icing conditions. A few examples of supercooled large droplet icing conditions were included. To verify the aerodynamic performance measurements, molds were made of selected ice shapes formed in the icing tunnel. Castings of the ice were made and placed on a model in a dry low-turbulence wind tunnel, and precision aerodynamic performance measurements were taken. Documentation is included in this report of all ice shapes produced and the aerodynamic performance measurements made during the icing tunnel tests. Results from the dry low-turbulence wind tunnel tests are also presented.

The report appendix data are available in full in ASCII (online: http://icedog.grc.nasa.gov); the appendix data are also available by request in ASCII on CD-ROM (contact: H.E. Addy, Jr., NASA Glenn Research Center, Cleveland, OH 44135, (216) 433–4000, Harold.E.Addy@grc.nasa.gov).

Summary

Design and certification of ice protection systems require prediction of ice accretions on aircraft surfaces that are unprotected or for which the ice protection system has failed. Analytical ice accretion computer codes represent an efficient means of prediction. It was recognized in the early 1990's that acceptance of these codes was somewhat limited by the lack of code validation data. Most of the ice accretion records available in the open literature were limited to ice shapes formed on a few basic airfoil sections, such as the two-dimensional NACA–0012 airfoil. Studies were needed of ice accretions on airfoils more typical of those being designed and used on today's aircraft. In response to this need, NASA Glenn Research Center and the Federal Aviation Administration (FAA) William J. Hughes Technical Center initiated the Modern Airfoils Program. This program uses icing and wind tunnel testing to determine ice accretion shapes and their aerodynamic effects. Understanding of aerodynamic effects is essential in identifying critical ice shapes that could cause problems in flight, which is an important part of icing certification.

Icing tests were conducted to document ice shapes and their aerodynamic effects on three different modern airfoils. The models, which were representative of current airfoil designs used in commercial transport, business jet, and general aviation aircraft, were subjected to a range of icing conditions in an icing wind tunnel. These conditions were selected primarily from the FAA's certification envelopes, but a few supercooled large droplet (SLD) cases were also included. To verify the aerodynamic performance measurements, molds were made of selected ice shapes formed in the icing tunnel. Simulated ice shapes based on the molds were placed on a model in a dry low-turbulence wind tunnel, and precision aerodynamic performance measurements were made. Documentation is included in this report of all the ice shapes and the aerodynamic performance measurements made during the icing tunnel tests, providing a new data base for modern airfoils. Results from the dry low-turbulence wind tunnel tests are also presented.

The icing tunnel data show that, for all three types of airfoil, an exposure to typical FAA Federal Aviation Regulations (FAR) 25 Appendix C atmospheric icing conditions for 2 min has a significant effect on the maximum lift coefficient as calculated from integrated surface pressure data, $c_{l\max}$, and the stall angle (the maximum lift coefficient as calculated from the force balance is designated $C_{l\max}$). This effect is more pronounced when the ice is accreted at temperatures closer to 32 °F than when it is accreted at lower temperatures. Longer exposures to icing conditions continue to degrade both $c_{l\max}$ and the stall angle.

The tests with simulated ice shapes in the dry low-turbulence wind tunnel support the trends in the performance data obtained in the icing tunnel. Moreover, the effect of the Reynolds number on aerodynamic performance was shown to be significantly reduced when the leading edge of an airfoil is contaminated with ice. Finally, the difference in aerodynamic effects between the two- and three-dimensional ice shapes indicates that the surface texture and surface irregularities present in natural aircraft ice are important.

Introduction

Aircraft icing has posed a hazard since powered flight became a practical means of transportation. Numerous tests have been conducted in icing wind tunnels not only to design effective and efficient ice protection systems, but also to study the ice accretion process itself and the effect of ice on aerodynamic performance. Valuable information can be gathered about aircraft icing by recording both the ice accretion's shape and its location on the airfoil.

Unfortunately, most of the ice accretion records available in the open literature are limited to ice accretions on a few, older airfoil sections, such as the two-dimensional NACA–0012 airfoil. Studies of ice accretions for airfoils more typical of those being designed and used on today's aircraft are needed to advance the state of the art in icing prediction tools for both aircraft design and certification.

In response to these needs, NASA Glenn Research Center and the FAA William J. Hughes Technical Center initiated the Modern Airfoils Program. The two objectives of this project were to document ice shapes on newer airfoils and to record their aerodynamic effects. The results of this effort, which are given in this report, form a data base of ice shapes and aerodynamic performance data for modern airfoils.

Research Approach

To accomplish the goals of this project, appropriate modern airfoil designs were selected and icing wind tunnel tests were conducted to collect ice shape and aerodynamic performance data. Selected ice shapes were made into molds that preserved the three-dimensional surface texture and roughness of the ice. Castings were then made from these molds, providing accurate replicas of the ice formed in the icing wind tunnel. Finally, selected ice castings were tested in an aerodynamic tunnel where more accurate and detailed aerodynamic performance measurements were made.

The NASA Glenn Icing Branch asked U.S. aircraft manufacturers to suggest airfoil sections to be used in the project. Only airfoils representative of those used in current aircraft design, production, and service were accepted. NASA chose one airfoil from each of the commercial transport, business jet, and general aviation categories of aircraft.

The icing tests were conducted in the Icing Research Tunnel (IRT) at Glenn Research Center. Icing conditions for these tests were selected from the FAA's FAR 25 Appendix C atmospheric icing conditions. Some SLD conditions were included due to the current interest in this area. The airfoils were subjected to icing conditions for fixed time periods ranging from 2 to 45 min. The shorter exposure periods were designed primarily to study the effects of initial ice buildup. The longer exposure periods allowed study of the effects of ice shapes like those used for aircraft icing certification. Air velocities and model attitudes for the tests were representative of the typical natural icing flight conditions for each airfoil.

Since the IRT has a relatively high level of air turbulence, tests were needed in an aerodynamic tunnel to verify the performance measurements made in the IRT. These detailed aerodynamic performance tests were conducted in the Low-Turbulence Pressure Tunnel (LTPT) at NASA Langley Research Center. The LTPT has a turbulence level of 0.1 percent or lower for most of its operating envelope. Because the tunnel can be pressurized, tests can be run over a range of Reynolds and Mach numbers. Since few studies have been done of the effects of Reynolds and Mach numbers on the aerodynamic performance of an ice-contaminated airfoil, this was an attractive feature.

Model Descriptions

Four models were built for this project: three that were selected from the different aircraft categories for tests in the IRT and one additional general aviation airfoil for tests in the LTPT. All were two-dimensional single-element models. Figure 1 shows the cross section of each airfoil. The business jet airfoil approximates an airfoil section found on the aircraft main wing, while the commercial transport model approximates an airfoil section found on the horizontal tailplane. The general aviation airfoil, the NLF–0414, is also a main wing design (ref. 1). It is a natural laminar flow design that was developed at NASA Langley and George Washington University in the early 1980's. Coordinates for each model are given in appendix A.

An indication of the differences in aerodynamic performance among the three airfoils is shown in figure 2. Here, curves are plotted with pressure coefficients calculated from surface pressure taps, c_p, for each airfoil at similar lift coefficients. It can be seen that the general aviation airfoil had the most aft pressure loading of the three airfoils. The business jet main wing airfoil had only slightly more aft loading at this level of lift coefficient than the commercial transport horizontal-tailplane

airfoil. Note also the wide range in angle of attack (*AOA*) required for these airfoils to achieve similar lift coefficients. Researchers were interested in how ice might accrete differently on these airfoils and how the ice would affect aerodynamic performance.

The three IRT models were designed and fabricated for vertical installation in the IRT. Each of the IRT airfoils had a span of 6 ft and a chord of 3 ft. The LTPT model was mounted horizontally and had a span of 3 ft and a chord of 3 ft. Photographs of the models installed in their respective tunnels are shown in figure 3. A description of the construction and instrumentation for each of the models follows.

Commercial Transport and Business Jet Models

The commercial transport and business jet models were made of fiberglass. The construction technique for both models consisted of several steps. First, two metal templates of each airfoil section were machined and used as cutting guides for wooden male patterns. The templates were mounted and aligned on the ends of blocks of laminated basswood. The blocks were then machined in the spanwise direction to produce male patterns of the two-dimensional airfoils. This pattern was used to create a female fiberglass mold for each model. The molds were made in two separate halves that intersected at the zero reference line of the airfoils. The model shells were then laid into the female molds to a 3/8-in. thickness using epoxy and fiberglass matting. After the skins dried, the ends were trimmed and the leading and trailing edges were machined flat to the zero-reference line (split line). Then, two 2-in.-thick wooden spars and seven 1-in.-thick wooden ribs were set into the two shell halves of each model. The spars and ribs were also surface cut along the split line. The top and bottom ribs were placed one-half inch from the end so that a 1/2-in. aluminum mounting plate could be installed. The ribs and spars were bonded to the shells using a mixture of colloidal silica and epoxy (this mixture fills in voids in the fiberglass to form a better bond), and the two shell halves were clamped together until the epoxy hardened. After the epoxy cured, the two halves were split apart to install pressure taps and thermocouples. The pressure tap and thermocouple locations are given in appendix B.

The static pressure taps were made with 0.040-in.-outside-diameter stainless steel tubing. Each type K thermocouple was embedded in the fiberglass skin. First, a hole was counterbored from the inner surface to a depth of five-sixteenths of an inch. Then the thermocouple was installed in the counterbore and backfilled with epoxy. The thermocouple leads were routed through the ceiling mount similarly to the pressure tubing. After the instrumentation was installed, the two halves of each model were bonded together with the epoxy silica mixture.

The first rib at each end of these models was recessed one-half inch so that an aluminum plate could be installed using the epoxy silica mixture. Holes were drilled and tapped through the outer surface into the aluminum plates so that the model could be mounted in the test section of the IRT.

IRT General Aviation Model

The general aviation model was created primarily of laminated mahogany similarly to the wooden male pattern for the commercial transport and business jet models. A 3-in. square tubular spar was installed at the quarter-chord location for added strength. The trailing edge, from the 30-percent chord to the end of the model, was also made of fiberglass like the commercial transport and business jet models. Aluminum plates were installed at each end of the model for mounting in the test section of the tunnel.

Seven pressure taps and three thermocouples were installed in the surface of the model. Their locations are given in appendix B. Channels were routed in the surface of the mahogany for the pressure taps and the thermocouples. The channels were backfilled with epoxy after the instrumentation was in place. The seven pressure taps were used as reference pressures for a chordwise strip of pressure-sensitive paint that was applied to the circumference of the model to measure surface pressures during the dry aerodynamic checkout runs.

LTPT General Aviation Model

The general aviation model for the LTPT was built of solid aluminum. It had a removable leading edge that intersected the main body of the model at the 16.5-percent chord on the upper surface and the 21-percent chord on the lower surface. Alternate leading edges were designed and built to accommodate the simulated ice shapes. A cross-sectional sketch of an alternate leading edge with a simulated ice shape attached is shown in figure 4. The removable leading edges were attached to the main body using ten 3/8-in.-diameter bolts and two 3/8-in.-diameter pins. These bolts were inserted through counterbored holes on the lower surface of the model and threaded into permanent steel-thread inserts (Keensert) mounted in the main body. The holes were backfilled with tissue and dental plaster to give a smooth aerodynamic surface for the baseline clean leading edge. The plaster could be easily removed to change the leading edge. For alternate leading edges, the simulated ice shapes covered these counterbored holes.

Surface pressure taps were mounted in the chordwise direction in the baseline leading edge and in both the chordwise and spanwise directions in the main body of the model. The spanwise taps were located on the upper surface at the 70-percent chord

and at the trailing edge and were used to monitor the two-dimensionality of the flow over the model. The chordwise taps were not placed in a straight row parallel to the chord. They were offset at a 15° angle from the upstream taps to ensure that flow disturbances caused by a tap would not affect the downstream pressures. This was a concern only for the clean wing, because the ice shapes at the leading edge formed a much larger flow disturbance than the surface pressure taps and dominated boundary layer flow over the model. The taps were angled back and forth across the model to limit their spanwise extent, as shown in figure 5. The alternate leading edges did not have surface pressure taps. Special instrumentation pieces were made to resemble the ice shapes. From digitized tracings of the original ice, a smoothed profile of the ice was generated using a smoothing procedure developed at Glenn Research Center (ref. 2). Various levels of smoothing can be obtained by specifying the number of control points used for the smoothing process. Smoothing was needed to ensure accurate pressure measurements. Twenty-percent control-point smoothing was used for the 22.5-min (run 621) ice shape instrumentation piece. Ten-percent control-point smoothing was used for both the 2- (run 622) and the 6-min (run 623) ice shapes. These instrumentation pieces are shown in figure 6. Pressure tap locations for the clean wing and the ice shapes are given in appendix B.

Test Description

IRT Tests

The IRT is an atmospheric closed-loop refrigerated wind tunnel capable of operating at temperatures as low as –40 °F (ref. 3). Airspeeds as high as 430 mph can be attained in the 6-ft-high, 9-ft-wide, 20-ft-long test section. The IRT has a water spray system capable of producing a uniform icing cloud with droplet sizes ranging from 15 to 40 μm in median volumetric diameter (*MVD*) and from 0.2 to 1.8 g/m^3 in liquid water content (*LWC*). The tunnel can produce clouds with larger *MVD's* under certain conditions. Several of these conditions were run for these tests to obtain data for SLD conditions.

The models were mounted vertically in the IRT test section and attached to an external force balance at both the top and bottom of each model. The lower portion of the force balance was mounted to the tunnel turntable and rotated with it. The upper portion of the force balance also rotated with the model. It was situated in a special bearing that permitted rotary movement while providing model support. The force balance was a three-component system measuring lift, drag, and pitching moment.

A wake survey system was used to measure model section drag. This system consisted of a movable Pitot probe that traversed the model wake at midspan and at a distance of one and one-half chords downstream of the model. Free-stream conditions were measured using the facility Pitot probe located two and one-half chords upstream of the model near the tunnel wall. Total pressures were measured using absolute pressure transducers; static pressures were measured using a differential pressure transducer.

Flow visualization with flow cones was used to observe the onset of flow separation during model rotation and icing. The flow cone was a white plastic cone 7/8 in. long and 9/32 in. in diameter at its base. The cones were attached to the model with a 7/8 in. length of string coming from the cone's apex. To affix the cone to the model, 1-in.-wide aluminum tape was applied over the string near the cone's apex. The extra string was doubled back and taped over with 2-in.-wide aluminum tape. A row of cones was affixed to each model in the chordwise direction on both the suction and pressure surfaces approximately 18 in. from the floor of the tunnel.

Icing conditions for tests in the IRT were selected primarily from the FAA's FAR 25 Appendix C atmospheric icing conditions and included glaze, mixed, and rime ice conditions. Glaze ice is transparent or translucent and typically has one or two horns. Rime ice has an opaque milk-white appearance and is usually thickest at or near the stagnation line. Mixed ice is transparent in the area of the stagnation line but has opaque white ice on both sides of the stagnation zone. Neither rime nor mixed ice has horns. Glaze ice is usually formed at total temperatures near 32 °F, rime ice usually forms at temperatures near 0 °F and below, and mixed ice forms at temperatures between these two. Because cloud liquid-water content and, to a lesser extent, droplet size also play a role in the determination of ice type, clear boundaries between ideal conditions of formation for different types of ice cannot be established. In tests where the icing exposure periods were too short to ascertain horn growth, the translucency of the ice was used to determine type. Test matrices for all the tests are given in appendix C. Air speeds and model attitudes were chosen to reflect natural icing flight conditions for each category of aircraft.

The targeted icing exposure times were 2, 3, 6, 22.5, and 45 min. Where actual icing exposure times deviated from these time periods, the IRT was unable to obtain the desired *LWC* at the desired airspeed and droplet size. In these cases, the icing exposure time was adjusted to approximate the appropriate amount of ice buildup for the desired set of conditions. For the commercial transport model, a Mach number of 0.45 was desired; however, it was found that the IRT could not sustain this airspeed with ice accreted on the model because the tunnel blockage became too great. Therefore, the Anderson scaling

methods were used to adjust the icing conditions to simulate the 0.45 Mach number icing conditions at a lower Mach number (ref. 4). The shorter icing exposure times of 2 and 6 min provided data on initial and early ice buildup and associated aerodynamic performance degradation. The longer icing exposure times corresponded to FAA certification requirements for flight in icing conditions with a failed ice protection system (22.5 min) and no ice protection system (45 min). At the request of NASA's industry partners, a few other icing exposure times were also included. Repeats of selected icing test runs were also conducted to check the reproducibility of the ice shapes and the performance data.

A typical test run in the IRT consisted of a number of steps. First, the tunnel and model were cooled to the desired temperature by operating the tunnel's fan and cooler. The fan was then brought to a stop so that a zero reading for the force balance could be taken. After restarting the fan, tunnel airspeed was brought to the desired level. At this point, force balance and wake survey measurements were made for the clean model. Then the icing portion of the test was executed for the set icing time period. Once the icing spray was terminated, force balance and wake survey measurements were taken for the iced model at the test point attitude. The model was rotated, and force balance measurements were made over a range of model attitudes. The typical attitude range was –4° to stall. Attempts to rotate the model past stall were not made due to heavy model buffeting. The model was returned to its set point attitude, and the fan was shut off. Another force balance zero measurement was made. Photographs of the ice were taken, and cuts were made in the ice so that tracings of the ice shape could be made. Normally, three tracings were made of the ice shape: one at the tunnel centerline, one 6 in. below, and one 6 in. above. Finally, the thickness of the ice at the cuts was measured using a depth gauge. The ice was then cleaned off the model and preparations were made for the next run.

LTPT Tests

The LTPT is a pressurized closed-loop wind tunnel (ref. 5). Its 3-ft-wide, 7.5-ft-high, 7.5-ft-long test section is capable of operating at Reynolds numbers as high as 15 million/ft and Mach numbers as high as 0.4. For the tests in this project, the tunnel turbulence was 0.1 percent of free-stream velocity or lower. The tunnel has a sidewall boundary layer control system that was used to promote a two-dimensional flow field around the model. Lift and pitching moment forces were measured by integrating static surface pressures on the model. A drag wake survey system was used to measure drag forces. A force balance system was also used to measure and monitor drag, lift, and pitching moment forces.

A second general aviation model was built for the LTPT tests. It was installed horizontally in the test section of the tunnel with the trailing edge of the model in the existing sidewall venting area of the tunnel turntable. The sidewall venting area consists of small closely spaced holes in the endplate of the turntable. The holes lead through the endplate to a system of flexible ducting and valves. This system was vented to atmospheric pressure outside the tunnel's pressure vessel. Venting of the pressurized air inside the tunnel out through the turntable endplates helped to control the sidewall flow over the model. The amount of venting for each test point was limited, however, by the tunnel operating pressure. At test points near atmospheric pressure, such as those near the Mach and Reynolds numbers of the IRT tests, a very limited amount of sidewall boundary layer control was available. The venting strip for this model was about 16 in. long and about three-fourths of an inch wide. It was tailored to follow the upper surface contour using strips of aluminum tape. The LTPT test engineers recommended this amount of venting on the basis of their past experience. A photograph of the vented area on one side of the tunnel is shown in figure 7.

Because the trailing edge of the model was intentionally placed in the venting area of the tunnel endplates, the leading edge of the model overhung the leading edge of the turntable by approximately 3 in. The small gap, approximately one-sixteenth of an inch, was sealed with room-temperature vulcanizing (RTV) silicone sealant. An RTV release agent was applied to the wall prior to application of the RTV to the gap. After the RTV had cured, a piano wire was run along the wall to ensure release of the RTV. This proved to be a good seal against excessive leakage around the ends of the leading edge but did not interfere with force balance measurements.

Ice shapes were accreted on the NLF–0414 airfoil in the IRT over a range of icing conditions chosen from the FAR 25 Appendix C atmospheric icing conditions. Airspeeds and model attitudes typical of general aviation aircraft were used in the ice accretion tests. Molds were made of selected ice shapes formed during these tests (ref. 6). From these molds, three different ice shapes were chosen for the aerodynamic tests in the LTPT that had been formed from three different exposure times to the same glaze ice conditions. The icing conditions included a static air temperature of –5 °C, a mean volumetric droplet diameter of 20 μm, a cloud liquid-water content of 0.54 g/m^3 at an airspeed of 66.9 m/sec (130 kn), and a model attitude of 2°. The three icing exposure times were 2 (run 621), 6 (run 622), and 22.5 (run 623) min. Figure 8 shows tracings of the three ice shapes that were used for castings for the LTPT tests. Aerodynamic performance data were not obtained for the 2-min ice shape in the LTPT due to a dimensional error in creating the casting.

In addition to the cast ice shapes, three smooth two-dimensional ice shapes were manufactured and tested. These two-dimensional shapes were made from the tracings of ice that were also used to make the castings for the three-dimensional ice shapes. The tracings were first digitized using a digitizing tablet, then smoothed using the computational routine used by Vickerman (ref. 2). The resulting smoothed tracings are shown in figure 9. Fifty-percent control-point smoothing was used for the 2- (run 621) and 6-min (run 622) shapes. Twenty-percent control-point smoothing was used for the 22.5-min (run 623) ice shape. These smoothed tracings were then projected in the spanwise direction using a computer-aided design (CAD) program to obtain a two-dimensional ice shape similar in concept to a two-dimensional airfoil model. A rapid-prototyping process known as stereo lithography was used to generate the two-dimensional ice shapes from the CAD models for the tests.

Ice shapes were installed on the model using a set of 10-32 flathead screws between the 10- and 14-percent chords on both the upper and lower surfaces. The screws were covered with dental plaster and then smoothed to match the surrounding surface. Body putty was used to fair in the interface between the ice shape and the main wing body. The interfaces between the ice shape and the main wing were sealed with an RTV, as well as the interfaces between adjacent ice shape pieces and the pressure instrumentation strip. The original mold spanned approximately 15 in. of the airfoil, so multiple casts of each mold were made and then pieced together to span the 3-ft-wide tunnel. The instrumentation strips were also secured to the leading edge of the model with screws.

After an ice shape was installed and the instrumentation was checked, the tunnel was pressurized and the fan was started. Once the set Mach and Reynolds numbers were reached, the model was rotated through a range of attitudes, usually from –4° to several degrees past stall. Then the new Mach and Reynolds numbers were set and the model was again rotated through the range of attitudes.

Results

Results from the IRT tests will be discussed first, followed by results from the LTPT tests. All of the data are given in appendix D. In this report, model attitude is the angle of the chord of the model with respect to the tunnel centerline. Where standard wind tunnel correction factors have been applied, the term "angle of attack" (*AOA*) is used (ref. 7). The maximum lift coefficient as calculated from the force balance is designated $C_{l\max}$. This overall lift coefficient takes lift generated over the entire model into account. The maximum lift coefficient as calculated from integrated surface pressure data, also known as the section lift, is designated $c_{l\max}$.

IRT Results

Data from the tests run in the IRT are shown in a composite form in appendix D. Included in this data are (1) actual tunnel icing conditions for each test run; (2) clean airfoil and iced airfoil drag coefficients for the *AOA*, airspeed, and temperature at which the ice was accreted as measured by the drag wake survey system: (3) clean airfoil and iced airfoil lift coefficients for the *AOA*, airspeed, and temperature at which the ice was accreted as measured by the tunnel's force balance; (4) digitized tracings of the ice at the locations shown; (5) ice thickness at the locations of the tracings; (6) photograph(s) of the ice; and (7) a plot of the clean and iced airfoil lift coefficients versus *AOA*. Force balance data were not available for all the test runs. This was either because the force balance was not installed or because time did not permit the acquisition of the full complement of force balance versus *AOA* data.

While the ability of the IRT to repeat ice shapes for a given set of icing conditions is well established, several repeat runs were made for each model (ref. 8). An example of the tunnel's repeatability is given in figure 10, where ice tracings taken at the tunnel centerline are given for several separate test runs.

An error analysis of the algorithm and the pressure instrumentation used to calculate the drag coefficients shows that the uncertainty for these values is ±12 drag counts, where one drag count is an increment of 0.0001 in drag coefficient. This is low for the drag of an airfoil with ice accretion, which ranges typically from several hundred to over a thousand counts of drag.

A static calibration of the force balance has shown the accuracy of this measurement system to be ±3 percent. It has been observed, however, that for two-dimensional wind tunnel tests where a constant chord model completely spans the test section, the spanwise distribution of lift caused by the tunnel walls typically diminishes lift by 10 to 15 percent at the maximum lift coefficient $c_{l\max}$ (ref. 9). As shown in figure 11, this effect was observed in the IRT. In this figure, lift coefficient versus *AOA* curves for the clean business jet model as measured by the IRT force balance and integrated surface pressure taps are shown. The business jet model was not rotated past stall in these tests due to severe buffeting. Stall was confirmed by observation of the tufts attached to the suction surface of the model.

The diminished lift at $C_{l\max}$ as measured by the force balance is also observed for the clean general aviation model when the lift curves from the IRT and the LTPT tests are compared, as shown in figure 12. The data for the LTPT shown in this figure are from integrating the surface pressure tap data, while the IRT data are from the force balance. It also should be noted that the stall angle is increased by about 2° in the IRT. This may also be due to the model-sidewall interaction.

An additional complication is present when making force balance performance measurements in an icing tunnel. Because the uniform icing cloud in the tunnel does not extend from floor to ceiling across the entire span of the model, the ice shapes taper off at each end. In the IRT, these nonuniform ends of the ice shapes extended about 12 in. from both the floor and the ceiling of the tunnel for the business jet airfoil and the commercial transport airfoil tests. The general aviation tests occurred after a new spray bar system was installed in the tunnel that enlarged the area of calibrated uniformity of the cloud. For these tests, the nonuniform ice shapes extended about 4 in. from the floor and ceiling.

Figure 13 shows lift coefficient versus *AOA* data for a 6-min (run 622) glaze ice shape from both the IRT and the LTPT for the general aviation model. The IRT lift coefficient data were obtained from the force balance after accreting the ice using the tunnel's icing cloud spray system. The LTPT lift coefficient data were obtained by integrating surface pressure data from the model with the casting of the ice shape attached. The mold of the original ice was approximately 15 in. long, so several of the castings were made and cut to fit across the 3-ft span of the model in the LTPT. Using this technique, the fully developed ice shape spanned the entire length of the model and was not tapered at the wall like the original ice shape in the IRT. Similar results for the 22.5-min (run 623) glaze ice shape are shown in figure 14. In addition to the diminished $C_{l\max}$ and higher stall angle measured by the force balance in the IRT, the slope of the lift curves at the lower *AOA* is slightly lower than those measured for the full-span ice shapes. The lower $C_{l\max}$ measured in the IRT may be caused by the tapered ice shapes at the ends of the model, although it is unknown precisely how the airflow is affected by the tapered ice at the walls. The measurements made by the IRT force balance system are nonetheless fairly accurate, especially when comparing the performance of the iced and clean airfoils.

A total of 84 icing runs were made with the business jet model. These were done in two separate entries in the IRT. In the first entry, the model was not mounted to the force balance, so lift data were not taken for this set of tests. The test matrix for the first set of business jet tests is given in appendix C1, while the test matrix for the second set is given in appendix C2. Results for the first set of tests are given in appendix D1 and results for the second set are given in appendix D2.

A total of 33 icing test runs were made in the IRT with the commercial transport model. Both the desired conditions at Mach number = 0.45, which were unattainable due to blockage in the tunnel, and the scaled conditions at Mach number = 0.40 used in the test are given in appendix C3. Results of the commercial transport airfoil IRT tests are given in appendix D3. Like the business jet model, the commercial transport model was not rotated past stall due to severe buffeting.

A total of 49 icing test runs were made with the general aviation airfoil in the IRT. The test matrix for these runs is given in appendix C4. Results for these tests are given in appendix D4.

The effect of varying icing exposure time is shown in figure 15. Here, lift coefficients are plotted versus *AOA* for each of the three models. In each case, the model was exposed to the same glaze ice conditions for three different periods of time. As can be seen in the figures, exposures to glaze icing conditions for time periods as short as 2 min has a significant effect on both $C_{l\max}$ and the stall angle, resulting in decreases of 25 to 30 percent in $C_{l\max}$ and of 1° to 8° in the stall angle.

The effects of various types of ice on $C_{l\max}$ and the stall angle for the airfoils are shown in figure 16. In these runs, each model was exposed to glaze, mixed, and rime icing conditions for the equivalent of 6 min. Lift versus *AOA* data were not obtained for rime ice accreted on the commercial transport model due to time constraints. For each model, glaze ice caused the largest degradation in $C_{l\max}$ and the stall angle, although there was not a large difference in the effects of the three ice types on the business jet model. This may be due to the higher *AOA* at which the ice was accreted for this model. All ice types degraded aerodynamic performance to the point where none should be overlooked as a hazard to safe flight.

A further analysis of the IRT data can be found in reference 10.

LTPT Results

Five different ice shapes were used in the dry tunnel tests at the LTPT. All were from ice shapes accreted during the general aviation icing tests in the IRT. Castings were made from ice accreted under icing conditions for IRT test runs 621, 622, and 623. As described earlier, corresponding two-dimensional ice shapes for these three test runs were manufactured and tested. During the testing at the LTPT, it was found that the casting for run 621 had not been manufactured properly. When the original mold of the ice was made in the IRT, the mold box had not been aligned correctly with the model. Steps were taken to compensate for the misalignment, but the resulting ice shape was much thicker than the original ice and did not resemble a natural ice accretion. Therefore, only a few data points were run and are not included in this report.

The matrices for the LTPT tests with the general aviation airfoil are given in appendix C6. Reynolds numbers varied from 1.0 to 12 million, while Mach numbers varied from 0.05 to 0.29. Results from tests of clean models and the five different ice shapes are given in appendix D5. Included in the results is lift coefficient versus *AOA* curves for each combination of Reynolds and Mach numbers in the test matrix. All of the lift coefficients shown are from integrated surface

pressure measurements. Drag coefficient data are also given for the runs. Wake survey data were used to calculate drag coefficients for most of the runs. Some problems with the wake survey system during the clean model and ice shape 623-2D tests, wake survey integrity concerns at the higher *AOA*, and time constraints prevented obtaining drag wake data for all of the runs. Where wake survey data were not available, drag data from the force balance are shown in italics. Where the drag forces on the model were low, typically about 300 drag counts or less, the force balance drag data were inconsistent. However, above 300 drag counts, the force balance drag data were consistent and agreed well with the wake survey data. Standard wind tunnel correction factors were applied to all of the lift and drag coefficient data (ref. 7). Pressure coefficient curves are shown for every other *AOA* for each of the runs.

Both force balance and surface pressure measurements were used to calculate lift coefficients. Surface pressure measurements are usually accepted as the more accurate method to determine lift coefficients for two-dimensional models. However, the three-dimensional character of the ice castings may have caused performance degradation that was not accurately reflected in the section lift coefficients derived from surface pressures. Therefore, force balance measurements, in which the lift over the entire model is taken into account, were also taken. It was found that the lift coefficients derived from the force balance and from the pressure taps agreed well. Figure 17 shows lift versus *AOA* curves derived from both force balance and surface pressure measurements for (a) 6-min and (b) 22.5-min three-dimensional ice shapes. A maximum 5-percent difference was typical. Because the lift coefficients calculated from the surface pressure measurements are more accurate, they will be used to discuss the results in the remainder of this report. The measurement error of the data indicates that the lift coefficients calculated from the surface pressures have an uncertainty of approximately ±2 percent up to the maximum lift coefficient $c_{l\max}$. Beyond $c_{l\max}$, the unsteady flow results in greater uncertainty in the lift coefficient values.

Figure 18 shows lift curves for the 6- and 22.5-min cast ice shapes attached to the general aviation model in the LTPT as well as for the clean model. The ice shapes again had a dramatic effect on both $c_{l\max}$ and the stall angle, as can be seen in the figure.

Figure 19 shows the effect of the Reynolds number at a Mach number of 0.21 for (a) the clean model, (b) 6-min ice shapes, and (c) 22.5-min ice shapes. Data for the clean model indicate a 5-percent increase in $c_{l\max}$ as the Reynolds number is increased from 4.6 to 10 million, while the stall angle remains unchanged. As was mentioned earlier, an increase in $c_{l\max}$ is typical of most airfoils. However, for both the 6-min and the 22.5-min ice shapes, there is no increase in $c_{l\max}$ and no change in the stall angle. This substantiates the idea that the presence of ice on an airfoil overrides the normal effect viscous forces have on airfoil boundary-layer behavior.

In figure 20, lift characteristics are compared of (a) 6-min and (b) 22.5-min two- and three-dimensional ice shapes. In both cases, the three-dimensional ice shapes show greater aerodynamic penalties than the corresponding two-dimensional ice shapes. For both ice shapes, $c_{l\max}$ is approximately 9 percent higher for the two-dimensional ice shapes and, for the 22.5-min ice shape, stall angle is increased by 1°. This indicates that, to obtain the proper aerodynamic effects, at least some of the complex, irregular surface features of the ice need to be included in any aircraft ice mockup.

Further analysis of the general aviation airfoil data from the LTPT tests can be found in reference 11.

Concluding Remarks

An extensive experimental study of various ice shapes on three modern airfoils was performed. The resulting data are useful for ice prediction code validation, as well as to gain insight into the effects of ice accretions on aerodynamic performance (ref. 12).

The icing tunnel data show that, for all three types of airfoils, an exposure to typical Federal Aviation Administration's Federal Aviation Regulations 25 Appendix C atmospheric icing conditions for as short a period as 2 min has a significant effect on $c_{l\max}$ and the stall angle. This is particularly true in the case of glaze ice. Longer exposures to icing conditions continue to degrade both $c_{l\max}$ and the stall angle.

Tests with the simulated ice shapes in the dry Low-Turbulence Pressure Tunnel (LTPT) support the performance data trends obtained in the Icing Research Tunnel (IRT). Moreover, the effect of the Reynolds number on aerodynamic performance was shown to be significantly reduced when the leading edge of an airfoil is contaminated with ice. This suggests that expensive testing for icing effects at full-scale Reynolds numbers may be reduced or may not be needed. Finally, the difference in aerodynamic effects between the two- and three-dimensional ice shapes indicates that the surface texture and irregularities present in natural aircraft ice are important.

With this data base in hand, hypotheses may be formed about the physical mechanisms that play significant roles in the observed behavior of iced airfoils. Detailed investigations into these mechanisms are needed to gain physical understanding and to produce better aircraft icing tools for prediction of critical ice shapes for airfoils.

National Aeronautics and Space Administration
John H. Glenn Research Center at Lewis Field
Cleveland, Ohio 44135, April 17, 2000

References

1. McGhee, R.J., et al.: Experimental Results for a Flapped Natural-Laminar-Flow Airfoil With High Lift/Drag Ratio. NASA TM–85788, 1984.
2. Vickerman, M: SmaggIce: Surface Modeling and Grid Generation for Iced Airfoils. AIAA Paper 2000–0235, 2000.
3. Soeder, R.H.: NASA Lewis Icing Research Tunnel User Manual. NASA TM–107159, 1996 (PDF available online: ftp://ftp-letrs.lerc.nasa.gov/LETRS/reports/1996/TM-107159.pdf)
4. Anderson, D.N.: Further Evaluation of Traditional Icing Scaling Methods. AIAA Paper 96–0633 (NASA TM–107140), 1996.
5. McGhee, R.J.; Beasley, W.D.; and Foster, J.M.: Recent Modifications and Calibration of the Langley Low-Turbulence Pressure Tunnel. NASA TP–2328, 1984.
6. Reehorst, A.L.; and Richter, G.P.: New Methods and Materials for Molding and Casting Ice Formations. NASA TM–100126, 1987.
7. Rae, W.H., Jr.; and Pope, A.: Low-Speed Wind Tunnel Testing. Second ed., John Wiley & Sons, New York, NY, 1984.
8. Shin, J. and Bond, T.H.: Results of an Icing Test on a NACA–0012 Airfoil in the NASA Lewis Icing Research Tunnel. NASA TM–105374 (AIAA Paper 92–0647), 1992.
9. Rae, W.H., Jr. and Pope, A.: Low-Speed Wind Tunnel Testing. Second ed., John Wiley & Sons, New York, NY, 1984.
10. Addy, H.E., Jr.; Potapczuk, M.G.; and Sheldon, D.W.: Modern Airfoil Ice Accretions. NASA TM–107423 (AIAA Paper 97–0174), 1997. (PDF available online: ftp://ftp-letrs.lerc.nasa.gov/LeTRS/reports/1997/TM–107423.pdf)
11. Addy, H.E., Jr.; and Chung, J.J.: A Wind Tunnel Study of Icing Effects on a Natural Laminar Flow Airfoil. AIAA Paper 2000–0095, 2000.
12. Wright, W.B.; and Rutkowski, A.: Validation Results for LEWICE 2.0. NASA/CR—1999-208690, 1999. (PDF available online: ftp://ftp-letrs.lerc.nasa.gov/LeTRS/reports/1999/CR–1999–208690.pdf)

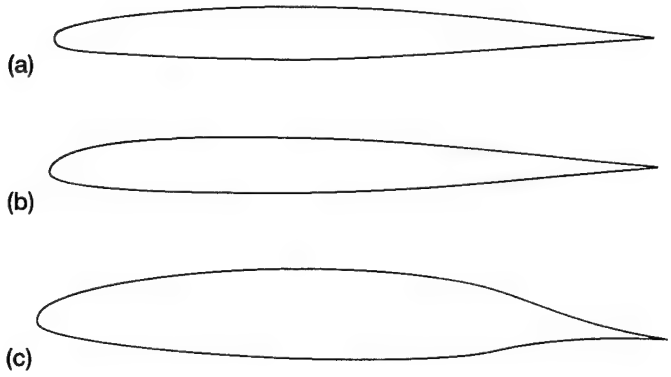

Figure 1.—Airfoils used in the Modern Airfoil Program.
(a) Business jet airfoil. (b) Commercial transport airfoil.
(c) General aviation airfoil.

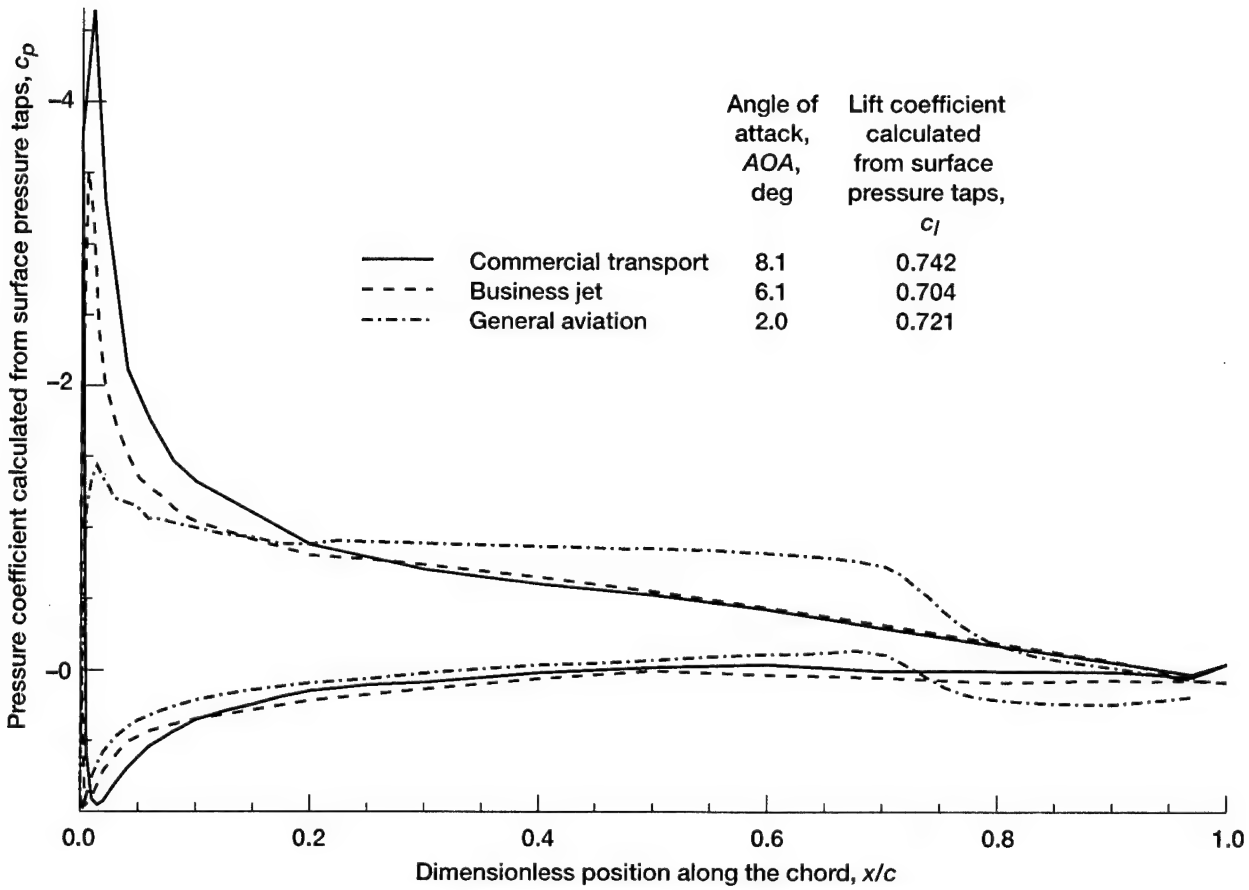

Figure 2.—Pressure coefficient curves for the three airfoils at similar lift coefficients.

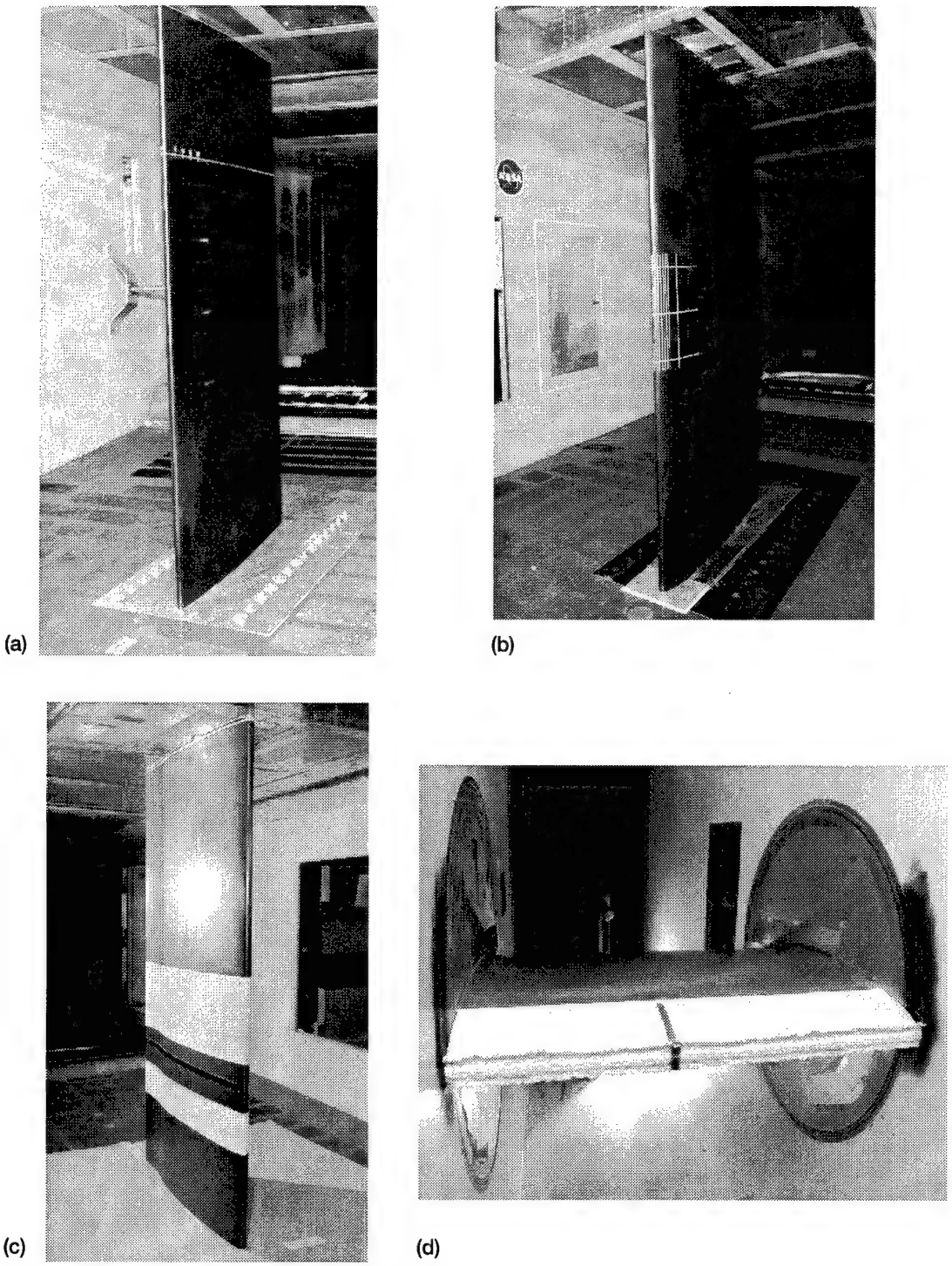

Figure 3.—Models used in the Modern Airfoil Program. (a) Business jet model. (b) Commercial transport model. (c) General aviation model. (d) General aviation model used in Low-Turbulence Pressure Tunnel (LTPT).

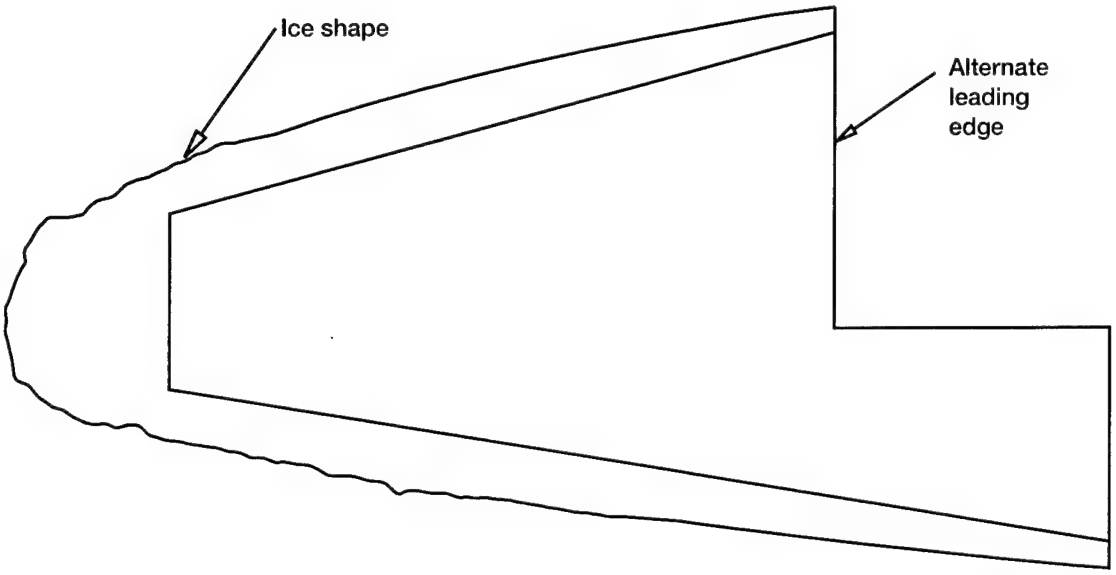

Figure 4.—Cross section of alternate leading edge with ice shape for LTPT general aviation model.

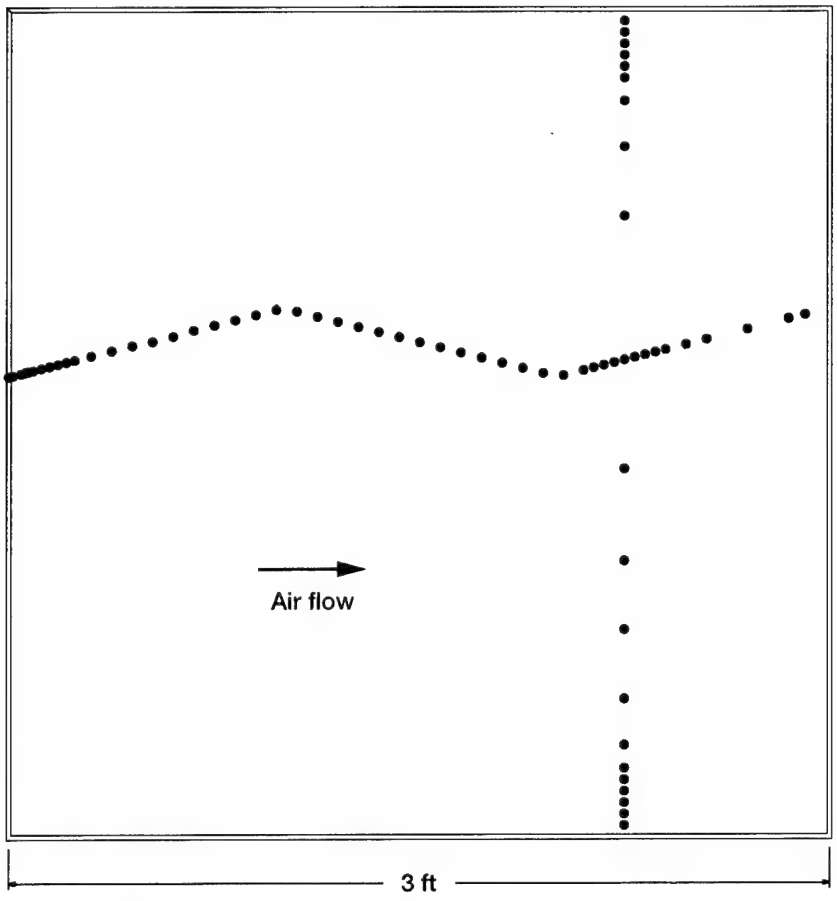

Figure 5.—Upper surface pressure taps on LTPT general aviation model.

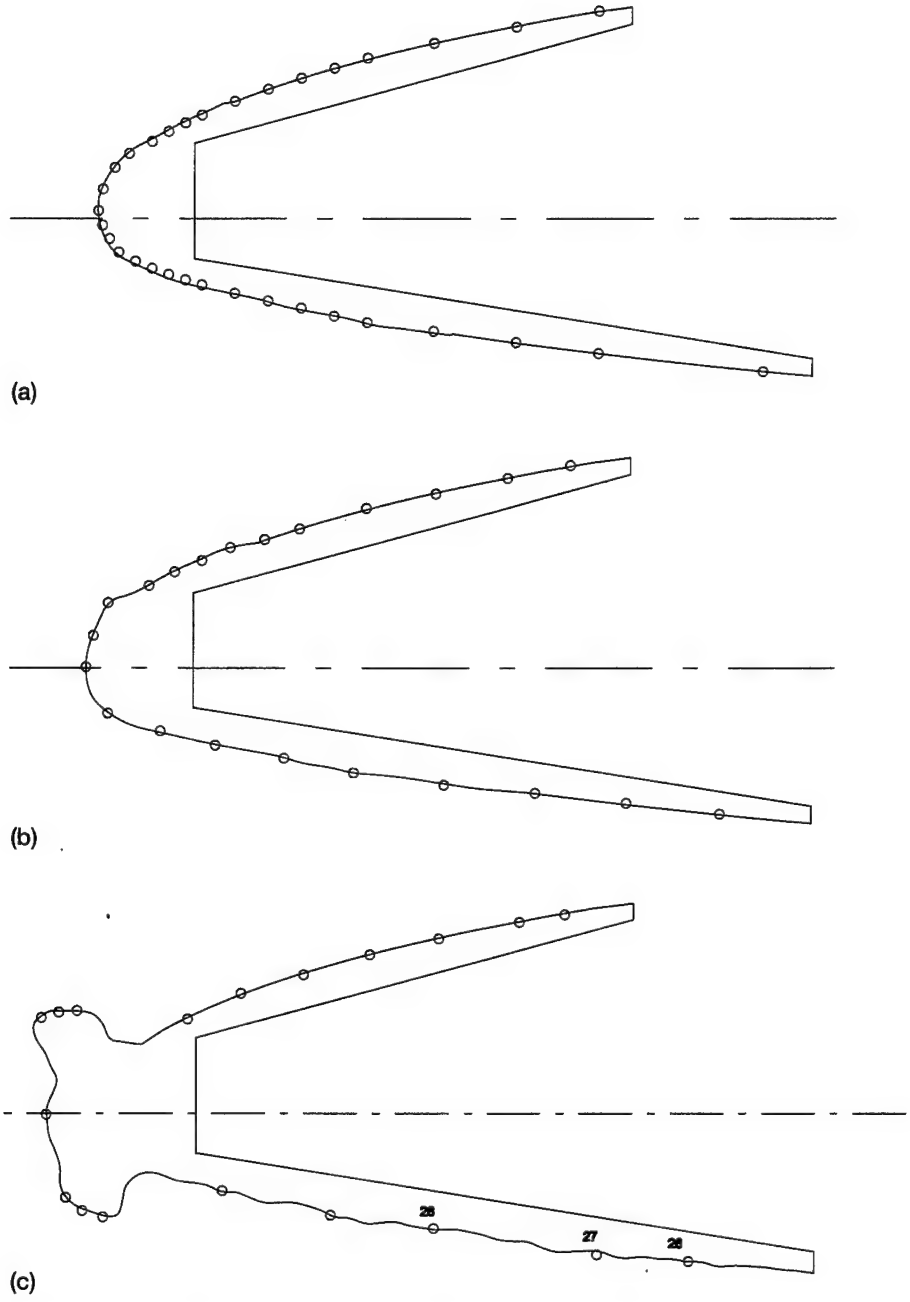

Figure 6.—Ice shape instrumentation pieces for LTPT general aviation model with tap locations shown. (a) 2-min (run 621). (b) 6-min (run 622). (c) 22.5-min (run 623).

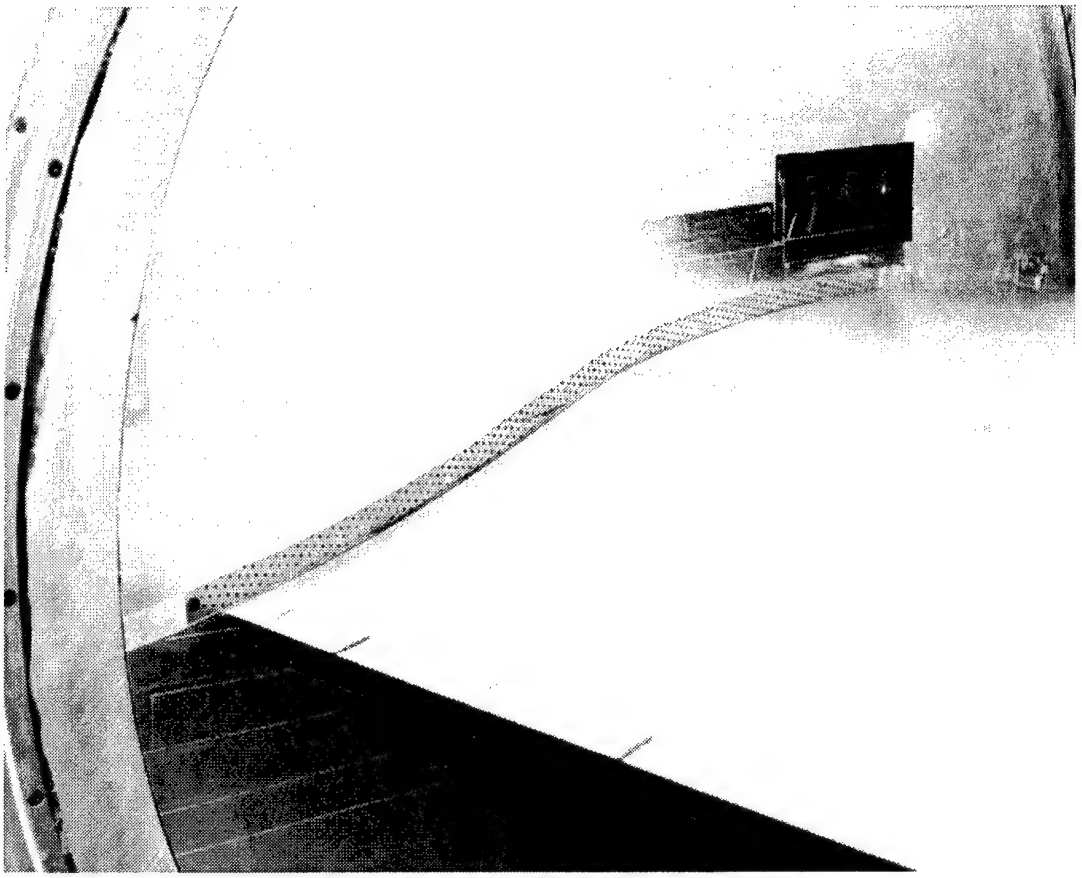

Figure 7.—Sidewall venting over trailing edge of general aviation model in LTPT.

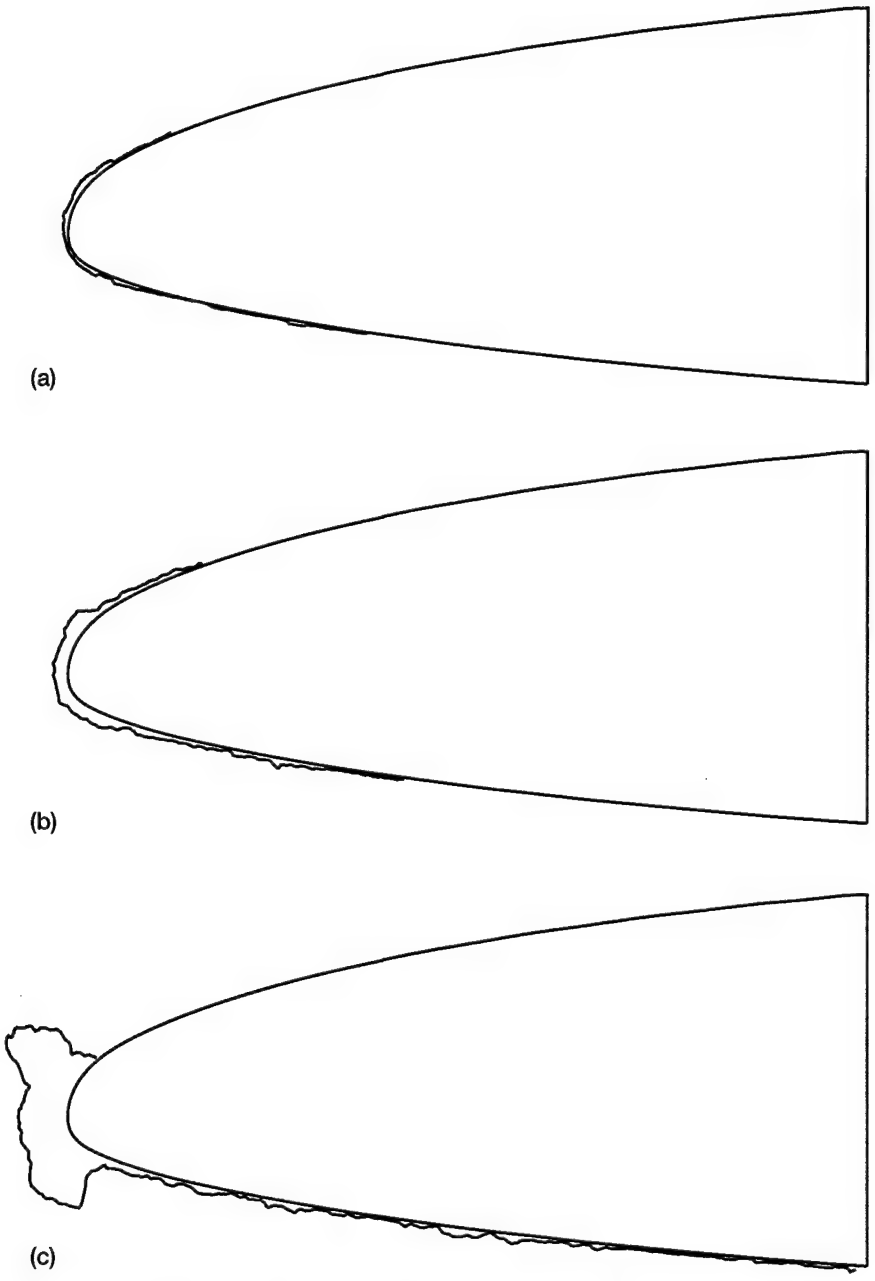

Figure 8.—Tracings of ice shapes for LTPT general aviation model tests. (a) 2-min (run 621). (b) 6-min (run 622). (c) 22.5-min (run 623). Speed, 130 kn; attitude, 2°; total temperature, T_t, 26.4 °F; median volumetric diameter, *MVD*, 20 μm; liquid water content, *LWC*, 0.54 g/m^3.

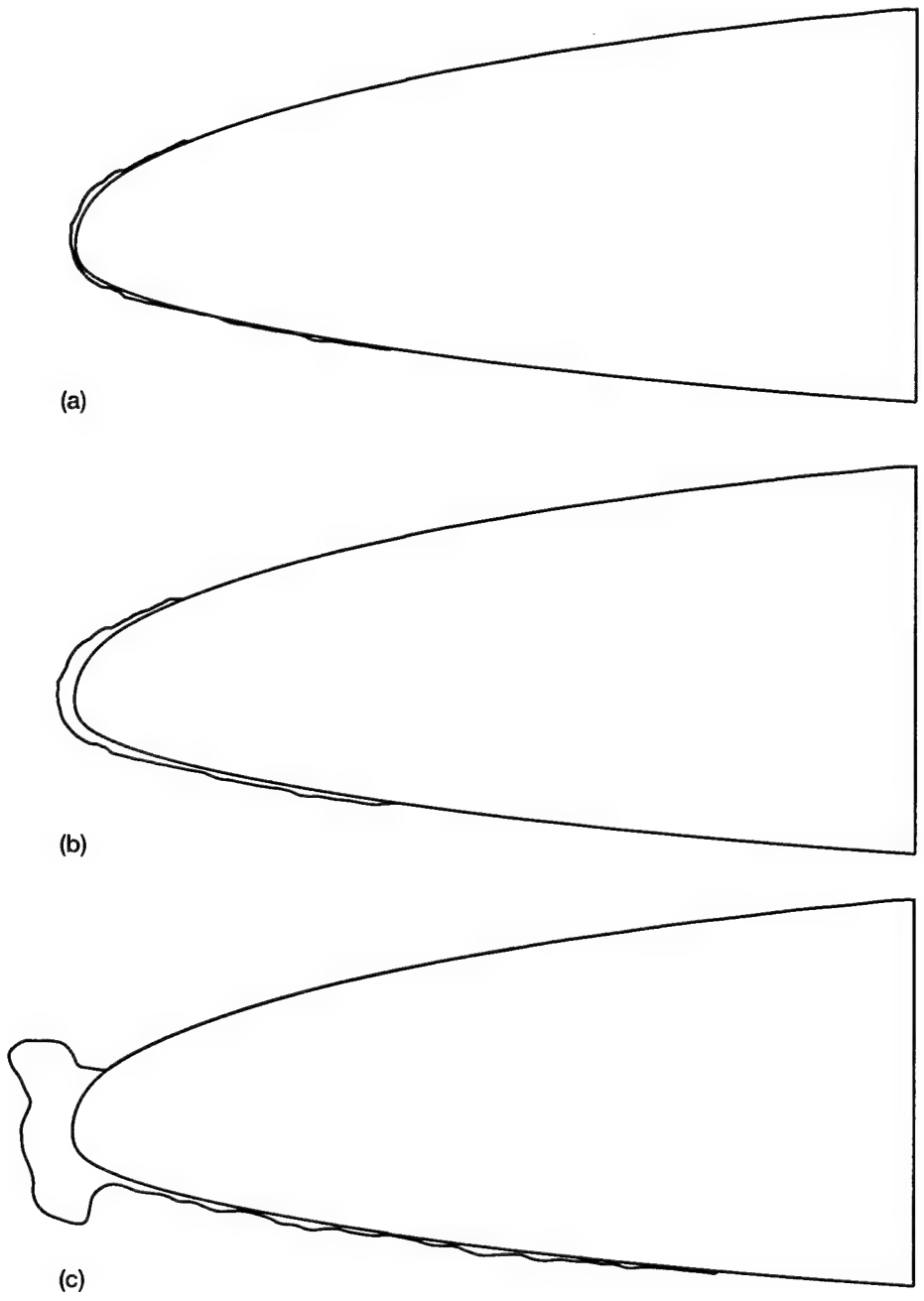

Figure 9.—Smoothed two-dimensional ice shapes for LTPT general aviation model tests. (a) 2-min (run 621). (b) 6-min (run 622). (c) 22.5-min (run 623). Speed, 130 kn; attitude, 2°; total temperature, T_t, 26.4 °F; median volumetric diameter, *MVD*, 20 μm; liquid water content, *LWC*, 0.54 g/m^3.

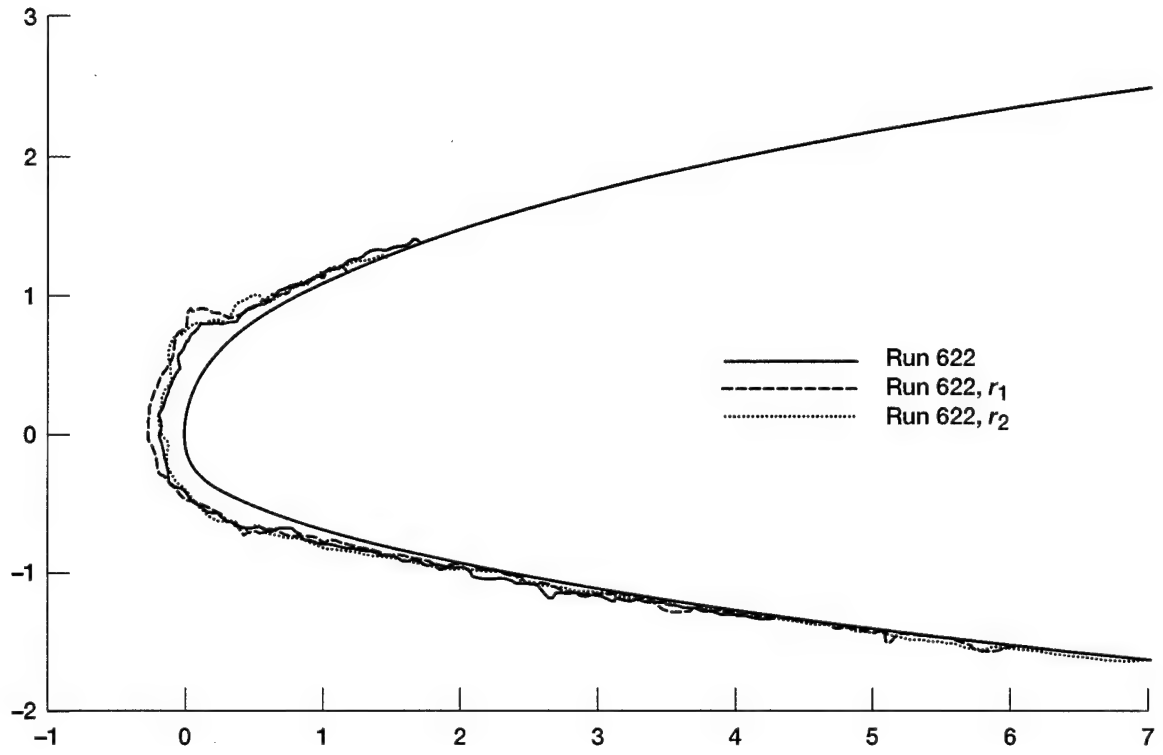

Figure 10.—Ice shape repeatability in Icing Research Tunnel (IRT) (6-min ice shape). First repetition, r_1; second repetition, r_2.

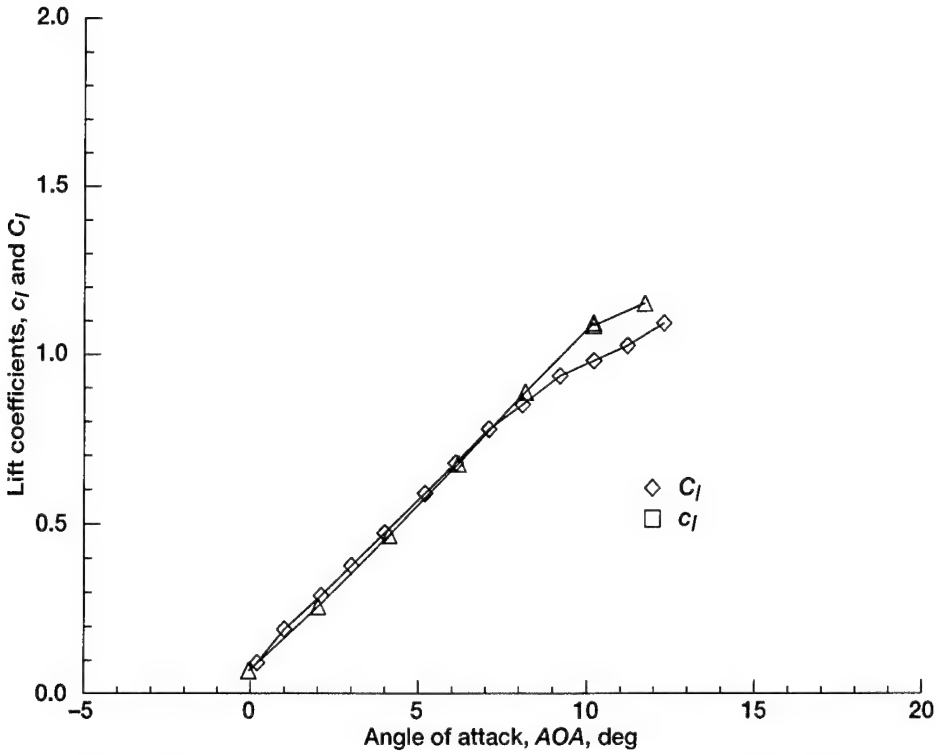

Figure 11.—Lift coefficients from force balance and pressure tap data for the clean business jet model (IRT). Lift coefficient calculated from surface pressure taps, c_l; lift coefficient calculated from force balance measurements, C_l.

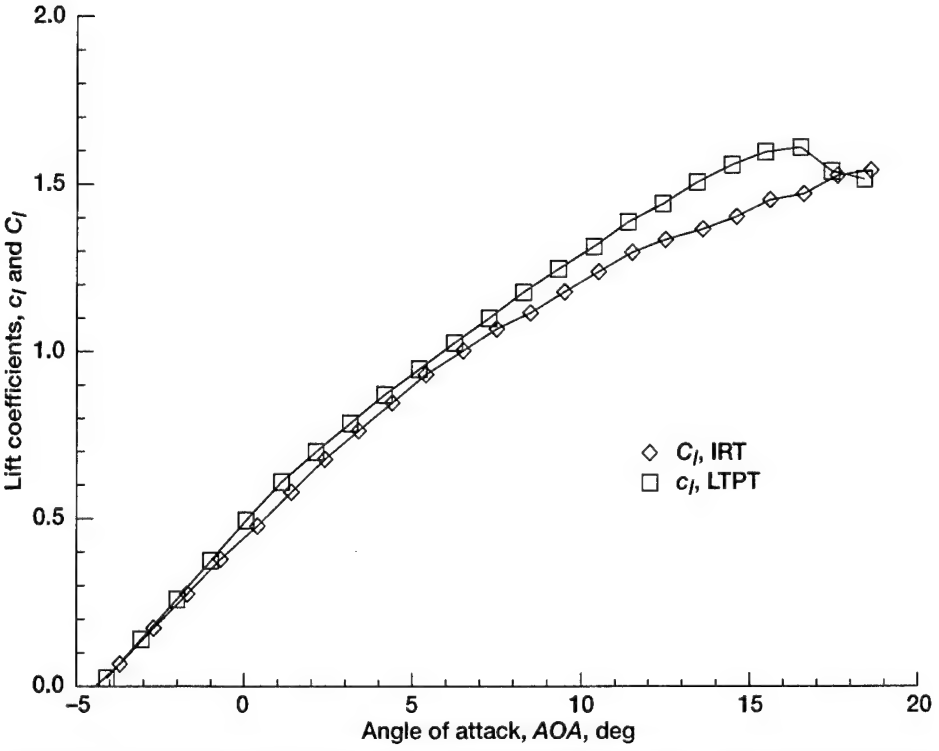

Figure 12.—Comparison of IRT and LTPT lift coefficients (C_l and c_l, respectively) for clean general aviation models. Lift coefficient C_l was calculated from force balance measurements; lift coefficient c_l was calculated from surface pressure taps.

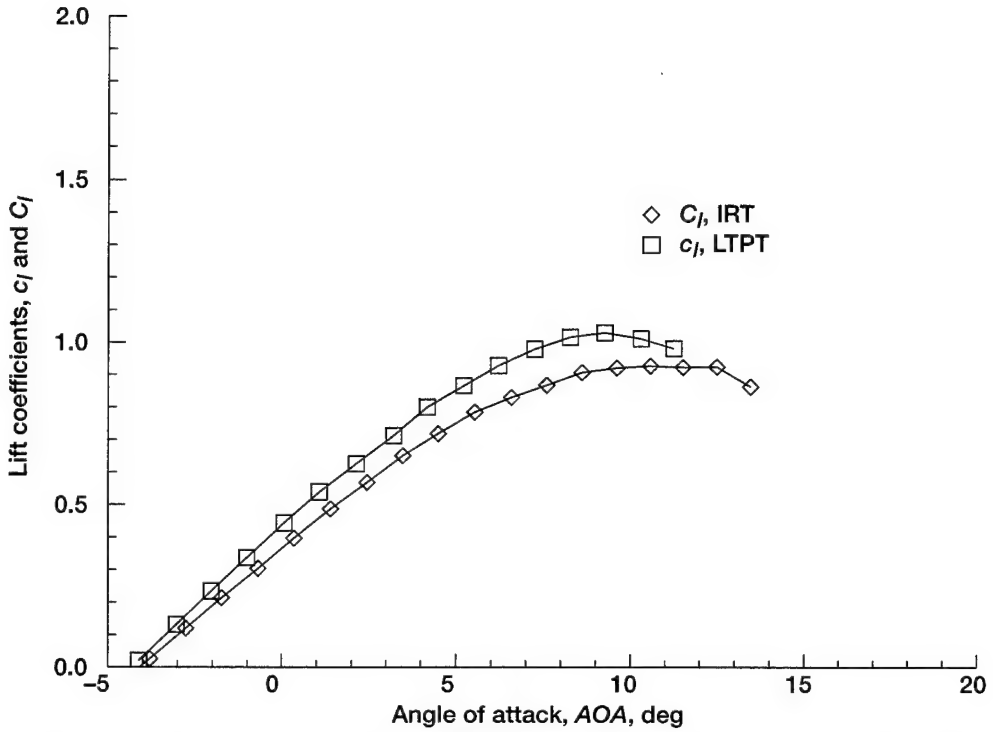

Figure 13.—Comparison of IRT and LTPT lift coefficients (C_l and c_l, respectively) for 6-min ice shape (run 622). Lift coefficient C_l was calculated from force balance measurements; lift coefficient c_l was calculated from surface pressure taps.

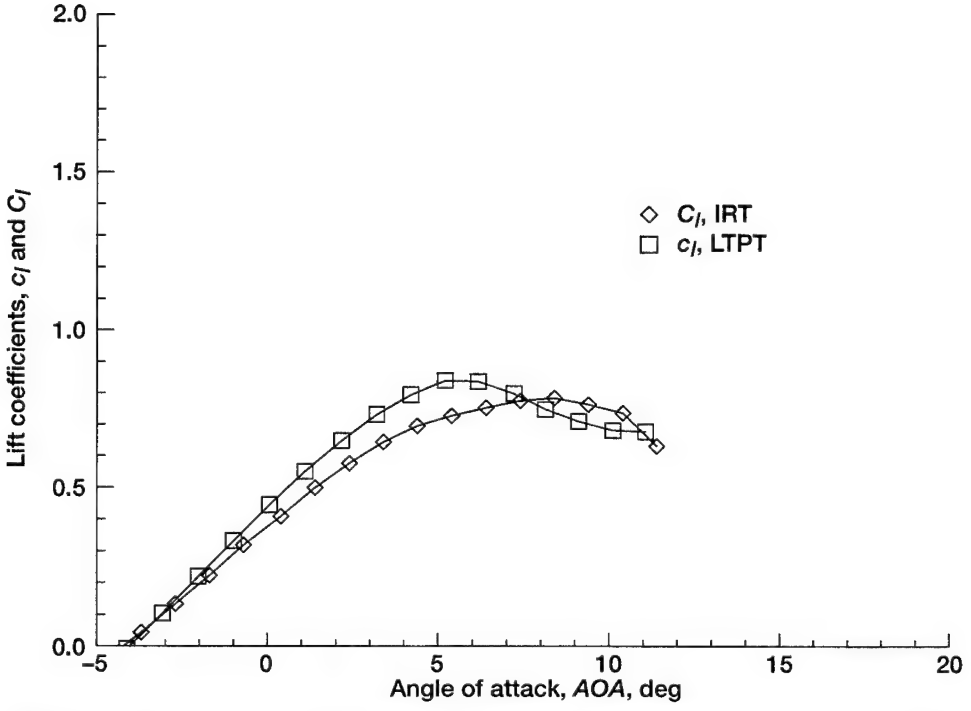

Figure 14.—Comparison of IRT and LTPT lift coefficients (C_l and c_l, respectively) for 22.5-min ice shape (run 623). Lift coefficient C_l was calculated from force balance measurements; lift coefficient c_l was calculated from surface pressure taps.

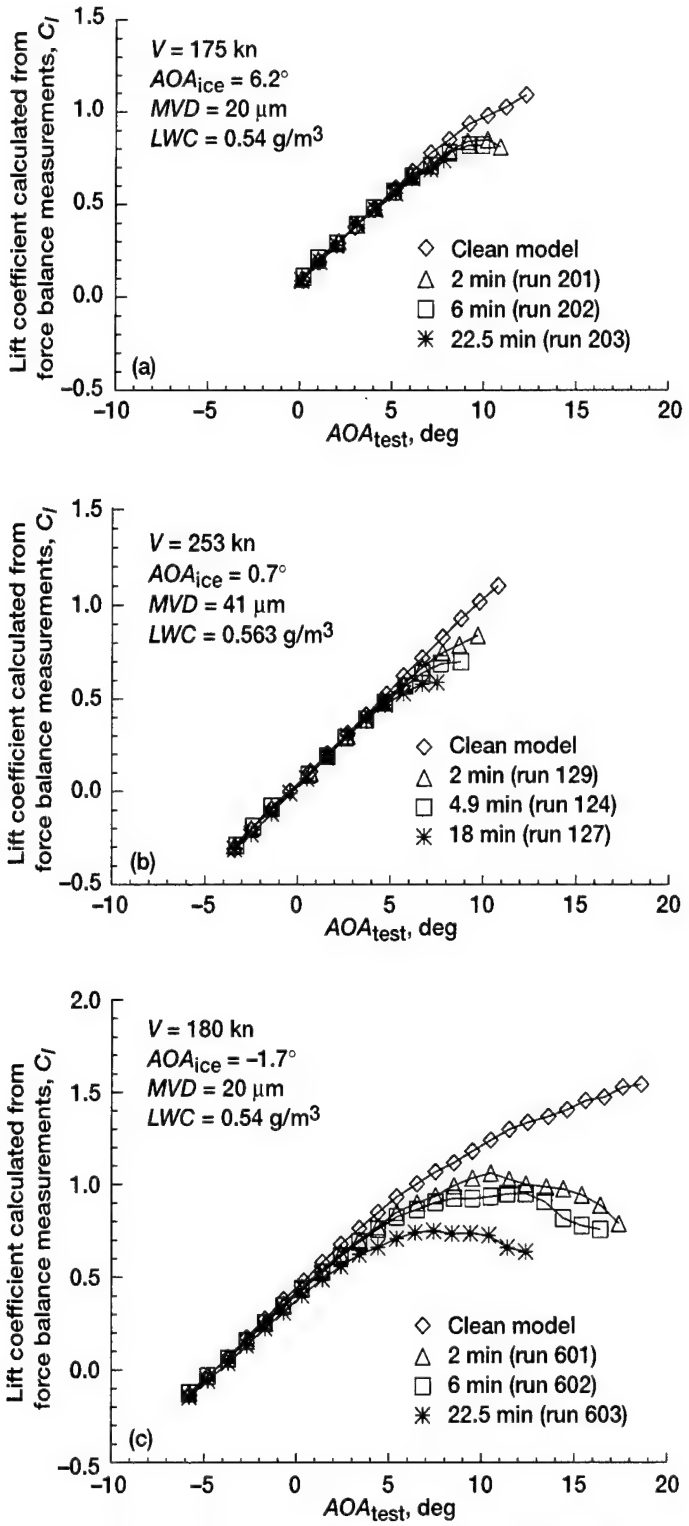

Figure 15.—Effect of various icing exposure times on lift for different models at a total temperature of 30 °F (IRT). (a) Business jet. (b) Commercial transport. (c) General aviation. Velocity, V; median volumetric diameter, MVD; liquid water content, LWC; angle of attack at which ice accretions were formed, AOA_{ice}; angle of attack during testing, AOA_{test}.

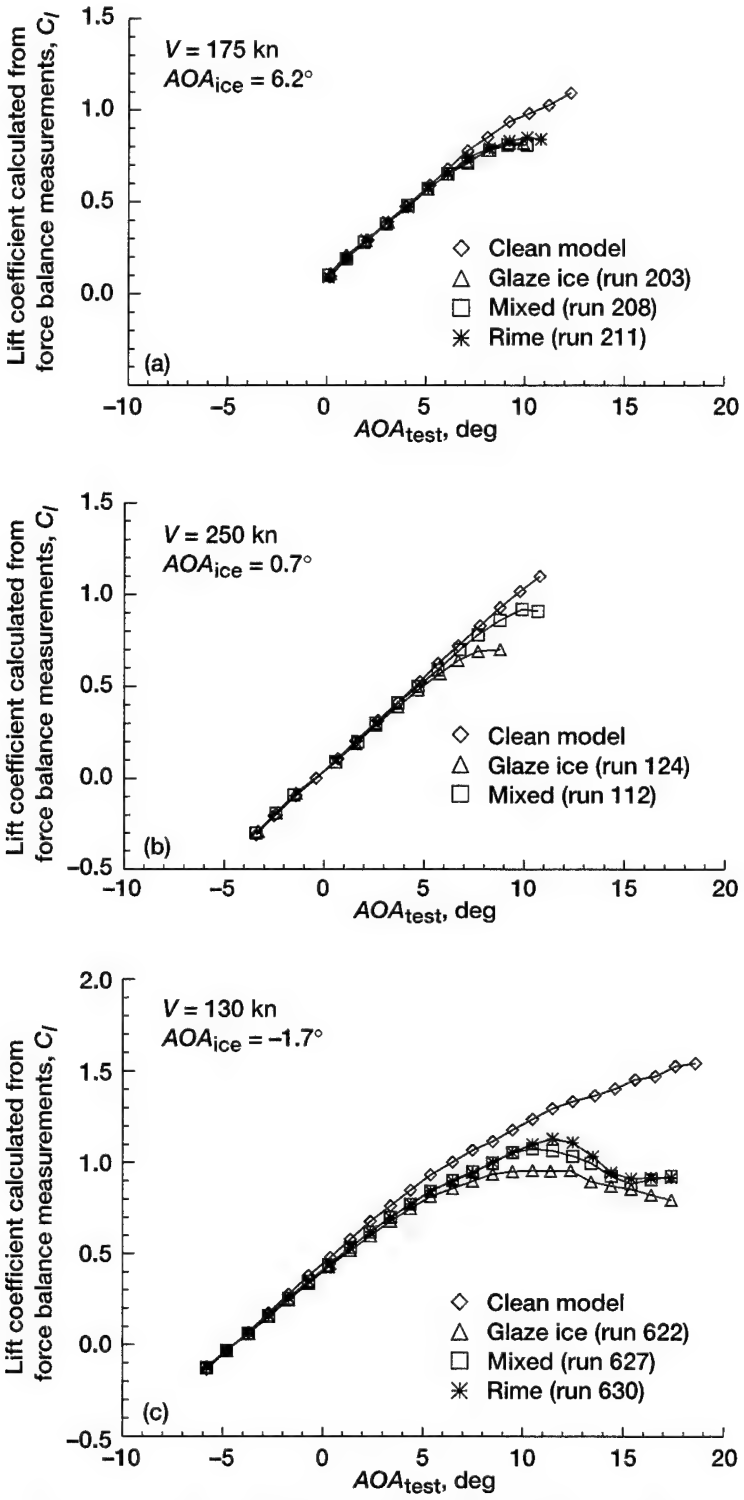

Figure 16.—Effects of different ice types on lift (IRT). (a) Business jet. (b) Commercial transport. (c) General aviation. Velocity, V; angle of attack at which ice accretions were formed, AOA_{ice}; angle of attack during testing, AOA_{test}.

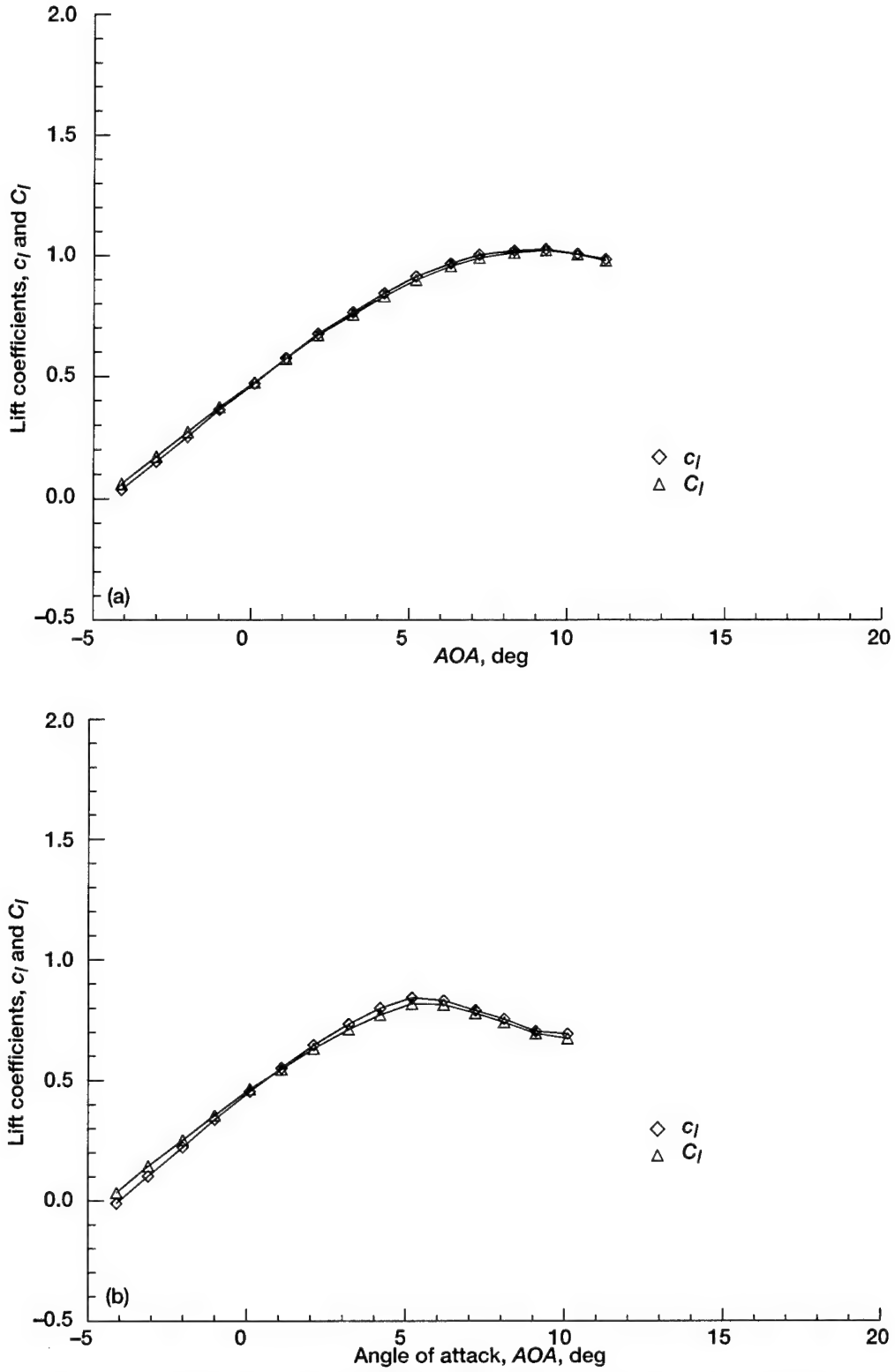

Figure 17.—Comparison of lift coefficients calculated from pressure taps and force balance measurements at a Mach number of 0.21 and a Reynolds number of 10×10^6 for three-dimensional ice shapes (LTPT). (a) 6-min. (b) 22.5-min. Lift coefficient calculated from surface pressure taps, c_l; lift coefficient calculated from force balance measurements, C_l.

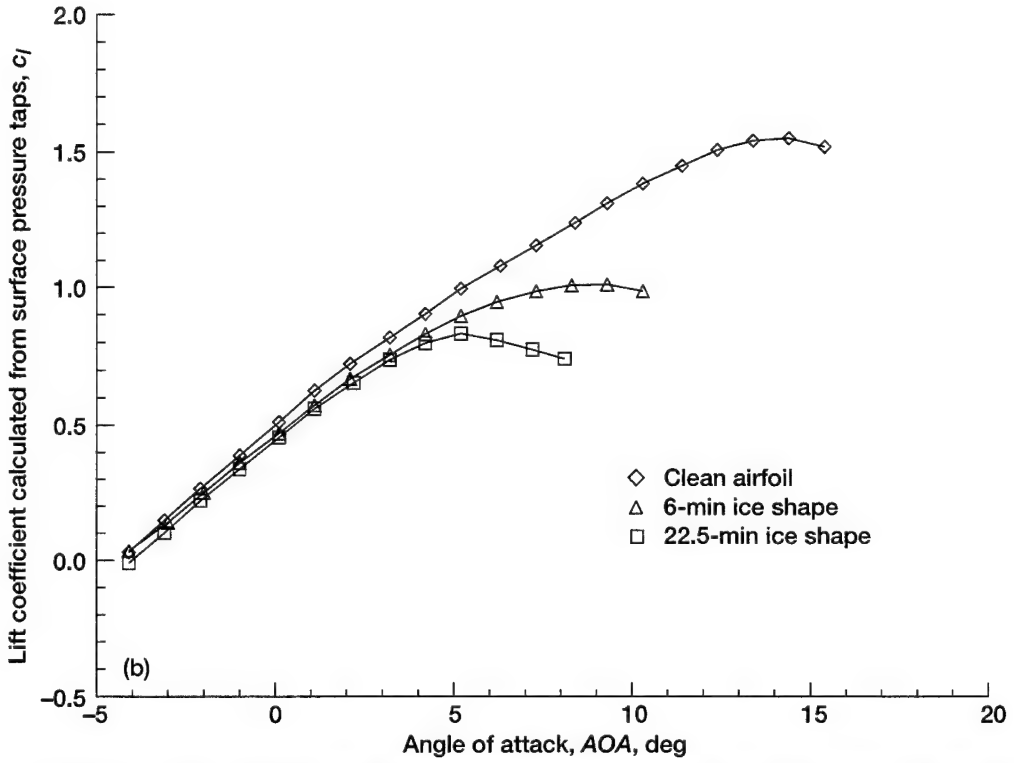

Figure 18.—Lift curves for castings of three-dimensional ice shapes at a Mach number of 0.2 and a Reynolds number of 6.4×10^6 on general aviation airfoil (LTPT).

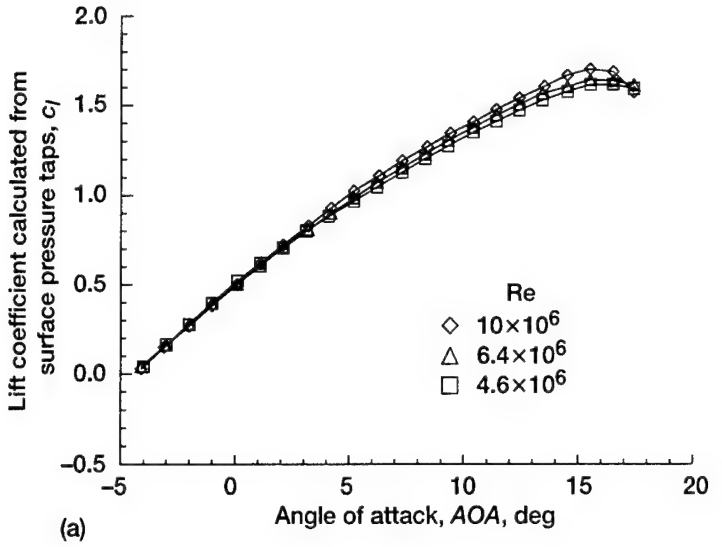

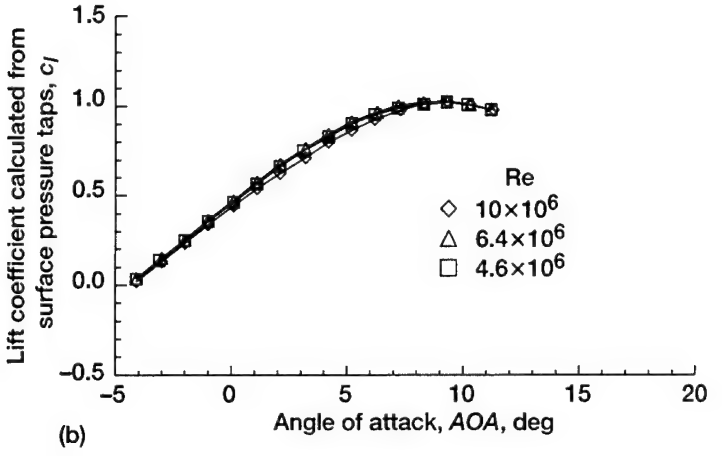

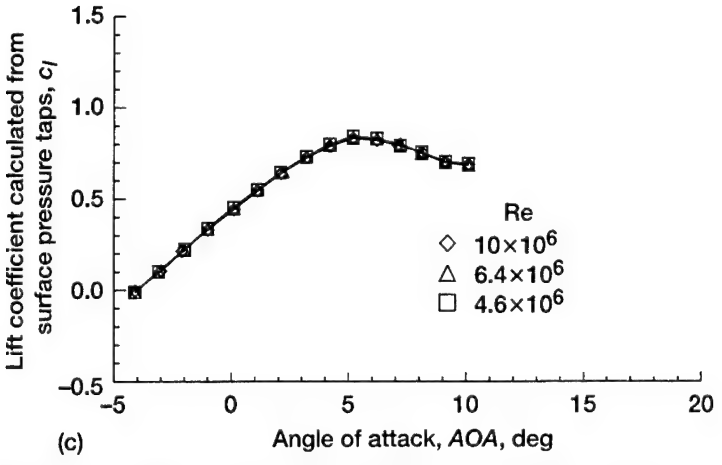

Figure 19.—Effect of Reynolds number, Re, on lift with a Mach number of 0.21 for (a) clean model, and (b) 6-min and (c) 22.5-min three-dimensional ice shapes on general aviation airfoil (LTPT).

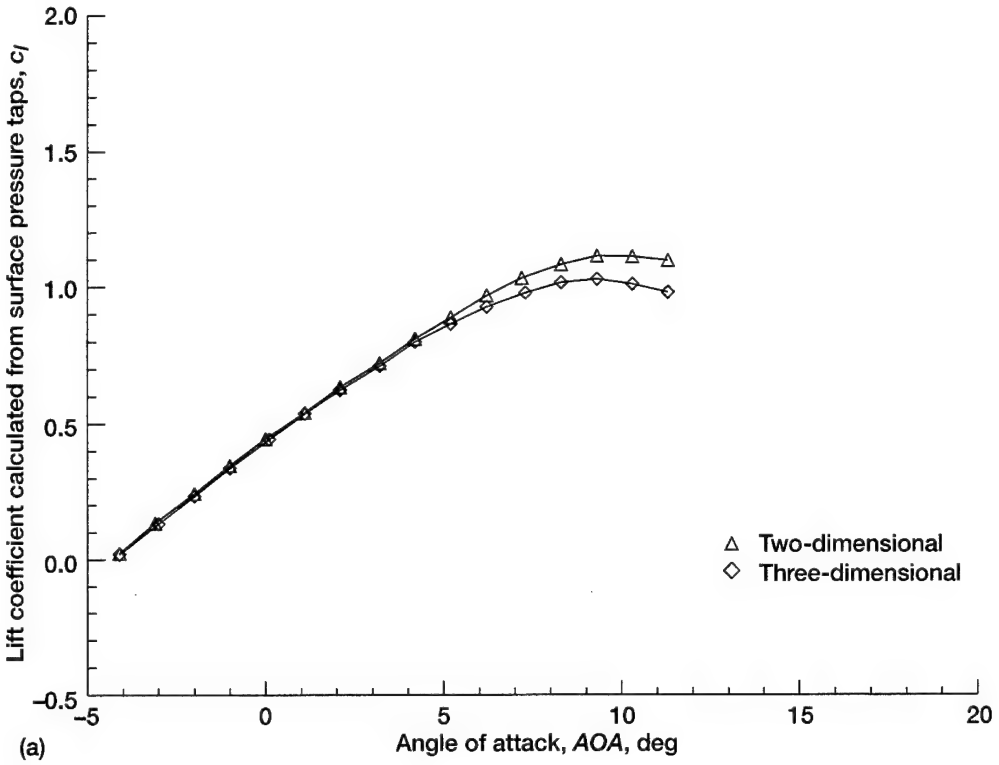

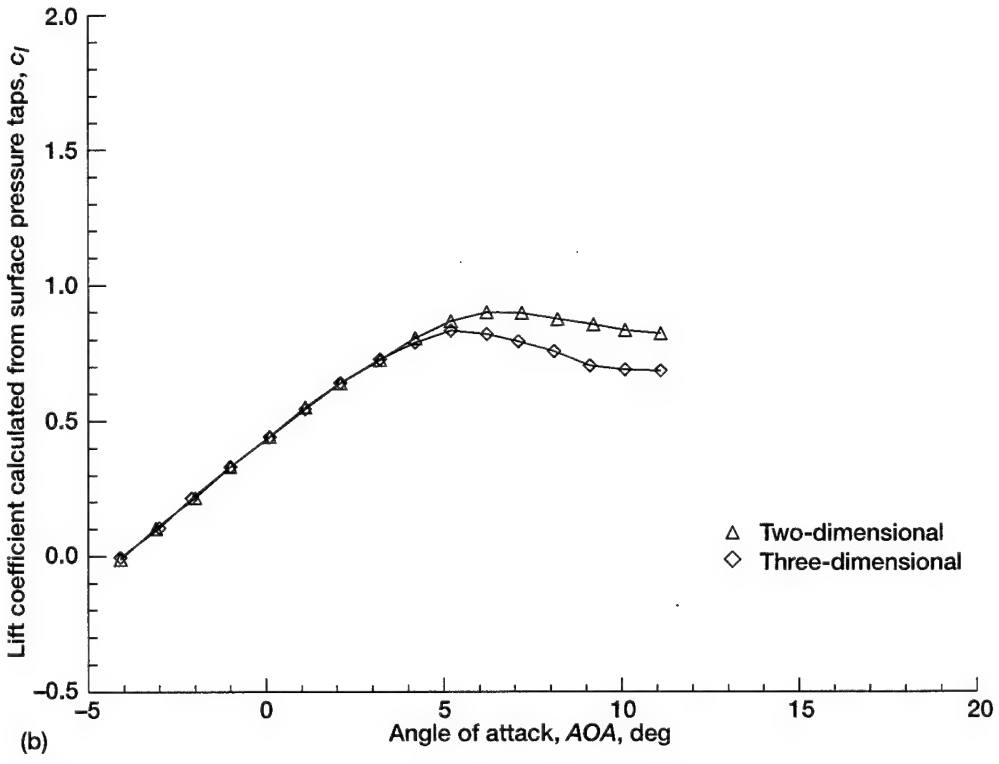

Figure 20.—Comparison of lift curves from (a) 6-min and (b) 22.5-min two- and three-dimensional ice shapes attached to general aviation airfoil at a Mach number of 0.21 and a Reynolds number of 4.6×10^6 (LTPT).

Appendix A
Model Coordinates

A1.—BUSINESS JET AIRFOIL COORDINATES

X / C	Z / C		X / C	Z / C
1.00000	-0.00033		0.00000	-0.00392
0.82500	-0.01321		0.00050	-0.00006
0.80000	-0.01506		0.00100	0.00137
0.77500	-0.01691		0.00150	0.00246
0.75000	-0.01876		0.00200	0.00337
0.72500	-0.02061		0.00300	0.00478
0.70000	-0.02244		0.00400	0.00594
0.67500	-0.02427		0.00500	0.00691
0.65000	-0.02610		0.00750	0.00870
0.62500	-0.02788		0.01000	0.00999
0.60000	-0.02953		0.01250	0.01108
0.57500	-0.03108		0.01500	0.01212
0.55000	-0.03252		0.02000	0.01388
0.52500	-0.03383		0.02500	0.01547
0.50000	-0.03501		0.03000	0.01694
0.47500	-0.03597		0.04000	0.01956
0.45000	-0.03666		0.05000	0.02184
0.42500	-0.03706		0.06000	0.02388
0.40000	-0.03718		0.07500	0.02670
0.37500	-0.03709		0.10000	0.03066
0.35000	-0.03681		0.12500	0.03404
0.32500	-0.03643		0.15000	0.03698
0.30000	-0.03598		0.17500	0.03951
0.27500	-0.03545		0.20000	0.04169
0.25000	-0.03482		0.22500	0.04359
0.22500	-0.03410		0.25000	0.04520
0.20000	-0.03322		0.27500	0.04654
0.17500	-0.03218		0.30000	0.04771
0.15000	-0.03094		0.32500	0.04862
0.12500	-0.02969		0.35000	0.04924
0.10000	-0.02833		0.37500	0.04951
0.07500	-0.02672		0.40000	0.04956
0.06000	-0.02551		0.42500	0.04942
0.05000	-0.02455		0.45000	0.04915
0.04000	-0.02338		0.47500	0.04863
0.03000	-0.02185		0.50000	0.04789
0.02500	-0.02090		0.52500	0.04685
0.02000	-0.01977		0.55000	0.04555
0.01500	-0.01833		0.57500	0.04404
0.01250	-0.01748		0.60000	0.04233
0.01000	-0.01656		0.62500	0.04042
0.00750	-0.01547		0.65000	0.03837
0.00500	-0.01386		0.67500	0.03623
0.00400	-0.01299		0.70000	0.03397
0.00300	-0.01192		0.72500	0.03154
0.00200	-0.01054		0.75000	0.02901
0.00150	-0.00967		0.77500	0.02629
0.00100	-0.00862		0.80000	0.02346
0.00050	-0.00723		0.82500	0.02058
0.00000	-0.00392		1.00000	0.00033

A2.—COMMERCIAL TRANSPORT AIRFOIL COORDINATES

X/C	Z/C	X/C	Z/C	X/C	Z/C	X/C	Z/C
1.000000	0.008649	0.349370	-0.033927	0.035223	0.029423	0.635551	0.043928
0.990740	0.007881	0.335871	-0.033921	0.041185	0.031511	0.648984	0.042839
0.980977	0.007064	0.322380	-0.033840	0.047581	0.033515	0.662418	0.041710
0.970724	0.006200	0.308910	-0.033732	0.054426	0.035429	0.675855	0.040544
0.960003	0.005287	0.295466	-0.033585	0.061730	0.037255	0.689294	0.039347
0.948844	0.004332	0.282057	-0.033411	0.069503	0.038992	0.702733	0.038120
0.937286	0.003333	0.268695	-0.033220	0.077750	0.040642	0.716173	0.036867
0.925373	0.002286	0.255396	-0.033018	0.086474	0.042203	0.729612	0.035592
0.913150	0.001195	0.242180	-0.032802	0.095671	0.043677	0.743047	0.034298
0.900662	0.000006	0.229070	-0.032567	0.105330	0.045066	0.756476	0.032989
0.887952	-0.001095	0.216091	-0.032306	0.115436	0.046372	0.769895	0.031670
0.875058	-0.002281	0.203272	-0.032010	0.125964	0.047594	0.783298	0.030345
0.862015	-0.003489	0.190642	-0.031669	0.136887	0.048731	0.796679	0.029018
0.848852	-0.004715	0.178234	-0.031278	0.148171	0.049785	0.810027	0.027689
0.835594	-0.005957	0.166084	-0.030817	0.159781	0.050754	0.823333	0.026365
0.822262	-0.007211	0.154228	-0.030289	0.171677	0.051649	0.836583	0.025048
0.808873	-0.008473	0.142703	-0.029705	0.183822	0.052471	0.849759	0.023742
0.795441	-0.009737	0.131547	-0.029071	0.196182	0.052321	0.862842	0.022453
0.781977	-0.011000	0.120795	-0.028388	0.208722	0.053863	0.875806	0.021182
0.768490	-0.012261	0.110477	-0.027658	0.221416	0.054424	0.888621	0.019933
0.754987	-0.013517	0.100617	-0.026881	0.234237	0.054900	0.901254	0.018711
0.741474	-0.014763	0.091231	-0.026063	0.247170	0.055276	0.913667	0.017521
0.727956	-0.015994	0.082328	-0.025204	0.260202	0.055525	0.925817	0.016370
0.714434	-0.017206	0.073906	-0.024309	0.273324	0.055658	0.937660	0.015266
0.700912	-0.018395	0.065958	-0.023373	0.286525	0.055719	0.949149	0.014211
0.687390	-0.019556	0.058473	-0.022407	0.299796	0.055754	0.960241	0.013201
0.673870	-0.020686	0.051434	-0.021387	0.313123	0.055776	0.970898	0.012236
0.660352	-0.021783	0.044823	-0.020314	0.326492	0.055788	0.981090	0.011321
0.646836	-0.022843	0.038616	-0.019194	0.339889	0.055780	0.990794	0.010457
0.633332	-0.023862	0.032792	-0.018027	0.353305	0.055740	0.999998	0.009644
0.619810	-0.024838	0.027333	-0.016797	0.366733	0.055654		
0.606300	-0.025769	0.022232	-0.015467	0.380170	0.055512		
0.592791	-0.026652	0.017490	-0.014001	0.393614	0.055318		
0.579282	-0.027486	0.013107	-0.012388	0.407064	0.055086		
0.565772	-0.028267	0.009090	-0.010609	0.420517	0.054819		
0.552262	-0.028998	0.005522	-0.008558	0.433973	0.054510		
0.538750	-0.029676	0.002576	-0.006619	0.447428	0.054154		
0.525237	-0.030300	0.000617	-0.003357	0.460880	0.053752		
0.511720	-0.030871	0.000002	-0.000278	0.474331	0.053300		
0.498201	-0.031389	0.000330	0.002726	0.487778	0.052799		
0.484678	-0.031856	0.000330	0.002726	0.501221	0.052248		
0.471153	-0.032270	0.001411	0.005723	0.514662	0.051645		
0.457624	-0.032635	0.003123	0.008853	0.528100	0.050990		
0.444092	-0.032952	0.005434	0.011807	0.541535	0.050282		
0.430558	-0.033221	0.008321	0.014781	0.554968	0.049523		
0.417026	-0.033445	0.011711	0.017531	0.568399	0.048712		
0.430487	-0.033624	0.015544	0.020162	0.581829	0.047851		
0.389952	-0.033760	0.019824	0.022656	0.595259	0.046940		
0.376420	-0.033855	0.024542	0.025013	0.608689	0.045981		
0.362894	-0.033910	0.029678	0.027260	0.622119	0.044977		

A3.—GENERAL AVIATION AIRFOIL COORDINATES

X/C	Z/C	X/C	Z/C	X/C	Z/C	X/C	Z/C
1.00000	-0.02751	0.47869	-0.05985	0.00286	0.01082	0.54838	0.07817
0.99471	-0.02723	0.46171	-0.05964	0.00653	0.01601	0.56558	0.07680
0.98894	-0.02695	0.44476	-0.05935	0.01154	0.02066	0.58268	0.07524
0.98271	-0.02669	0.42788	-0.05897	0.01762	0.02472	0.59967	0.07346
0.97602	-0.02645	0.41107	-0.05851	0.02450	0.02836	0.61653	0.07147
0.96886	-0.02624	0.39435	-0.05796	0.03202	0.03177	0.63322	0.06926
0.96123	-0.02604	0.37775	-0.05732	0.04009	0.03506	0.64974	0.06682
0.95316	-0.02587	0.36128	-0.05661	0.04869	0.03823	0.66605	0.06414
0.94463	-0.02573	0.34495	-0.05583	0.05782	0.04127	0.68211	0.06115
0.93565	-0.02562	0.32879	-0.05497	0.06745	0.04418	0.69790	0.05777
0.92623	-0.02556	0.31282	-0.05405	0.07757	0.04696	0.71336	0.05394
0.91638	-0.02556	0.29704	-0.05307	0.08816	0.04962	0.72845	0.04963
0.90611	-0.02565	0.28148	-0.05203	0.09921	0.05218	0.74315	0.04491
0.89542	-0.02586	0.26616	-0.05094	0.11070	0.05463	0.75749	0.03993
0.88432	-0.02621	0.25108	-0.04980	0.12261	0.05699	0.77149	0.03484
0.87283	-0.02671	0.23627	-0.04860	0.13494	0.05926	0.78519	0.02979
0.86096	-0.02739	0.22174	-0.04736	0.14766	0.06147	0.79860	0.02488
0.84872	-0.02825	0.20751	-0.04607	0.16076	0.06360	0.81175	0.02016
0.83613	-0.02930	0.19358	-0.04474	0.17423	0.06566	0.82461	0.01567
0.82319	-0.03053	0.17998	-0.04335	0.18805	0.06763	0.83719	0.01142
0.80993	-0.03196	0.16672	-0.04193	0.20221	0.06950	0.84947	0.00744
0.79635	-0.03359	0.15381	-0.04047	0.21671	0.07128	0.86143	0.00372
0.78249	-0.03548	0.14126	-0.03896	0.23151	0.07294	0.87308	0.00027
0.76838	-0.03772	0.12909	-0.03742	0.24661	0.07449	0.88438	-0.00293
0.75404	-0.04036	0.11730	-0.03584	0.26198	0.07591	0.89533	-0.00587
0.73948	-0.04333	0.10592	-0.03422	0.27762	0.07720	0.90591	-0.00859
0.72468	-0.04641	0.09494	-0.03255	0.29351	0.07837	0.91611	-0.01108
0.70959	-0.04929	0.08438	-0.03084	0.30962	0.07940	0.92591	-0.01337
0.69418	-0.05170	0.07426	-0.02909	0.32594	0.08030	0.93530	-0.01546
0.67849	-0.05357	0.06457	-0.02731	0.34245	0.08107	0.94426	-0.01737
0.66255	-0.05501	0.05533	-0.02549	0.35913	0.08169	0.95280	-0.01912
0.64641	-0.05617	0.04655	-0.02363	0.37597	0.08216	0.96090	-0.02070
0.63010	-0.05715	0.03824	-0.02169	0.39294	0.08248	0.96856	-0.02211
0.61363	-0.05798	0.03043	-0.01966	0.41002	0.08265	0.97577	-0.02338
0.59703	-0.05865	0.02312	-0.01749	0.42720	0.08267	0.98252	-0.02451
0.58031	-0.05917	0.01635	-0.01515	0.44445	0.08252	0.98881	-0.02550
0.56350	-0.05955	0.01016	-0.01257	0.46175	0.08221	0.99464	-0.02636
0.54661	-0.05982	0.00475	-0.00949	0.47909	0.08175		
0.52967	-0.05997	0.00104	-0.00516	0.49645	0.08112		
0.51269	-0.06002	0.00000	0.00000	0.51379	0.08032		
0.49569	-0.05998	0.00069	0.00536	0.53111	0.07934		

Appendix B
Pressure Tap and Thermocouple Coordinates

B1.—BUSINESS JET PRESSURE TAP LOCATIONS
[Y measured from tunnel centerline]

No.	X/C	Y/C	Z/C	X, (in)	Y, (in)	Z, (in)
1	0.9700	-0.0833	-0.0026	34.920	-3.000	-0.094
2	0.9300	-0.0833	-0.0055	33.480	-3.000	-0.198
3	0.9000	-0.0833	-0.0077	32.400	-3.000	-0.277
4	0.8000	-0.0833	-0.0151	28.800	-3.000	-0.544
5	0.7000	-0.0833	-0.0224	25.200	-3.000	-0.806
6	0.6000	-0.0833	-0.0295	21.600	-3.000	-1.062
7	0.5000	-0.0833	-0.0350	18.000	-3.000	-1.260
8	0.4000	-0.0833	-0.0372	14.400	-3.000	-1.339
9	0.3000	-0.0833	-0.0360	10.800	-3.000	-1.296
10	0.2000	-0.0833	-0.0332	7.200	-3.000	-1.195
11	0.1000	-0.0833	-0.0284	3.600	-3.000	-1.022
12	0.0800	-0.0833	-0.0271	2.880	-3.000	-0.976
13	0.0600	-0.0833	-0.0255	2.160	-3.000	-0.918
14	0.0400	-0.0833	-0.0233	1.440	-3.000	-0.839
15	0.0200	-0.0833	-0.0197	0.720	-3.000	-0.709
16	0.0100	-0.0833	-0.0165	0.360	-3.000	-0.594
17	0.0040	-0.0833	-0.0128	0.144	-3.000	-0.461
18	0.0005	-0.0833	-0.0073	0.018	-3.000	-0.263
19	0.0000	-0.0833	0.0000	0.000	-3.000	0.000
20	0.0050	-0.0833	0.0065	0.180	-3.000	0.234
21	0.0100	-0.0833	0.0100	0.360	-3.000	0.360
22	0.0150	-0.0833	0.0121	0.540	-3.000	0.436
23	0.0200	-0.0833	0.0138	0.720	-3.000	0.497
24	0.0300	-0.0833	0.0170	1.080	-3.000	0.612
25	0.0400	-0.0833	0.0196	1.440	-3.000	0.706
26	0.0500	-0.0833	0.0218	1.800	-3.000	0.785
27	0.0600	-0.0833	0.0239	2.160	-3.000	0.860
28	0.0700	-0.0833	0.0257	2.520	-3.000	0.925
29	0.0800	-0.0833	0.0274	2.880	-3.000	0.986
30	0.0900	-0.0833	0.0290	3.240	-3.000	1.044
31	0.1000	-0.0833	0.0307	3.600	-3.000	1.105
32	0.1500	-0.0833	0.0370	5.400	-3.000	1.332
33	0.2000	-0.0833	0.0417	7.200	-3.000	1.501
34	0.2500	-0.0833	0.0452	9.000	-3.000	1.627
35	0.3000	-0.0833	0.0476	10.800	-3.000	1.714
36	0.4000	-0.0833	0.0496	14.400	-3.000	1.786
37	0.5000	-0.0833	0.0478	18.000	-3.000	1.721
38	0.6000	-0.0833	0.0424	21.600	-3.000	1.526
39	0.7000	-0.0833	0.0340	25.200	-3.000	1.224
40	0.8000	-0.0833	0.0234	28.800	-3.000	0.842
41	0.9000	-0.0833	0.0119	32.400	-3.000	0.428
42	0.9300	-0.0833	0.0090	33.480	-3.000	0.324
43	0.9700	-0.0833	0.0038	34.920	-3.000	0.137
44	1.0000	-0.0833	0.0000	36.000	-3.000	0.000
	Thermocouple Locations					
	X/C	Y/C	Z/C	X, (in)	Y, (in)	Z, (in)
1	0.1000	0.0833	-0.0284	3.600	3.000	-1.022
2	0.0500	0.0833	-0.0241	1.800	3.000	-0.868
3	0.1000	0.0833	0.0307	3.600	3.000	1.104
4	0.0500	0.0833	0.0218	1.800	3.000	0.786
5	0.0000	0.0833	0.0000	0.000	3.000	0.000
6	0.0000	-0.2500	0.0000	0.000	-9.000	0.000

B2.—COMMERCIAL TRANSPORT PRESSURE TAP LOCATIONS

No.	X/C	Y/C	Z/C	X, (in.)	Y, (in.)	Z, (in.)
1	0.9700	-0.0833	0.0061	34.920	-3.000	0.221
2	0.9278	-0.0833	0.0027	33.400	-3.000	0.097
3	0.9000	-0.0833	0.0000	32.400	-3.000	0.000
4	0.8000	-0.0833	-0.0093	28.800	-3.000	-0.335
5	0.7000	-0.0833	-0.0185	25.200	-3.000	-0.665
6	0.6000	-0.0833	-0.0262	21.600	-3.000	-0.943
7	0.5000	-0.0833	-0.0313	18.000	-3.000	-1.128
8	0.4000	-0.0833	-0.0337	14.400	-3.000	-1.212
9	0.3000	-0.0833	-0.0336	10.800	-3.000	-1.211
10	0.2000	-0.0833	-0.0319	7.200	-3.000	-1.149
11	0.1000	-0.0833	-0.0268	3.600	-3.000	-0.966
12	0.0800	-0.0833	-0.0250	2.880	-3.000	-0.898
13	0.0600	-0.0833	-0.0226	2.160	-3.000	-0.814
14	0.0400	-0.0833	-0.0194	1.440	-3.000	-0.700
15	0.0200	-0.0833	-0.0148	0.720	-3.000	-0.532
16	0.0100	-0.0833	-0.0110	0.360	-3.000	-0.396
17	0.0000	-0.0833	-0.0003	0.000	-3.000	-0.010
18	0.0050	-0.0833	0.0113	0.180	-3.000	0.408
19	0.0100	-0.0833	0.0161	0.360	-3.000	0.581
20	0.0150	-0.0833	0.0198	0.540	-3.000	0.712
21	0.0200	-0.0833	0.0227	0.720	-3.000	0.819
22	0.0300	-0.0833	0.0274	1.080	-3.000	0.986
23	0.0400	-0.0833	0.0311	1.440	-3.000	1.120
24	0.0500	-0.0833	0.0342	1.800	-3.000	1.231
25	0.0600	-0.0833	0.0368	2.160	-3.000	1.326
26	0.0700	-0.0833	0.0391	2.520	-3.000	1.407
27	0.0800	-0.0833	0.0410	2.880	-3.000	1.478
28	0.0900	-0.0833	0.0428	3.240	-3.000	1.540
29	0.1000	-0.0833	0.0443	3.600	-3.000	1.595
30	0.1250	-0.0833	0.0475	4.500	-3.000	1.709
31	0.1500	-0.0833	0.0499	5.400	-3.000	1.798
32	0.1750	-0.0833	0.0519	6.300	-3.000	1.867
33	0.2000	-0.0833	0.0534	7.200	-3.000	1.923
34	0.2500	-0.0833	0.0553	9.000	-3.000	1.992
35	0.3000	-0.0833	0.0558	10.800	-3.000	2.007
36	0.4000	-0.0833	0.0552	14.400	-3.000	1.988
37	0.5000	-0.0833	0.0523	18.000	-3.000	1.883
38	0.6000	-0.0833	0.0466	21.600	-3.000	1.678
39	0.7000	-0.0833	0.0384	25.200	-3.000	1.381
40	0.8000	-0.0833	0.0287	28.800	-3.000	1.033
41	0.9000	-0.0833	0.0188	32.400	-3.000	0.678
42	0.9300	-0.0833	0.0160	33.480	-3.000	0.575
43	0.9700	-0.0833	0.0123	34.920	-3.000	0.443
44	1.0000	-0.0833	0.0087	36.000	-3.000	0.311
	Thermocouple Locations					
	X/C	Y/C	Z/C	X, (in.)	Y, (in.)	Z, (in.)
1	0.1000	0.0833	-0.0284	3.600	3.000	-1.022
2	0.0500	0.0833	-0.0241	1.800	3.000	-0.868
3	0.1000	0.0833	-0.0307	3.600	3.000	-1.104
4	0.0500	0.0833	-0.0218	1.800	3.000	-0.786
5	0.0000	0.0833	0.0000	0.000	3.000	0.000
6	0.0000	-0.2500	0.0000	0.000	-9.000	0.000

B3.—GENERAL AVIATION PRESSURE TAP LOCATIONS
[Y measured from tunnel centerline]

No.	X/C	Y/C	Z/C	X, (in.)	Y, (in.)	Z, (in.)
1	0.59703	-0.08333	-0.05865	21.493	-3.000	-2.112
2	0.09494	-0.13889	-0.03255	3.418	-5.000	-1.172
3	0.00475	-0.16111	-0.00949	0.171	-5.800	-0.342
4	0.00000	-0.16667	0.00000	0.000	-6.000	0.000
5	0.00653	-0.17222	0.01601	0.235	-6.200	0.576
6	0.08816	-0.13889	0.04962	3.174	-5.000	1.786
7	0.59967	-0.08333	0.07346	21.588	-3.000	2.645
	General Aviation Thermocouple Locations					
	X/C	Y/C	Z/C	X, (in.)	Y, (in.)	Z, (in.)
1	0.00000	0.50000	0.00000	0.000	18.000	0.000
2	0.59967	0.50000	0.07346	21.588	18.000	2.645

B4.—GENERAL AVIATION (LTPT) PRESSURE TAP LOCATIONS
[Baseline leading edge and main body]

No.	x/c	y/c	z/c	x, in.	y, in.	z, in.	
1	0.97000	0.13074	-0.02630	34.920	4.707	-0.947	
2	0.95000	0.12575	-0.02580	34.200	4.527	-0.929	
3	0.90000	0.11328	-0.02570	32.400	4.078	-0.925	
4	0.85000	0.10082	-0.02820	30.600	3.629	-1.015	
5	0.82500	0.09459	-0.03053	29.700	3.405	-1.099	
6	0.80000	0.08835	-0.03320	28.800	3.181	-1.195	
7	0.78750	0.08524	-0.03500	28.350	3.068	-1.260	
8	0.77500	0.08212	-0.03670	27.900	2.956	-1.321	
9	0.76250	0.07900	-0.03890	27.450	2.844	-1.400	
10	0.75000	0.07589	-0.04110	27.000	2.732	-1.480	
11	0.73750	0.07277	-0.04370	26.550	2.620	-1.573	
12	0.72500	0.06965	-0.04640	26.100	2.507	-1.670	
13	0.71250	0.06654	-0.04860	25.650	2.395	-1.750	
14	0.70000	0.06342	-0.05090	25.200	2.283	-1.832	
15	0.67500	0.05719	-0.05390	24.300	2.059	-1.940	
16	0.65000	0.05971	-0.05600	23.400	2.150	-2.016	
17	0.62500	0.06594	-0.05750	22.500	2.374	-2.070	
18	0.60000	0.07218	-0.05860	21.600	2.598	-2.110	
19	0.55000	0.08464	-0.05980	19.800	3.047	-2.153	
20	0.50000	0.09711	-0.06000	18.000	3.496	-2.160	
21	0.45000	0.10958	-0.05950	16.200	3.945	-2.142	
22	0.40000	0.12204	-0.05820	14.400	4.394	-2.095	
23	0.35000	0.13451	-0.05610	12.600	4.842	-2.020	
24	0.30000	0.13035	-0.05330	10.800	4.693	-1.919	
25	0.25000	0.11789	-0.04970	9.000	4.244	-1.789	
26	0.20000	0.10542	-0.04540	7.200	3.795	-1.634	Baseline
27	0.15000	0.09296	-0.04000	5.400	3.346	-1.440	Leading
28	0.12500	0.08672	-0.03670	4.500	3.122	-1.321	Edge
29	0.10000	0.08049	-0.03340	3.600	2.898	-1.202	
30	0.08000	0.07550	-0.03080	2.880	2.718	-1.109	
31	0.07000	0.07301	-0.02890	2.520	2.628	-1.040	
32	0.06000	0.07052	-0.02650	2.160	2.539	-0.954	
33	0.05000	0.06802	-0.02440	1.800	2.449	-0.878	
34	0.04000	0.06553	-0.02210	1.440	2.359	-0.796	
35	0.03000	0.06304	-0.01960	1.080	2.269	-0.706	
36	0.02500	0.06179	-0.01810	0.900	2.224	-0.652	
37	0.02000	0.06054	-0.01650	0.720	2.180	-0.594	
38	0.01500	0.05930	-0.01470	0.540	2.135	-0.529	
39	0.01000	0.05805	-0.01260	0.360	2.090	-0.454	
40	0.00500	0.05680	-0.00990	0.180	2.045	-0.356	
41	0.00220	0.05618	-0.00590	0.079	2.022	-0.212	
42	0.00010	0.05558	-0.00190	0.004	2.001	-0.068	
43	0.00010	0.05558	0.00220	0.004	2.001	0.079	
44	0.00220	0.05618	0.00830	0.079	2.022	0.299	
45	0.00500	0.05680	0.01440	0.180	2.045	0.518	
46	0.01000	0.05558	0.01950	0.360	2.001	0.702	
47	0.01500	0.05930	0.02310	0.540	2.135	0.832	
48	0.02000	0.06054	0.02610	0.720	2.180	0.940	
49	0.02500	0.06179	0.02870	0.900	2.224	1.033	
50	0.03000	0.06304	0.03100	1.080	2.269	1.116	
51	0.04000	0.06553	0.03510	1.440	2.359	1.264	
52	0.05000	0.06802	0.03870	1.800	2.449	1.393	
53	0.06000	0.07052	0.04200	2.160	2.539	1.512	
54	0.07000	0.07301	0.04500	2.520	2.628	1.620	
55	0.08000	0.07550	0.04800	2.880	2.718	1.728	End
56	0.10000	0.08049	0.05240	3.600	2.898	1.886	Baseline
57	0.12500	0.08672	0.05720	4.500	3.122	2.059	Leading
58	0.15000	0.09296	0.06190	5.400	3.346	2.228	Edge

B4.—Continued.
[Baseline leading edge and main body]

59	0.17500	0.09794	0.06560	6.300	3.526	2.362
60	0.20000	0.10418	0.06930	7.200	3.750	2.495
61	0.22500	0.11165	0.07210	8.100	4.020	2.596
62	0.25000	0.11789	0.07490	9.000	4.244	2.696
63	0.27500	0.12412	0.07690	9.900	4.468	2.768
64	0.30000	0.13035	0.07890	10.800	4.693	2.840
65	0.32500	0.13659	0.08020	11.700	4.917	2.887
66	0.35000	0.13451	0.08140	12.600	4.842	2.930
67	0.37500	0.12828	0.08200	13.500	4.618	2.952
68	0.40000	0.12204	0.08260	14.400	4.394	2.974
69	0.42500	0.11581	0.08255	15.300	4.169	2.972
70	0.45000	0.10958	0.08250	16.200	3.945	2.970
71	0.47500	0.10334	0.08180	17.100	3.720	2.945
72	0.50000	0.09711	0.08100	18.000	3.496	2.916
73	0.52500	0.09088	0.07960	18.900	3.272	2.866
74	0.55000	0.08464	0.07810	19.800	3.047	2.812
75	0.57500	0.07841	0.07580	20.700	2.823	2.729
76	0.60000	0.07218	0.07350	21.600	2.598	2.646
77	0.62500	0.06594	0.07040	22.500	2.374	2.534
78	0.65000	0.05971	0.06680	23.400	2.150	2.405
79	0.67500	0.05719	0.06260	24.300	2.059	2.254
80	0.70000	0.06342	0.05730	25.200	2.283	2.063
81	0.71250	0.06654	0.05400	25.650	2.395	1.944
82	0.72500	0.06965	0.05080	26.100	2.507	1.829
83	0.73750	0.07277	0.04670	26.550	2.620	1.681
84	0.75000	0.07589	0.04260	27.000	2.732	1.534
85	0.76250	0.07900	0.03800	27.450	2.844	1.368
86	0.77500	0.08212	0.03350	27.900	2.956	1.206
87	0.78750	0.08524	0.02890	28.350	3.068	1.040
88	0.80000	0.08835	0.02440	28.800	3.181	0.878
89	0.82500	0.09459	0.01580	29.700	3.405	0.569
90	0.85000	0.10082	0.00730	30.600	3.629	0.263
91	0.90000	0.11328	-0.00710	32.400	4.078	-0.256
92	0.95000	0.12575	-0.01850	34.200	4.527	-0.666
93	0.97000	0.13074	-0.02240	34.920	4.707	-0.806
94	0.70000	0.25000	0.05730	25.200	9.000	2.063
95	0.70000	0.33333	0.05730	27.000	12.000	2.063
96	0.70000	0.38889	0.05730	25.200	14.000	2.063
97	0.70000	0.41667	0.05730	25.200	15.000	2.063
98	0.70000	0.43056	0.05730	25.200	15.500	2.063
99	0.70000	0.44444	0.05730	25.200	16.000	2.063
100	0.70000	0.45833	0.05730	25.200	16.500	2.063
101	0.70000	0.47222	0.05730	25.200	17.000	2.063
102	0.70000	0.48611	0.05730	25.200	17.500	2.063
103	0.70000	-0.05556	0.05730	25.200	-2.000	2.063
104	0.70000	-0.16667	0.05730	25.200	-6.000	2.063
105	0.70000	-0.25000	0.05730	25.200	-9.000	2.063
106	0.70000	-0.33333	0.05730	25.200	-12.000	2.063
107	0.70000	-0.38889	0.05730	25.200	-14.000	2.063
108	0.70000	-0.41667	0.05730	25.200	-15.000	2.063
109	0.70000	-0.43056	0.05730	25.200	-15.500	2.063
110	0.70000	-0.44444	0.05730	25.200	-16.000	2.063
111	0.70000	-0.45833	0.05730	25.200	-16.500	2.063
112	0.70000	-0.47222	0.05730	25.200	-17.000	2.063
113	0.70000	-0.48611	0.05730	25.200	-17.500	2.063
114	1.00000	0.25000	-0.02751	36.000	9.000	-0.990
115	1.00000	0.33333	-0.02751	36.000	12.000	-0.990
116	1.00000	0.41667	-0.02751	36.000	15.000	-0.990

B4.—Continued.
[Baseline leading edge and main body]

117	1.00000	0.47222	-0.02751	36.000	17.000	-0.990	
118	1.00000	-0.05556	-0.02751	36.000	-2.000	-0.990	
119	1.00000	-0.16667	-0.02751	36.000	-6.000	-0.990	
120	1.00000	-0.25000	-0.02751	36.000	-9.000	-0.990	
121	1.00000	-0.33333	-0.02751	36.000	-12.000	-0.990	
122	1.00000	-0.41667	-0.02751	36.000	-15.000	-0.990	
123	1.00000	-0.47222	-0.02751	36.000	-17.000	-0.990	

B4.—Continued.
[Leading edge for ice shape 621]

No.	x/c	y/c	z/c	x, in.	y, in.	z, in.
26	0.18721	0.08333	-0.04417	6.740	3.000	-1.590
27	0.15944	0.08333	-0.04111	5.740	3.000	-1.480
28	0.13167	0.08333	-0.03778	4.740	3.000	-1.360
29	0.10390	0.08333	-0.03444	3.740	3.000	-1.240
30	0.07610	0.08333	-0.03028	2.740	3.000	-1.090
31	0.05528	0.08333	-0.02611	1.990	3.000	-0.940
32	0.04139	0.08333	-0.02278	1.490	3.000	-0.820
33	0.02839	0.08333	-0.02000	1.022	3.000	-0.720
34	0.01536	0.08333	-0.01611	0.553	3.000	-0.580
35	0.00494	0.08333	-0.01139	0.178	3.000	-0.410
36	-0.00119	0.08333	0.00028	-0.043	3.000	0.010
37	0.00072	0.08333	0.01083	0.026	3.000	0.390
38	0.00550	0.08333	0.01833	0.198	3.000	0.660
39	0.01417	0.08333	0.02389	0.510	3.000	0.860
40	0.02458	0.08333	0.02917	0.885	3.000	1.050
41	0.03500	0.08333	0.03361	1.260	3.000	1.210
42	0.04889	0.08333	0.03833	1.760	3.000	1.380
43	0.06278	0.08333	0.04278	2.260	3.000	1.540
44	0.08014	0.08333	0.04778	2.885	3.000	1.720
45	0.10097	0.08333	0.05278	3.635	3.000	1.900
46	0.12180	0.08333	0.05694	4.385	3.000	2.050
47	0.14264	0.08333	0.06083	5.135	3.000	2.190

B4.—Continued.
[Leading edge for ice shape 622]

No.	x/c	y/c	z/c	x, in.	y, in.	z, in.
26	0.18721	0.08333	-0.04417	6.740	3.000	-1.590
27	0.15944	0.08333	-0.04111	5.740	3.000	-1.480
28	0.13167	0.08333	-0.03778	4.740	3.000	-1.360
29	0.10390	0.08333	-0.03722	3.740	3.000	-1.340
30	0.07610	0.08333	-0.03139	2.740	3.000	-1.130
31	0.05528	0.08333	-0.02667	1.990	3.000	-0.960
32	0.03444	0.08333	-0.02306	1.240	3.000	-0.830
33	0.01708	0.08333	-0.01917	0.615	3.000	-0.690
34	0.00180	0.08333	-0.01333	0.065	3.000	-0.480
35	-0.00464	0.08333	0.00028	-0.167	3.000	0.010
36	-0.00230	0.08333	0.01000	-0.083	3.000	0.360
37	0.00236	0.08333	0.01944	0.085	3.000	0.700
38	0.01417	0.08333	0.02500	0.510	3.000	0.900
39	0.02200	0.08333	0.02917	0.792	3.000	1.050
40	0.02980	0.08333	0.03278	1.073	3.000	1.180
41	0.03847	0.08333	0.03611	1.385	3.000	1.300
42	0.04889	0.08333	0.03833	1.760	3.000	1.380
43	0.05930	0.08333	0.04167	2.135	3.000	1.500
44	0.08014	0.08333	0.04750	2.885	3.000	1.710
45	0.10097	0.08333	0.05250	3.635	3.000	1.890
46	0.12180	0.08333	0.05694	4.385	3.000	2.050
47	0.14125	0.08333	0.06056	5.085	3.000	2.180

B4.—Concluded.
[Leading edge for ice shape 623]

No.	x/c	y/c	z/c	x, in.	y, in.	z, in.
26	0.17680	0.08330	-0.04444	6.365	2.999	-1.600
27	0.14900	0.08330	-0.04139	5.364	2.999	-1.490
28	0.10040	0.08330	-0.03472	3.614	2.999	-1.250
29	0.06920	0.08330	-0.03056	2.491	2.999	-1.100
30	0.03620	0.08330	-0.02333	1.303	2.999	-0.840
31	-0.00028	0.08330	-0.03056	-0.010	2.999	-1.100
32	-0.00550	0.08330	-0.02861	-0.198	2.999	-1.030
33	-0.01160	0.08330	-0.02500	-0.418	2.999	-0.900
34	-0.01880	0.08330	0.00028	-0.677	2.999	0.010
35	-0.01880	0.08330	0.02889	-0.677	2.999	1.040
36	-0.01360	0.08330	0.03056	-0.490	2.999	1.100
37	-0.00840	0.08330	0.03056	-0.302	2.999	1.100
38	0.02460	0.08330	0.02861	0.886	2.999	1.030
39	0.04110	0.08330	0.03556	1.480	2.999	1.280
40	0.06020	0.08330	0.04194	2.167	2.999	1.510
41	0.08010	0.08330	0.04750	2.884	2.999	1.710
42	0.10100	0.08330	0.05250	3.636	2.999	1.890
43	0.12530	0.08330	0.05750	4.511	2.999	2.070
44	0.13920	0.08330	0.06000	5.011	2.999	2.160

Appendix C
Test Matrices

C1.—COMPLETED BUSINESS JET (1st ENTRY) TEST MATRIX

Run No.	Mach No.	Airspd (kts)	Attitude desired	Tt (F)	Tt (C)	Ts (F)	Ts (C)	MVD (um)	LWC (g/m^3) desired	LWC (g/m^3) act	Pair (psig)	Pwat (psid)	Spray (min)	Notes
072595.01	0.28	175	6.0	30.6	-0.8	23.0	-5.0	20	0.540	0.540	17.0	37.9	6.0	
072595.02	0.28	175	6.0	30.6	-0.8	23.0	-5.0	20	0.540	0.540	17.0	37.9	6.0	repeat of 072595.01
072595.03	0.28	175	6.0	30.6	-0.8	23.0	-5.0	20	0.540	0.540	17.0	37.9	22.5	
072595.04	0.28	175	6.0	30.6	-0.8	23.0	-5.0	20	0.540	0.540	17.0	37.9	45.0	
072695.01	0.28	175	6.0	28.9	-1.7	21.4	-5.9	20	0.300	0.405	10.3	18.6	4.4	
072695.02	0.28	175	6.0	28.9	-1.8	21.2	-6.0	20	0.300	0.405	10.3	18.6	16.7	
072695.03	0.28	175	6.0	28.9	-1.7	21.4	-5.9	20	0.300	0.405	10.3	18.6	33.3	
072695.04	0.28	175	6.0	21.4	-5.9	14.0	-10.0	20	0.430	0.430	11.6	21.6	6.0	
072695.05	0.28	175	6.0	21.4	-5.9	14.0	-10.0	20	0.430	0.430	11.6	21.6	45.0	mold
072795.01	0.28	175	6.0	21.4	-5.9	14.0	-10.0	20	0.430	0.430	11.6	21.6	22.5	
072795.02	0.28	175	6.0	21.4	-5.9	14.0	-10.0	15	0.600	0.600	60.0	66.7	6.0	
072795.03	0.28	175	6.0	21.4	-5.9	14.0	-10.0	15	0.600	0.600	60.0	66.7	22.5	
072795.04	0.28	175	6.0	21.4	-6.0	14.0	-10.0	15	0.600	0.600	60.0	66.7	45.0	
072795.05	0.28	175	6.0	12.3	-11.0	5.0	-15.0	20	0.300	0.405	10.3	18.6	4.4	
072795.06	0.28	175	6.0	12.3	-11.0	5.0	-15.0	20	0.300	0.405	10.3	18.6	33.3	mold
072895.02	0.39	250	1.5	29.7	-1.3	15.3	-9.3	15	0.600	0.500	71.2	82.7	3.9	
072895.03	0.39	250	1.5	29.7	-1.3	15.3	-9.3	15	0.600	0.500	71.2	82.7	7.2	
072895.04	0.39	250	1.5	28.0	-2.2	13.7	-10.2	20	0.430	0.430	18.2	41.8	3.0	
072895.05	0.39	250	1.5	28.0	-2.2	13.7	-10.2	20	0.430	0.430	18.2	41.8	6.0	
072895.06	0.39	250	1.5	28.0	-2.2	13.7	-10.2	20	0.540	0.540	29.1	75.1	3.0	
072895.07	0.39	250	1.5	28.0	-2.2	13.7	-10.2	20	0.540	0.540	29.1	75.1	6.0	
072895.08	0.39	175	6.0	12.3	-11.0	5.0	-15.0	20	0.540	0.540	17.0	37.9	45.0	mold
073195.01	0.39	250	1.5	18.9	-7.3	4.7	-15.1	20	0.300	0.310	10.3	18.5	2.9	
073195.02	0.39	250	1.5	18.9	-7.3	4.7	-15.1	20	0.300	0.310	10.3	18.5	5.8	
073195.03	0.28	175	6.0	12.3	-11.0	5.0	-15.0	20	0.300	0.405	10.3	18.6	16.7	
073195.04	0.28	175	6.0	12.3	-11.0	5.0	-15.0	20	0.540	0.540	17.0	37.9	6.0	
073195.05	0.28	175	6.0	12.3	-11.0	5.0	-15.0	20	0.540	0.540	17.0	37.9	22.5	
080195.01	0.39	250	1.5	9.5	-12.5	-4.3	-20.2	40	0.100	0.410	10.6	32.6	0.7	
080195.02	0.39	250	1.5	9.5	-12.5	-4.3	-20.2	40	0.100	0.410	10.6	32.6	1.5	
080195.03	0.28	175	6.0	6.8	-14.0	-0.4	-18.0	20	0.540	0.535	17.0	37.9	6.0	
080195.04	0.28	175	4.0	6.8	-14.0	-0.4	-18.0	20	0.540	0.535	17.0	37.9	6.0	repeat of 080195.03
080195.05	0.28	175	4.0	6.8	-14.0	-0.4	-18.0	40	0.540	0.535	10.6	32.6	6.0	
080195.06	0.34	212	4.0	6.8	-14.0	-3.7	-19.9	40	0.540	0.535	10.6	32.6	6.0	
080195.07	0.34	212	4.0	6.8	-14.0	-3.7	-19.9	20	0.540	0.540	17.0	37.9	6.0	
080195.08	0.28	175	6.0	6.8	-14.0	-0.4	-18.0	40	0.540	0.540	10.6	32.6	6.0	
080195.09	0.28	175	6.0	6.8	-14.0	-0.4	-18.0	40	0.100	0.535	10.6	32.6	4.2	
080295.01	0.28	175	6.0	30.6	-0.8	23.0	-5.0	20	0.540	0.540	17.0	37.9	12.0	
080295.02	0.28	175	4.0	30.6	-0.8	23.0	-5.0	20	0.540	0.540	17.0	37.9	22.5	
080295.04	0.28	175	4.0	30.6	-0.8	23.0	-5.0	20	0.540	0.540	17.0	37.9	22.5	
080295.05	0.34	212	4.0	24.9	-3.9	14.0	-10.0	20	0.430	0.430	11.6	21.6	22.5	
080295.06	0.28	175	4.0	30.6	-0.8	23.0	-5.0	20	0.540	0.540	17.0	37.9	22.5	mold
080395.01	0.39	250	1.5	30.8	-0.7	16.4	-8.7	15	2.500	0.750	28.9	9.9	10.0	
080395.02	0.39	250	1.5	30.8	-0.7	16.4	-8.7	20	2.250	1.250	68.0	57.5	5.4	
080395.03	0.28	175	6.0	28.4	-2.0	20.9	-6.2	15	2.500	1.000	28.3	9.8	15.0	
080395.04	0.28	175	6.0	24.2	-4.4	16.7	-8.5	20	2.250	1.600	70.8	61.3	8.4	
080395.05	0.39	250	1.5	18.8	-7.4	4.7	-15.2	15	2.500	0.750	28.9	9.9	10.0	
080395.06	0.39	250	1.5	18.8	-7.4	4.7	-15.2	20	2.250	1.250	68.0	57.5	5.4	
080395.07	0.28	175	6.0	12.3	-11.0	5.0	-15.0	20	2.250	1.600	70.8	9.8	8.4	
080495.01	0.28	175	6.0	-18.0	-27.8	-24.9	-31.6	160	0.830	0.830	5.0	50.0	6.0	
080495.02	0.28	175	4.0	-18.0	-27.8	-24.9	-31.6	160	0.830	0.830	5.0	50.0	6.0	
080495.03	0.28	175	6.0	12.2	-11.0	4.9	-15.0	160	0.830	0.830	5.0	50.0	20.0	
080495.04	0.28	175	4.0	12.2	-11.0	4.9	-15.0	160	0.830	0.830	5.0	50.0	20.0	
080495.05	0.28	175	6.0	30.6	-0.8	23.0	-5.0	160	0.830	0.830	5.0	50.0	20.0	
080495.06	0.28	175	6.0	30.6	-0.8	23.0	-5.0	20	0.540	0.540	17.0	37.9	22.5	mold

C2.—COMPLETED BUSINESS JET (2nd ENTRY) TEST MATRIX

Run	Mach	Airspd	Attitude	Tt	Tt	Ts	Ts	MVD	LWC	LWC	Pair	Pwat	Spray	Notes
No.	No.	(kts)	desired	(F)	(C)	(F)	(C)	(um)	(g/m^3)	(g/m^3)	(psig)	(psid)	(min)	
									desired	act				
201	0.28	175	6.0	30.0	-0.8	22.4	-5.0	20	0.300	0.405	10.3	18.6	4.4	
202	0.28	175	6.0	30.0	-0.8	22.4	-5.0	20	0.540	0.540	17.0	37.9	2.0	
202r	0.28	175	6.0	30.0	-0.8	22.4	-5.0	20	0.540	0.540	17.0	37.9	2.0	repeat
202m	0.28	175	6.0	30.0	-0.8	22.4	-5.0	20	0.540	0.540	17.0	37.9	2.0	mold
203	0.28	175	6.0	30.0	-0.8	22.4	-5.0	20	0.540	0.540	17.0	37.9	6.0	
204	0.28	175	6.0	30.0	-0.8	22.4	-5.0	20	0.540	0.540	17.0	37.9	22.5	
205	0.28	175	6.0	20.8	-5.9	13.4	-10.0	40	0.100	0.535	10.6	32.6	1.1	
205r	0.28	175	6.0	20.8	-5.9	13.4	-10.0	40	0.100	0.535	10.6	32.6	1.1	repeat
206	0.28	175	6.0	20.8	-5.9	13.4	-10.0	40	0.100	0.535	10.6	32.6	4.2	
207	0.28	175	6.0	20.8	-5.9	13.4	-10.0	20	0.430	0.430	11.6	21.6	2.0	
208	0.28	175	6.0	20.8	-5.9	13.4	-10.0	20	0.430	0.430	11.6	21.6	6.0	
209	0.28	175	6.0	20.8	-5.9	13.4	-10.0	20	0.430	0.430	11.6	21.6	22.5	
210	0.28	175	6.0	11.7	-11.0	4.4	-15.0	20	0.300	0.405	10.3	18.6	2.0	
211	0.28	175	6.0	11.7	-11.0	4.4	-15.0	20	0.300	0.405	10.3	18.6	4.4	
212	0.28	175	6.0	11.7	-11.0	4.4	-15.0	20	0.300	0.405	10.3	18.6	16.7	
213	0.28	175	6.0	20.8	-5.9	13.4	-10.0	15	0.600	0.600	60.0	66.7	2.0	
214	0.28	175	6.0	20.8	-5.9	13.4	-10.0	15	0.600	0.600	60.0	66.7	6.0	
221	0.39	250	1.5	30.0	-0.8	22.4	-5.0	20	0.540	0.540	29.1	75.1	3.0	
222	0.39	250	1.5	30.0	-0.8	22.4	-5.0	20	0.540	0.540	29.1	75.1	6.0	
223	0.39	250	1.5	30.0	-0.8	22.4	-5.0	20	0.300	0.310	10.3	18.5	2.9	
224	0.39	250	1.5	30.0	-0.8	22.4	-5.0	20	0.300	0.310	10.3	18.5	5.8	
225	0.39	250	1.5	20.8	-5.9	13.4	-10.0	15	0.600	0.500	71.2	82.7	3.6	
226	0.39	250	1.5	20.8	-5.9	13.4	-10.0	15	0.600	0.500	71.2	82.7	7.2	
231	0.28	175	4.0	30.0	-0.8	22.4	-5.0	20	0.540	0.540	17.0	37.9	2.0	
232	0.28	175	4.0	30.0	-0.8	22.4	-5.0	20	0.540	0.540	17.0	37.9	6.0	
233	0.28	175	4.0	20.8	-5.9	13.4	-10.0	15	0.600	0.600	60.0	66.7	2.0	
234	0.28	175	4.0	20.8	-5.9	13.4	-10.0	15	0.600	0.600	60.0	66.7	6.0	
235	0.28	175	4.0	20.8	-5.9	13.4	-10.0	40	0.100	0.535	10.6	32.6	1.1	
236	0.28	175	4.0	20.8	-5.9	13.4	-10.0	40	0.100	0.535	10.6	32.6	4.2	
237	0.28	175	4.0	11.7	-11.0	4.4	-15.0	20	0.300	0.405	10.3	18.6	1.5	
238	0.28	175	4.0	11.7	-11.0	4.4	-15.0	20	0.300	0.405	10.3	18.6	4.4	

C3.—PLANNED COMMERCIAL TRANSPORT TEST MATRIX

Run No.	Mach No.	Airspd (kts)	Attitude	Tt (F)	Tt (C)	Ts (F)	Ts (C)	MVD (um)	LWC (g/m^3)	Spray (min)
101	0.45	284	0.0	32.0	0.0	12.8	-10.6	20	0.410	6.0
102	0.45	284	0.0	32.0	0.0	12.8	-10.6	20	0.410	6.0
103	0.45	284	0.0	32.0	0.0	12.8	-10.6	20	0.410	22.5
104	0.45	279	-1.0	14.0	-10.0	-4.4	-20.2	15	0.295	6.0
105	0.45	279	-1.0	14.0	-10.0	-4.4	-20.2	15	0.295	22.5
106	0.45	279	0.0	14.0	-10.0	-4.4	-20.2	15	0.295	6.0
107	0.45	279	0.0	14.0	-10.0	-4.4	-20.2	15	0.295	22.5
108	0.45	279	0.0	14.0	-10.0	-4.4	-20.2	15	0.295	30.0
110	0.45	282	-1.0	23.0	-5.0	4.2	-15.4	20	0.285	6.0
111	0.45	282	-1.0	23.0	-5.0	4.2	-15.4	20	0.285	22.5
112	0.45	282	0.0	23.0	-5.0	4.2	-15.4	20	0.285	6.0
113	0.45	282	0.0	23.0	-5.0	4.2	-15.4	20	0.285	45.0
114	0.45	282	0.0	23.0	-5.0	4.2	-15.4	20	0.285	30.0
115	0.45	282	0.0	23.0	-5.0	4.2	-15.4	20	0.285	22.5
116	0.45	284	0.0	32.0	0.0	12.8	-10.6	20	0.410	6.0
122	0.45	284	-1.0	32.0	0.0	12.8	-10.6	20	0.410	6.0
123	0.45	284	-1.0	32.0	0.0	12.8	-10.6	20	0.410	22.5
124	0.45	284	0.0	32.0	0.0	12.8	-10.6	20	0.410	6.0
126	0.45	284	0.0	32.0	0.0	12.8	-10.6	20	0.410	30.0
127	0.45	284	0.0	32.0	0.0	12.8	-10.6	20	0.410	22.5
128	0.45	282	0.0	23.0	-5.0	4.2	-15.4	20	0.285	2.0
129	0.45	284	0.0	32.0	0.0	12.8	-10.6	20	0.410	2.0
130	0.40	253	0.0	32.0	0.0	16.7	-8.4	56	0.420	22.5
131	0.40	253	0.0	33.0	0.6	17.7	-7.9	56	0.420	22.5
132	0.40	253	0.0	35.0	1.7	19.7	-6.8	56	0.420	6.0
133	0.40	253	0.0	34.0	1.1	18.7	-7.4	56	0.420	22.5
141	0.45	284	0.0	18.0	-7.7	-0.6	-18.1	40	0.100	7.5
142	0.45	284	0.0	18.0	-7.7	-0.6	-18.1	40	0.100	2.0
143	0.45	284	0.0	32.0	0.0	12.8	-10.6	40	0.512	6.0
144	0.45	284	0.0	32.0	0.0	12.8	-10.6	40	0.200	6.0
145	0.45	284	0.0	32.0	0.0	12.8	-10.6	40	0.200	22.5

C4.—COMPLETED COMMERCIAL TRANSPORT TEST MATRIX

Run	Mach	Airspd	Attitude	Tt	Tt	Ts	Ts	MVD	LWC	LWC	Pair	Pwat	Spray	Notes
No.	No.	(kts)	desired	(F)	(C)	(F)	(C)	(um)	(g/m^3)	(g/m^3)	(psig)	(psid)	(min)	
									desired	act				
101	0.45	284	0.0	32.0	0.0	13.0	-10.0	20	0.410	0.410	20.0	47.0	6.0	not scaled
102	0.40	250	0.0	32.0	0.0	13.0	-10.0	20	0.410	0.460	20.0	47.0	6.0	not scaled
103	0.40	250	0.0	32.0	0.0	13.0	-10.0	20	0.410	0.460	20.0	47.0	22.5	not scaled
104	0.40	248	-1.0	10.5	-12.0	-4.0	-20.0	15	0.295	0.339	17.3	25.3	5.9	
105	0.40	248	-1.0	10.5	-12.0	-4.0	-20.0	15	0.295	0.339	17.3	25.3	22.0	
106	0.40	248	0.0	10.5	-12.0	-4.0	-20.0	15	0.295	0.339	17.3	25.3	5.9	
106r1	0.40	248	0.0	10.5	-12.0	-4.0	-20.0	15	0.295	0.339	17.3	25.3	5.9	
107	0.40	248	0.0	10.5	-12.0	-4.0	-20.0	15	0.295	0.339	17.3	25.3	22.0	
108	0.40	248	0.0	10.5	-12.0	-4.0	-20.0	15	0.295	0.339	17.3	25.3	29.3	
110	0.40	250	-1.0	20.0	-6.3	5.1	-14.6	21	0.285	0.341	11.8	23.2	5.7	
111	0.40	250	-1.0	20.0	-6.3	5.1	-14.6	21	0.285	0.341	11.8	23.2	21.1	
112	0.40	250	0.0	20.0	-6.3	5.1	-14.6	21	0.285	0.341	11.8	23.2	5.7	
113	0.40	250	0.0	20.0	-6.3	5.1	-14.6	21	0.285	0.341	11.8	23.2	42.4	
114	0.40	250	0.0	20.0	-6.3	5.1	-14.6	21	0.285	0.341	11.8	23.2	28.3	
115	0.40	250	0.0	20.0	-6.3	5.1	-14.6	21	0.285	0.341	11.8	23.2	21.1	mold made
116	0.40	255	-1.0	38.6	4.0	23.1	-4.6	21	0.410	0.500	23.8	62.6	5.5	ice shed - no data
122	0.40	253	-1.0	29.5	-1.1	14.3	-9.5	21	0.410	0.563	29.7	83.2	4.9	
123	0.40	253	-1.0	29.5	-1.1	14.3	-9.5	21	0.410	0.563	29.7	83.2	18.5	
124	0.40	253	0.0	29.5	-1.1	14.3	-9.5	21	0.410	0.563	29.7	83.2	4.9	
126	0.40	253	0.0	29.5	-1.1	14.3	-9.5	21	0.410	0.563	29.7	83.2	24.6	
127	0.40	253	0.0	29.5	-1.1	14.3	-9.5	21	0.410	0.563	29.7	83.2	18.5	mold made
128	0.40	250	0.0	20.0	-6.3	5.1	-14.6	21	0.285	0.341	11.8	23.2	2.0	
129	0.40	253	0.0	29.5	-1.1	14.3	-9.5	21	0.410	0.563	29.7	83.2	2.0	
130	0.40	253	0.0	32.0	0.3	16.7	-8.1	56	0.420	unk	8.2	32.0	18.0	not scaled
131	0.40	253	0.0	33.0	0.9	17.7	-7.6	56	0.420	unk	8.2	32.0	18.0	not scaled
132	0.40	253	0.0	35.0	2.0	19.7	-6.5	56	0.420	unk	8.2	32.0	5.2	not scaled, ice shed - no data
133	0.40	253	0.0	34.0	1.4	18.7	-7.1	56	0.420	unk	8.2	32.0	18.0	not scaled
141	0.40	249	0.0	15.0	-9.1	0.3	-17.3	42	0.100	0.400	10.1	30.3	6.7	
142	0.40	249	0.0	15.0	-9.1	0.3	-17.3	42	0.100	0.400	10.1	30.3	2.0	
143	0.40	253	0.0	29.0	-1.3	13.8	-9.8	42	0.512	0.650	21.8	101.8	5.3	
144	0.40	253	0.0	25.5	-3.3	10.4	-11.6	42	0.200	0.400	10.4	31.3	3.0	
145	0.40	253	0.0	25.5	-3.3	10.4	-11.6	42	0.200	0.400	10.4	31.3	11.2	
145m	0.40	253	0.0	25.5	-3.3	10.4	-11.6	42	0.200	0.400	10.4	31.3	11.2	mold made

C5.—GENERAL AVIATION AIRFOIL TEST MATRIX

Run No.	Mach No.	Airspd (kts)	Attitude desired	Tt (F)	Tt (C)	Ts (F)	Ts (C)	MVD (um)	LWC (g/m^3) desired	LWC (g/m^3) act	Pair (psig)	Pwat (psid)	Spray (min)	Notes
601	0.29	180	0.0	30.0	-0.8	22.4	-5.0	20	0.540	0.540	19.0	41.0	2.0	
602	0.29	180	0.0	30.0	-0.8	22.4	-5.0	20	0.540	0.540	19.0	41.0	6.0	
602m	0.29	180	0.0	30.0	-0.8	22.4	-5.0	20	0.540	0.540	19.0	41.0	6.0	mold
603	0.29	180	0.0	30.0	-0.8	22.4	-5.0	20	0.540	0.540	19.0	41.0	22.5	
606	0.29	180	0.0	20.8	-5.9	13.4	-10.0	20	0.430	0.430	14.5	25.0	2.0	
607	0.29	180	0.0	20.8	-5.9	13.4	-10.0	20	0.430	0.430	14.5	25.0	6.0	
607m	0.29	180	0.0	20.8	-5.9	13.4	-10.0	20	0.430	0.430	14.5	25.0	6.0	mold
608	0.29	180	0.0	20.8	-5.9	13.4	-10.0	20	0.430	0.430	14.5	25.0	22.5	
609	0.29	180	0.0	11.7	-11.0	4.4	-15.0	20	0.300	0.330	10.0	14.5	2.0	
610	0.29	180	0.0	11.7	-11.0	4.4	-15.0	20	0.300	0.330	10.0	14.5	6.0	
611	0.29	180	0.0	11.7	-11.0	4.4	-15.0	20	0.300	0.330	10.0	14.5	22.5	
612	0.29	180	0.0	20.8	-5.9	13.4	-10.0	15	0.600	0.560	80.0	80.0	2.0	
612r	0.29	180	0.0	20.8	-5.9	13.4	-10.0	15	0.600	0.560	80.0	80.0	2.0	repeat
613	0.29	180	0.0	20.8	-5.9	13.4	-10.0	15	0.600	0.560	80.0	80.0	6.0	
621	0.21	130	2.0	26.4	-2.8	22.4	-5.0	20	0.540	0.540	14.0	23.0	2.0	
621m	0.21	130	2.0	26.4	-2.8	22.4	-5.0	20	0.540	0.540	14.0	23.0	2.0	mold
622	0.21	130	2.0	26.4	-2.8	22.4	-5.0	20	0.540	0.540	14.0	23.0	6.0	
622r	0.21	130	2.0	26.4	-2.8	22.4	-5.0	20	0.540	0.540	14.0	23.0	6.0	repeat
622r2	0.21	130	2.0	26.4	-2.8	22.4	-5.0	20	0.540	0.540	14.0	23.0	6.0	repeat
622m	0.21	130	2.0	26.4	-2.8	22.4	-5.0	20	0.540	0.540	14.0	23.0	6.0	mold
623	0.21	130	2.0	26.4	-2.8	22.4	-5.0	20	0.540	0.540	14.0	23.0	22.5	
623m	0.21	130	2.0	26.4	-2.8	22.4	-5.0	20	0.540	0.540	14.0	23.0	22.5	mold
625	0.21	130	2.0	17.3	-7.8	13.4	-10.0	40	0.100	0.660	10.0	34.0	0.9	
626	0.21	130	2.0	17.3	-7.8	13.4	-10.0	20	0.430	0.440	10.0	15.0	2.0	
627	0.21	130	2.0	17.3	-7.8	13.4	-10.0	20	0.430	0.440	10.0	15.0	5.9	
627m	0.21	130	2.0	17.3	-7.8	13.4	-10.0	20	0.430	0.440	10.0	15.0	5.9	mold
627r	0.21	130	2.0	17.3	-7.8	13.4	-10.0	20	0.430	0.440	10.0	15.0	5.9	repeat
627r2	0.21	130	2.0	17.3	-7.8	13.4	-10.0	20	0.430	0.440	10.0	15.0	5.9	repeat
628	0.21	130	2.0	17.3	-7.8	13.4	-10.0	20	0.430	0.440	10.0	15.0	22.0	
629	0.21	130	2.0	8.3	-12.9	4.4	-15.0	20	0.300	0.440	10.0	15.0	1.4	
630	0.21	130	2.0	8.3	-12.9	4.4	-15.0	20	0.300	0.440	10.0	15.0	4.1	
631	0.21	130	2.0	8.3	-12.9	4.4	-15.0	20	0.300	0.440	10.0	15.0	15.3	
632	0.21	130	2.0	17.3	-7.8	13.4	-10.0	15	0.600	0.600	35.0	35.0	2.0	
633	0.21	130	2.0	17.3	-7.8	13.4	-10.0	15	0.600	0.600	35.0	35.0	6.0	
633m	0.21	130	2.0	17.3	-7.8	13.4	-10.0	15	0.600	0.600	35.0	35.0	6.0	mold
641	0.21	130	0.0	17.3	-7.8	13.4	-10.0	20	0.430	0.440	10.0	15.0	2.0	
642	0.21	130	0.0	17.3	-7.8	13.4	-10.0	20	0.430	0.440	10.0	15.0	5.9	
643	0.21	130	0.0	17.3	-7.8	13.4	-10.0	20	0.430	0.440	10.0	15.0	22.0	
644	0.21	130	4.0	17.3	-7.8	13.4	-10.0	20	0.430	0.440	10.0	15.0	2.0	
645	0.21	130	4.0	17.3	-7.8	13.4	-10.0	20	0.430	0.440	10.0	15.0	5.9	
645m	0.21	130	4.0	17.3	-7.8	13.4	-10.0	20	0.430	0.440	10.0	15.0	5.9	mold
646	0.21	130	4.0	17.3	-7.8	13.4	-10.0	20	0.430	0.440	10.0	15.0	22.0	
647	0.21	130	6.0	17.3	-7.8	13.4	-10.0	20	0.430	0.440	10.0	15.0	2.0	
648	0.21	130	6.0	17.3	-7.8	13.4	-10.0	20	0.430	0.440	10.0	15.0	5.9	
649	0.21	130	6.0	17.3	-7.8	13.4	-10.0	20	0.430	0.440	10.0	15.0	22.0	
655	0.13	83	6.0	15.0	-9.1	13.4	-10.0	20	0.430	0.650	10.0	15.0	2.0	
656	0.13	83	6.0	15.0	-9.1	13.4	-10.0	20	0.430	0.650	10.0	15.0	6.0	
657	0.13	83	6.0	24.1	-4.1	22.4	-5.0	20	0.700	0.650	11.0	18.0	5.0	
661	0.21	130	0.0	28.2	-1.8	24.2	-4.0	20.5	1.000	1.000	35.5	100.0	15.0	

C6.—LaRC/LeRC ICING CONTAMINATION TESTS NOVEMBER 1998

Run nos. 23–35 clean wing

Reynolds number	Mach number			
	0.05	0.12	0.21	0.29
1	35			
3		25		
4.6			26	
6.4		24	28	27
8.1			29	
10		23	30	
12			32	

Run nos. 101–112 ice shape 623-2D (SLA)

Reynolds number	Mach number			
	0.05	0.12	0.21	0.29
1	112			
3		109		
4.6			103	
6.4		106	108	111
8.1			107	
10		101	102	
12			105	

Run nos. 201–211 ice shape 623-3D (casting)

Reynolds number	Mach number			
	0.05	0.12	0.21	0.29
1	211			
3		208		
4.6			204	
6.4		202	207	210
8.1				
10		201	203	
12				

Run nos. 701–705 clean wing

Reynolds number	Mach number			
	0.05	0.12	0.21	0.29
1				
3		705		
4.6			702	
6.4				704
8.1				
10		701	703	
12				

Run nos. 301–310 ice shape 622-2D (SLA)

Reynolds number	Mach number			
	0.05	0.12	0.21	0.29
1	310			
3		308		
4.6			309	
6.4		302	307	304
8.1				
10		301	306	
12				

Run nos. 401–410 ice shape 622-3D (casting)

Reynolds number	Mach number			
	0.05	0.12	0.21	0.29
1	410			
3		409		
4.6			403	
6.4		402	407	404
8.1				
10		401	406	
12				

Run nos. 501–510 ice shape 621-2D (SLA)

Reynolds number	Mach number			
	0.05	0.12	0.21	0.29
1	510			
3		508		
4.6			504	
6.4		502	507	505
8.1				
10		501	503	
12				

Appendix D1
Test Results, Business Jet—1st Entry

Business Jet - Run 072595.01

T_t = -0.8°C (30.6°F)
T_s = -5.0°C (23.0°F)
V = 90 m/s (175 kts)
Attitude = 6.1°

LWC = 0.54 g/m^3
MVD = 20 μm
Spray = 6.0 min
chord = 90 cm (36 in)

$C_{d\text{-clean}}$ = 0.0093
$C_{d\text{-iced}}$ = 0.0481

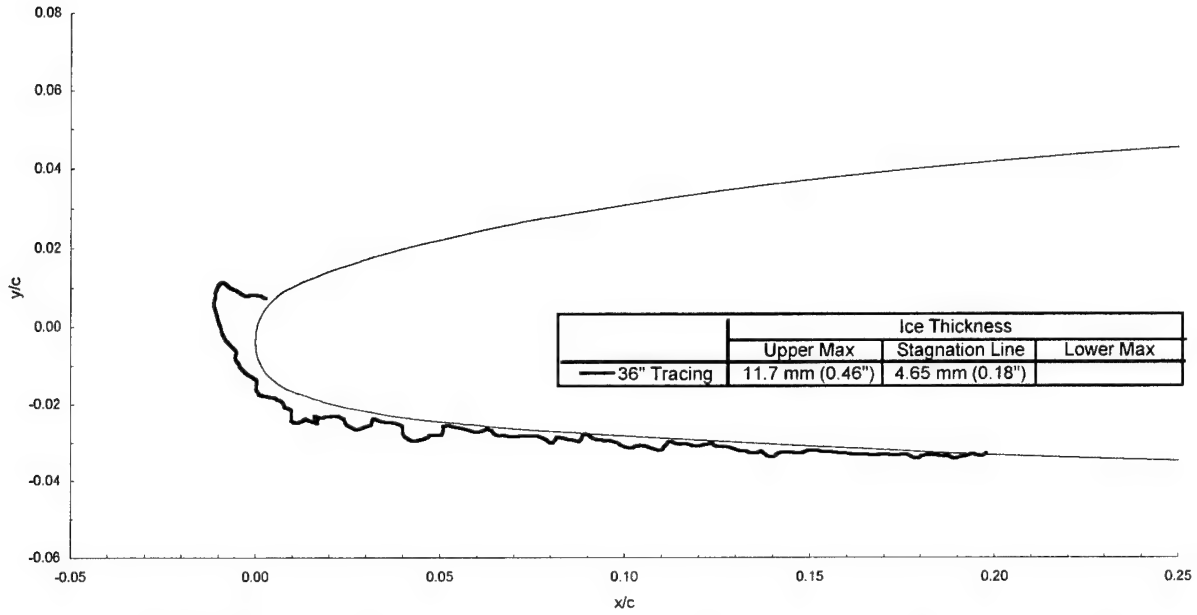

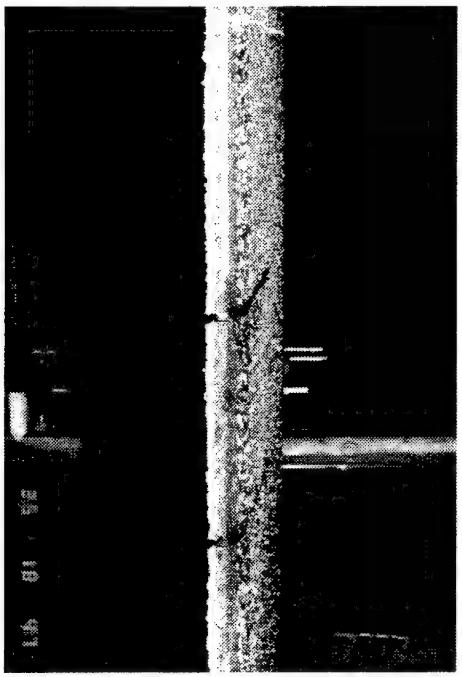

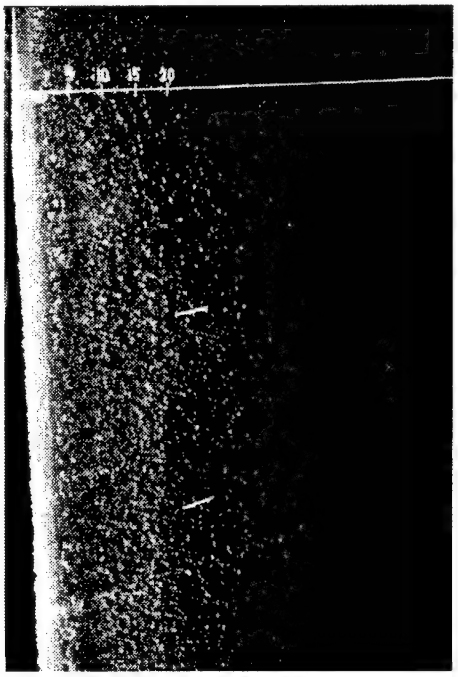

Business Jet - Run 072595.02

T_t = -0.8°C (30.6°F)
T_s = -5.0°C (23.0°F)
V = 90 m/s (175 kts)
Attitude = 6.1°

LWC = 0.54 g/m^3
MVD = 20 μm
Spray = 6.0 min
chord = 90 cm (36 in)

$C_{d\text{-}clean}$ = 0.0093
$C_{d\text{-}iced}$ = 0.0478

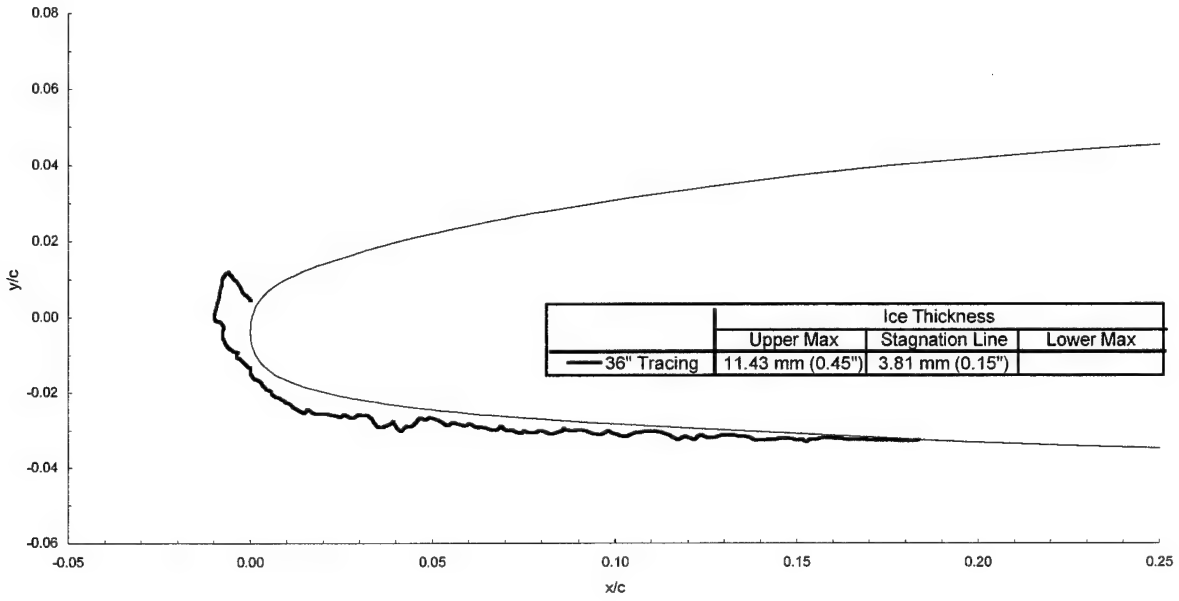

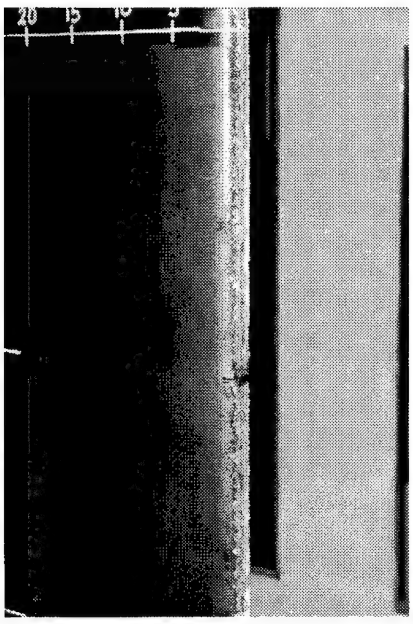

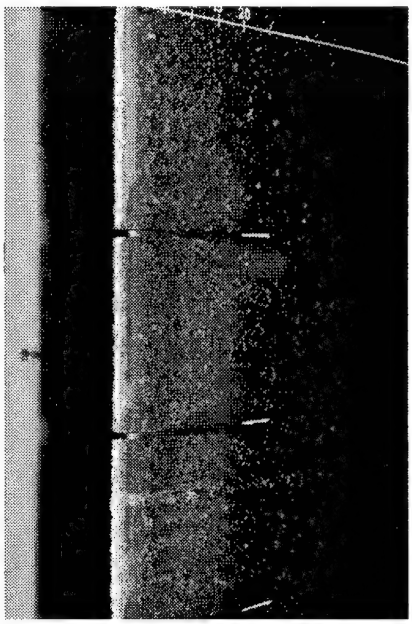

Business Jet - Run 072595.03

T_t = -0.8°C (30.6°F)
T_s = -5.0°C (23.0°F)
V = 90 m/s (175 kts)
Attitude = 6.1°

LWC = 0.54 g/m^3
MVD = 20 μm
Spray = 22.5 min
chord = 90 cm (36 in)

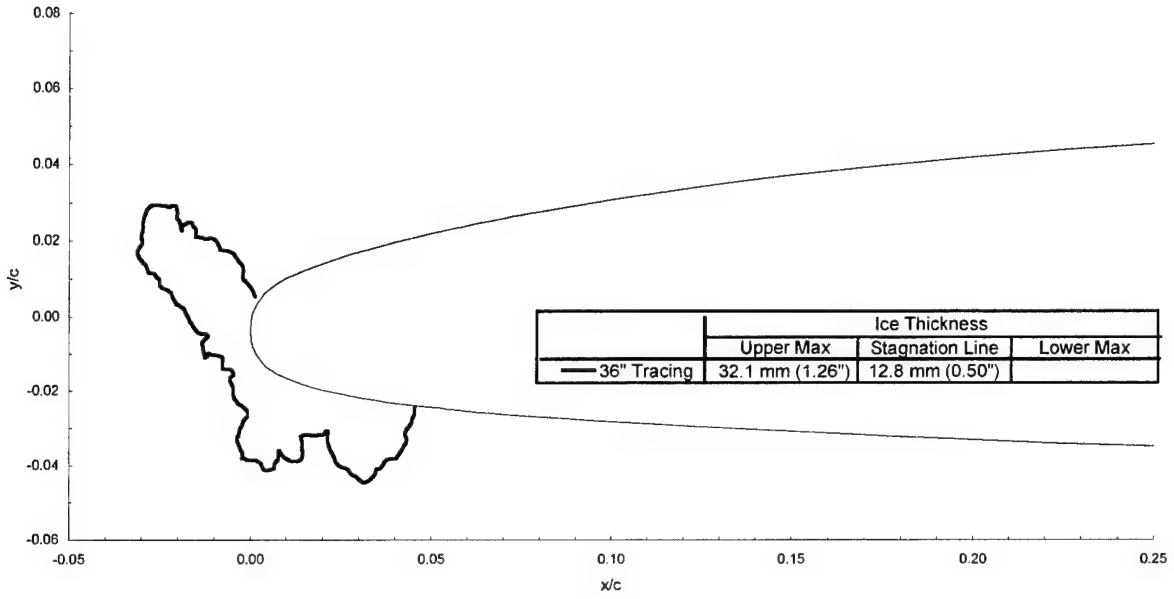

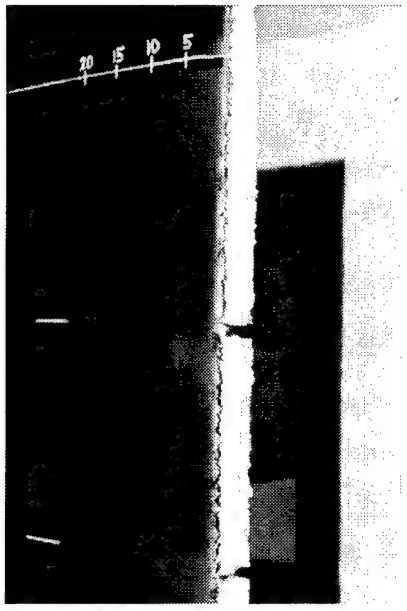

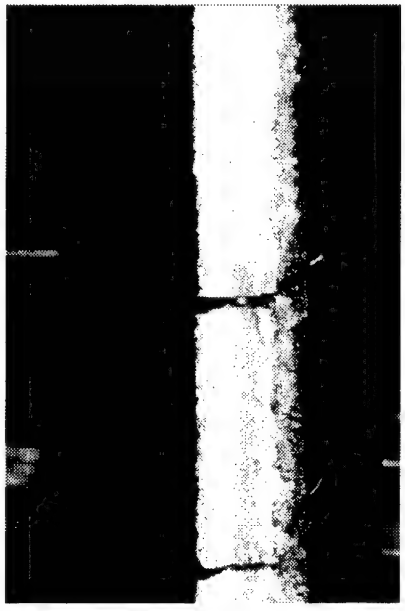

Business Jet - Run 072595.04

T_t = -0.800°C (30.6°F)
T_s = -5.0°C (23.0°F)
V = 90 m/s (175 kts)
Attitude = 6.1°3

LWC = 0.54 g/m^3
MVD = 20 μm
Spray = 45.0 min
chord = 90 cm (36 in)

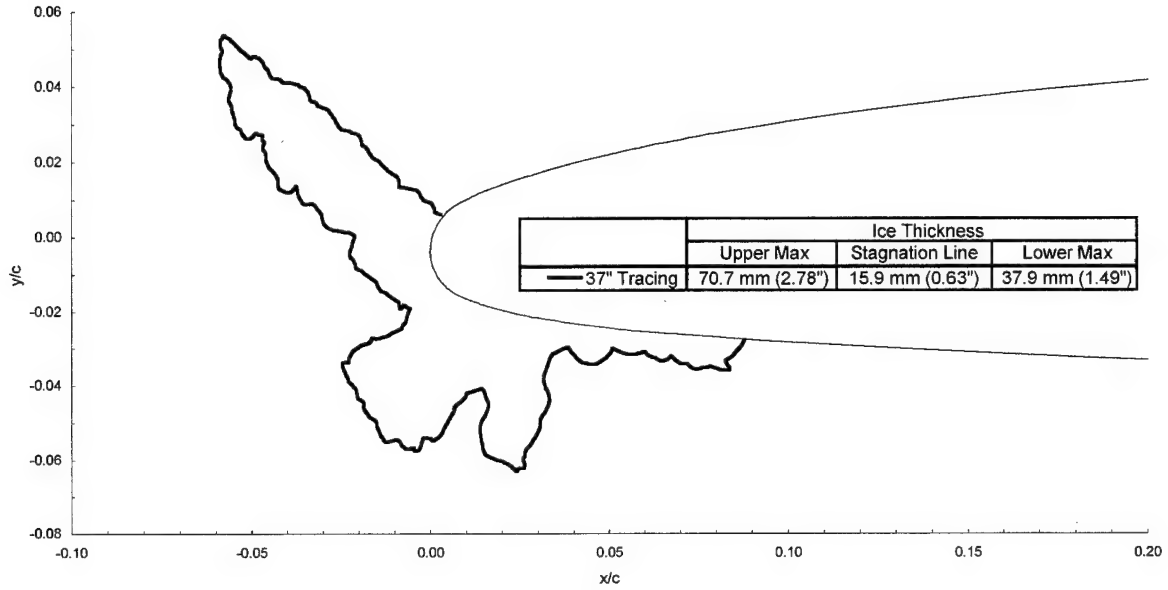

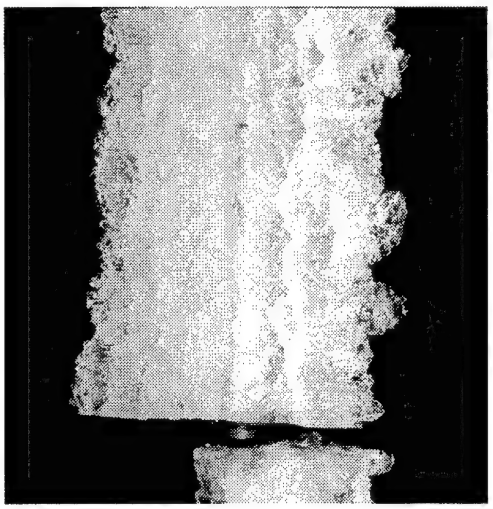

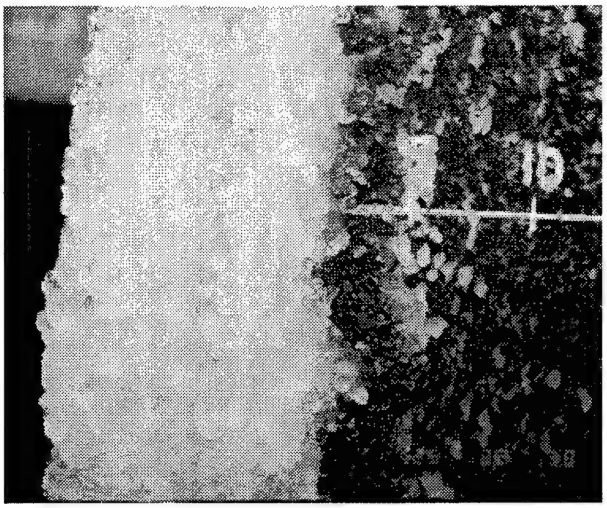

Business Jet - Run 072695.01

T_t = -1.7°C (28.9°F)
T_s = -5.9°C (21.4°F)
V = 90 m/s (175 kts)
Attitude = 6.1°

LWC = 0.405 g/m^3
MVD = 20 μm
Spray = 4.4 min
chord = 90 cm (36 in)

$C_{d\text{-clean}}$ = 0.0093
$C_{d\text{-iced}}$ = 0.0258

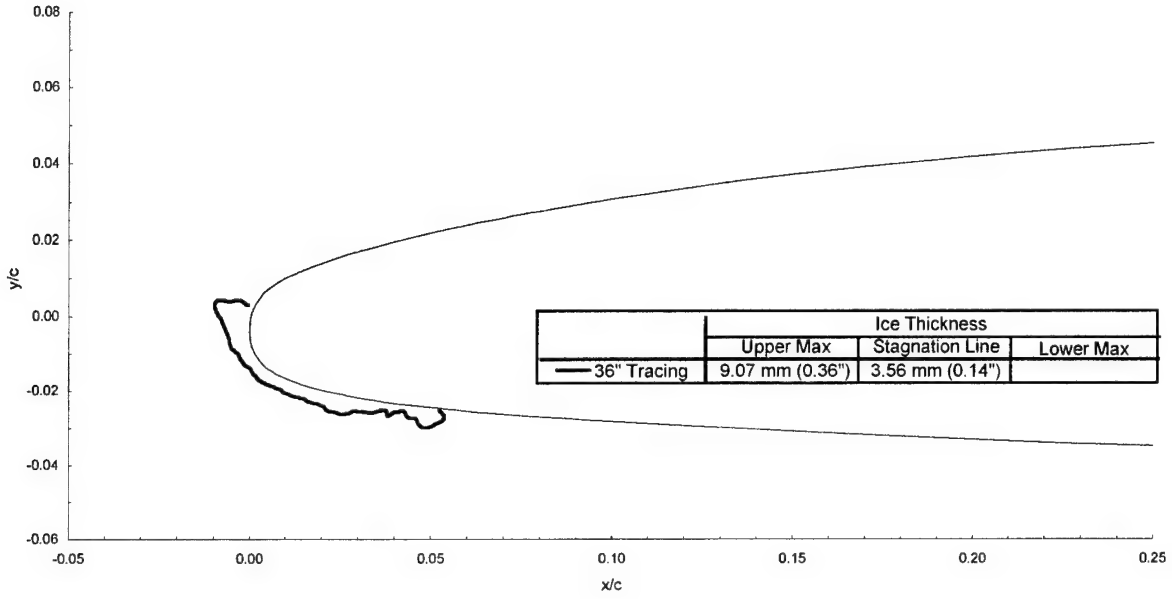

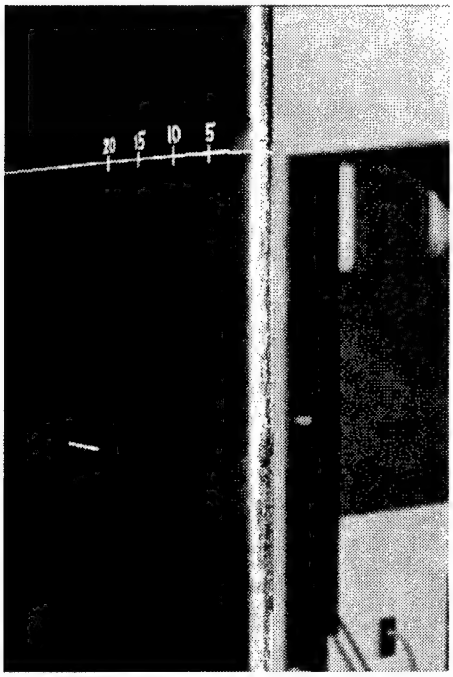

Business Jet - Run 072695.02

T_t = -1.8°C (28.9°F)
T_s = -6.0°C (21.2°F)
V = 90 m/s (175 kts)
Attitude = 6.1°

LWC = 0.405 g/m^3
MVD = 20 μm
Spray = 16.7 min
chord = 90 cm (36 in)

$C_{d\text{-clean}}$ = 0.0093
$C_{d\text{-iced}}$ = 0.0526

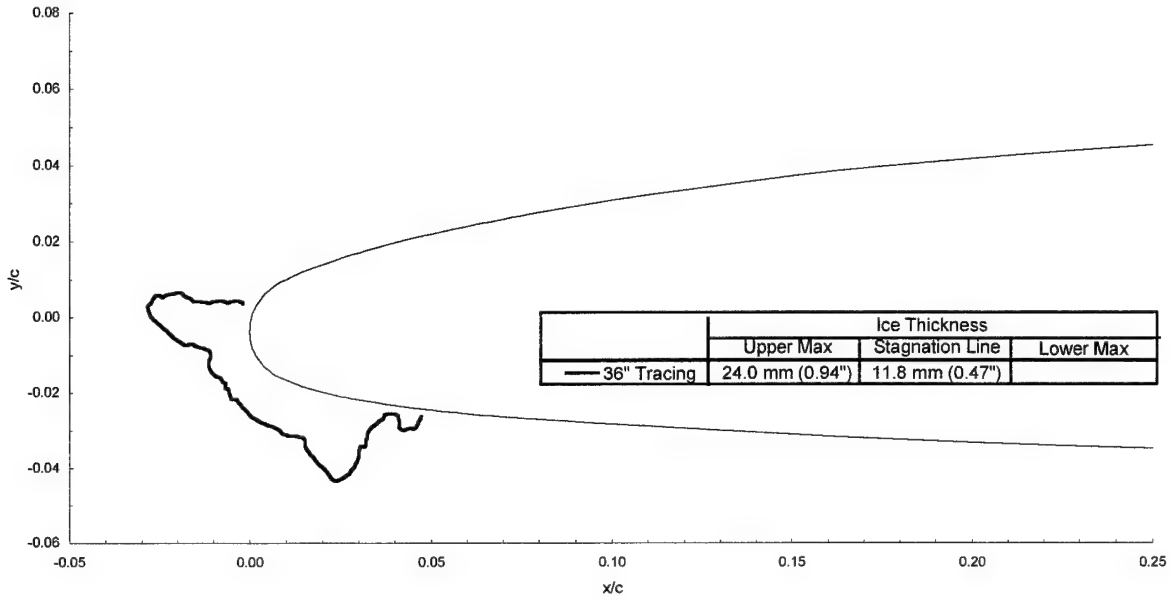

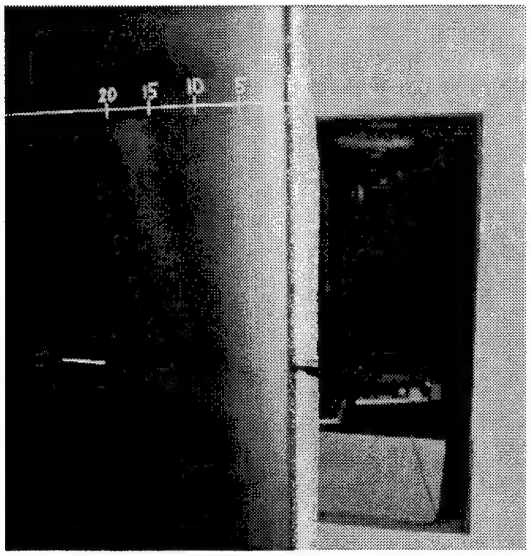

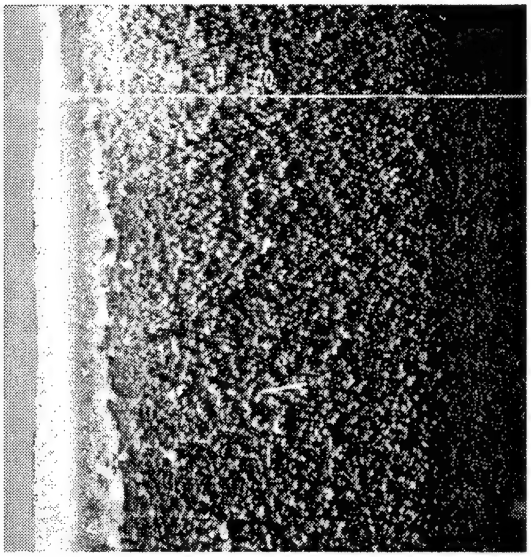

Business Jet - Run 072695.03

T_t = -1.7°C (28.9°F)
T_s = -5.9°C (21.4°F)
V = 90 m/s (175 kts)
Attitude = 6.1°

LWC = 0.405 g/m^3
MVD = 20 μm
Spray = 33.3 min
chord = 90 cm (36 in)

$C_{d\text{-clean}}$ = 0.0093
$C_{d\text{-iced}}$ = 0.1001

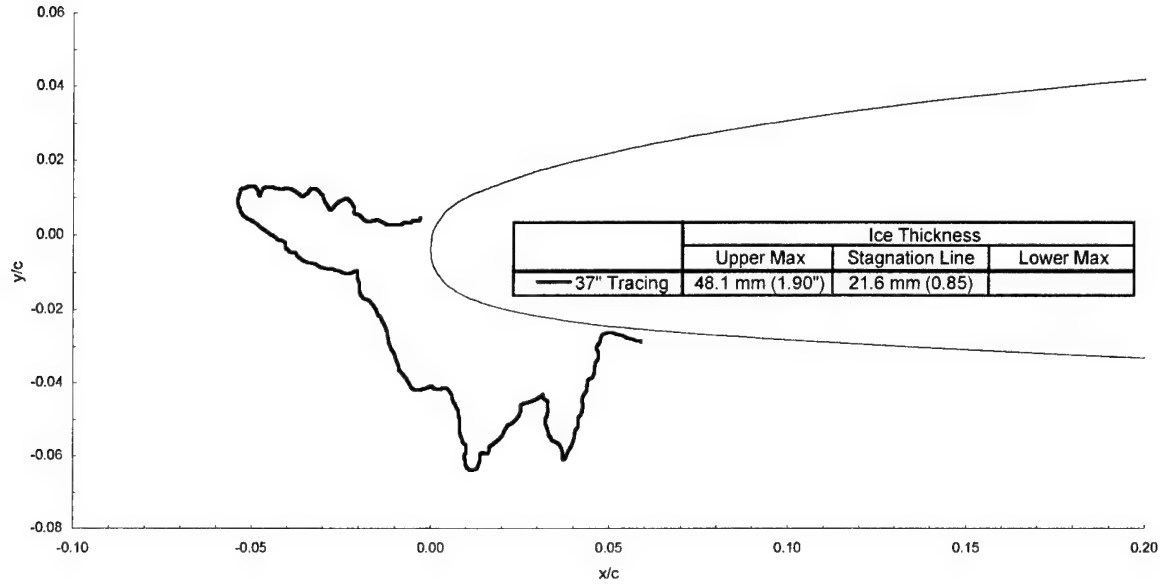

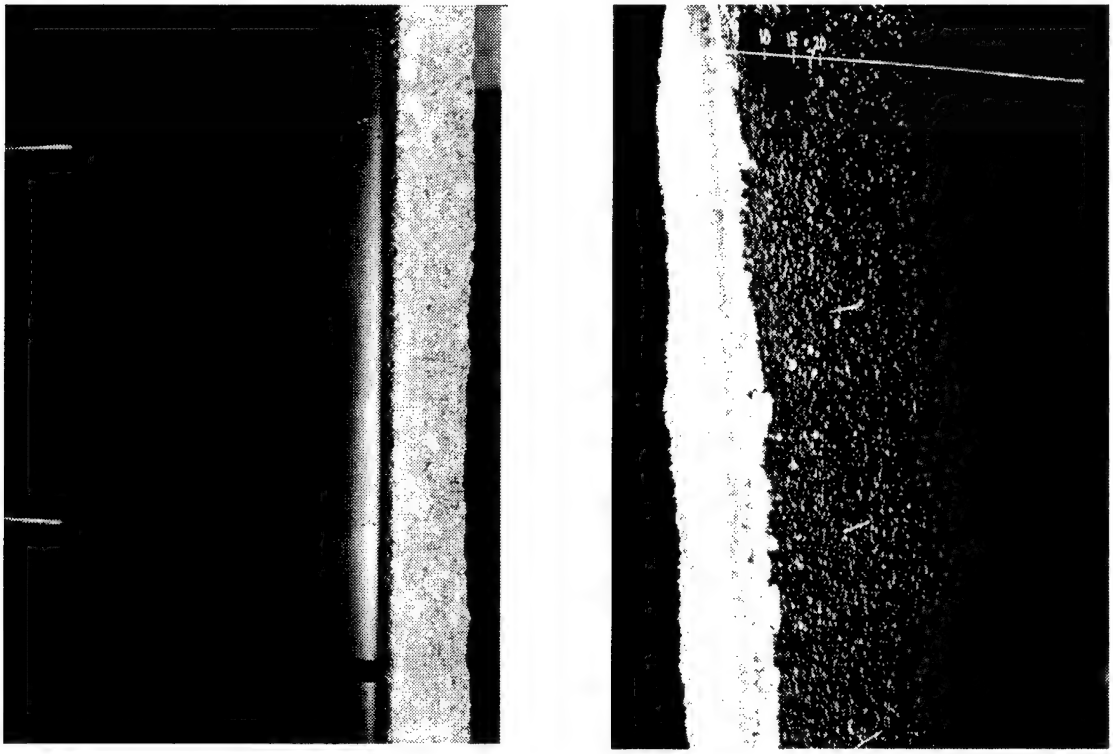

Business Jet - Run 072695.04

T_t = -5.9°C (21.4°F)
T_s = -10.0°C (14.0°F)
V = 90 m/s (175 kts)
Attitude = 6.1°

LWC = 0.43 g/m^3
MVD = 20 μm
Spray = 6.0 min
chord = 90 cm (36 in)

$C_{d\text{-clean}}$ = 0.0093
$C_{d\text{-iced}}$ = 0.0202

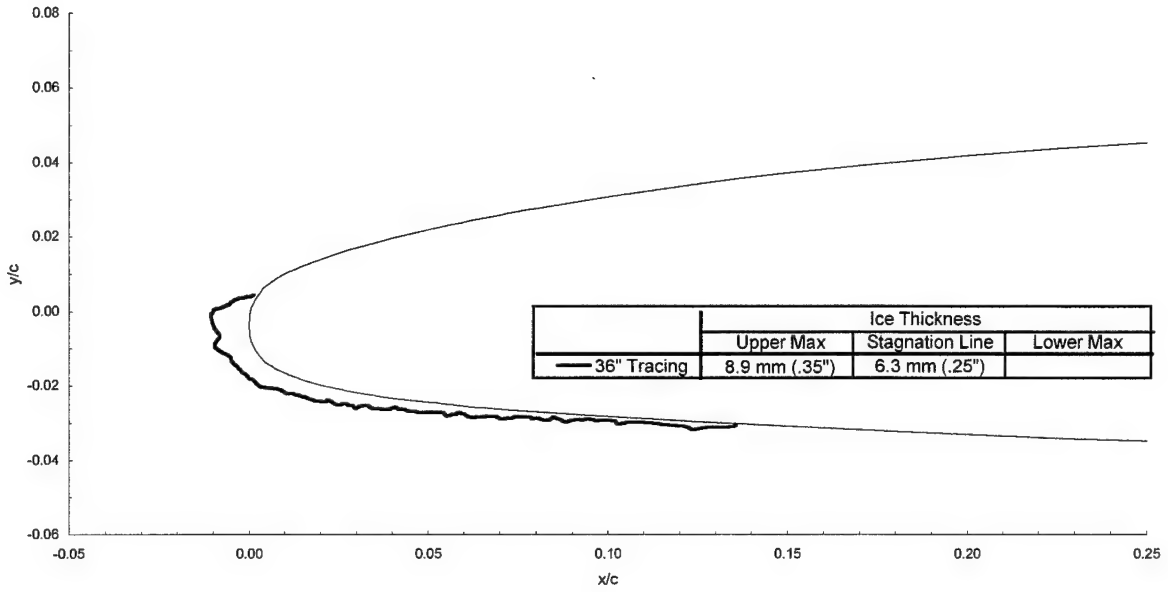

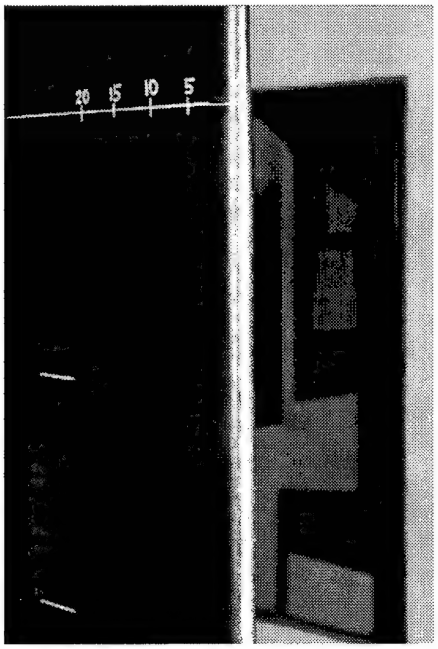

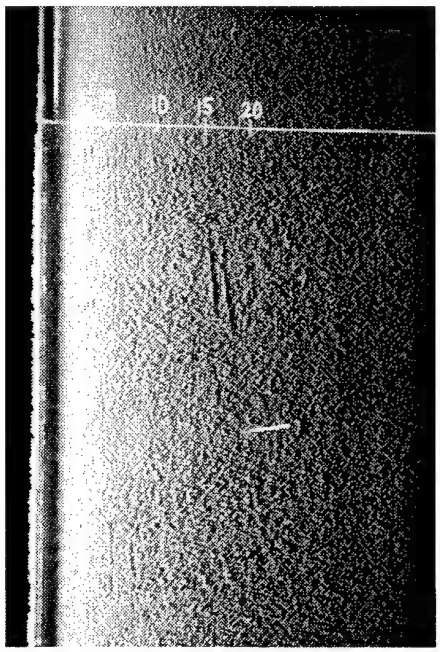

Business Jet - Run 072695.05

T_t = -5.9°C (21.4°F)
T_s = -10.0°C (14.0°F)
V = 90 m/s (175 kts)
Attitude = 6.1°

LWC = 0.43 g/m^3
MVD = 20 μm
Spray = 45.0 min
chord = 90 cm (36 in)

$C_{d\text{-clean}}$ = 0.0093
$C_{d\text{-iced}}$ = 0.0412

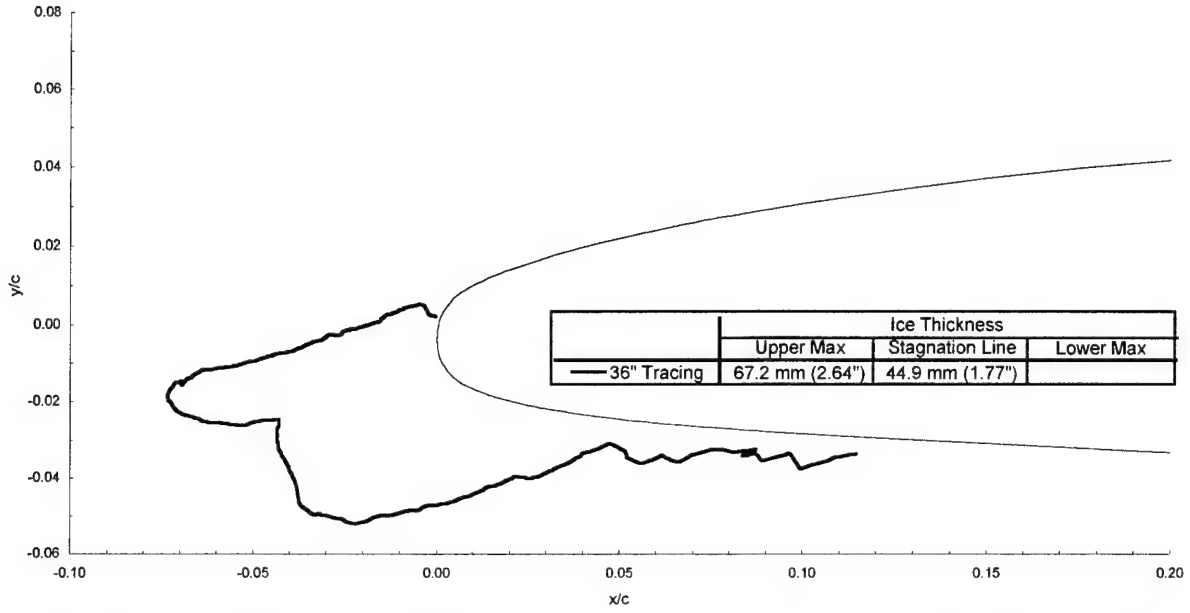

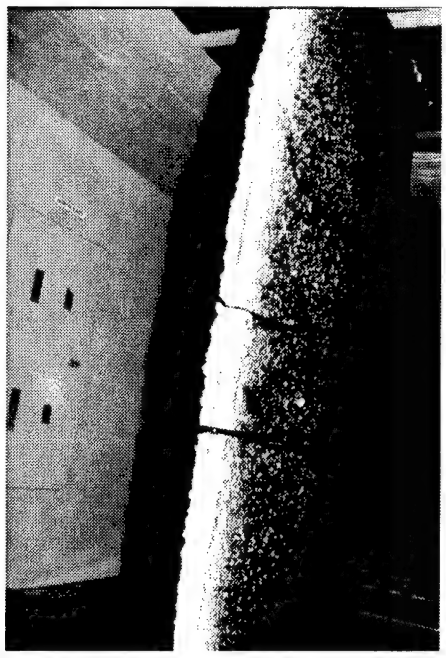

Business Jet - Run 072795.01

T_t = -5.9°C (21.4°F)
T_s = -10.0°C (14.0°F)
V = 90 m/s (175 kts)
Attitude = 6.1°

LWC = 0.43 g/m^3
MVD = 20 μm
Spray = 22.5 min
chord = 90 cm (36 in)

$C_{d\text{-clean}}$ = 0.0093
$C_{d\text{-iced}}$ = 0.0277

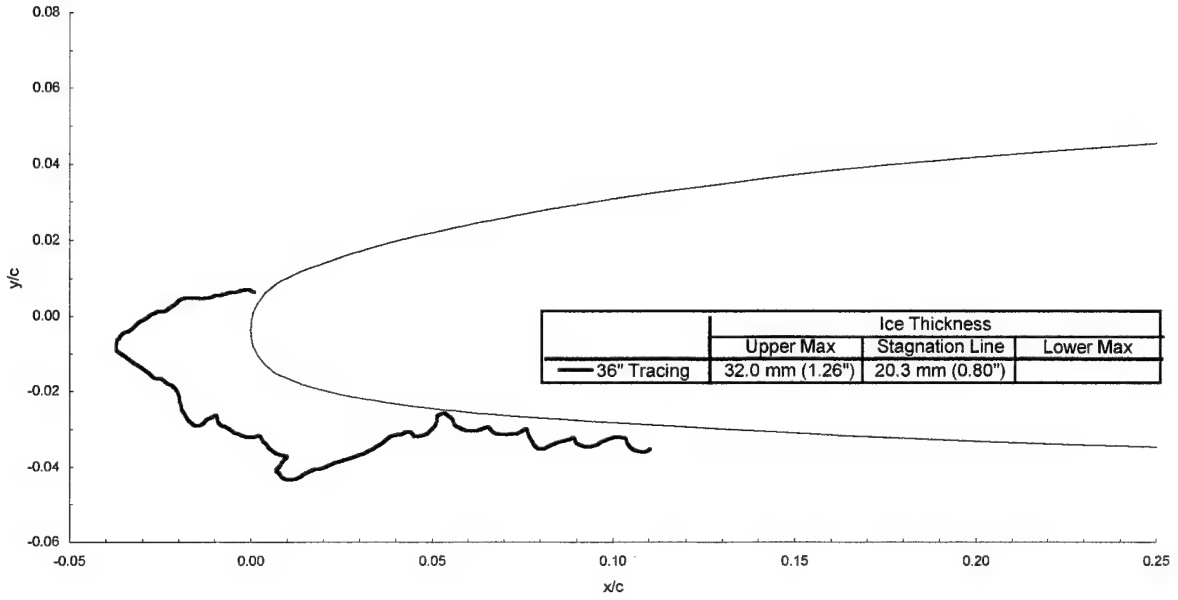

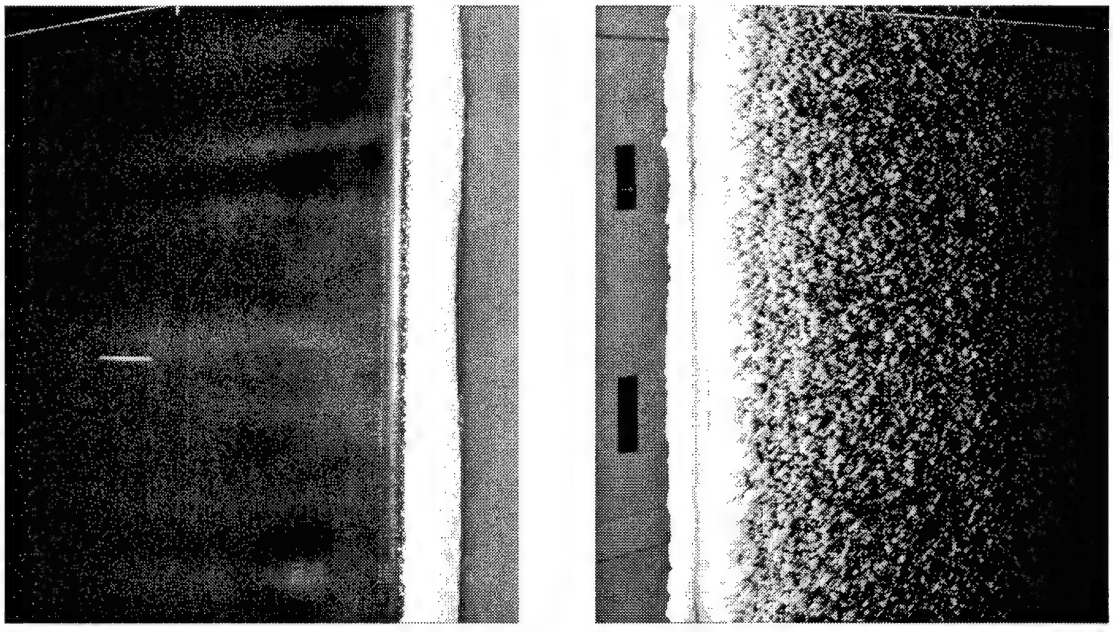

Business Jet - Run 072795.02

T_t = -5.9°C (21.4°F)
T_s = -10.0°C (14.0°F)
V = 90 m/s (175 kts)
Attitude = 6.1°

LWC = 0.60 g/m^3
MVD = 15 μm
Spray = 6.0 min
chord = 90 cm (36 in)

$C_{d\text{-}clean}$ = 0.0093
$C_{d\text{-}iced}$ = 0.0125

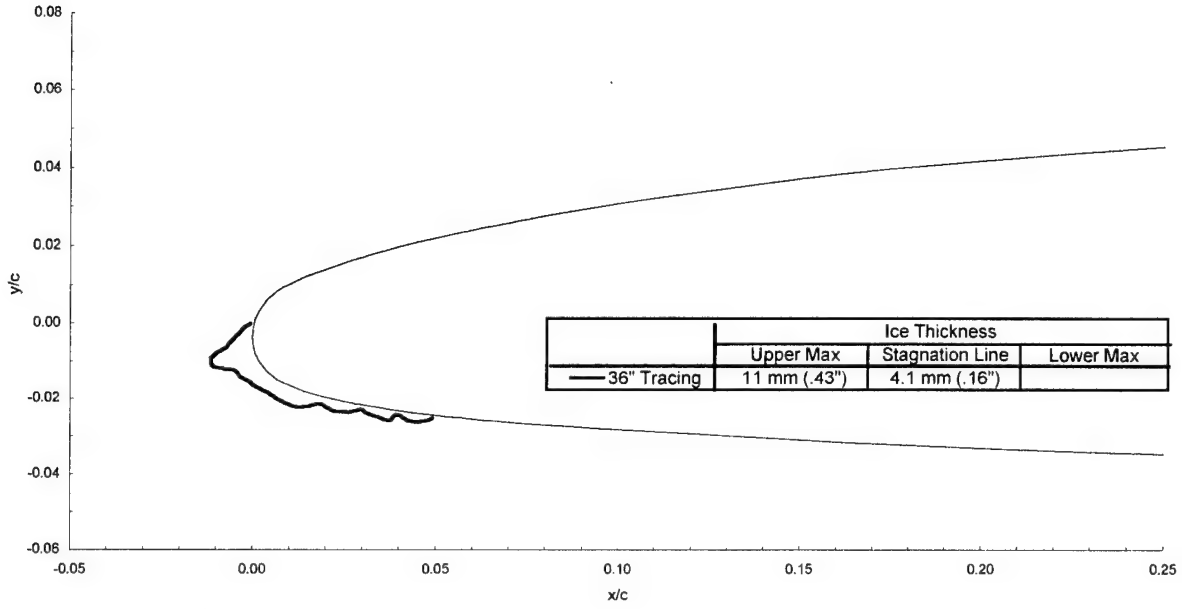

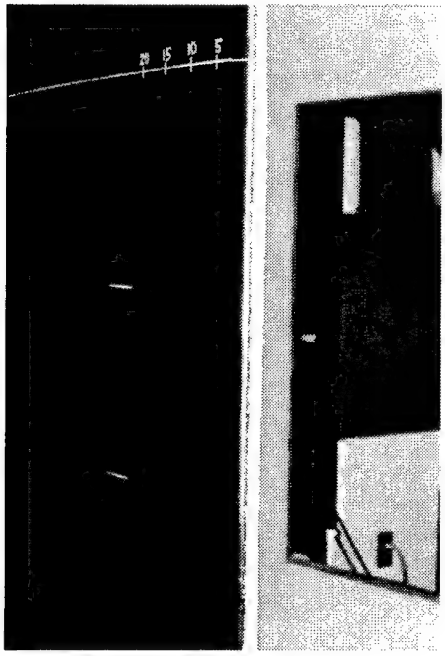

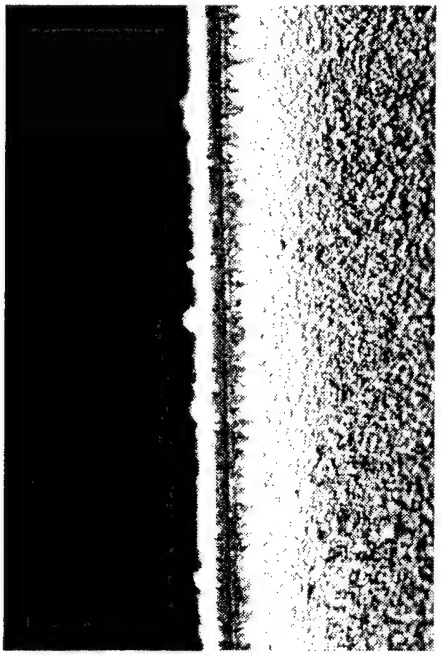

Business Jet - Run 072795.03

T_t = -5.9°C (21.4°F)
T_s = -10.0°C (14.0°F)
V = 90 m/s (175 kts)
Attitude = 6.1°

LWC = 0.60 g/m^3
MVD = 15 μm
Spray = 22.5 min
chord = 90 cm (36 in)

$C_{d\text{-}clean}$ = 0.0093
$C_{d\text{-}iced}$ = 0.0251

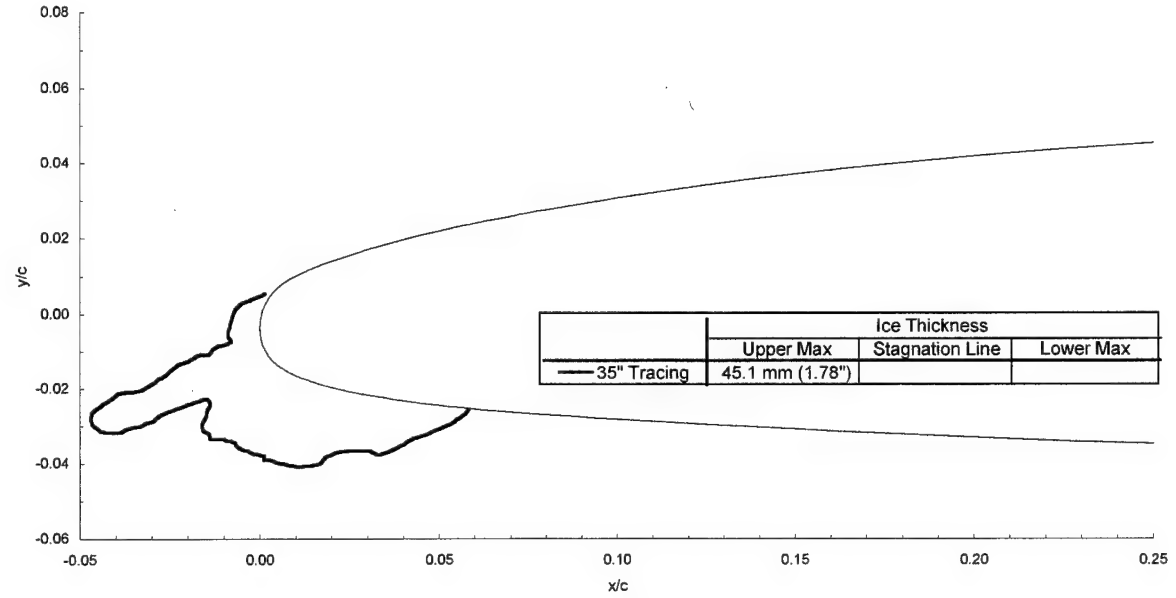

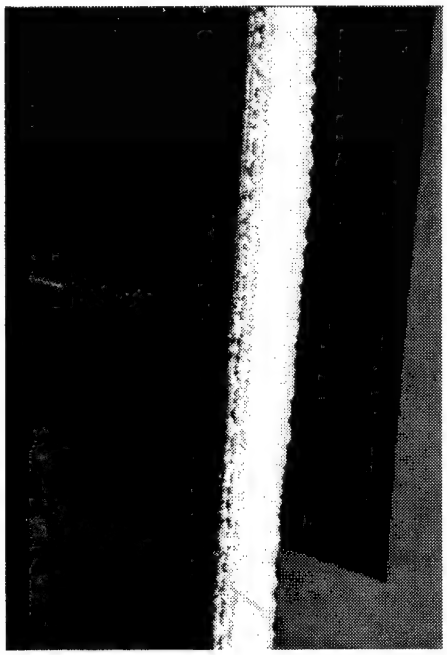

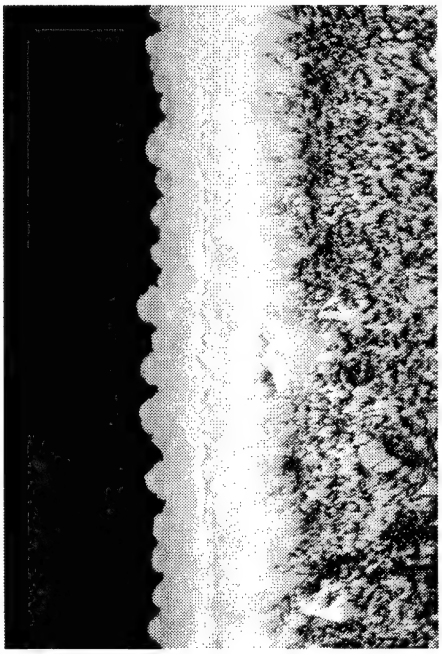

Business Jet - Run 072795.04

T_t = -6.0°C (21.4°F)
T_s = -10.0°C (14.0°F)
V = 90 m/s (175 kts)
Attitude = 6.1°

LWC = 0.60 g/m^3
MVD = 15 μm
Spray = 45.0 min
chord = 90 cm (36 in)

$C_{d\text{-clean}}$ = 0.0093
$C_{d\text{-iced}}$ = 0.0266

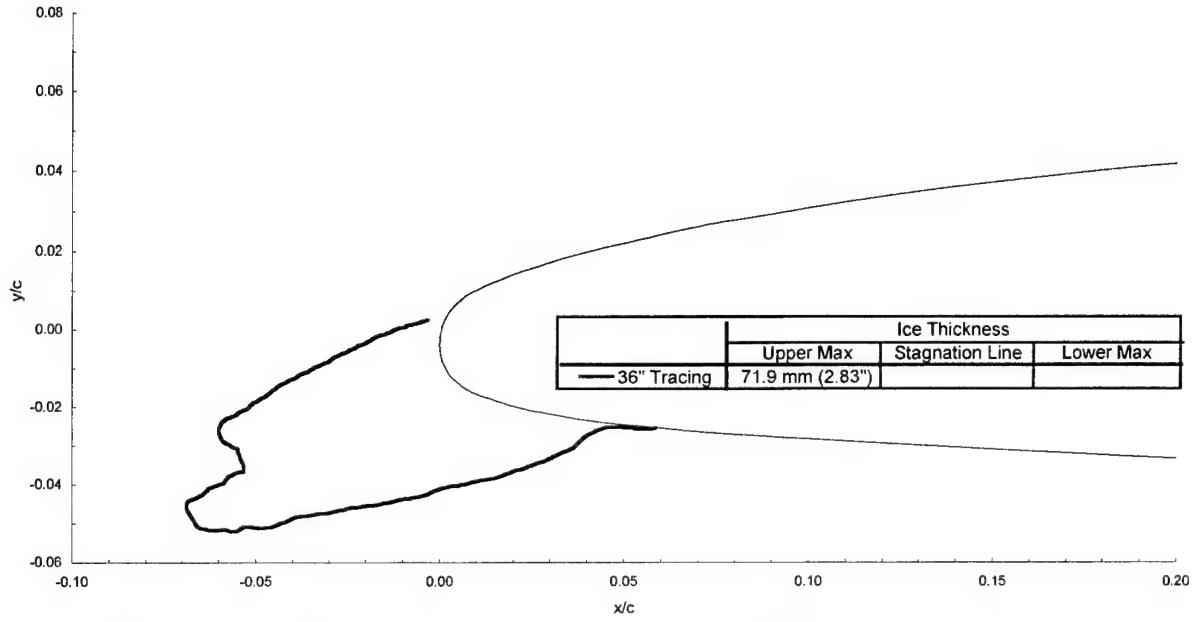

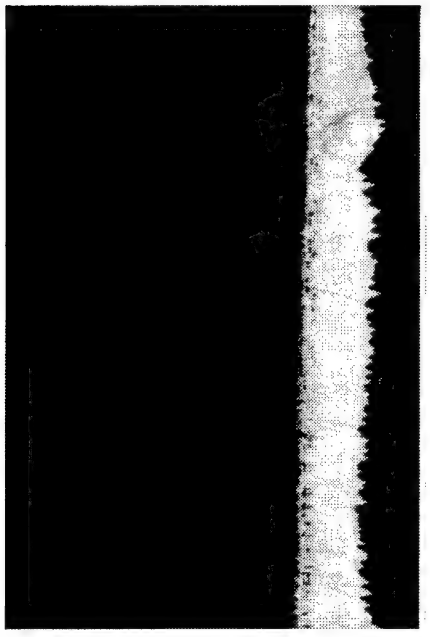

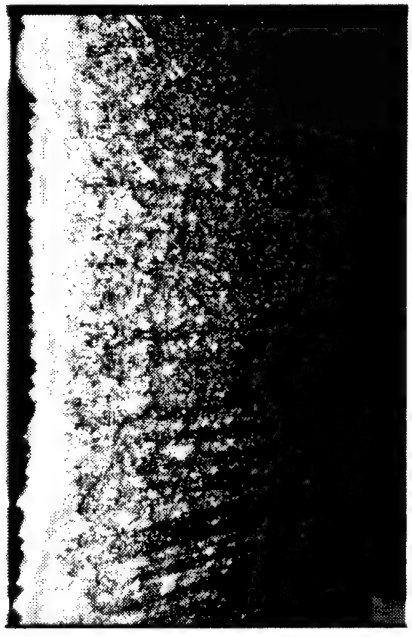

Business Jet - Run 072795.05

T_t = -11.0°C (12.3°F)
T_s = -15.0°C (5.0°F)
V = 90 m/s (175 kts)
Attitude = 6.1°

LWC = 0.405 g/m^3
MVD = 20 μm
Spray = 4.4 min
chord = 90 cm (36 in)

$C_{d\text{-}clean}$ = 0.0093
$C_{d\text{-}iced}$ = 0.0197

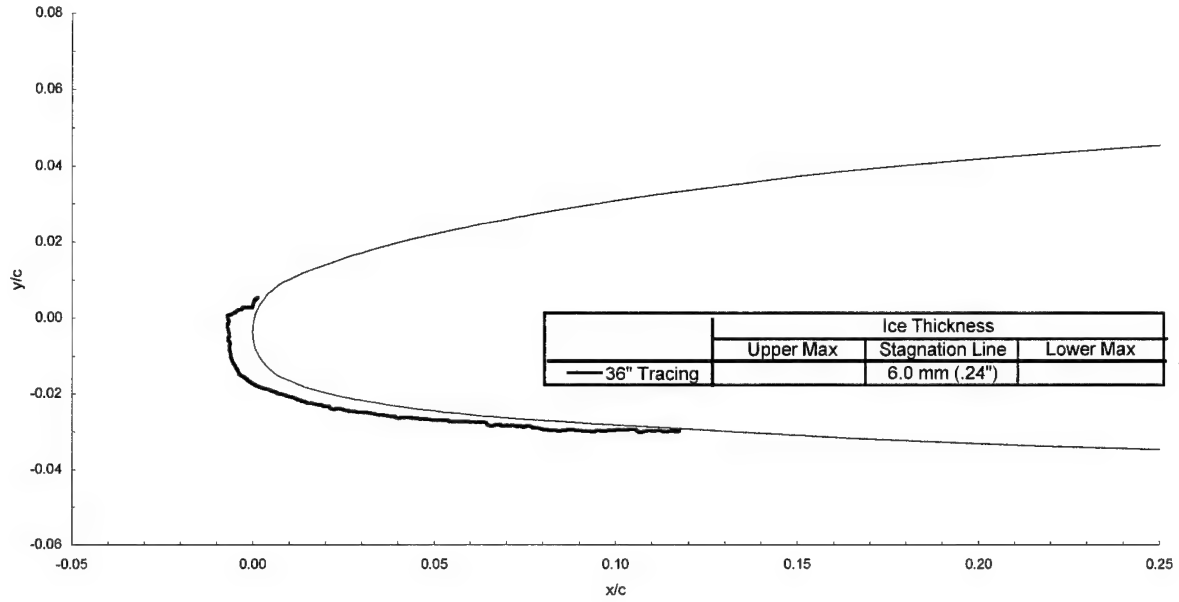

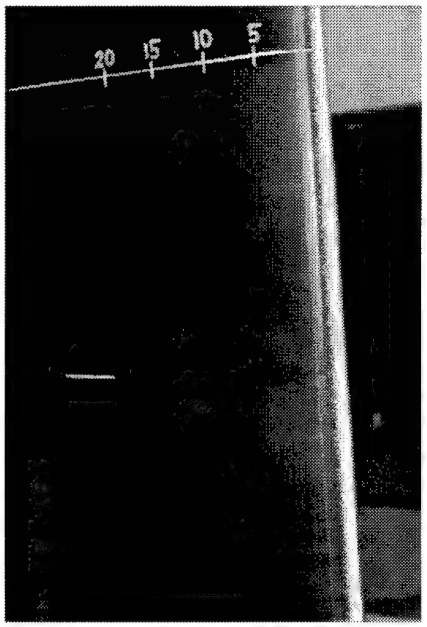

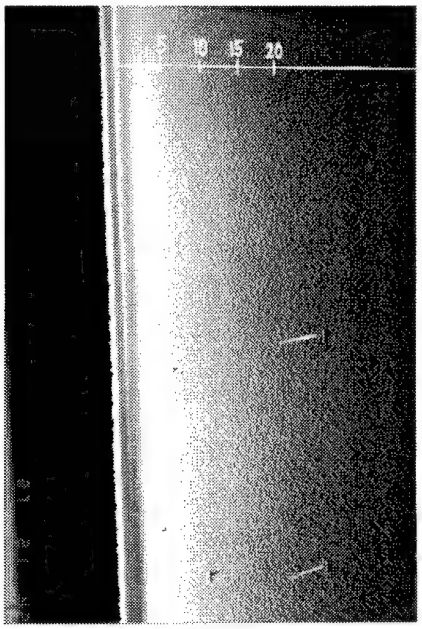

Business Jet - Run 072795.06

T_t = -11.0°C (12.3°F)
T_s = -15.0°C (5.0°F)
V = 90 m/s (175 kts)
Attitude = 6.1°

LWC = 0.405 g/m^3
MVD = 20 μm
Spray = 33.3 min
chord = 90 cm (36 in)

$C_{d\text{-clean}}$ = 0.0093
$C_{d\text{-iced}}$ = 0.0218

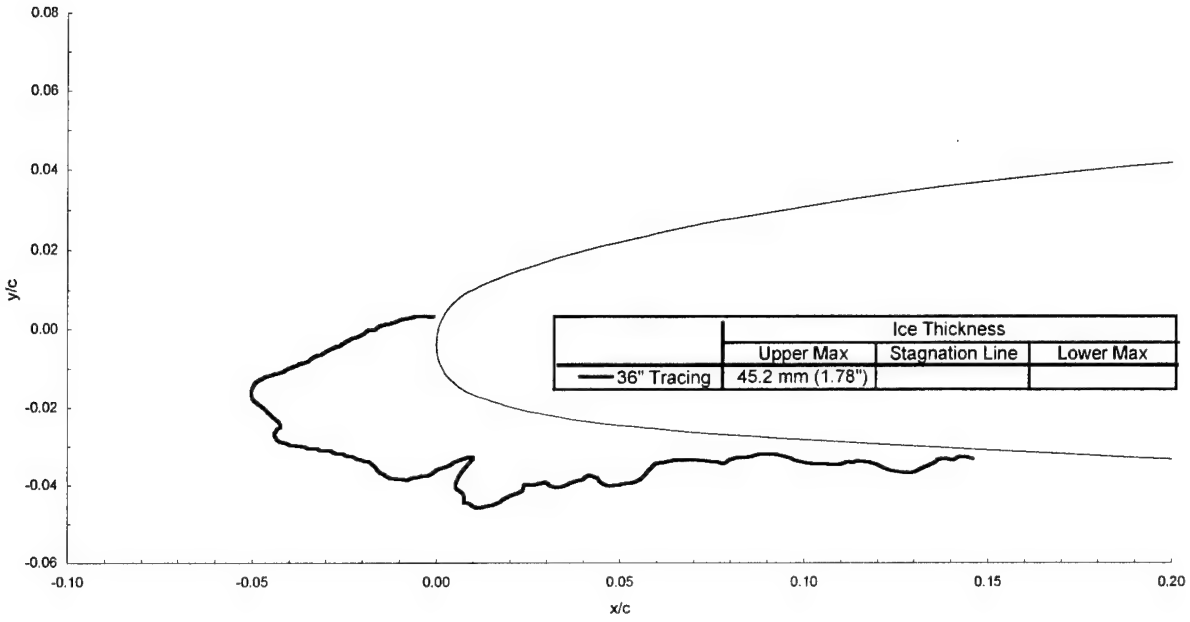

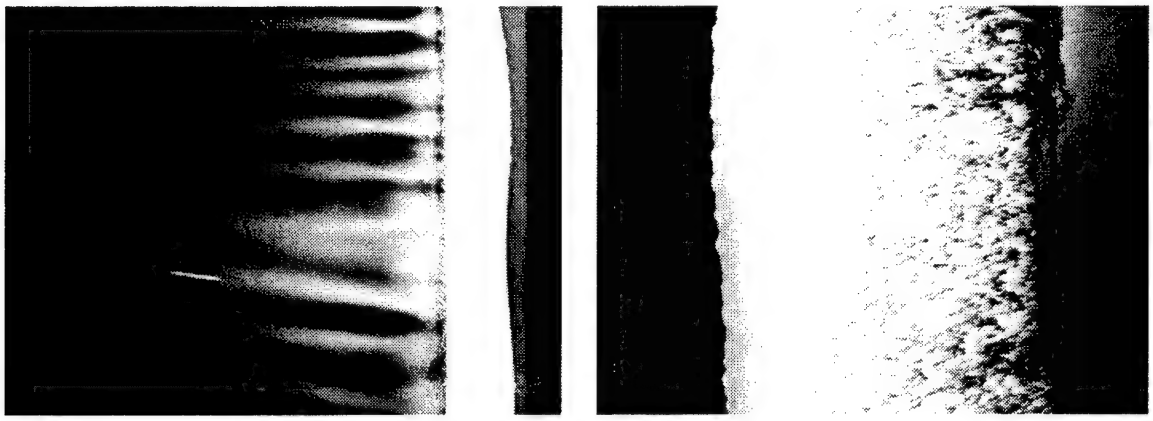

Business Jet - Run 072895.02

T_t = -1.3°C (29.7°F)
T_s = -9.3°C (15.3°F)
V = 129 m/s (250 kts)
Attitude = 1.6°

LWC = 0.50 g/m^3
MVD = 15 μm
Spray = 3.9 min
chord = 90 cm (36 in)

$C_{d\text{-clean}}$ = 0.0082
$C_{d\text{-iced}}$ = 0.0132

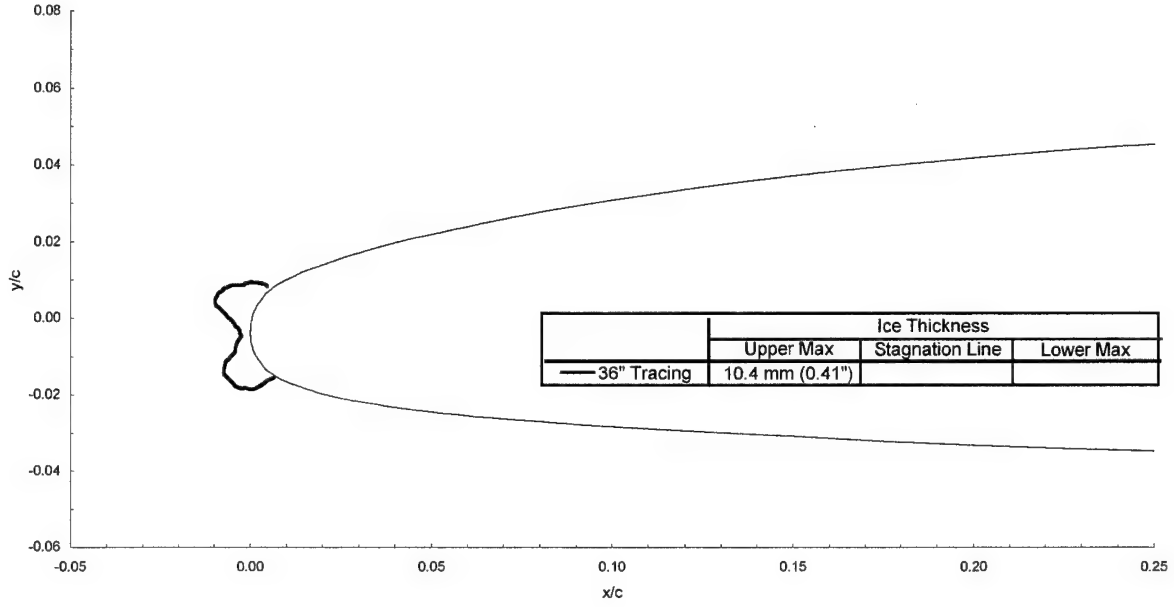

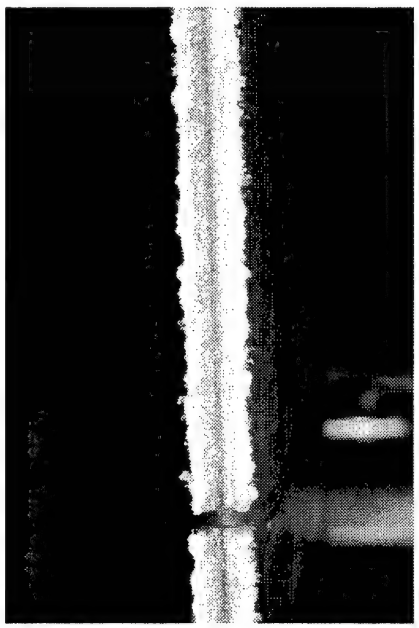

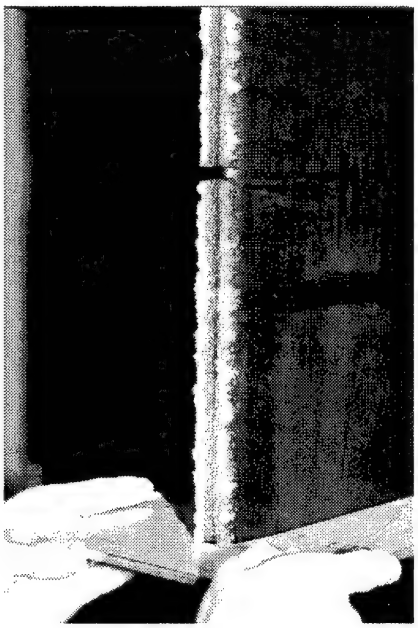

Business Jet - Run 072895.03

T_t = -1.3°C (29.7°F)
T_s = -9.3°C (15.3°F)
V = 129 m/s (250 kts)
Attitude = 1.6°

LWC = 0.50 g/m^3
MVD = 15 μm
Spray = 7.2 min
chord = 90 cm (36 in)

$C_{d\text{-clean}}$ = 0.0082
$C_{d\text{-iced}}$ = 0.0161

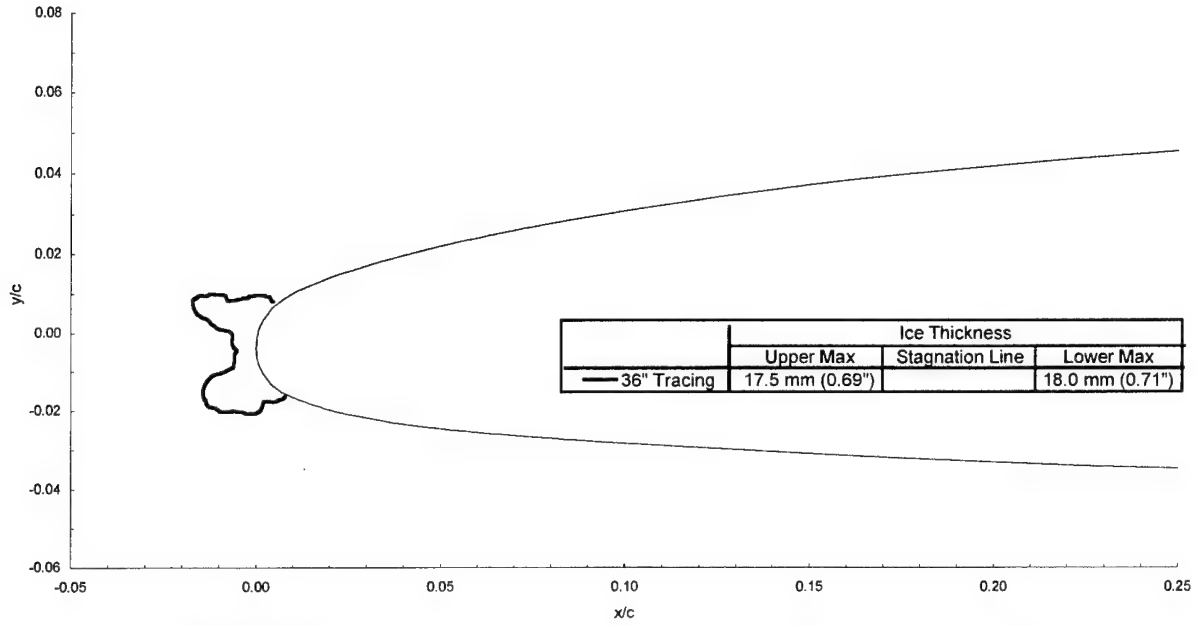

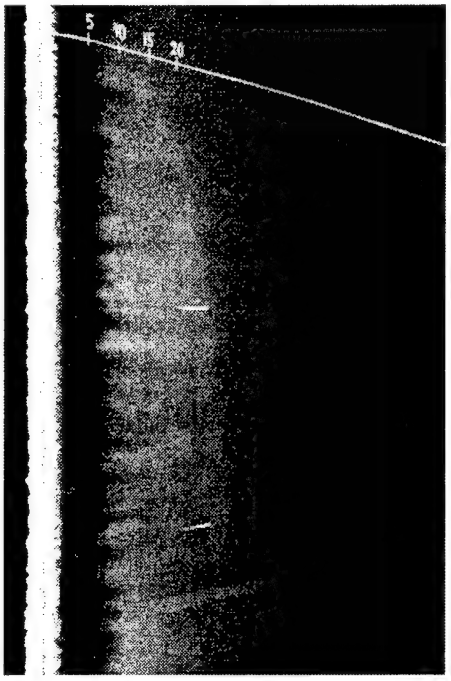

Business Jet - Run 072895.04

T_t = -2.2°C (28°F)
T_s = -10.2°C (13.7°F)
V = 129 m/s (250 kts)
Attitude = 1.6°

LWC = 0.43 g/m^3
MVD = 20 μm
Spray = 3.0 min
chord = 90 cm (36 in)

$C_{d\text{-}clean}$ = 0.0082
$C_{d\text{-}iced}$ = 0.0170

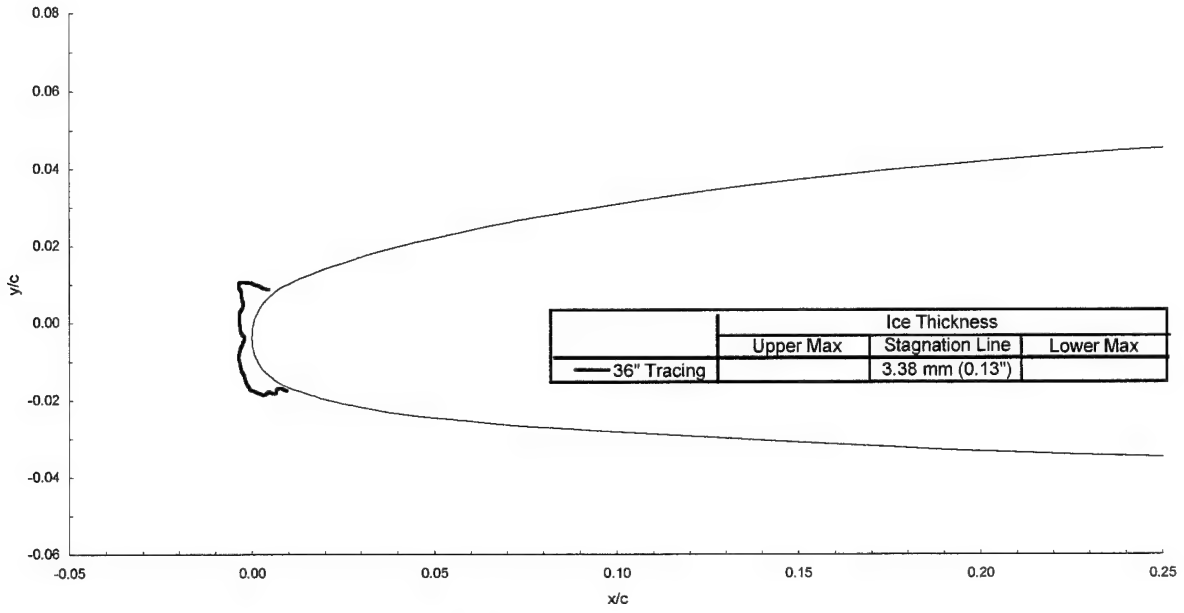

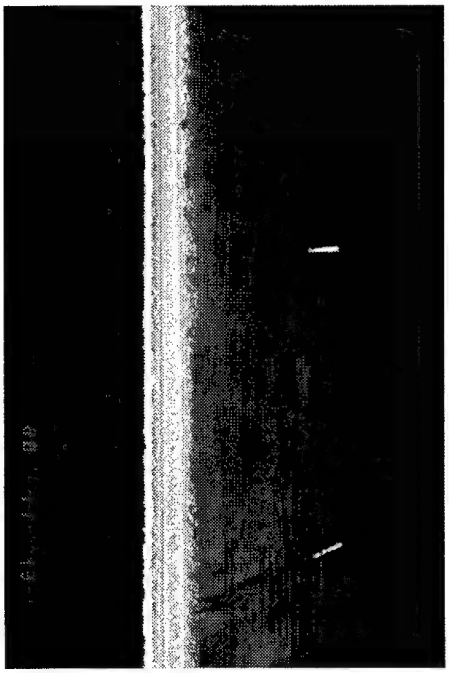

Business Jet - Run 072895.05

T_t = -2.2°C (28.0°F)
T_s = -10.2°C (13.7°F)
V = 129 m/s (250 kts)
Attitude = 1.6°

LWC = 0.43 g/m^3
MVD = 20 μm
Spray = 6.0 min
chord = 90 cm (36 in)

$C_{d\text{-clean}}$ = 0.0082
$C_{d\text{-iced}}$ = 0.0264

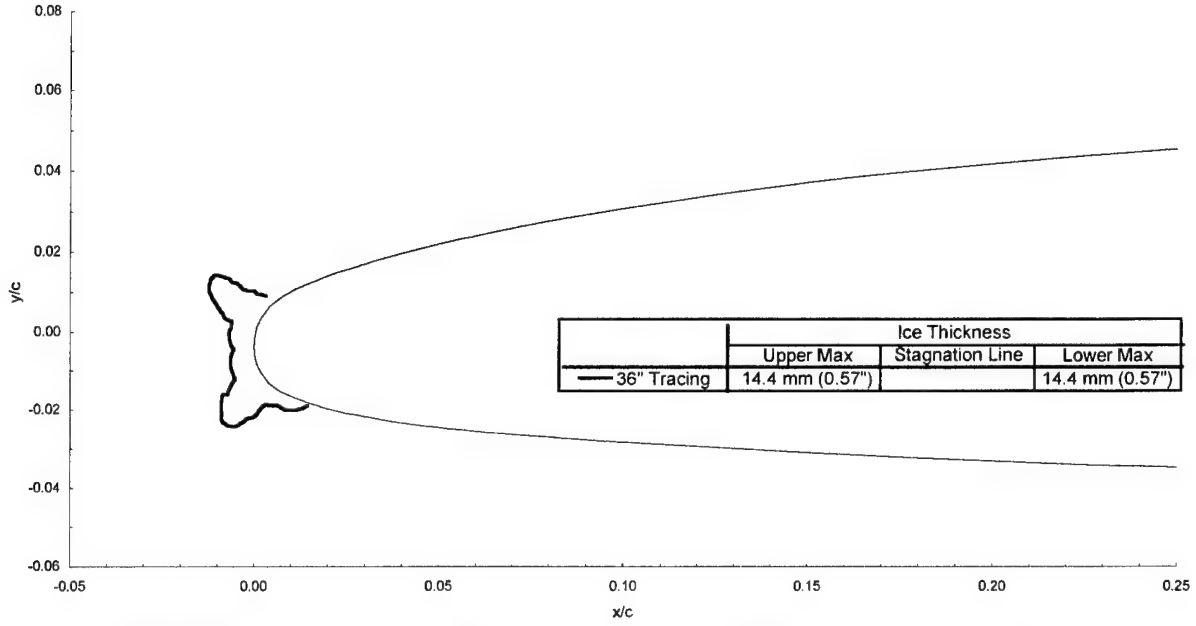

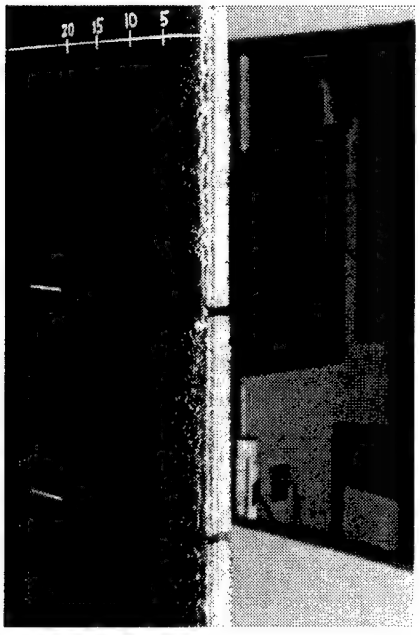

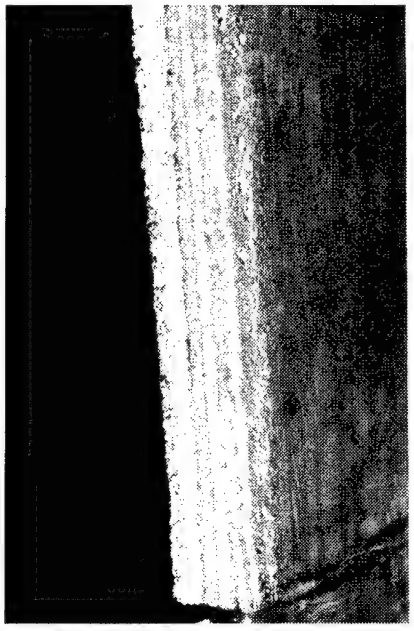

Business Jet - Run 072895.06

T_t = -2.2°C (28.0°F)
T_s = -10.2°C (13.7°F)
V = 129 m/s (250 kts)
Attitude = 1.6°

LWC = 0.54 g/m^3
MVD = 20 μm
Spray = 3.0 min
chord = 90 cm (36 in)

$C_{d\text{-}clean}$ = 0.0082
$C_{d\text{-}iced}$ = 0.0188

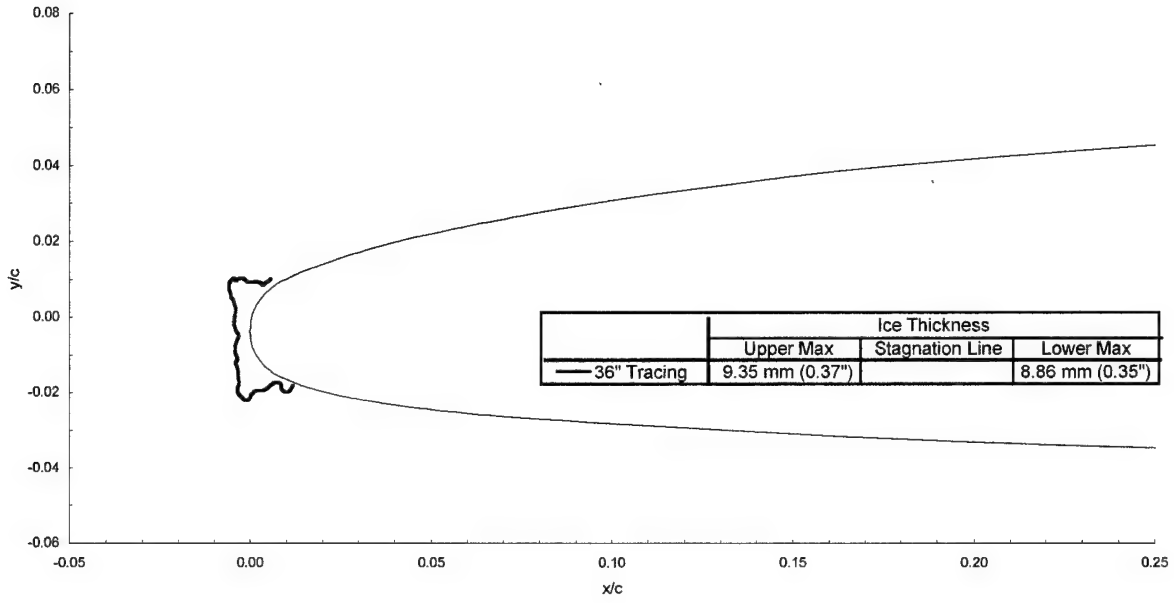

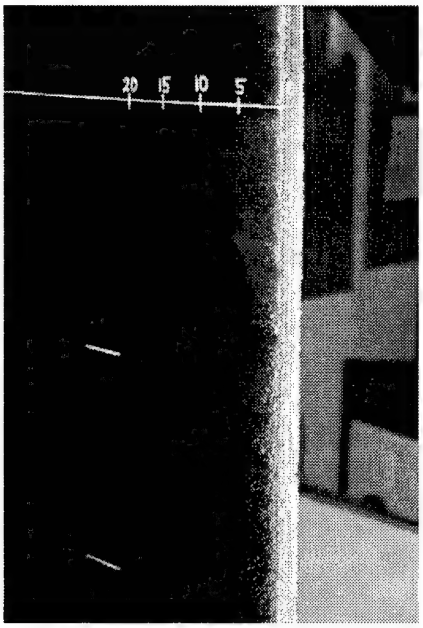

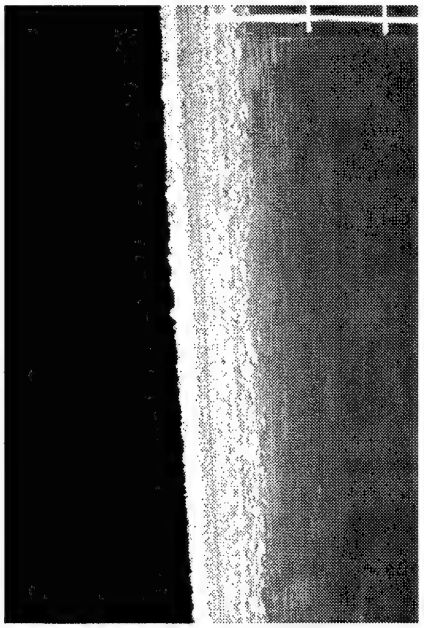

Business Jet - Run 072895.07

T_t = -2.2°C (28.0°F)
T_s = -10.2°C (13.7°F)
V = 129 m/s (250 kts)
Attitude = 1.6°

LWC = 0.54 g/m^3
MVD = 20 μm
Spray = 6.0 min
chord = 90 cm (36 in)

$C_{d\text{-clean}}$ = 0.0082
$C_{d\text{-iced}}$ = 0.0315

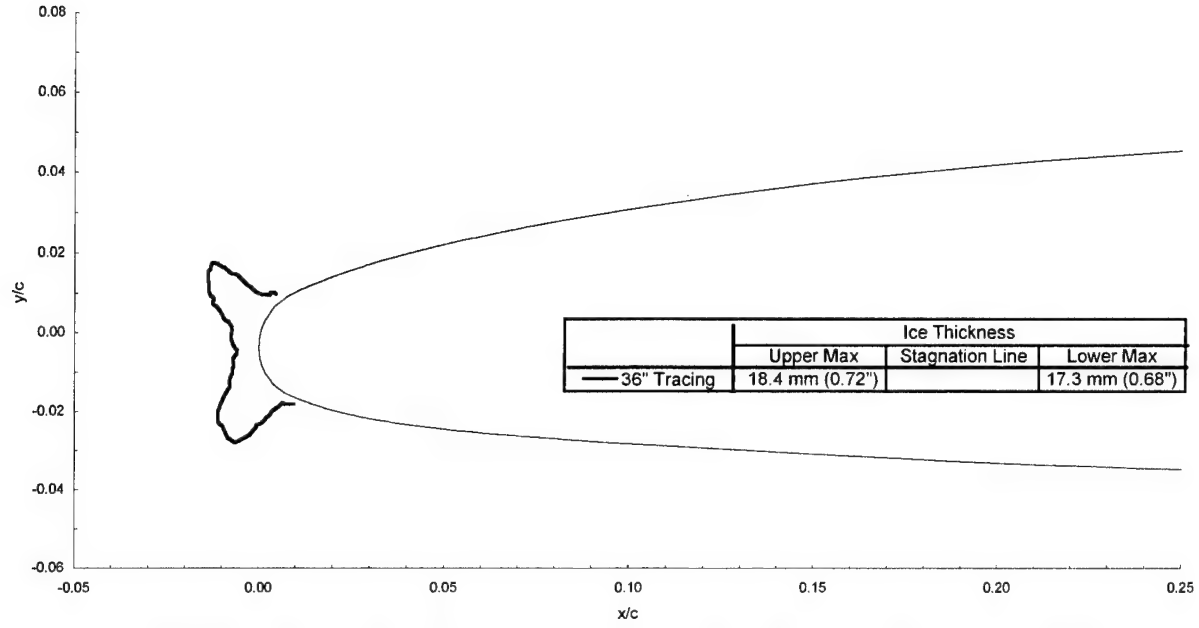

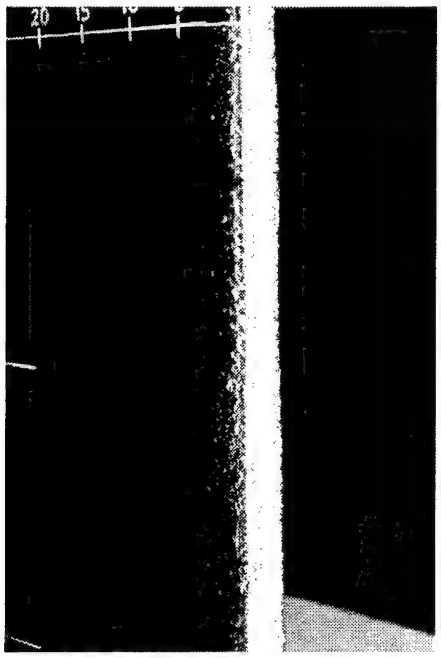

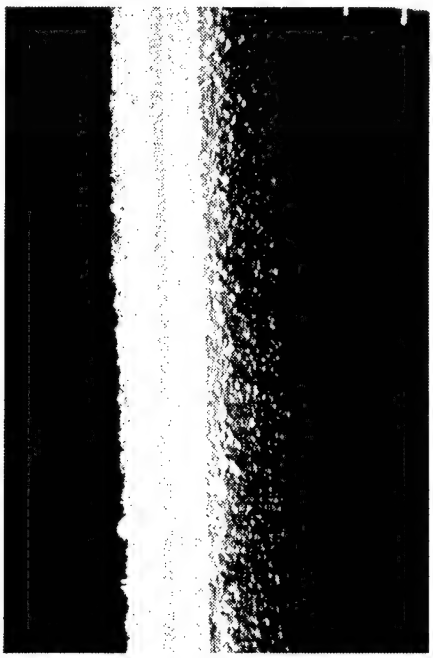

Business Jet - Run 072895.08

T_t = -11.0°C (12.3°F)
T_s = -15.0°C (5.0°F)
V = 90 m/s (175 kts)
Attitude = 6.1°

LWC = 0.54 g/m^3
MVD = 20 μm
Spray = 45.0 min
chord = 90 cm (36 in)

$C_{d\text{-clean}}$ = 0.0093
$C_{d\text{-iced}}$ = 0.0220

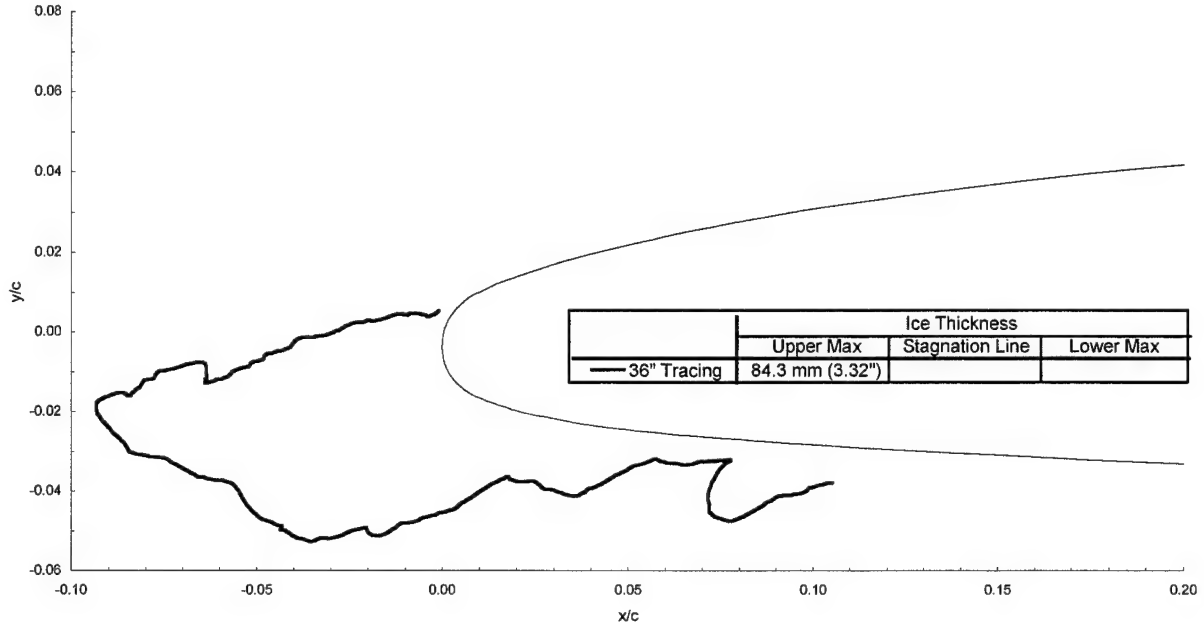

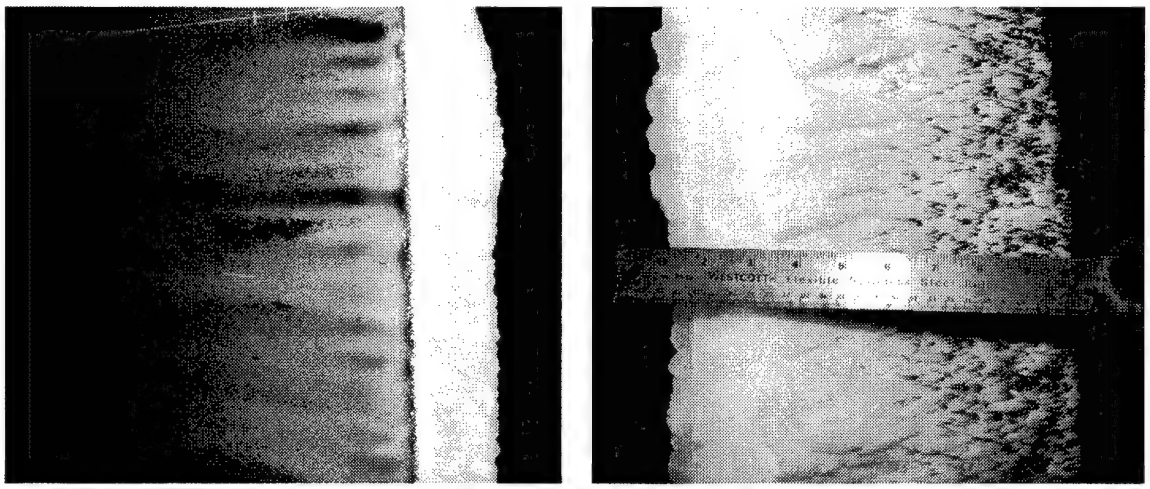

Business Jet - Run 073195.01

T_t = -7.3°C (18.9°F)
T_s = -15.0°C (5.0°F)
V = 129 m/s (250 kts)
Attitude = 1.5°

LWC = 0.31 g/m^3
MVD = 20 μm
Spray = 2.9 min
chord = 90 cm (36 in)

$C_{d\text{-}clean}$ = 0.0082
$C_{d\text{-}iced}$ = 0.0125

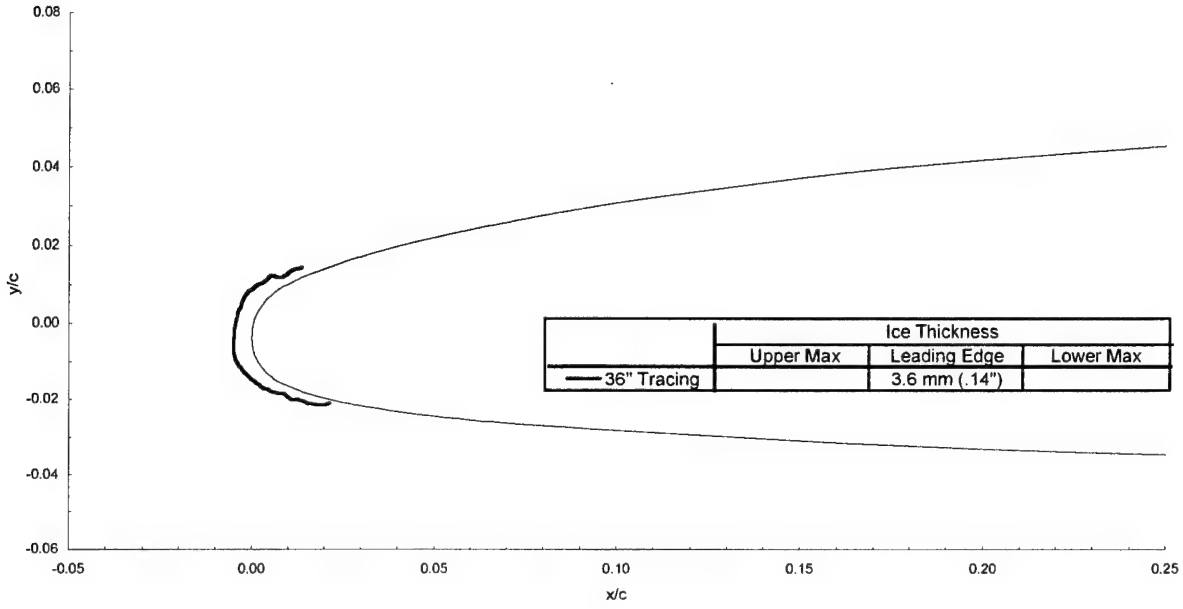

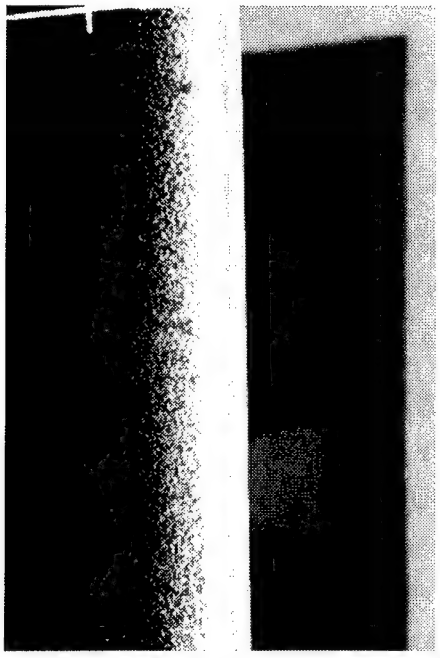

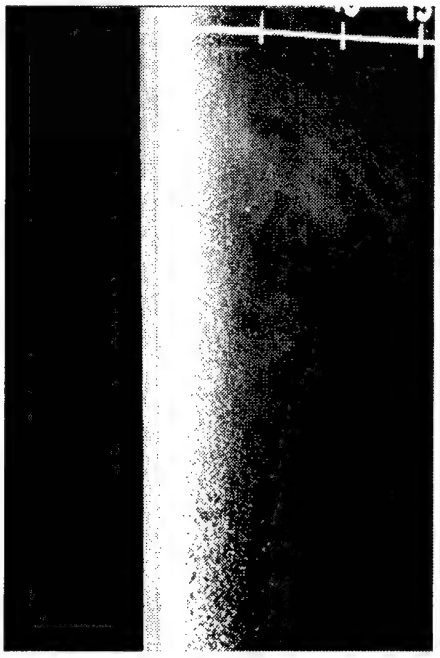

Business Jet - Run 073195.02

T_t = -7.3°C (18.9°F)
T_s = -15.0°C (5.0°F)
V = 129 m/s (250 kts)
Attitude = 1.5°

LWC = 0.31 g/m^3
MVD = 20 μm
Spray = 5.8 min
chord = 90 cm (36 in)

$C_{d\text{-clean}}$ = 0.0082
$C_{d\text{-iced}}$ = 0.0134

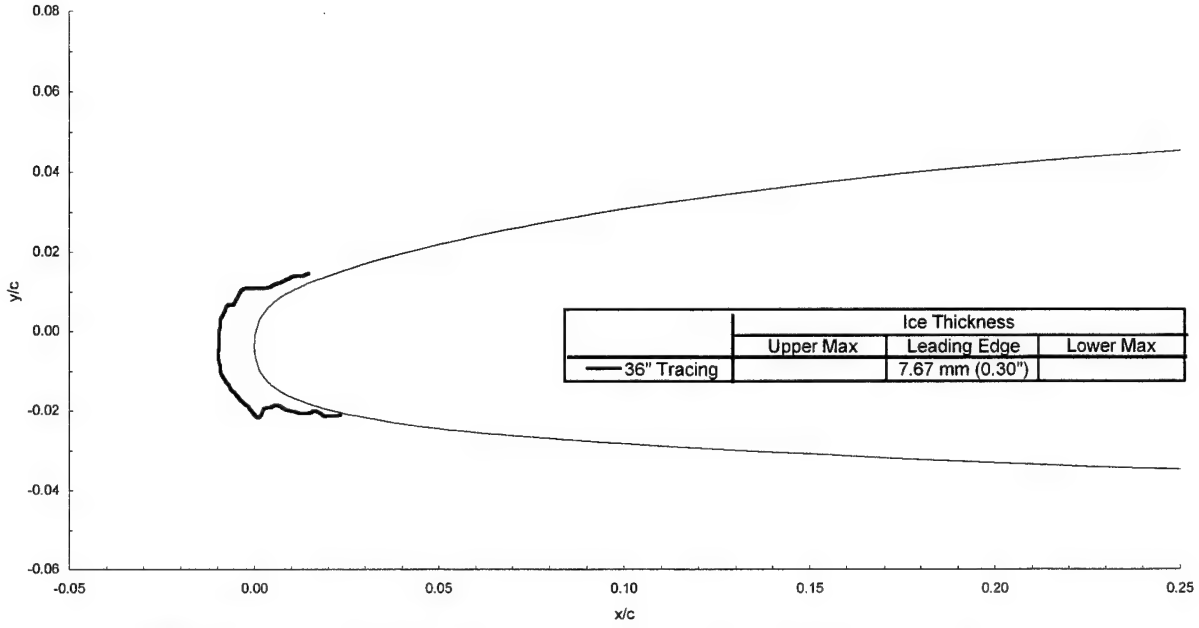

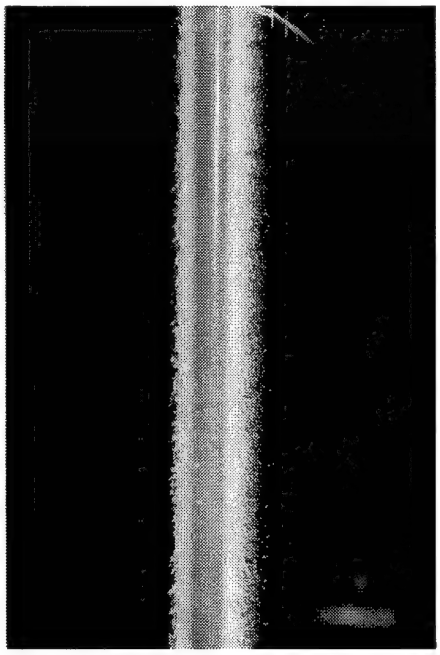

Business Jet - Run 073195.03

T_t = -11.0°C (12.3°F)
T_s = -15.0°C (5.0°F)
V = 90 m/s (175 kts)
Attitude = 6.1°

LWC = 0.405 g/m^3
MVD = 20 μm
Spray = 16.7 min
chord = 90 cm (36 in)

$C_{d\text{-clean}}$ = 0.0093
$C_{d\text{-iced}}$ = 0.0220

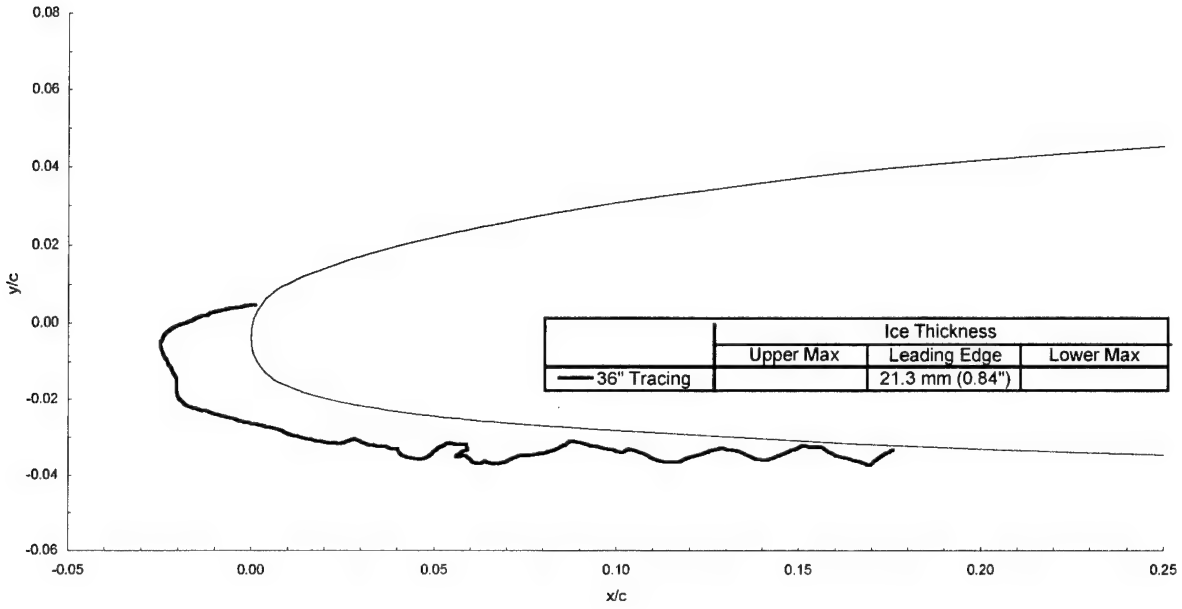

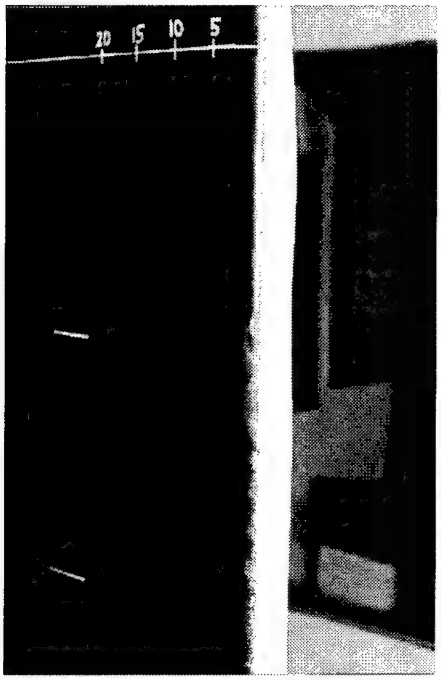

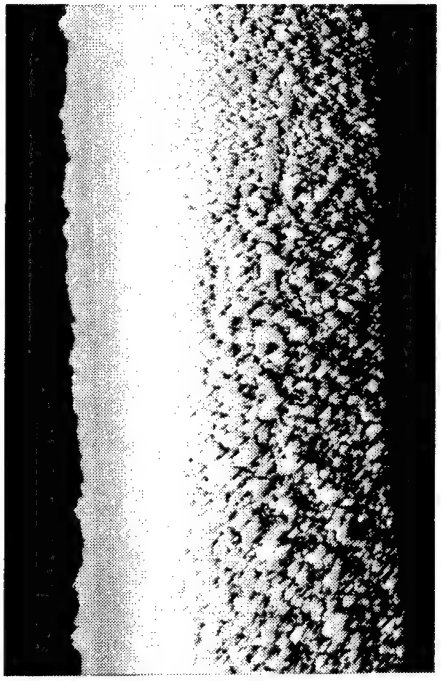

Business Jet - Run 073195.04

T_t = -11.0°C (12.3°F)
T_s = -15.0°C (5.0°F)
V = 90 m/s (175 kts)
Attitude = 6.1°

LWC = 0.54 g/m^3
MVD = 20 μm
Spray = 6.0 min
chord = 90 cm (36 in)

$C_{d\text{-}clean}$ = 0.0093
$C_{d\text{-}iced}$ = 0.0212

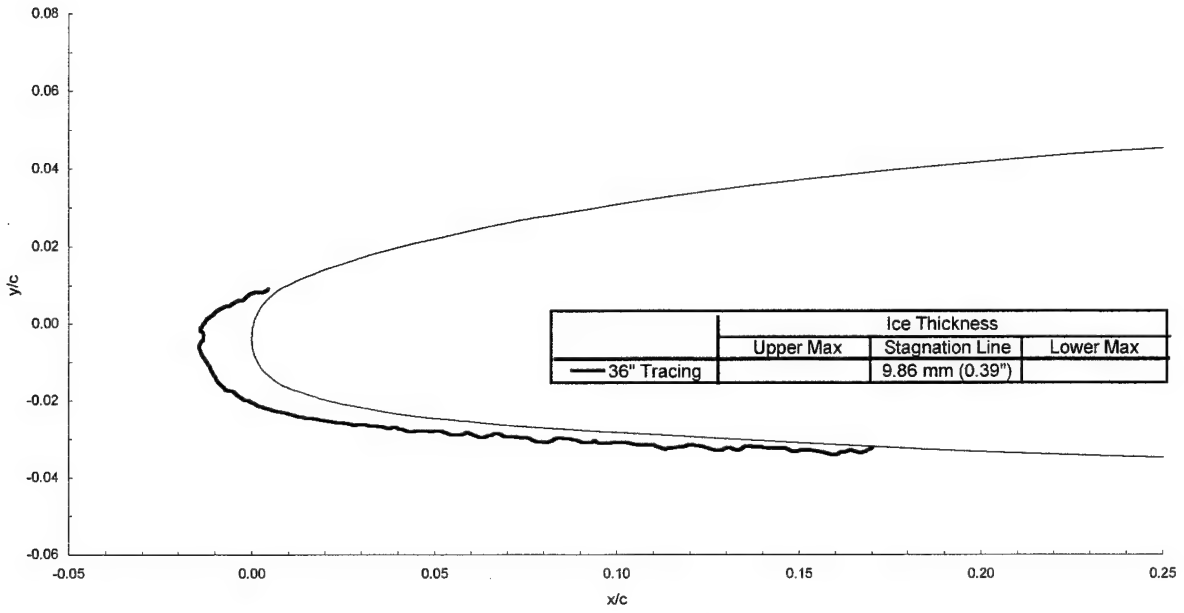

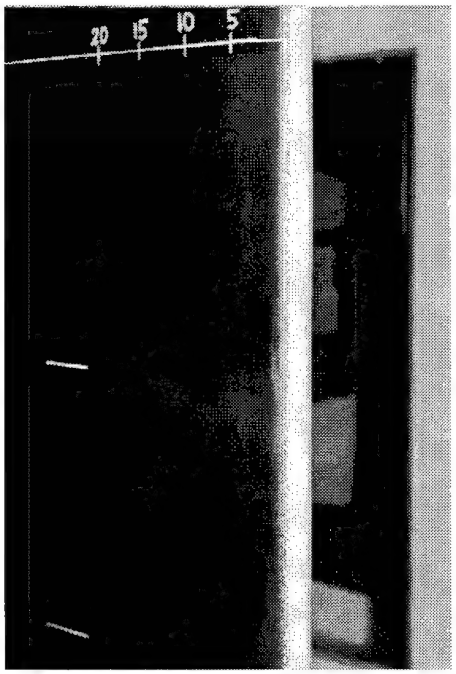

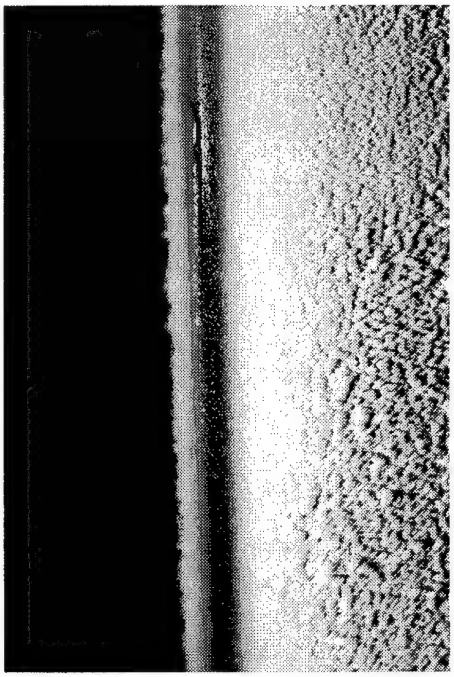

Business Jet - Run 073195.05

T_t = -11.0°C (12.3°F)
T_s = -15.0°C (5.0°F)
V = 90 m/s (175 kts)
Attitude = 6.1°

LWC = 0.54 g/m^3
MVD = 20 μm
Spray = 22.5 min
chord = 90 cm (36 in)

$C_{d\text{-}clean}$ = 0.0093
$C_{d\text{-}iced}$ = 0.0299

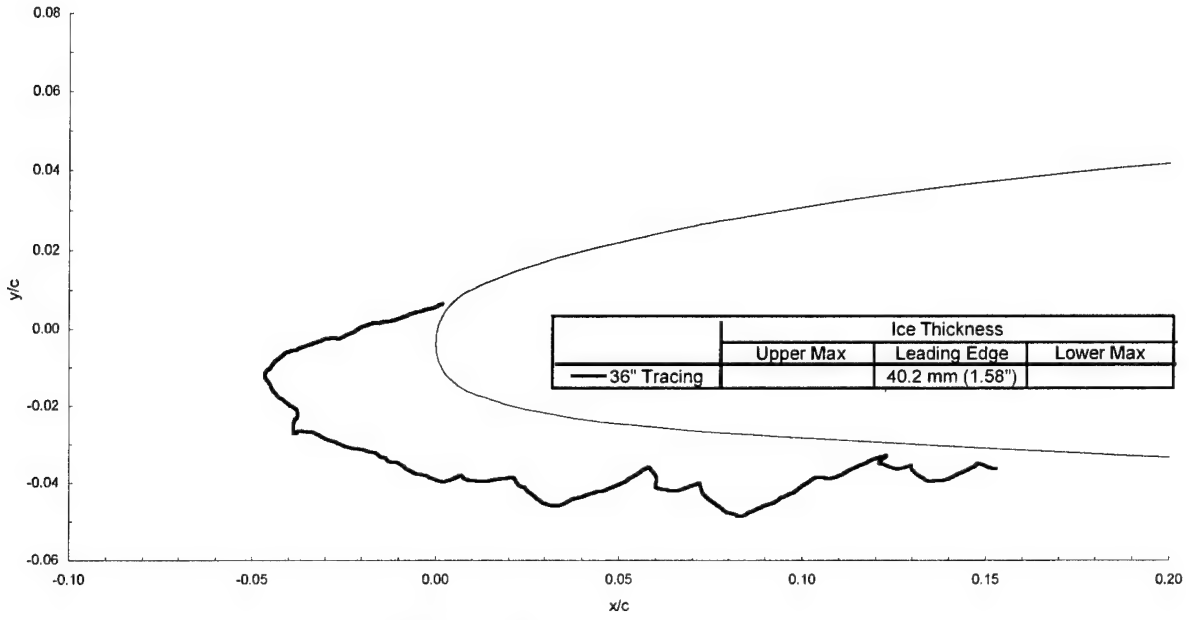

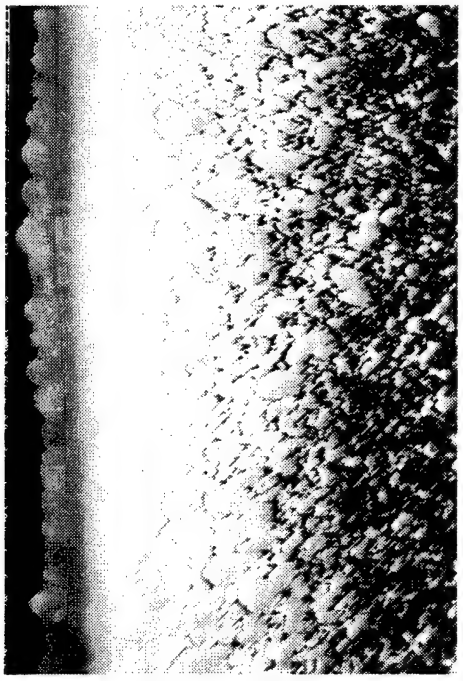

Business Jet - Run 080195.01

T_t = -12.5°C (9.5°F)
T_s = -20.0°C (4.3°F)
V = 129 m/s (250 kts)
Attitude = 1.5°

LWC = 0.41 g/m^3
MVD = 40 μm
Spray = 0.7 min
chord = 90 cm (36 in)

$C_{d\text{-clean}}$ = 0.0082
$C_{d\text{-iced}}$ = 0.0091

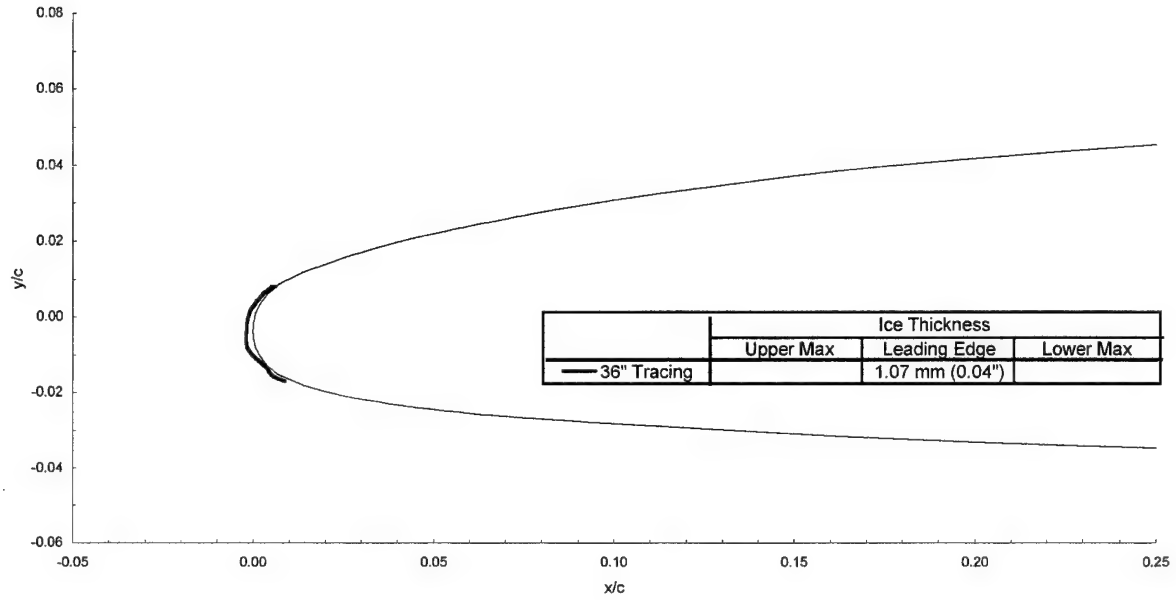

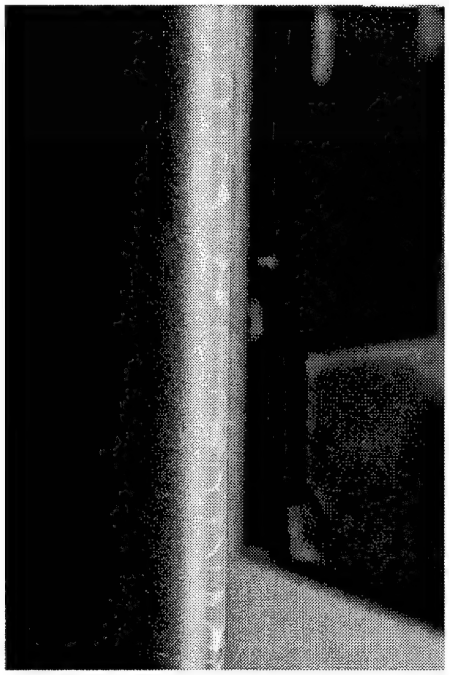

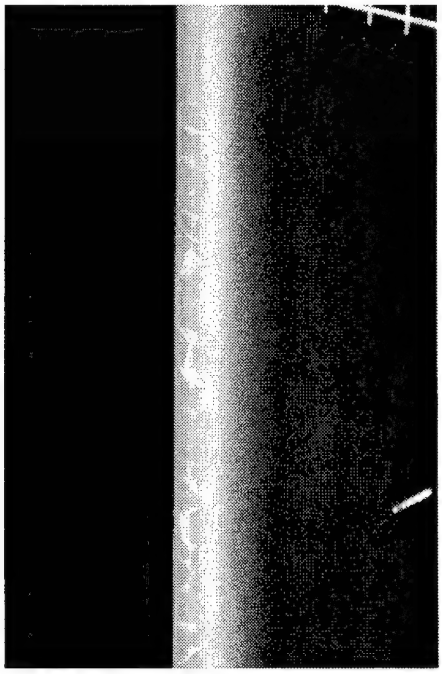

Business Jet - Run 080195.02

T_t = -12.5°C (9.5°F)
T_s = -20.0°C (-4.3°F)
V = 129 m/s (250 kts)
Attitude = 1.5°

LWC = 0.41 g/m^3
MVD = 40 μm
Spray = 1.5 min
chord = 90 cm (36 in)

$C_{d\text{-clean}}$ = 0.0082
$C_{d\text{-iced}}$ = 0.0112

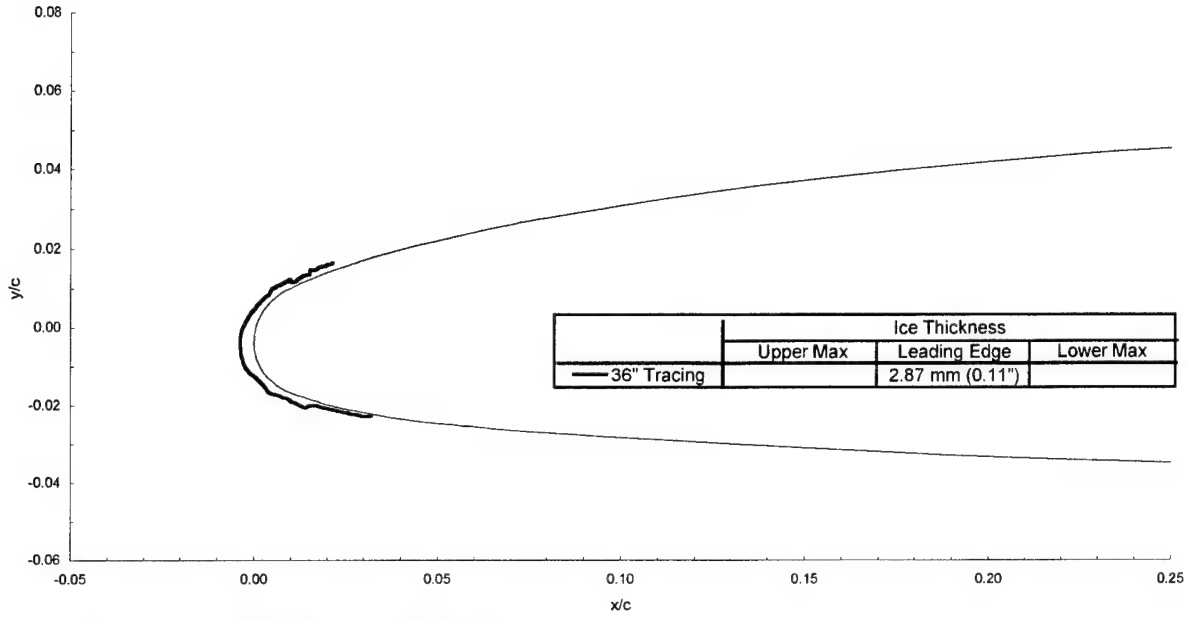

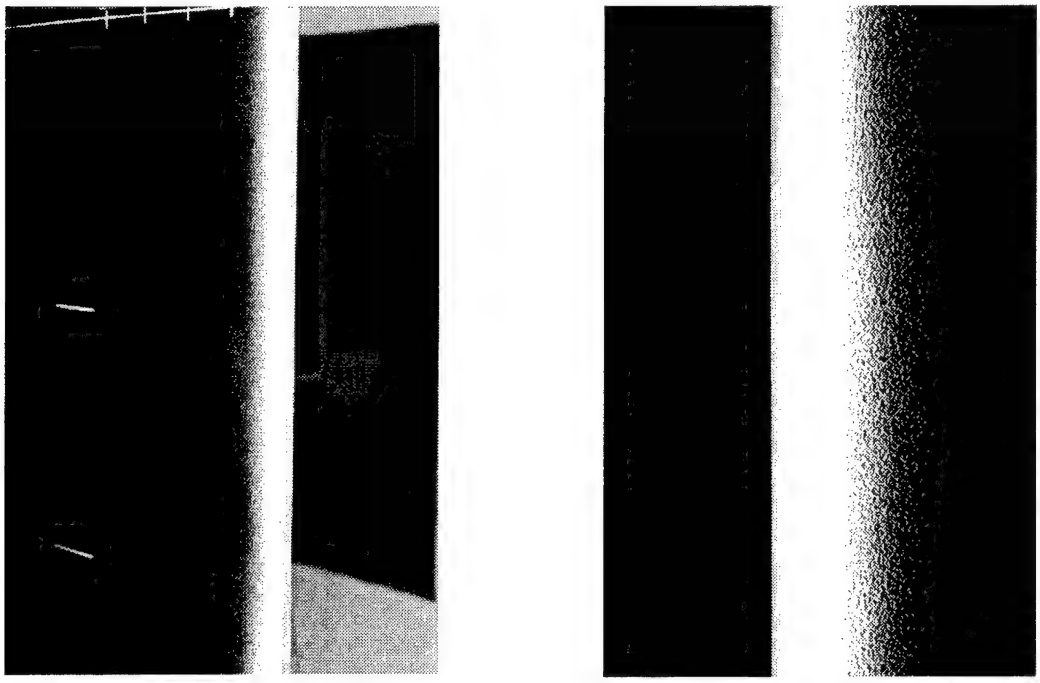

Business Jet - Run 080195.03

T_t = -14.0°C (6.8°F)
T_s = -18.0°C (-0.4°F)
V = 90 m/s (175 kts)
Attitude = 6.1°

LWC = 0.535 g/m^3
MVD = 20 μm
Spray = 6.0 min
chord = 90 cm (36 in)

$C_{d\text{-}clean}$ = 0.0093
$C_{d\text{-}iced}$ = 0.0188

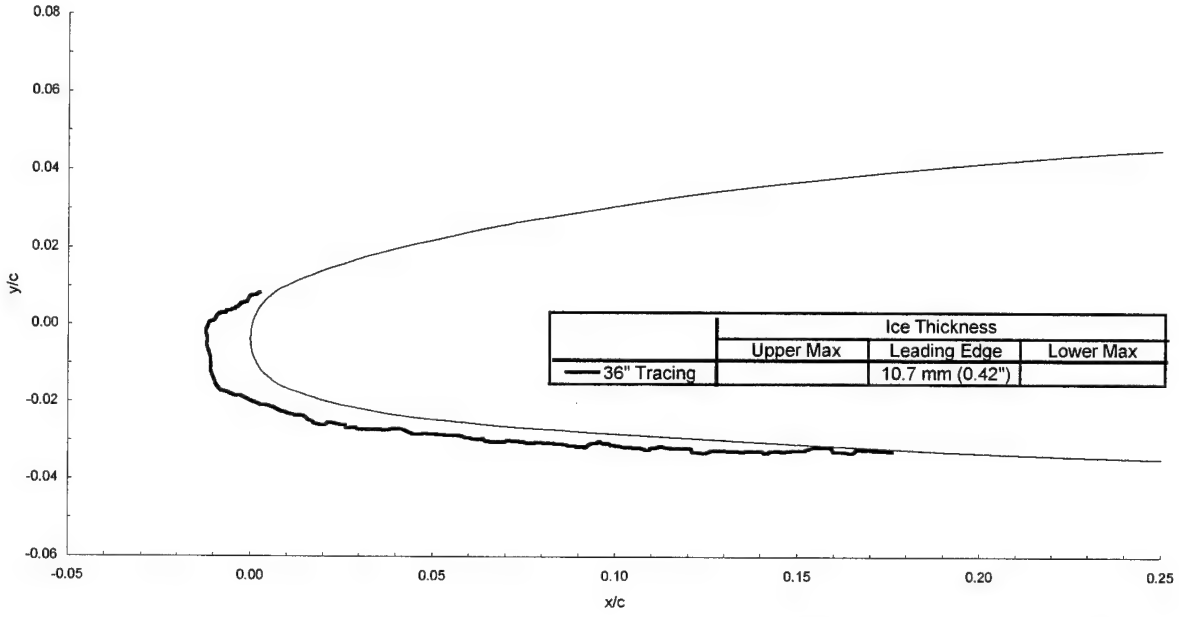

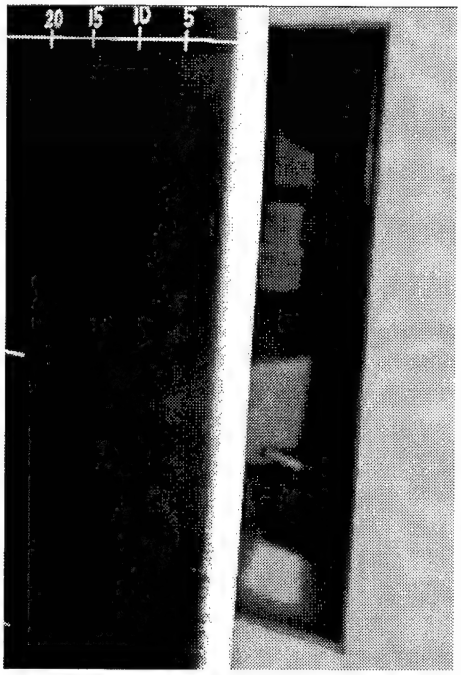

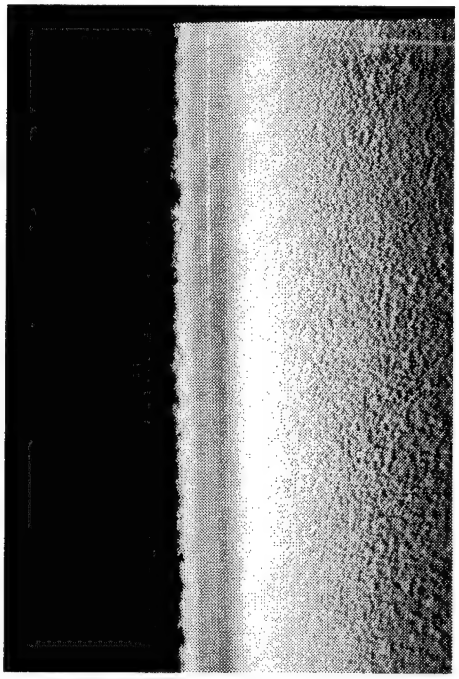

Business Jet - Run 080195.04

T_t = -14.0°C (6.8°F)
T_s = -18.0°C (-0.4°F)
V = 90 m/s (175 kts)
Attitude = 4.0°

LWC = 0.535 g/m^3
MVD = 20 μm
Spray = 6.0 min
chord = 90 cm (36 in)

$C_{d\text{-}clean}$ = 0.0087
$C_{d\text{-}iced}$ = 0.0151

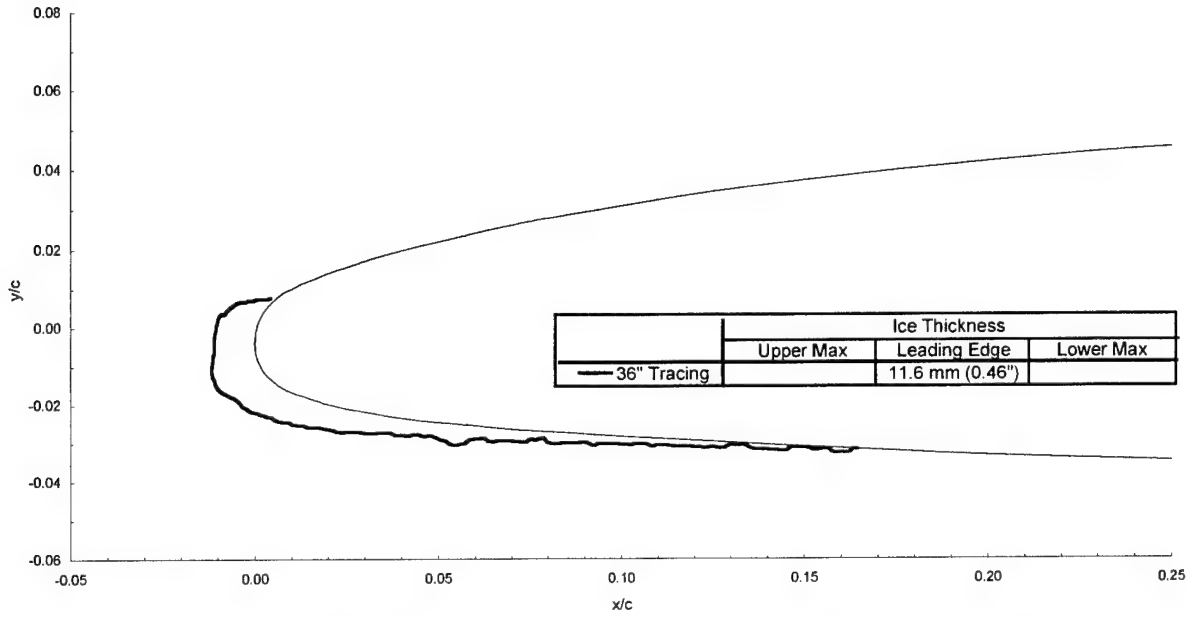

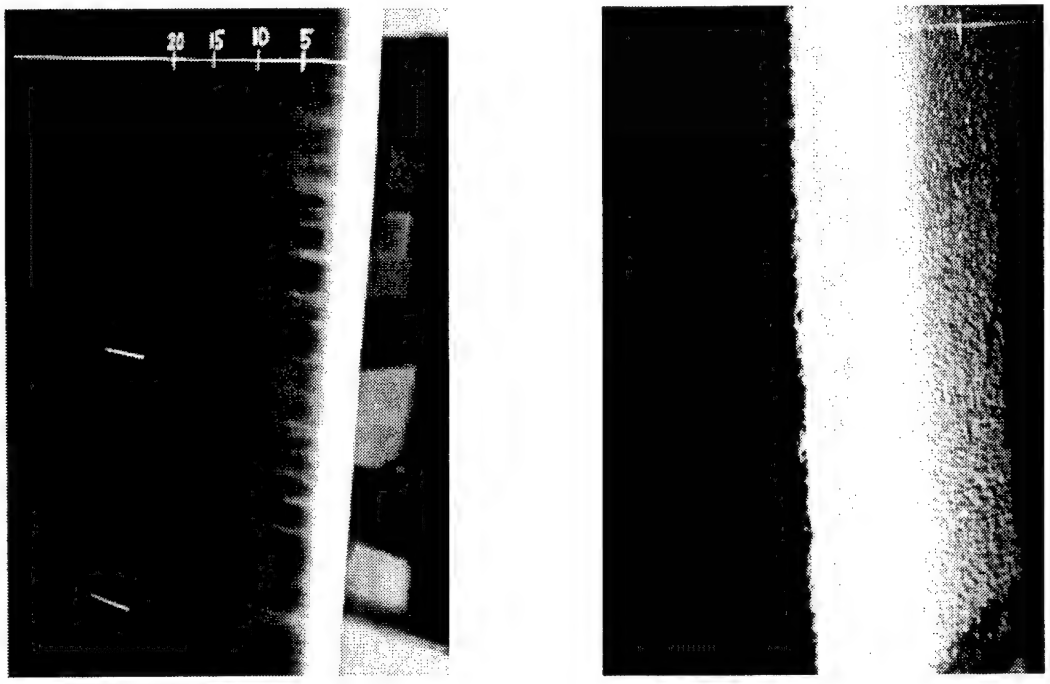

Business Jet - Run 080195.05

T_t = -14.0°C (6.8°F)
T_s = -18.0°C (-0.4°F)
V = 90 m/s (175 kts)
Attitude = 4.0°

LWC = 0.535 g/m^3
MVD = 40 μm
Spray = 6.0 min
chord = 90 cm (36 in)

$C_{d\text{-}clean}$ = 0.0087
$C_{d\text{-}iced}$ = 0.0201

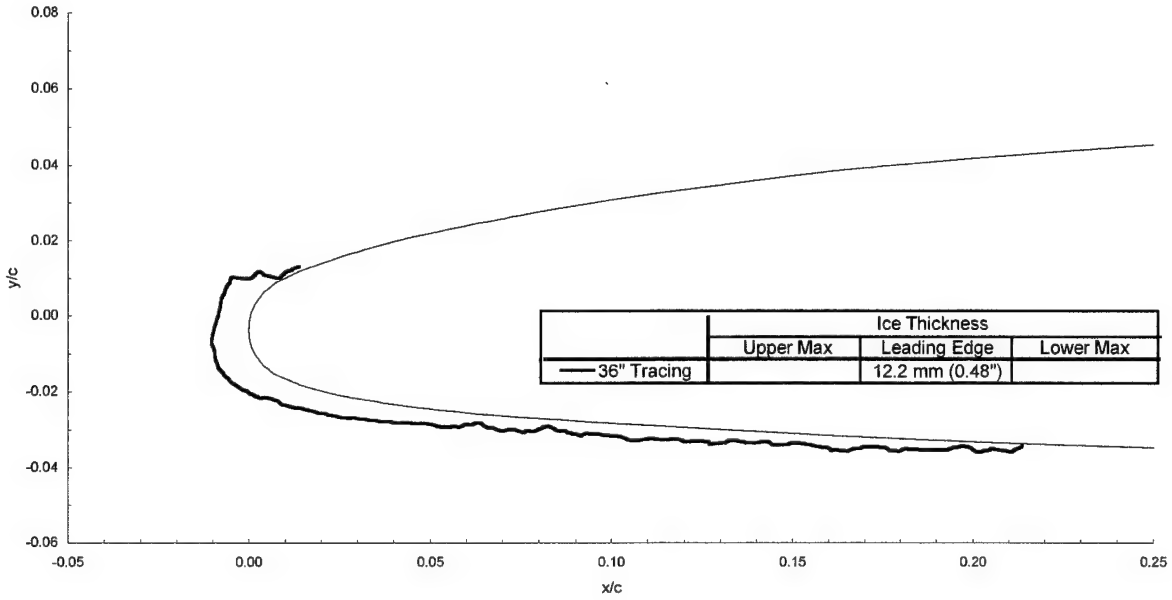

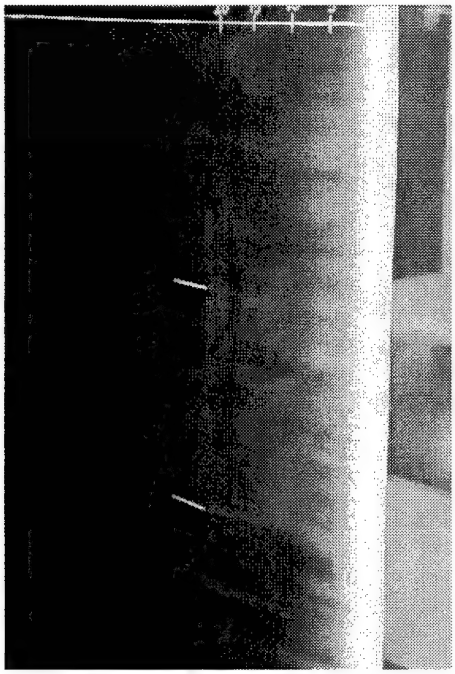

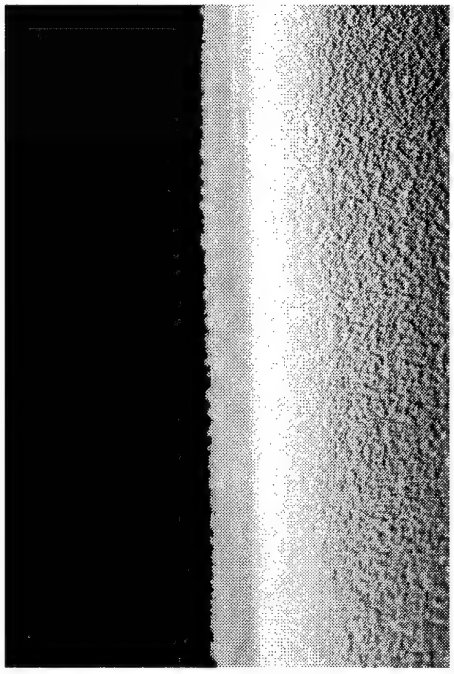

Business Jet - Run 080195.06

T_t = -14.0°C (6.8°F)
T_s = -19.9°C (-3.7°F)
V = 109 m/s (212 kts)
Attitude = 4.0°

LWC = 0.535 g/m^3
MVD = 40 μm
Spray = 6.0 min
chord = 90 cm (36 in)

$C_{d\text{-}clean}$ = 0.0087
$C_{d\text{-}iced}$ = 0.0192

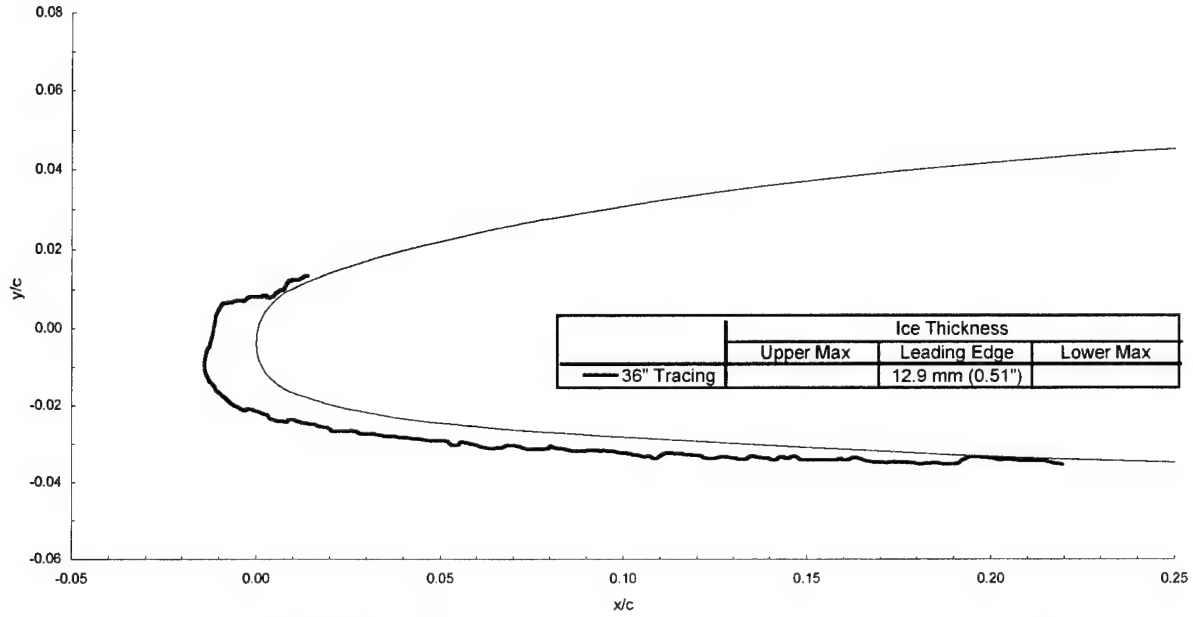

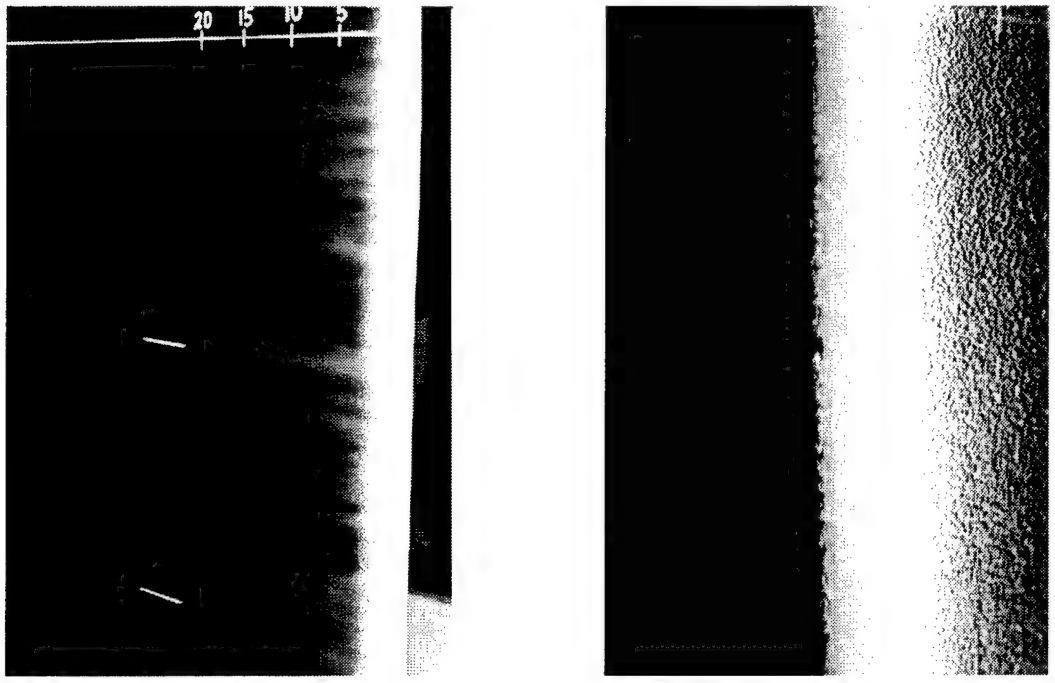

Business Jet - Run 080195.07

T_t = -14.0°C (6.8°F)
T_s = -19.9°C (-3.7°F)
V = 109 m/s (212 kts)
Attitude = 4.0°

LWC = 0.535 g/m^3
MVD = 20 μm
Spray = 6.0 min
chord = 90 cm (36 in)

$C_{d\text{-}clean}$ = 0.0087
$C_{d\text{-}iced}$ = 0.0174

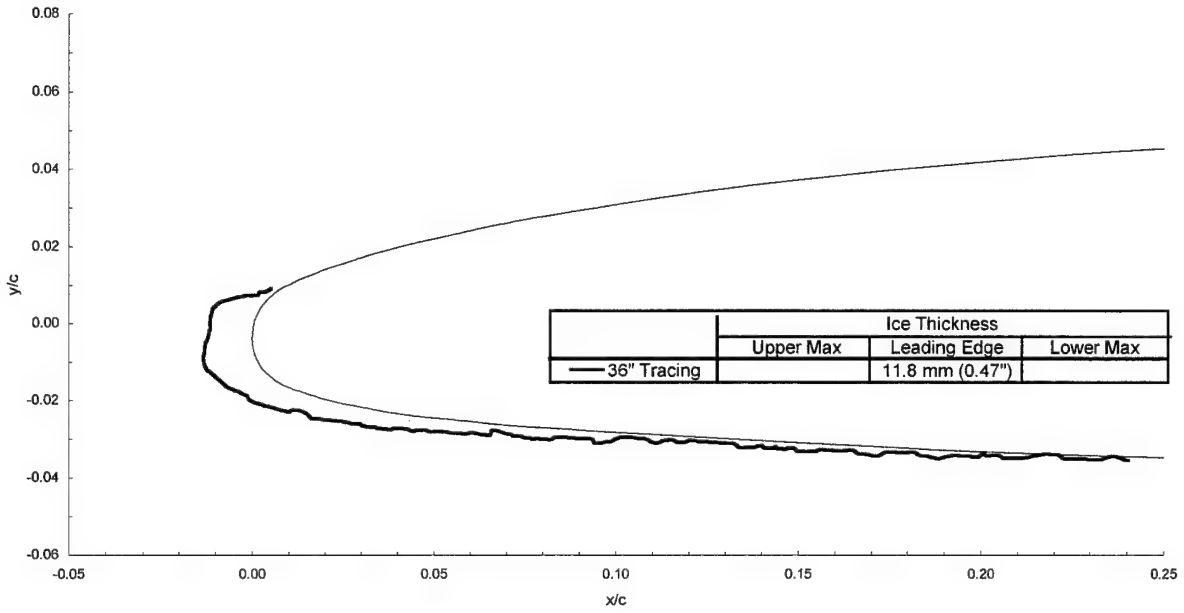

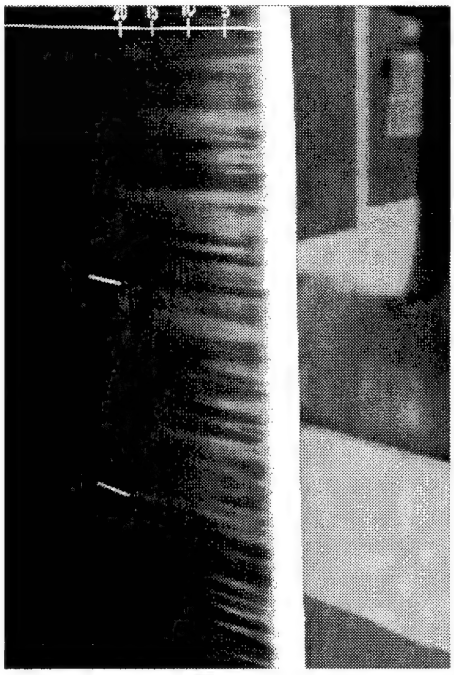

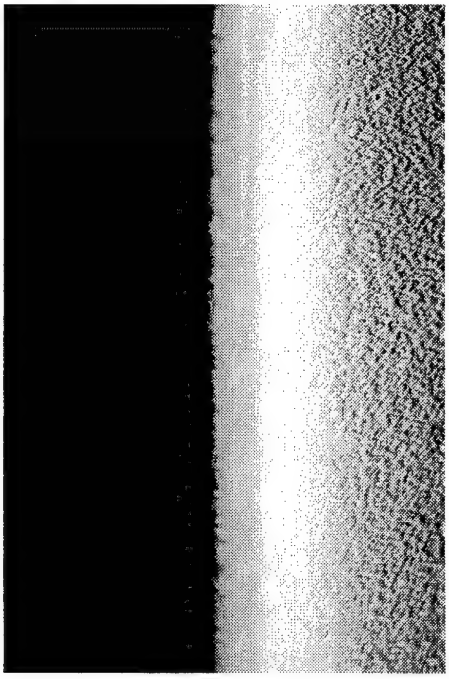

Business Jet - Run 080195.08

T_t = -14.0°C (6.8°F)
T_s = -18.0°C (-0.4°F)
V = 90 m/s (175 kts)
Attitude = 6.2°

LWC = 0.535 g/m^3
MVD = 40 μm
Spray = 6.0 min
chord = 90 cm (36 in)

$C_{d\text{-clean}}$ = 0.0093
$C_{d\text{-iced}}$ = 0.0302

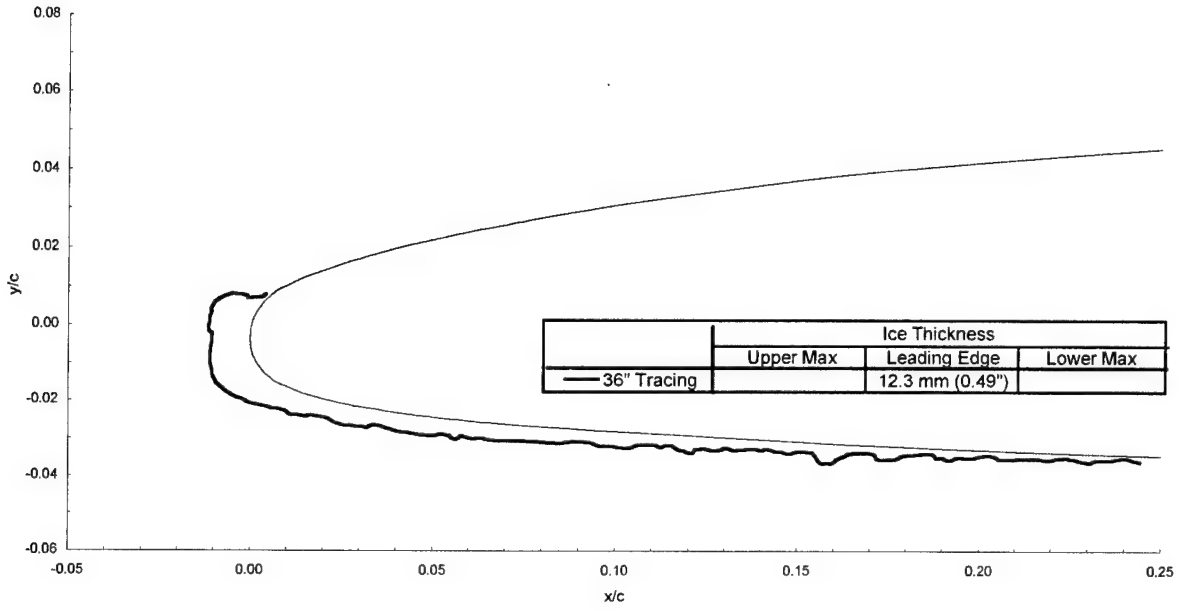

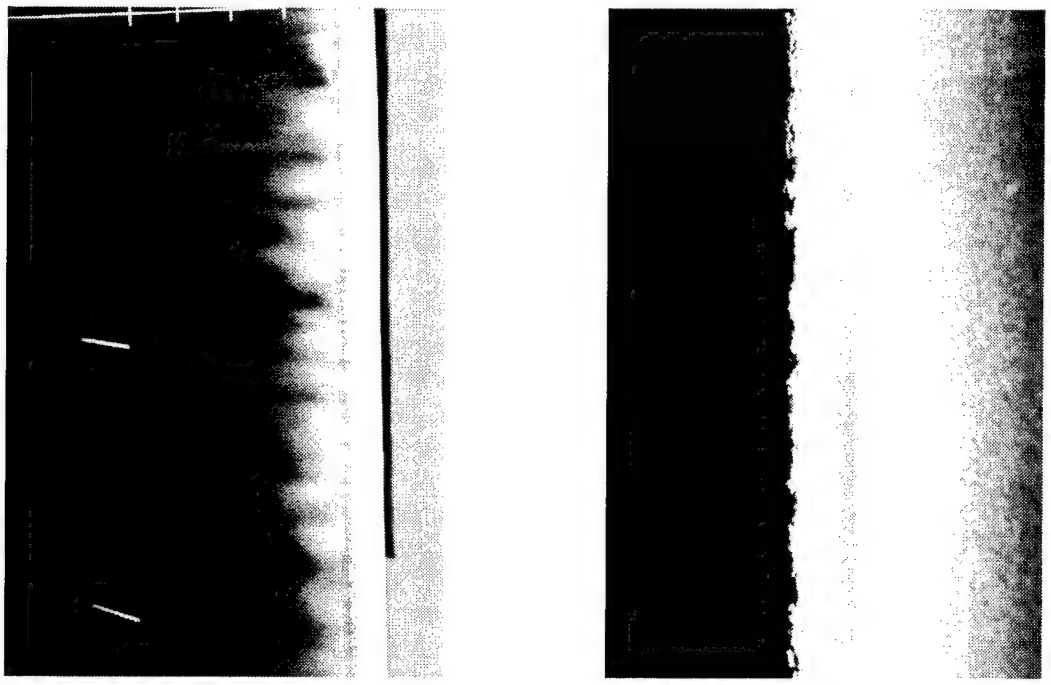

Business Jet - Run 080195.09

T_t = -14.0°C (6.8°F)
T_s = -18.0°C (-0.4°F)
V = 90 m/s (175 kts)
Attitude = 6.2°

LWC = 0.535 g/m^3
MVD = 40 μm
Spray = 4.2 min
chord = 90 cm (36 in)

$C_{d\text{-clean}}$ = 0.0093
$C_{d\text{-iced}}$ = 0.0275

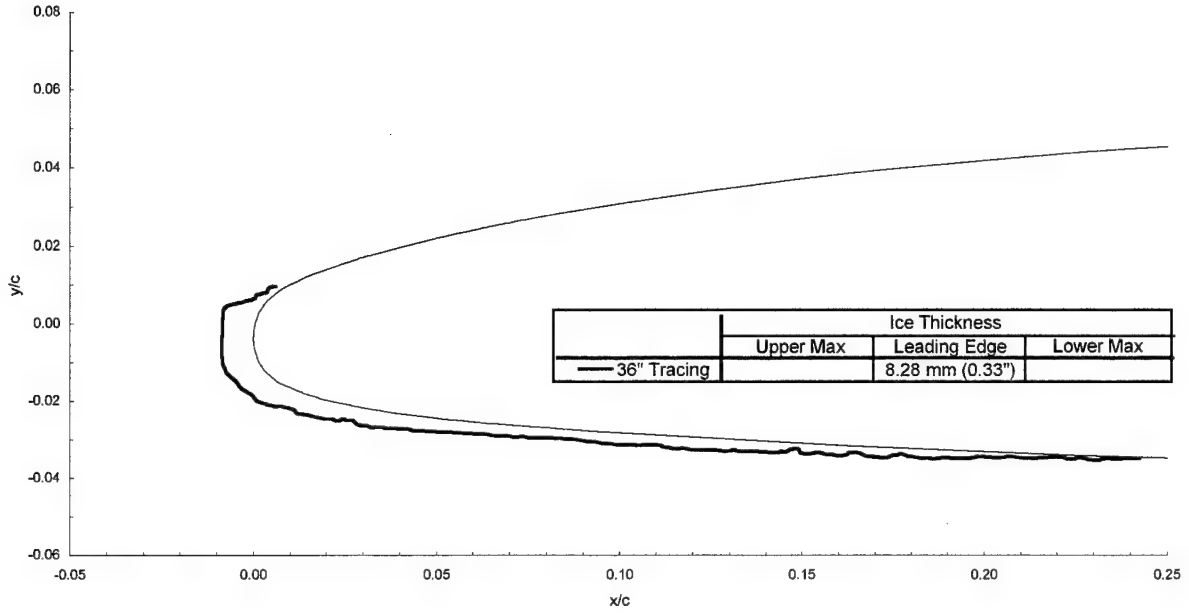

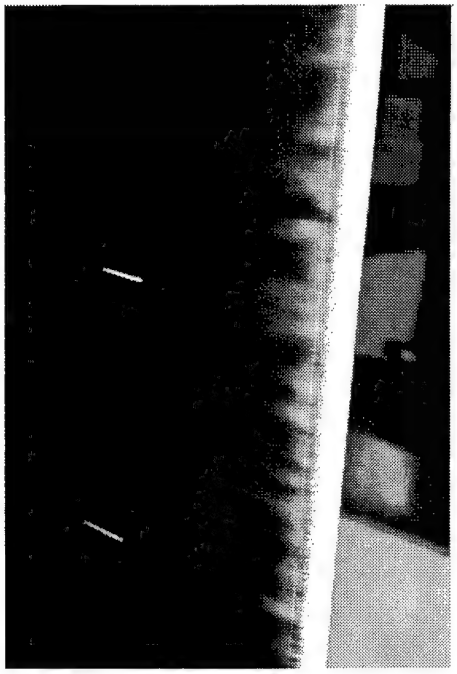

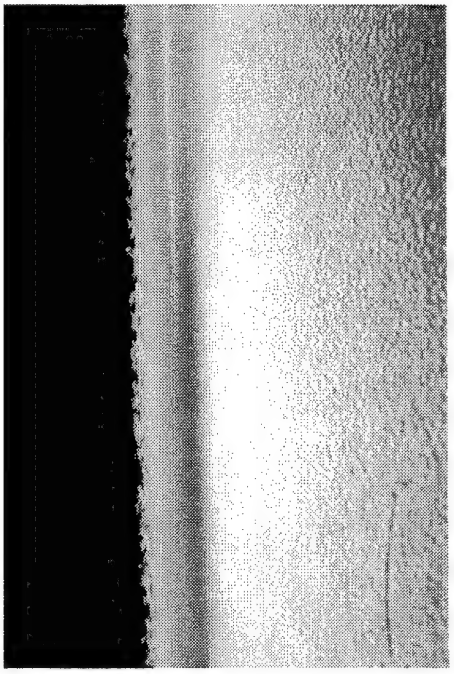

Business Jet - Run 080295.01

T_t = -0.8°C (31.0°F)
T_s = -5.0°C (23.0°F)
V = 90 m/s (175 kts)
Attitude = 6.0°

LWC = 0.54 g/m^3
MVD = 20 μm
Spray = 12.0 min
chord = 90 cm (36 in)

$C_{d\text{-clean}}$ = 0.0093
$C_{d\text{-iced}}$ = 0.0679

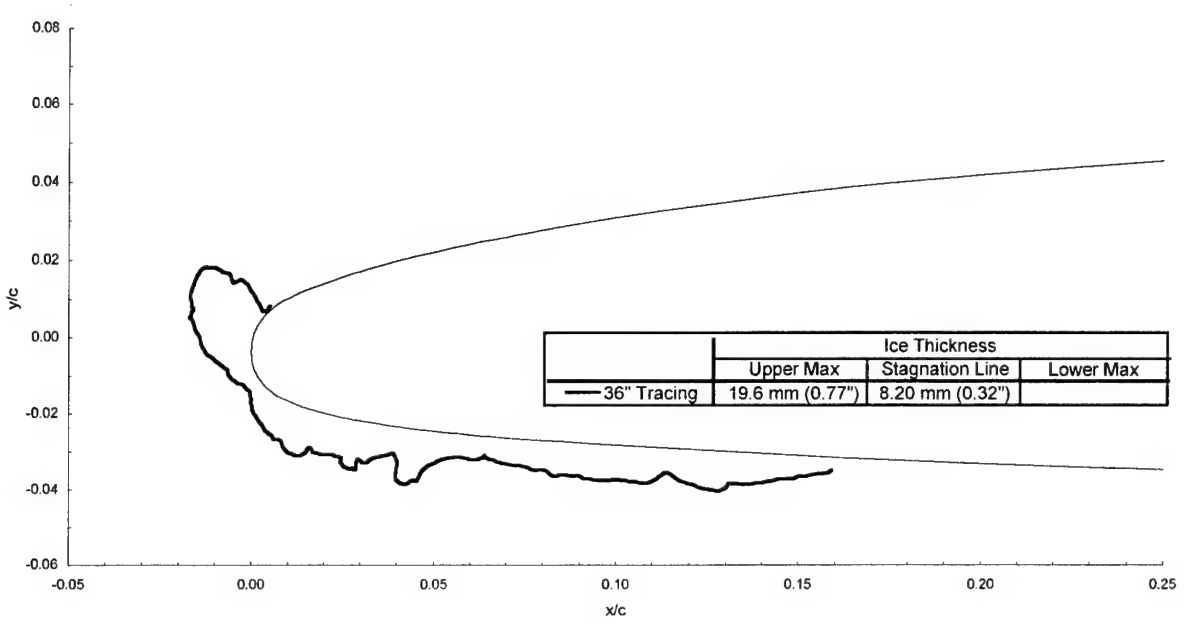

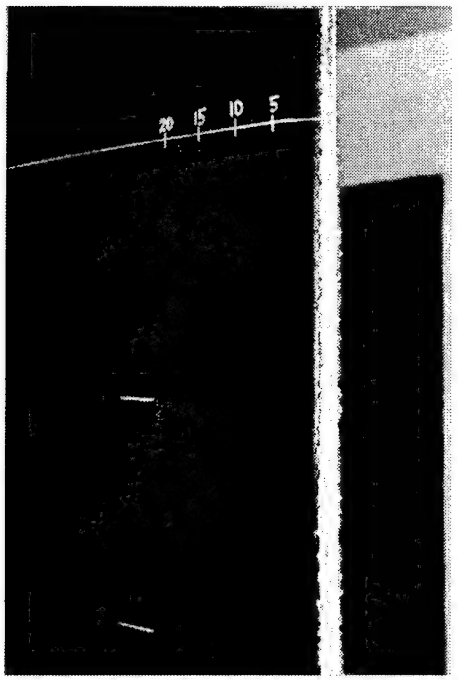

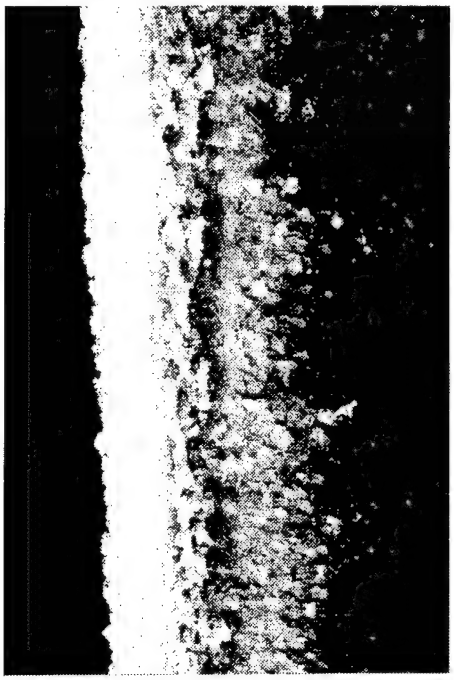

Business Jet - Run 080295.02

T_t = -0.8°C (31.0°F)
T_s = -5.0°C (23.0°F)
V = 90 m/s (175 kts)
Attitude = 4.1°

LWC = 0.54 g/m^3
MVD = 20 μm
Spray = 22.5 min
chord = 90 cm (36 in)

$C_{d\text{-clean}}$ = 0.0087
$C_{d\text{-iced}}$ = 0.0014

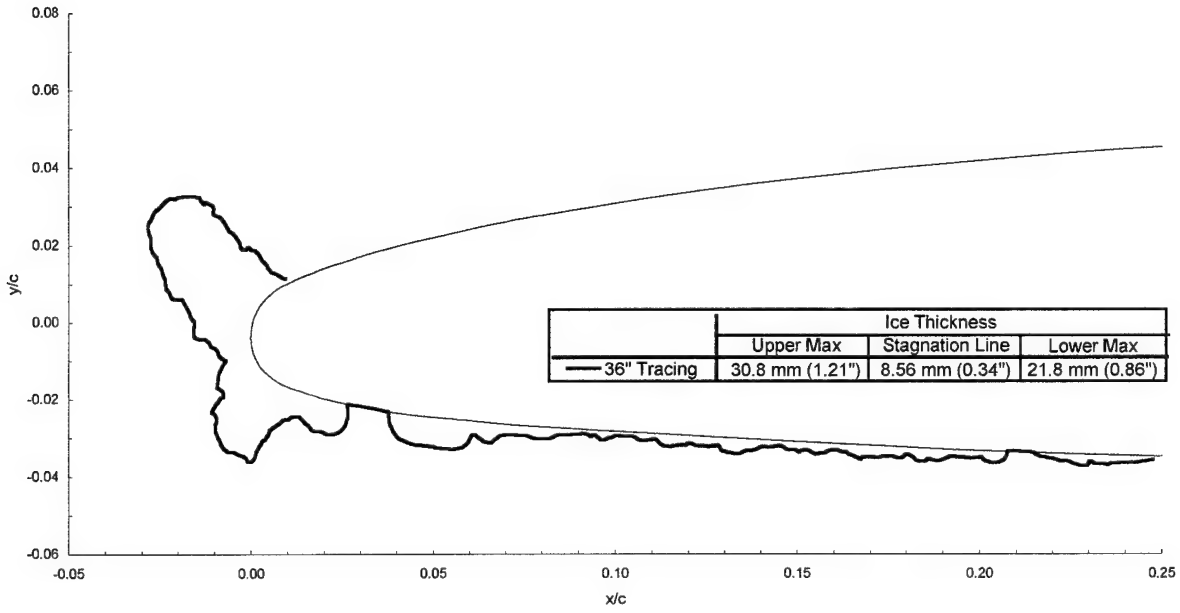

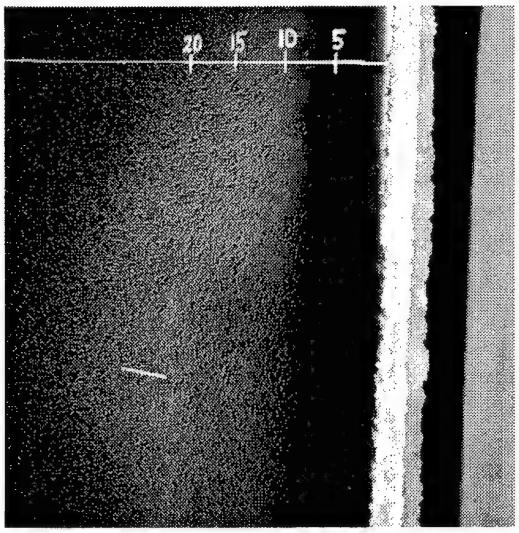

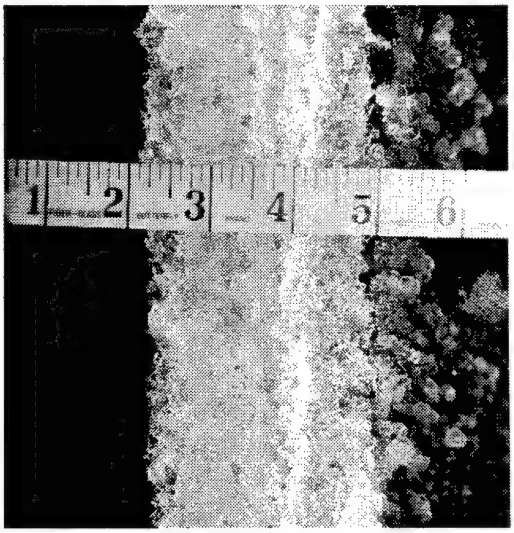

Business Jet - Run 080295.04

T_t = -0.8°C (31.0°F)
T_s = -5.0°C (23.0°F)
V = 90 m/s (175 kts)
Attitude = 4.1°

LWC = 0.54 g/m^3
MVD = 20 μm
Spray = 6.0 min
chord = 90 cm (36 in)

$C_{d\text{-}clean}$ = 0.0087
$C_{d\text{-}iced}$ = 0.0217

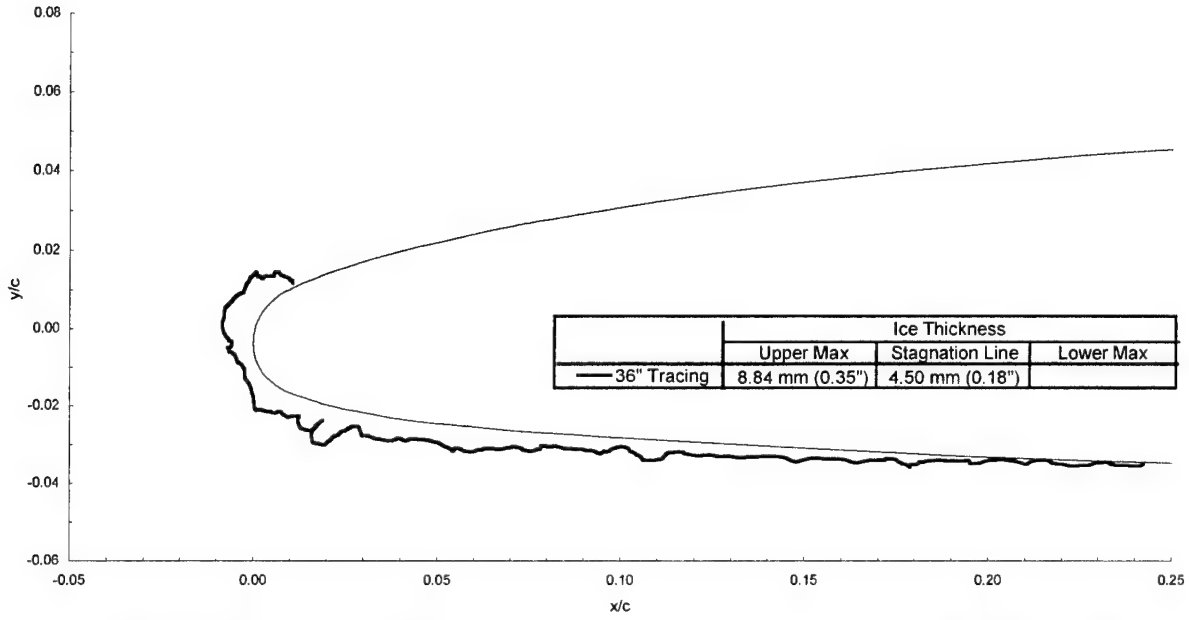

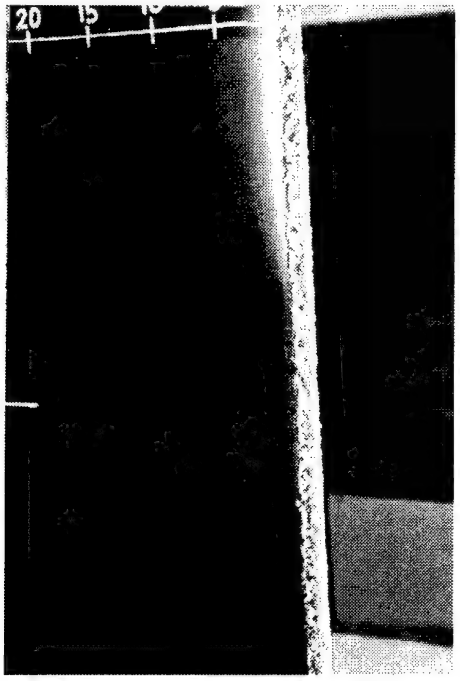

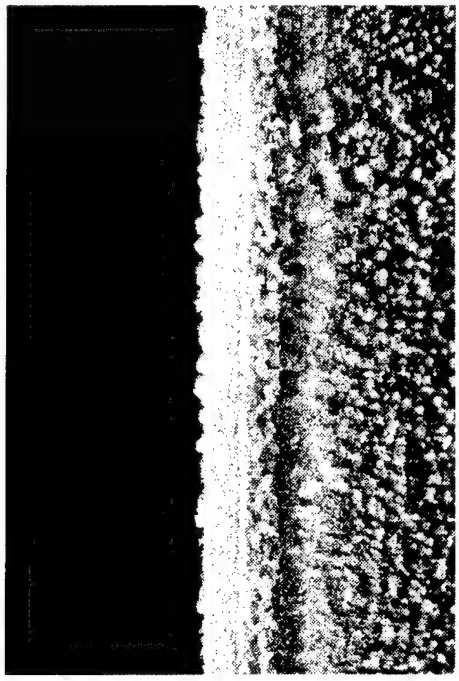

Business Jet - Run 080295.05

T_t = -3.9°C (24.9°F)
T_s = -10.0°C (14.0°F)
V = 109 m/s (212 kts)
Attitude = 4.1°

LWC = 0.43 g/m^3
MVD = 20 μm
Spray = 22.5 min
chord = 90 cm (36 in)

$C_{d\text{-}clean}$ = 0.0087
$C_{d\text{-}iced}$ = 0.0352

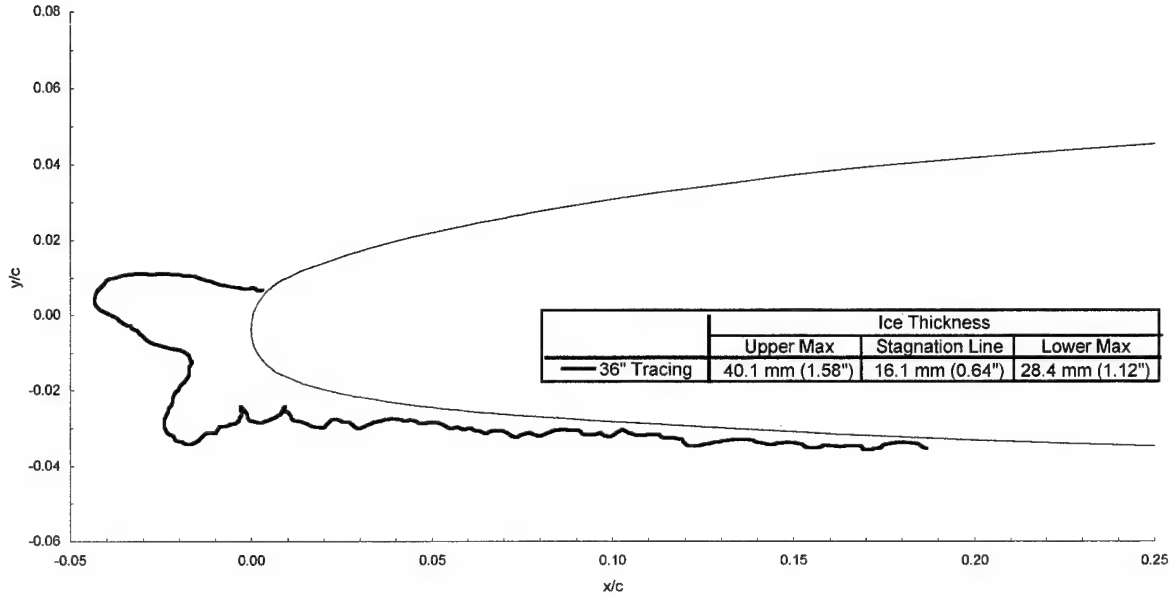

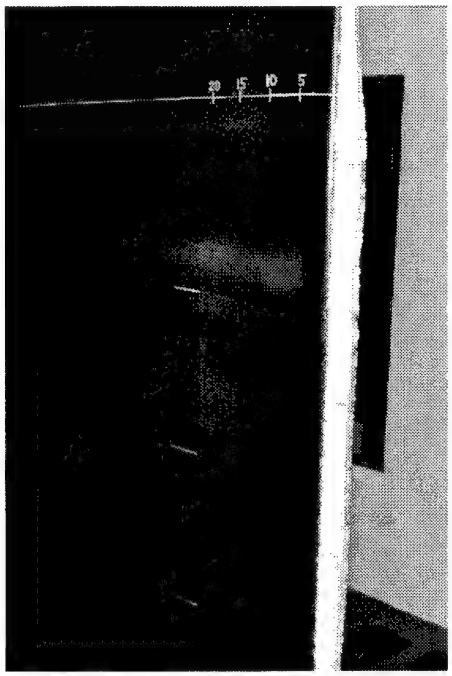

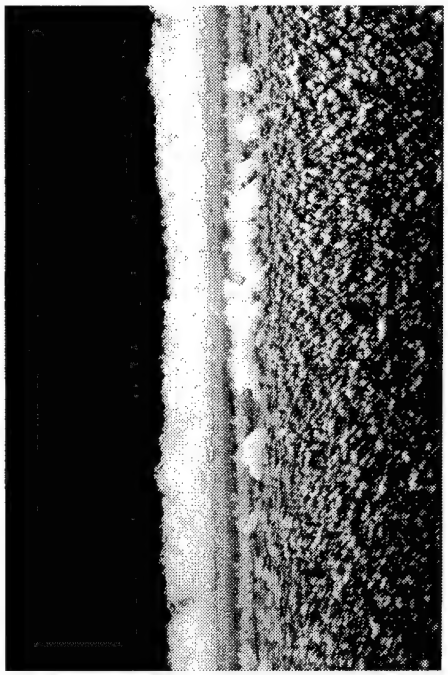

Business Jet - Run 080295.06

T_t = -0.8°C (31.0°F)
T_s = -5.0°C (23.0°F)
V = 90 m/s (175 kts)
Attitude = 4.1°

LWC = 0.54 g/m^3
MVD = 20 μm
Spray = 22.5 min
chord = 90 cm (36 in)

$C_{d\text{-clean}}$ = 0.0087
$C_{d\text{-iced}}$ = 0.0679

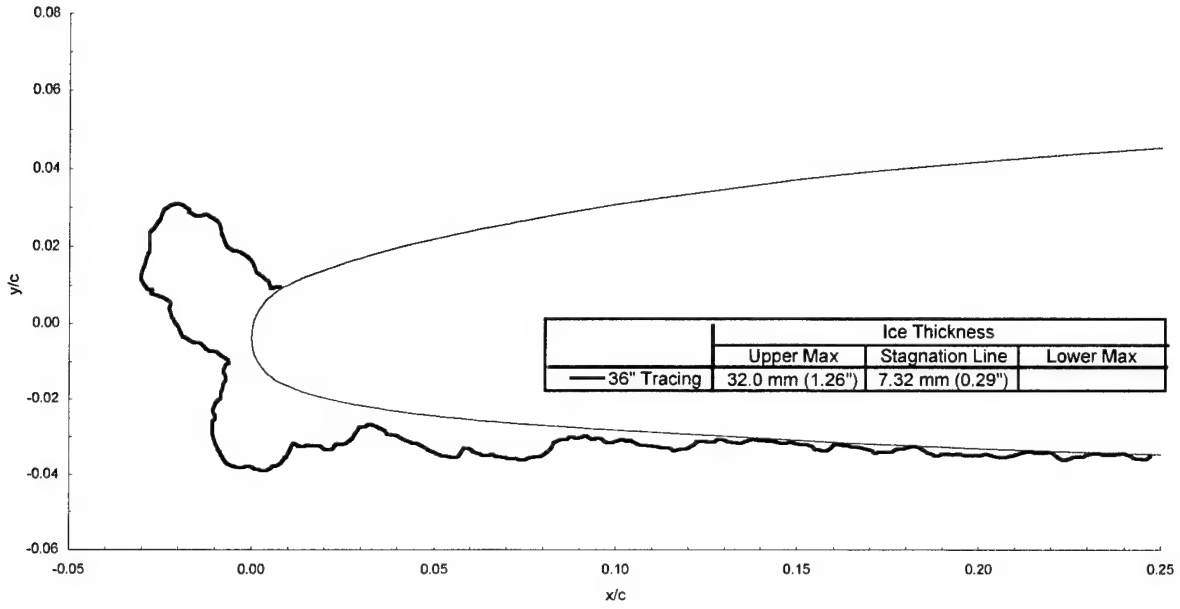

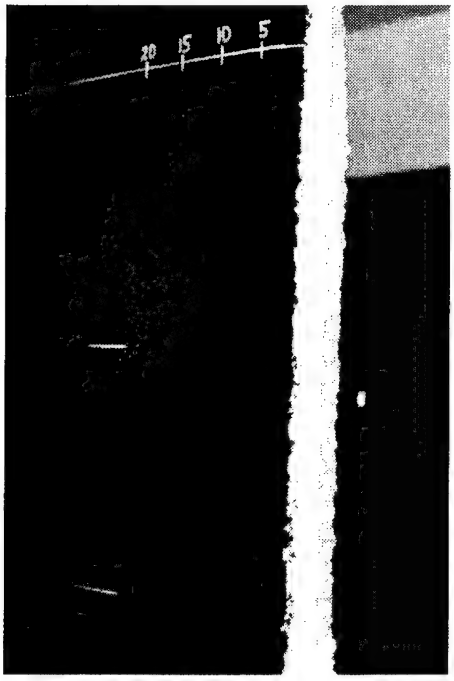

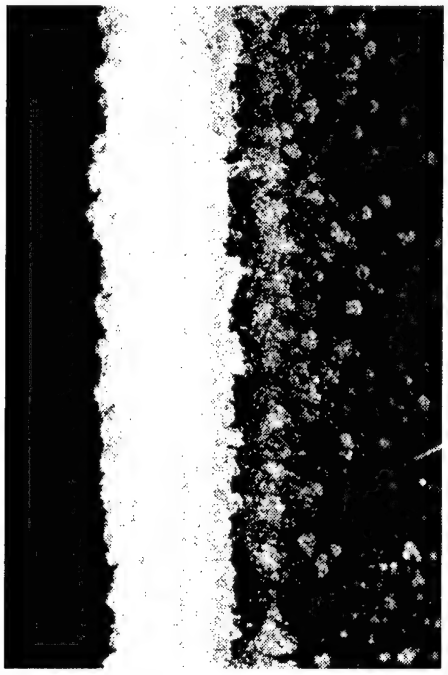

Business Jet - Run 080395.01

T_t = -0.7°C (30.8°F)
T_s = -8.7°C (16.3°F)
V = 129 m/s (250 kts)
Attitude = 1.5°

LWC = 0.75 g/m^3
MVD = 15 μm
Spray = 10.0 min
chord = 90 cm (36 in)

$C_{d\text{-clean}}$ = 0.0082
$C_{d\text{-iced}}$ = 0.0380

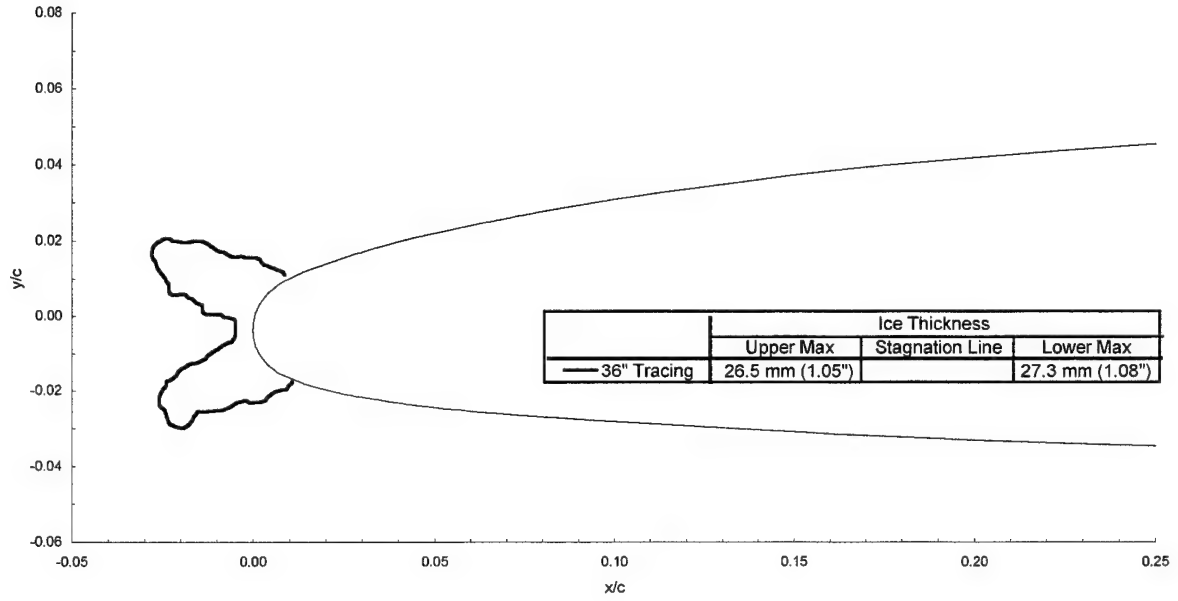

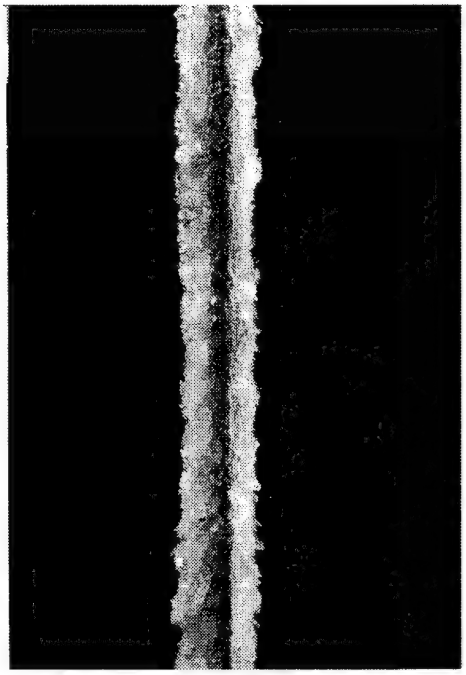

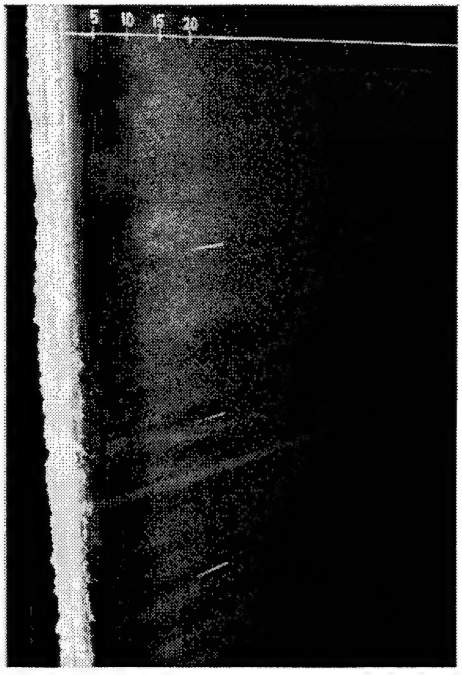

Business Jet - Run 080395.02

T_t = -0.7°C (30.8°F)
T_s = -8.7°C (16.3°F)
V = 129 m/s (250 kts)
Attitude = 1.5°

LWC = 1.25 g/m^3
MVD = 20 μm
Spray = 5.4 min
chord = 90 cm (36 in)

$C_{d\text{-clean}}$ = 0.0082
$C_{d\text{-iced}}$ = 0.0247

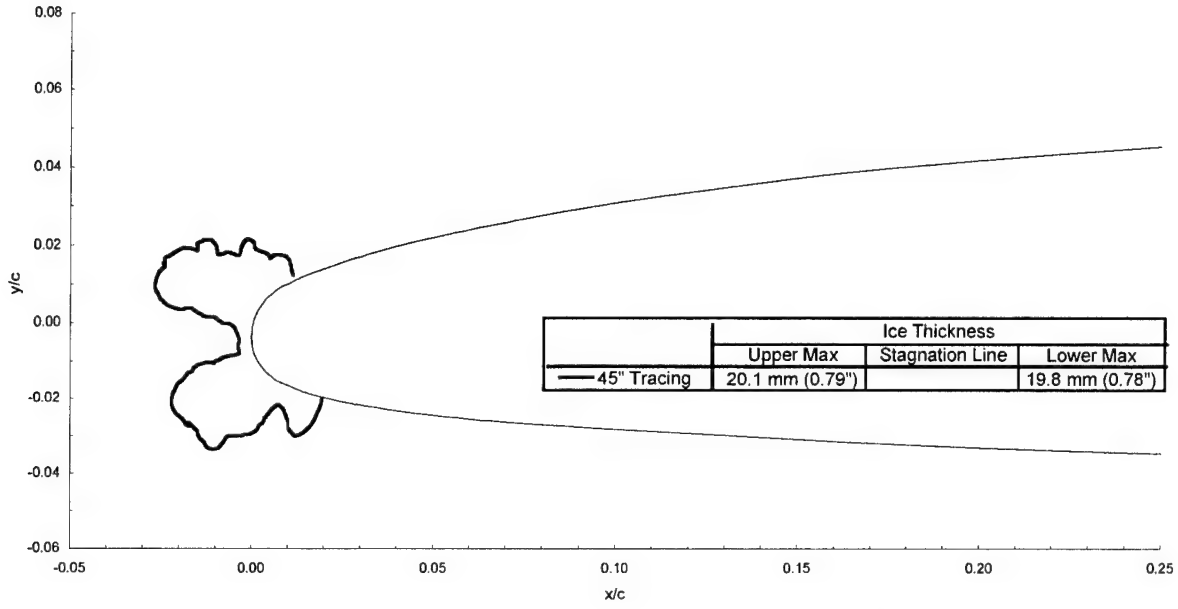

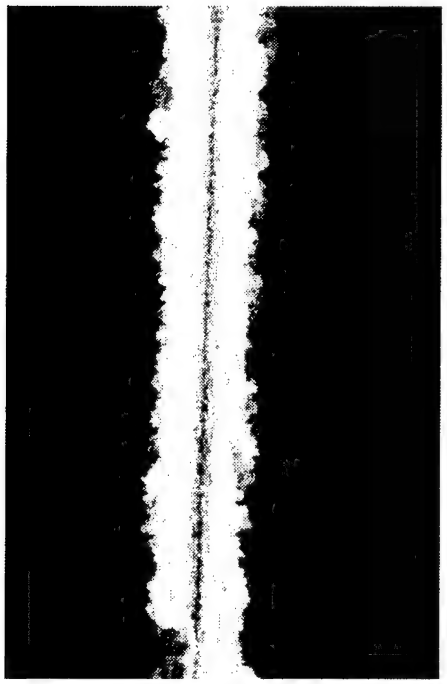

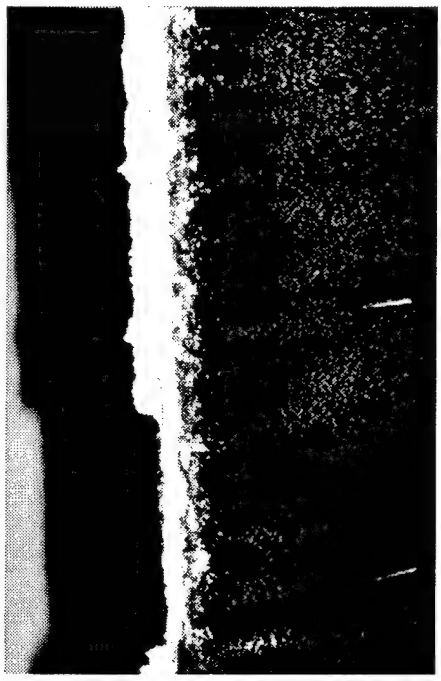

Business Jet - Run 080395.03

T_t = -2.0°C (28.4°F)
T_s = -6.2°C (20.9°F)
V = 90 m/s (175 kts)
AOA = 6.1°

LWC = 1.00 g/m^3
MVD = 15 μm
Spray = 15.0 min
chord = 90 cm (36 in)

$C_{d\text{-clean}}$ = 0.0093
$C_{d\text{-iced}}$ = 0.0775

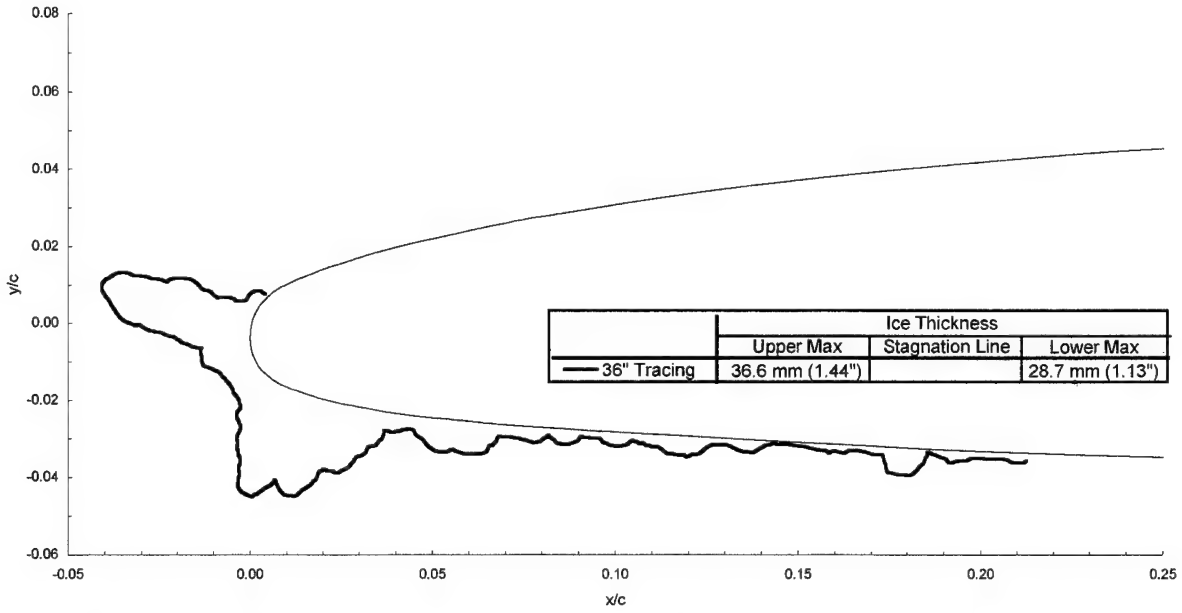

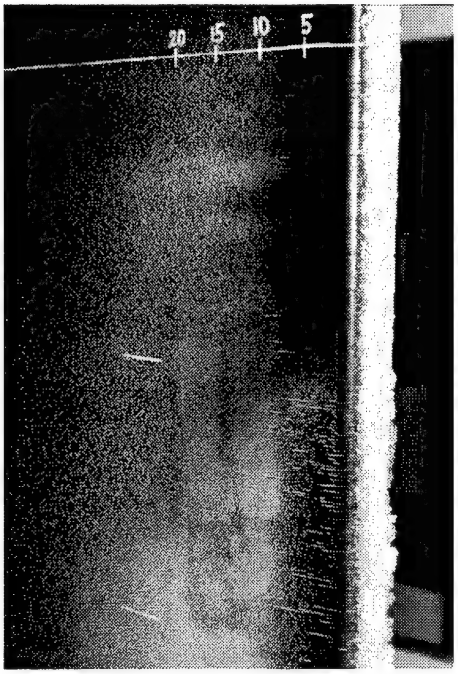

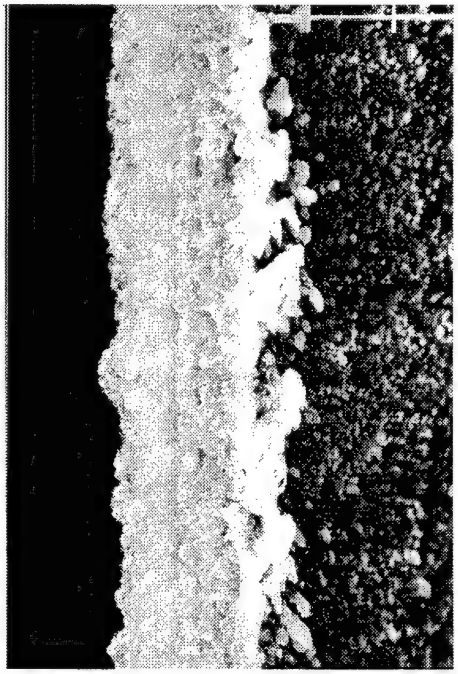

Business Jet - Run 080395.04

T_t = -4.4°C (24.2°F)
T_s = -8.5°C (16.7°F)
V = 90 m/s (175 kts)
Attitude = 6.1°

LWC = 1.60 g/m^3
MVD = 20 μm
Spray = 8.4 min
chord = 90 cm (36 in)

$C_{d\text{-}clean}$ = 0.0093
$C_{d\text{-}iced}$ = 0.1027

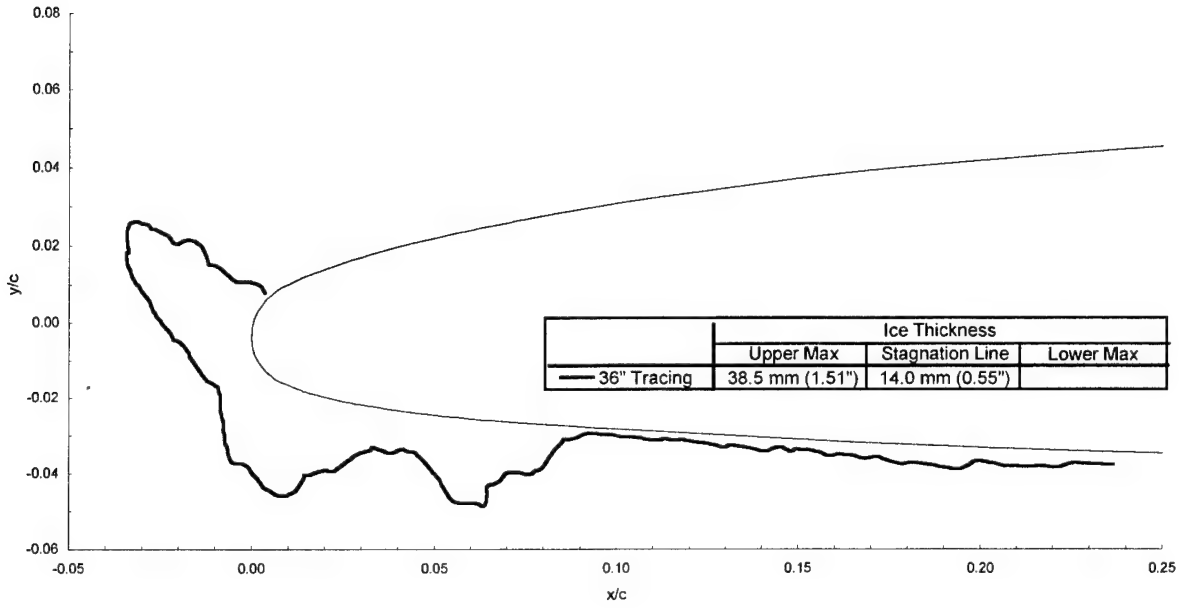

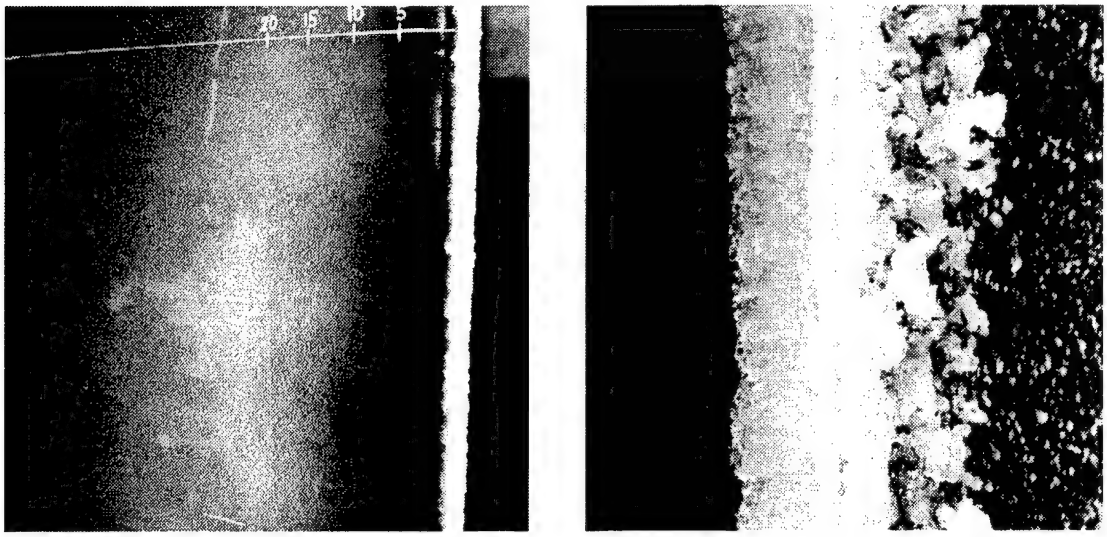

Business Jet - Run 080395.05

T_t = -7.4°C (18.8°F)
T_s = -15.2°C (4.7°F)
V = 129 m/s (250 kts)
Attitude = 1.6°

LWC = 0.75 g/m^3
MVD = 15 μm
Spray = 10.0 min
chord = 90 cm (36 in)

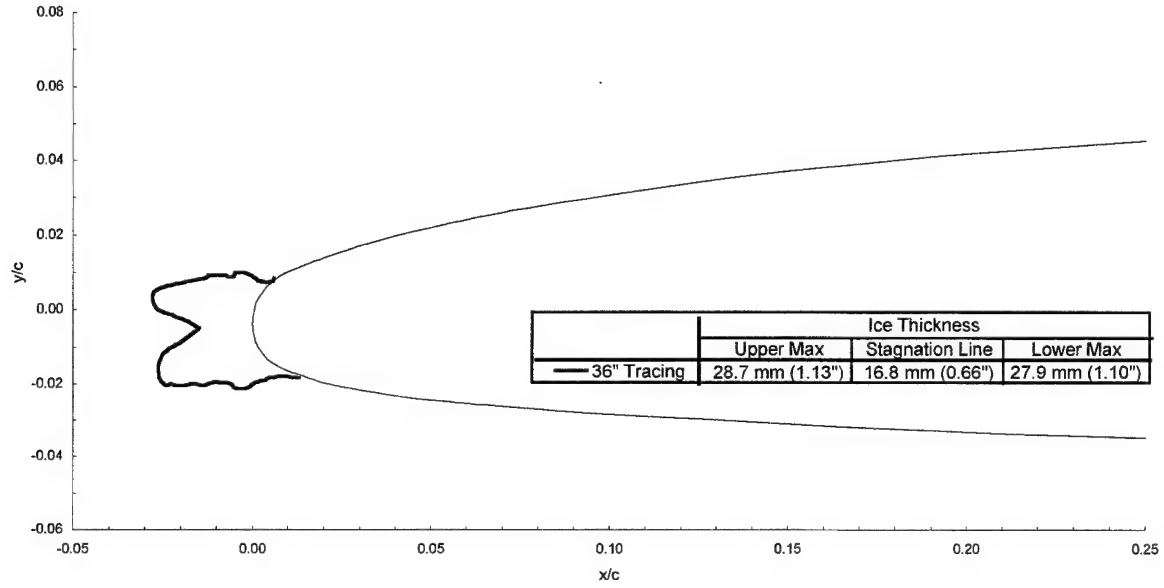

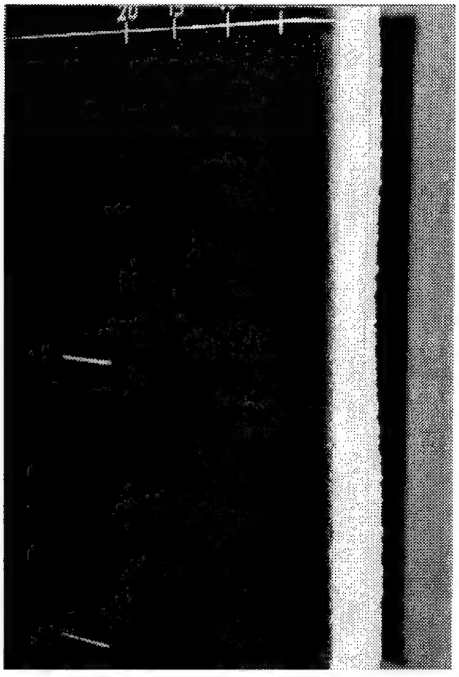

Business Jet - Run 080395.06

T_t = -7.4°C (18.8°F)
T_s = -15.2°C (4.7°F)
V = 129 m/s (250 kts)
Attitude = 1.6°

LWC = 1.25 g/m^3
MVD = 20 μm
Spray = 5.4 min
chord = 90 cm (36 in)

$C_{d\text{-clean}}$ = 0.0082
$C_{d\text{-iced}}$ = 0.0577

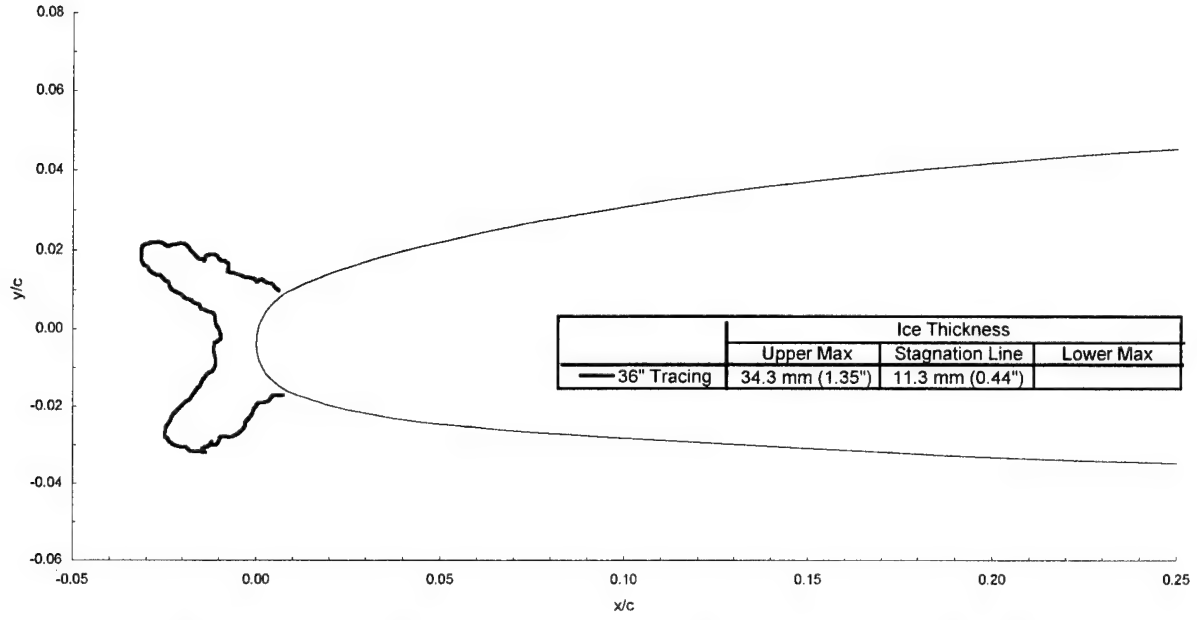

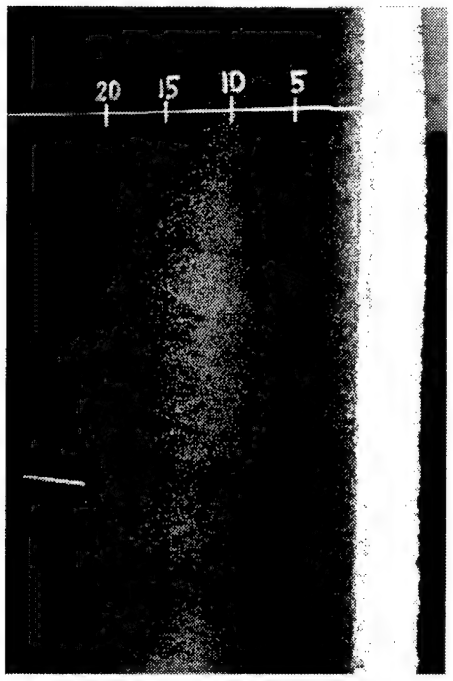

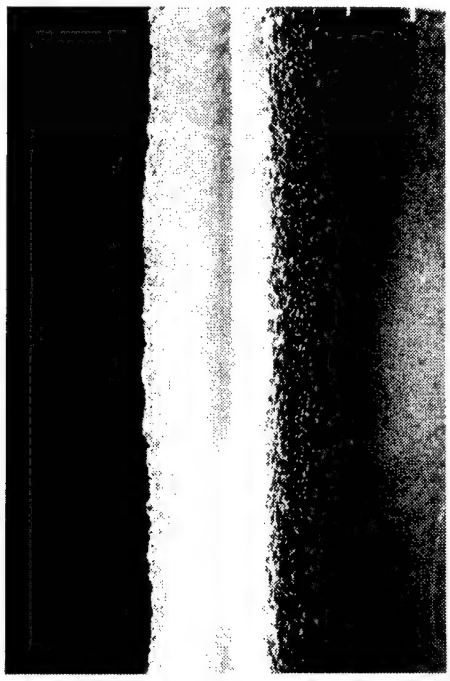

Business Jet - Run 080395.07

T_t = -11.0°C (12.3°F)
T_s = -15.0°C (5.0°F)
V = 90 m/s (175 kts)
Attitude = 6.1°

LWC = 1.60 g/m^3
MVD = 20 μm
Spray = 8.4 min
chord = 90 cm (36 in)

$C_{d\text{-}clean}$ = 0.0093
$C_{d\text{-}iced}$ = 0.0433

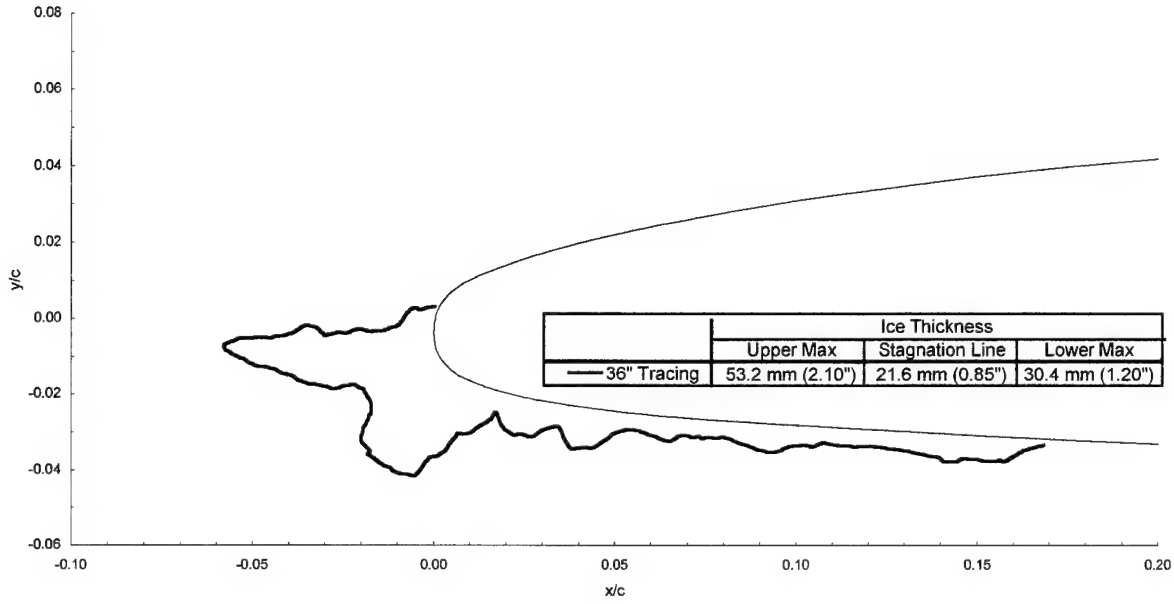

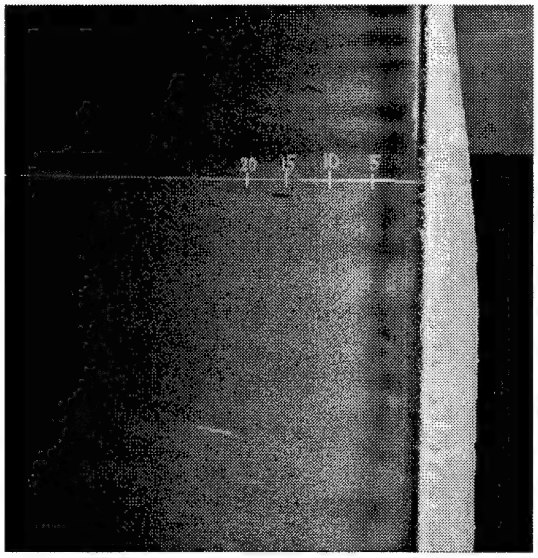

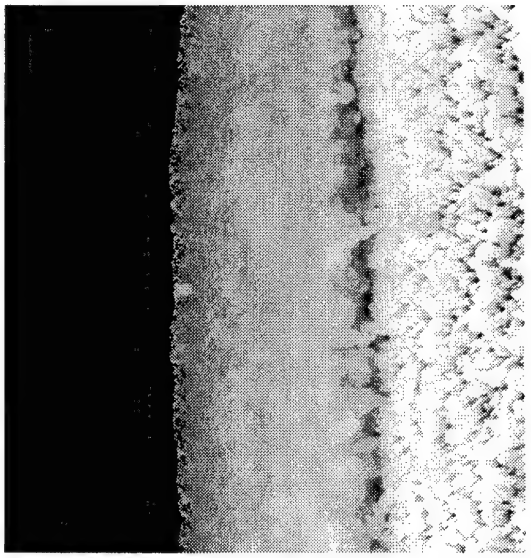

Business Jet - Run 080495.01

T_t = -27.8°C (-18.0°F)
T_s = -31.6°C (-24.9°F)
V = 90 m/s (175 kts)
Attitude = 6.1°

LWC = 0.83 g/m^3
MVD = 160 μm
Spray = 6.0 min
chord = 90 cm (36 in)

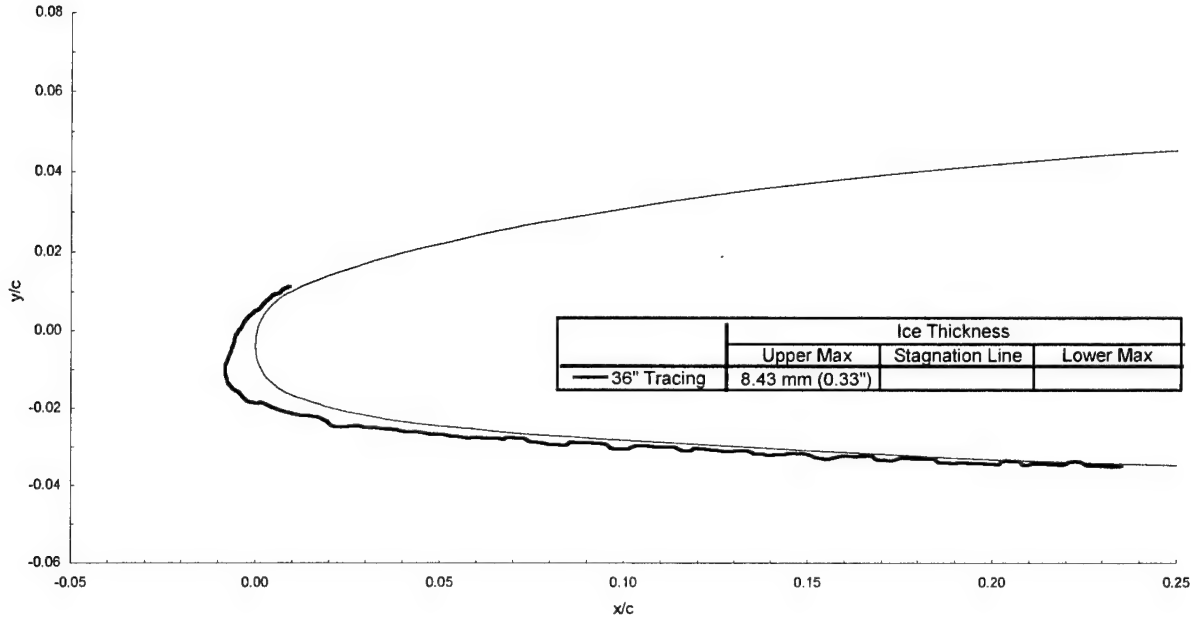

Business Jet - Run 080495.02

T_t = -27.8°C (-18.0°F)
T_s = -31.6°C (-24.9°F)
V = 90 m/s (175 kts)
Attitude = 4.1°

LWC = 0.83 g/m^3
MVD = 160 μm
Spray = 6.0 min
chord = 90 cm (36 in)

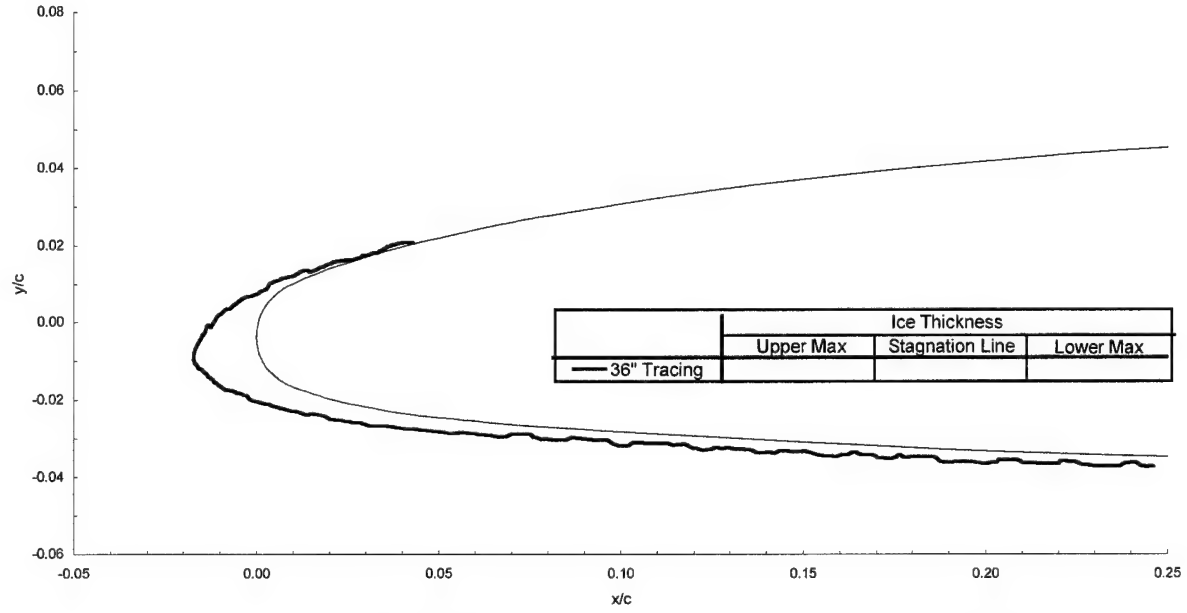

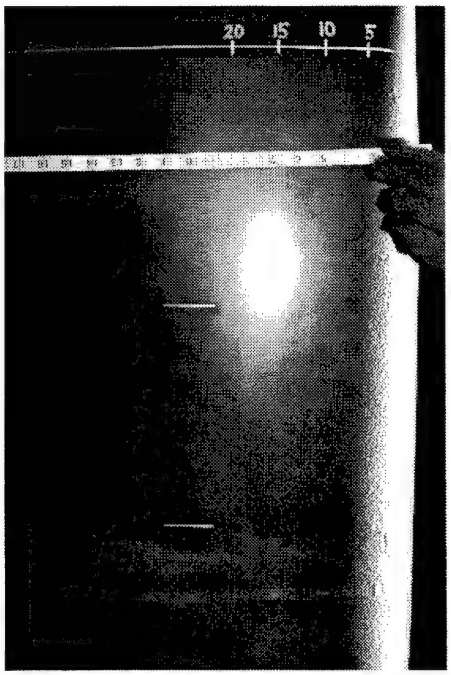

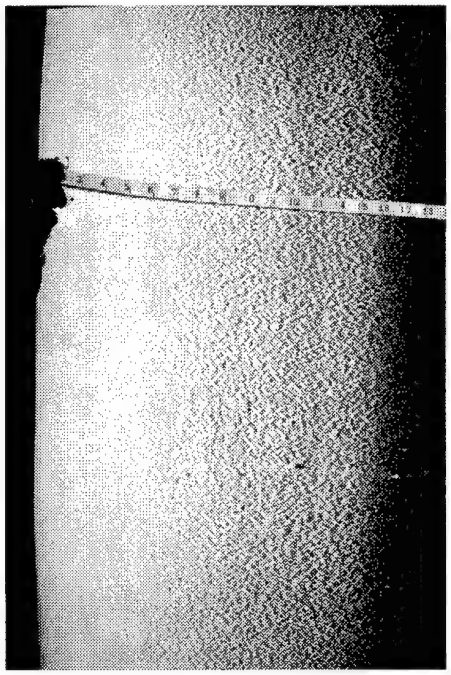

Business Jet - Run 080495.04

T_t = -11.0°C (12.2°F)
T_s = -15.0°C (5.0°F)
V = 90 m/s (175 kts)
Attitude = 4.1°

LWC = 0.83 g/m^3
MVD = 160 μm
Spray = 20.0 min
chord = 90 cm (36 in)

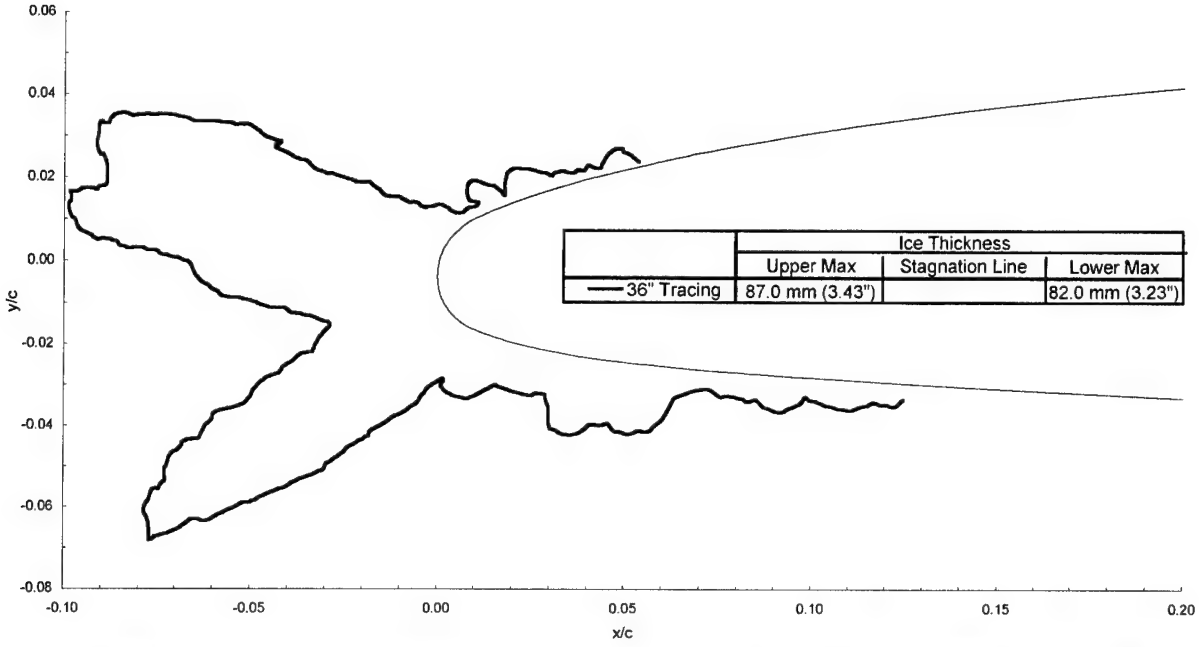

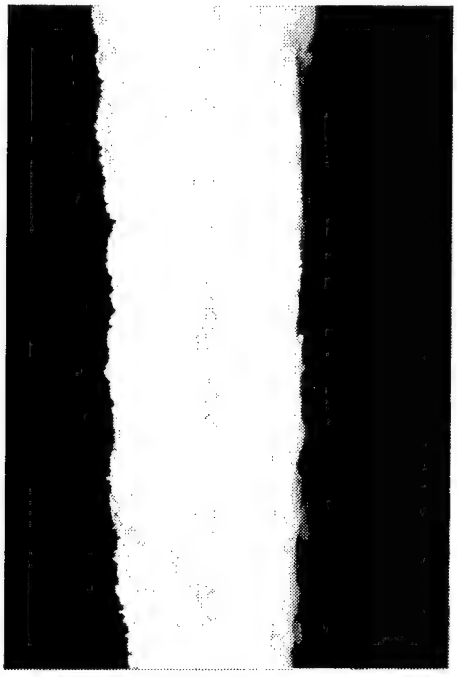

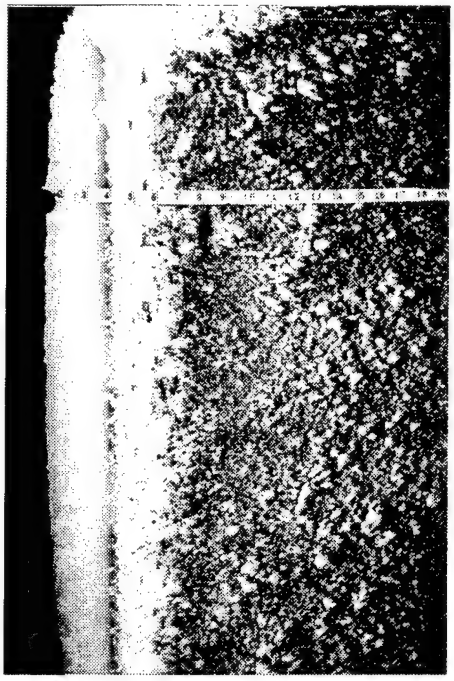

Business Jet - Run 080495.05

T_t = -0.8°C (30.6°F)
T_s = -5.0°C (23.0°F)
V = 90 m/s (175 kts)
Attitude = 6.2°

LWC = 0.83 g/m^3
MVD = 160 μm
Spray = 20.0 min
chord = 90 cm (36 in)

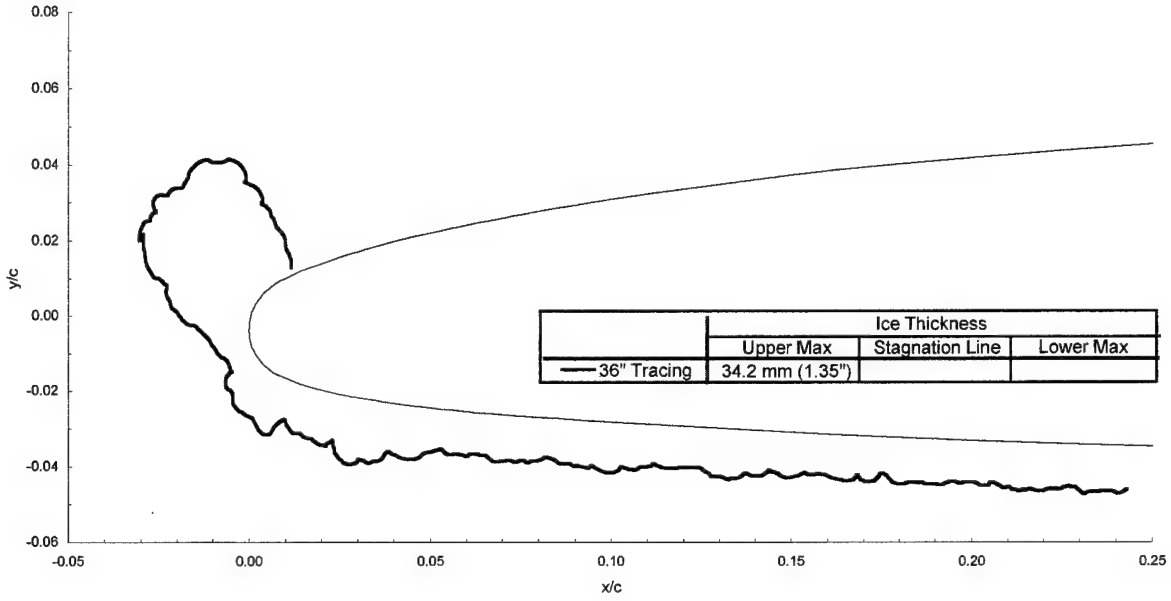

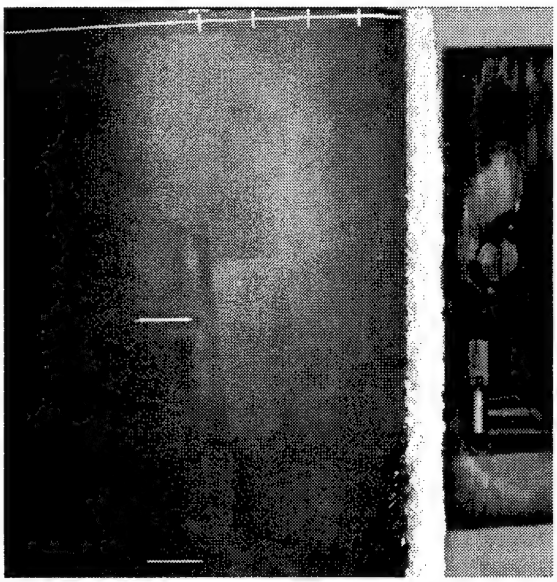

Business Jet - Run 080495.06

T_t = -0.8°C (30.6°F)
T_s = -5.0°C (23.0°F)
V = 90 m/s (175 kts)
Attitude = 6.2°

LWC = 0.54 g/m^3
MVD = 20 μm
Spray = 22.5 min
chord = 90 cm (36 in)

$C_{d\text{-}clean}$ = 0.0093
$C_{d\text{-}iced}$ = 0.1201

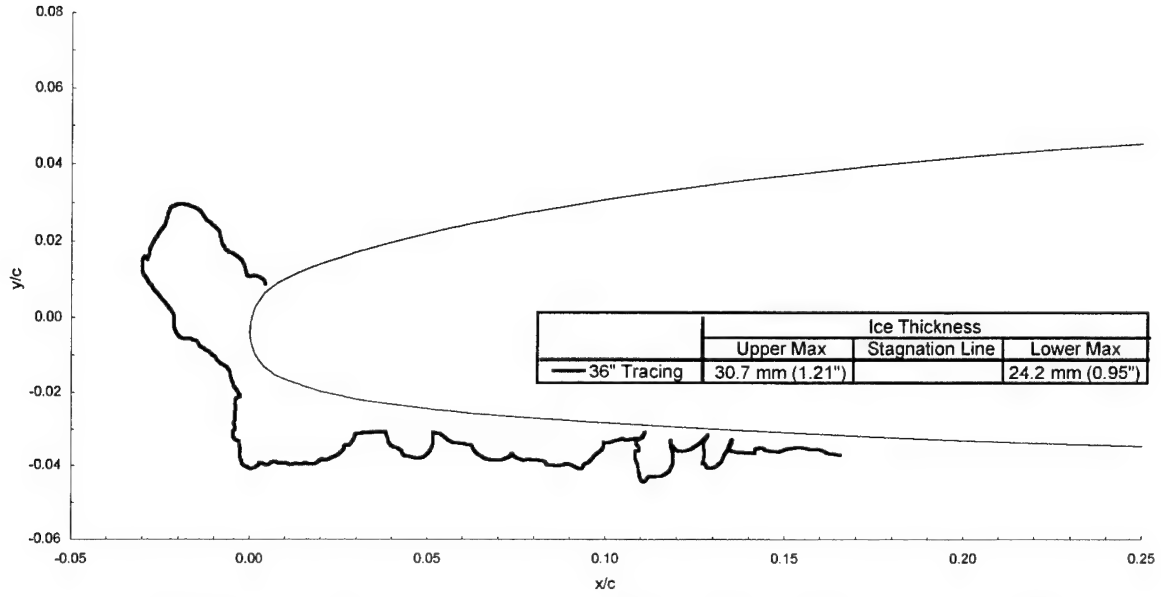

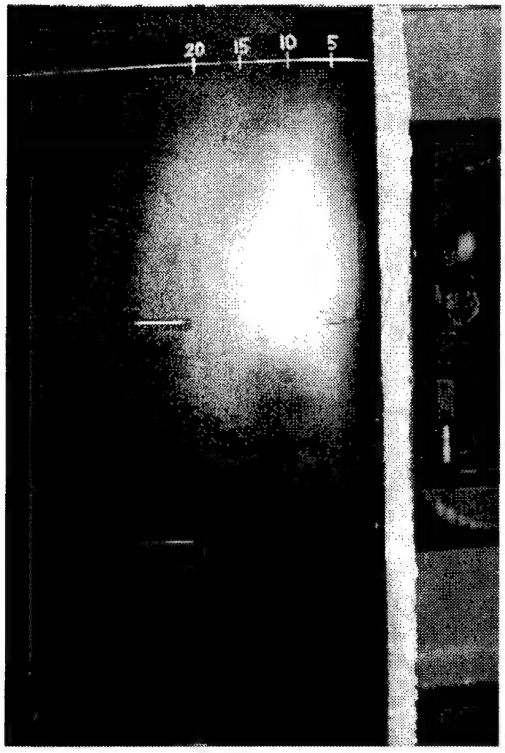

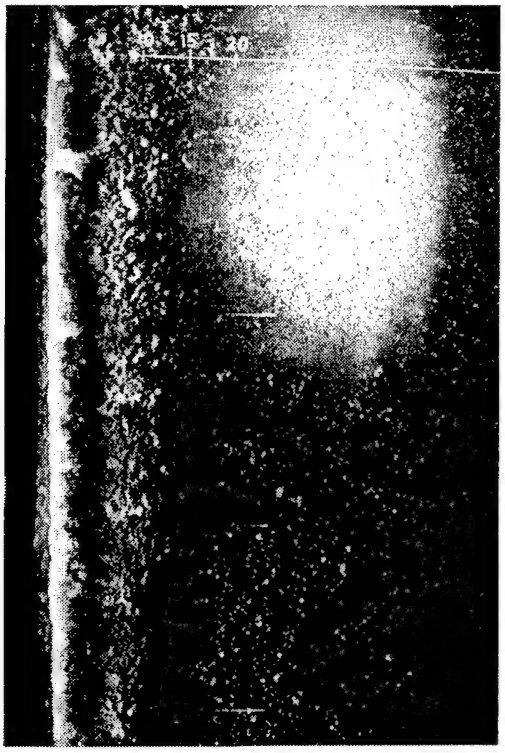

Appendix D2
Test Results, Business Jet—2nd Entry

Business Jet - Run 201

T_t = -0.8°C (30°F)
T_s = -5.0°C (22°F)
V = 90.0 m/s (175 kts)
AOA = 6.2°

LWC = 0.405 g/m^3
MVD = 20 μm
Spray = 4.4 min
chord = 90 cm (36 in)

$C_{d\text{-clean}}$ = 0.0092
$C_{d\text{-iced}}$ = 0.0353
$C_{l\text{-clean}}$ = 0.676
$C_{l\text{-iced}}$ = 0.654

	Ice Thickness		
	Upper Max	Leading Edge	Lower Max
42" Tracing	6.7 mm (.27")	4.3 mm (.17")	2.5 mm (0.10")
36" Tracing	5.6 mm (.22")	3.5 mm (.14")	1.8 mm (0.07")
30" Tracing	6.7 mm (.26")	4.4 mm (.17")	3.7 mm (0.15")

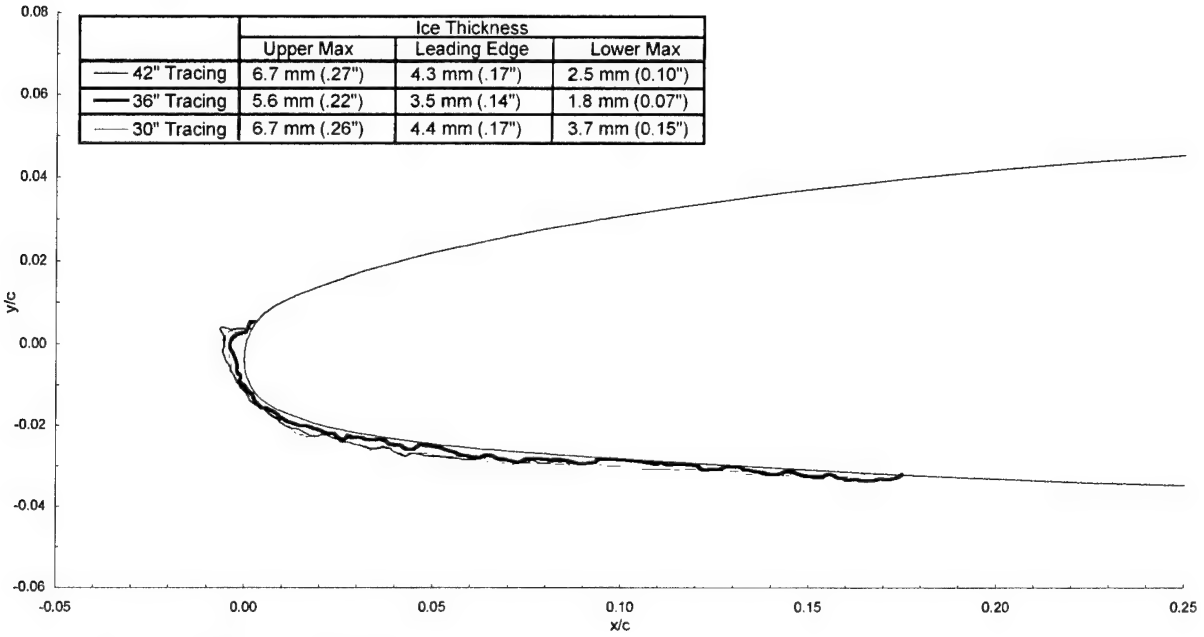

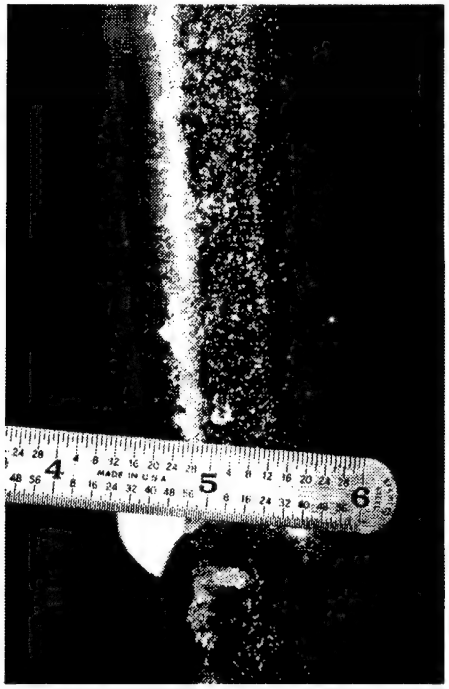

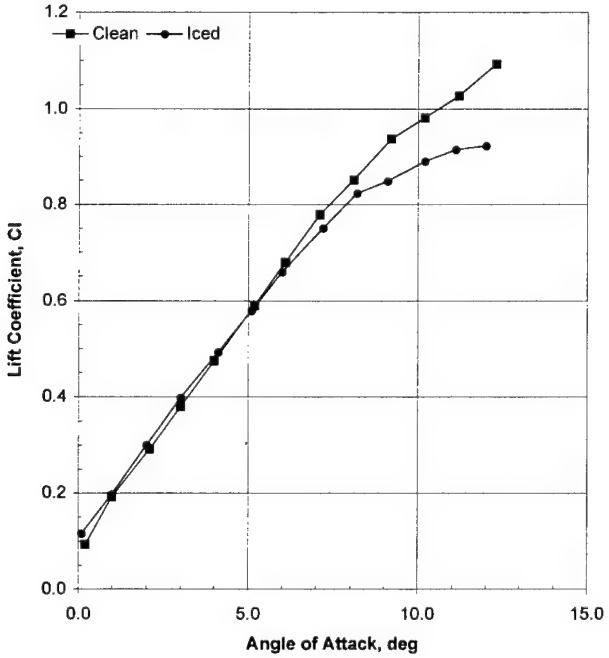

Business Jet - Run 202

T_t = -0.8°C (30°F)
T_s = -5.0°C (22°F)
V = 90.0 m/s (175 kts)
AOA = 6.2°

LWC = 0.54 g/m^3
MVD = 20 μm
Spray = 2.0 min
chord = 90 cm (36 in)

$C_{d\text{-}clean}$ = 0.0092
$C_{d\text{-}iced}$ = 0.0293
$C_{l\text{-}clean}$ = 0.676
$C_{l\text{-}iced}$ = 0.646

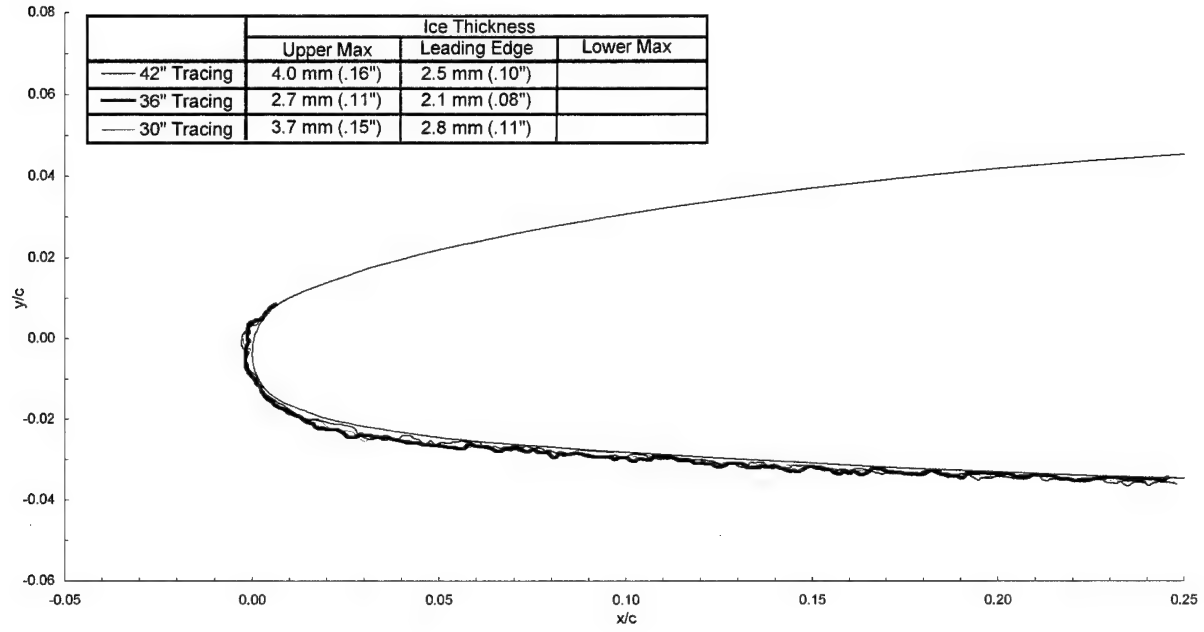

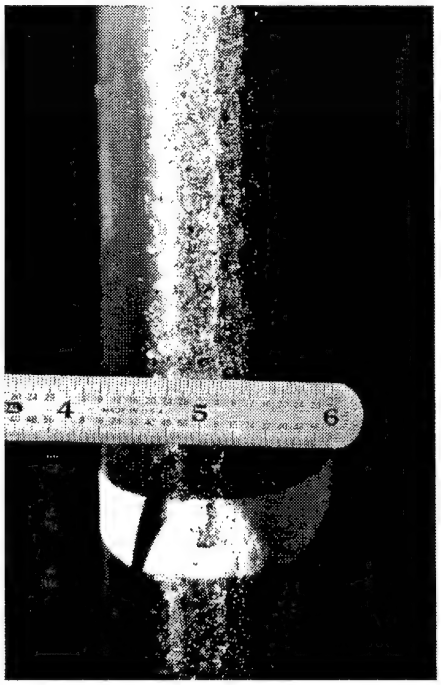

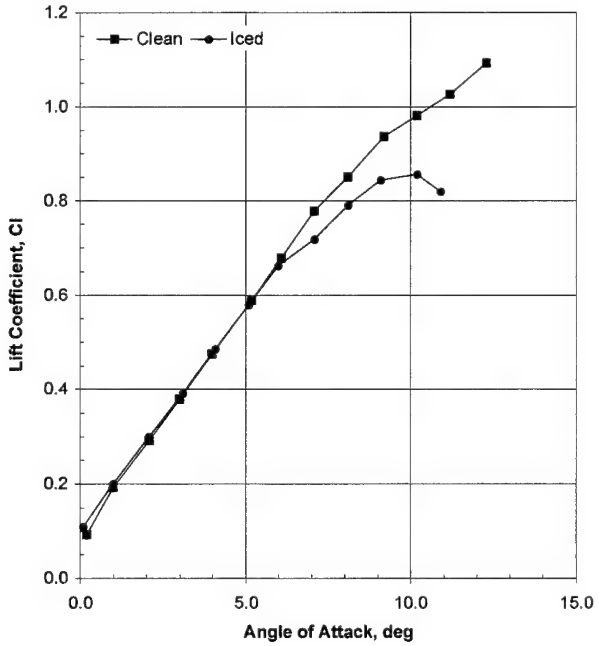

Business Jet - Run 202m

T_t = -0.8°C (30°F)
T_s = -5.0°C (22°F)

V = 90.0 m/s (175 kts)
AOA = 6.2°

LWC = 0.54 g/m^3
MVD = 20 μm
Spray = 2.0 min
chord = 90 cm (36 in)

$C_{d\text{-}clean}$ = 0.0092
$C_{d\text{-}iced}$ = 0.0292

$C_{l\text{-}clean}$ = 0.676
$C_{l\text{-}iced}$ = 0.661

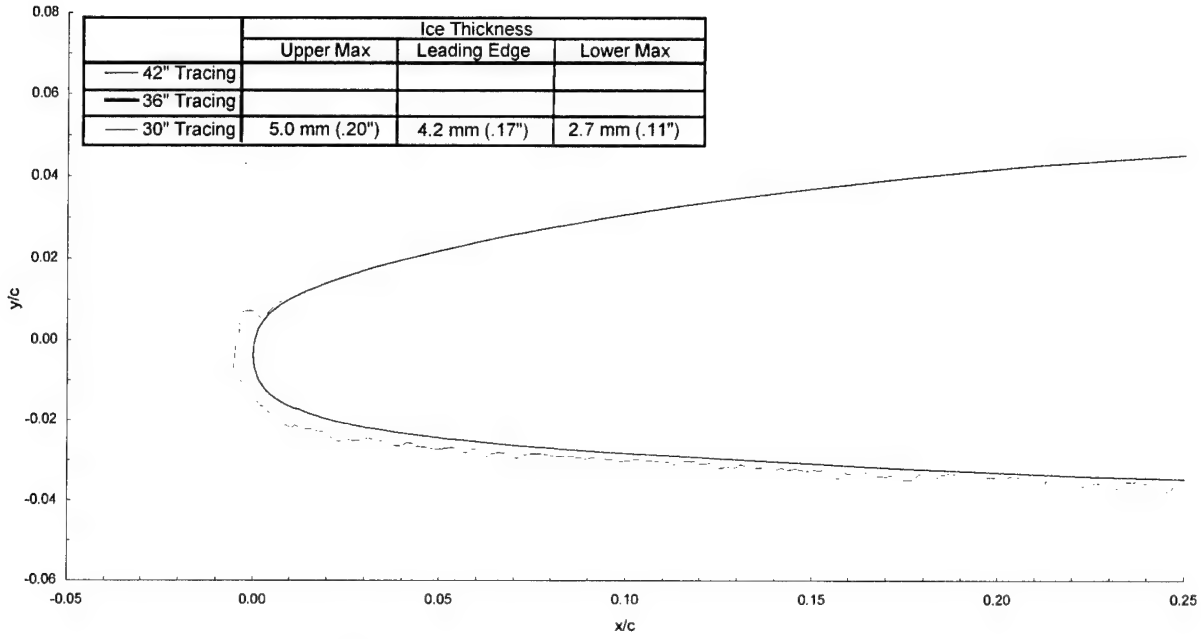

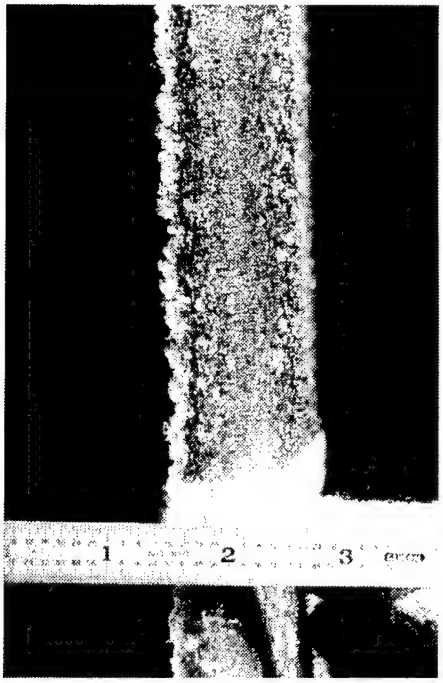

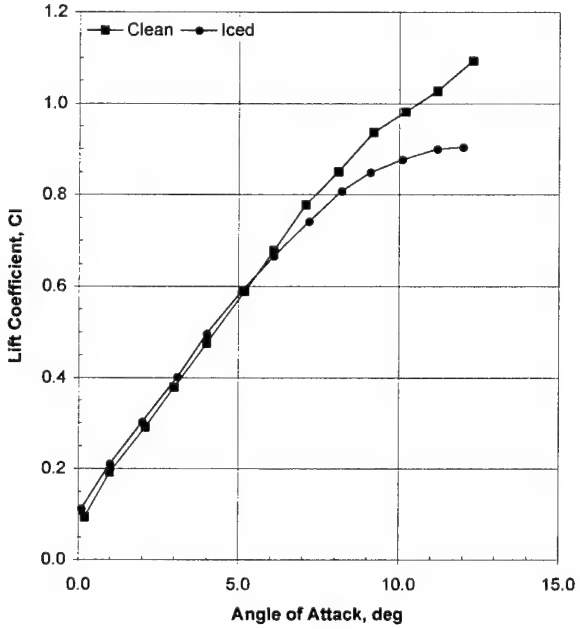

Business Jet - Run 202r

T_t = -0.8°C (30°F)
T_s = -5.0°C (22°F)
V = 90.0 m/s (175 kts)
AOA = 6.2°

LWC = 0.54 g/m^3
MVD = 20 μm
Spray = 2.0 min
chord = 90 cm (36 in)

$C_{d\text{-}clean}$ = 0.0092
$C_{d\text{-}iced}$ = 0.0291
$C_{l\text{-}clean}$ = 0.676
$C_{l\text{-}iced}$ = 0.651

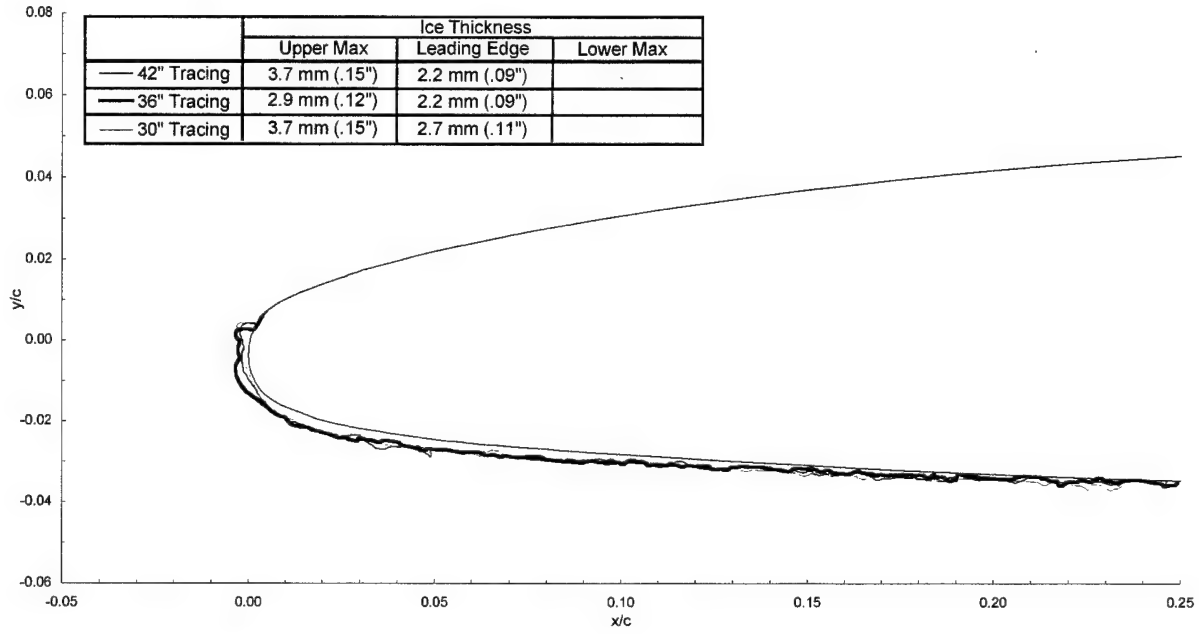

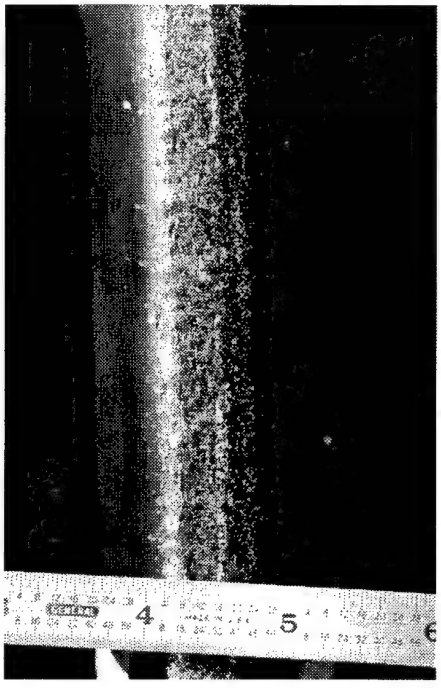

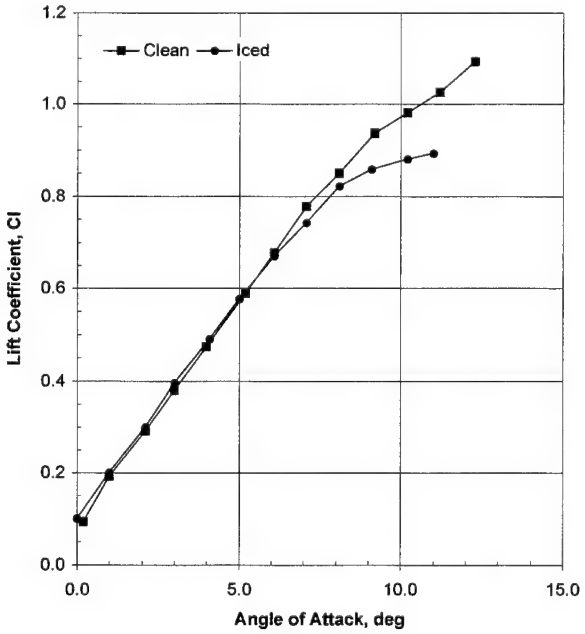

Business Jet - Run 203

T_t = -0.8°C (30°F)
T_s = -5.0°C (22°F)
V = 90.0 m/s (175 kts)
AOA = 6.2°

LWC = 0.54 g/m^3
MVD = 20 μm
Spray = 6.0 min
chord = 90 cm (36 in)

$C_{d\text{-}clean}$ = 0.0092
$C_{d\text{-}iced}$ = 0.0158
$C_{l\text{-}clean}$ = 0.676
$C_{l\text{-}iced}$ = 0.631

	Ice Thickness		
	Upper Max	Leading Edge	Lower Max
—— 42" Tracing	11.1 mm (0.44")	5.60 mm (0.22")	
—— 36" Tracing	11.0 mm (0.43")	5.20 mm (0.21")	
—— 30" Tracing	11.9 mm (0.47")	5.30 mm (0.21")	

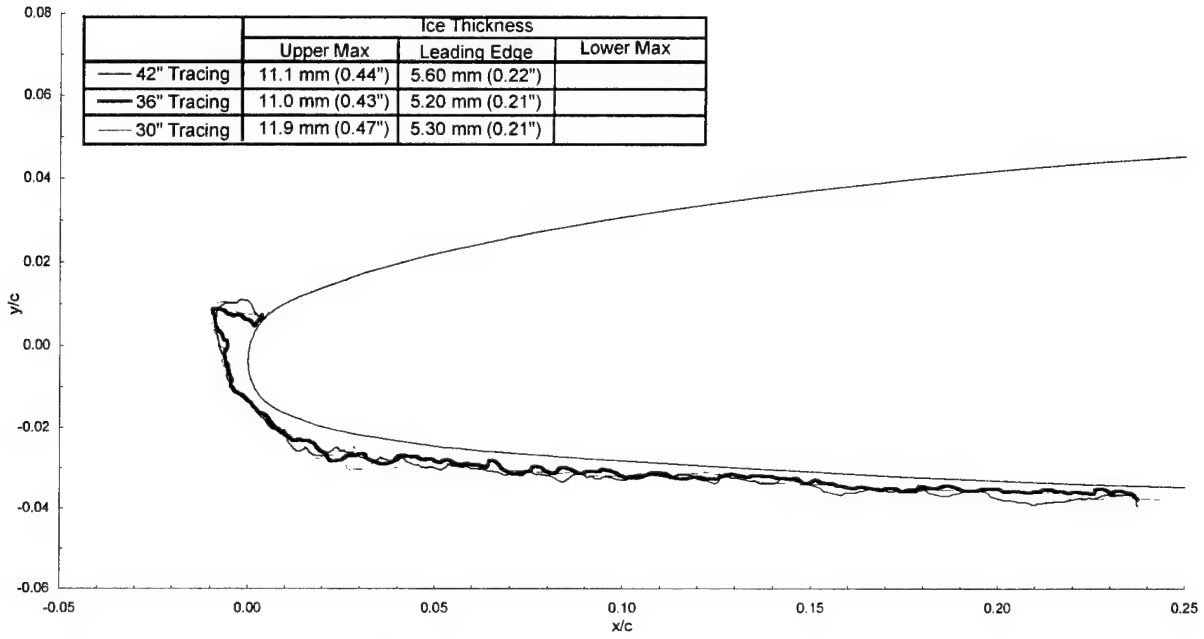

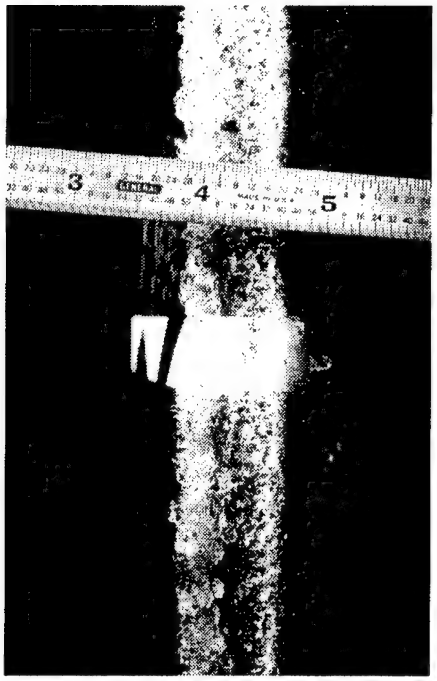

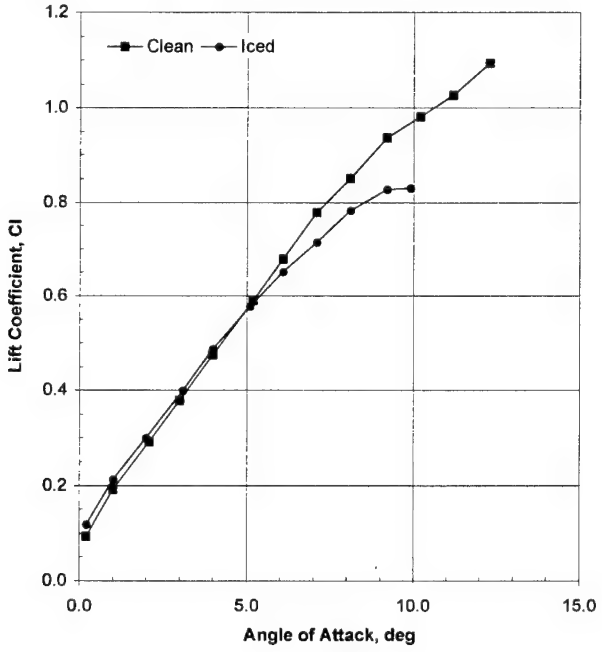

Business Jet - Run 204

T_t = -0.8°C (30°F)
T_s = -5.0°C (22°F)
V = 90.0 m/s (175 kts)
AOA = 6.2°

LWC = 0.54 g/m^3
MVD = 20 μm
Spray = 22.5 min
chord = 90 cm (36 in)

$C_{d\text{-}clean}$ = 0.0092
$C_{d\text{-}iced}$ = 0.1104
$C_{l\text{-}clean}$ = 0.676
$C_{l\text{-}iced}$ = 0.632

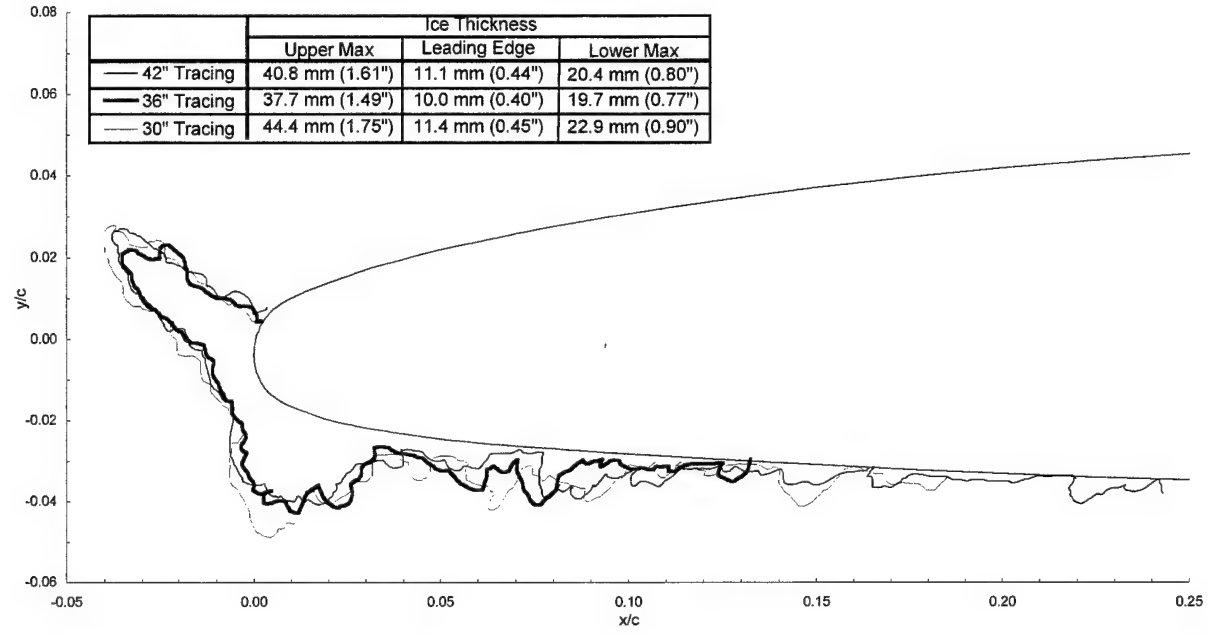

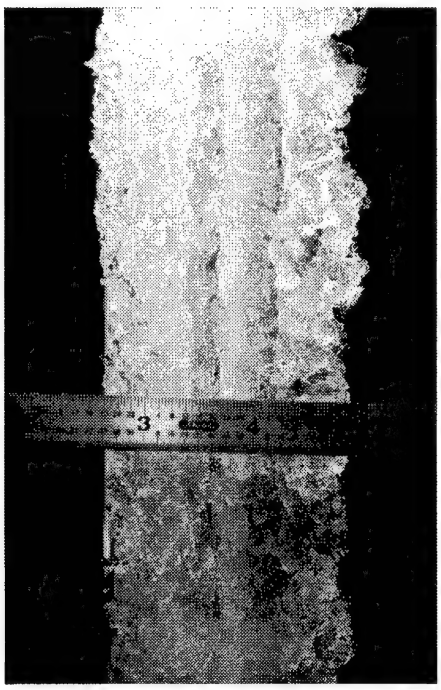

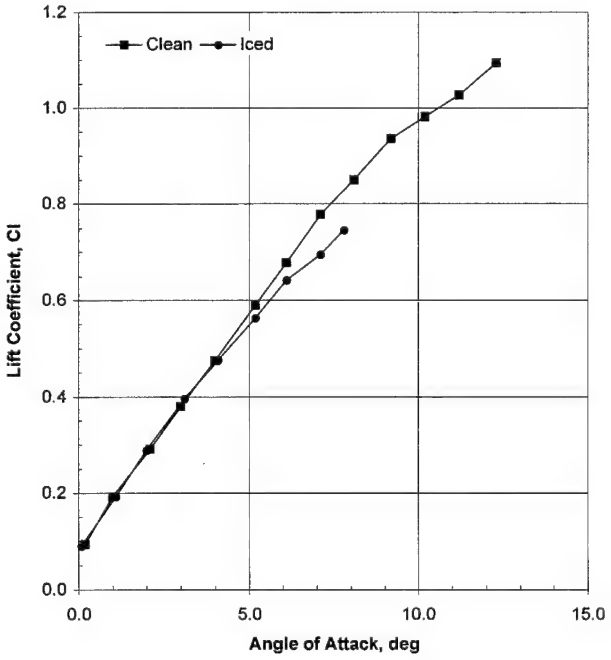

Business Jet - Run 205

T_t = -5.9°C (20.8°F)
T_s = -10.0°C (13.4°F)

V = 90.0 m/s (175 kts)
AOA = 6.2°

LWC = 0.535 g/m^3
MVD = 40 μm
Spray = 1.1 min
chord = 90 cm (36 in)

$C_{d\text{-}clean}$ = 0.0092
$C_{d\text{-}iced}$ = 0.0173

$C_{l\text{-}clean}$ = 0.676
$C_{l\text{-}iced}$ = 0.668

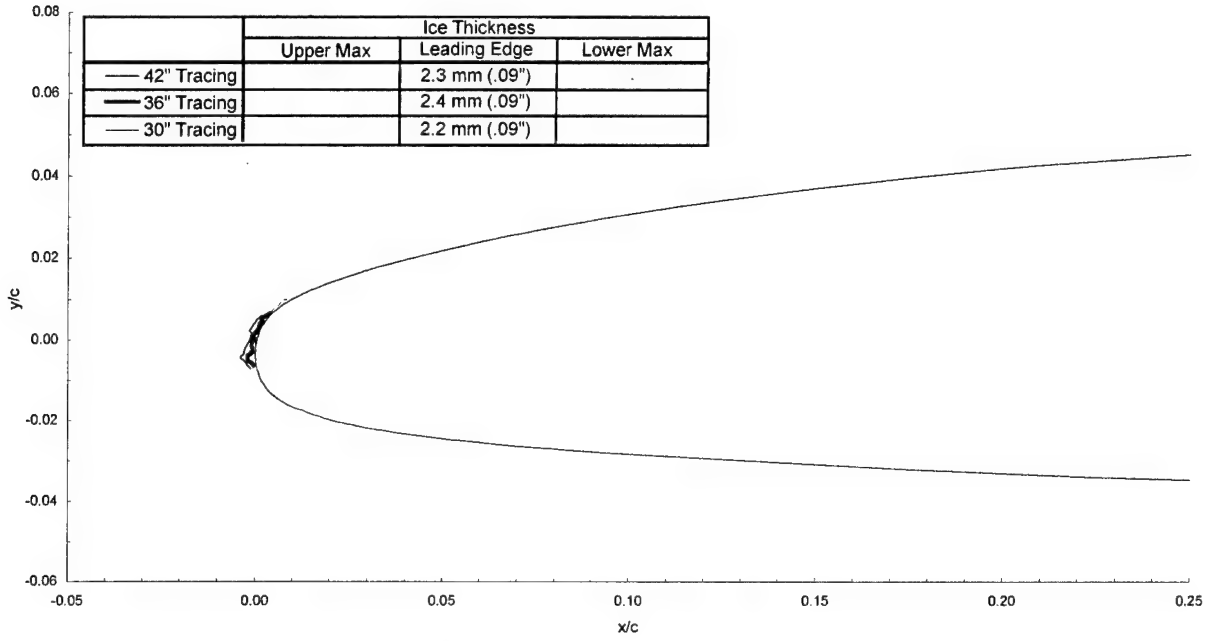

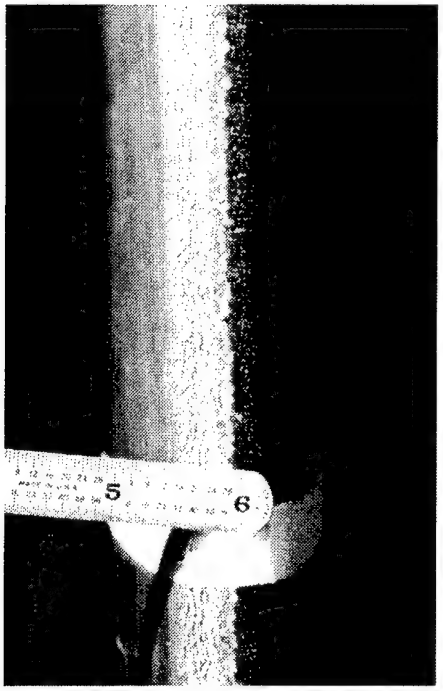

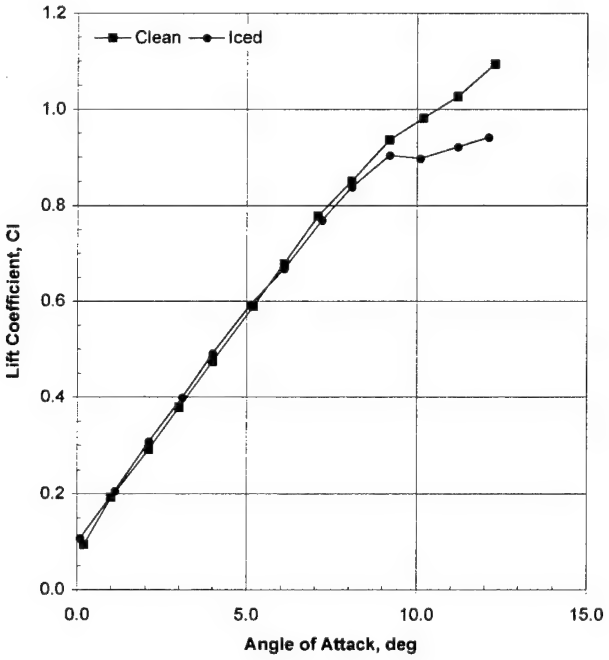

Business Jet - Run 205r

T_t = -5.9°C (20.8°F)
T_s = -10.0°C (13.4°F)
V = 90.0 m/s (175 kts)
AOA = 6.2°

LWC = 0.535 g/m^3
MVD = 40 μm
Spray = 1.1 min
chord = 90 cm (36 in)

$C_{d\text{-clean}}$ = 0.0092
$C_{d\text{-iced}}$ = 0.0176
$C_{l\text{-clean}}$ = 0.676
$C_{l\text{-iced}}$ = 0.662

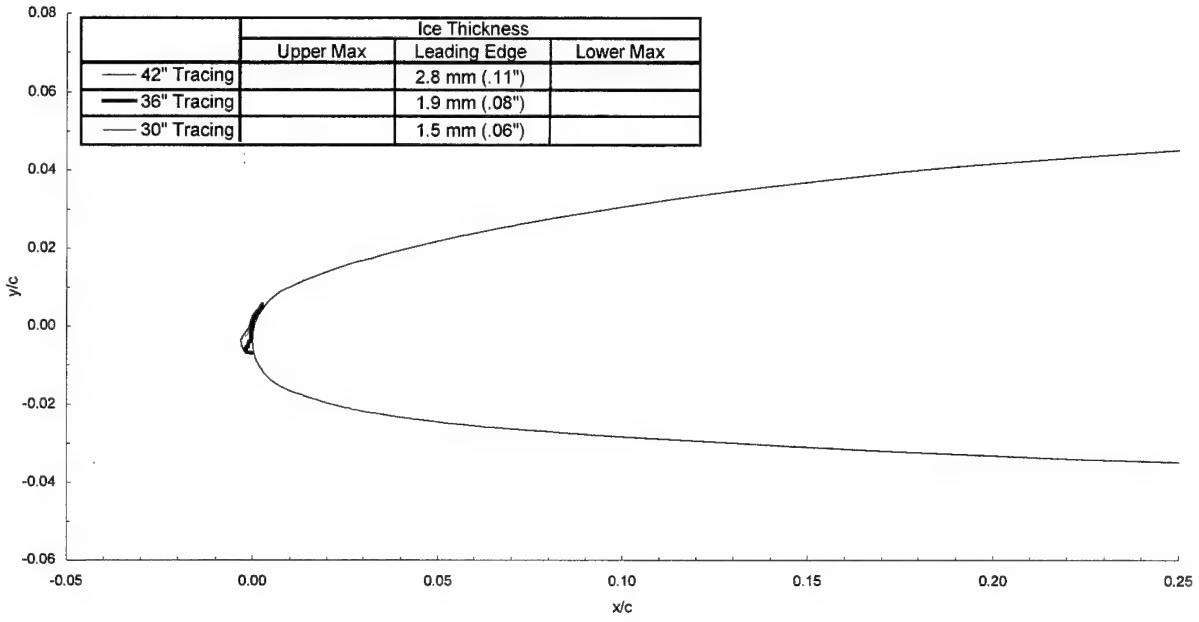

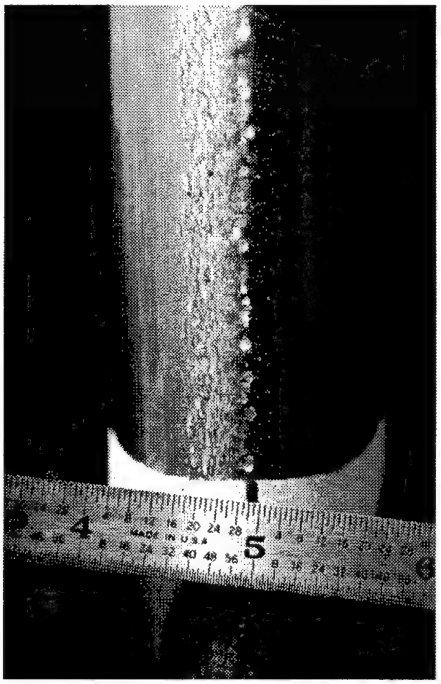

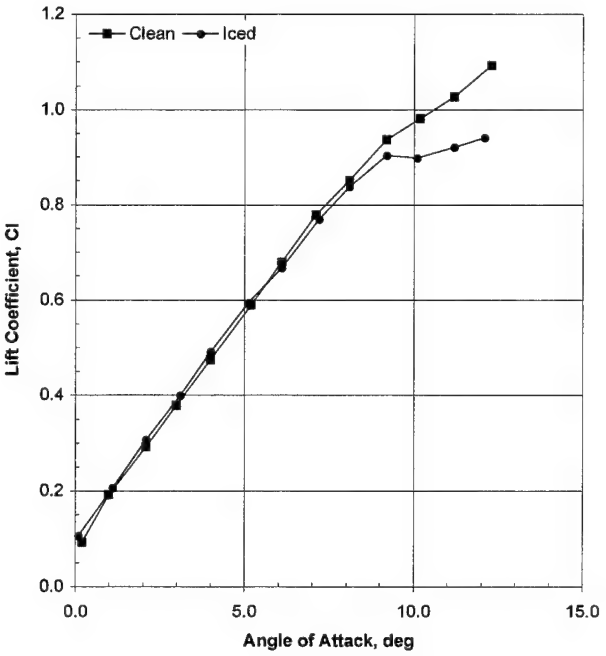

Business Jet - Run 206

T_t = -5.9°C (20.8°F)
T_s = -10.0°C (13.4°F)

V = 90.0 m/s (175 kts)
AOA = 6.2°

LWC = 0.535 g/m^3
MVD = 40 μm
Spray = 4.2 min
chord = 90 cm (36 in)

$C_{d\text{-}clean}$ = 0.0092
$C_{d\text{-}iced}$ = 0.0176

$C_{l\text{-}clean}$ = 0.676
$C_{l\text{-}iced}$ = 0.637

	Ice Thickness		
	Upper Max	Leading Edge	Lower Max
42" Tracing	10.2 mm (0.40")	11.0 mm (0.44")	6.9 mm (0.27")
36" Tracing	8.8 mm (0.35")	9.1 mm (0.36")	5.6 mm (0.22")
30" Tracing	9.9 mm (0.39")	10.5 mm (0.41")	6.6 mm (0.26")

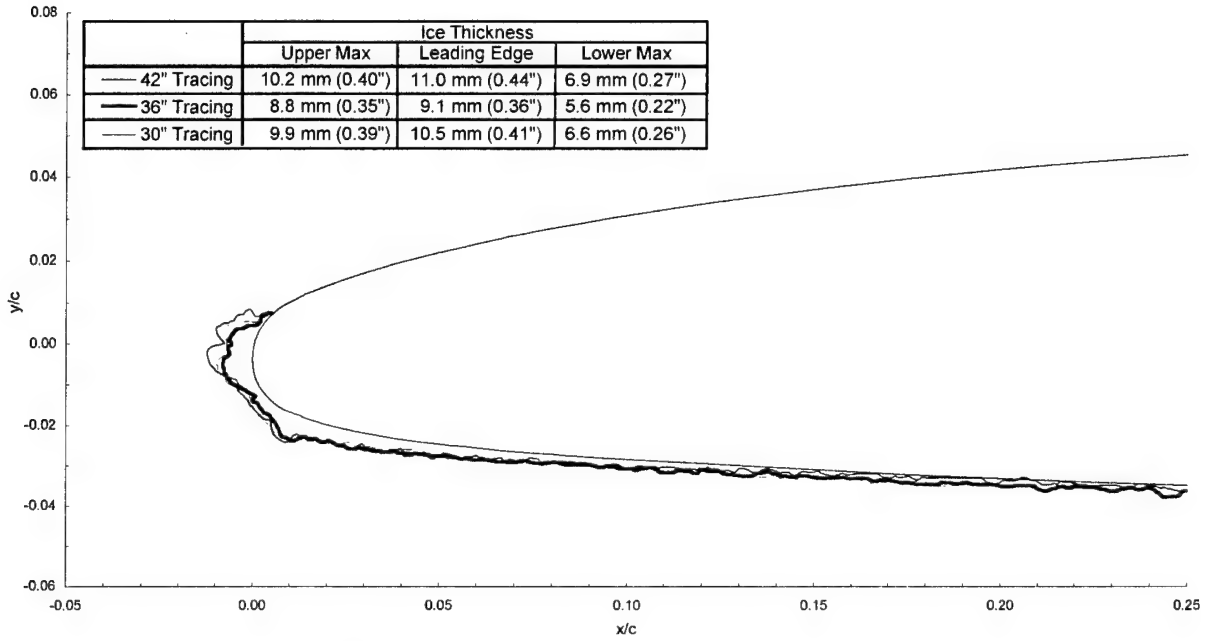

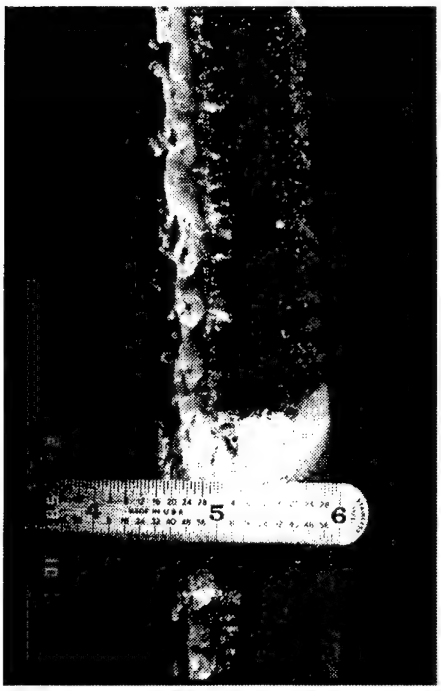

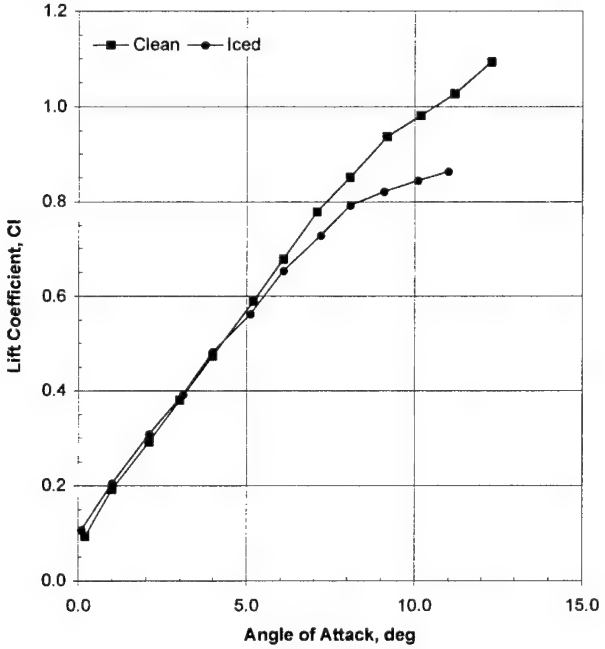

Business Jet - Run 207

T_t = -5.9°C (20.8°F)
T_s = -10.0°C (13.4°F)

V = 90.0 m/s (175 kts)
AOA = 6.2°

LWC = 0.43 g/m^3
MVD = 20 μm
Spray = 2.0 min
chord = 90 cm (36 in)

$C_{d\text{-}clean}$ = 0.0092
$C_{d\text{-}iced}$ = 0.0186

$C_{l\text{-}clean}$ = 0.676
$C_{l\text{-}iced}$ = 0.657

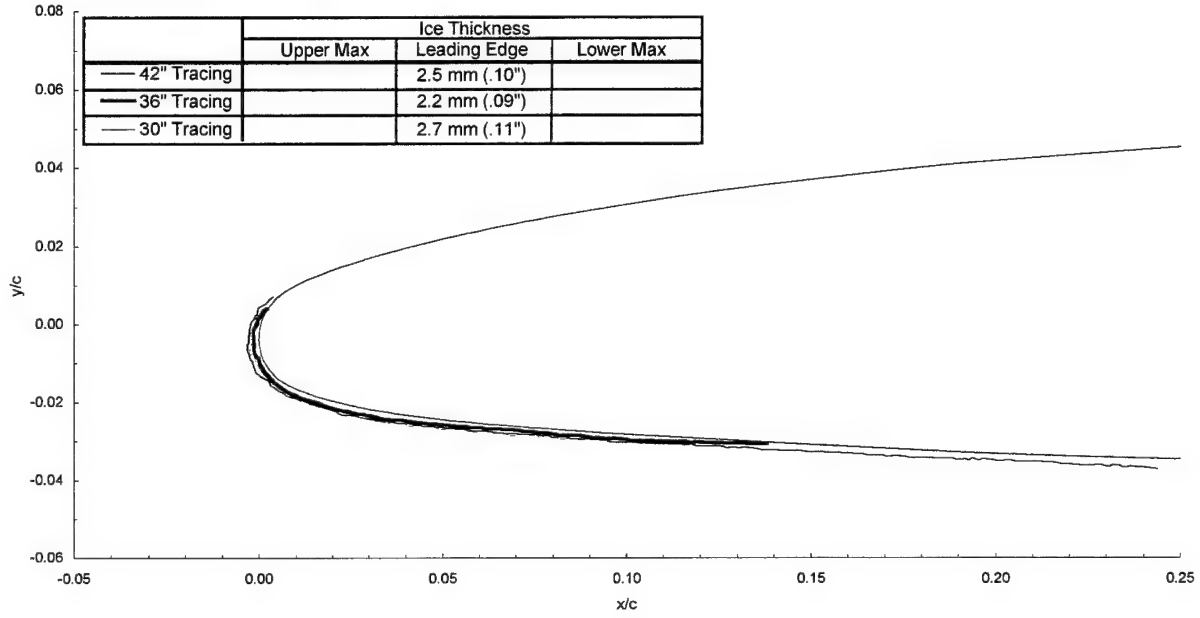

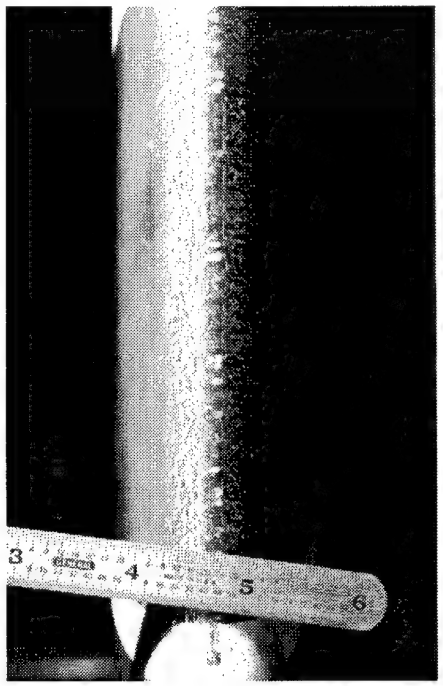

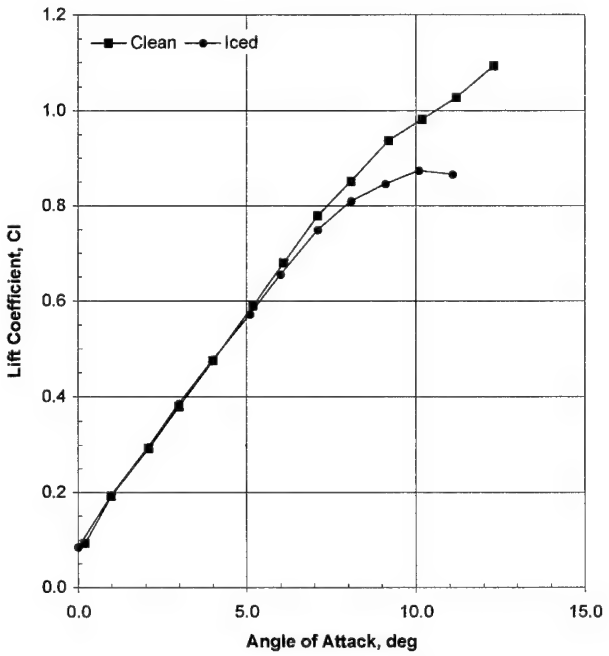

Business Jet - Run 208

T_t = -5.9°C (20.8°F)
T_s = -10.0°C (13.4°F)
V = 90.0 m/s (175 kts)
AOA = 6.2°

LWC = 0.43 g/m^3
MVD = 20 μm
Spray = 6.0 min
chord = 90 cm (36 in)

$C_{d\text{-clean}}$ = 0.0092
$C_{d\text{-iced}}$ = 0.0301
$C_{l\text{-clean}}$ = 0.676
$C_{l\text{-iced}}$ = 0.641

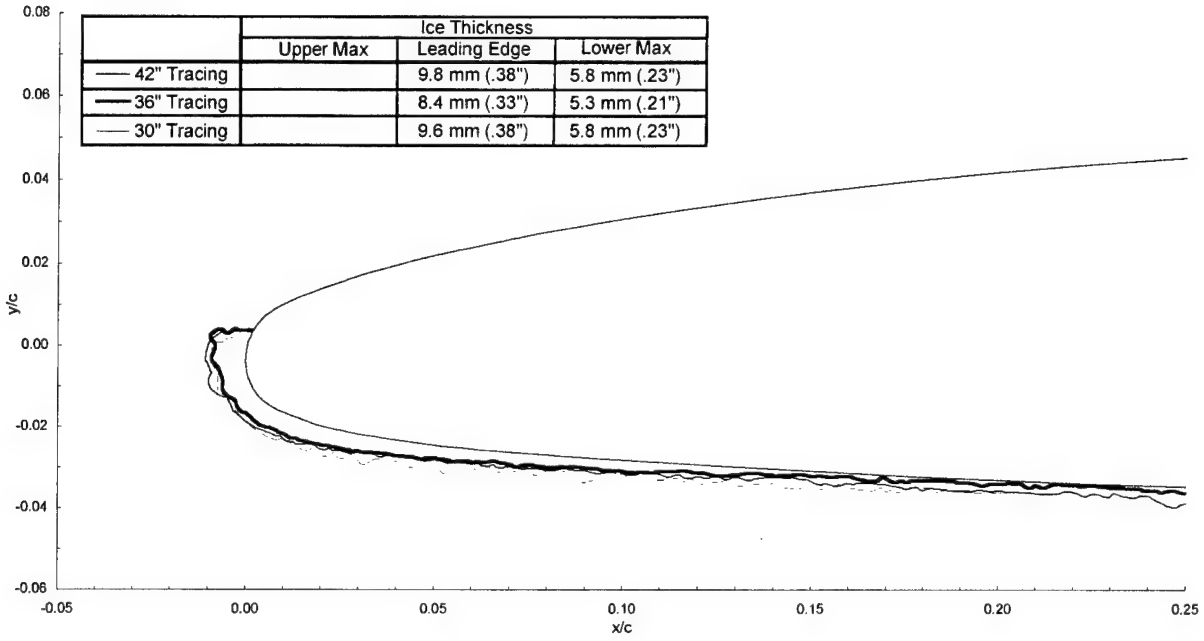

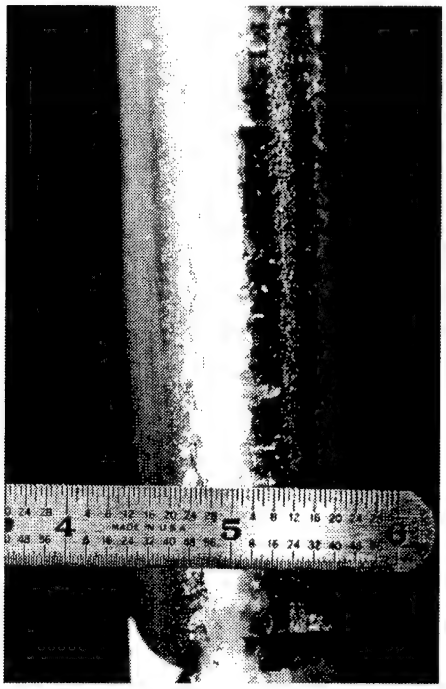

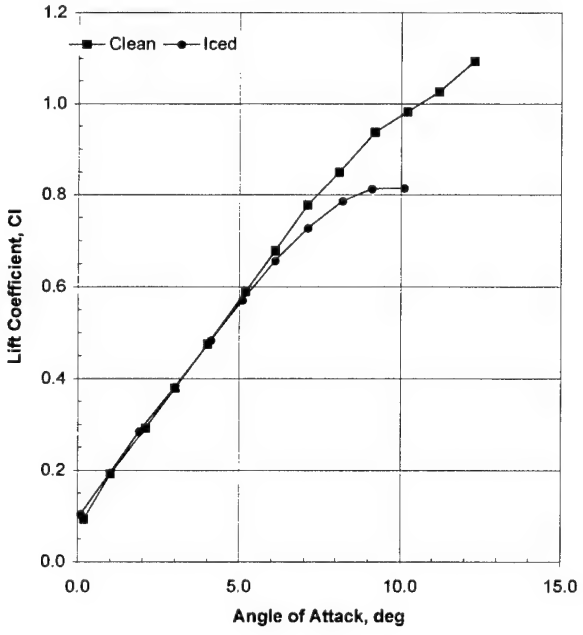

Business Jet - Run 209

T_t = -5.9°C (20.8°F)
T_s = -10.0°C (13.4°F)

V = 90.0 m/s (175 kts)
AOA = 6.2°

LWC = 0.43 g/m^3
MVD = 20 μm
Spray = 22.5 min
chord = 90 cm (36 in)

$C_{d\text{-}clean}$ = 0.0092
$C_{d\text{-}iced}$ = 0.0343

$C_{l\text{-}clean}$ = 0.676
$C_{l\text{-}iced}$ = 0.655

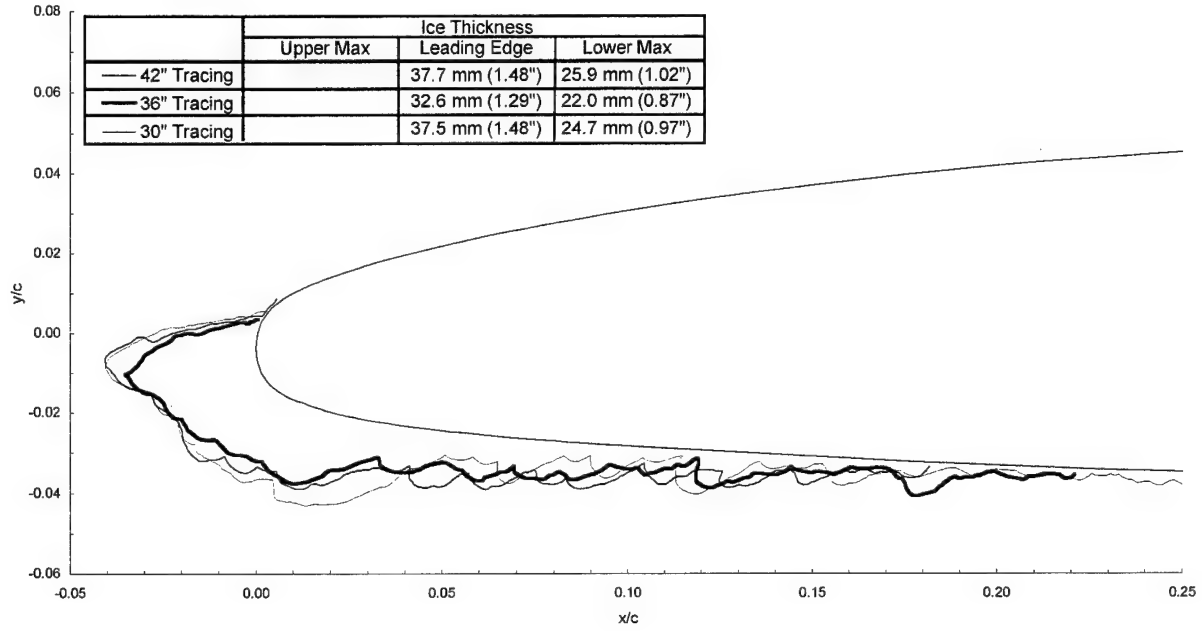

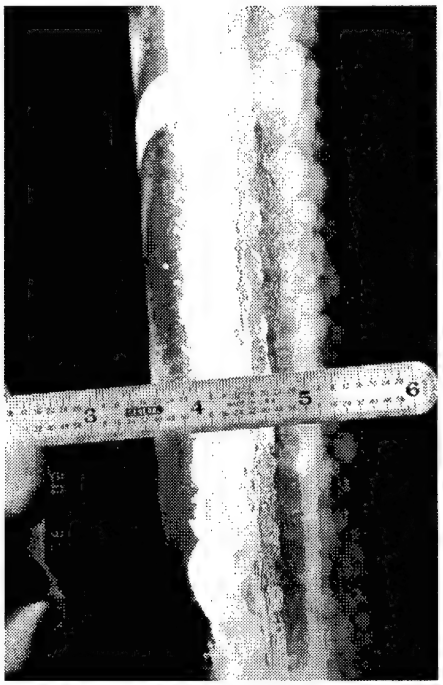

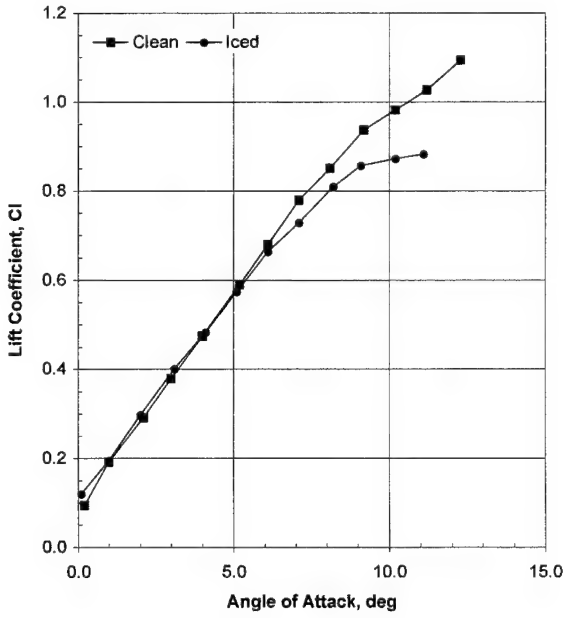

Business Jet - Run 210

T_t = -11.0°C (11.7°F)
T_s = -15°C (4.4°F)

V = 90.0 m/s (175 kts)
AOA = 6.2°

LWC = 0.405 g/m^3
MVD = 20 μm
Spray = 2.0 min
chord = 90 cm (36 in)

$C_{d\text{-}clean}$ = 0.0092
$C_{d\text{-}iced}$ = 0.0171

$C_{l\text{-}clean}$ = 0.676
$C_{l\text{-}iced}$ = 0.660

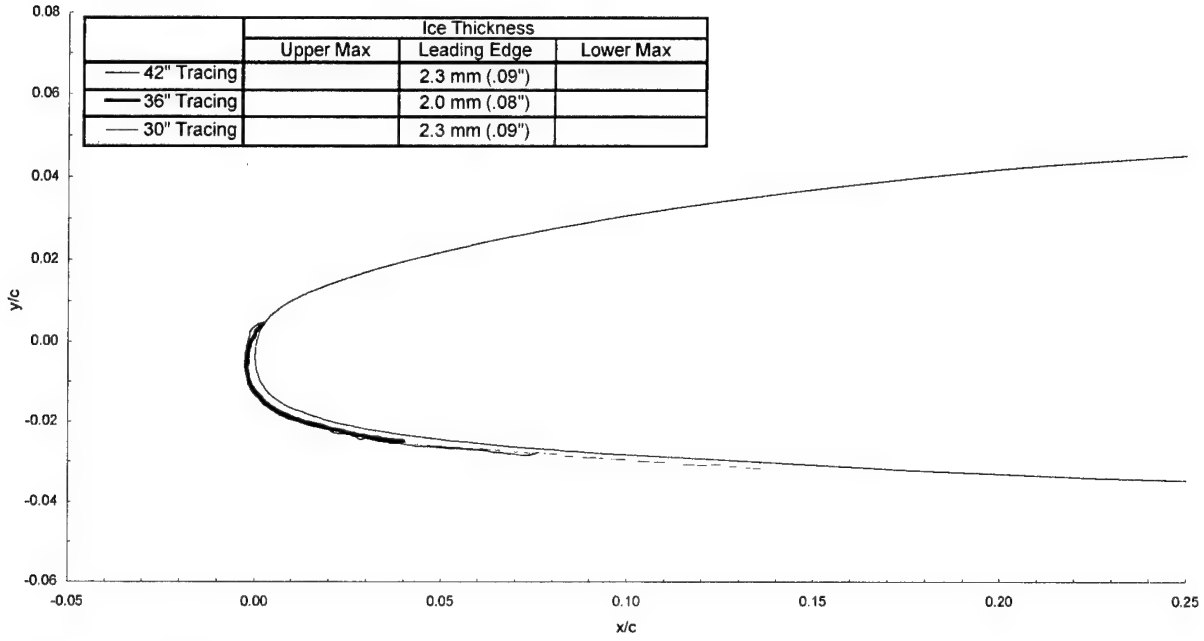

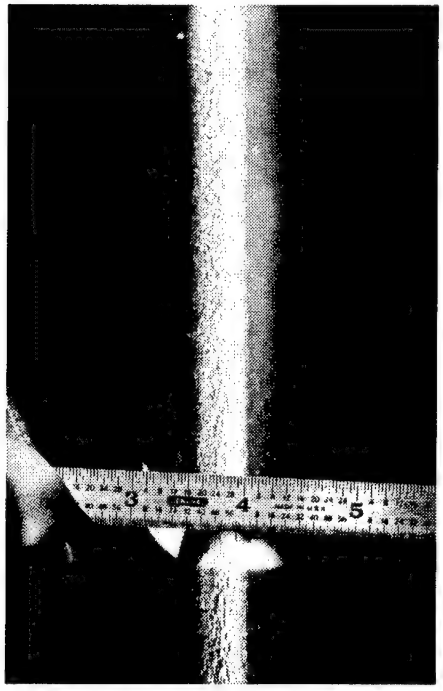

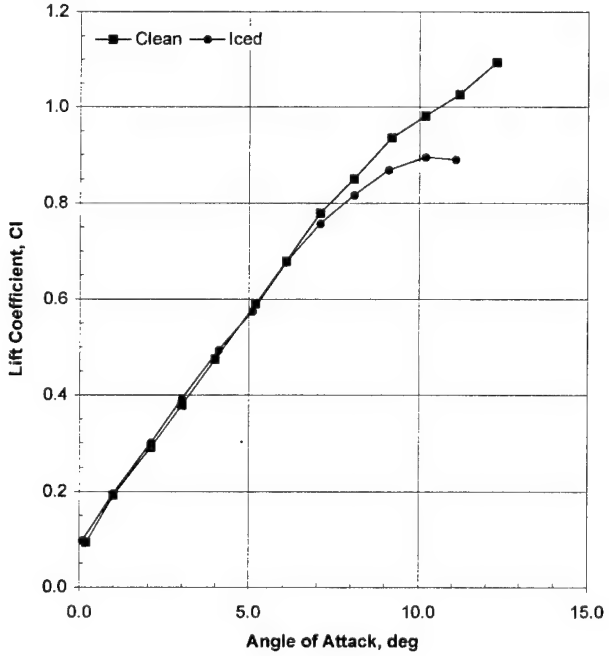

Business Jet - Run 211

T_t = -11.0°C (11.7°F)
T_s = -15°C (4.4°F)

V = 90.0 m/s (175 kts)
AOA = 6.2°

LWC = 0.405 g/m^3
MVD = 20 μm
Spray = 4.4 min
chord = 90 cm (36 in)

$C_{d\text{-clean}}$ = 0.0092
$C_{d\text{-iced}}$ = 0.0252

$C_{l\text{-clean}}$ = 0.676
$C_{l\text{-iced}}$ = 0.647

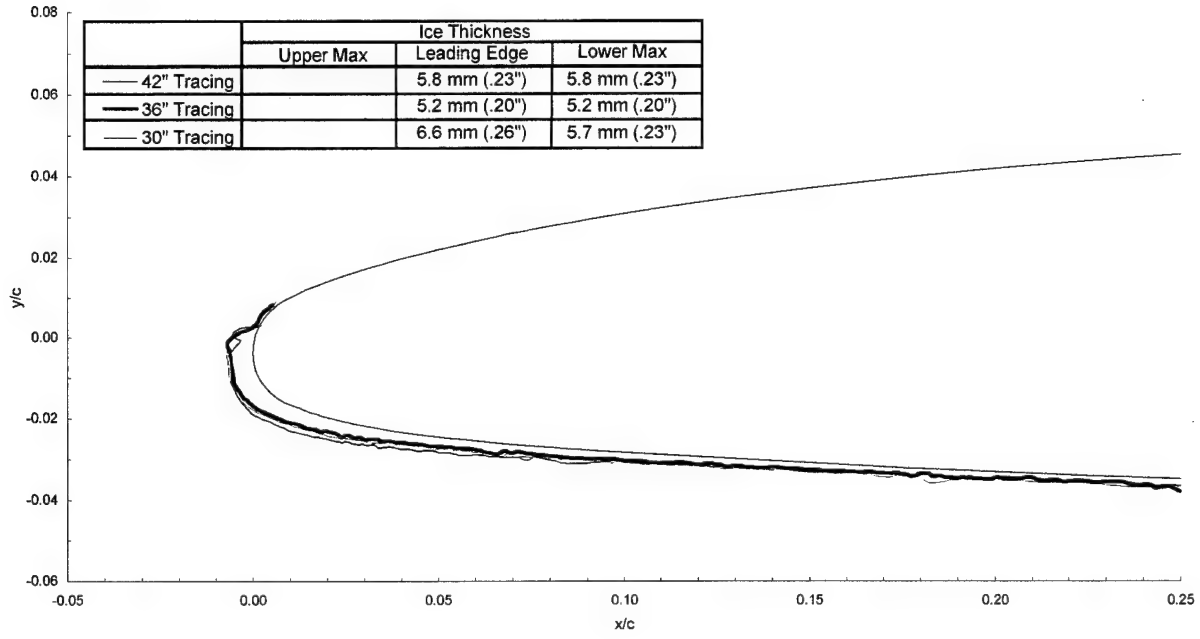

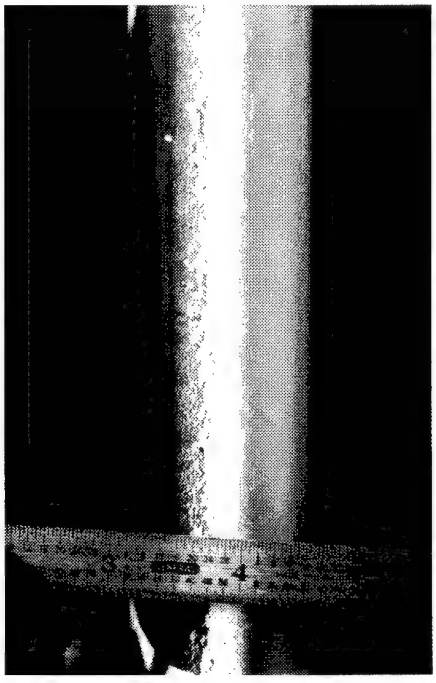

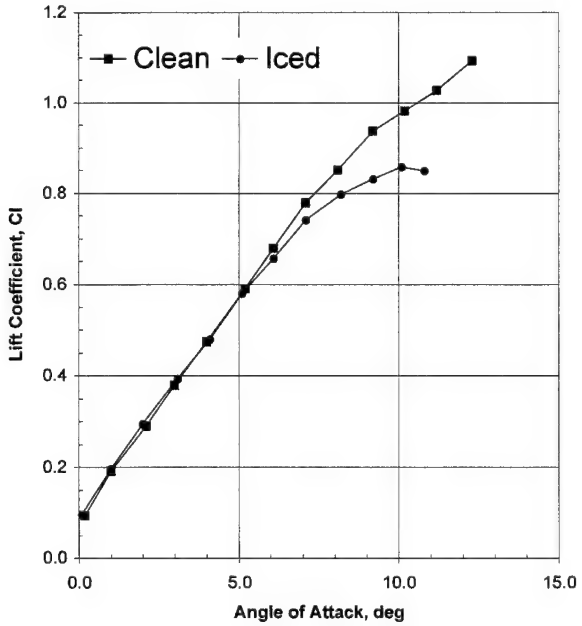

Business Jet - Run 212

T_t = -11.0°C (11.7°F)
T_s = -15°C (4.4°F)

V = 90.0 m/s (175 kts)
AOA = 6.2°

LWC = 0.405 g/m^3
MVD = 20 μm
Spray = 16.7 min
chord = 90 cm (36 in)

$C_{d\text{-clean}}$ = 0.0092
$C_{d\text{-iced}}$ = 0.0287

$C_{l\text{-clean}}$ = 0.676
$C_{l\text{-iced}}$ = 0.658

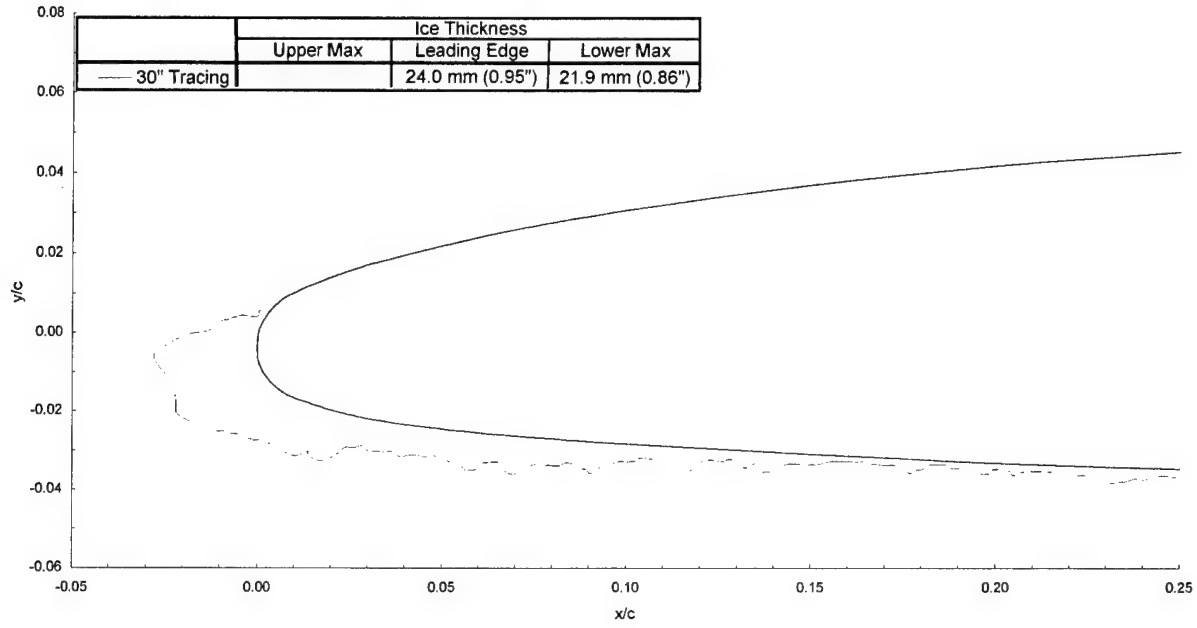

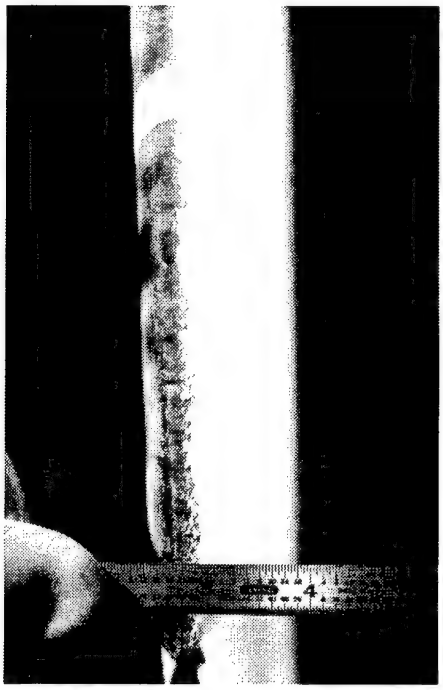

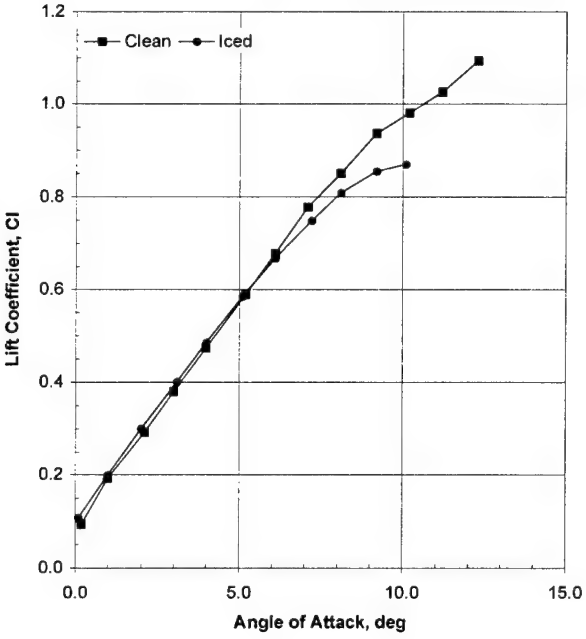

Business Jet - Run 213

T_t = -5.9°C (20.8°F)
T_s = -10.0°C (13.4°F)

V = 90.0 m/s (175 kts)
AOA = 6.2°

LWC = 0.60 g/m^3
MVD = 15 μm
Spray = 2.0 min
chord = 90 cm (36 in)

$C_{d\text{-}clean}$ = 0.0092
$C_{d\text{-}iced}$ = 0.0129

$C_{l\text{-}clean}$ = 0.676
$C_{l\text{-}iced}$ = 0.660

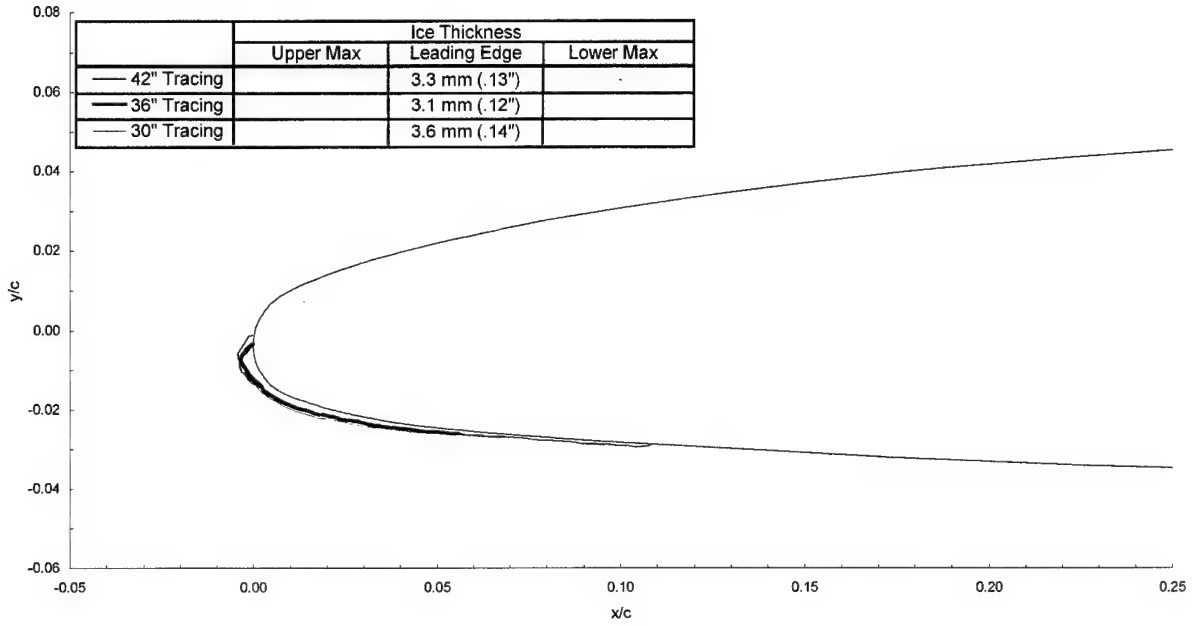

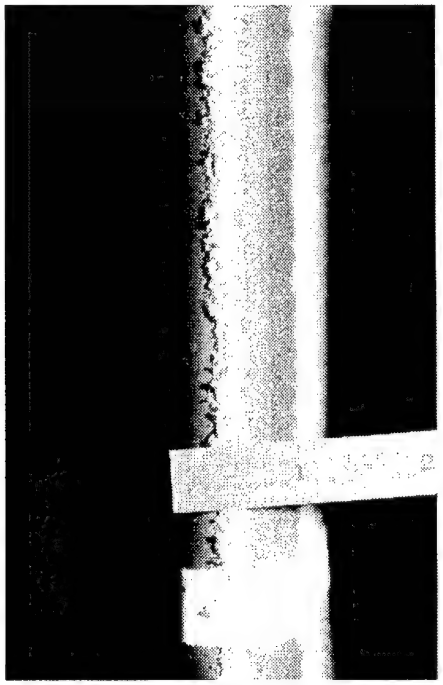

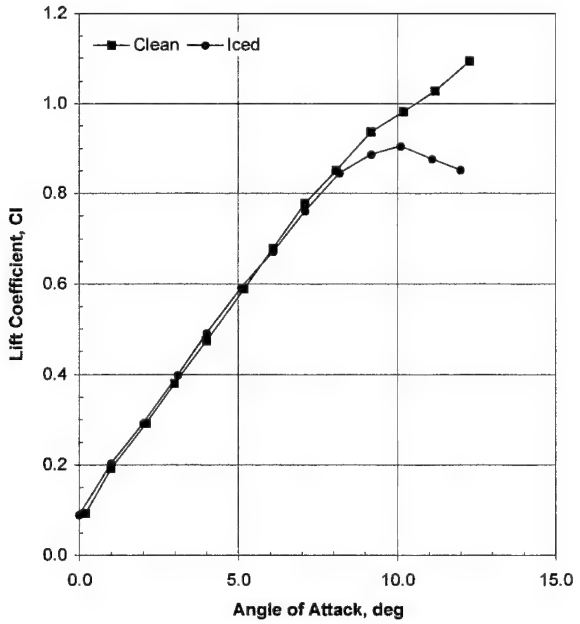

Business Jet - Run 214

T_t = -5.9°C (20.8°F)
T_s = -10.0°C (13.4°F)

V = 90.0 m/s (175 kts)
AOA = 6.2°

LWC = 0.60 g/m^3
MVD = 15 μm
Spray = 6.0 min
chord = 90 cm (36 in)

$C_{d\text{-}clean}$ = 0.0092
$C_{d\text{-}iced}$ = 0.0158

$C_{l\text{-}clean}$ = 0.676
$C_{l\text{-}iced}$ = 0.675

	Ice Thickness		
	Upper Max	Stagnation Line	Lower Max
42" Tracing		12.1 mm (0.48")	
36" Tracing		11.1 mm (0.44")	
30" Tracing		12.6 mm (0.50")	

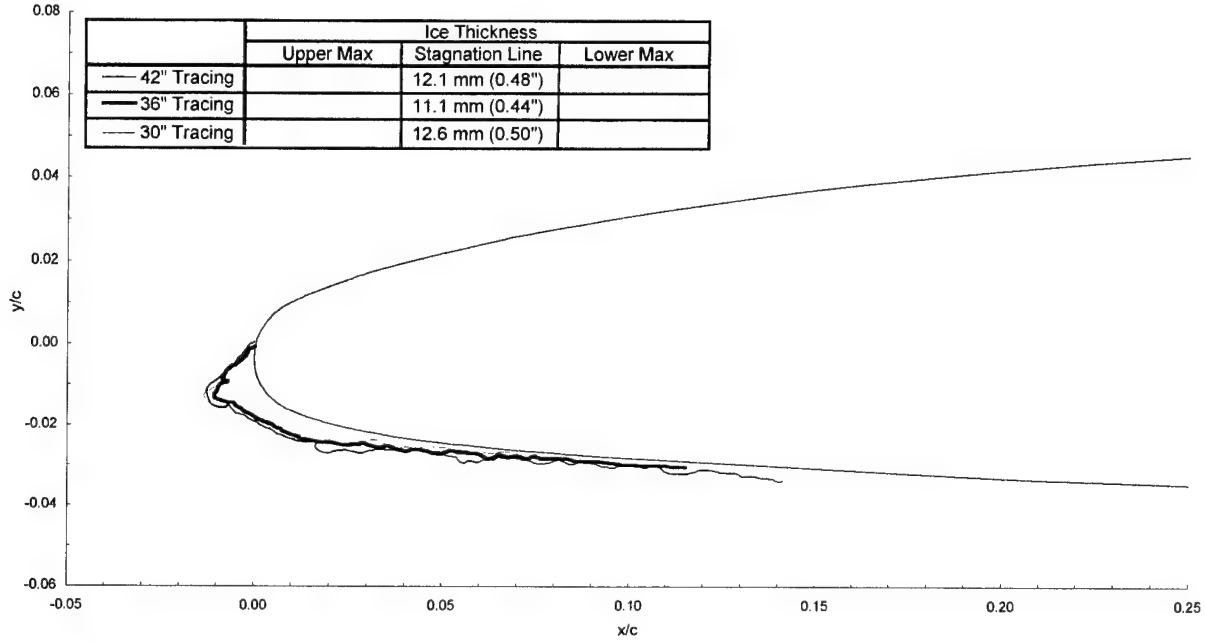

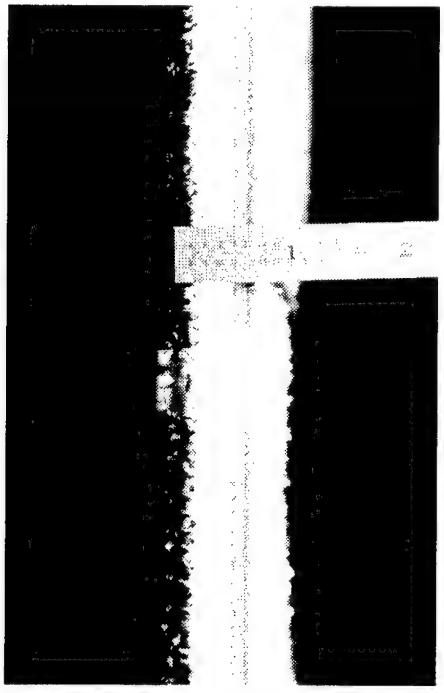

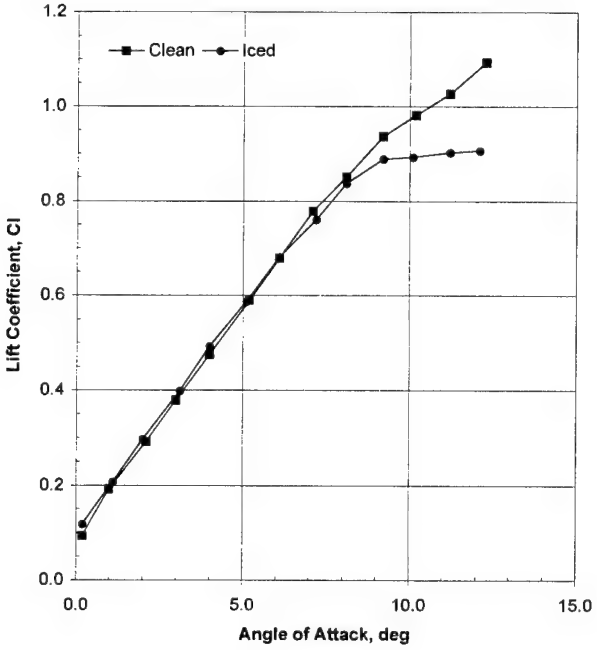

Business Jet - Run 221

T_t = -0.8°C (30°F)
T_s = -5.0°C (22°F)

V = 129 m/s (250 kts)
AOA = 1.5°

LWC = 0.54 g/m^3
MVD = 20 μm

Spray = 3.0 min
chord = 90 cm (36 in)

$C_{d\text{-}clean}$ = 0.0081
$C_{d\text{-}iced}$ = 0.0151

$C_{l\text{-}clean}$ = 0.228
$C_{l\text{-}iced}$ = 0.220

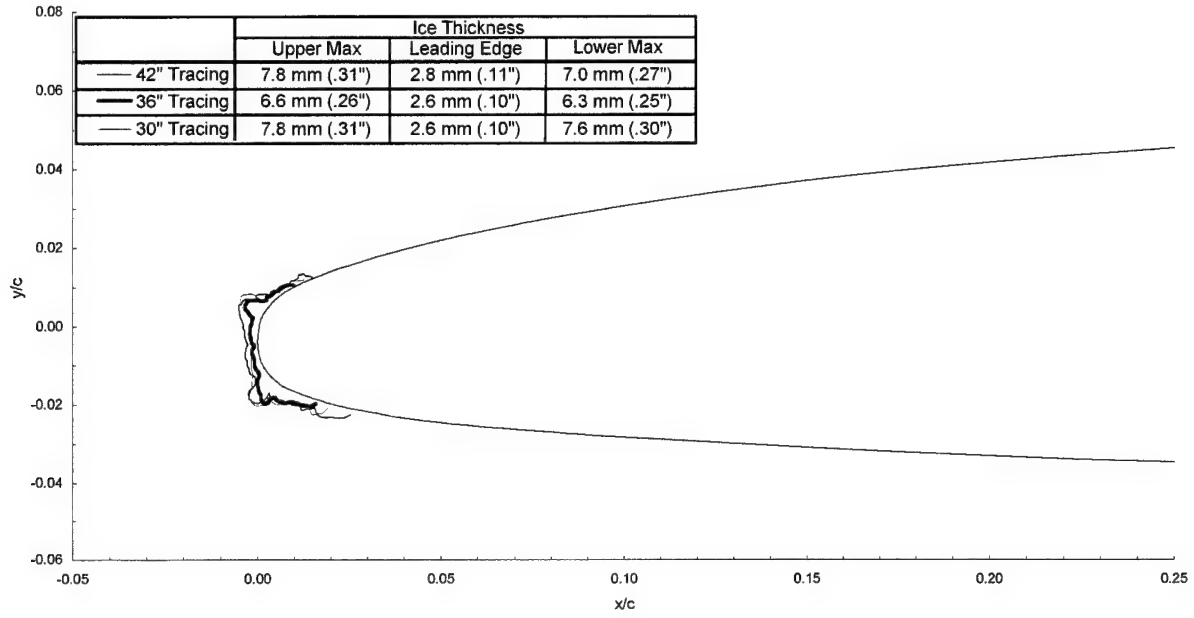

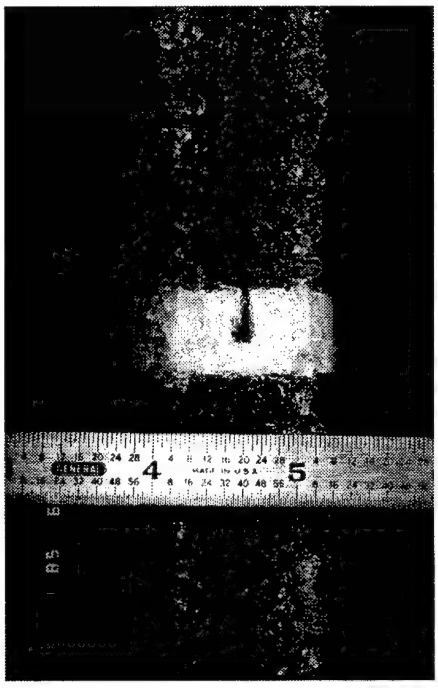

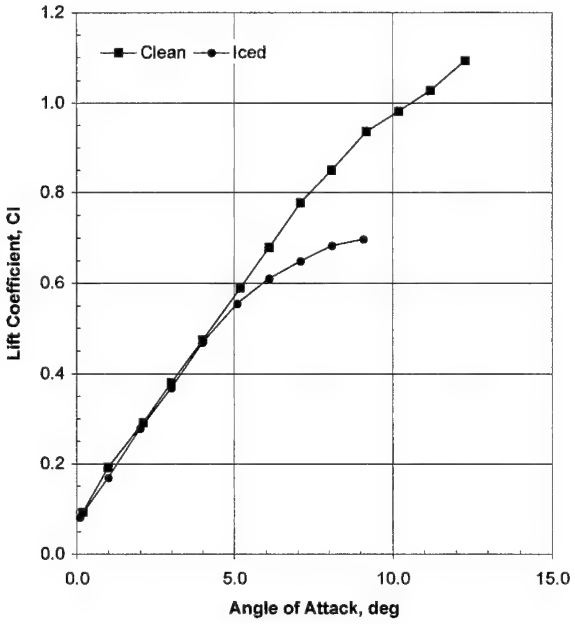

Business Jet - Run 222

T_t = -0.8°C (30°F)
T_s = -5.0°C (22°F)

V = 129 m/s (250 kts)
AOA = 1.5°

LWC = 0.54 g/m^3
MVD = 20 μm
Spray = 6.0 min
chord = 90 cm (36 in)

$C_{d\text{-}clean}$ = 0.0081
$C_{d\text{-}iced}$ = 0.0238

$C_{l\text{-}clean}$ = 0.228
$C_{l\text{-}iced}$ = 0.222

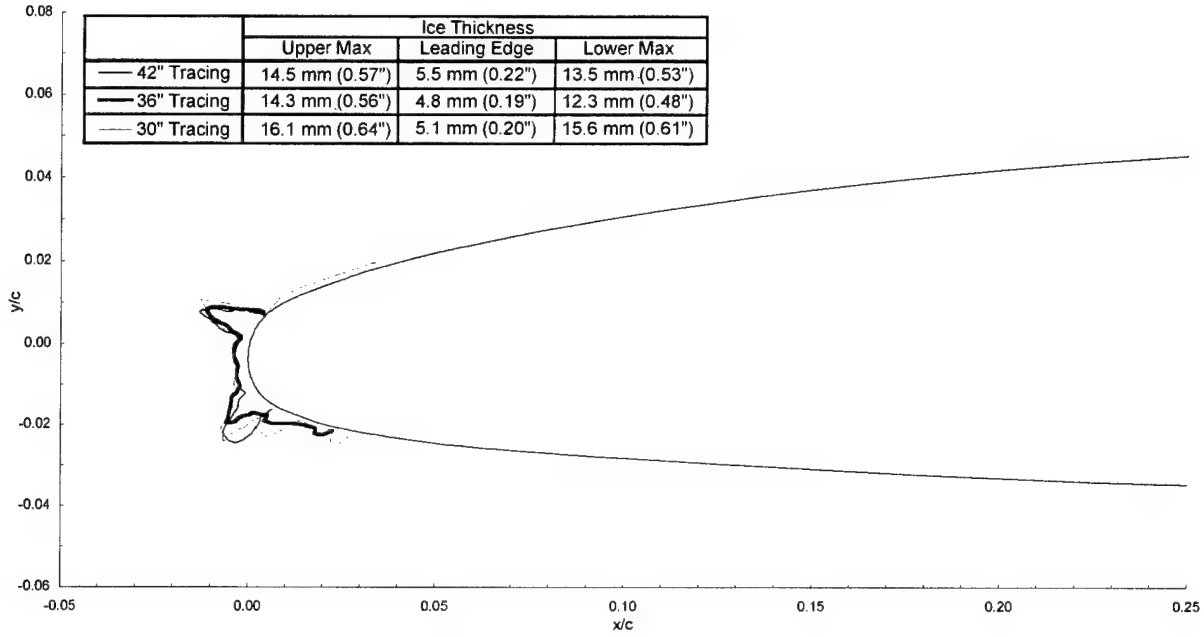

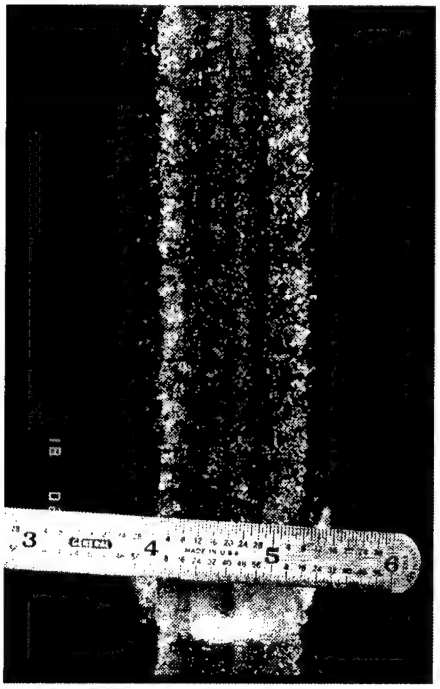

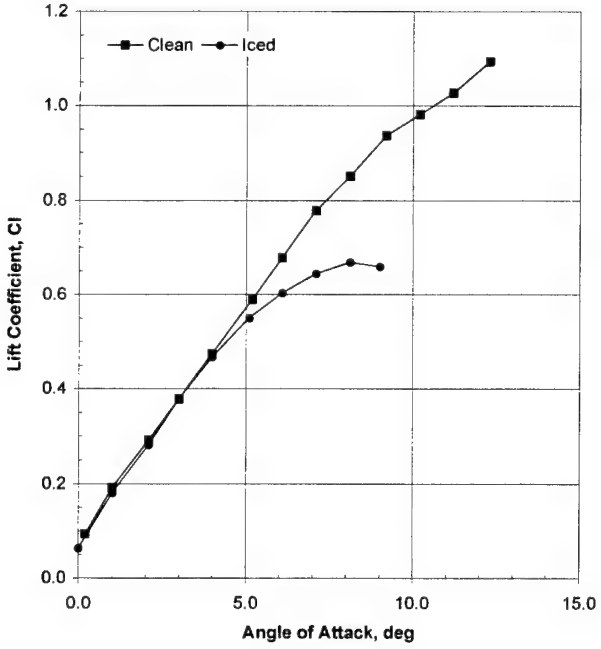

Business Jet - Run 223

T_t = -0.8°C (30°F)
T_s = -5.0°C (22°F)
V = 129 m/s (250 kts)
AOA = 1.5°

LWC = 0.31 g/m^3
MVD = 20 μm
Spray = 2.9 min
chord = 90 cm (36 in)

$C_{d\text{-clean}}$ = 0.0081
$C_{d\text{-iced}}$ = 0.0125
$C_{l\text{-clean}}$ = 0.228
$C_{l\text{-iced}}$ = 0.226

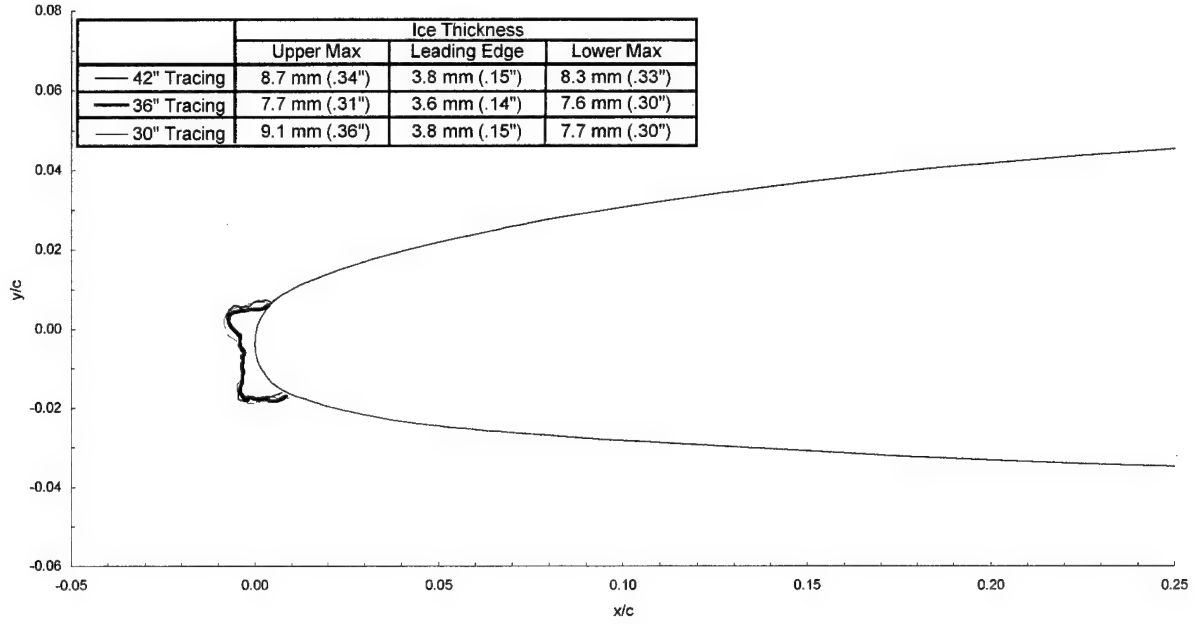

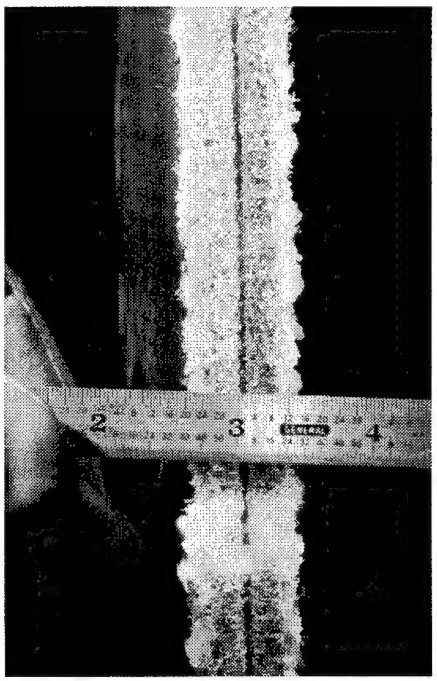

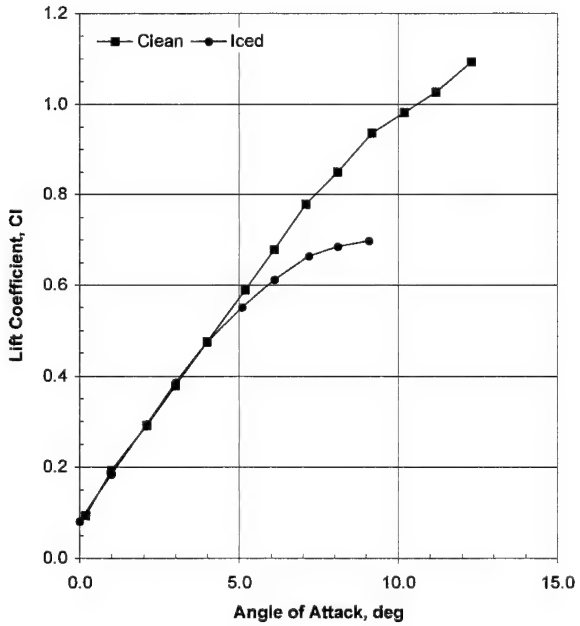

Business Jet - Run 224

T_t = -0.8°C (30°F)
T_s = -5.0°C (22°F)

V = 129 m/s (250 kts)
AOA = 1.5°

LWC = 0.31 g/m^3
MVD = 20 μm
Spray = 5.8 min
chord = 90 cm (36 in)

$C_{d\text{-clean}}$ = 0.0081
$C_{d\text{-iced}}$ = 0.0179

$C_{l\text{-clean}}$ = 0.228
$C_{l\text{-iced}}$ = 0.232

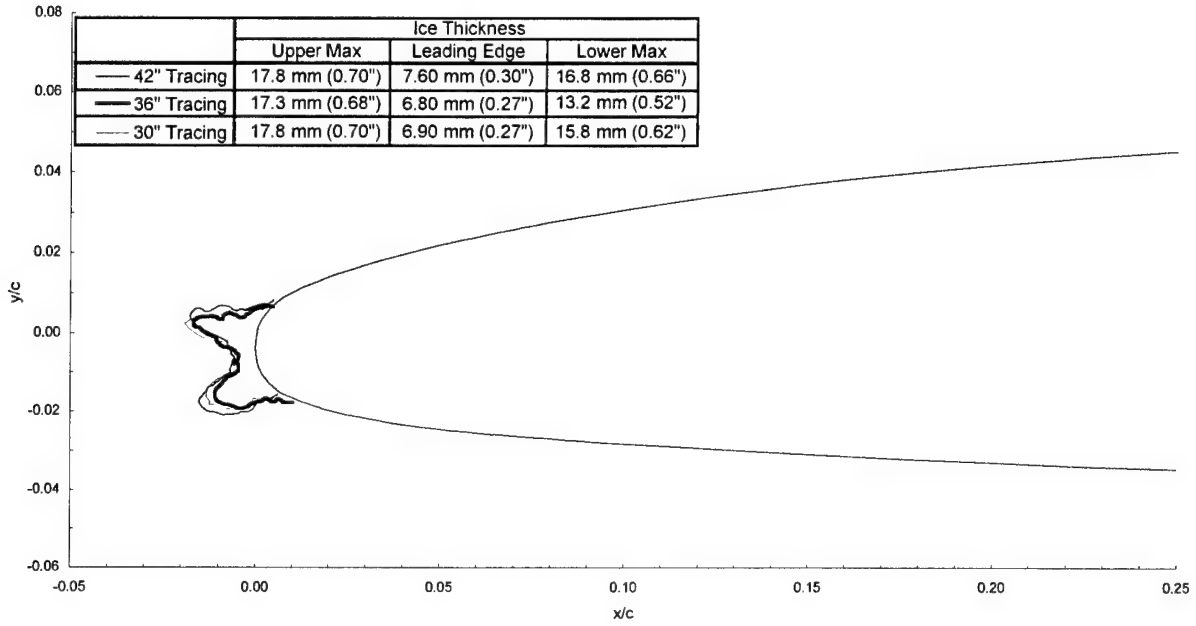

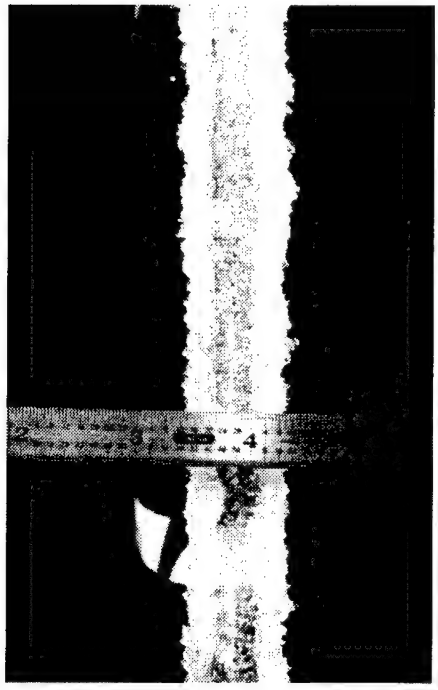

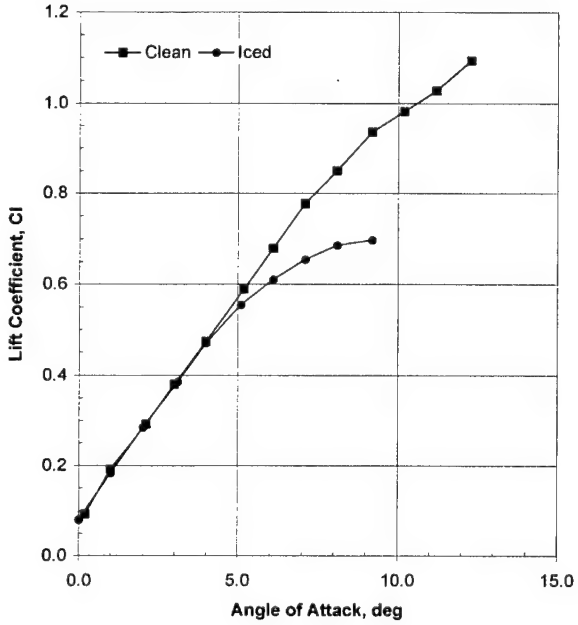

Business Jet - Run 225

T_t = -5.9°C (20.8°F)
T_s = -10.0°C (13.4°F)
V = 129 m/s (250 kts)
AOA = 1.5°

LWC = 0.50 g/m^3
MVD = 15 μm
Spray = 3.6 min
chord = 90 cm (36 in)

$C_{d\text{-}clean}$ = 0.0081
$C_{d\text{-}iced}$ = 0.0096
$C_{l\text{-}clean}$ = 0.228
$C_{l\text{-}iced}$ = 0.217

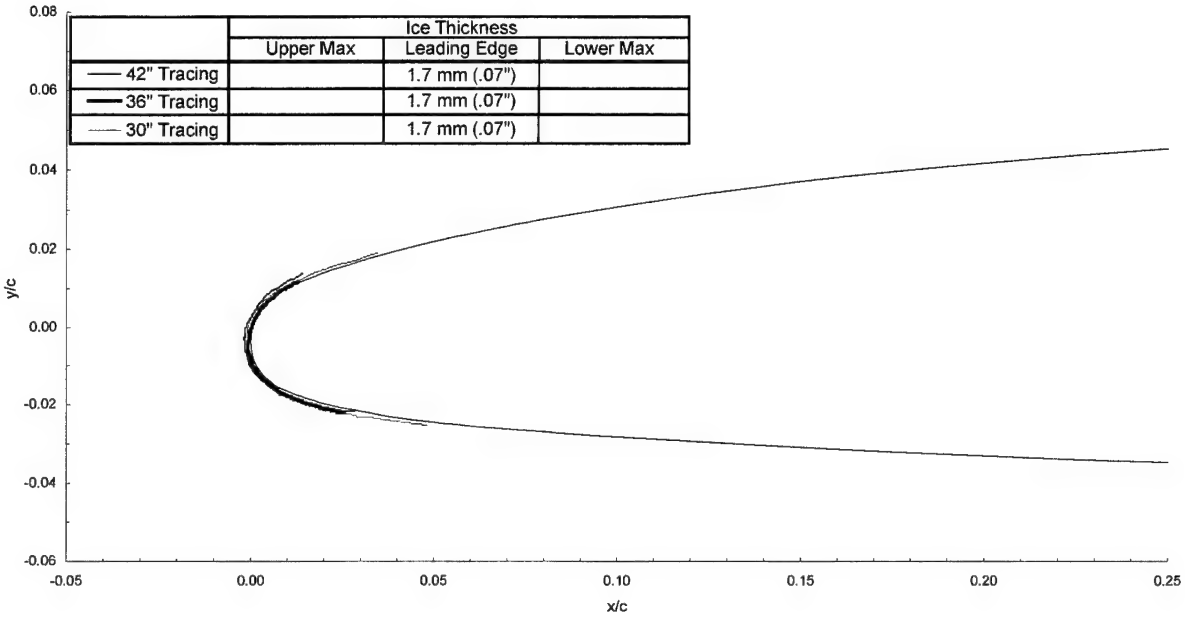

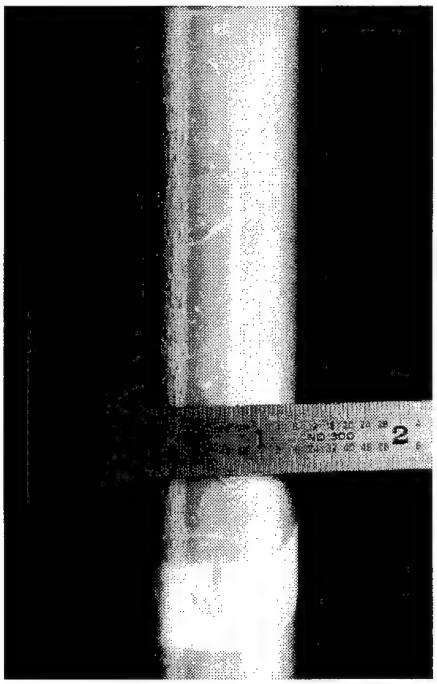

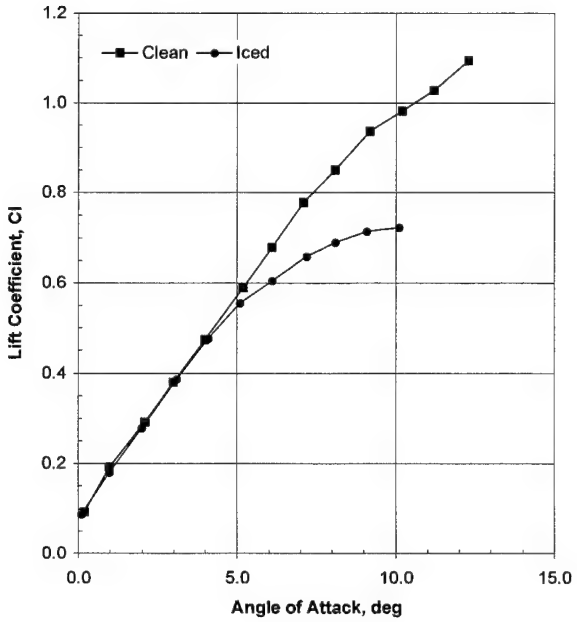

Business Jet - Run 226

T_t = -5.9°C (20.8°F)
T_s = -10.0°C (13.4°F)

V = 129 m/s (250 kts)
AOA = 1.5°

LWC = 0.50 g/m^3
MVD = 15 μm
Spray = 7.2 min
chord = 90 cm (36 in)

$C_{d\text{-clean}}$ = 0.0081
$C_{d\text{-iced}}$ = 0.0113

$C_{l\text{-clean}}$ = 0.228
$C_{l\text{-iced}}$ = 0.227

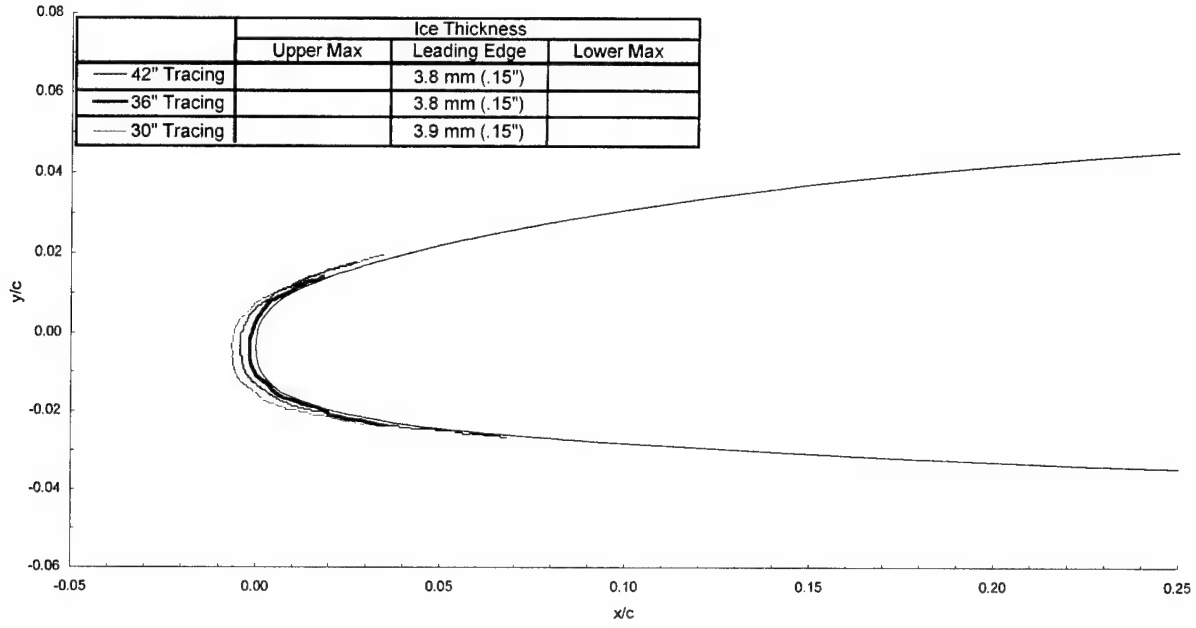

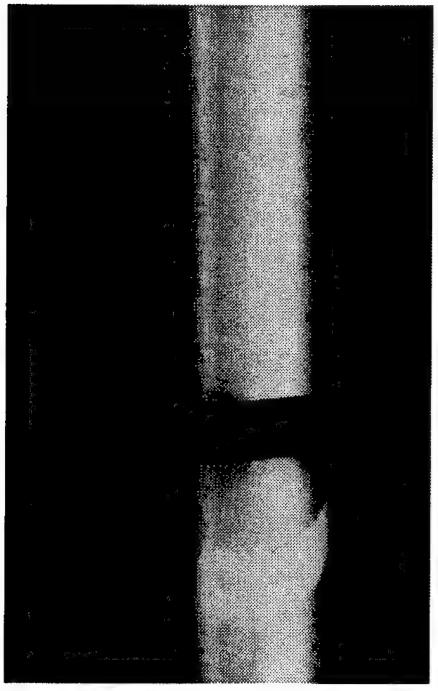

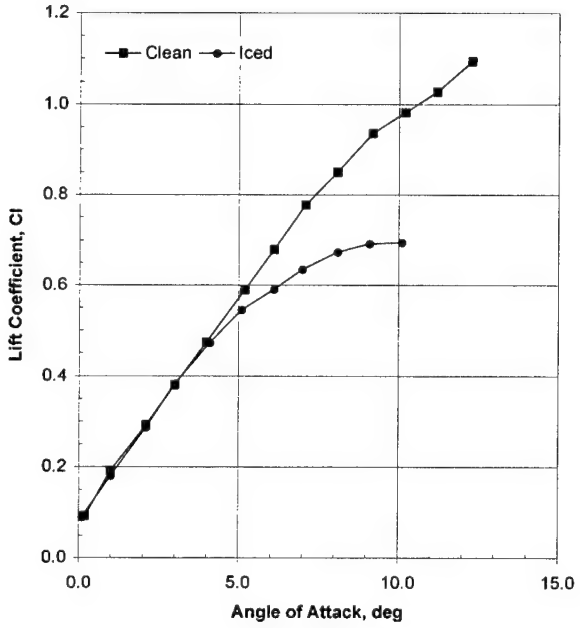

Business Jet - Run 231

T_t = -0.8°C (30°F)
T_s = -5.0°C (22°F)
V = 90.0 m/s (175 kts)
AOA = 4.0°

LWC = 0.54 g/m^3
MVD = 20 μm
Spray = 2.0 min
chord = 90 cm (36 in)

$C_{d\text{-}clean}$ = 0.0086
$C_{d\text{-}iced}$ = 0.0196
$C_{l\text{-}clean}$ = 0.472
$C_{l\text{-}iced}$ = 0.463

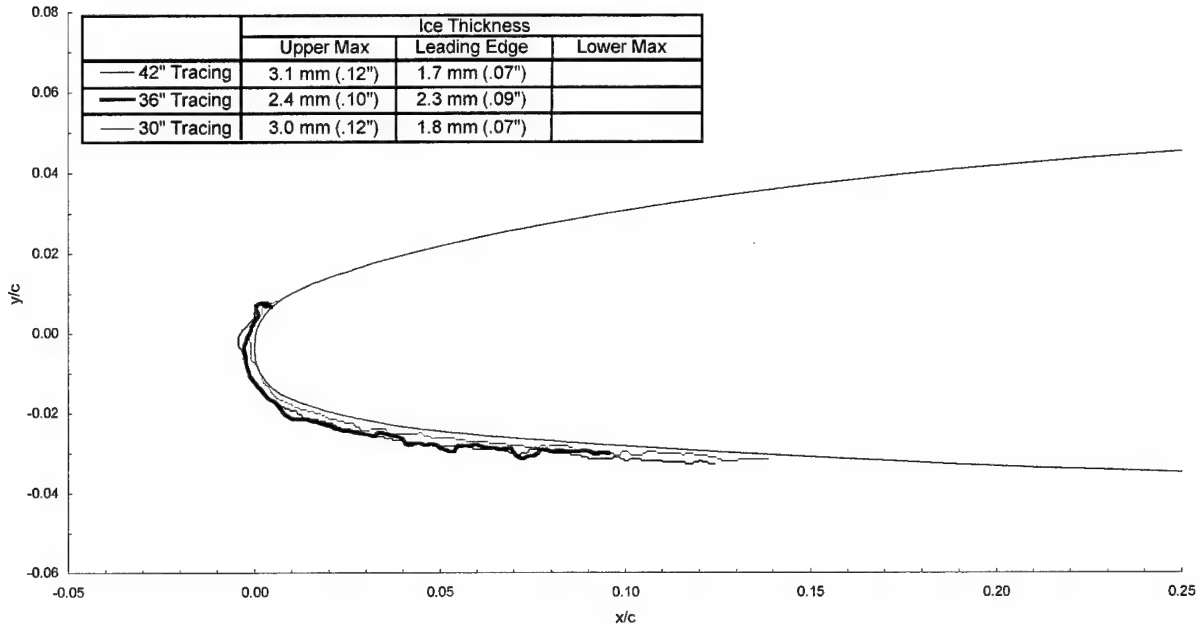

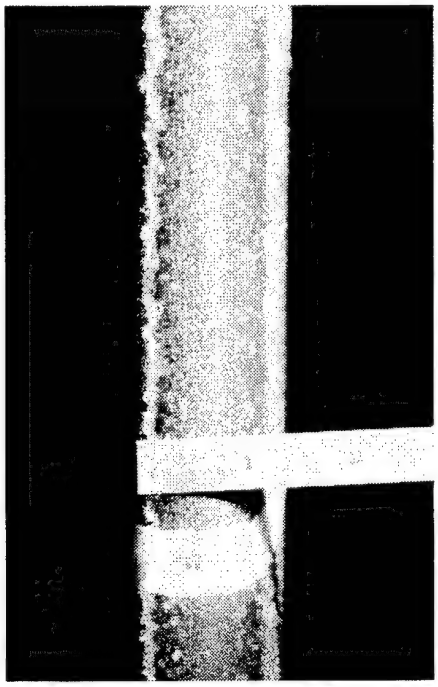

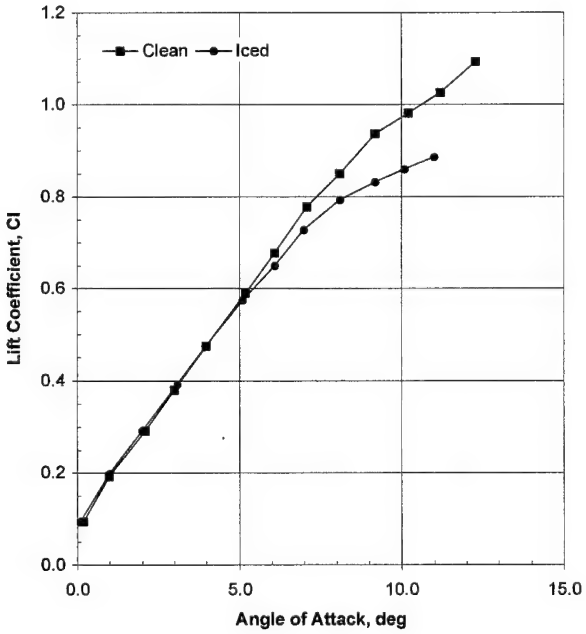

Business Jet - Run 232

T_t = -0.8°C (30°F)
T_s = -5.0°C (22°F)

V = 90.0 m/s (175 kts)
AOA = 4.0°

LWC = 0.54 g/m^3
MVD = 20 μm
Spray = 6.0 min
chord = 90 cm (36 in)

$C_{d\text{-}clean}$ = 0.0086
$C_{d\text{-}iced}$ = 0.0394

$C_{l\text{-}clean}$ = 0.472
$C_{l\text{-}iced}$ = 0.470

	Ice Thickness		
	Upper Max	Leading Edge	Lower Max
42" Tracing	11.3 mm (0.44")	4.50 mm (0.18")	6.30 mm (0.25")
36" Tracing	11.4 mm (0.45")	3.80 mm (0.15")	5.40 mm (0.21")
30" Tracing	11.8 mm (0.47")	5.10 mm (0.20")	5.50 mm (0.22")

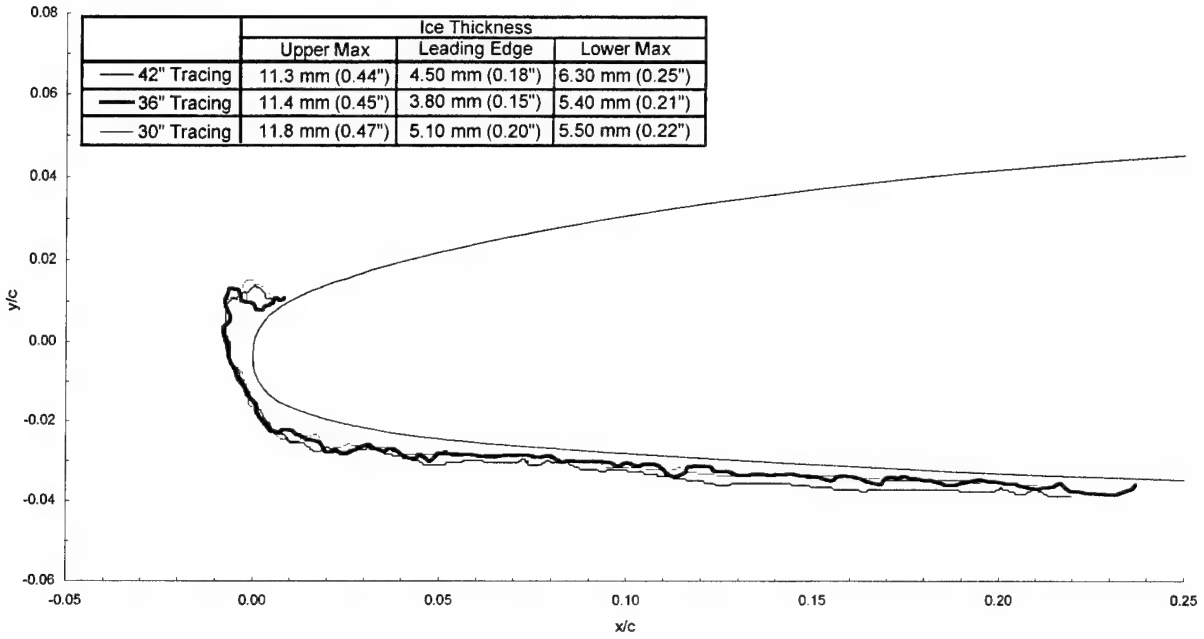

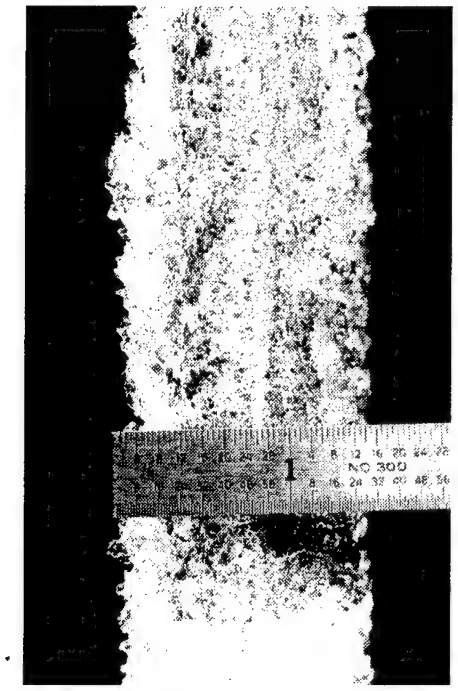

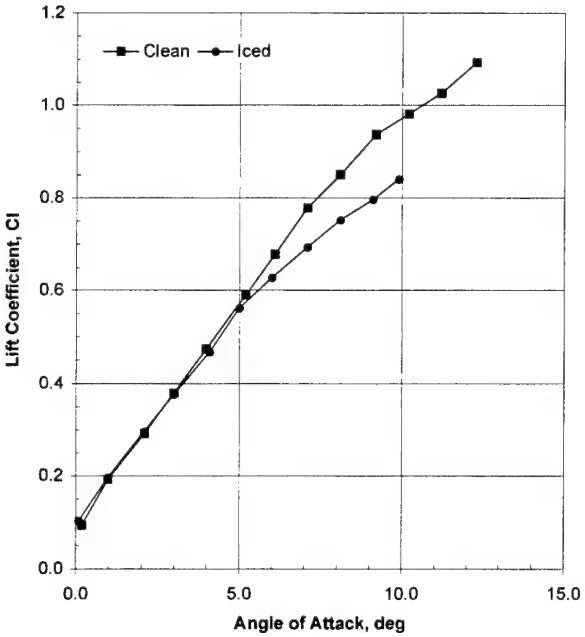

Business Jet - Run 233

T_t = -5.9°C (20.8°F)
T_s = -10.0°C (13.4°F)

V = 90.0 m/s (175 kts)
AOA = 4.0°

LWC = 0.60 g/m^3
MVD = 15 μm
Spray = 2.0 min
chord = 90 cm (36 in)

$C_{d\text{-}clean}$ = 0.0086
$C_{d\text{-}iced}$ = 0.0116

$C_{l\text{-}clean}$ = 0.472
$C_{l\text{-}iced}$ = 0.480

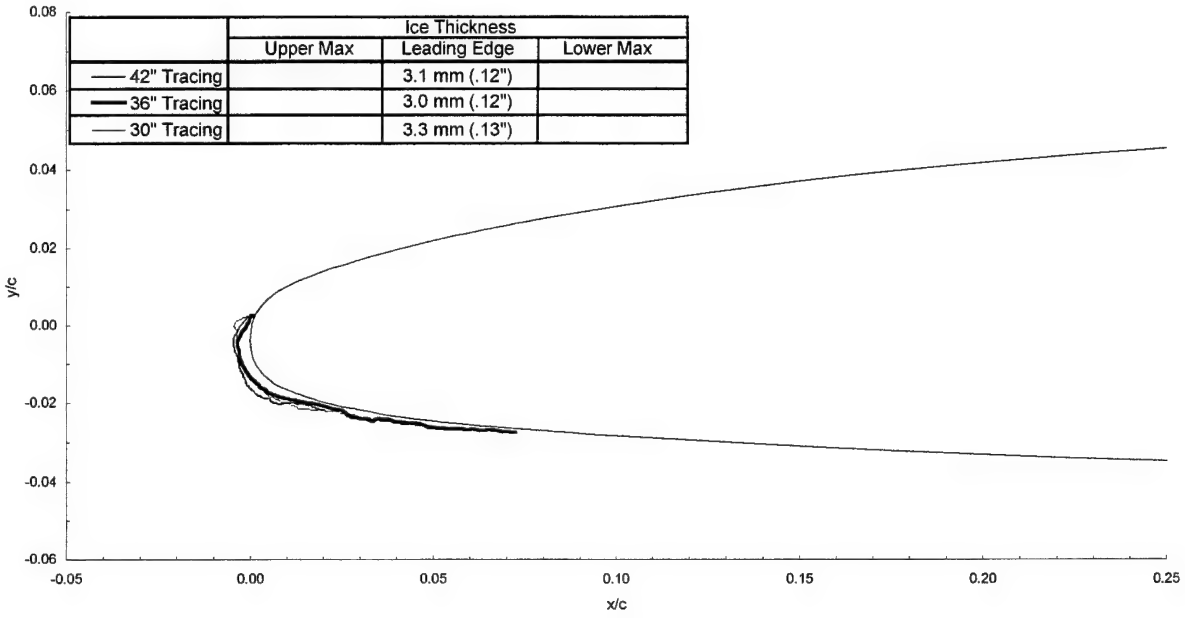

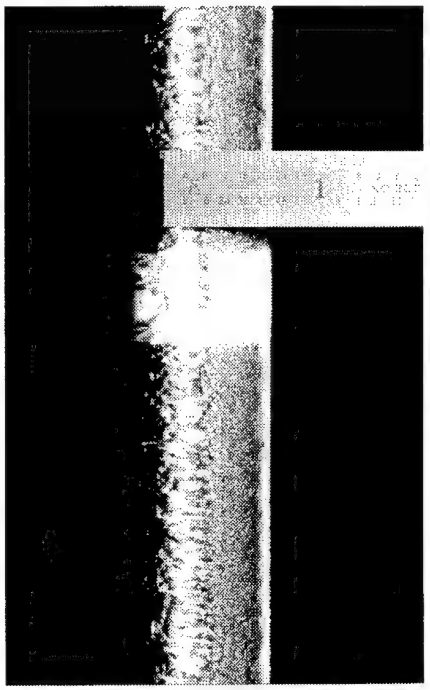

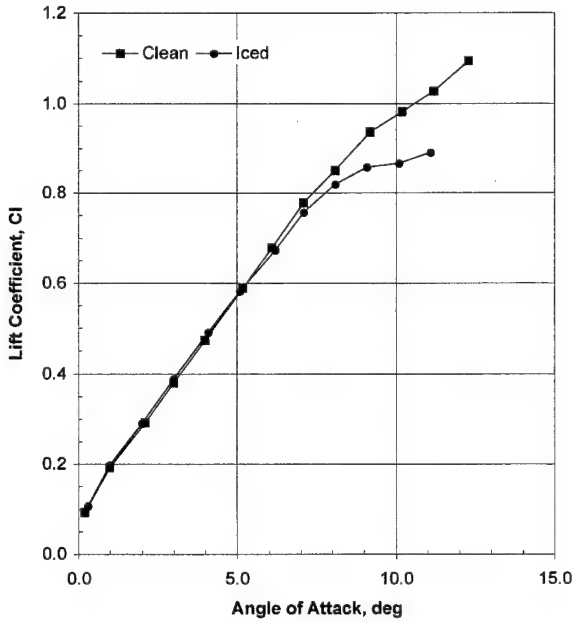

Business Jet - Run 234

T_t = -5.9°C (20.8°F)
T_s = -10.0°C (13.4°F)

V = 90.0 m/s (175 kts)
AOA = 4.0°

LWC = 0.60 g/m^3
MVD = 15 μm
Spray = 6.0 min
chord = 90 cm (36 in)

$C_{d\text{-}clean}$ = 0.0086
$C_{d\text{-}iced}$ = 0.0142

$C_{l\text{-}clean}$ = 0.472
$C_{l\text{-}iced}$ = 0.472

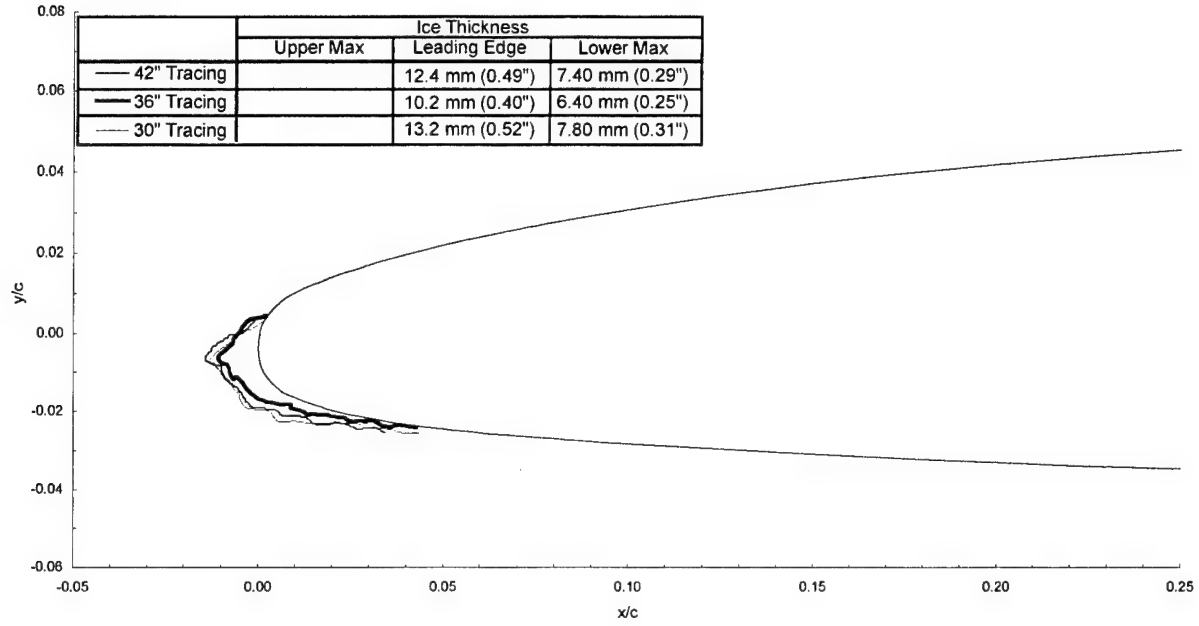

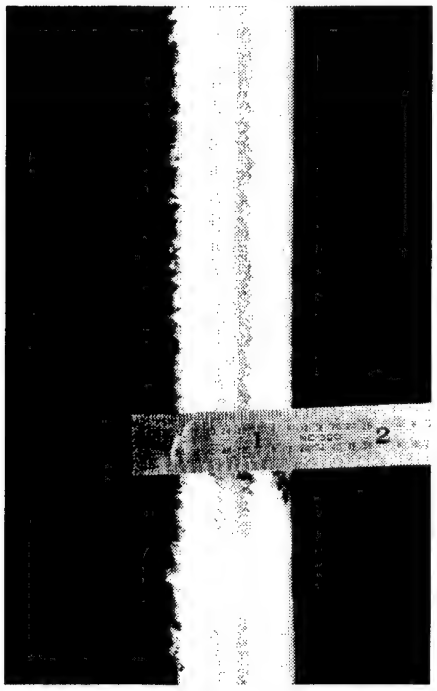

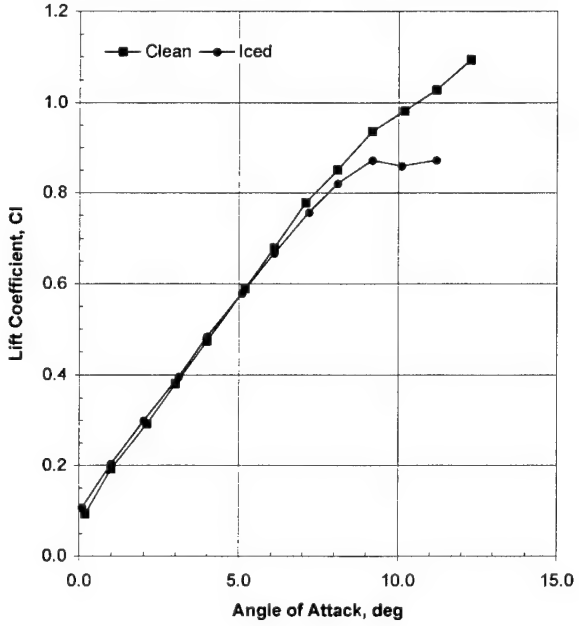

Business Jet - Run 235

T_t = -5.9°C (20.8°F)
T_s = -10.0°C (13.4°F)
V = 90.0 m/s (175 kts)
AOA = 4.0°

LWC = 0.535 g/m^3
MVD = 40 μm
Spray = 1.1 min
chord = 90 cm (36 in)

$C_{d\text{-}clean}$ = 0.0086
$C_{d\text{-}iced}$ = 0.0.132
$C_{l\text{-}clean}$ = 0.472
$C_{l\text{-}iced}$ = 0.467

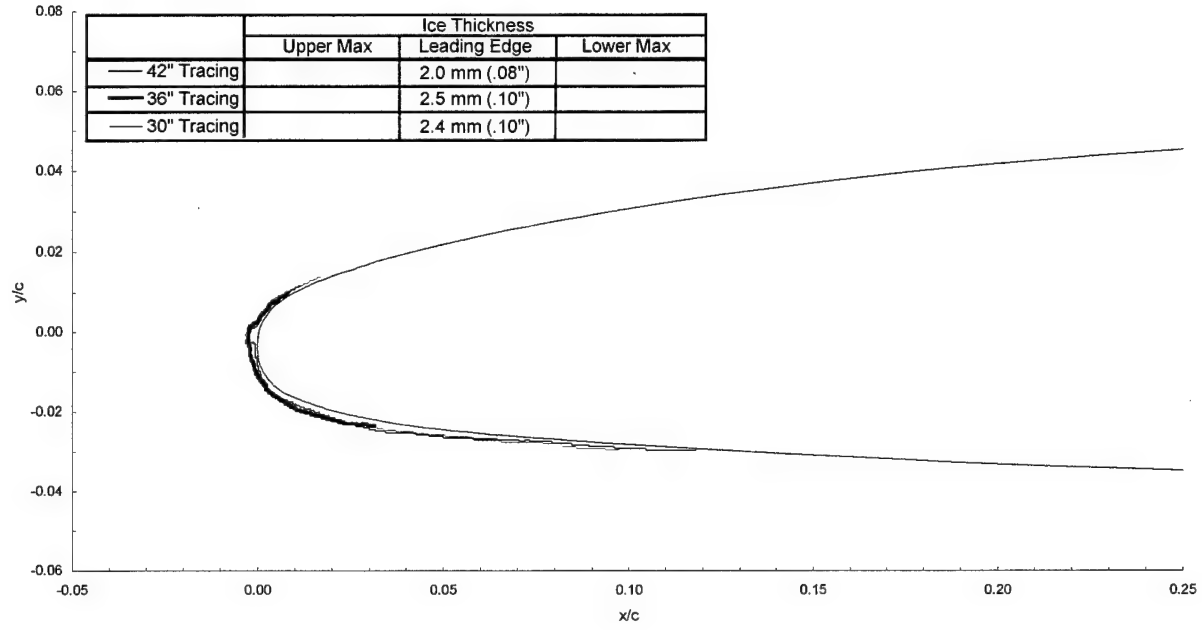

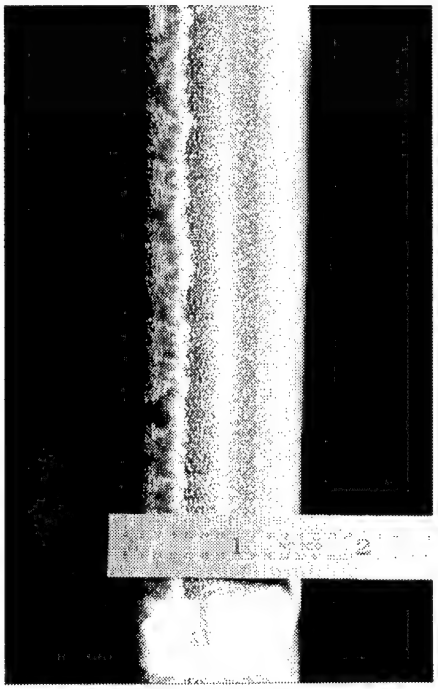

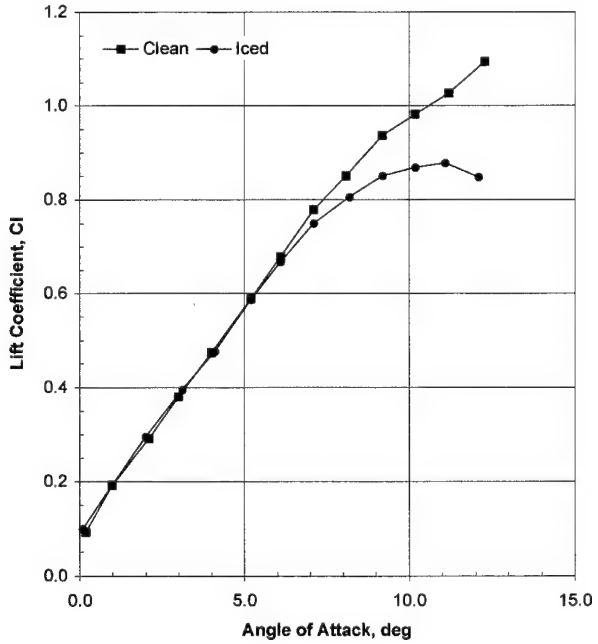

Business Jet - Run 236

T_t = -5.9°C (20.8°F)
T_s = -10.0°C (13.4°F)

V = 90.0 m/s (175 kts)
AOA = 4.0°

LWC = 0.535 g/m^3
MVD = 40 μm
Spray = 4.2 min
chord = 90 cm (36 in)

$C_{d\text{-}clean}$ = 0.0086
$C_{d\text{-}iced}$ = 0.0252

$C_{l\text{-}clean}$ = 0.472
$C_{l\text{-}iced}$ = 0.455

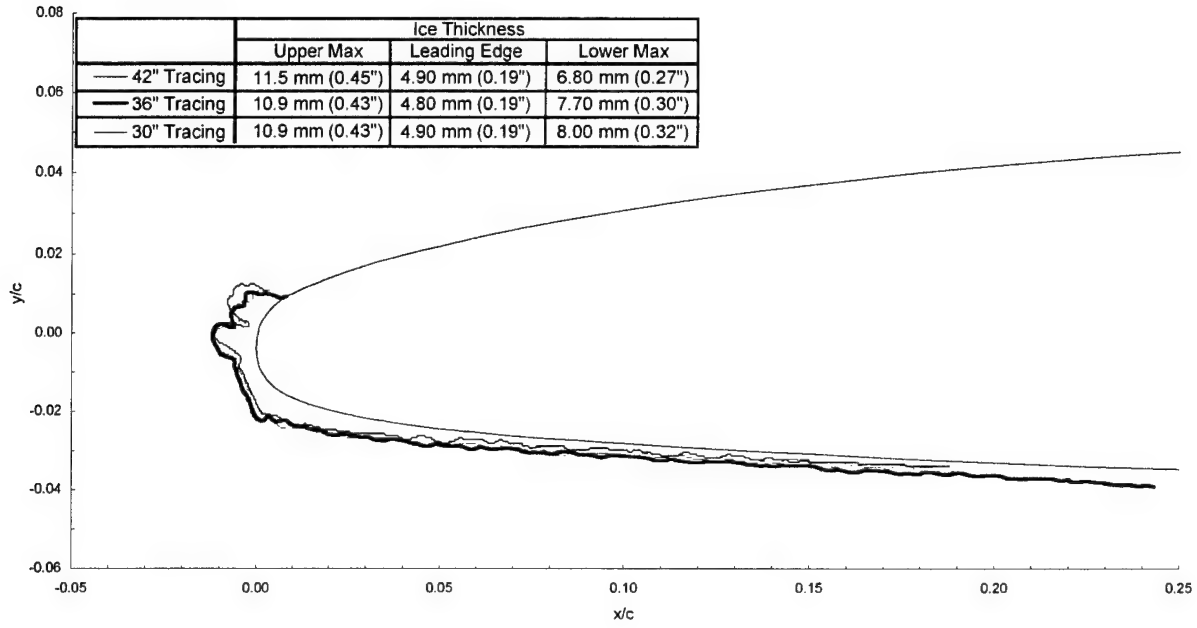

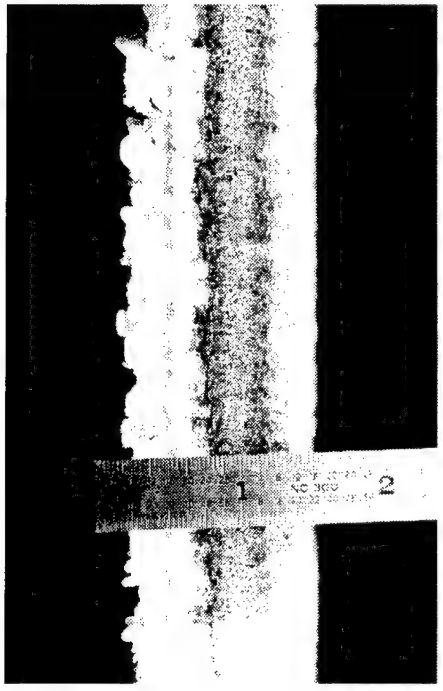

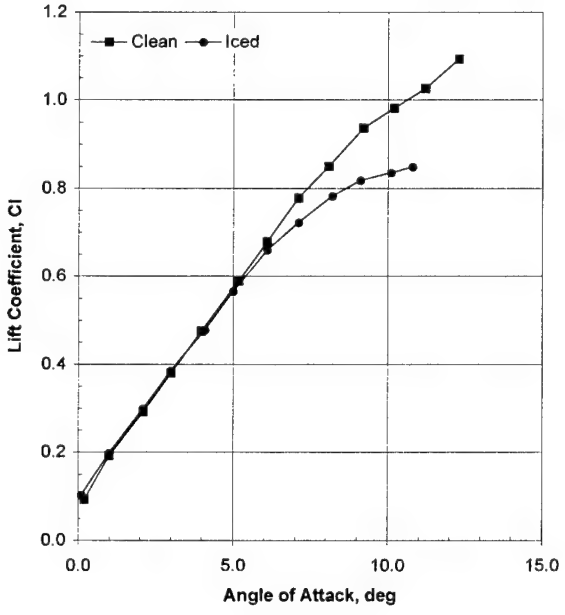

Business Jet - Run 237

T_t = -11.0°C (11.7°F)
T_s = -15°C (4.4°F)
V = 90.0 m/s (175 kts)
AOA = 4.0°

LWC = 0.405 g/m^3
MVD = 20 μm
Spray = 1.5 min
chord = 90 cm (36 in)

$C_{d\text{-}clean}$ = 0.0086
$C_{d\text{-}iced}$ = 0.0113
$C_{l\text{-}clean}$ = 0.472
$C_{l\text{-}iced}$ = 0.462

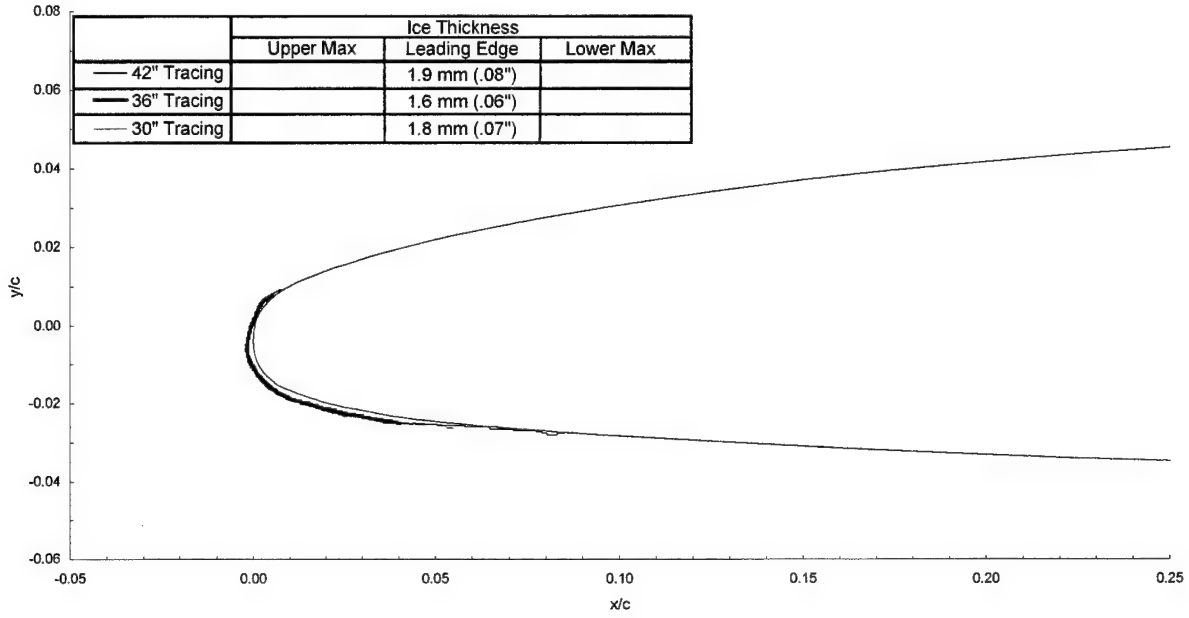

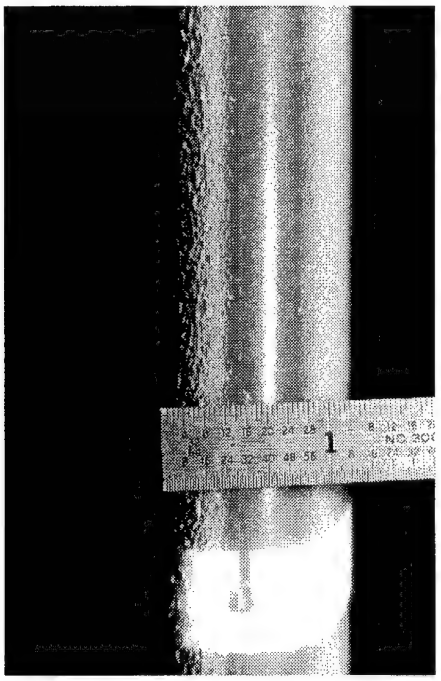

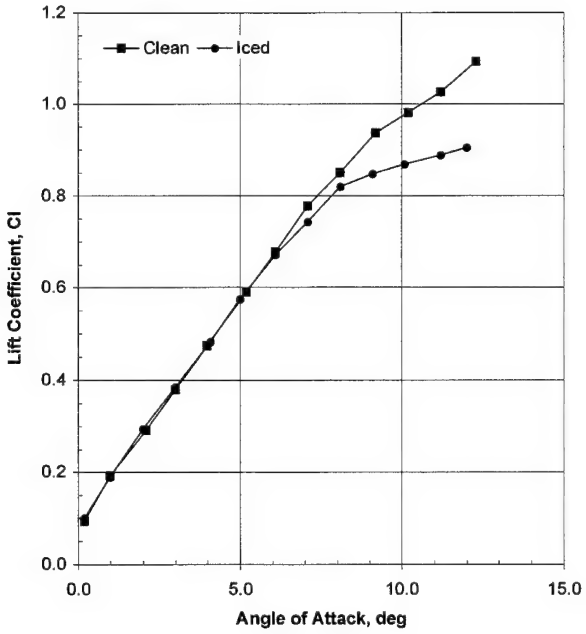

Business Jet - Run 238

T_t = -11.0°C (11.7°F)
T_s = -15°C (4.4°F)

V = 90.0 m/s (175 kts)
AOA = 4.0°

LWC = 0.405 g/m^3
MVD = 20 μm
Spray = 4.4 min
chord = 90 cm (36 in)

$C_{d\text{-}clean}$ = 0.0086
$C_{d\text{-}iced}$ = 0.0169

$C_{l\text{-}clean}$ = 0.472
$C_{l\text{-}iced}$ = 0.453

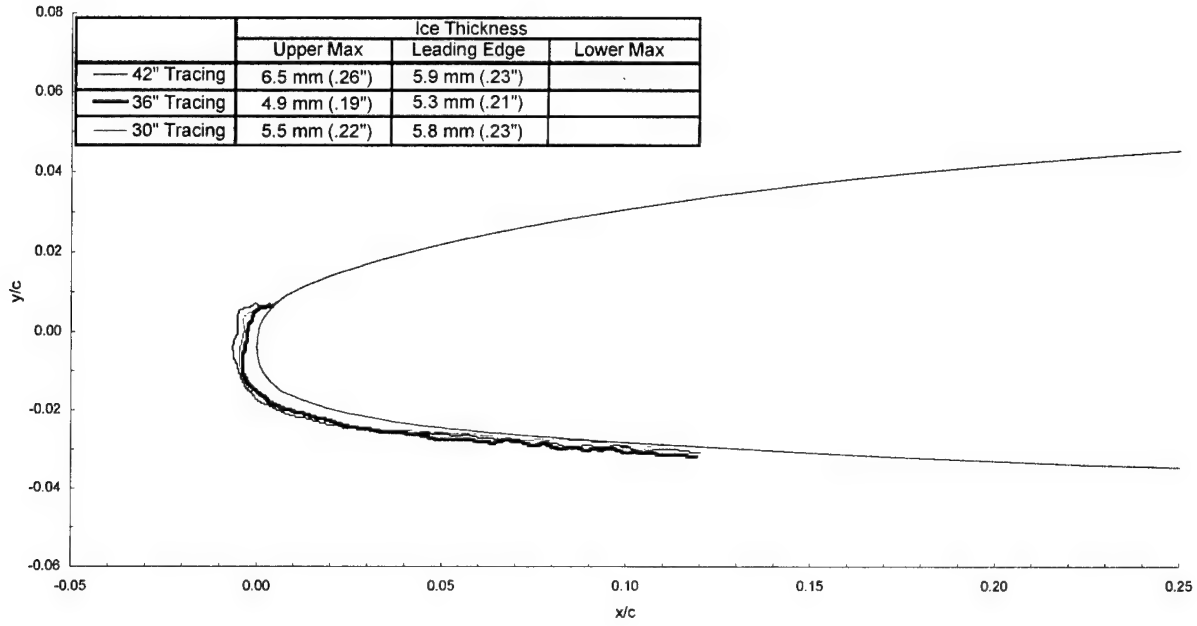

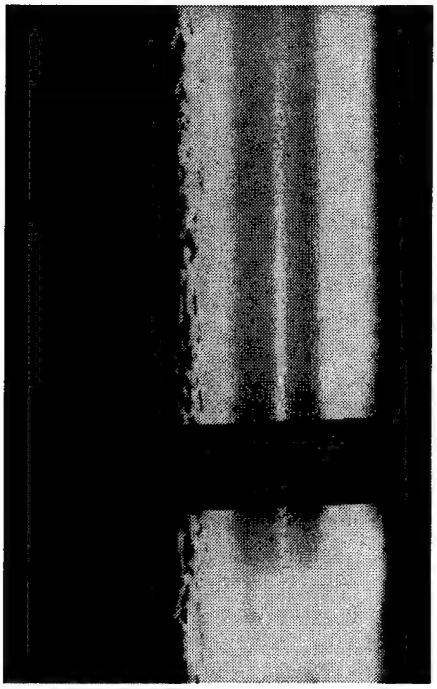

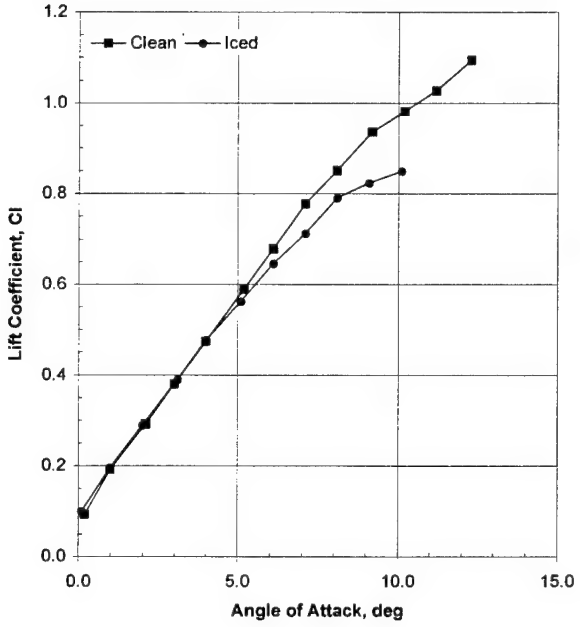

Appendix D3
Test Results, Commercial Transport

Commercial Transport - Run 101

T_t = 0.0°C (32°F)
T_s = -10°C (13°F)
V = 146 m/s (284 kts)
AOA = 0.7°

LWC = 0.41 g/m^3
MVD = 20 μm
Spray = 6.0 min
chord = 90 cm (36 in)

$C_{l\text{-clean}}$ = 0.097
$C_{l\text{-iced}}$ = 0.100

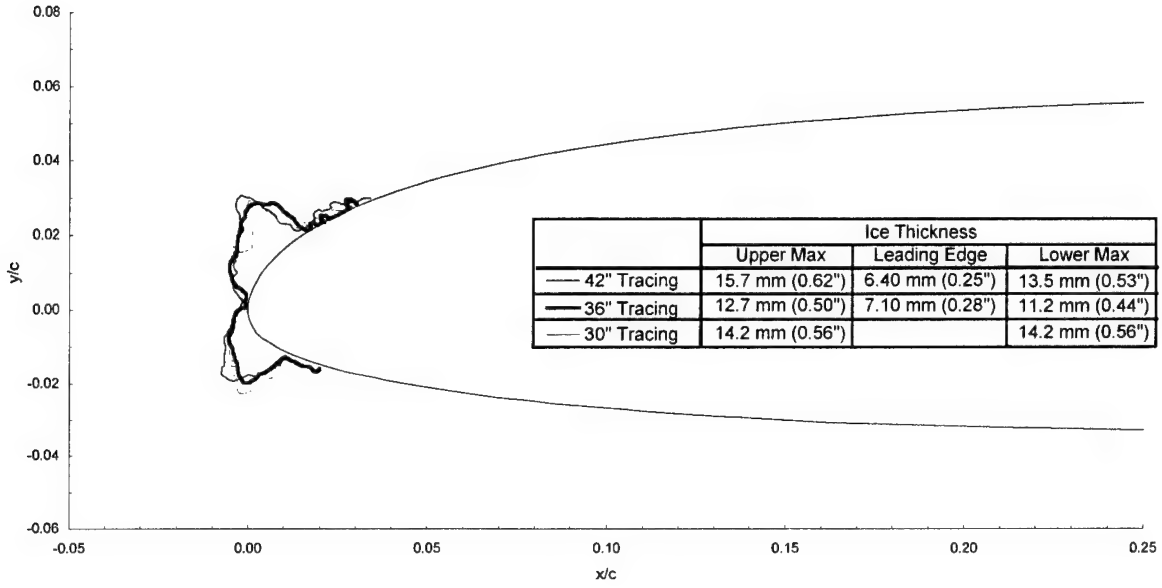

	Ice Thickness		
	Upper Max	Leading Edge	Lower Max
42" Tracing	15.7 mm (0.62")	6.40 mm (0.25")	13.5 mm (0.53")
36" Tracing	12.7 mm (0.50")	7.10 mm (0.28")	11.2 mm (0.44")
30" Tracing	14.2 mm (0.56")		14.2 mm (0.56")

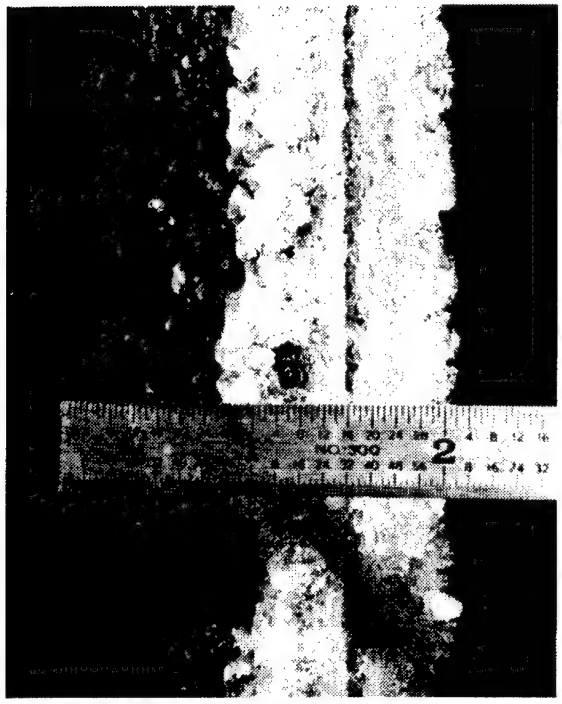

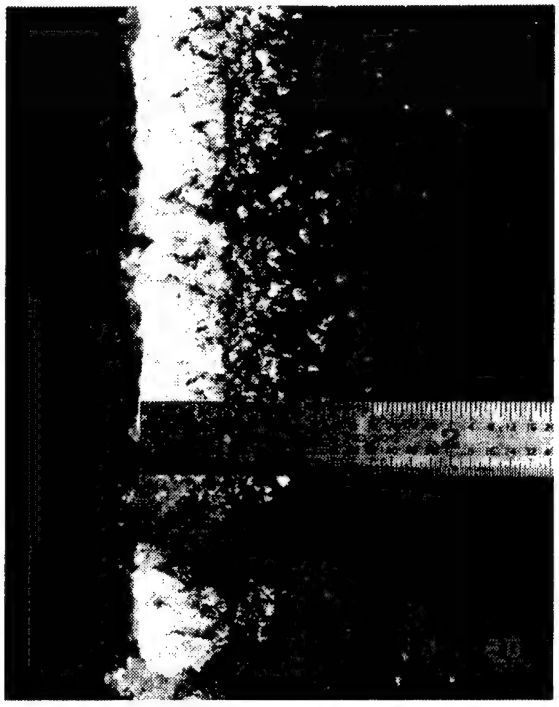

Commercial Transport - Run 102

T_t = 0.0°C (32°F)
T_s = -10°C (13°F)
V = 129 m/s (250 kts)
AOA = 0.7°

LWC = 0.46 g/m^3
MVD = 20 μm
Spray = 6.0 min
chord = 90 cm (36 in)

$C_{l\text{-clean}}$ = 0.097
$C_{l\text{-iced}}$ = 0.090

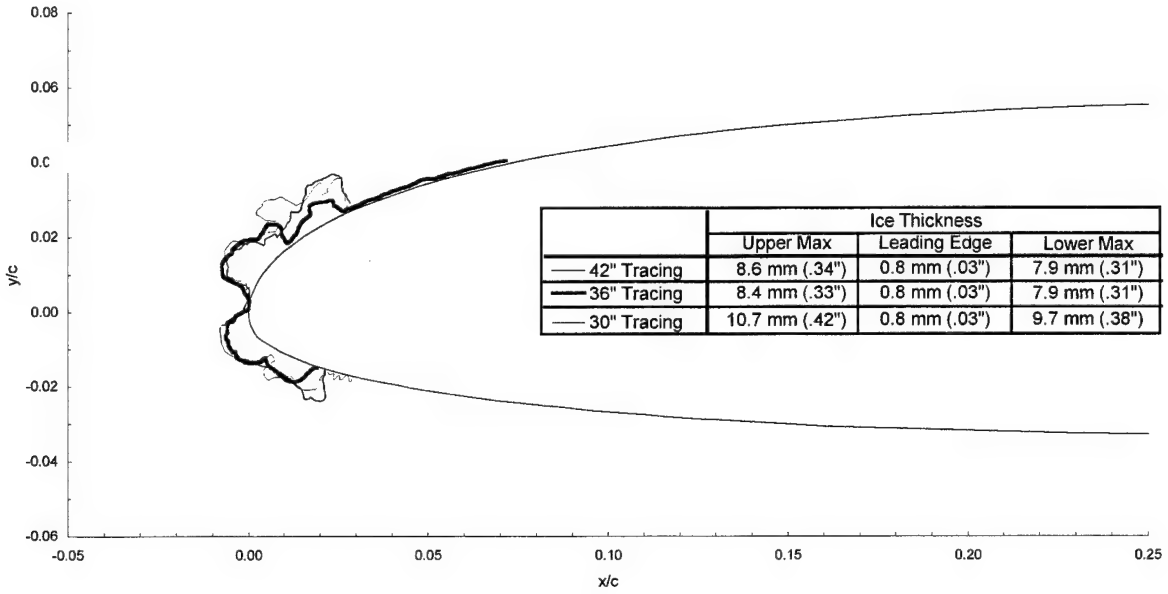

	Ice Thickness		
	Upper Max	Leading Edge	Lower Max
42" Tracing	8.6 mm (.34")	0.8 mm (.03")	7.9 mm (.31")
36" Tracing	8.4 mm (.33")	0.8 mm (.03")	7.9 mm (.31")
30" Tracing	10.7 mm (.42")	0.8 mm (.03")	9.7 mm (.38")

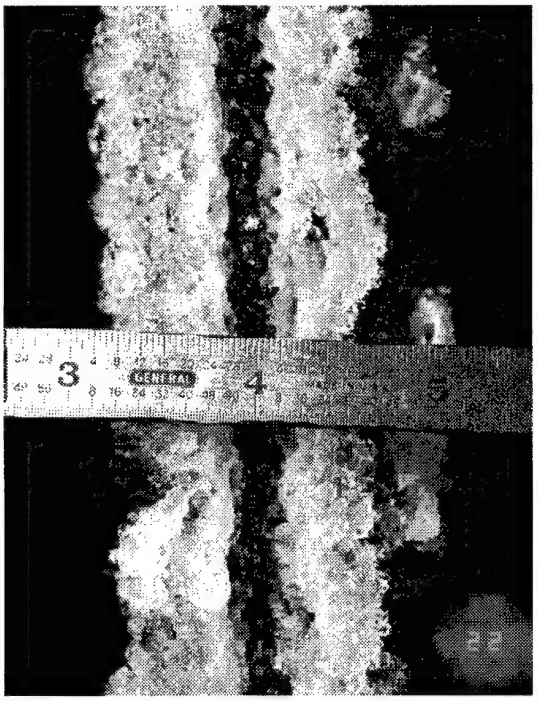

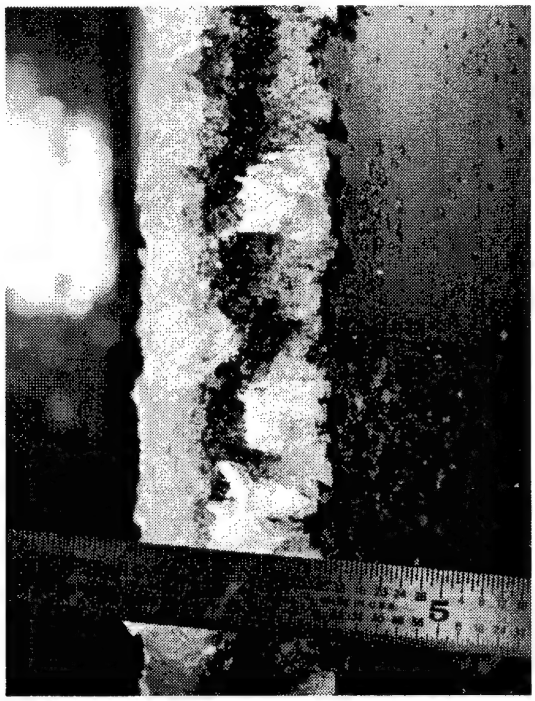

Commercial Transport - Run 103

T_t = 0.0°C (32°F)
T_s = -10°C (13°F)
V = 129 m/s (250 kts)
AOA = 0.7°

LWC = 0.46 g/m^3
MVD = 20 μm
Spray = 22.5 min
chord = 90 cm (36 in)

$C_{l\text{-clean}}$ = 0.097
$C_{l\text{-iced}}$ = 0.083

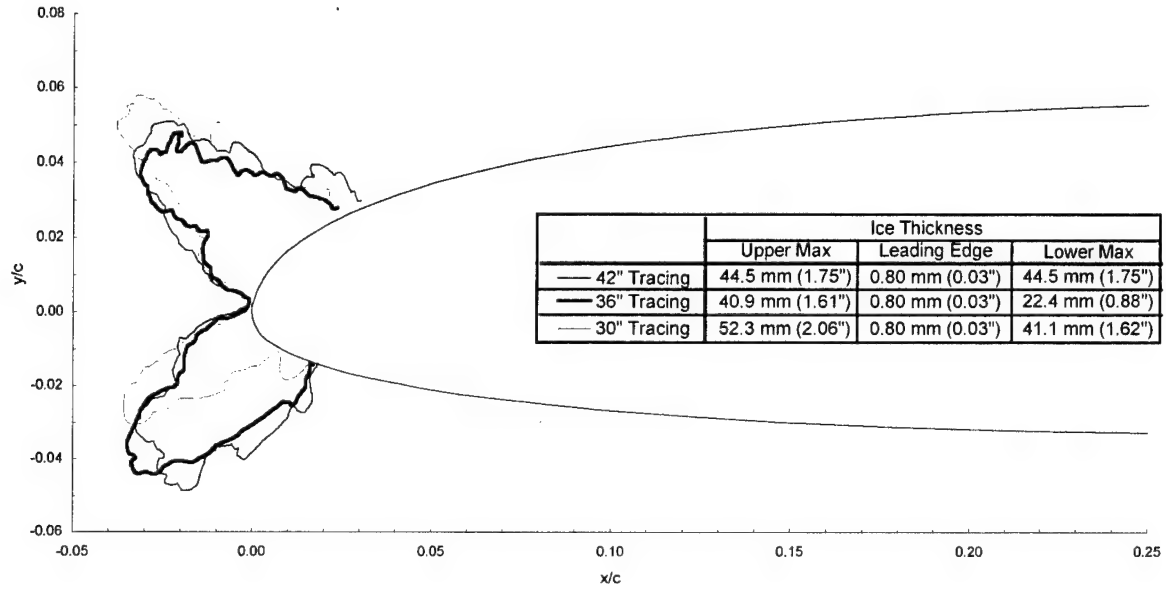

	Ice Thickness		
	Upper Max	Leading Edge	Lower Max
42" Tracing	44.5 mm (1.75")	0.80 mm (0.03")	44.5 mm (1.75")
36" Tracing	40.9 mm (1.61")	0.80 mm (0.03")	22.4 mm (0.88")
30" Tracing	52.3 mm (2.06")	0.80 mm (0.03")	41.1 mm (1.62")

Commercial Transport - Run 104

T_t = -12.0°C (10.5°F)
T_s = -20°C (4.0°F)
V = 128 m/s (248 kts)
AOA = 1.7°

LWC = 0.339 g/m^3
MVD = 15 μm
Spray = 5.9 min
chord = 90 cm (36 in)

$C_{l\text{-clean}}$ = 0.215
$C_{l\text{-iced}}$ = 0.211

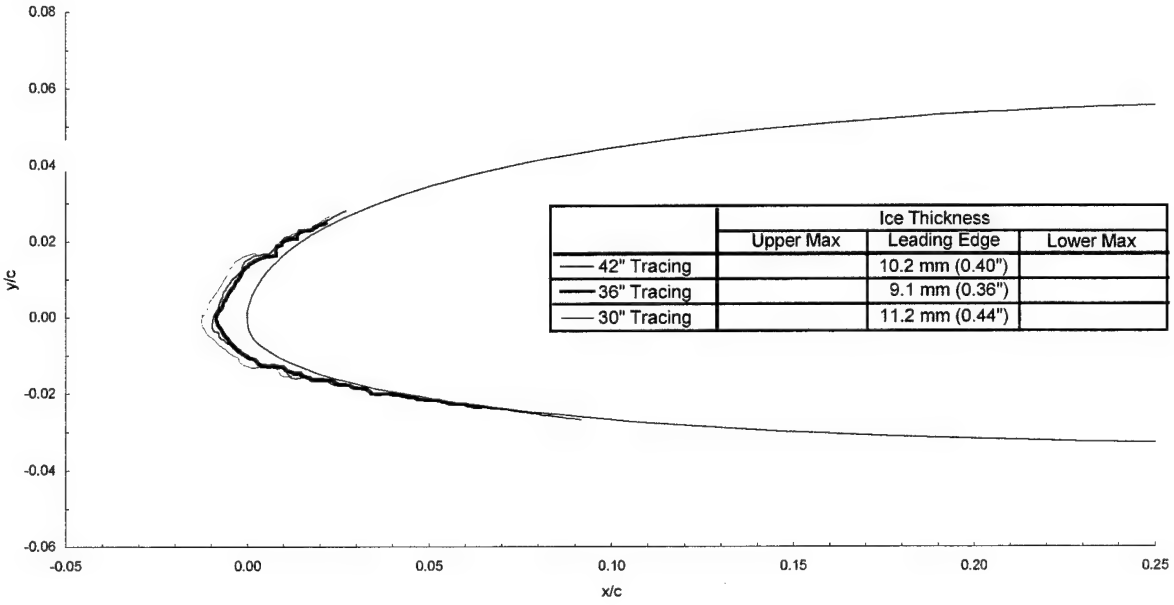

	Ice Thickness		
	Upper Max	Leading Edge	Lower Max
42" Tracing		10.2 mm (0.40")	
36" Tracing		9.1 mm (0.36")	
30" Tracing		11.2 mm (0.44")	

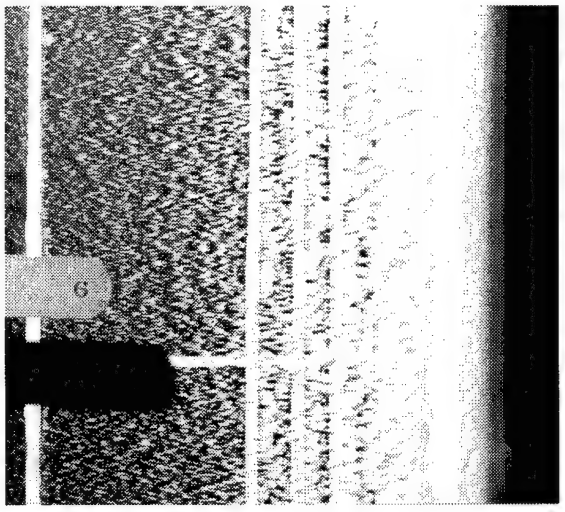

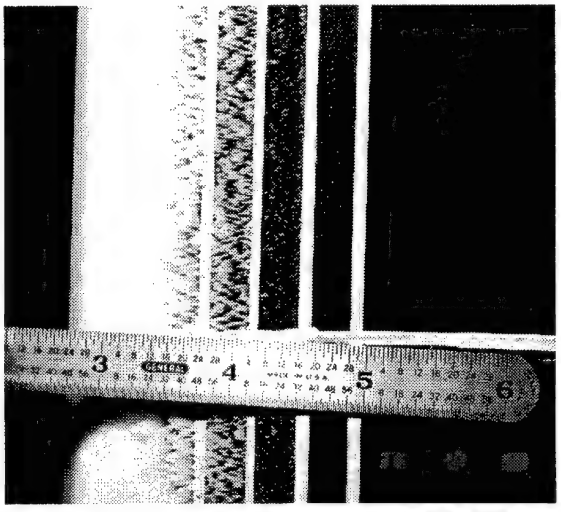

Commercial Transport - Run 105

T_t = -12.0°C (10.5°F)
T_s = -20°C (-4.0°F)
V = 128 m/s (248 kts)
AOA = 1.7°

LWC = 0.339 g/m^3
MVD = 15 μm
Spray = 22 min
chord = 90 cm (36 in)

$C_{l\text{-clean}}$ = 0.215
$C_{l\text{-iced}}$ = 0.209

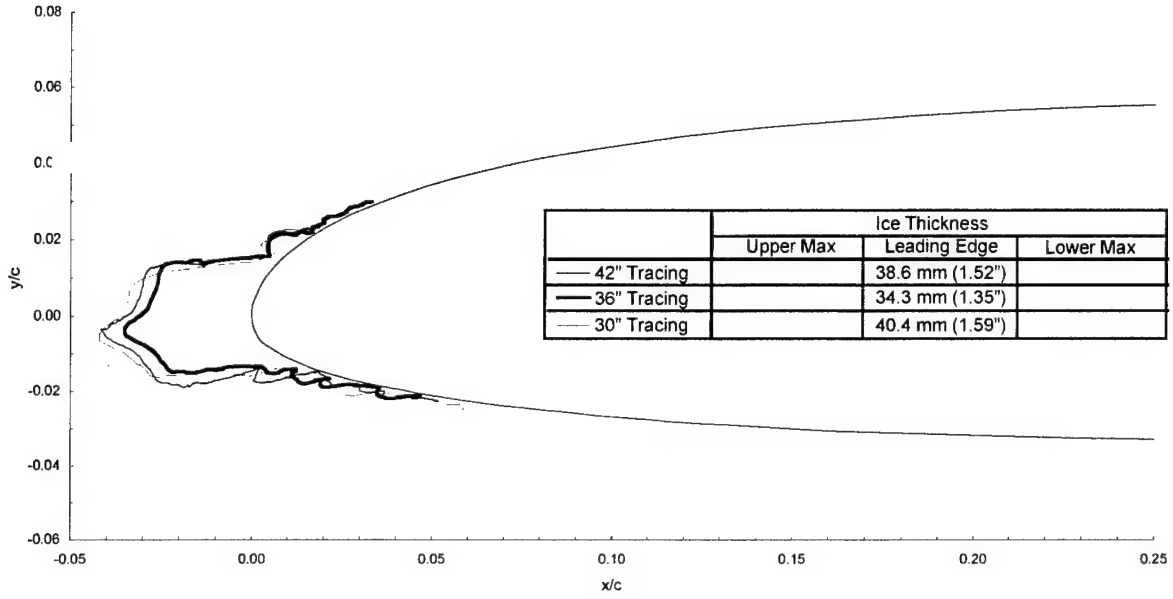

	Ice Thickness		
	Upper Max	Leading Edge	Lower Max
42" Tracing		38.6 mm (1.52")	
36" Tracing		34.3 mm (1.35")	
30" Tracing		40.4 mm (1.59")	

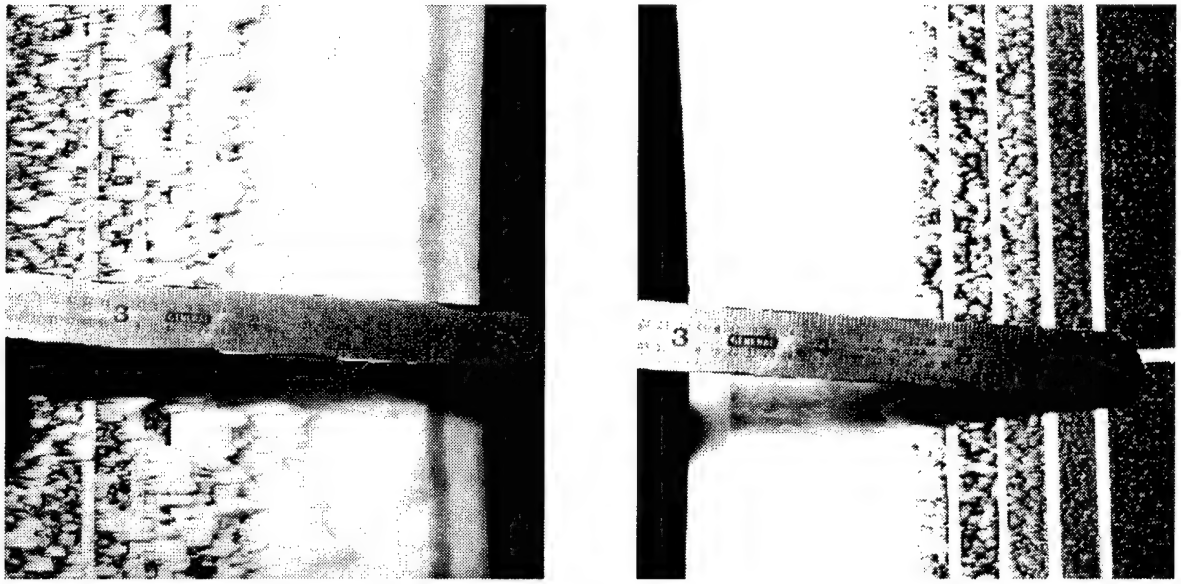

Commercial Transport - Run 106

T_t = -12.0°C (10.5°F)
T_s = -20°C (-4.0°F)
V = 128 m/s (248 kts)
AOA = 0.7°

LWC = 0.339 g/m^3
MVD = 15 μm
Spray = 5.9 min
chord = 90 cm (36 in)

$C_{d\text{-}clean}$ = 0.0085
$C_{d\text{-}iced}$ = 0.0120
$C_{l\text{-}clean}$ = 0.097
$C_{l\text{-}iced}$ = 0.100

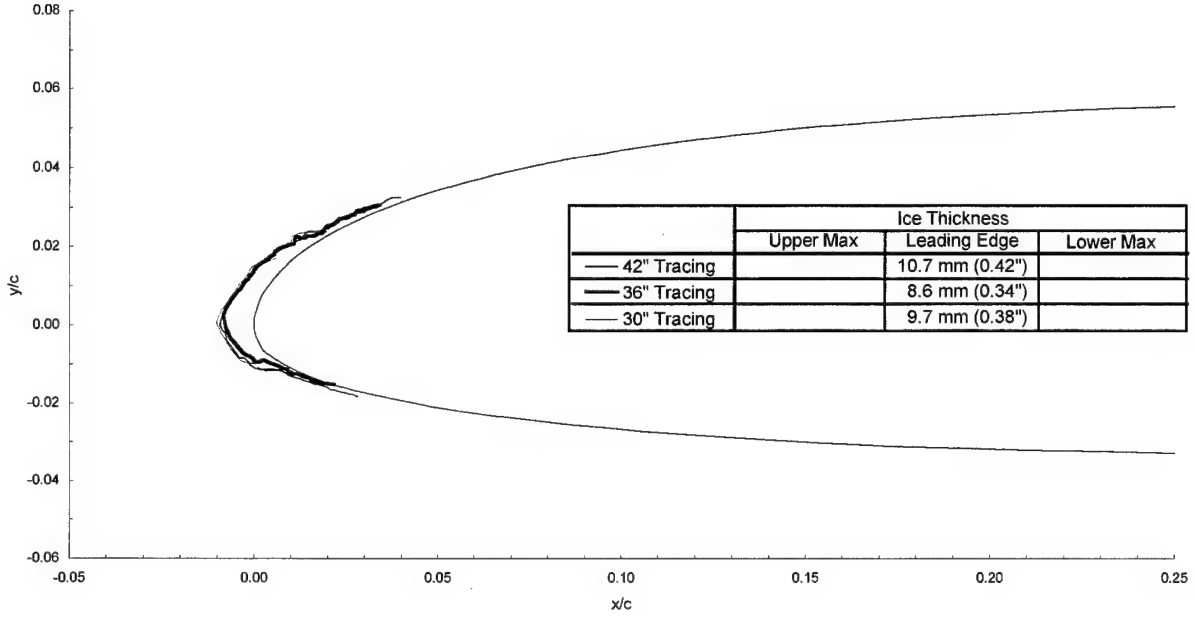

	Ice Thickness		
	Upper Max	Leading Edge	Lower Max
42" Tracing		10.7 mm (0.42")	
36" Tracing		8.6 mm (0.34")	
30" Tracing		9.7 mm (0.38")	

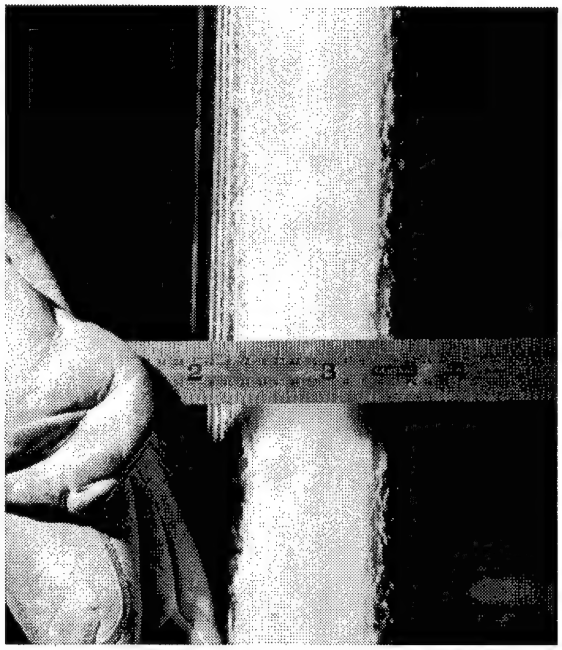

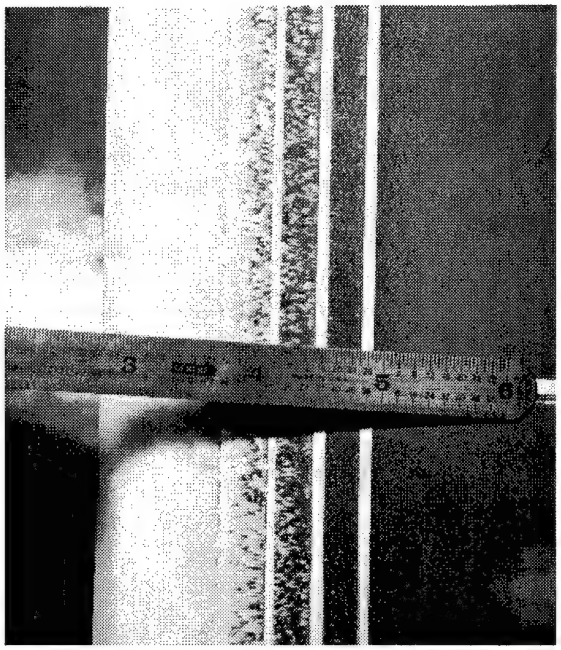

Commercial Transport - Run 106r1

T_t = -12.0°C (10.5°F)
T_s = -20°C (-4.0°F)

V = 128 m/s (248 kts)
AOA = 0.7°

LWC = 0.339 g/m^3
MVD = 15 μm
Spray = 5.9 min
chord = 90 cm (36 in)

$C_{d\text{-clean}}$ = 0.0085
$C_{d\text{-iced}}$ = 0.0120

$C_{l\text{-clean}}$ = 0.097
$C_{l\text{-iced}}$ = 0.099

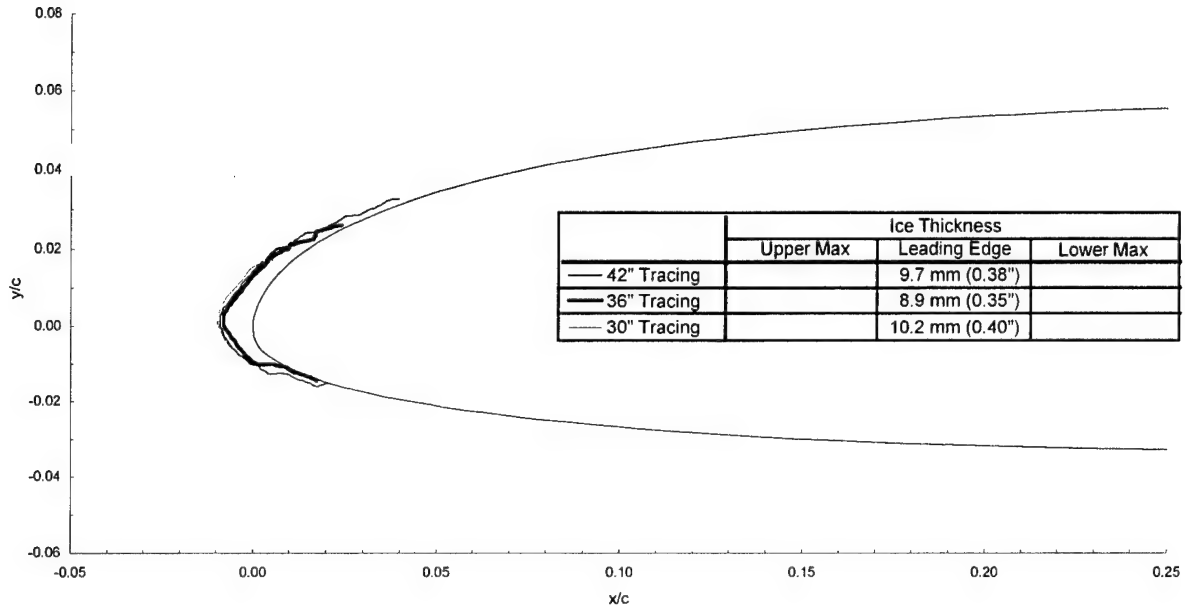

	Ice Thickness		
	Upper Max	Leading Edge	Lower Max
42" Tracing		9.7 mm (0.38")	
36" Tracing		8.9 mm (0.35")	
30" Tracing		10.2 mm (0.40")	

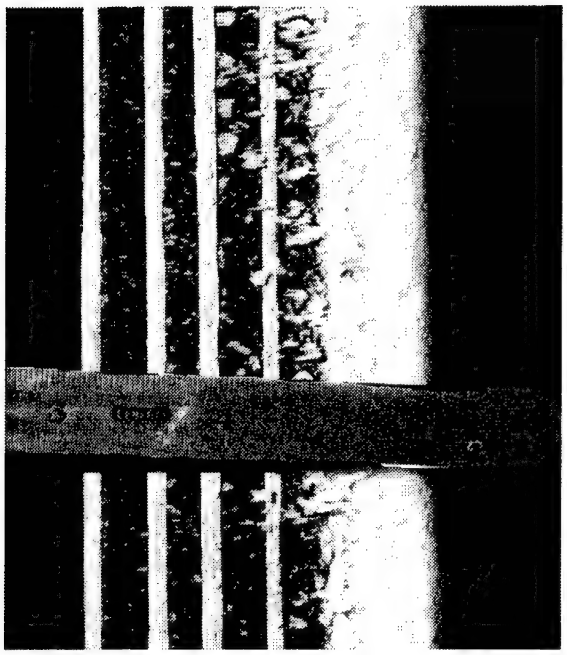

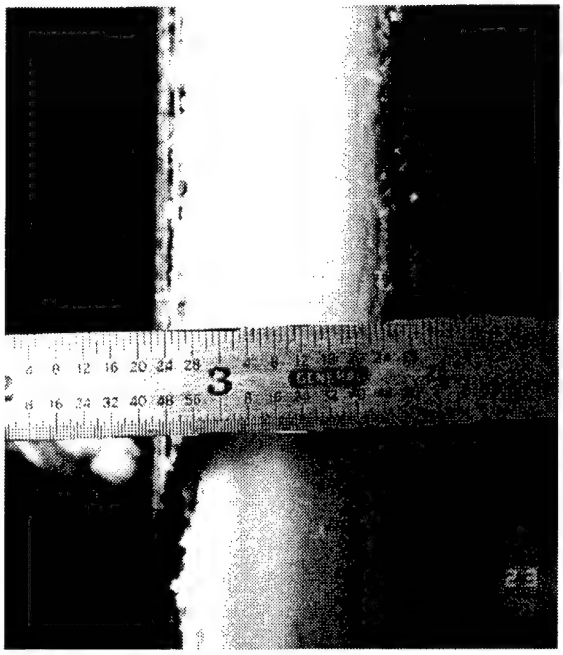

Commercial Transport - Run 107

T_t = -12.0°C (10.5°F)
T_s = -20°C (-4.0°F)

V = 128 m/s (248 kts)
AOA = 0.7°

LWC = 0.339 g/m^3
MVD = 15 μm
Spray = 22 min
chord = 90 cm (36 in)

$C_{d\text{-}clean}$ = 0.0085
$C_{d\text{-}iced}$ = 0.0163

$C_{l\text{-}clean}$ = 0.097
$C_{l\text{-}iced}$ = 0.099

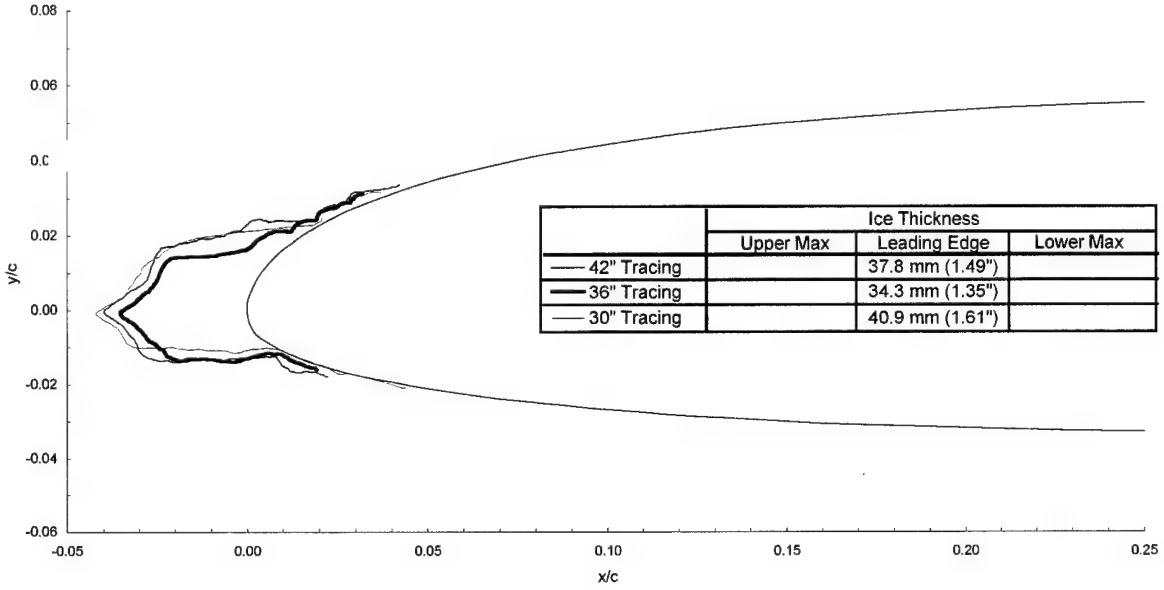

	Ice Thickness		
	Upper Max	Leading Edge	Lower Max
42" Tracing		37.8 mm (1.49")	
36" Tracing		34.3 mm (1.35")	
30" Tracing		40.9 mm (1.61")	

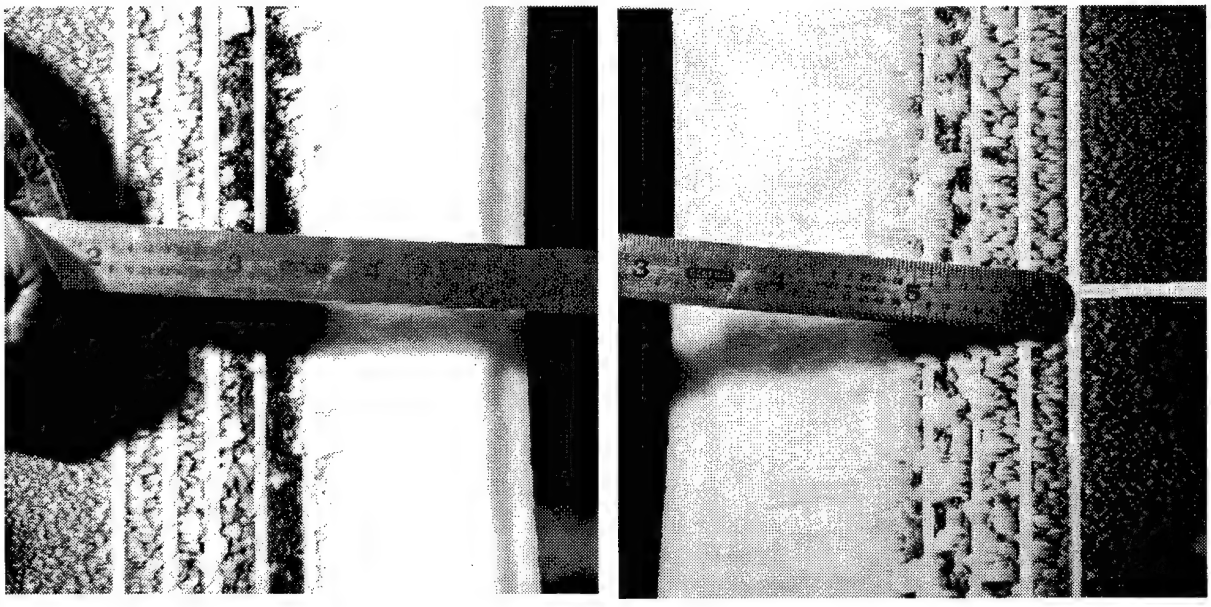

Commercial Transport - Run 108

T_t = -12.0°C (10.5°F)
T_s = -20°C (-4.0°F)

V = 128 m/s (248 kts)
AOA = 0.7°

LWC = 0.339 g/m^3
MVD = 15 μm
Spray = 29.3 min
chord = 90 cm (36 in)

$C_{d\text{-}clean}$ = 0.0085
$C_{d\text{-}iced}$ = 0.0163

$C_{l\text{-}clean}$ = 0.097
$C_{l\text{-}iced}$ = 0.098

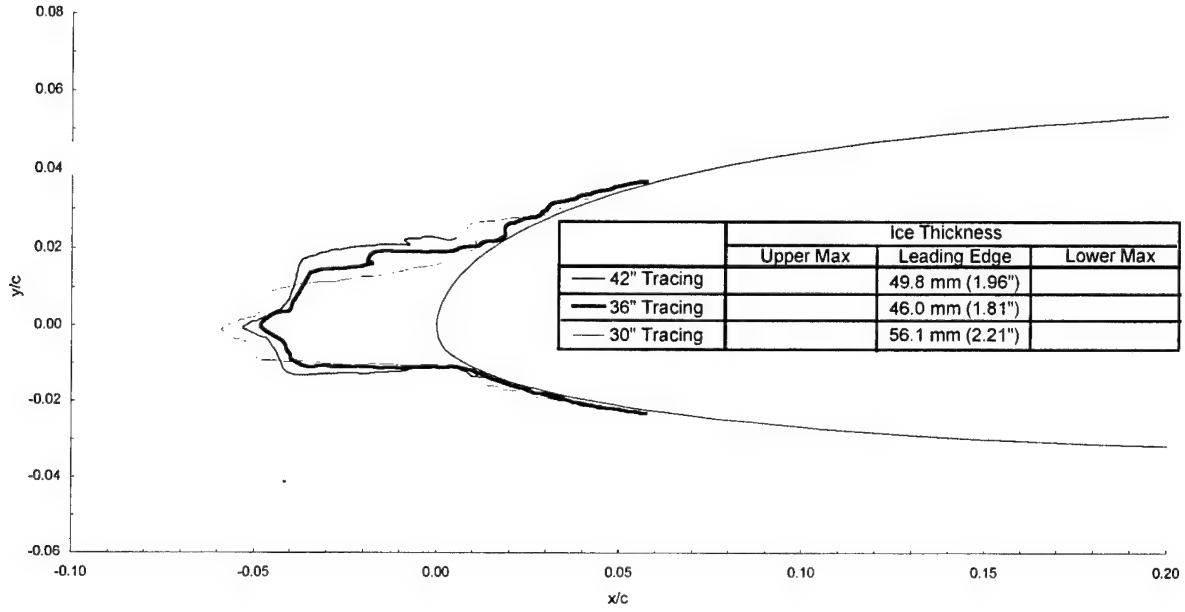

	Ice Thickness		
	Upper Max	Leading Edge	Lower Max
42" Tracing		49.8 mm (1.96")	
36" Tracing		46.0 mm (1.81")	
30" Tracing		56.1 mm (2.21")	

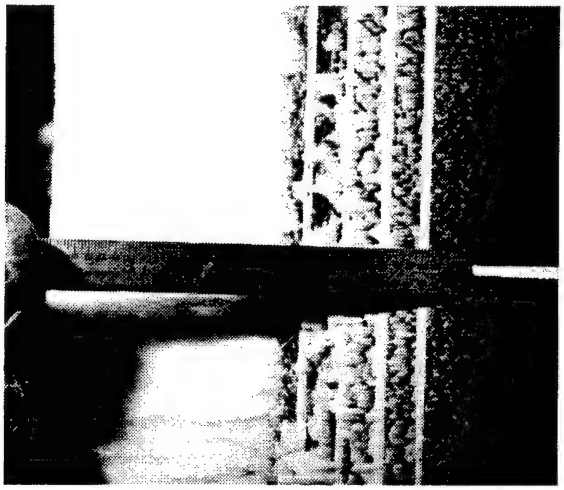

Commercial Transport - Run 110

T_t = -6.33°C (20.0°F)
T_s = -14.6°C (5.1°F)

V = 129 m/s (250 kts)
AOA = 1.7°

LWC = 0.341 g/m^3
MVD = 21 μm
Spray = 5.7 min
chord = 90 cm (36 in)

$C_{d\text{-}clean}$ = 0.0087
$C_{d\text{-}iced}$ = 0.0154

$C_{l\text{-}clean}$ = 0.215
$C_{l\text{-}iced}$ = 0.201

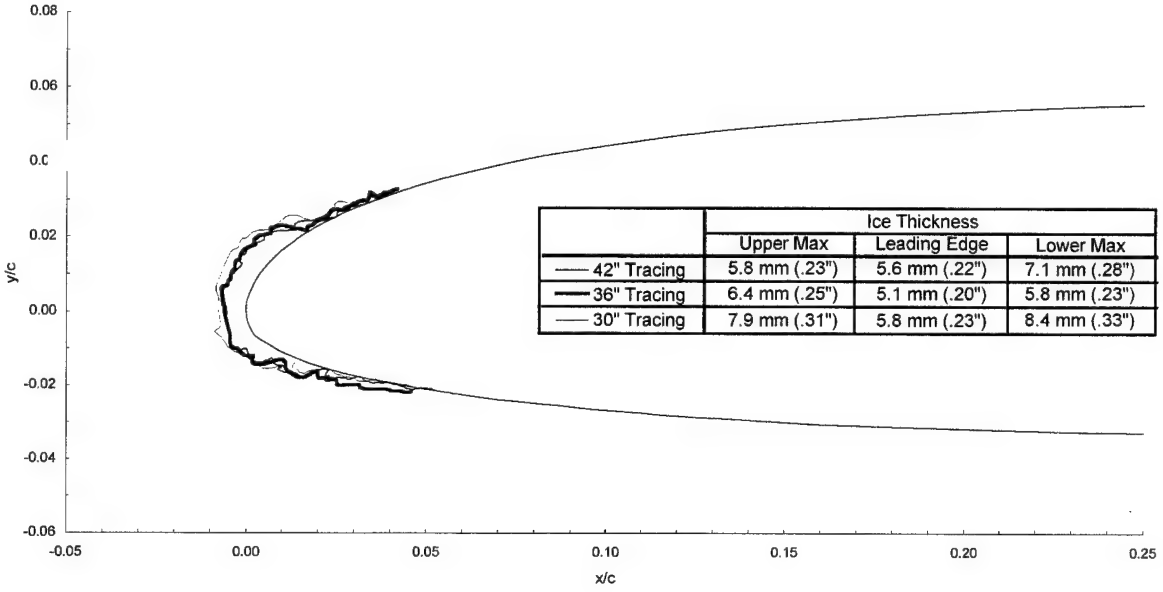

	Ice Thickness		
	Upper Max	Leading Edge	Lower Max
42" Tracing	5.8 mm (.23")	5.6 mm (.22")	7.1 mm (.28")
36" Tracing	6.4 mm (.25")	5.1 mm (.20")	5.8 mm (.23")
30" Tracing	7.9 mm (.31")	5.8 mm (.23")	8.4 mm (.33")

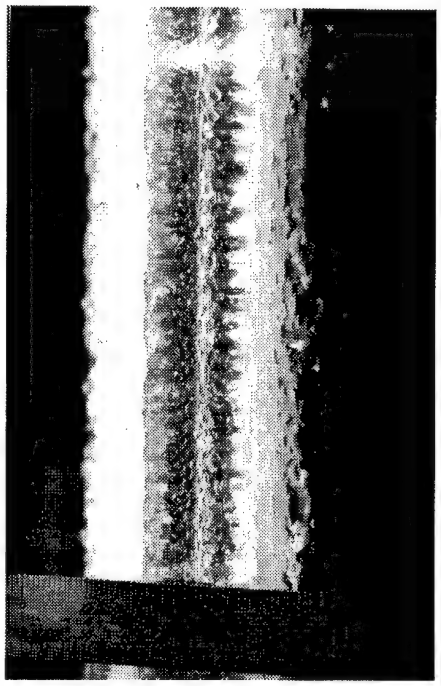

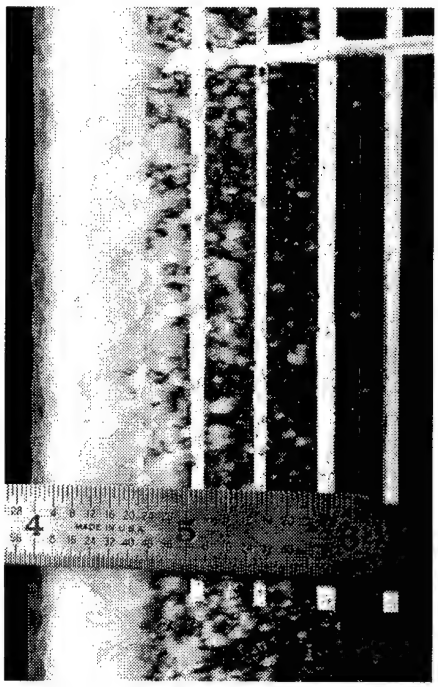

Commercial Transport - Run 111

T_t = -6.33°C (20.0°F)
T_s = -14.6°C (5.1°F)

V = 129 m/s (250 kts)
AOA = 1.5°

LWC = 0.341 g/m^3
MVD = 21 μm
Spray = 21.1 min
chord = 90 cm (36 in)

$C_{d\text{-}clean}$ = 0.0087
$C_{d\text{-}iced}$ = 0.0288

$C_{l\text{-}clean}$ = 0.203
$C_{l\text{-}iced}$ = 0.196

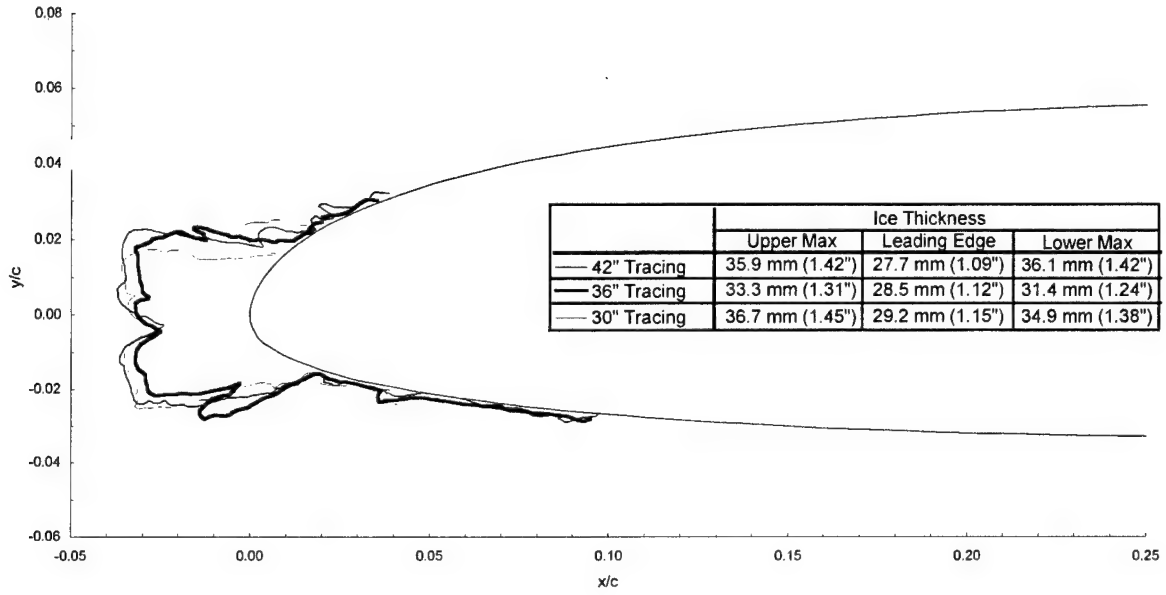

	Ice Thickness		
	Upper Max	Leading Edge	Lower Max
42" Tracing	35.9 mm (1.42")	27.7 mm (1.09")	36.1 mm (1.42")
36" Tracing	33.3 mm (1.31")	28.5 mm (1.12")	31.4 mm (1.24")
30" Tracing	36.7 mm (1.45")	29.2 mm (1.15")	34.9 mm (1.38")

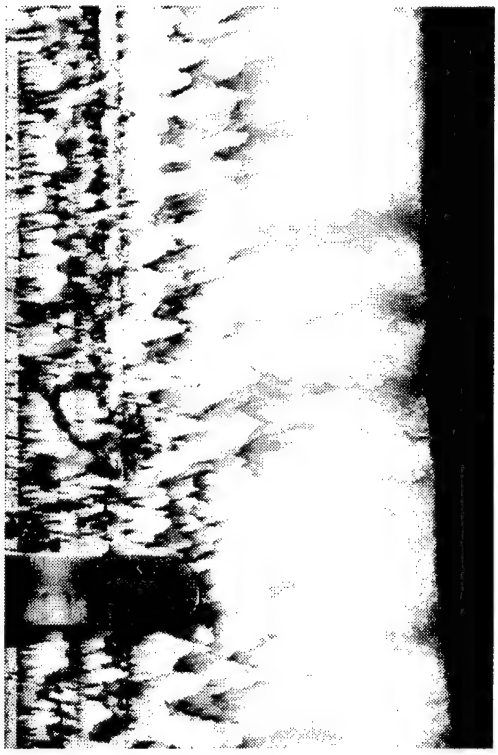

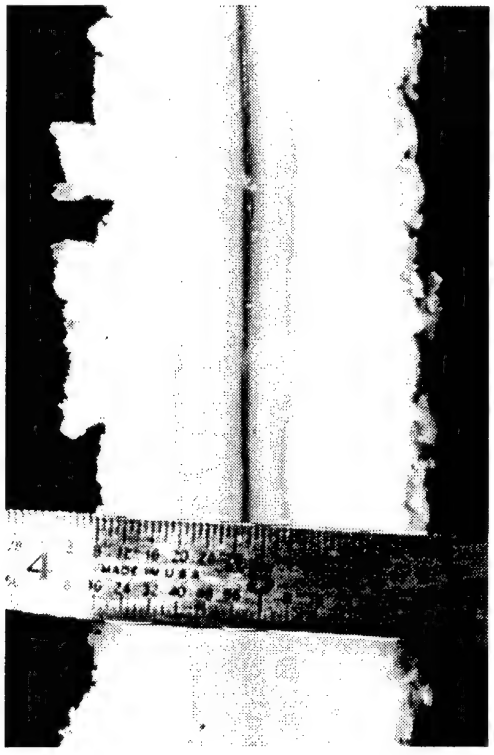

Commercial Transport - Run 112

T_t = -6.33°C (20.0°F)
T_s = -14.6°C (5.1°F)

V = 129 m/s (250 kts)
AOA = 0.7°

LWC = 0.341 g/m^3
MVD = 21 μm
Spray = 5.7 min
chord = 90 cm (36 in)

$C_{d\text{-}clean}$ = 0.0085
$C_{d\text{-}iced}$ = 0.0148

$C_{l\text{-}clean}$ = 0.097
$C_{l\text{-}iced}$ = 0.096

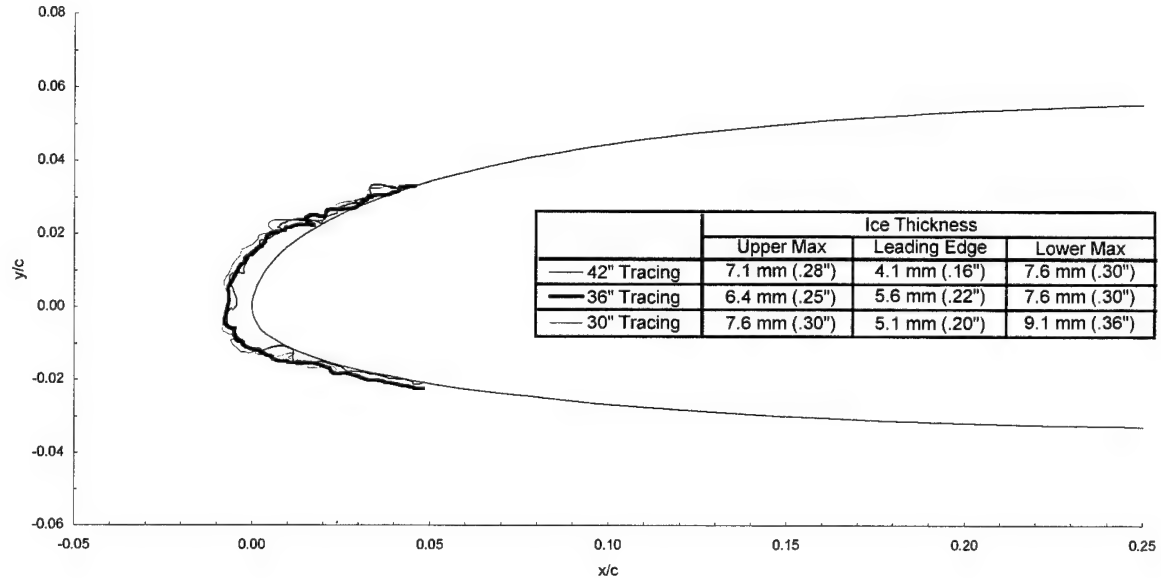

	Ice Thickness		
	Upper Max	Leading Edge	Lower Max
42" Tracing	7.1 mm (.28")	4.1 mm (.16")	7.6 mm (.30")
36" Tracing	6.4 mm (.25")	5.6 mm (.22")	7.6 mm (.30")
30" Tracing	7.6 mm (.30")	5.1 mm (.20")	9.1 mm (.36")

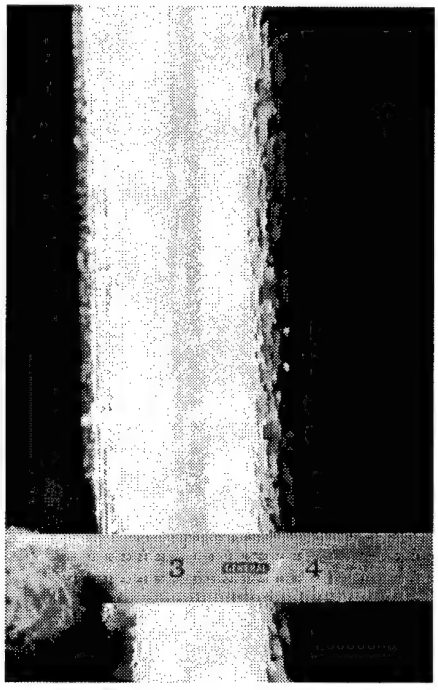

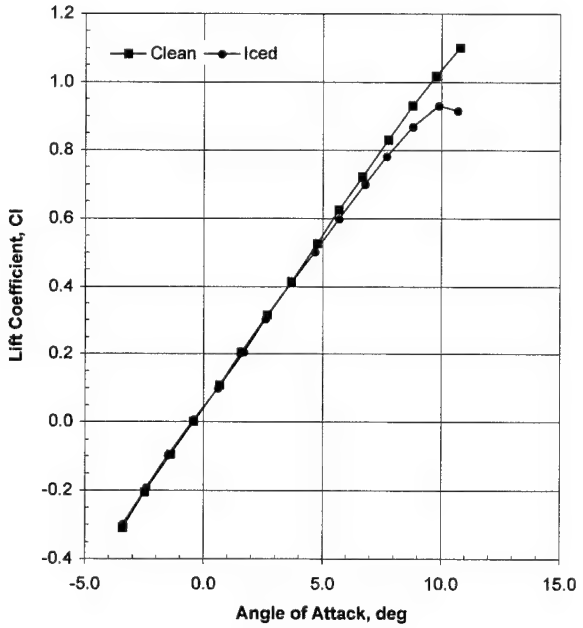

Commercial Transport - Run 113

T_t = -6.33°C (20.0°F)
T_s = -14.6°C (5.1°F)

V = 129 m/s (250 kts)
AOA = 0.7°

LWC = 0.341 g/m^3
MVD = 21 μm
Spray = 42.4 miin
chord = 90 cm (36 in)

$C_{d\text{-}clean}$ = 0.0085
$C_{d\text{-}iced}$ = 0.0209

$C_{l\text{-}clean}$ = 0.097
$C_{l\text{-}iced}$ = 0.096

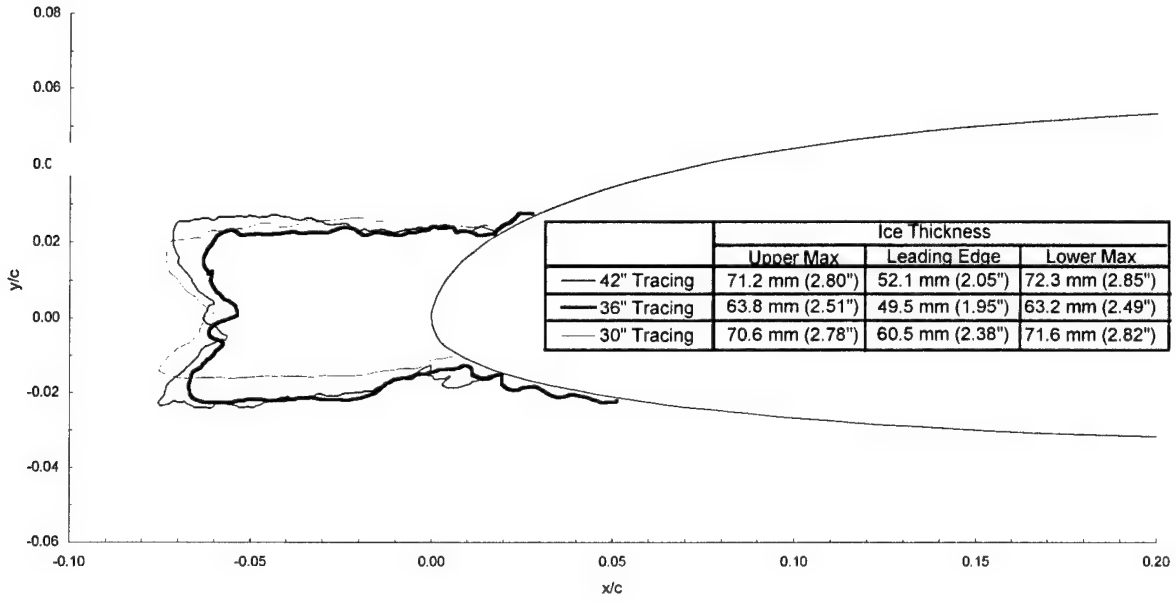

	Ice Thickness		
	Upper Max	Leading Edge	Lower Max
42" Tracing	71.2 mm (2.80")	52.1 mm (2.05")	72.3 mm (2.85")
36" Tracing	63.8 mm (2.51")	49.5 mm (1.95")	63.2 mm (2.49")
30" Tracing	70.6 mm (2.78")	60.5 mm (2.38")	71.6 mm (2.82")

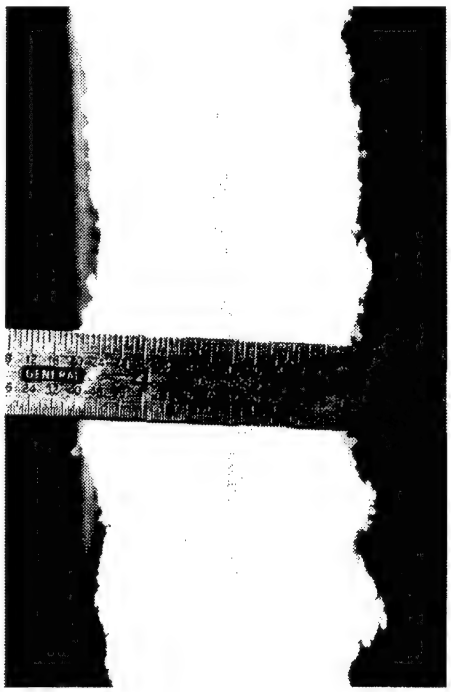

Commercial Transport - Run 114

T_t = -6.33°C (20.0°F)
T_s = -14.6°C (5.1°F)

V = 129 m/s (250 kts)
AOA = 0.7°

LWC = 0.341 g/m^3
MVD = 21 μm
Spray = 28.3 miin
chord = 90 cm (36 in)

$C_{d\text{-}clean}$ = 0.0085
$C_{d\text{-}iced}$ = 0.0286

$C_{l\text{-}clean}$ = 0.097
$C_{l\text{-}iced}$ = 0.100

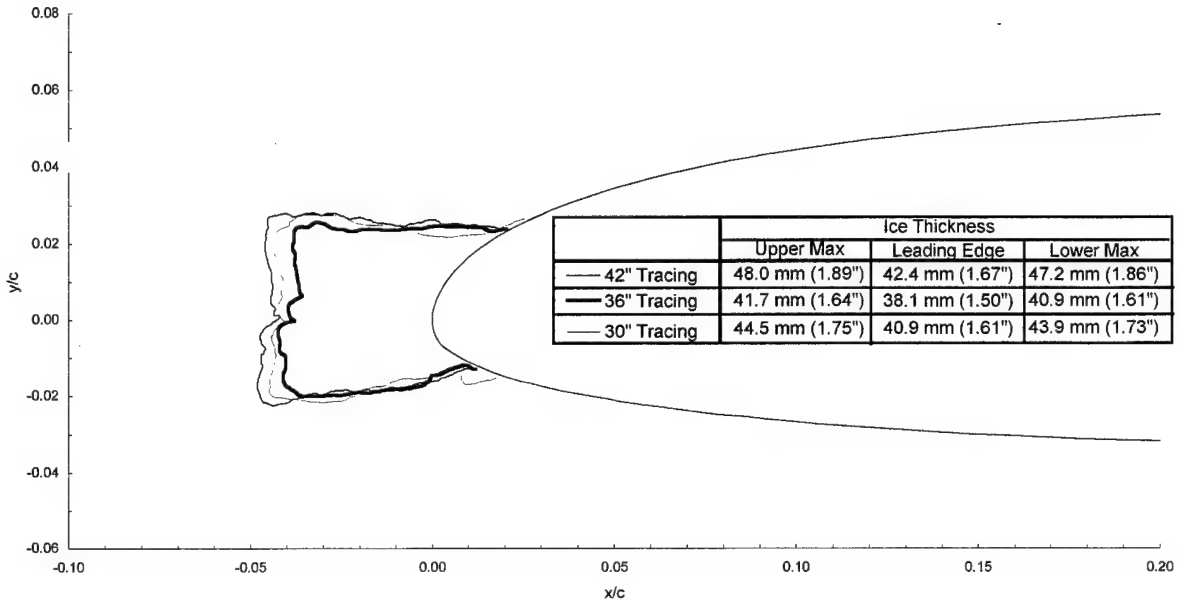

	Ice Thickness		
	Upper Max	Leading Edge	Lower Max
42" Tracing	48.0 mm (1.89")	42.4 mm (1.67")	47.2 mm (1.86")
36" Tracing	41.7 mm (1.64")	38.1 mm (1.50")	40.9 mm (1.61")
30" Tracing	44.5 mm (1.75")	40.9 mm (1.61")	43.9 mm (1.73")

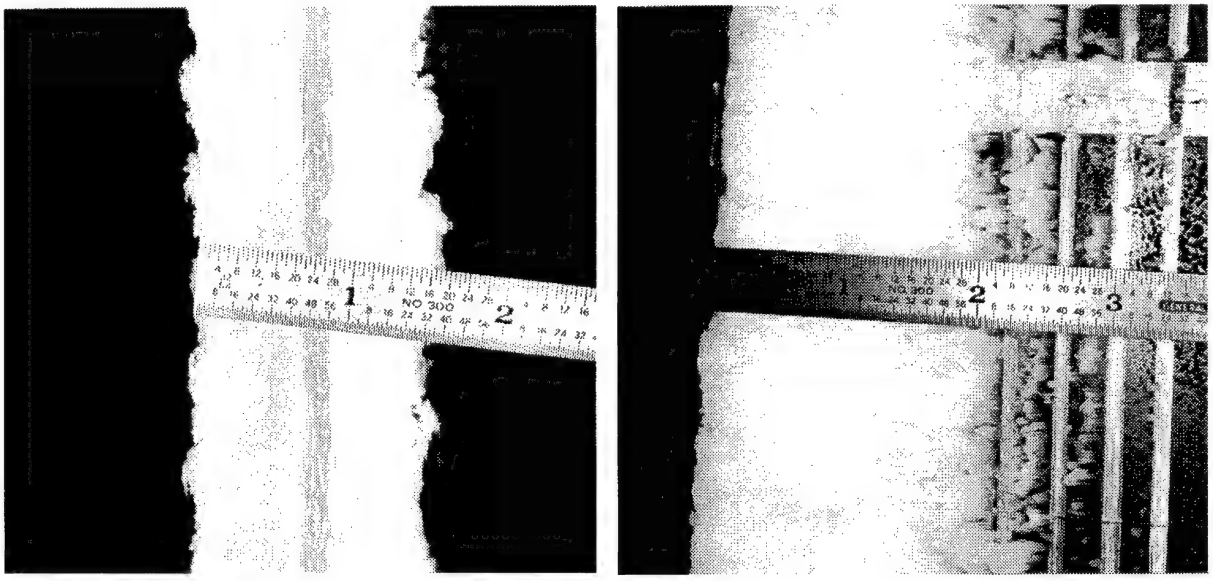

Commercial Transport - Run 115

T_t = -6.33°C (20.0°F)
T_s = -14.6°C (5.1°F)

V = 129 m/s (250 kts)
AOA = 0.7°

LWC = 0.341 g/m^3
MVD = 21 μm
Spray = 21.1 min
chord = 90 cm (36 in)

$C_{d\text{-}clean}$ = 0.0085
$C_{d\text{-}iced}$ = 0.0209

$C_{l\text{-}clean}$ = 0.097
$C_{l\text{-}iced}$ = 0.095

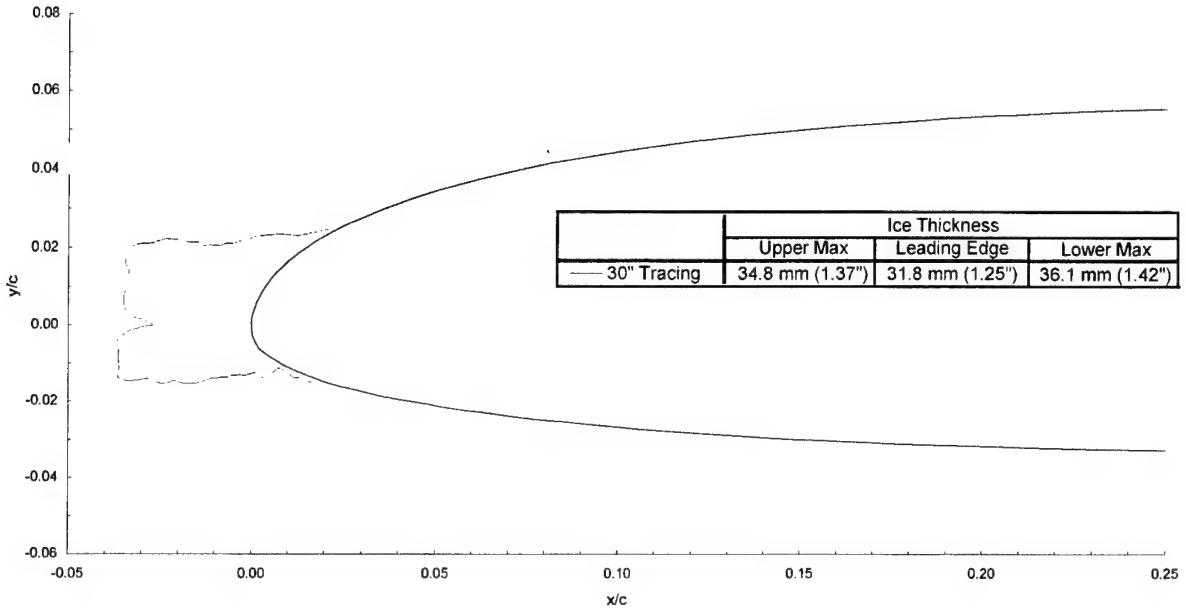

	Ice Thickness		
	Upper Max	Leading Edge	Lower Max
30" Tracing	34.8 mm (1.37")	31.8 mm (1.25")	36.1 mm (1.42")

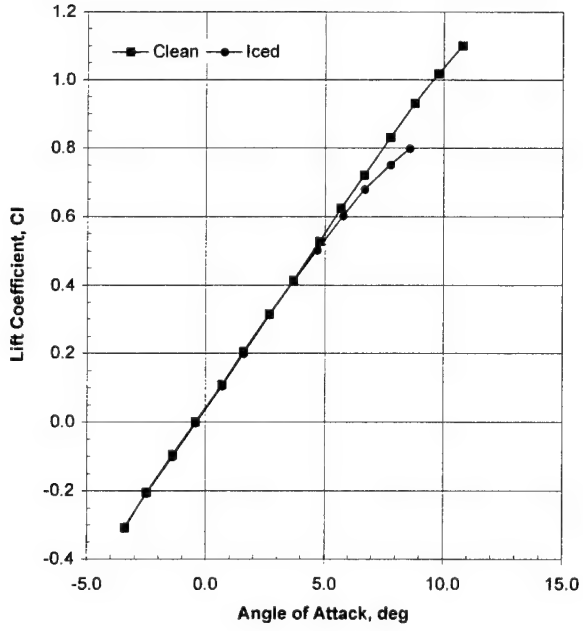

Commercial Transport - Run 122

T_t = -1.06°C (29.5°F)
T_s = -9.49°C (14.3°F)

V = 130 m/s (253 kts)
AOA = 1.6°

LWC = 0.563 g/m^3
MVD = 21 μm
Spray = 4.9 min
chord = 90 cm (36 in)

$C_{d\text{-}clean}$ = 0.0087
$C_{d\text{-}iced}$ = 0.0280

$C_{l\text{-}clean}$ = 0.208
$C_{l\text{-}iced}$ = 0.202

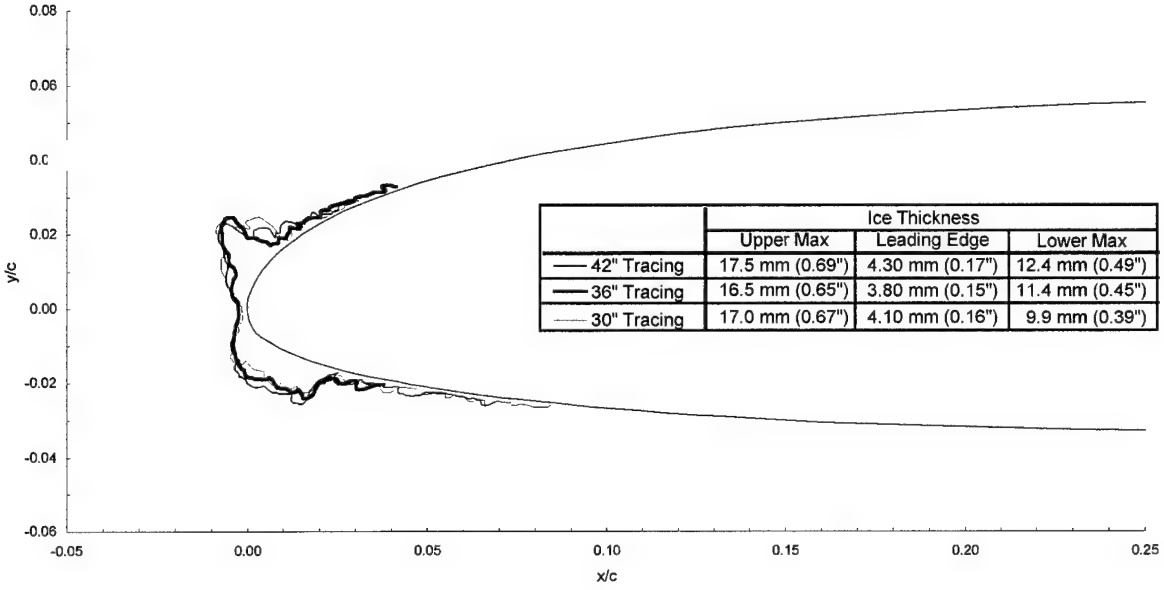

	Ice Thickness		
	Upper Max	Leading Edge	Lower Max
42" Tracing	17.5 mm (0.69")	4.30 mm (0.17")	12.4 mm (0.49")
36" Tracing	16.5 mm (0.65")	3.80 mm (0.15")	11.4 mm (0.45")
30" Tracing	17.0 mm (0.67")	4.10 mm (0.16")	9.9 mm (0.39")

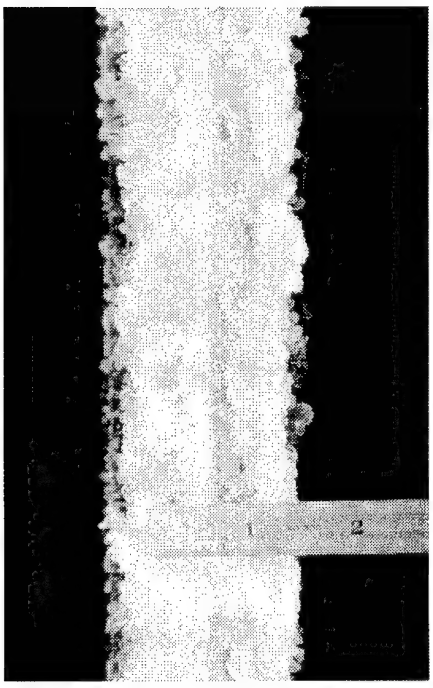

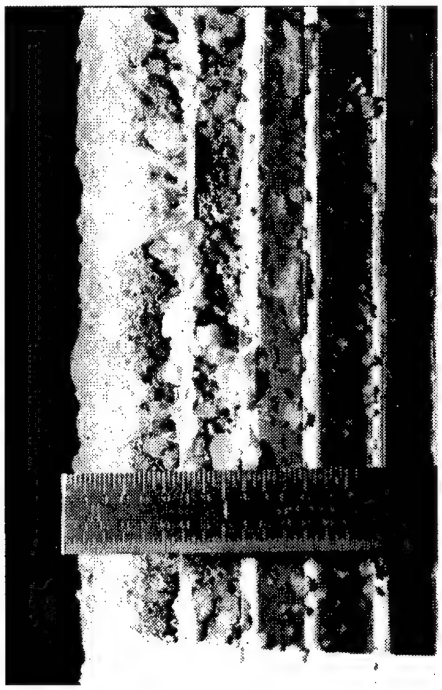

Commercial Transport - Run 123

T_t = -1.06°C (29.5°F)
T_s = -9.49°C (14.3°F)

V = 130 m/s (253 kts)
AOA = 1.6°

LWC = 0.563 g/m^3
MVD = 21 μm
Spray = 18.5 miin
chord = 90 cm (36 in)

$C_{d\text{-}clean}$ = 0.0087
$C_{d\text{-}iced}$ = 0.0799

$C_{l\text{-}clean}$ = 0.208
$C_{l\text{-}iced}$ = 0.184

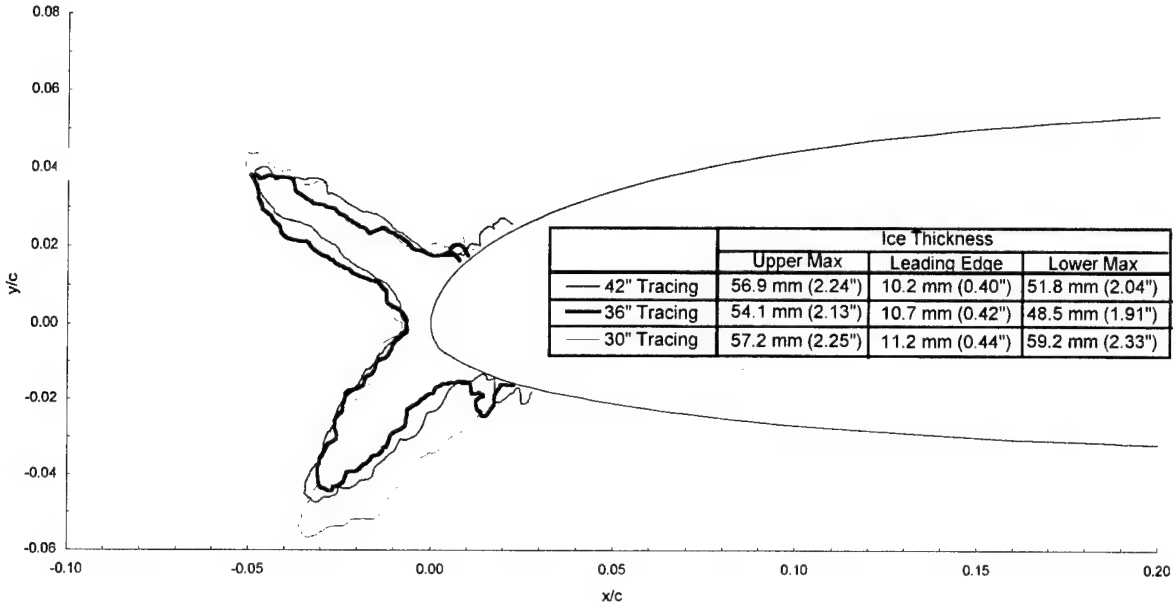

	Ice Thickness		
	Upper Max	Leading Edge	Lower Max
42" Tracing	56.9 mm (2.24")	10.2 mm (0.40")	51.8 mm (2.04")
36" Tracing	54.1 mm (2.13")	10.7 mm (0.42")	48.5 mm (1.91")
30" Tracing	57.2 mm (2.25")	11.2 mm (0.44")	59.2 mm (2.33")

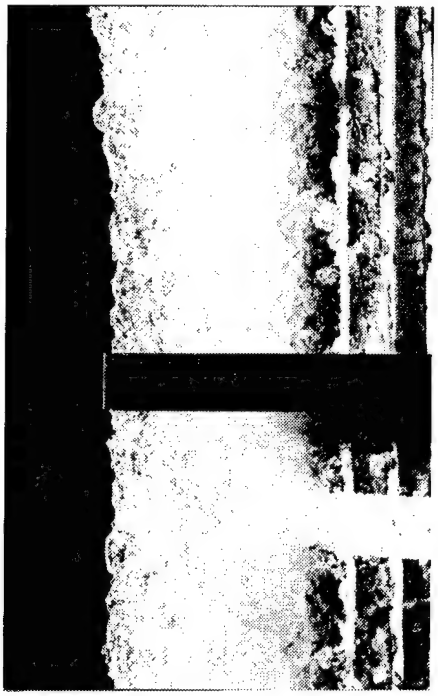

Commercial Transport - Run 124

T_t = -1.06°C (29.5°F)
T_s = -9.49°C (14.3°F)

V = 130 m/s (253 kts)
AOA = 0.7°

LWC = 0.563 g/m^3
MVD = 21 μm
Spray = 4.9 min
chord = 90 cm (36 in)

$C_{d\text{-}clean}$ = 0.0085
$C_{d\text{-}iced}$ = 0.0269

$C_{l\text{-}clean}$ = 0.097
$C_{l\text{-}iced}$ = 0.088

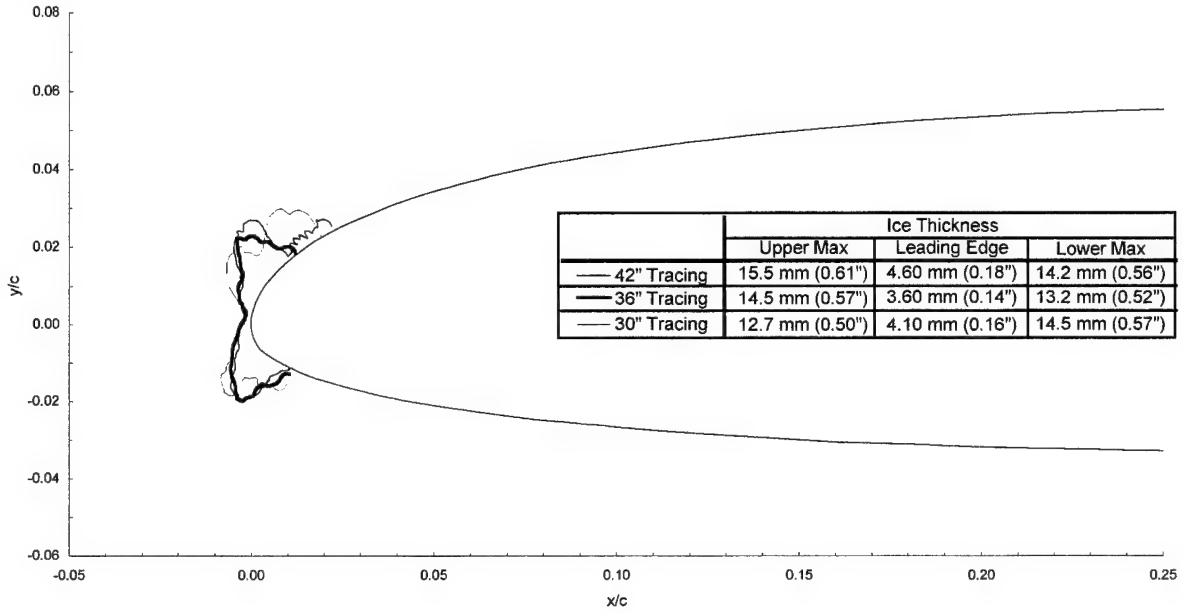

	Ice Thickness		
	Upper Max	Leading Edge	Lower Max
42" Tracing	15.5 mm (0.61")	4.60 mm (0.18")	14.2 mm (0.56")
36" Tracing	14.5 mm (0.57")	3.60 mm (0.14")	13.2 mm (0.52")
30" Tracing	12.7 mm (0.50")	4.10 mm (0.16")	14.5 mm (0.57")

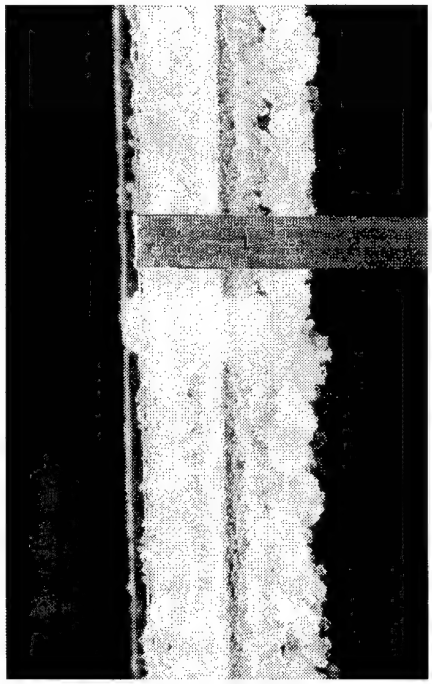

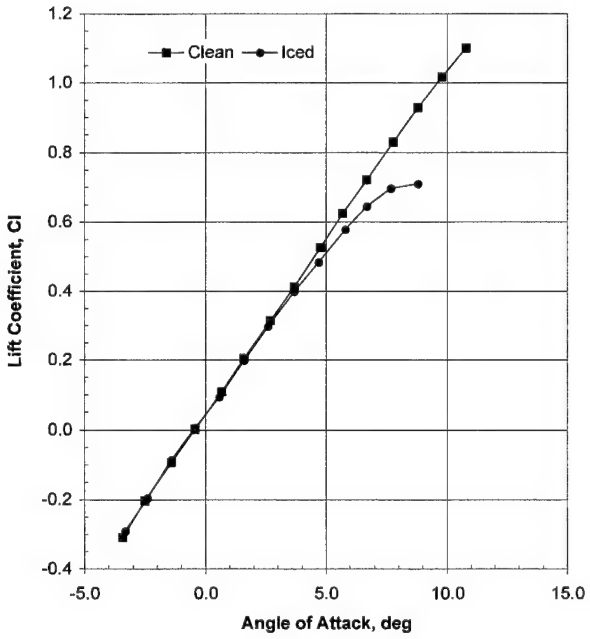

Commercial Transport - Run 126

T_t = -1.06°C (29.5°F)
T_s = -9.49°C (14.3°F)

V = 130 m/s (253 kts)
AOA = 0.6°

LWC = 0.563 g/m^3
MVD = 21 μm
Spray = 24.6 min
chord = 90 cm (36 in)

$C_{d\text{-}clean}$ = 0.0085
$C_{d\text{-}iced}$ = 0.1422

$C_{l\text{-}clean}$ = 0.095
$C_{l\text{-}iced}$ = 0.072

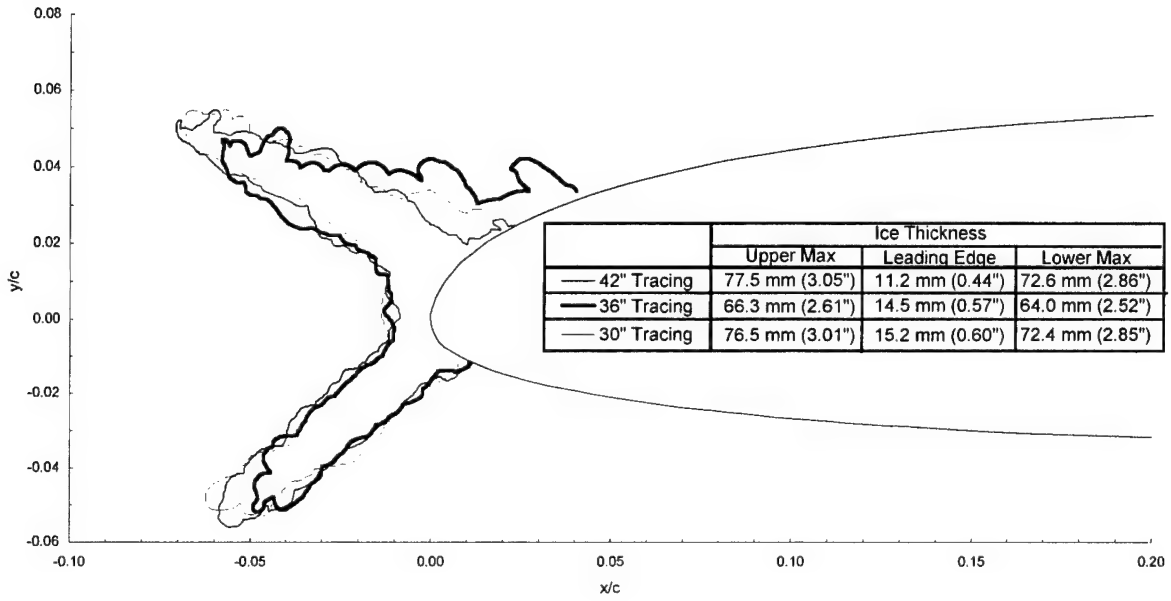

	Ice Thickness		
	Upper Max	Leading Edge	Lower Max
42" Tracing	77.5 mm (3.05")	11.2 mm (0.44")	72.6 mm (2.86")
36" Tracing	66.3 mm (2.61")	14.5 mm (0.57")	64.0 mm (2.52")
30" Tracing	76.5 mm (3.01")	15.2 mm (0.60")	72.4 mm (2.85")

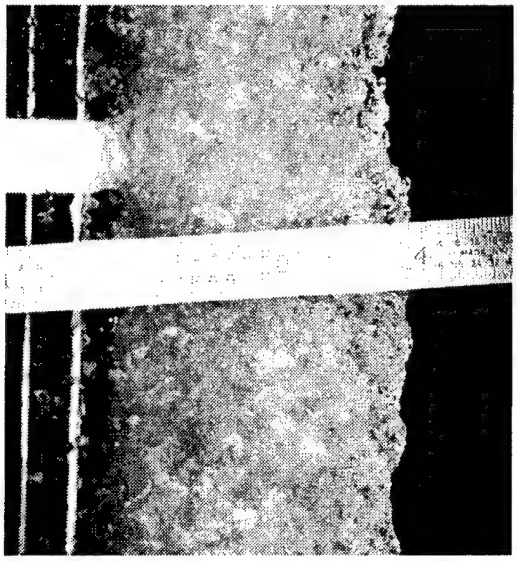

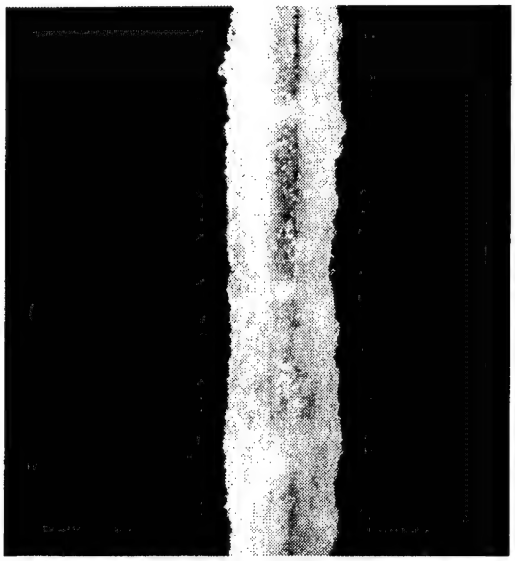

Commercial Transport - Run 127

T_t = -1.06°C (29.5°F)
T_s = -9.49°C (14.3°F)

V = 130 m/s (253 kts)
AOA = 0.7°

LWC = 0.563 g/m^3
MVD = 21 μm
Spray = 18.5 min
chord = 90 cm (36 in)

$C_{d\text{-}clean}$ = 0.0085
$C_{d\text{-}iced}$ = 0.1398

$C_{l\text{-}clean}$ = 0.097
$C_{l\text{-}iced}$ = 0.079

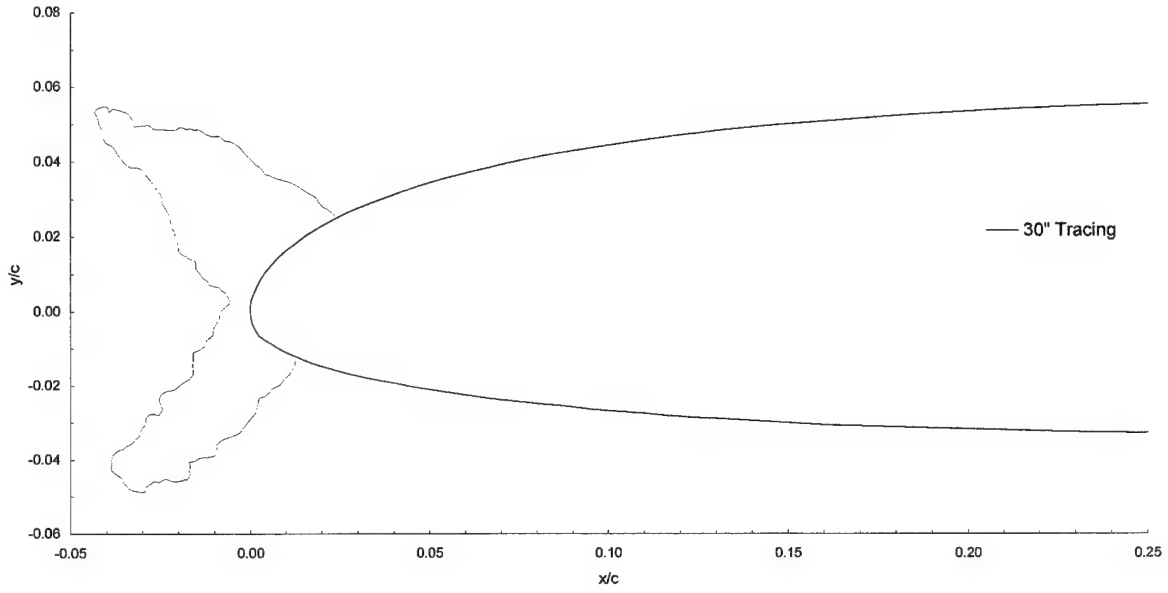

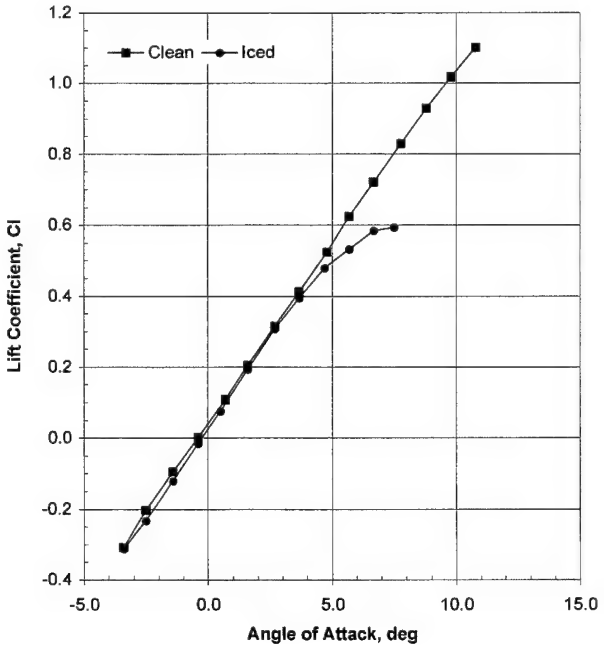

Commercial Transport - Run 128

T_t = -6.33°C (20.0°F)
T_s = -14.6°C (5.1°F)

V = 129 m/s (250 kts)
AOA = 0.6°

LWC = 0.341 g/m^3
MVD = 21 μm
Spray = 2.0 min
chord = 90 cm (36 in)

$C_{d\text{-}clean}$ = 0.0085
$C_{d\text{-}iced}$ = 0.0112

$C_{l\text{-}clean}$ = 0.095
$C_{l\text{-}iced}$ = 0.098

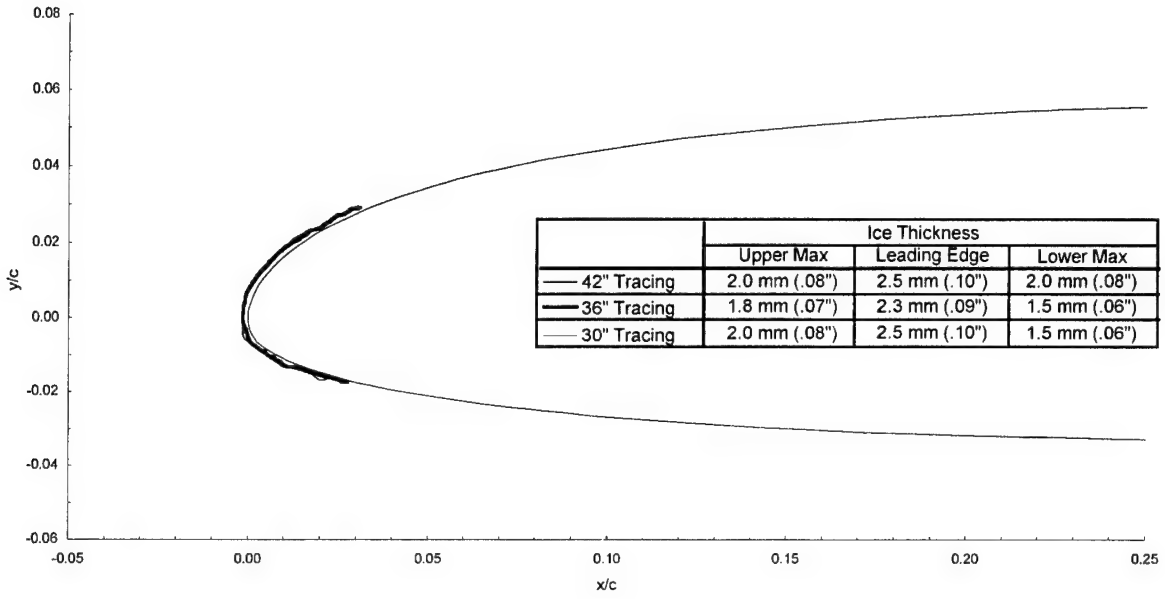

	Ice Thickness		
	Upper Max	Leading Edge	Lower Max
42" Tracing	2.0 mm (.08")	2.5 mm (.10")	2.0 mm (.08")
36" Tracing	1.8 mm (.07")	2.3 mm (.09")	1.5 mm (.06")
30" Tracing	2.0 mm (.08")	2.5 mm (.10")	1.5 mm (.06")

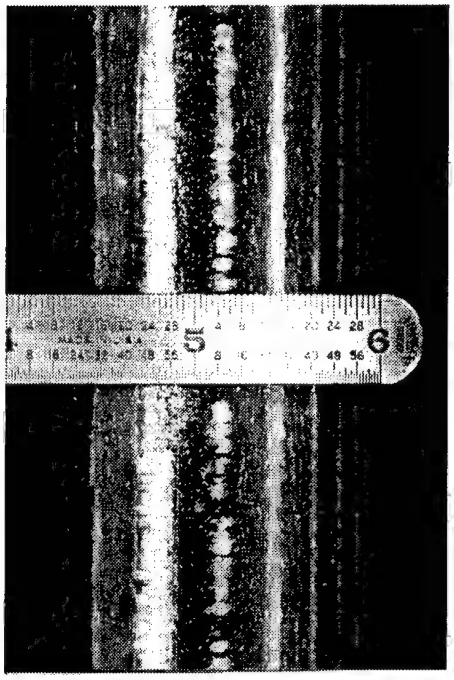

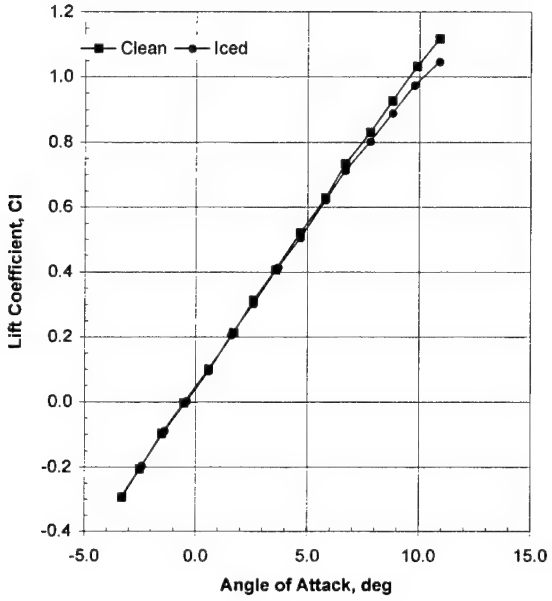

Commercial Transport - Run 129

T_t = -1.06°C (29.5°F)
T_s = -9.49°C (14.3°F)

V = 130 m/s (253 kts)
AOA = 0.7°

LWC = 0.563 g/m^3
MVD = 21 μm
Spray = 2.0 min
chord = 90 cm (36 in)

$C_{d\text{-}clean}$ = 0.0085
$C_{d\text{-}iced}$ = 0.0154

$C_{l\text{-}clean}$ = 0.097
$C_{l\text{-}iced}$ = 0.092

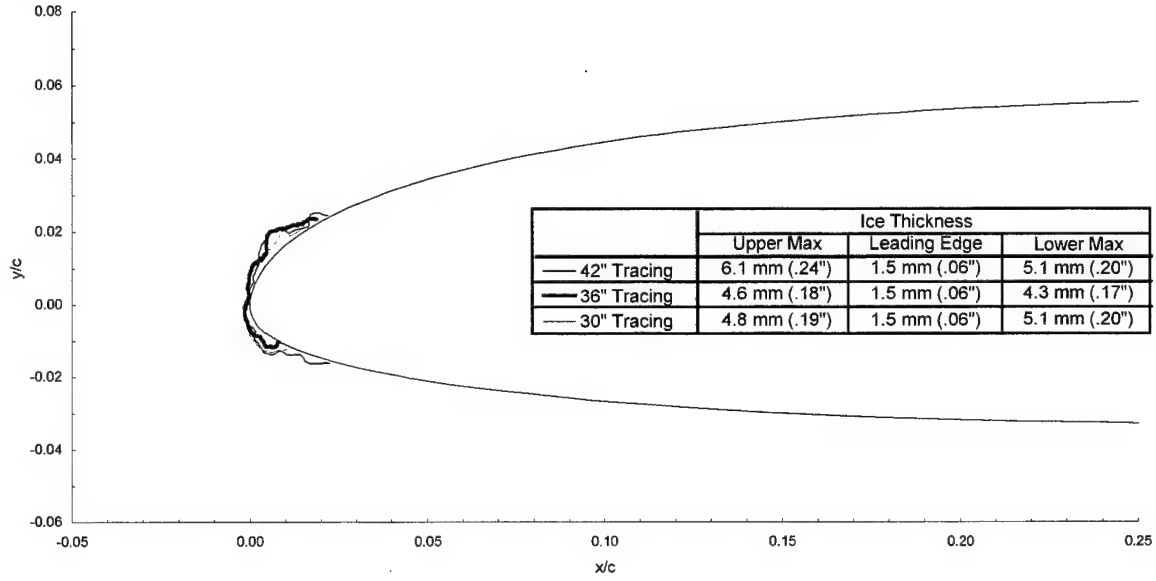

	Ice Thickness		
	Upper Max	Leading Edge	Lower Max
42" Tracing	6.1 mm (.24")	1.5 mm (.06")	5.1 mm (.20")
36" Tracing	4.6 mm (.18")	1.5 mm (.06")	4.3 mm (.17")
30" Tracing	4.8 mm (.19")	1.5 mm (.06")	5.1 mm (.20")

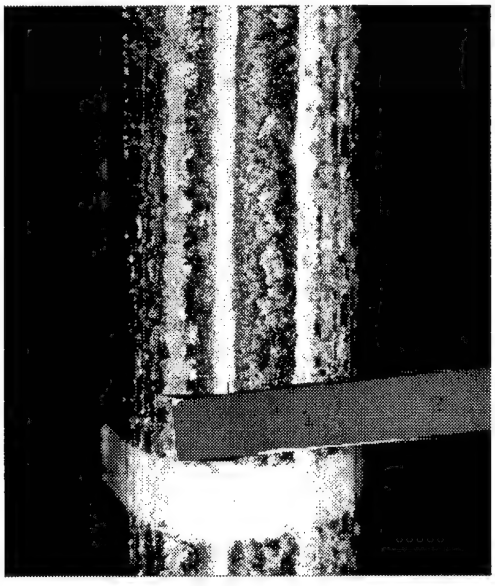

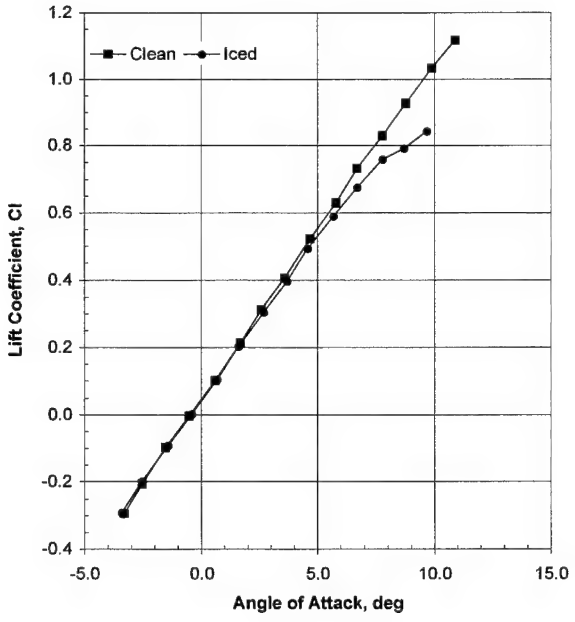

Commercial Transport - Run 130

T_t = 0.33°C (32.0°F)
T_s = -8.14°C (16.7°F)

V = 130 m/s (253 kts)
AOA = 0.6°

LWC = 0.42 g/m^3
MVD = 56 μm
Spray = 18.0 min
chord = 90 cm (36 in)

$C_{d\text{-}clean}$ = 0.0085
$C_{d\text{-}iced}$ = 0.1168

$C_{l\text{-}clean}$ = 0.095
$C_{l\text{-}iced}$ = 0.078

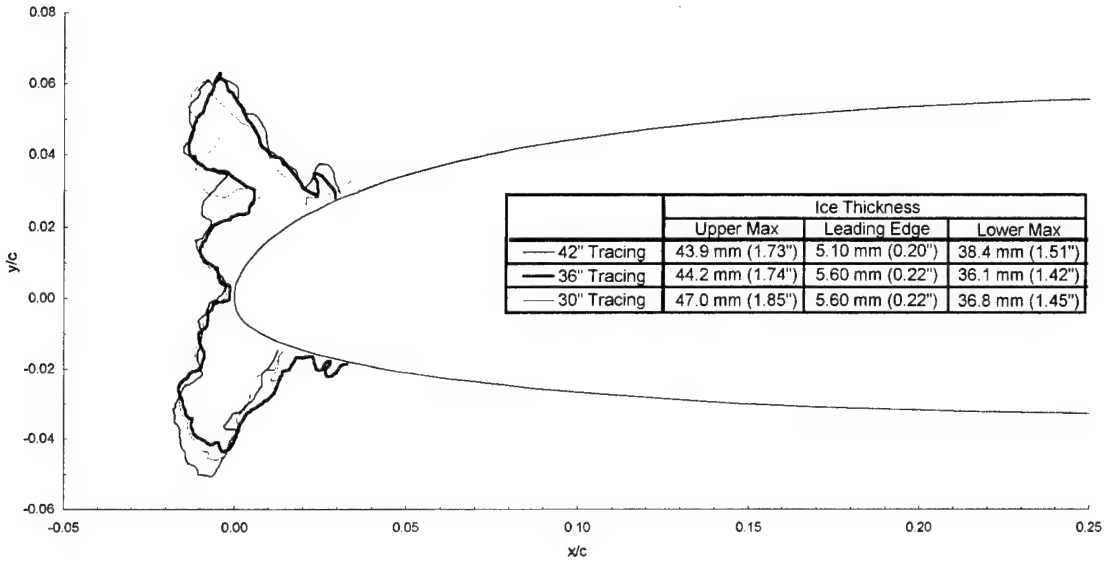

	Ice Thickness		
	Upper Max	Leading Edge	Lower Max
42" Tracing	43.9 mm (1.73")	5.10 mm (0.20")	38.4 mm (1.51")
36" Tracing	44.2 mm (1.74")	5.60 mm (0.22")	36.1 mm (1.42")
30" Tracing	47.0 mm (1.85")	5.60 mm (0.22")	36.8 mm (1.45")

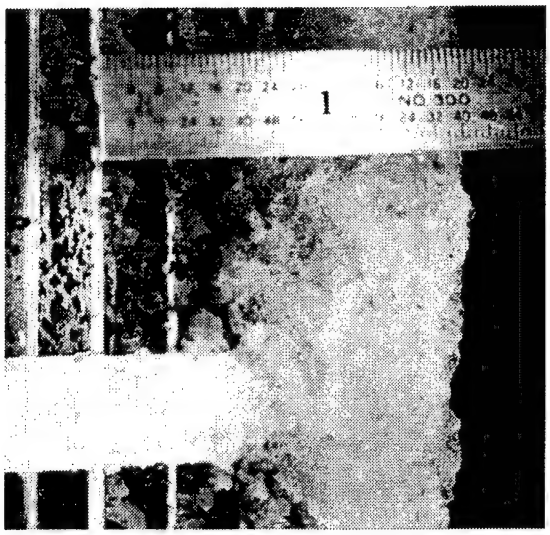

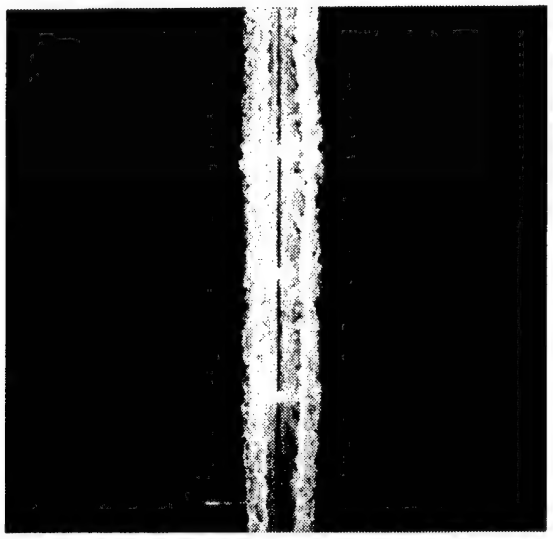

Commercial Transport - Run 131

T_t = 0.89°C (33.0°F)
T_s = -7.60°C (17.7°F)

V = 130 m/s (253 kts)
AOA = 0.6°

LWC = 0.42 g/m^3
MVD = 56 μm
Spray = 18.0 min
chord = 90 cm (36 in)

$C_{d\text{-}clean}$ = 0.0085
$C_{d\text{-}iced}$ = 0.1027

$C_{l\text{-}clean}$ = 0.095
$C_{l\text{-}iced}$ = 0.082

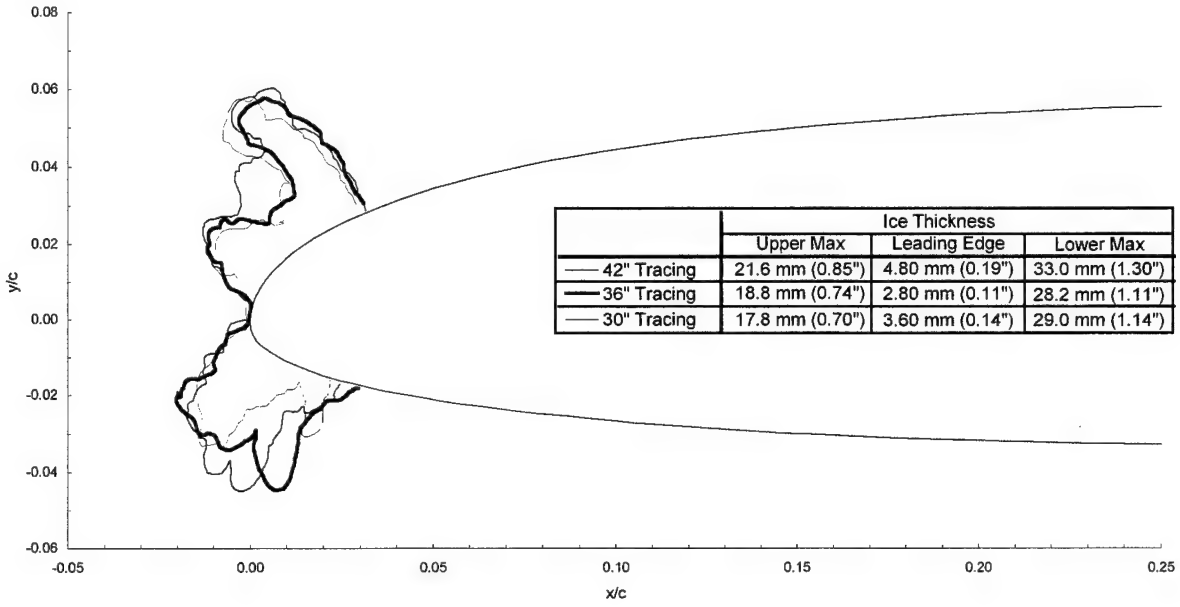

	Ice Thickness		
	Upper Max	Leading Edge	Lower Max
42" Tracing	21.6 mm (0.85")	4.80 mm (0.19")	33.0 mm (1.30")
36" Tracing	18.8 mm (0.74")	2.80 mm (0.11")	28.2 mm (1.11")
30" Tracing	17.8 mm (0.70")	3.60 mm (0.14")	29.0 mm (1.14")

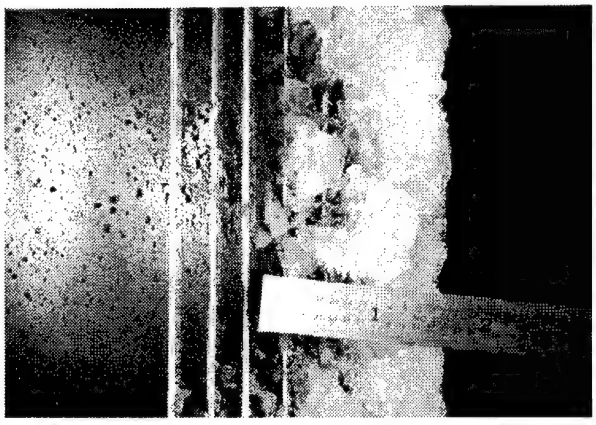

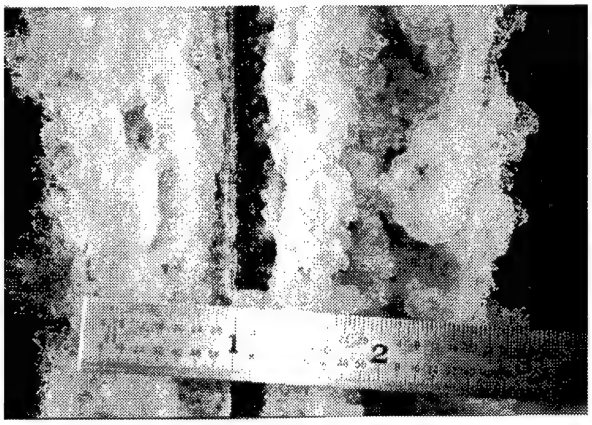

Commercial Transport - Run 133

T_t = 1.44°C (34.0°F)
T_s = -7.07°C (18.7°F)
V = 130 m/s (253 kts)
AOA = 0.5°

LWC = 0.42 g/m^3
MVD = 56 μm
Spray = 18.0 min
chord = 90 cm (36 in)

$C_{d\text{-clean}}$ = 0.0085
$C_{d\text{-iced}}$ = 0.0251
$C_{l\text{-clean}}$ = 0.093
$C_{l\text{-iced}}$ = 0.083

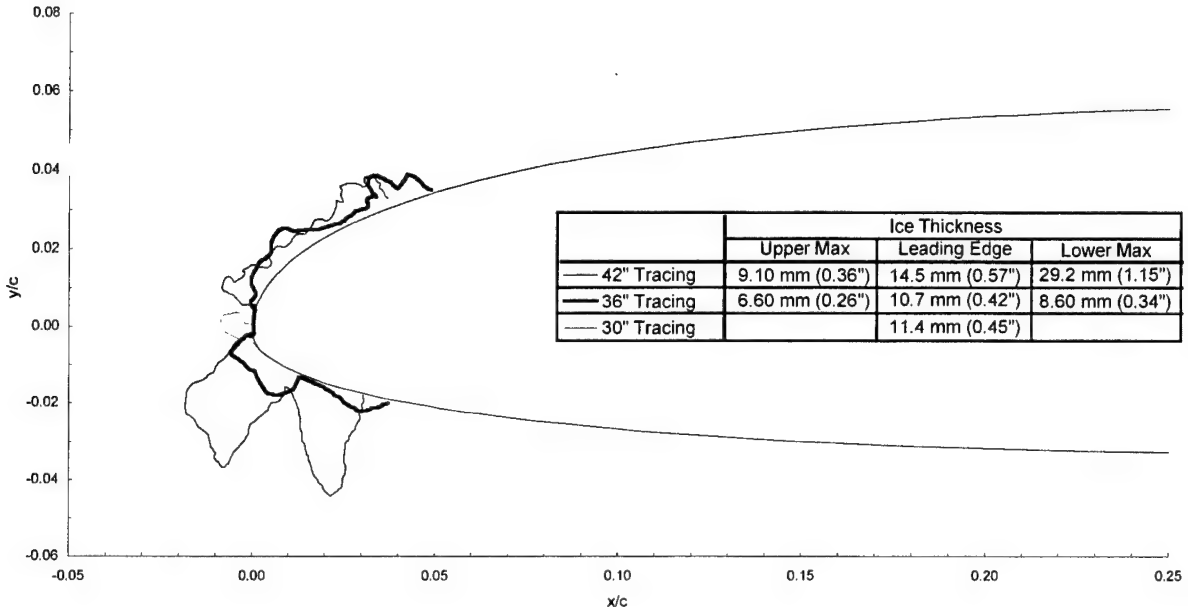

	Ice Thickness		
	Upper Max	Leading Edge	Lower Max
42" Tracing	9.10 mm (0.36")	14.5 mm (0.57")	29.2 mm (1.15")
36" Tracing	6.60 mm (0.26")	10.7 mm (0.42")	8.60 mm (0.34")
30" Tracing		11.4 mm (0.45")	

Commercial Transport - Run 141

T_t = -9.11°C (15.0°F)
T_s = -17.3°C (0.3°F)
V = 128 m/s (249 kts)
AOA = 0.7°

LWC = 0.40 g/m^3
MVD = 42 μm
Spray = 6.7 min
chord = 90 cm (36 in)

$C_{d\text{-}clean}$ = 0.0085
$C_{d\text{-}iced}$ = 0.0177
$C_{l\text{-}clean}$ = 0.097
$C_{l\text{-}iced}$ = 0.091

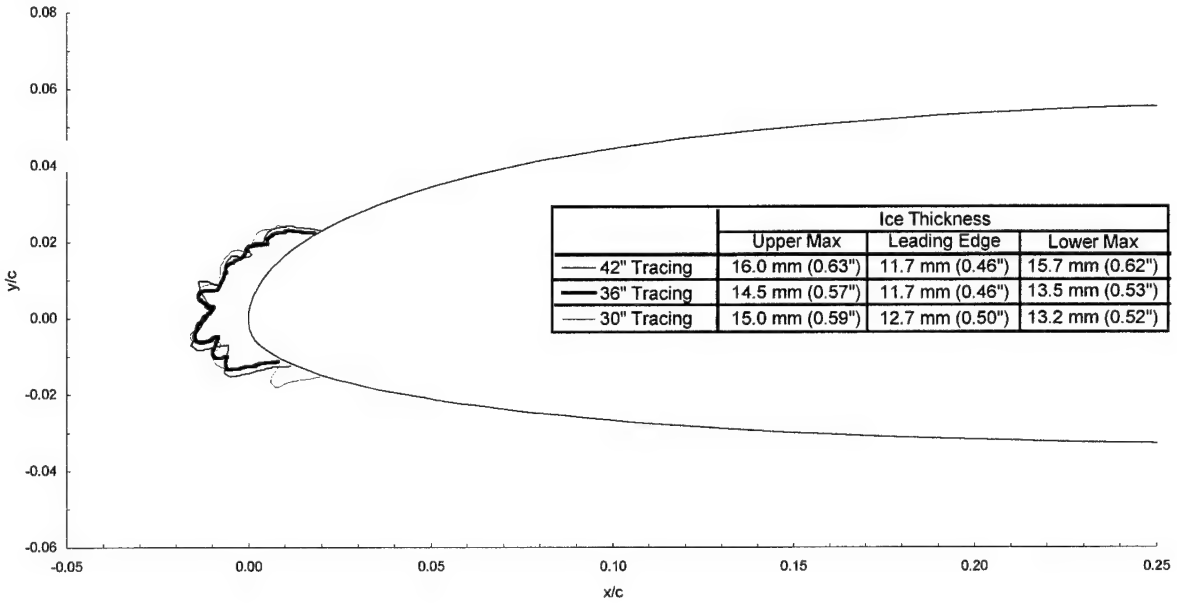

	Ice Thickness		
	Upper Max	Leading Edge	Lower Max
42" Tracing	16.0 mm (0.63")	11.7 mm (0.46")	15.7 mm (0.62")
36" Tracing	14.5 mm (0.57")	11.7 mm (0.46")	13.5 mm (0.53")
30" Tracing	15.0 mm (0.59")	12.7 mm (0.50")	13.2 mm (0.52")

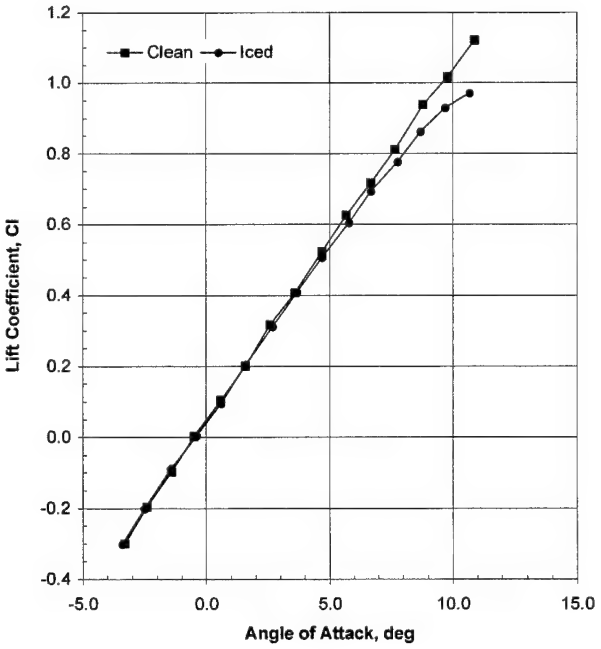

Commercial Transport - Run 142

T_t = -9.11°C (15.0°F)
T_s = -17.3°C (0.3°F)
V = 128 m/s (249 kts)
AOA = 0.6°

LWC = 0.40 g/m^3
MVD = 42 μm
Spray = 2.0 min
chord = 90 cm (36 in)

$C_{d\text{-clean}}$ = 0.0085
$C_{d\text{-iced}}$ = 0.0127
$C_{l\text{-clean}}$ = 0.095
$C_{l\text{-iced}}$ = 0.087

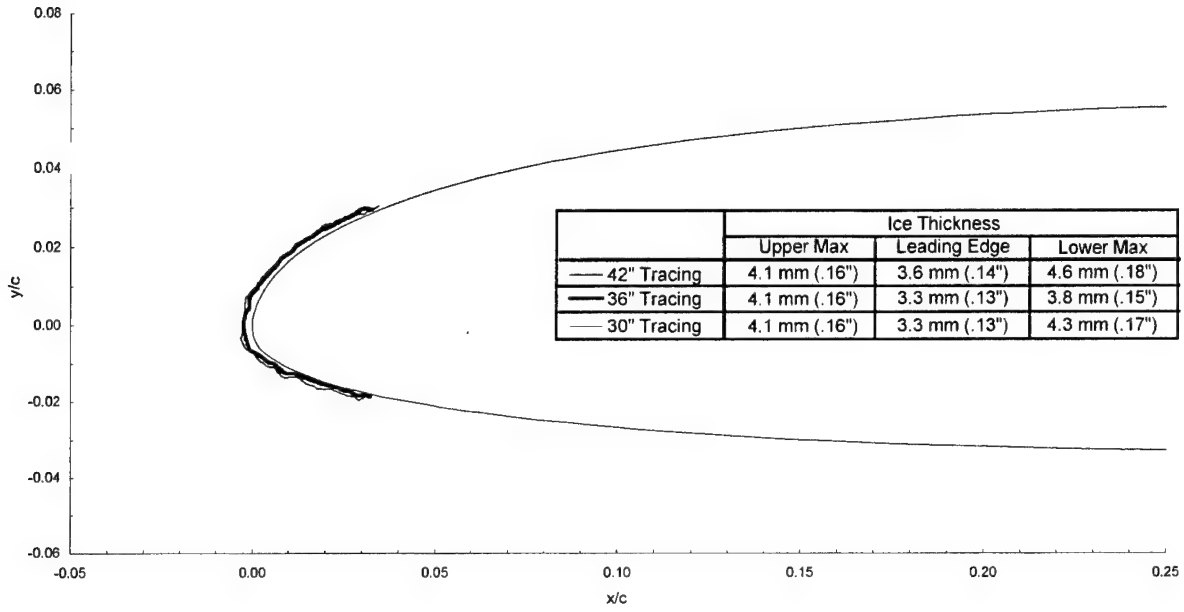

	Ice Thickness		
	Upper Max	Leading Edge	Lower Max
42" Tracing	4.1 mm (.16")	3.6 mm (.14")	4.6 mm (.18")
36" Tracing	4.1 mm (.16")	3.3 mm (.13")	3.8 mm (.15")
30" Tracing	4.1 mm (.16")	3.3 mm (.13")	4.3 mm (.17")

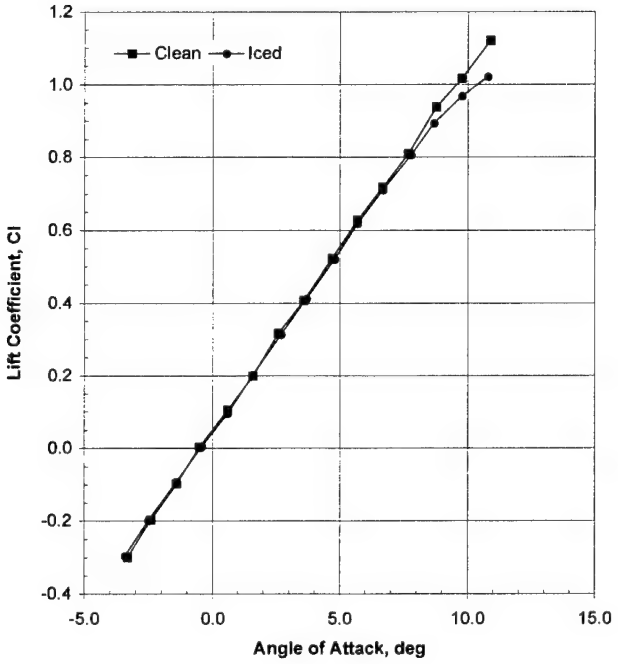

Commercial Transport - Run 143

T_t = -1.33°C (29.0°F)
T_s = -9.76°C (13.8°F)
V = 130 m/s (253 kts)
AOA = 0.6°

LWC = 0.65 g/m^3
MVD = 42 μm
Spray = 5.3 min
chord = 90 cm (36 in)

$C_{d\text{-}clean}$ = 0.0085
$C_{d\text{-}iced}$ = 0.0443
$C_{l\text{-}clean}$ = 0.095
$C_{l\text{-}iced}$ = 0.085

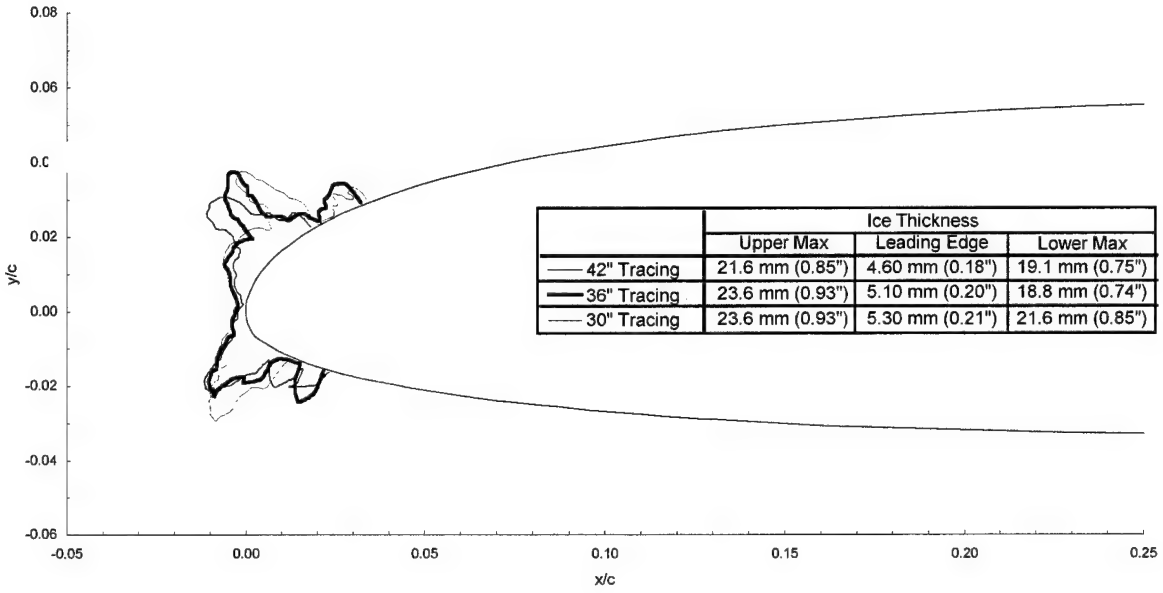

	Ice Thickness		
	Upper Max	Leading Edge	Lower Max
42" Tracing	21.6 mm (0.85")	4.60 mm (0.18")	19.1 mm (0.75")
36" Tracing	23.6 mm (0.93")	5.10 mm (0.20")	18.8 mm (0.74")
30" Tracing	23.6 mm (0.93")	5.30 mm (0.21")	21.6 mm (0.85")

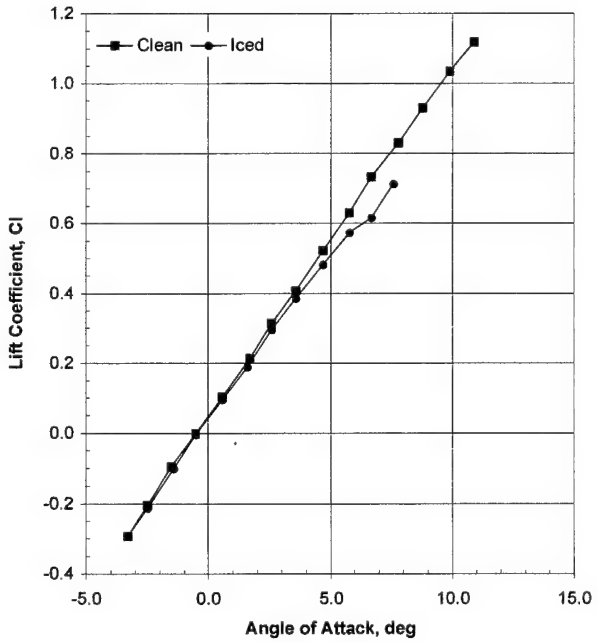

Commercial Transport - Run 144

T_t = -3.28°C (25.5°F)
T_s = -11.6°C (10.4°F)
V = 130 m/s (253 kts)
AOA = 0.7°

LWC = 0.40 g/m^3
MVD = 42 μm
Spray = 3.0 min
chord = 90 cm (36 in)

$C_{d\text{-}clean}$ = 0.0085
$C_{d\text{-}iced}$ = 0.0181
$C_{l\text{-}clean}$ = 0.097
$C_{l\text{-}iced}$ = 0.093

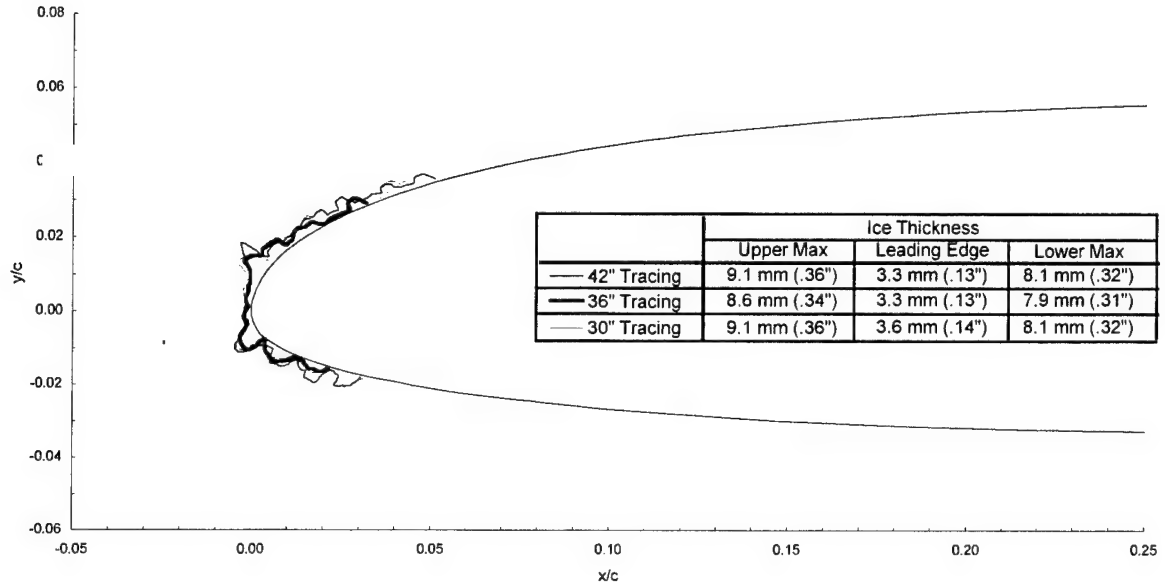

	Ice Thickness		
	Upper Max	Leading Edge	Lower Max
42" Tracing	9.1 mm (.36")	3.3 mm (.13")	8.1 mm (.32")
36" Tracing	8.6 mm (.34")	3.3 mm (.13")	7.9 mm (.31")
30" Tracing	9.1 mm (.36")	3.6 mm (.14")	8.1 mm (.32")

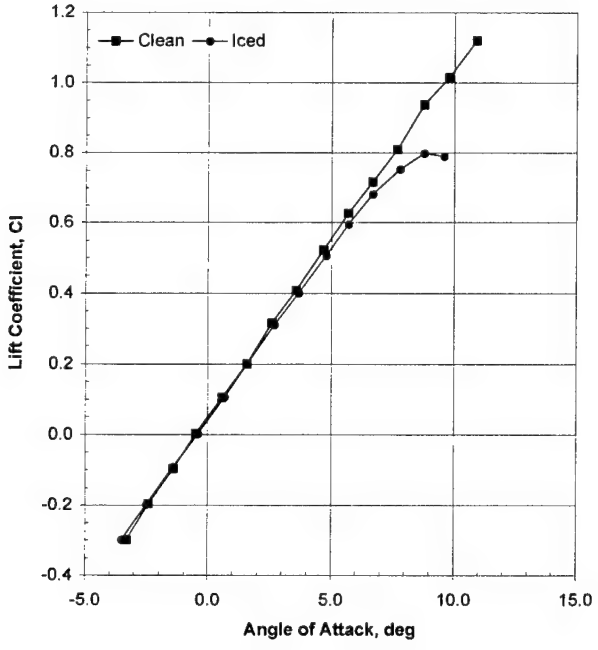

Commercial Transport - Run 145

T_t = -3.28°C (25.5°F)
T_s = -11.6°C (10.4°F)
V = 130 m/s (253 kts)
AOA = 0.7°

LWC = 0.40 g/m^3
MVD = 42 μm
Spray = 11.2 min
chord = 90 cm (36 in)

$C_{d\text{-}clean}$ = 0.0085
$C_{d\text{-}iced}$ = 0.0320
$C_{l\text{-}clean}$ = 0.097
$C_{l\text{-}iced}$ = 0.085

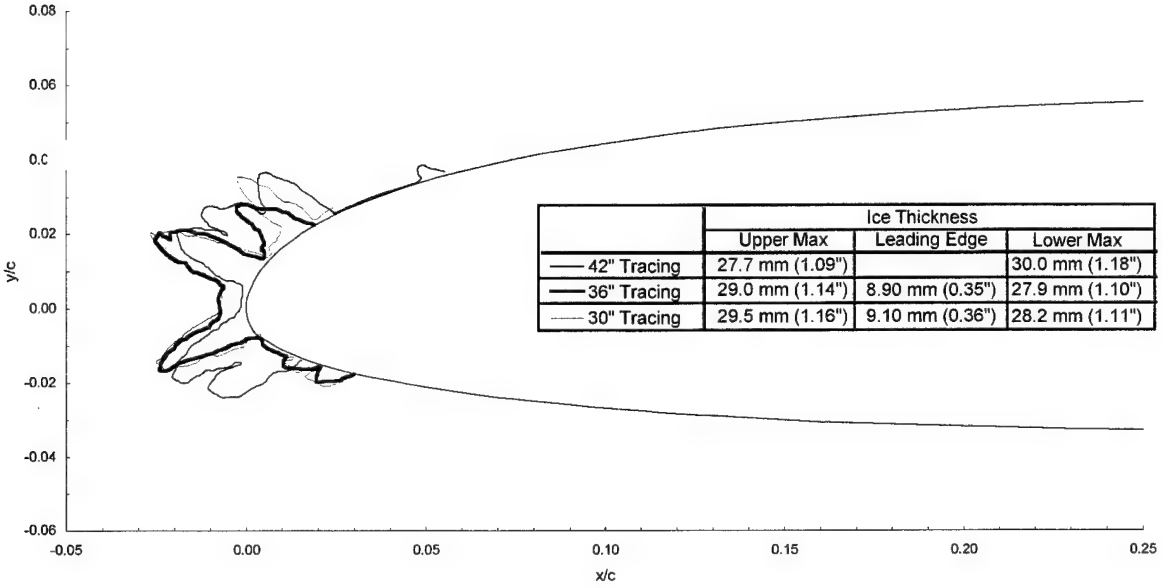

	Ice Thickness		
	Upper Max	Leading Edge	Lower Max
42" Tracing	27.7 mm (1.09")		30.0 mm (1.18")
36" Tracing	29.0 mm (1.14")	8.90 mm (0.35")	27.9 mm (1.10")
30" Tracing	29.5 mm (1.16")	9.10 mm (0.36")	28.2 mm (1.11")

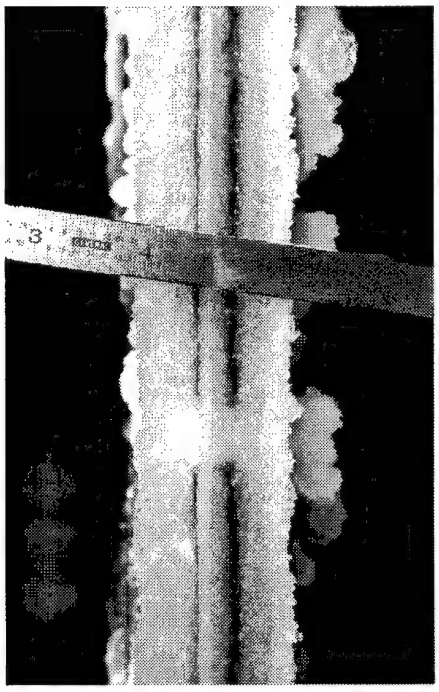

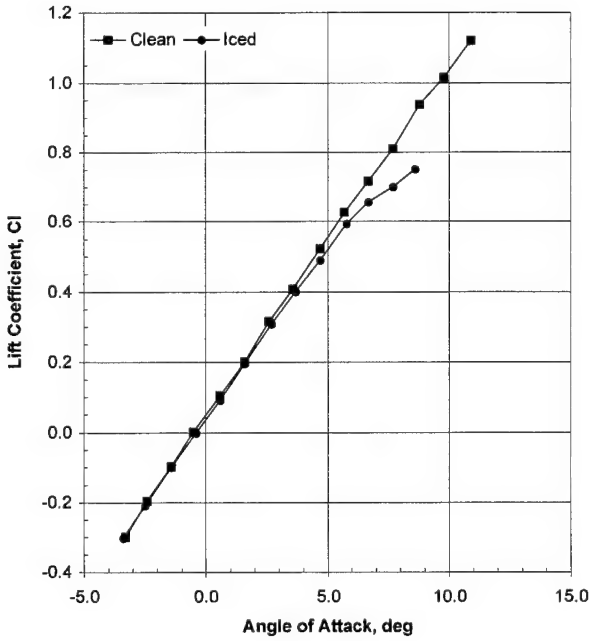

Commercial Transport - Run 145m

T_t = -3.28°C (25.5°F)
T_s = -11.6°C (10.4°F)

V = 130 m/s (253 kts)
AOA = 0.6°

LWC = 0.40 g/m^3
MVD = 42 μm
Spray = 11.2 min
chord = 90 cm (36 in)

$C_{d\text{-}clean}$ = 0.0085
$C_{d\text{-}iced}$ = 0.0301

$C_{l\text{-}clean}$ = 0.095
$C_{l\text{-}iced}$ = 0.086

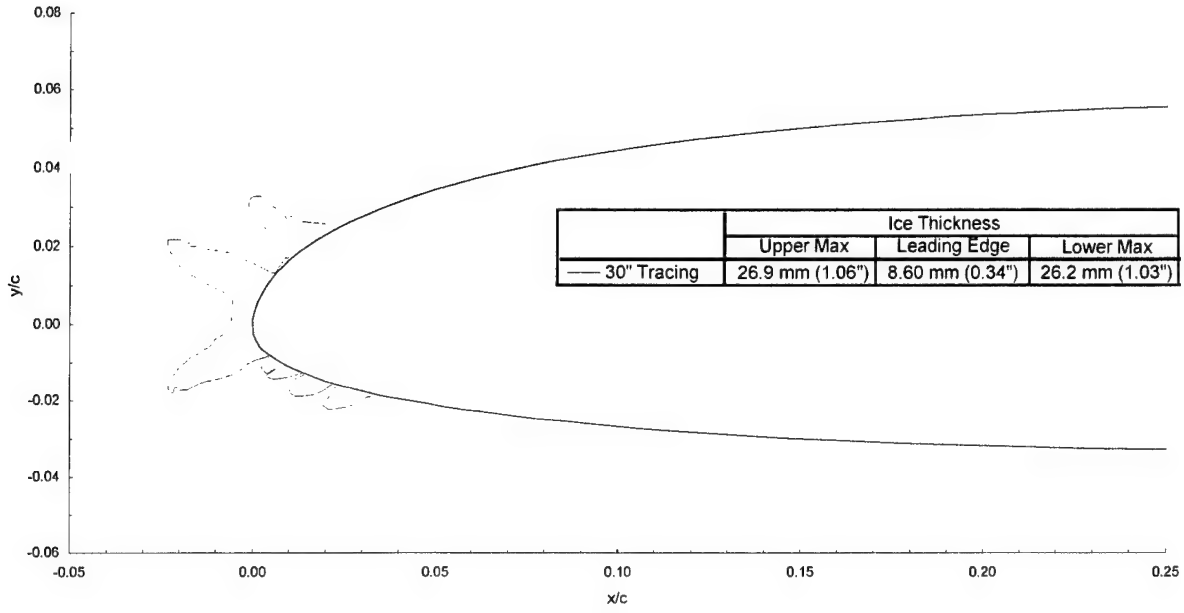

	Ice Thickness		
	Upper Max	Leading Edge	Lower Max
—— 30" Tracing	26.9 mm (1.06")	8.60 mm (0.34")	26.2 mm (1.03")

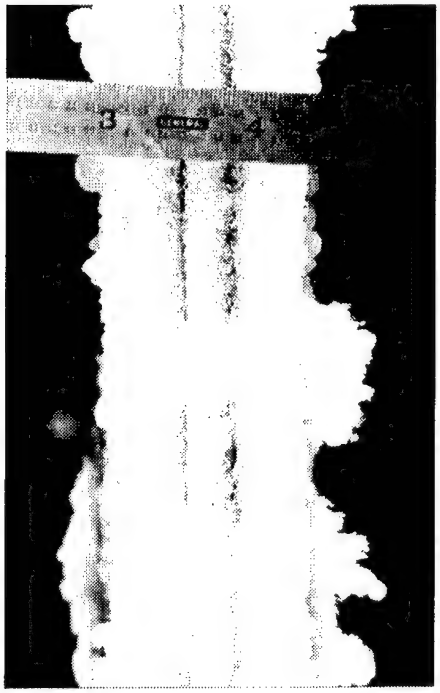

Appendix D4
Test Results, General Aviation

General Aviation - Run 601

T_t = -0.8°C (30°F)
T_s = -5.0°C (22°F)

V = 93.0 m/s (180 kts)
AOA = -1.7°

LWC = 0.54 g/m^3
MVD = 20 μm
Spray = 2.0 min
chord = 90 cm (36 in)

$C_{d\text{-clean}}$ = 0.0099
$C_{d\text{-iced}}$ = 0.0155

$C_{l\text{-clean}}$ = 0.272
$C_{l\text{-iced}}$ = 0.253

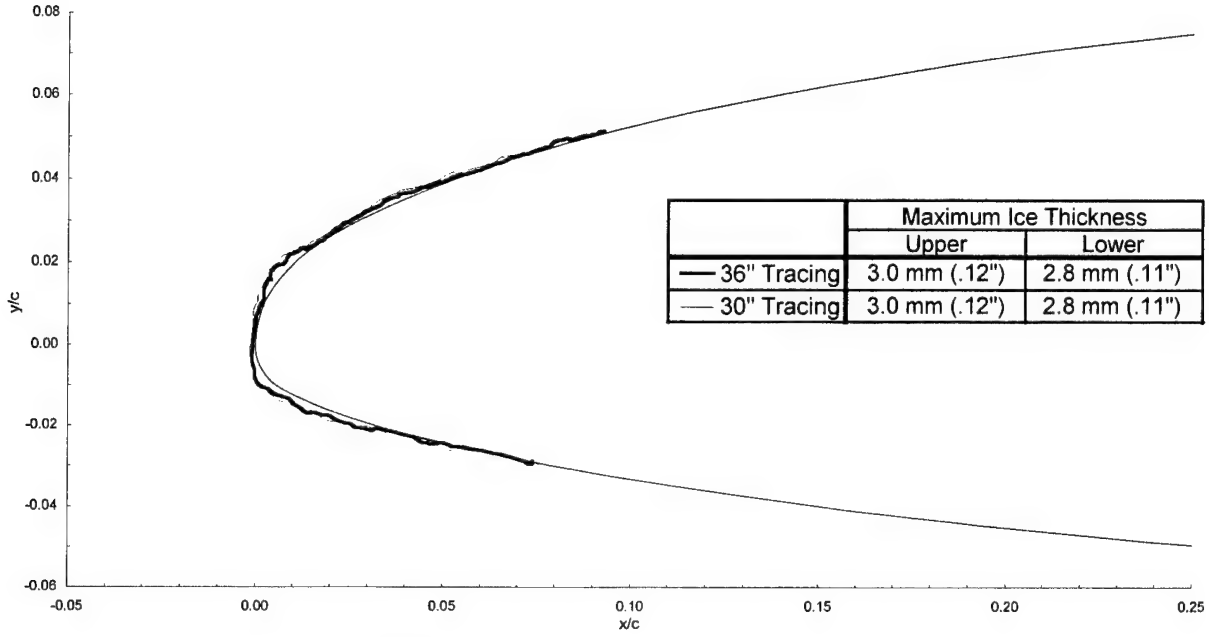

	Maximum Ice Thickness	
	Upper	Lower
— 36" Tracing	3.0 mm (.12")	2.8 mm (.11")
— 30" Tracing	3.0 mm (.12")	2.8 mm (.11")

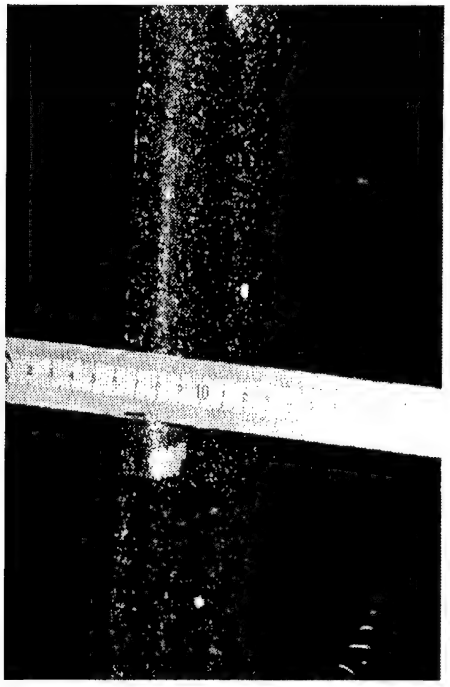

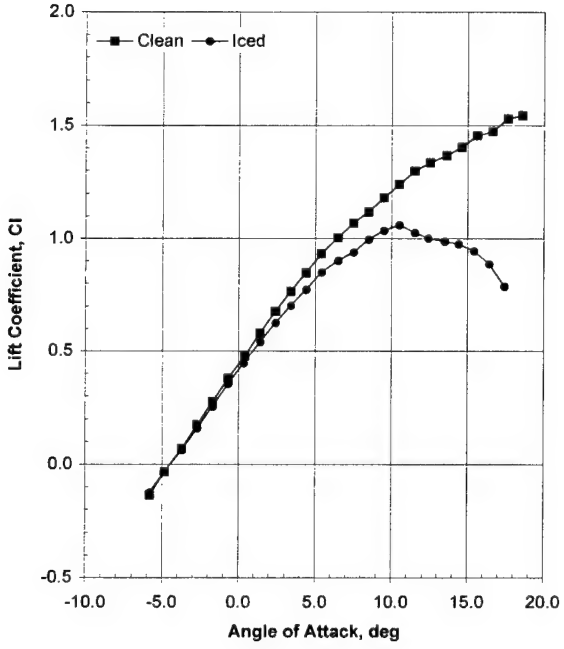

General Aviation - Run 602

T_t = -0.8°C (30°F)
T_s = -5.0°C (22°F)
V = 93.0 m/s (180 kts)
AOA = -1.7°

LWC = 0.54 g/m^3
MVD = 20 μm
Spray = 6.0 min
chord = 90 cm (36 in)

$C_{d\text{-}clean}$ = 0.0099
$C_{d\text{-}iced}$ = 0.0201
$C_{l\text{-}clean}$ = 0.273
$C_{l\text{-}iced}$ = 0.243

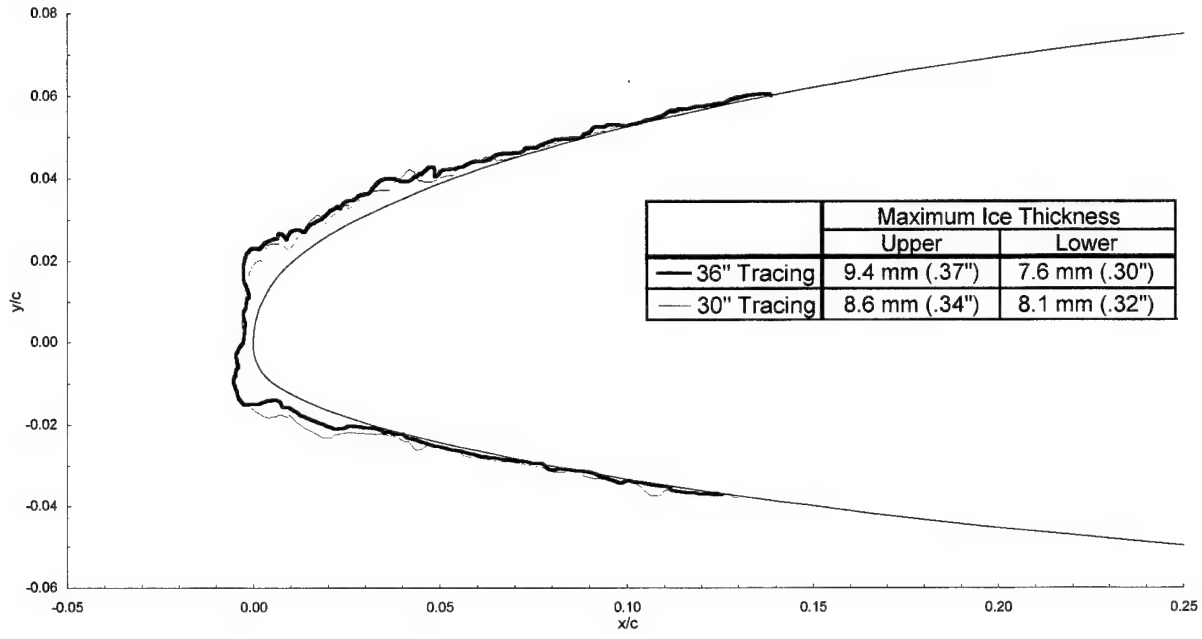

	Maximum Ice Thickness	
	Upper	Lower
—— 36" Tracing	9.4 mm (.37")	7.6 mm (.30")
—— 30" Tracing	8.6 mm (.34")	8.1 mm (.32")

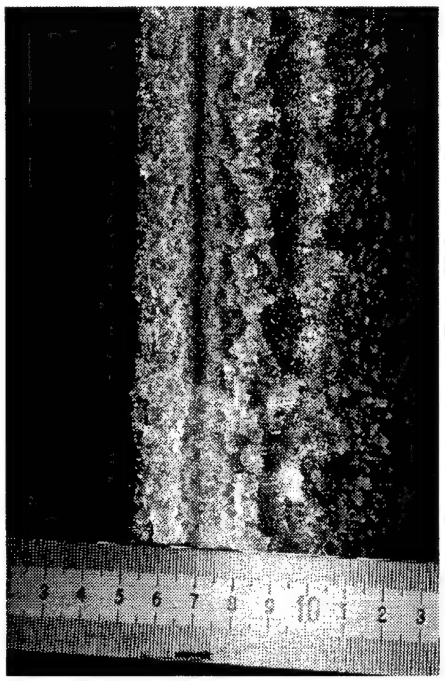

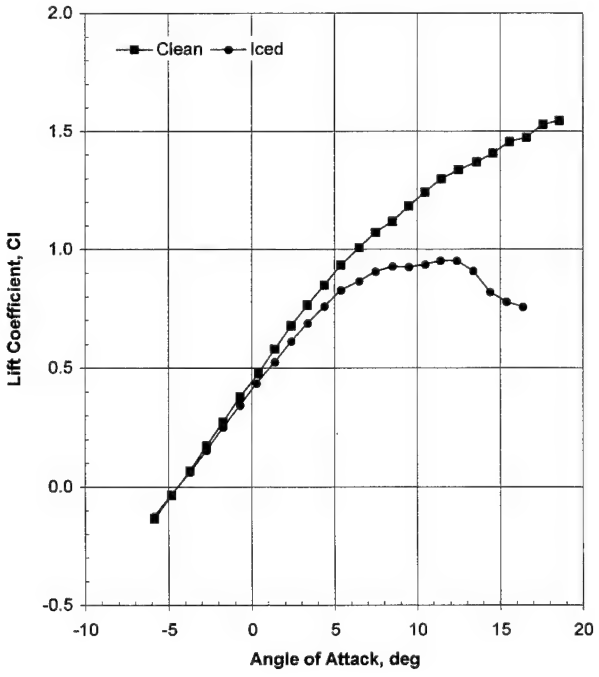

General Aviation - Run 602m

T_t = -0.8°C (30.0°F)
T_s = -5.0°C (22.0°F)
V = 93.0 m/s (180 kts)
AOA = -1.7°

LWC = 0.54 g/m^3
MVD = 20 μm
Spray = 6.0 min
chord = 90 cm (36 in)

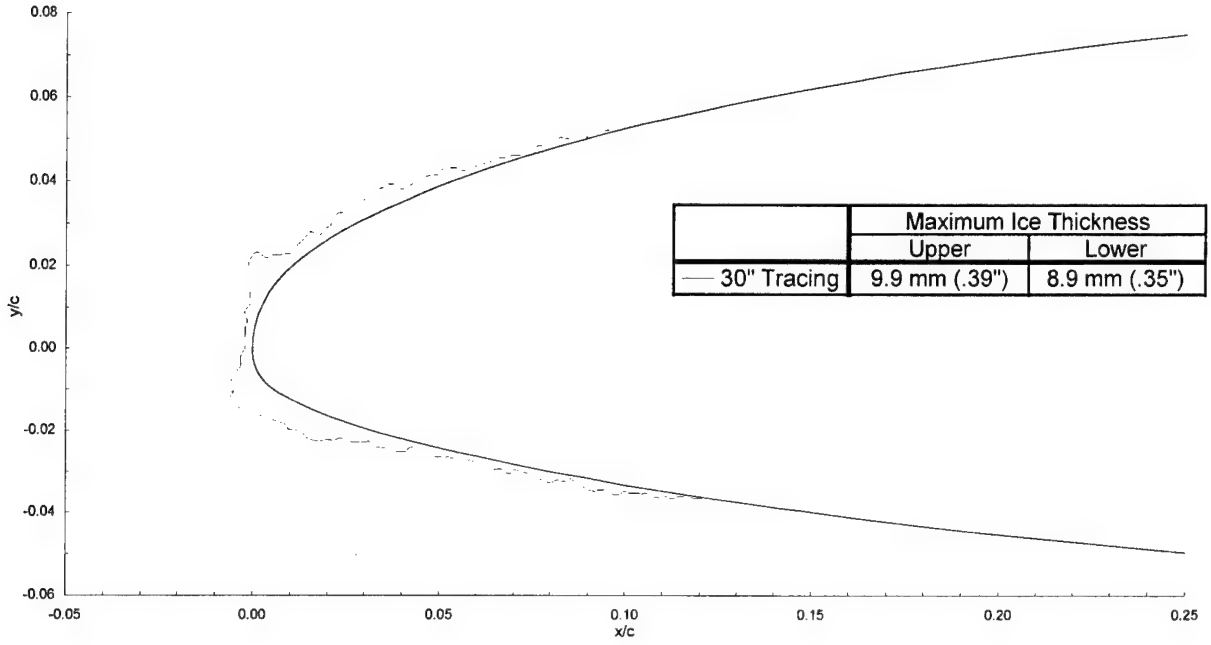

	Maximum Ice Thickness	
	Upper	Lower
— 30" Tracing	9.9 mm (.39")	8.9 mm (.35")

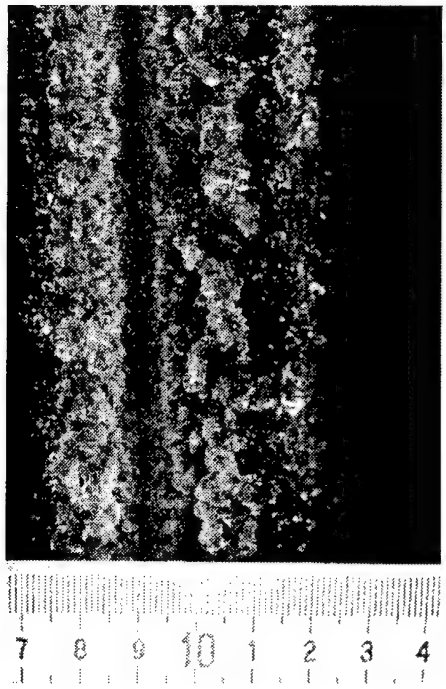

General Aviation - Run 603

T_t = -0.8°C (30.0°F)
T_s = -5.0°C (22.0°F)

V = 93.0 m/s (180 kts)
AOA = -1.7°

LWC = 0.54 g/m^3
MVD = 20 μm
Spray = 22.5 min
chord = 90 cm (36 in)

$C_{d\text{-}clean}$ = 0.0099
$C_{d\text{-}iced}$ = 0.0466

$C_{l\text{-}clean}$ = 0.274
$C_{l\text{-}iced}$ = 0.221

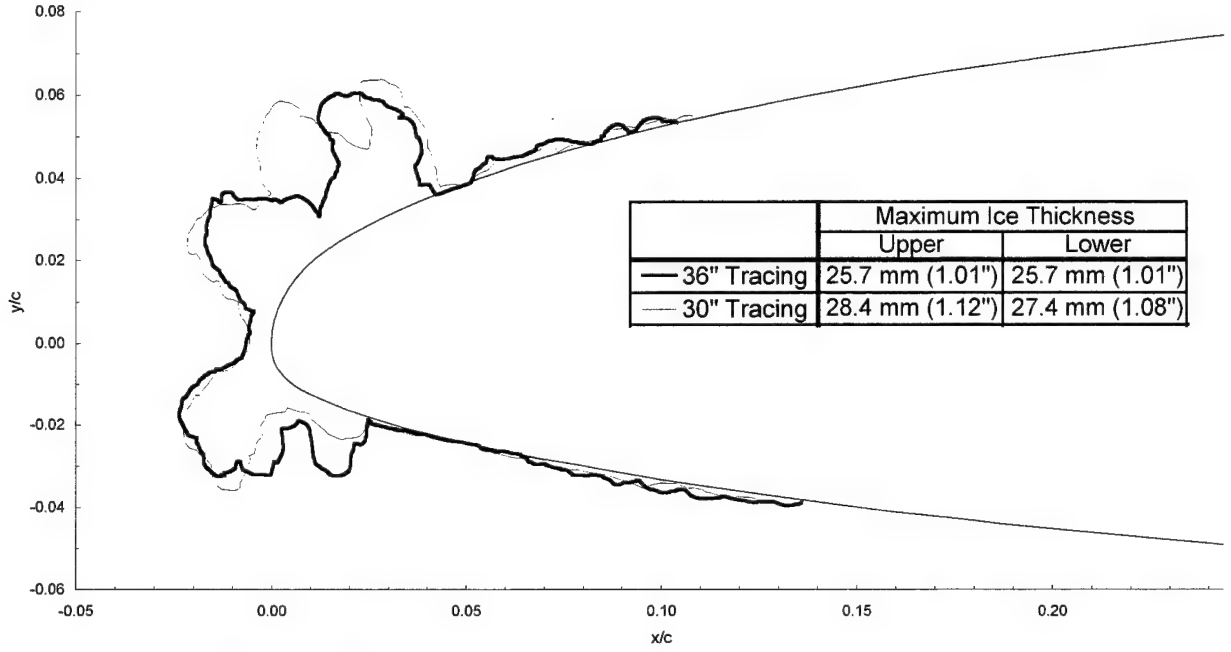

	Maximum Ice Thickness	
	Upper	Lower
36" Tracing	25.7 mm (1.01")	25.7 mm (1.01")
30" Tracing	28.4 mm (1.12")	27.4 mm (1.08")

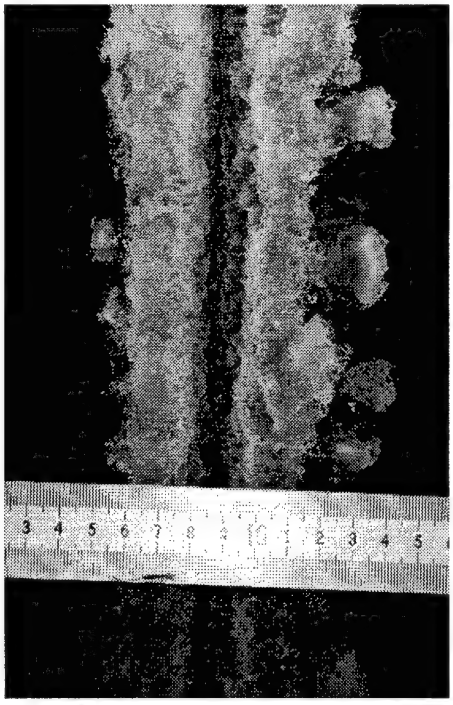

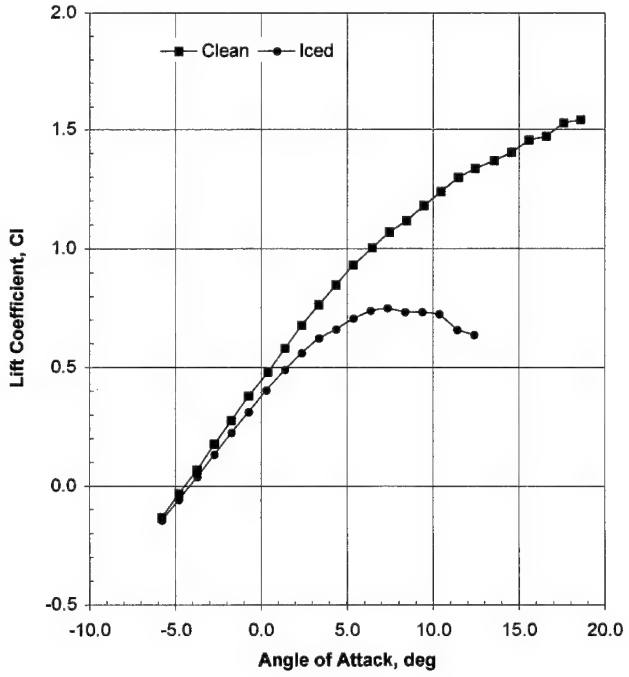

General Aviation - Run 606

T_t = -5.9°C (20.8°F)
T_s = -10.0°C (13.4°F)

V = 93.0 m/s (180 kts)
AOA = -1.7°

LWC = 0.43 g/m^3
MVD = 20 μm
Spray = 2.0 min
chord = 90 cm (36 in)

$C_{d\text{-}clean}$ = 0.0099
$C_{d\text{-}iced}$ = 0.0124

$C_{l\text{-}clean}$ = 0.274
$C_{l\text{-}iced}$ = 0.258

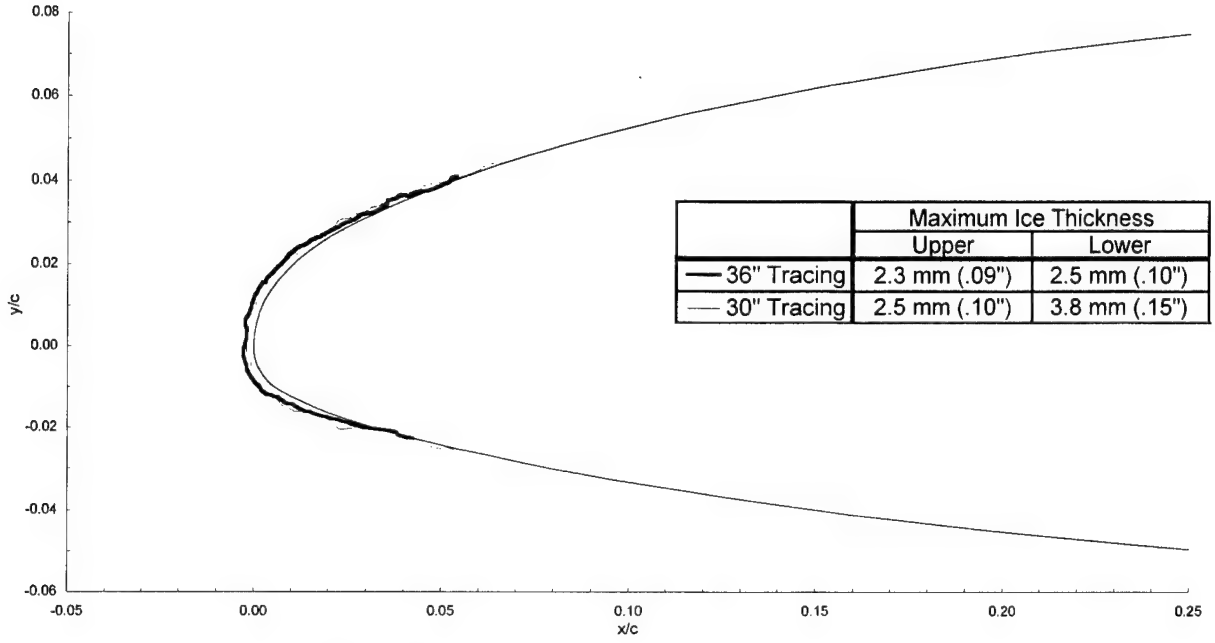

	Maximum Ice Thickness	
	Upper	Lower
36" Tracing	2.3 mm (.09")	2.5 mm (.10")
30" Tracing	2.5 mm (.10")	3.8 mm (.15")

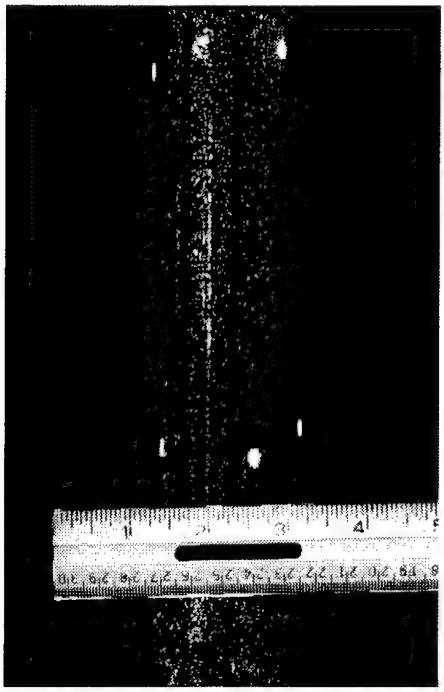

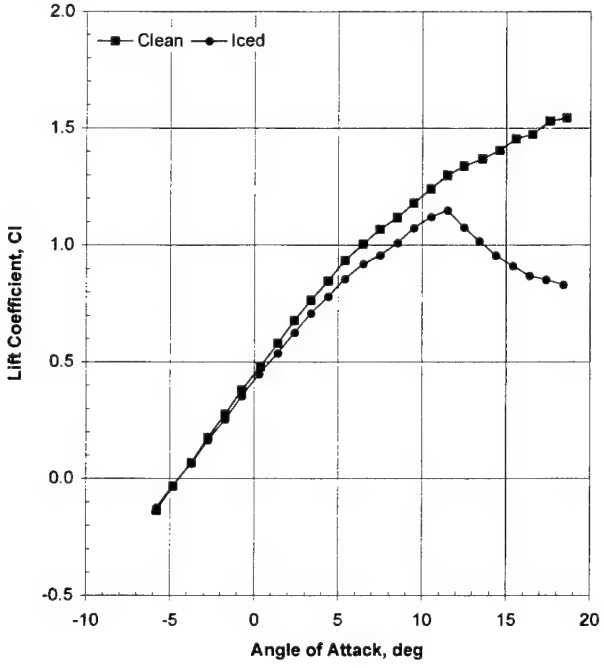

General Aviation - Run 607

T_t = -5.9°C (20.8°F)
T_s = -10.0°C (13.4°F)
V = 93.0 m/s (180 kts)
AOA = -1.7°

LWC = 0.43 g/m^3
MVD = 20 μm
Spray = 6.0 min
chord = 90 cm (36 in)

$C_{d\text{-}clean}$ = 0.0099
$C_{d\text{-}iced}$ = 0.0158
$C_{l\text{-}clean}$ = 0.274
$C_{l\text{-}iced}$ = 0.253

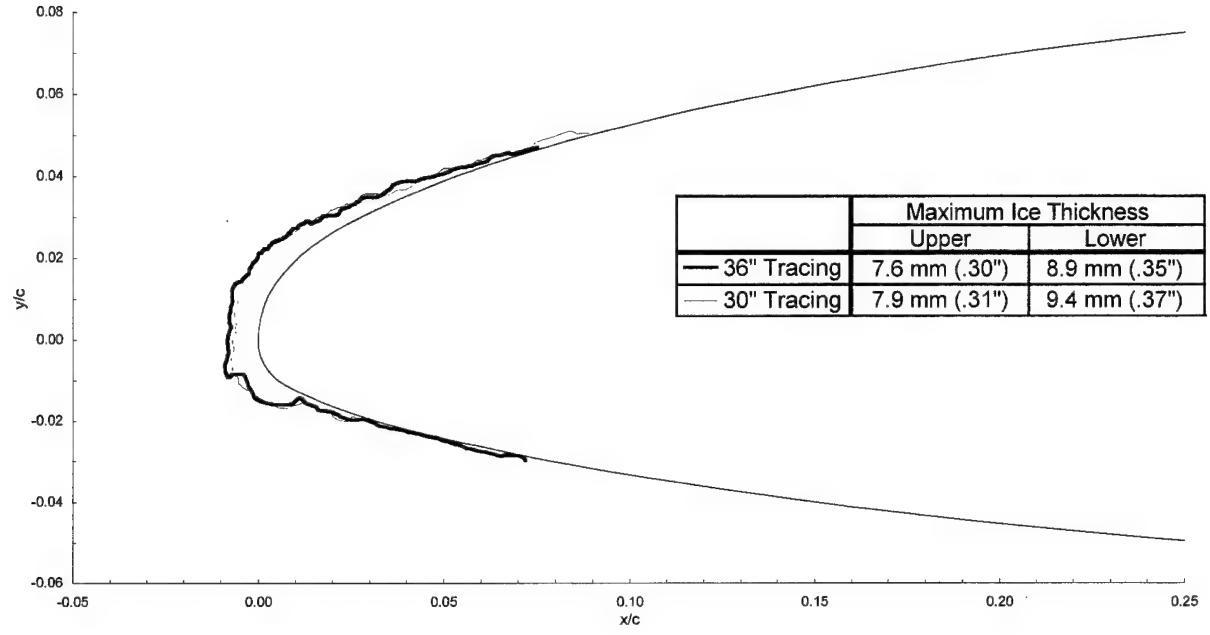

	Maximum Ice Thickness	
	Upper	Lower
36" Tracing	7.6 mm (.30")	8.9 mm (.35")
30" Tracing	7.9 mm (.31")	9.4 mm (.37")

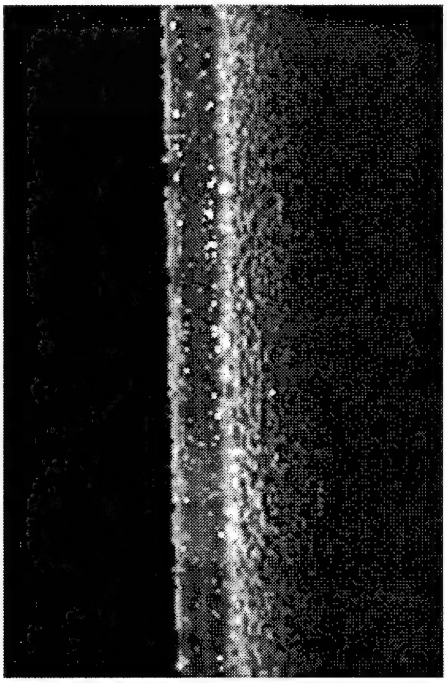

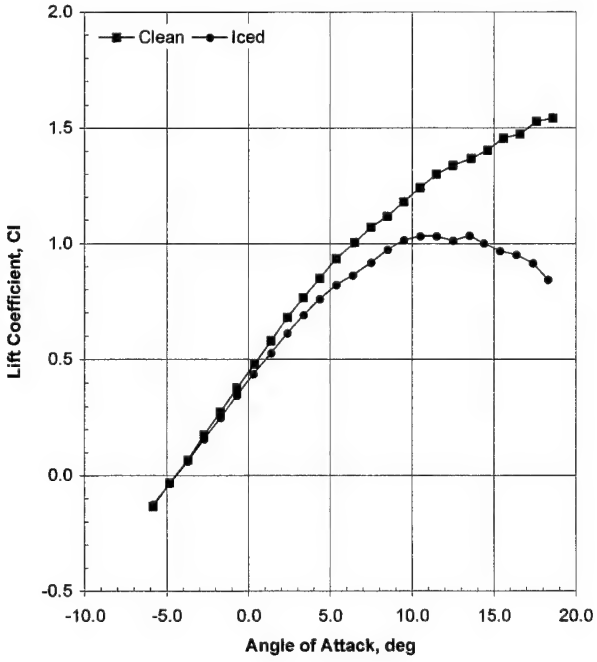

General Aviation - Run 608

T_t = -5.9°C (20.8°F)
T_s = -10.0°C (13.4°F)

V = 93.0 m/s (180 kts)
AOA = -1.7°

LWC = 0.43 g/m^3
MVD = 20 μm
Spray = 22.5 min
chord = 90 cm (36 in)

$C_{d\text{-}clean}$ = 0.0099
$C_{d\text{-}iced}$ = 0.0241

$C_{l\text{-}clean}$ = 0.275
$C_{l\text{-}iced}$ = 0.244

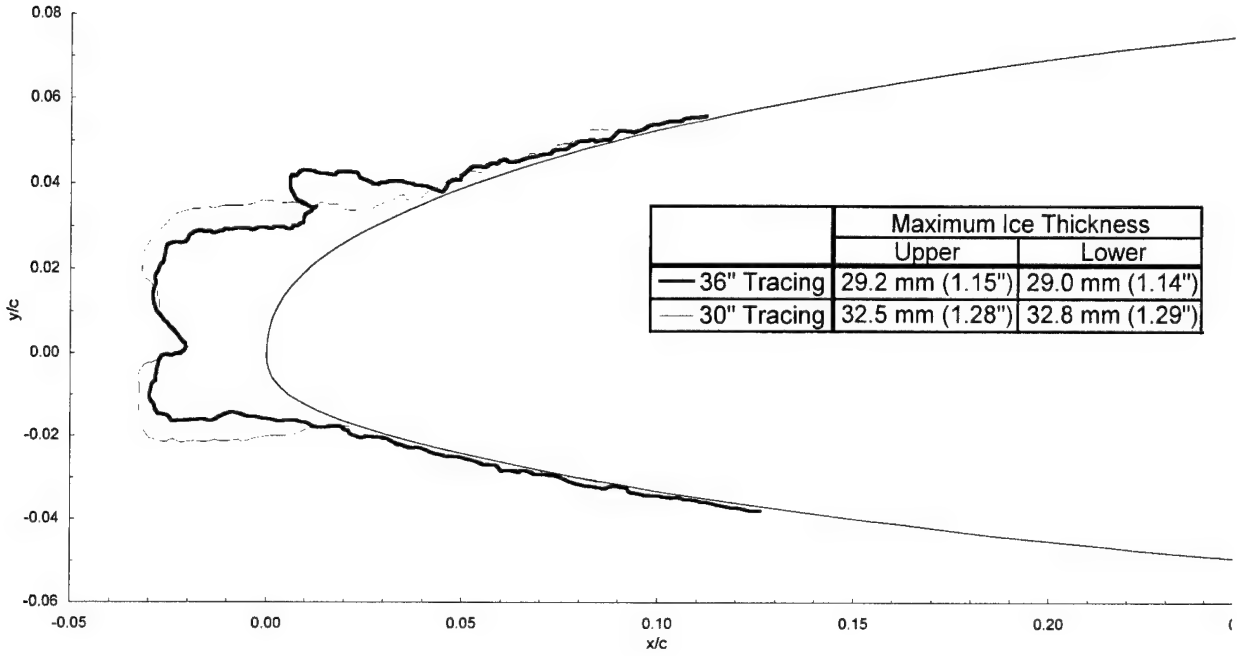

	Maximum Ice Thickness	
	Upper	Lower
—— 36" Tracing	29.2 mm (1.15")	29.0 mm (1.14")
—— 30" Tracing	32.5 mm (1.28")	32.8 mm (1.29")

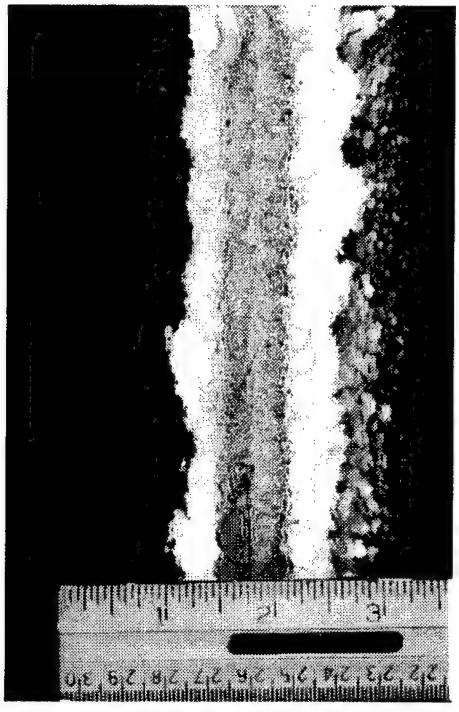

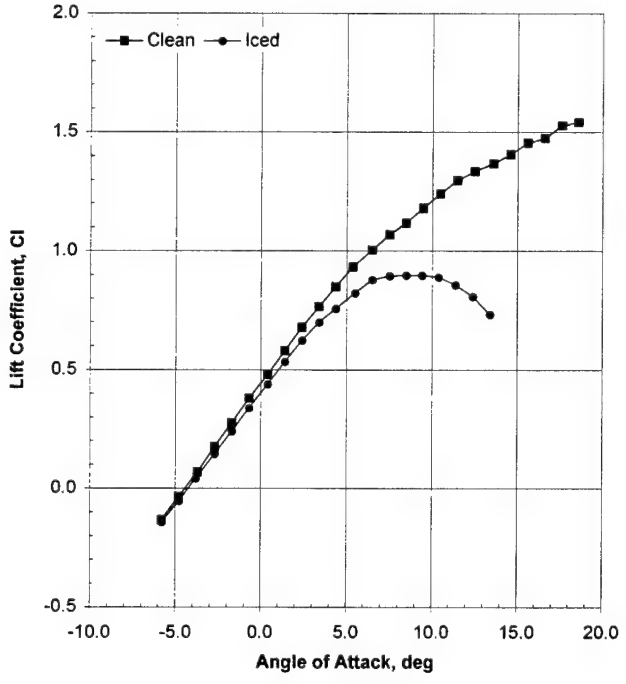

General Aviation - Run 609

T_t = -11.0°C (11.7°F)
T_s = -15.0°C (4.4°F)
V = 93.0 m/s (180 kts)
AOA = -1.7°

LWC = 0.33 g/m^3
MVD = 20 μm
Spray = 2.0 min
chord = 90 cm (36 in)

$C_{d\text{-clean}}$ = 0.0099
$C_{d\text{-iced}}$ = 0.0126
$C_{l\text{-clean}}$ = 0.272
$C_{l\text{-iced}}$ = 0.258

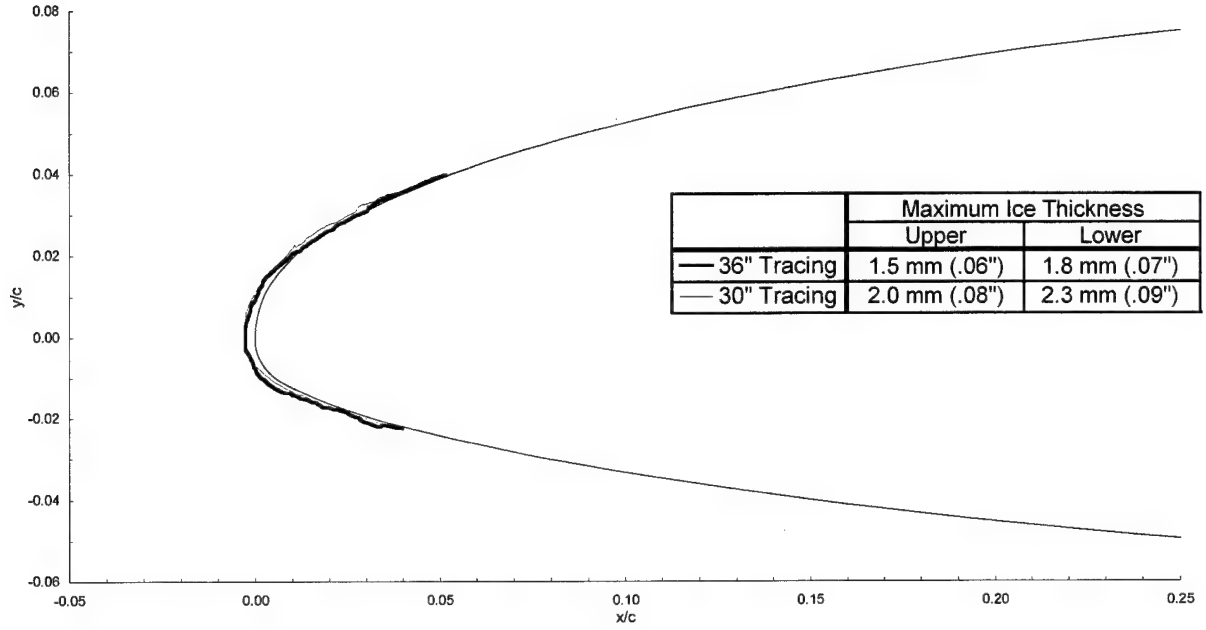

	Maximum Ice Thickness	
	Upper	Lower
— 36" Tracing	1.5 mm (.06")	1.8 mm (.07")
— 30" Tracing	2.0 mm (.08")	2.3 mm (.09")

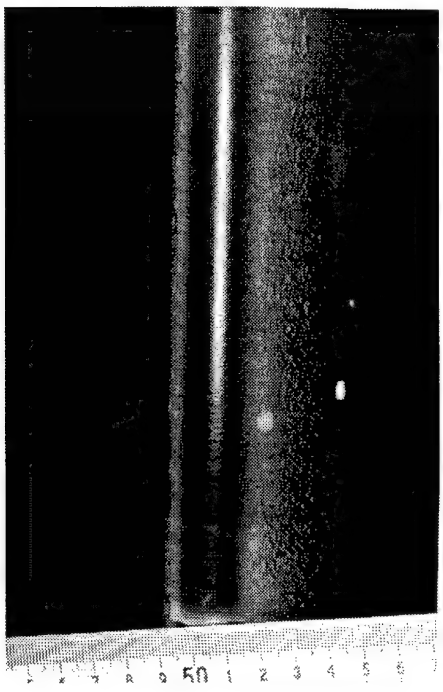

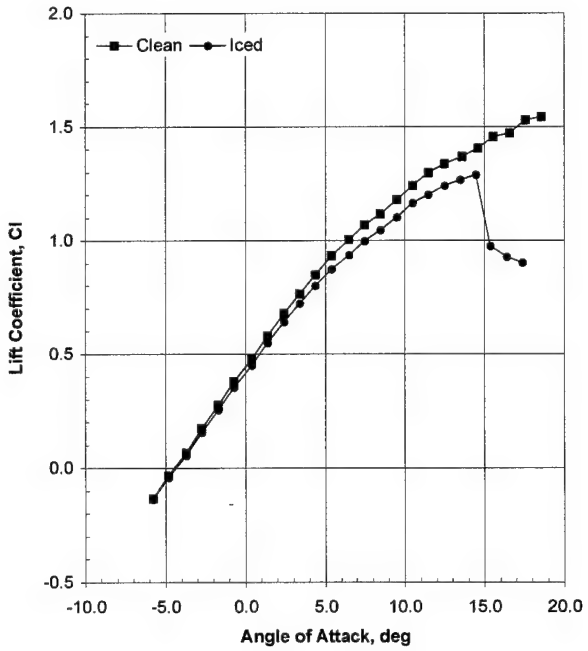

General Aviation - Run 610

T_t = -11.0°C (11.7°F)
T_s = -15.0°C (4.4°F)

V = 93.0 m/s (180 kts)
AOA = -1.7°

LWC = 0.33 g/m^3
MVD = 20 μm
Spray = 6.0 min
chord = 90 cm (36 in)

$C_{d\text{-clean}}$ = 0.0099
$C_{d\text{-iced}}$ = 0.0147

$C_{l\text{-clean}}$ = 0.268
$C_{l\text{-iced}}$ = 0.253

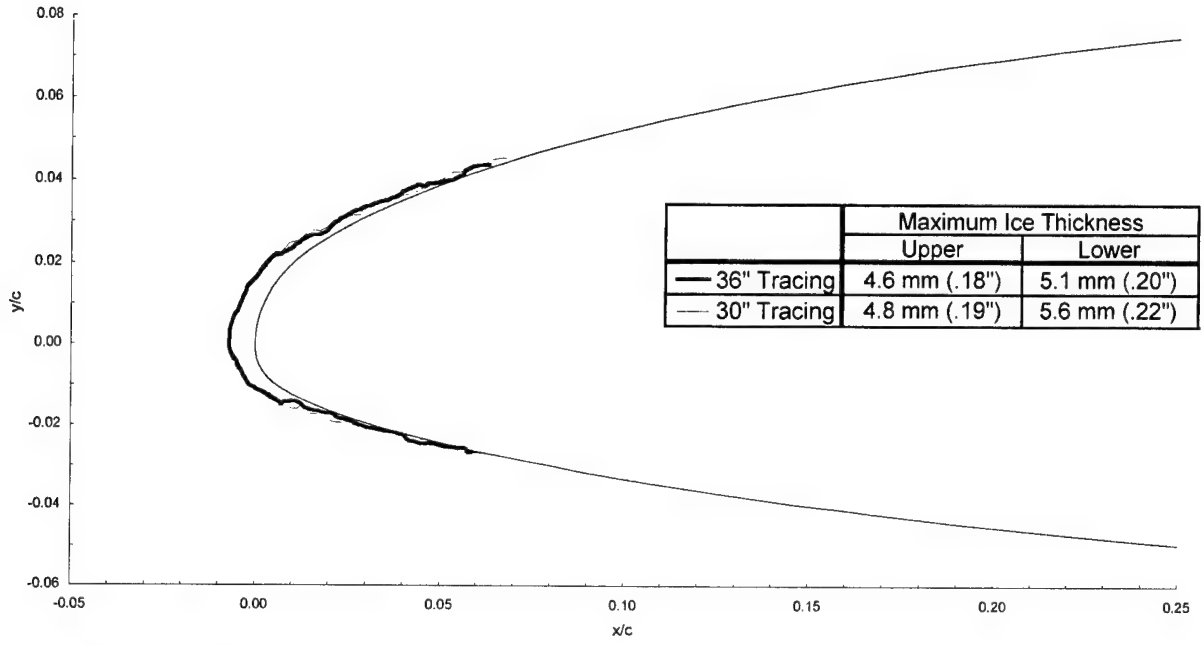

	Maximum Ice Thickness	
	Upper	Lower
—— 36" Tracing	4.6 mm (.18")	5.1 mm (.20")
—— 30" Tracing	4.8 mm (.19")	5.6 mm (.22")

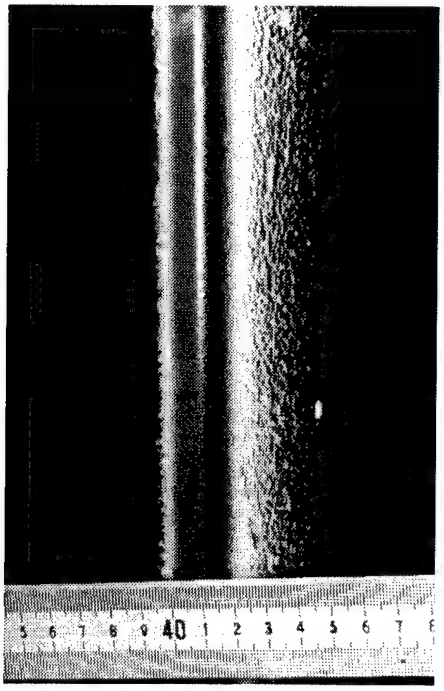

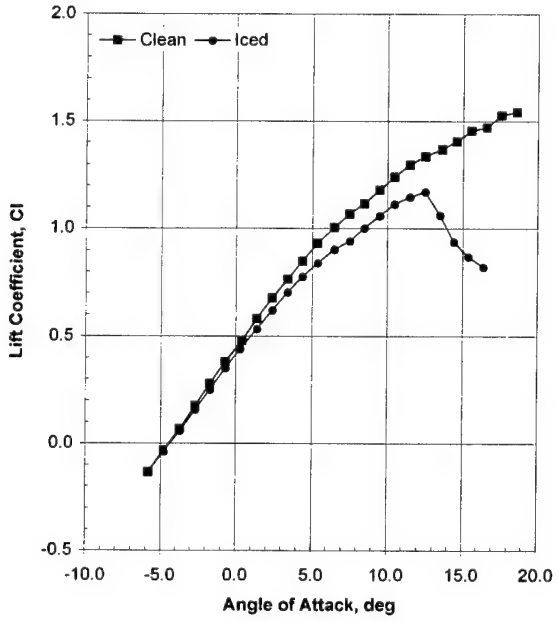

General Aviation - Run 611

T_t = -11.0°C (11.7°F)
T_s = -15.0°C (4.4°F)
V = 93.0 m/s (180 kts)
AOA = -1.7°

LWC = 0.33 g/m^3
MVD = 20 μm
Spray = 22.5 min
chord = 90 cm (36 in)

$C_{d\text{-}clean}$ = 0.0099
$C_{d\text{-}iced}$ = 0.0192
$C_{l\text{-}clean}$ = 0.272
$C_{l\text{-}iced}$ = 0.242

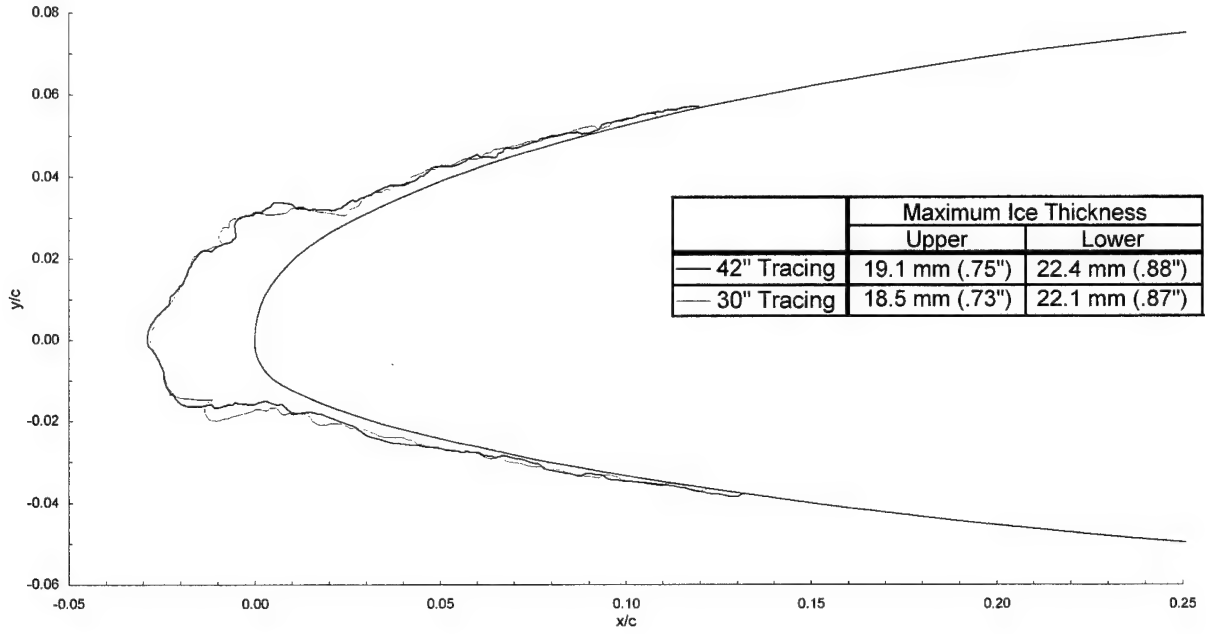

	Maximum Ice Thickness	
	Upper	Lower
— 42" Tracing	19.1 mm (.75")	22.4 mm (.88")
— 30" Tracing	18.5 mm (.73")	22.1 mm (.87")

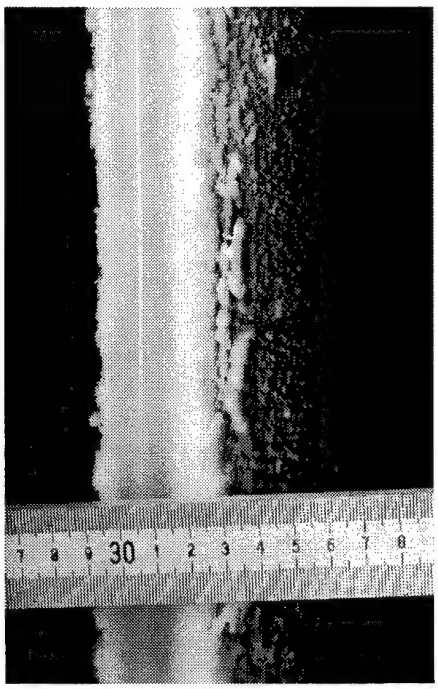

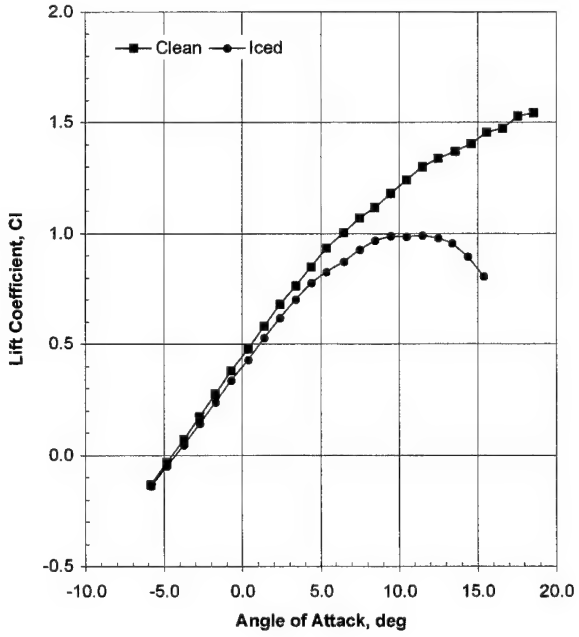

General Aviation - Run 612

T_t = -5.9°C (20.8°F)
T_s = -10.0°C (13.4°F)

V = 93.0 m/s (180 kts)
AOA = -1.7°

LWC = 0.56 g/m^3
MVD = 15 μm
Spray = 2.0 min
chord = 90 cm (36 in)

$C_{d\text{-}clean}$ = 0.0099
$C_{d\text{-}iced}$ = 0.0121

$C_{l\text{-}clean}$ = 0.272
$C_{l\text{-}iced}$ = 0.257

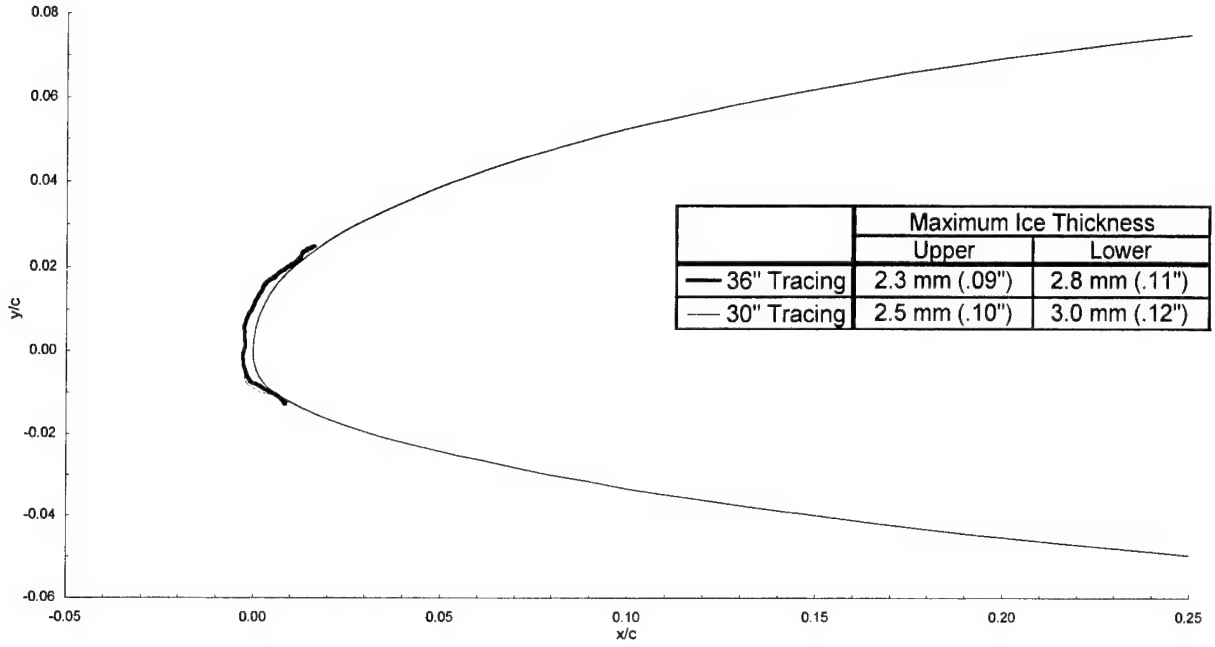

	Maximum Ice Thickness	
	Upper	Lower
— 36" Tracing	2.3 mm (.09")	2.8 mm (.11")
— 30" Tracing	2.5 mm (.10")	3.0 mm (.12")

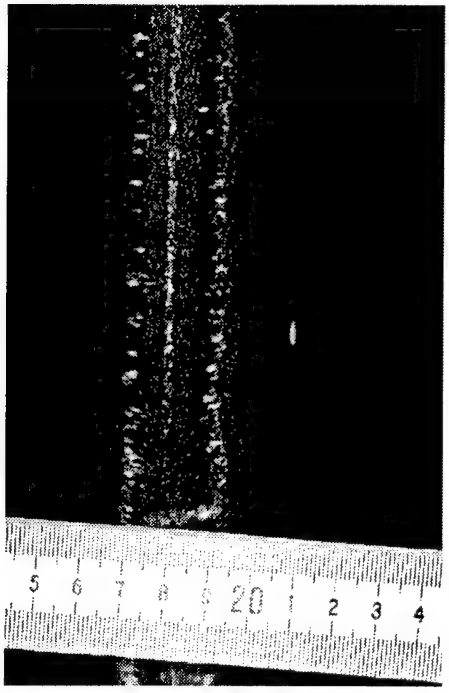

General Aviation - Run 612r

T_t = -5.9°C (20.8°F)
T_s = -10.0°C (13.4°F)

V = 93.0 m/s (180 kts)
AOA = -1.7°

LWC = 0.56 g/m^3
MVD = 15 μm
Spray = 2.0 min
chord = 90 cm (36 in)

$C_{d\text{-}clean}$ = 0.0099
$C_{d\text{-}iced}$ = 0.0124

$C_{l\text{-}clean}$ = 0.272
$C_{l\text{-}iced}$ = 0.261

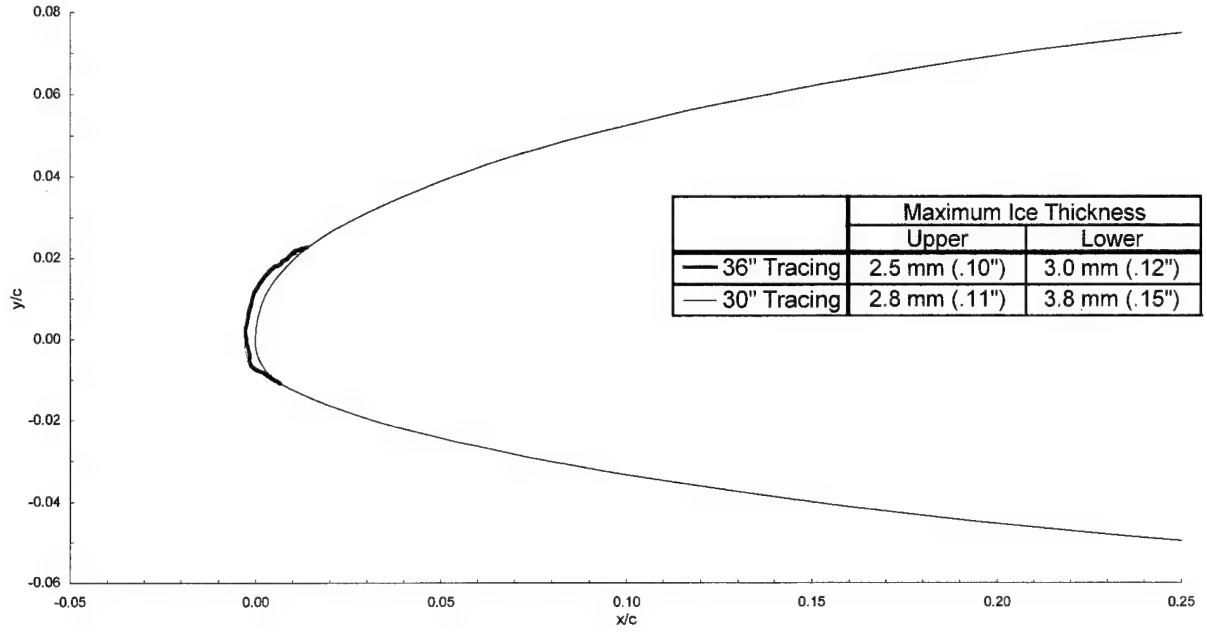

	Maximum Ice Thickness	
	Upper	Lower
—— 36" Tracing	2.5 mm (.10")	3.0 mm (.12")
—— 30" Tracing	2.8 mm (.11")	3.8 mm (.15")

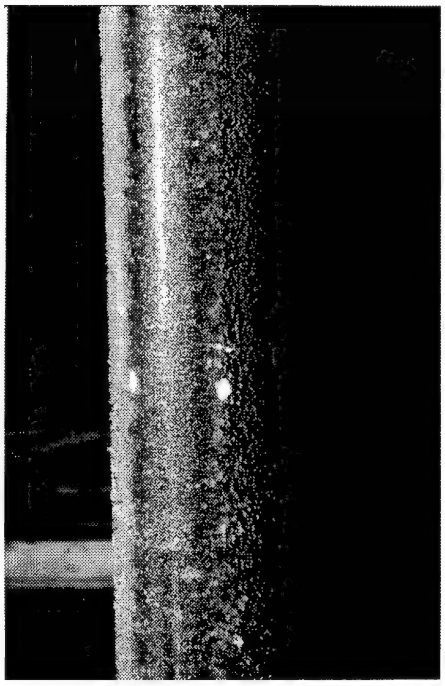

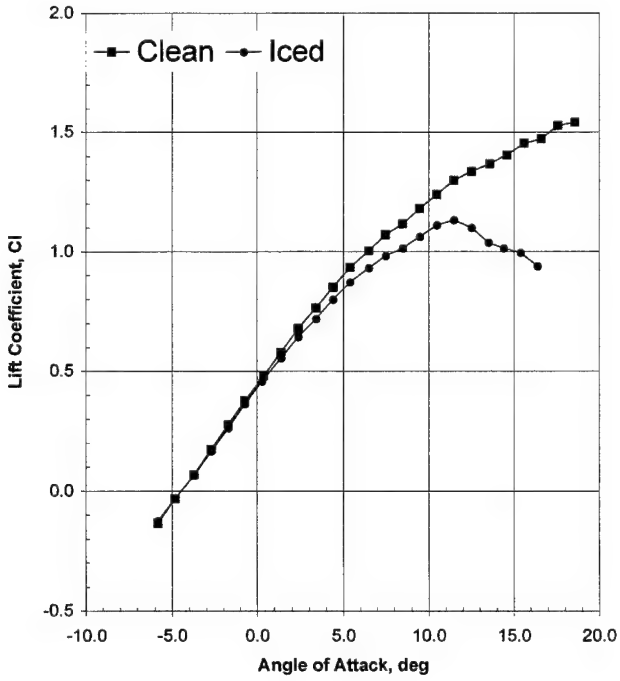

General Aviation - Run 613

T_t = -5.9°C (20.8°F)
T_s = -10.0°C (13.4°F)

V = 93.0 m/s (180 kts)
AOA = -1.7°

LWC = 0.56 g/m^3
MVD = 15 μm
Spray = 6.0 min
chord = 90 cm (36 in)

$C_{d\text{-}clean}$ = 0.0099
$C_{d\text{-}iced}$ = 0.0146

$C_{l\text{-}clean}$ = 0.273
$C_{l\text{-}iced}$ = 0.239

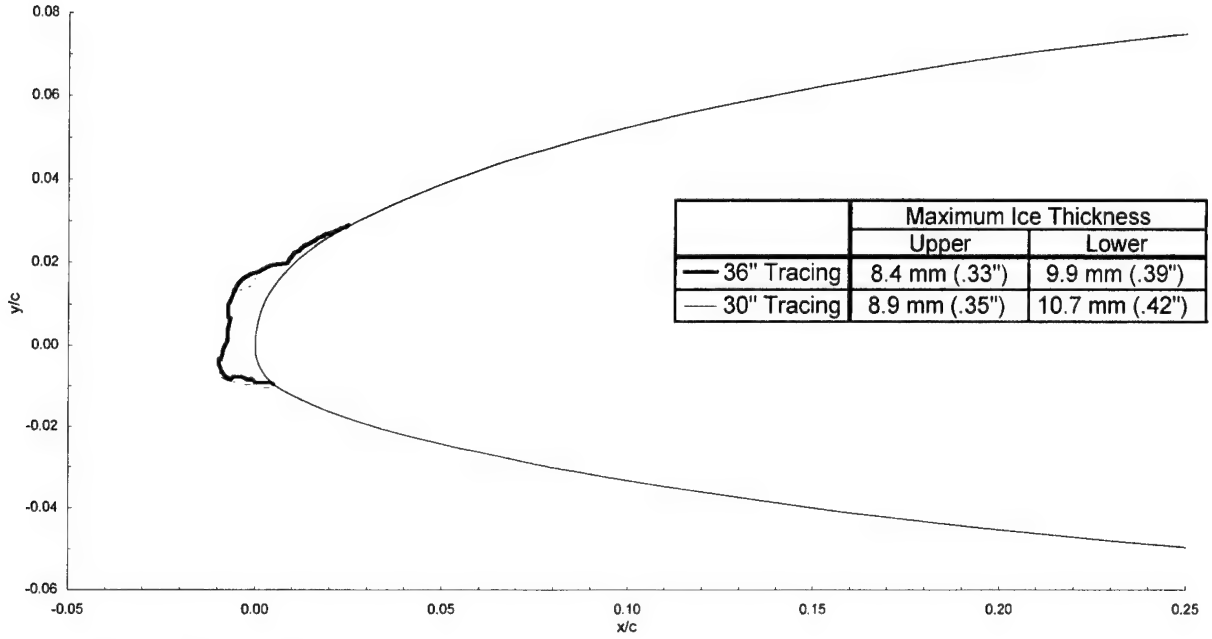

	Maximum Ice Thickness	
	Upper	Lower
36" Tracing	8.4 mm (.33")	9.9 mm (.39")
30" Tracing	8.9 mm (.35")	10.7 mm (.42")

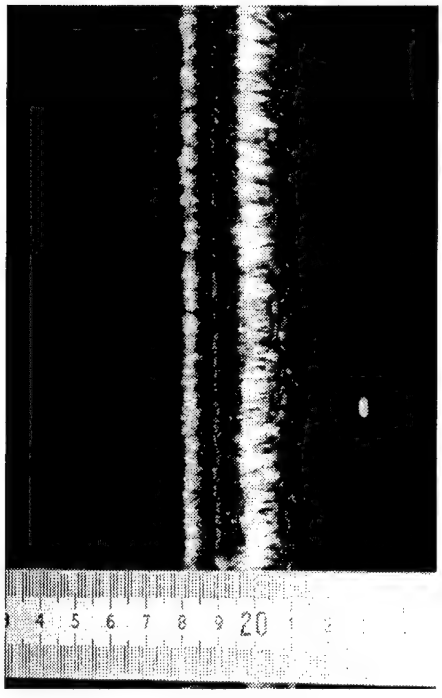

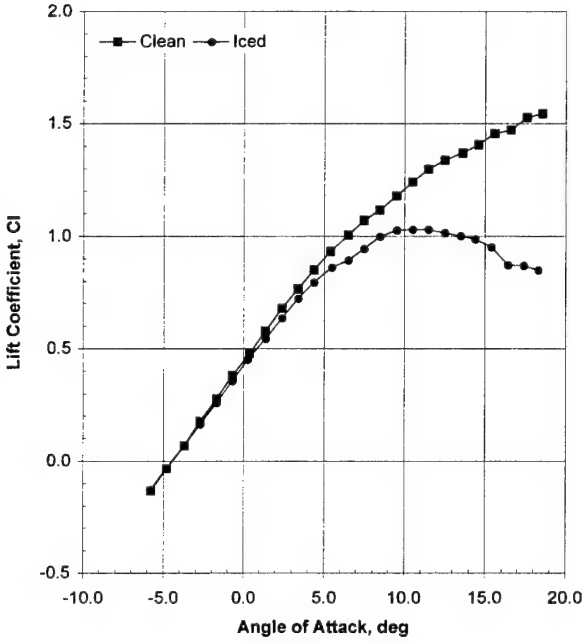

General Aviation - Run 621

T_t = -2.8°C (26.4°F)
T_s = -5.0°C (22.4°F)

V = 66.9 m/s (130 kts)
AOA = 0.4°

LWC = 0.54 g/m^3
MVD = 20 μm
Spray = 2.0 min
chord = 90 cm (36 in)

$C_{d\text{-}clean}$ = 0.0105
$C_{d\text{-}iced}$ = 0.0153

$C_{l\text{-}clean}$ = 0.483
$C_{l\text{-}iced}$ = 0.453

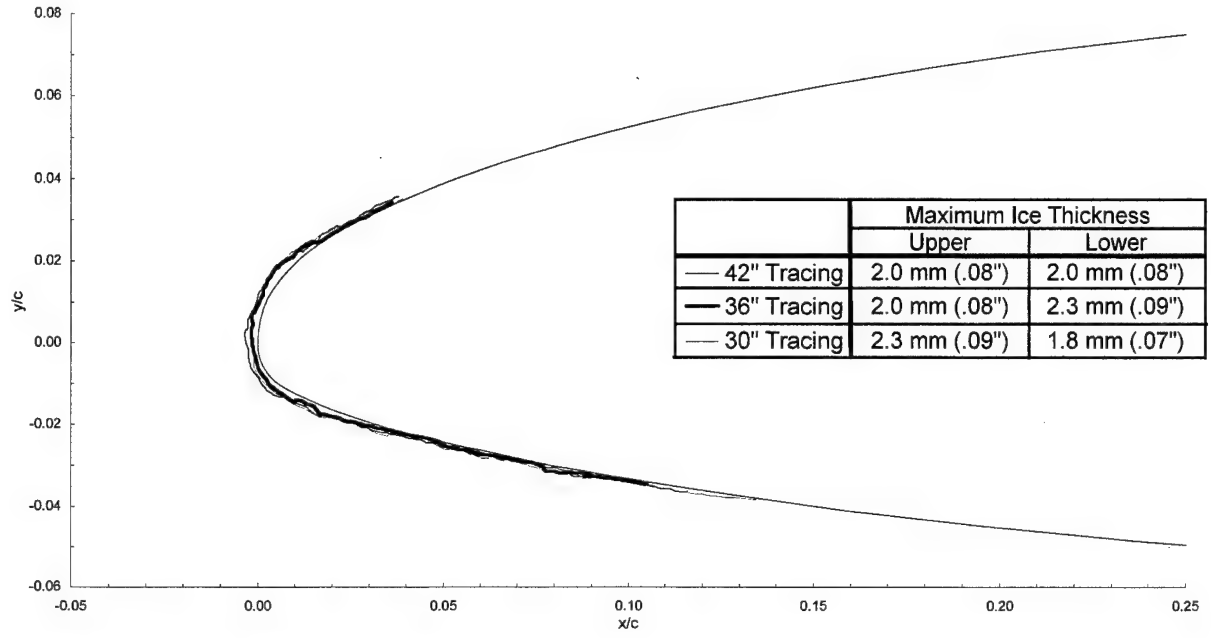

	Maximum Ice Thickness	
	Upper	Lower
42" Tracing	2.0 mm (.08")	2.0 mm (.08")
36" Tracing	2.0 mm (.08")	2.3 mm (.09")
30" Tracing	2.3 mm (.09")	1.8 mm (.07")

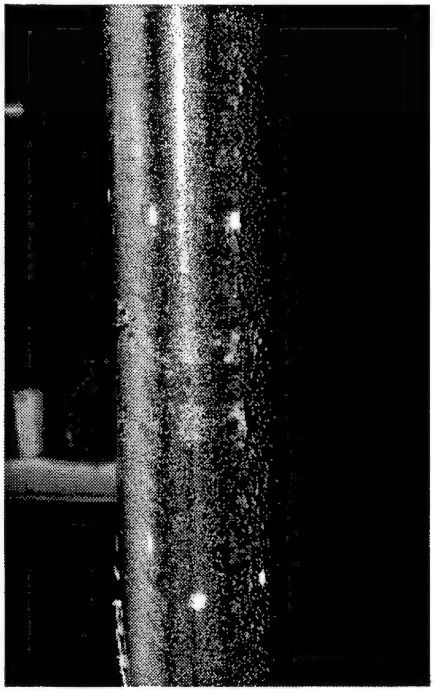

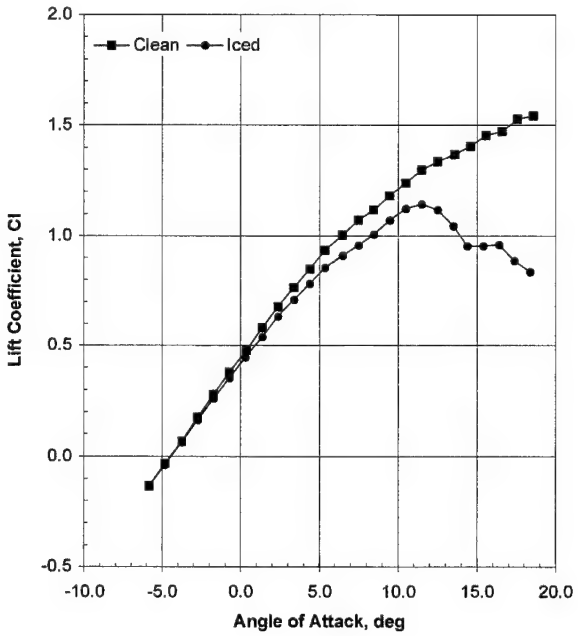

General Aviation - Run 621m

T_t = -2.8°C (26.4°F)
T_s = -5.0°C (22.4°F)
V = 66.9 m/s (130 kts)
AOA = 0.4°

LWC = 0.54 g/m^3
MVD = 20 μm
Spray = 2.0 min
chord = 90 cm (36 in)

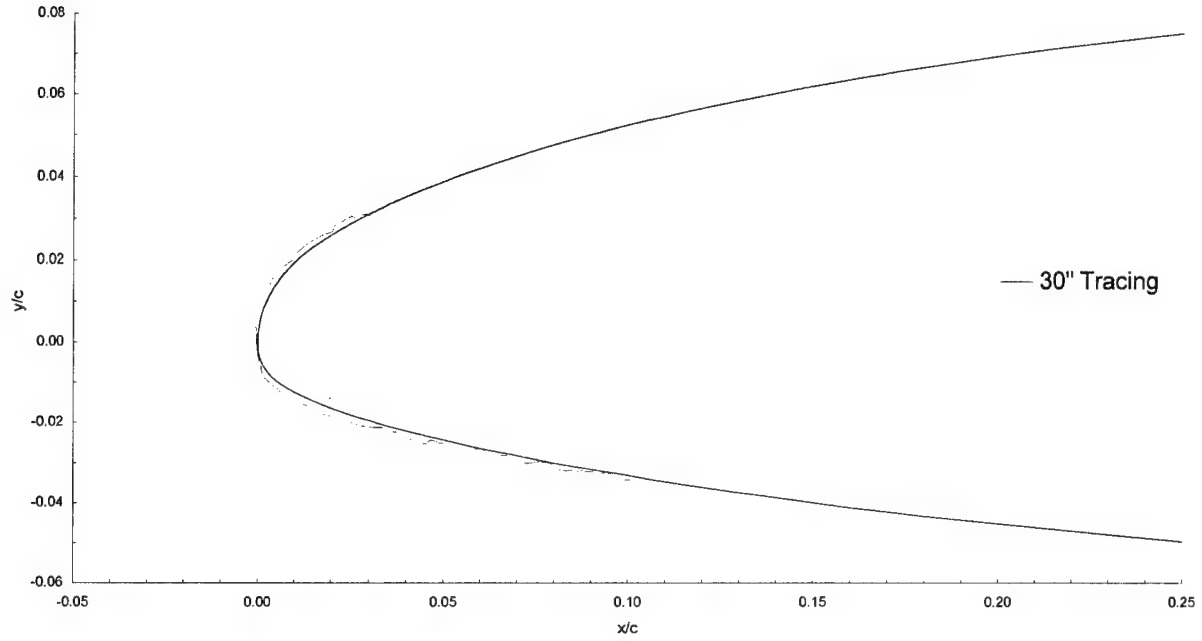

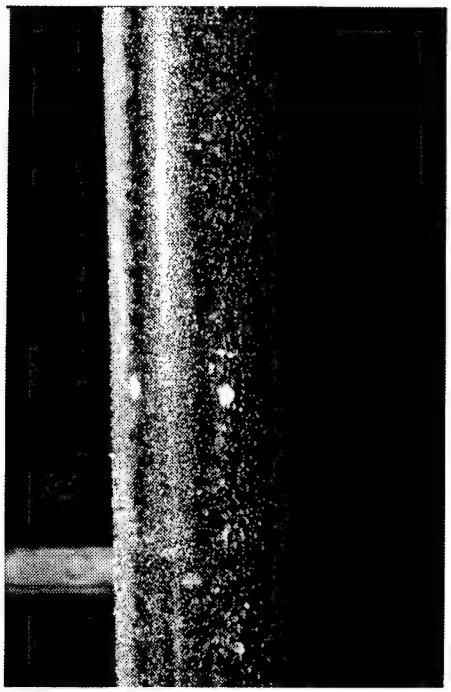

General Aviation - Run 622

T_t = -2.8°C (26.4°F)
T_s = -5.0°C (22.4°F)
V = 66.9 m/s (130 kts)
AOA = 0.3°

LWC = 0.54 g/m^3
MVD = 20 μm
Spray = 6.0 min
chord = 90 cm (36 in)

$C_{d\text{-}clean}$ = 0.0105
$C_{d\text{-}iced}$ = 0.0202
$C_{l\text{-}clean}$ = 0.463
$C_{l\text{-}iced}$ = 0.418

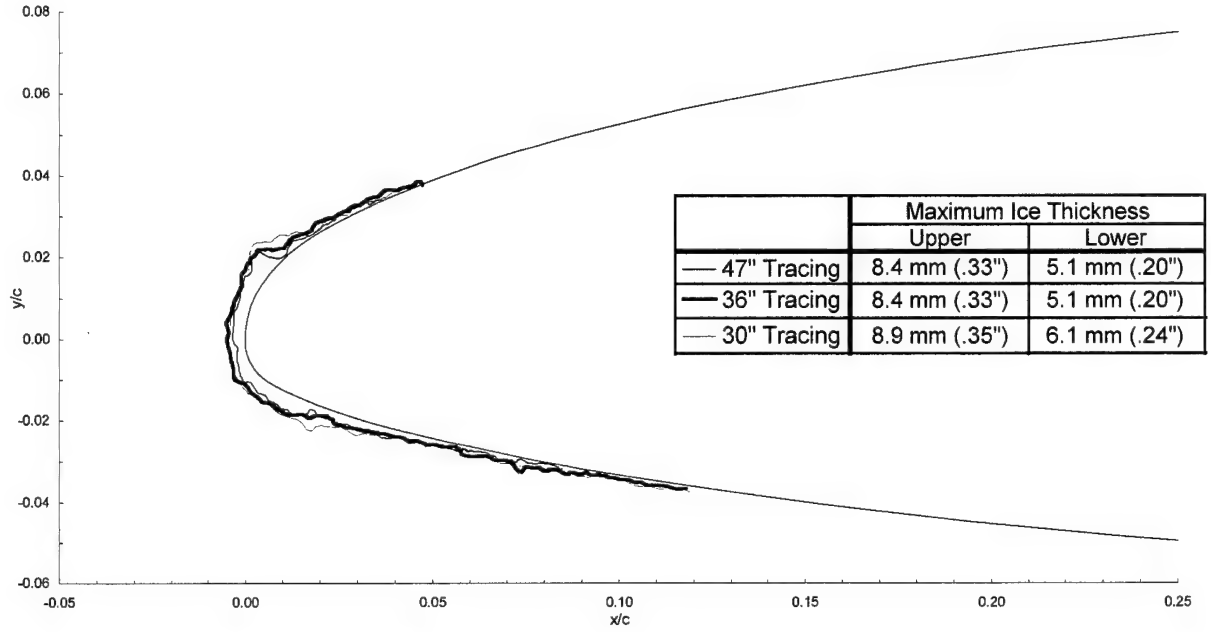

	Maximum Ice Thickness	
	Upper	Lower
47" Tracing	8.4 mm (.33")	5.1 mm (.20")
36" Tracing	8.4 mm (.33")	5.1 mm (.20")
30" Tracing	8.9 mm (.35")	6.1 mm (.24")

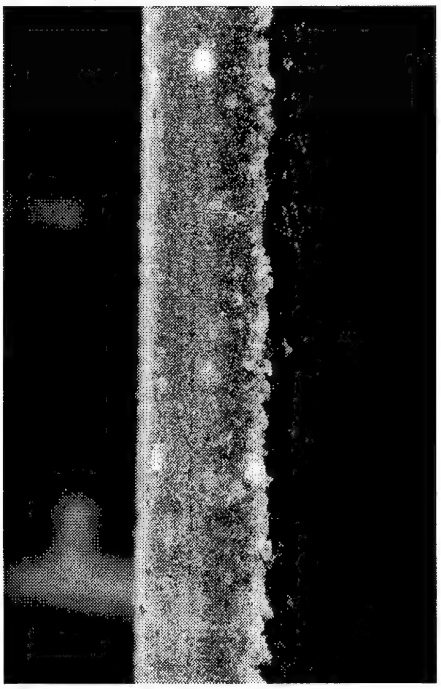

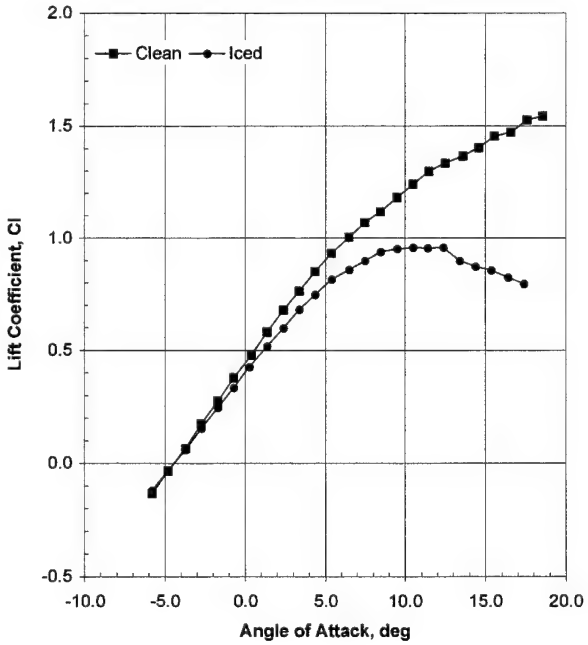

General Aviation - Run 622r

T_t = -2.8°C (26.4°F)
T_s = -5.0°C (22.4°F)

V = 66.9 m/s (130 kts)
AOA = 0.3°

LWC = 0.54 g/m^3
MVD = 20 μm
Spray = 6.0 min
chord = 90 cm (36 in)

$C_{d\text{-clean}}$ = 0.0105
$C_{d\text{-iced}}$ = 0.0204

$C_{l\text{-clean}}$ = 0.461
$C_{l\text{-iced}}$ = 0.425

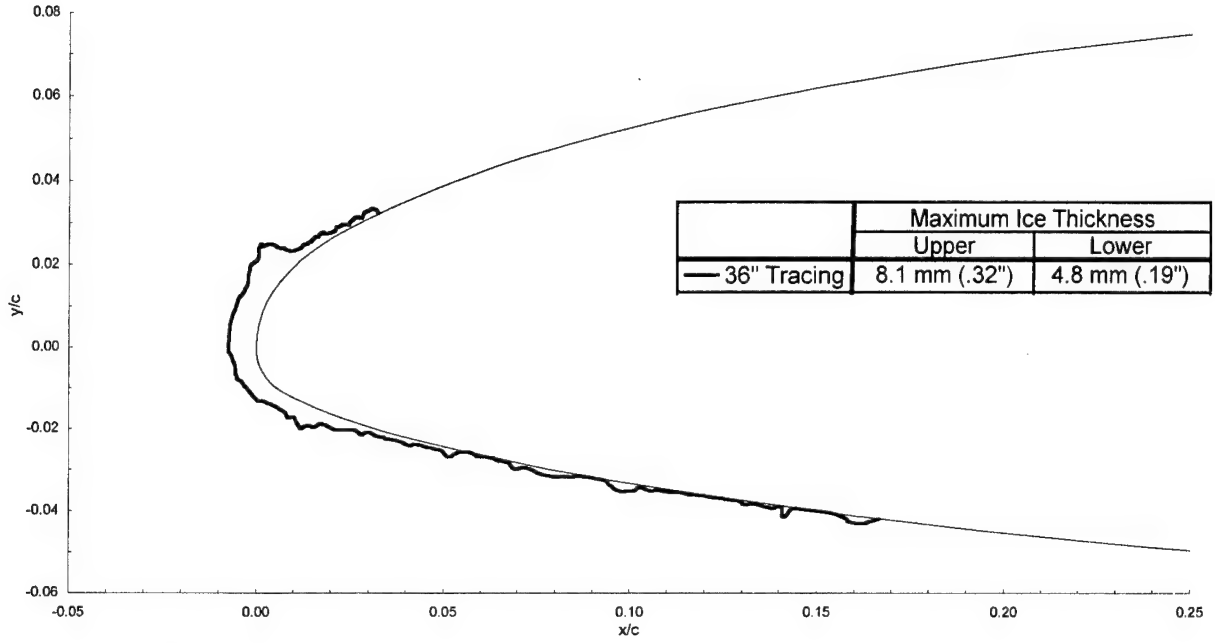

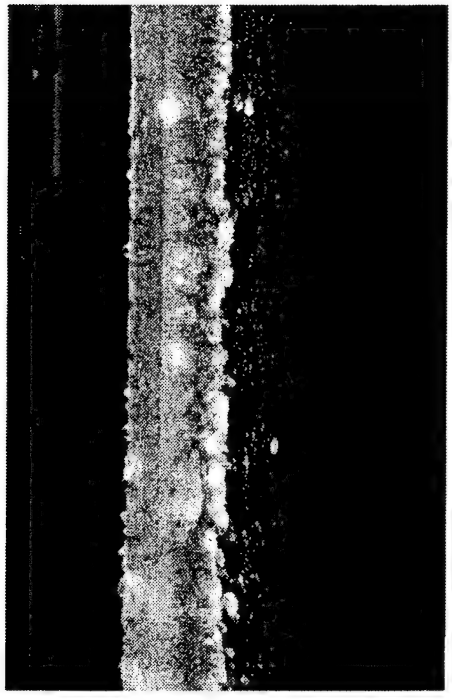

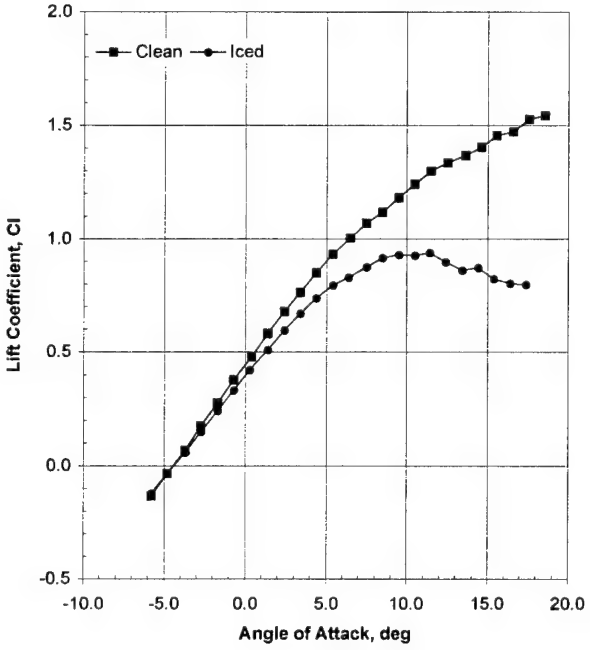

General Aviation - Run 622r2

T_t = -2.8°C (26.4°F)
T_s = -5.0°C (22.4°F)
V = 66.9 m/s (130 kts)
AOA = 0.3°

LWC = 0.54 g/m^3
MVD = 20 μm
Spray = 6.0 min
chord = 90 cm (36 in)

$C_{d\text{-}clean}$ = 0.0105
$C_{d\text{-}iced}$ = 0.0204
$C_{l\text{-}clean}$ = 0.479
$C_{l\text{-}iced}$ = 0.440

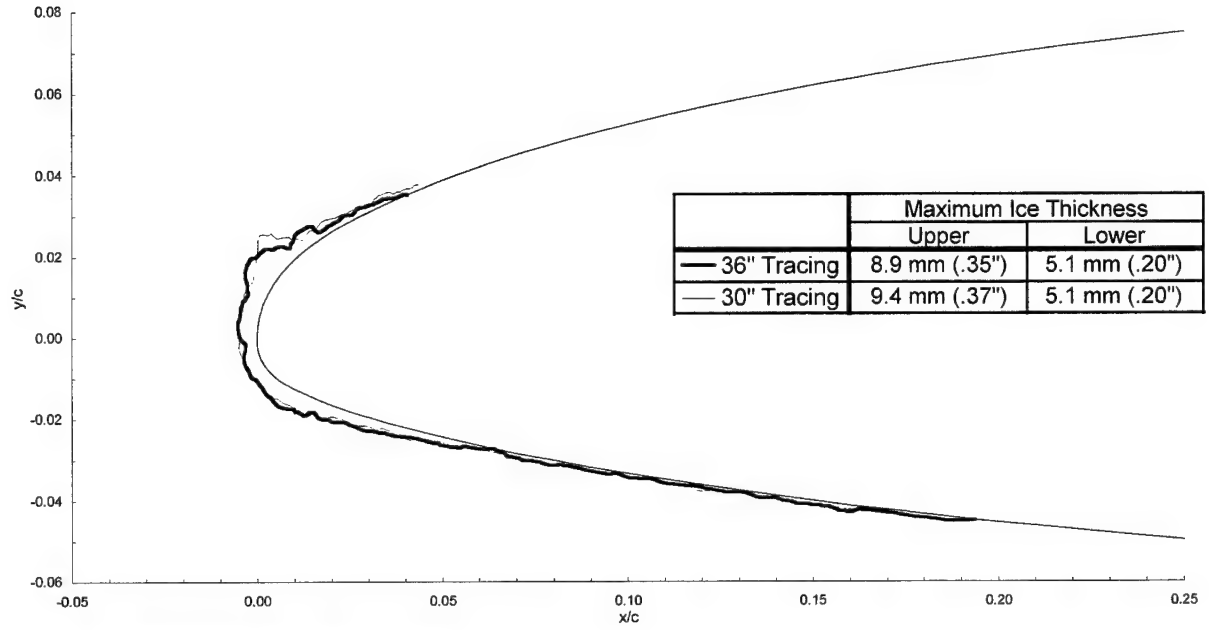

	Maximum Ice Thickness	
	Upper	Lower
— 36" Tracing	8.9 mm (.35")	5.1 mm (.20")
— 30" Tracing	9.4 mm (.37")	5.1 mm (.20")

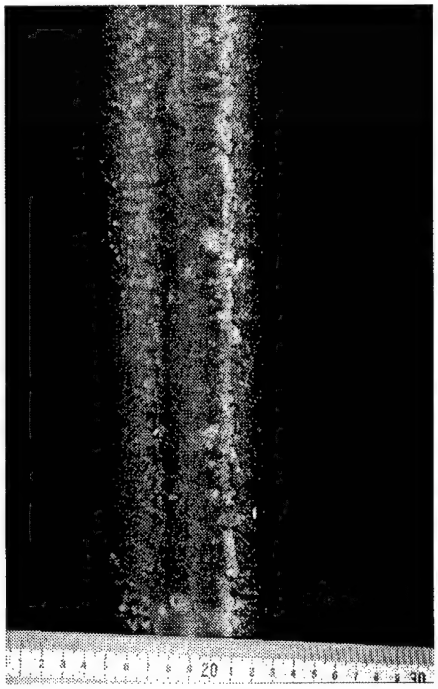

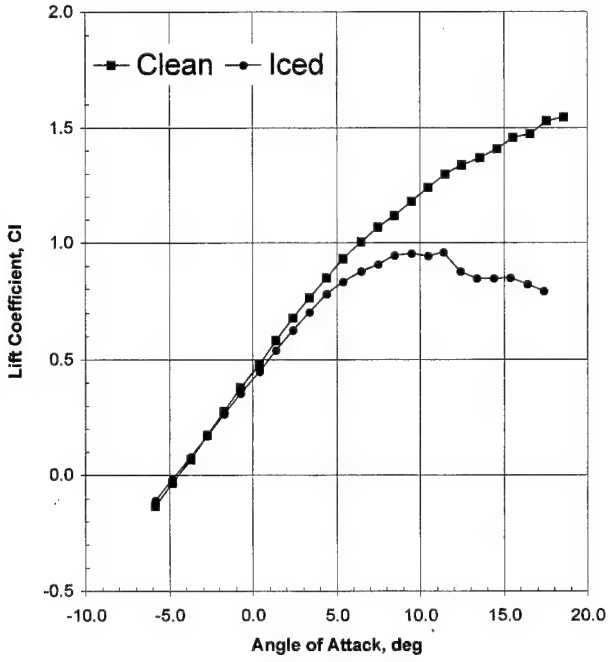

General Aviation - Run 622m

T_t = -2.8°C (26.4°F)
T_s = -5.0°C (22.4°F)
V = 66.9 m/s (130 kts)
AOA = 0.3°

LWC = 0.54 g/m^3
MVD = 20 μm
Spray = 6.0 min
chord = 90 cm (36 in)

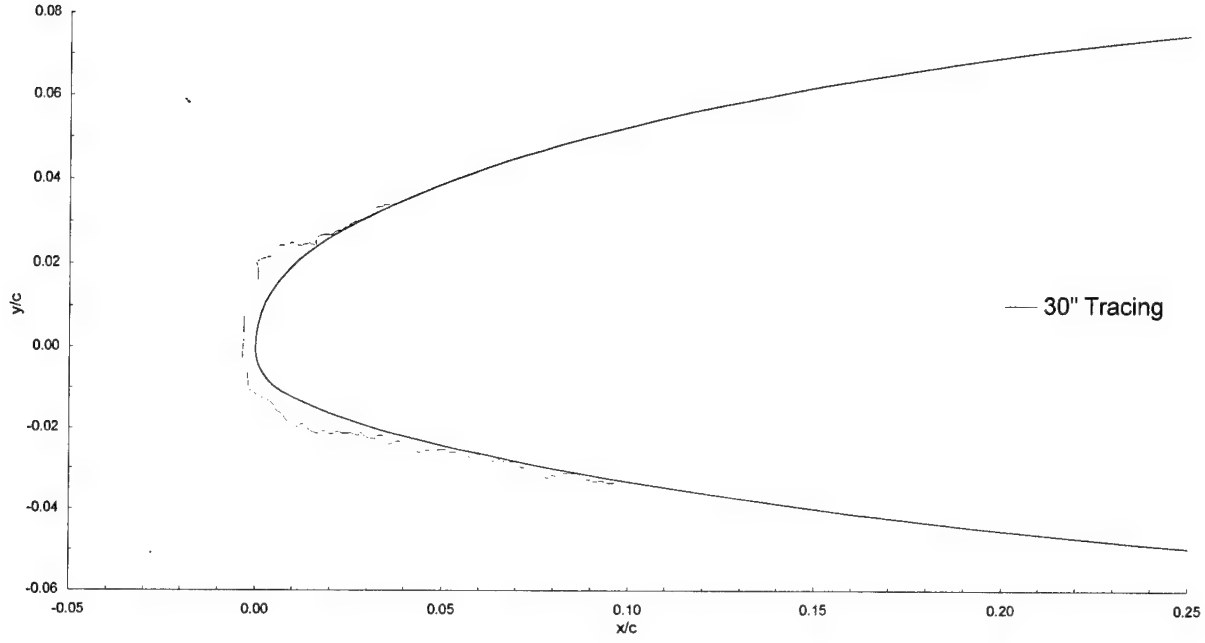

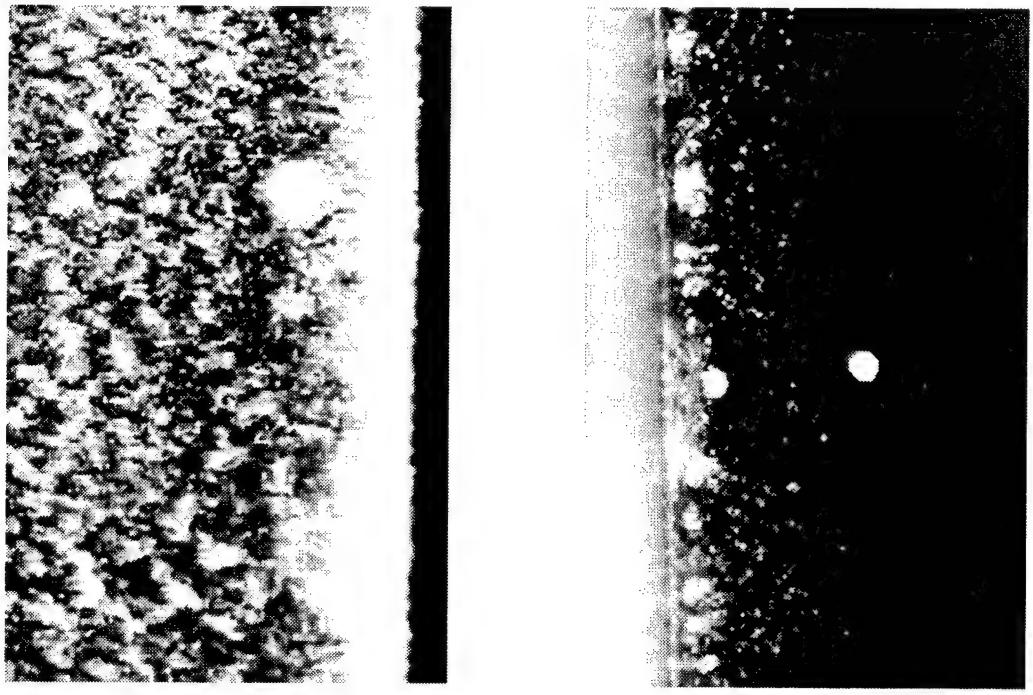

General Aviation - Run 623

T_t = -2.8°C (26.4°F)
T_s = -5.0°C (22.4°F)

V = 66.9 m/s (130 kts)
AOA = 0.3°

LWC = 0.54 g/m^3
MVD = 20 μm
Spray = 22.5 min
chord = 90 cm (36 in)

$C_{d\text{-}clean}$ = 0.0105
$C_{d\text{-}iced}$ = 0.0459

$C_{l\text{-}clean}$ = 0.460
$C_{l\text{-}iced}$ = 0.401

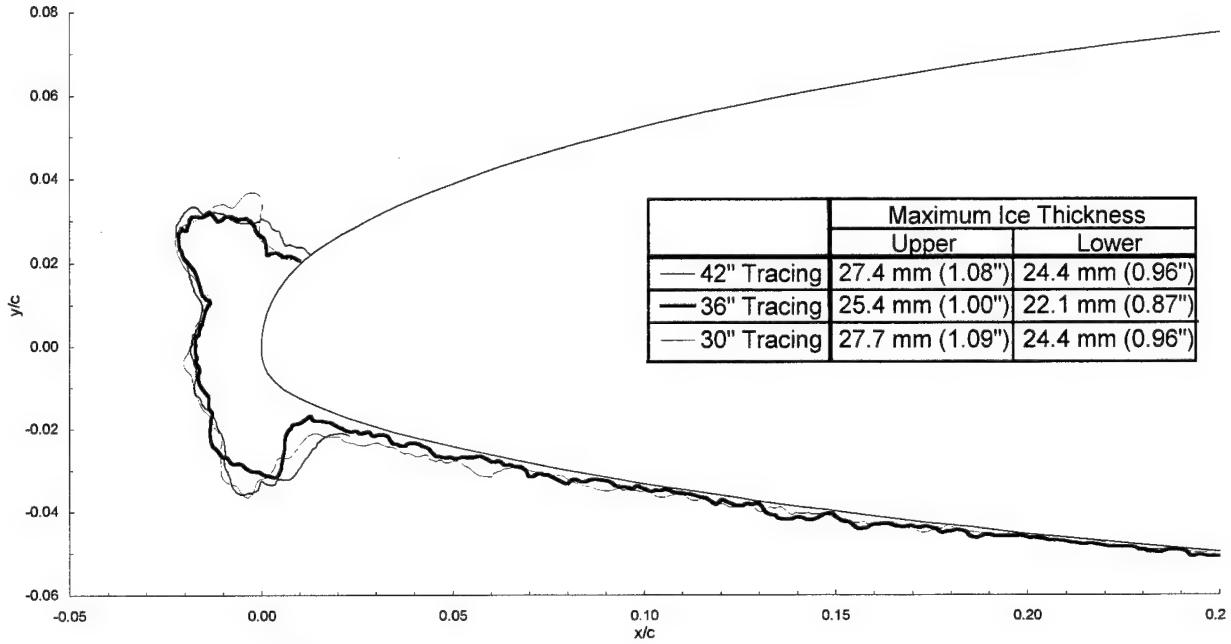

	Maximum Ice Thickness	
	Upper	Lower
42" Tracing	27.4 mm (1.08")	24.4 mm (0.96")
36" Tracing	25.4 mm (1.00")	22.1 mm (0.87")
30" Tracing	27.7 mm (1.09")	24.4 mm (0.96")

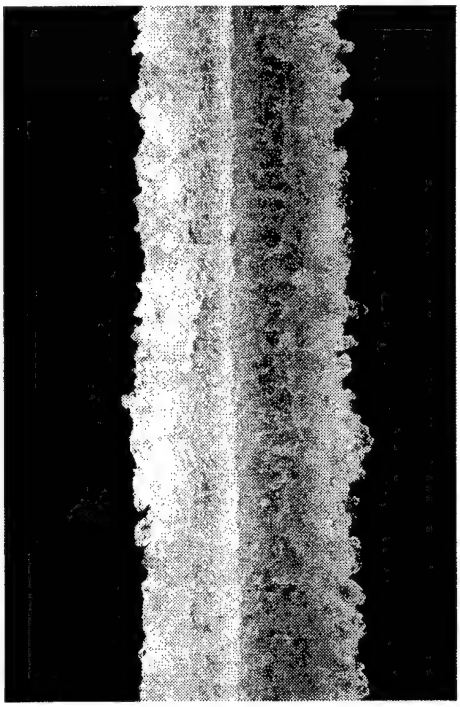

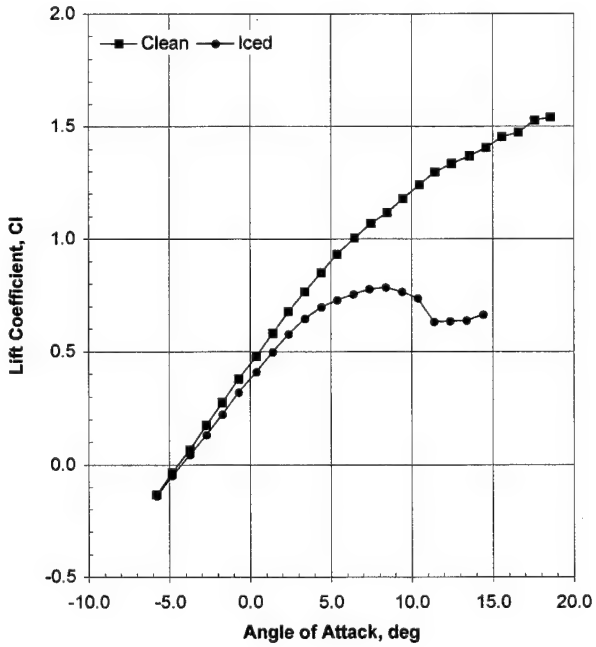

General Aviation - Run 623m

T_t = -2.8°C (26.4°F)
T_s = -5.0°C (22.4°F)
V = 66.9 m/s (130 kts)
AOA = 0.3°

LWC = 0.54 g/m^3
MVD = 20 μm
Spray = 22.5 min
chord = 90 cm (36 in)

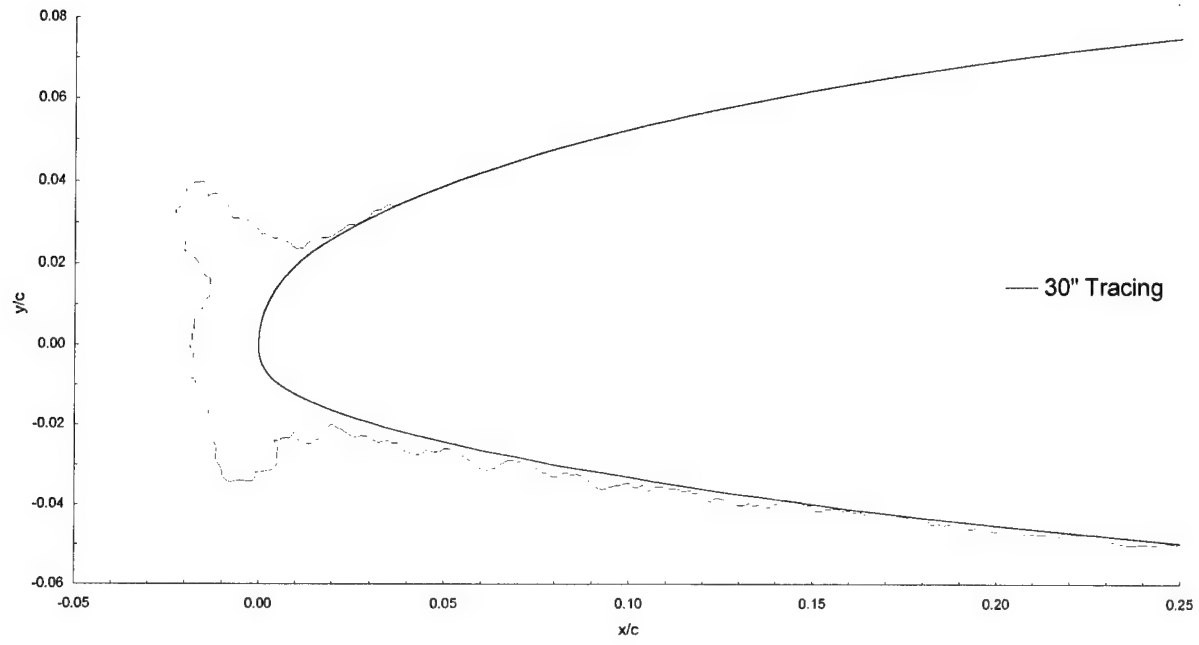

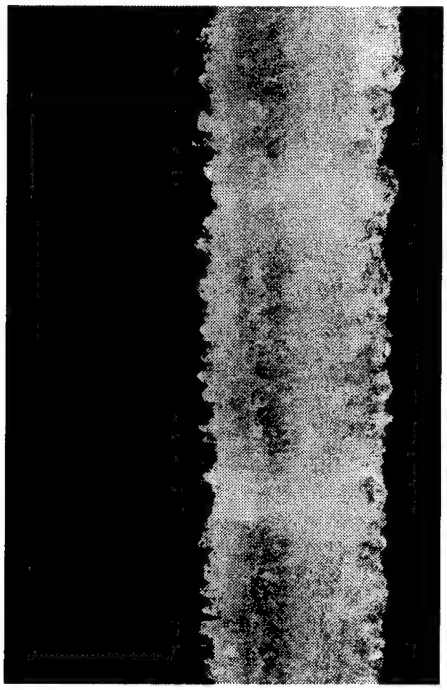

General Aviation - Run 625

T_t = -7.8°C (17.3°F)
T_s = -10.0°C (13.4°F)

V = 66.9 m/s (130 kts)
AOA = 0.3°

LWC = 0.66 g/m^3
MVD = 40 μm
Spray = 0.9 min
chord = 90 cm (36 in)

$C_{d\text{-}clean}$ = 0.0105
$C_{d\text{-}iced}$ = 0.0152

$C_{l\text{-}clean}$ = 0.475
$C_{l\text{-}iced}$ = 0.447

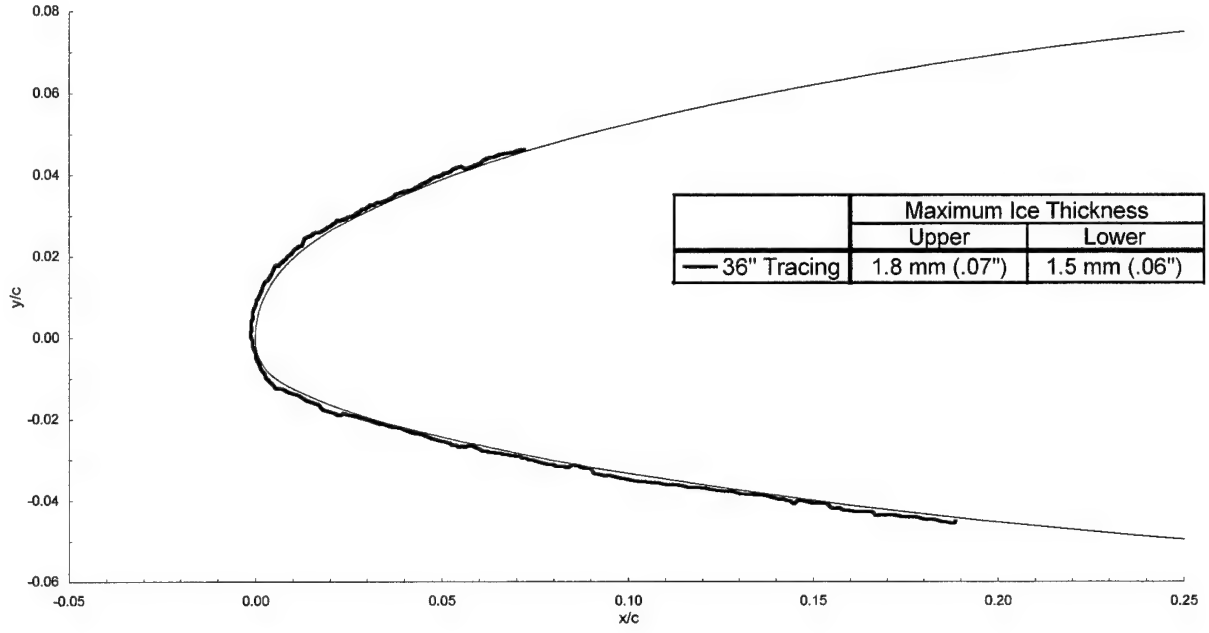

	Maximum Ice Thickness	
	Upper	Lower
—36" Tracing	1.8 mm (.07")	1.5 mm (.06")

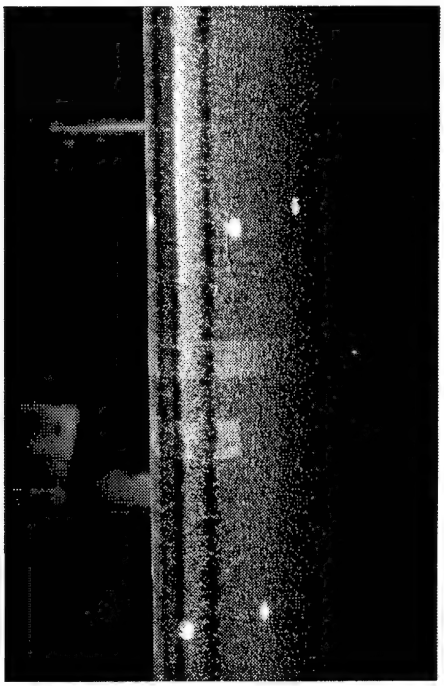

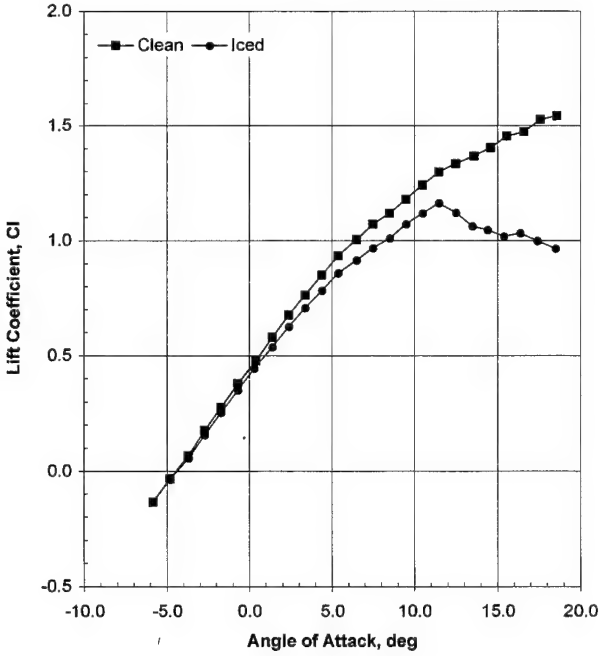

General Aviation - Run 626

T_t = -7.8°C (17.3°F)
T_s = -10.0°C (13.4°F)

V = 66.9 m/s (130 kts)
AOA = 0.3°

LWC = 0.44 g/m^3
MVD = 20 μm
Spray = 2.0 min
chord = 90 cm (36 in)

$C_{d\text{-}clean}$ = 0.0105
$C_{d\text{-}iced}$ = 0.0142

$C_{l\text{-}clean}$ = 0.476
$C_{l\text{-}iced}$ = 0.451

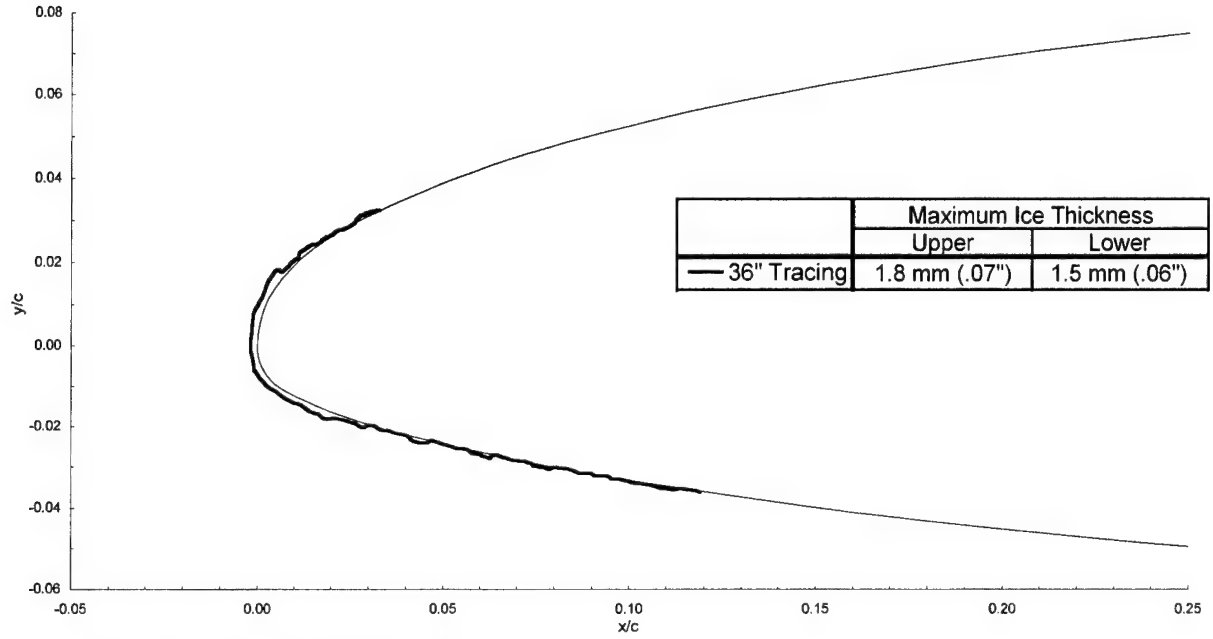

	Maximum Ice Thickness	
	Upper	Lower
—36" Tracing	1.8 mm (.07")	1.5 mm (.06")

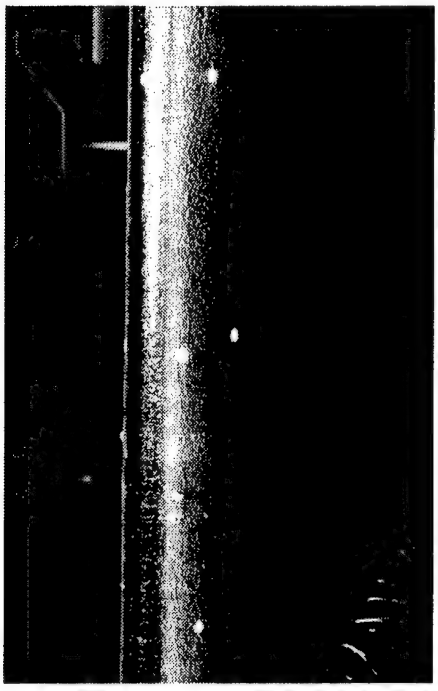

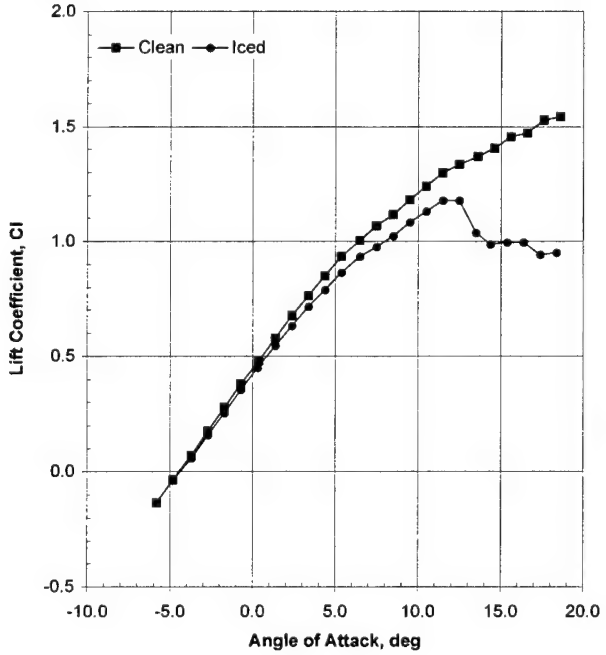

General Aviation - Run 627

T_t = -7.8°C (17.3°F)
T_s = -10.0°C (13.4°F)

V = 66.9 m/s (130 kts)
AOA = 0.3°

LWC = 0.44 g/m^3
MVD = 20 μm
Spray = 5.9 min
chord = 90 cm (36 in)

$C_{d\text{-}clean}$ = 0.0105
$C_{d\text{-}iced}$ = 0.0169

$C_{l\text{-}clean}$ = 0.462
$C_{l\text{-}iced}$ = 0.433

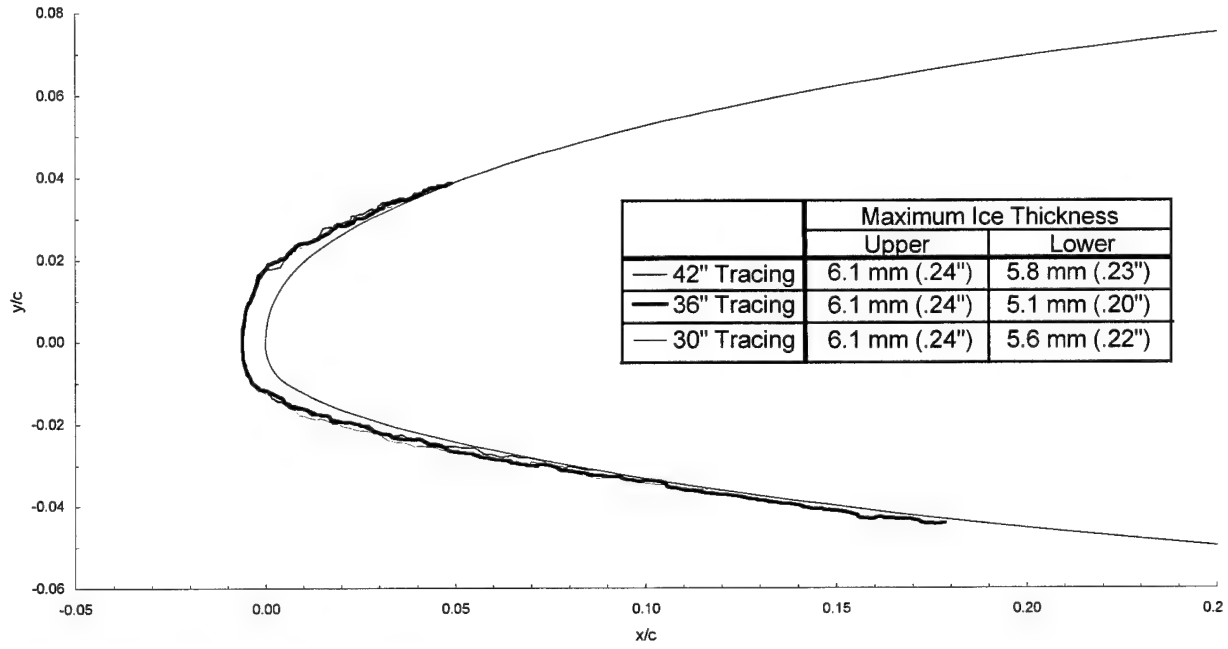

	Maximum Ice Thickness	
	Upper	Lower
— 42" Tracing	6.1 mm (.24")	5.8 mm (.23")
— 36" Tracing	6.1 mm (.24")	5.1 mm (.20")
— 30" Tracing	6.1 mm (.24")	5.6 mm (.22")

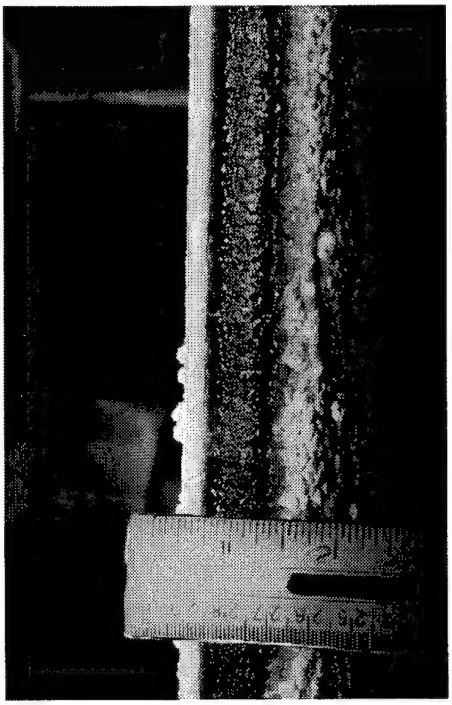

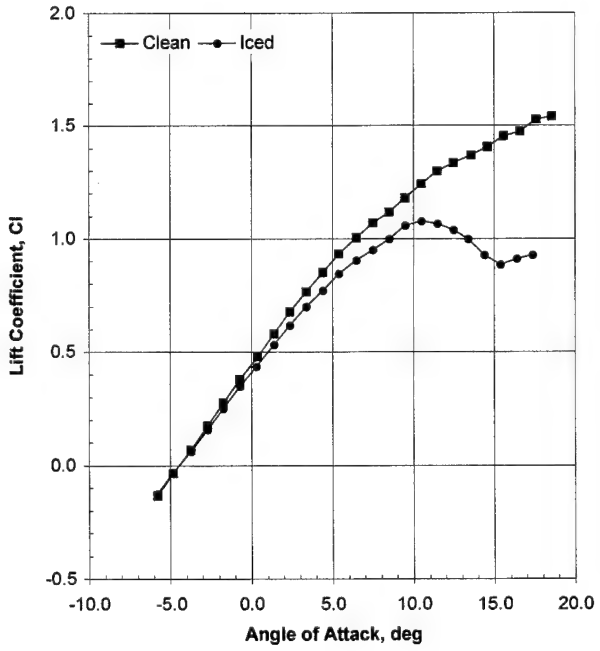

General Aviation - Run 627r

T_t = -7.8°C (17.3°F)
T_s = -10.0°C (13.4°F)

V = 66.9 m/s (130 kts)
AOA = 0.3°

LWC = 0.44 g/m^3
MVD = 20 μm
Spray = 5.9 min
chord = 90 cm (36 in)

$C_{d\text{-}clean}$ = 0.0105
$C_{d\text{-}iced}$ = 0.0167

$C_{l\text{-}clean}$ = 0.478
$C_{l\text{-}iced}$ = 0.443

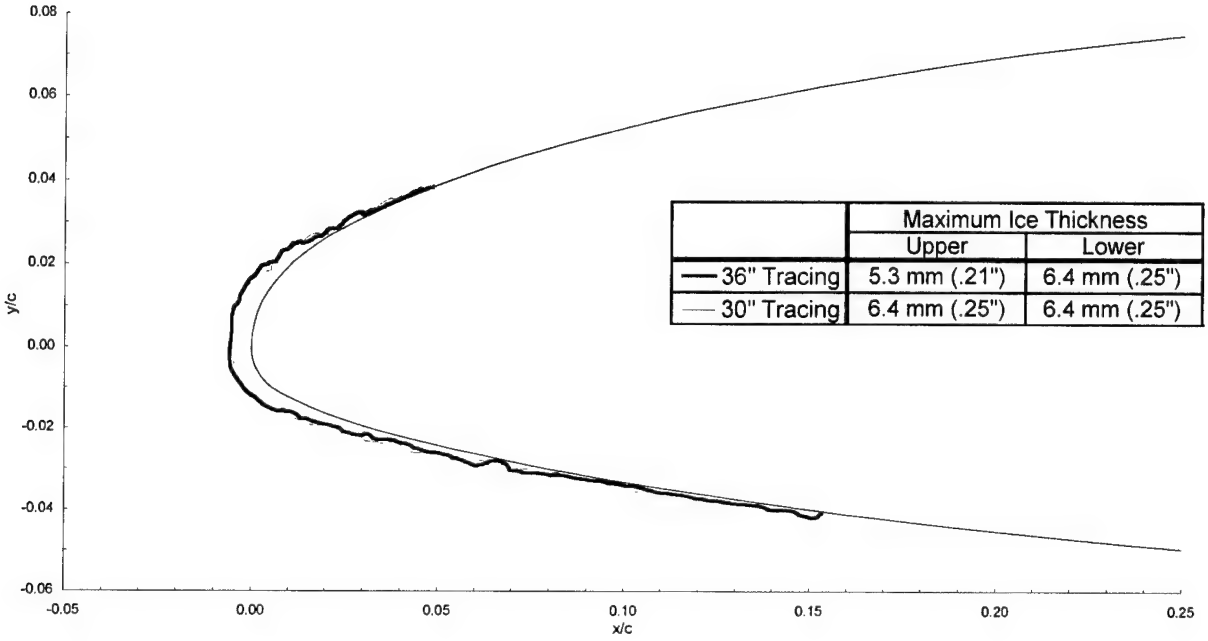

	Maximum Ice Thickness	
	Upper	Lower
36" Tracing	5.3 mm (.21")	6.4 mm (.25")
30" Tracing	6.4 mm (.25")	6.4 mm (.25")

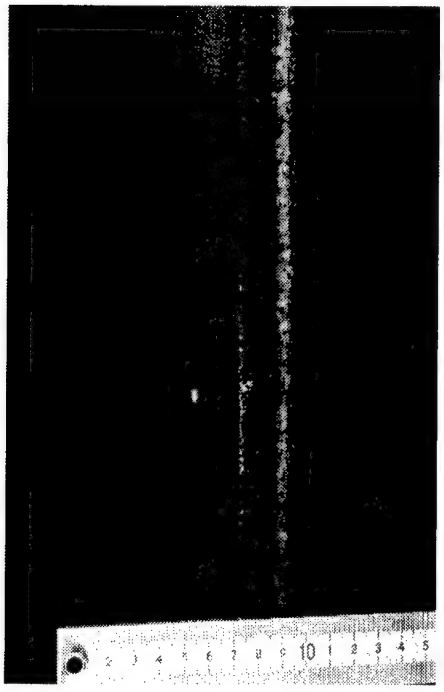

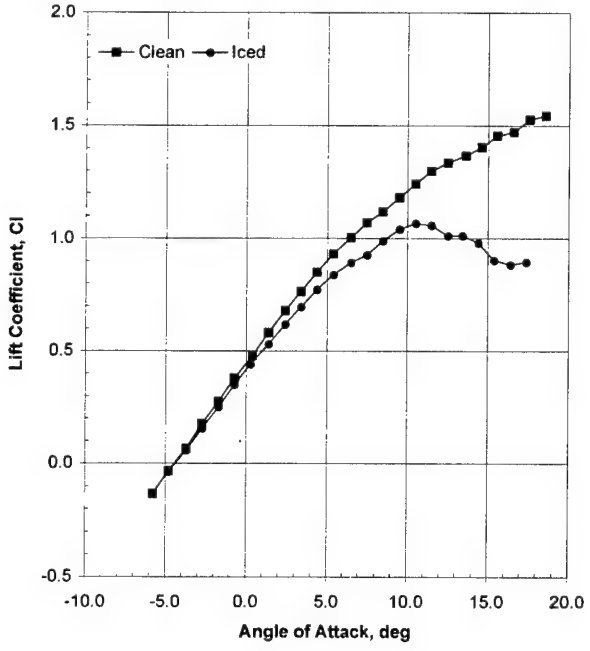

General Aviation - Run 627r2

T_t = -7.8°C (17.3°F)
T_s = -10.0°C (13.4°F)
V = 66.9 m/s (130 kts)
AOA = 0.3°

LWC = 0.44 g/m^3
MVD = 20 μm
Spray = 5.9 min
chord = 90 cm (36 in)

$C_{d\text{-}clean}$ = 0.0105
$C_{d\text{-}iced}$ = 0.0172
$C_{l\text{-}clean}$ = 0.476
$C_{l\text{-}iced}$ = 0.435

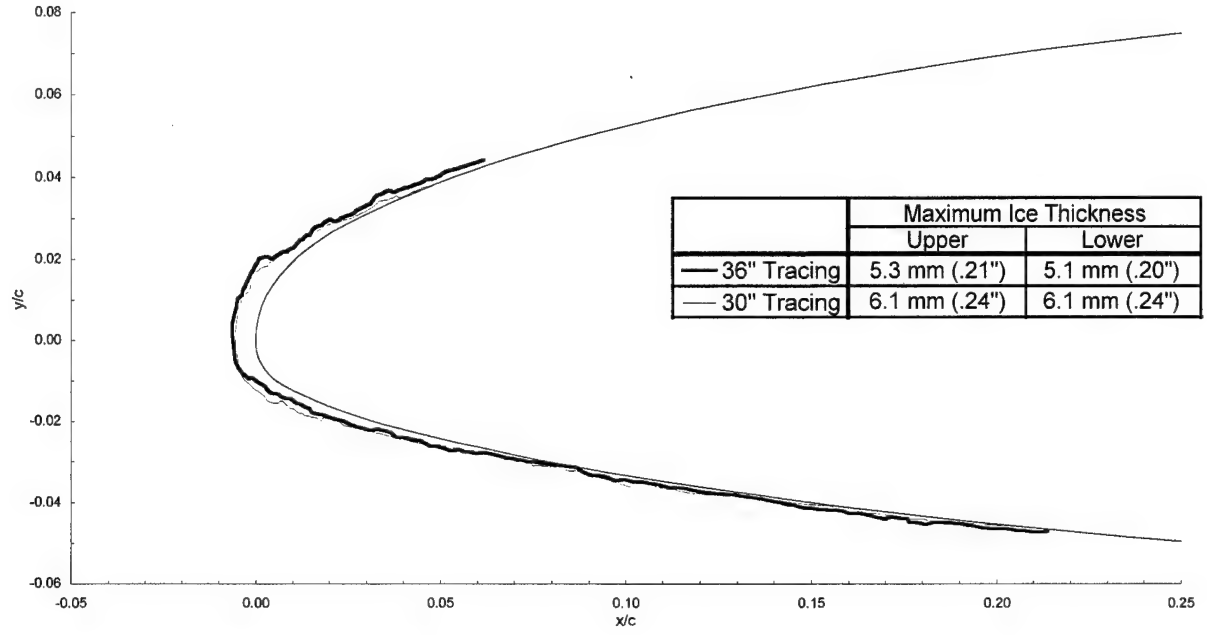

	Maximum Ice Thickness	
	Upper	Lower
—36" Tracing	5.3 mm (.21")	5.1 mm (.20")
—30" Tracing	6.1 mm (.24")	6.1 mm (.24")

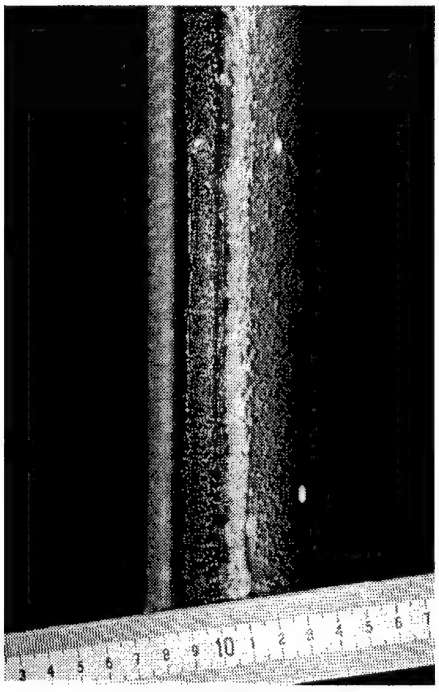

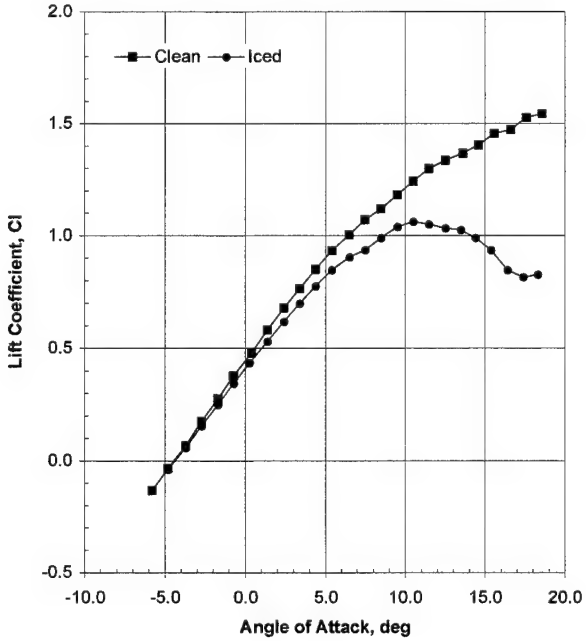

General Aviation - Run 627m

T_t = -7.8°C (17.3°F)
T_s = -10.0°C (13.4°F)
V = 66.9 m/s (130 kts)
AOA = 0.3°

LWC = 0.44 g/m^3
MVD = 20 μm
Spray = 5.9 min
chord = 90 cm (36 in)

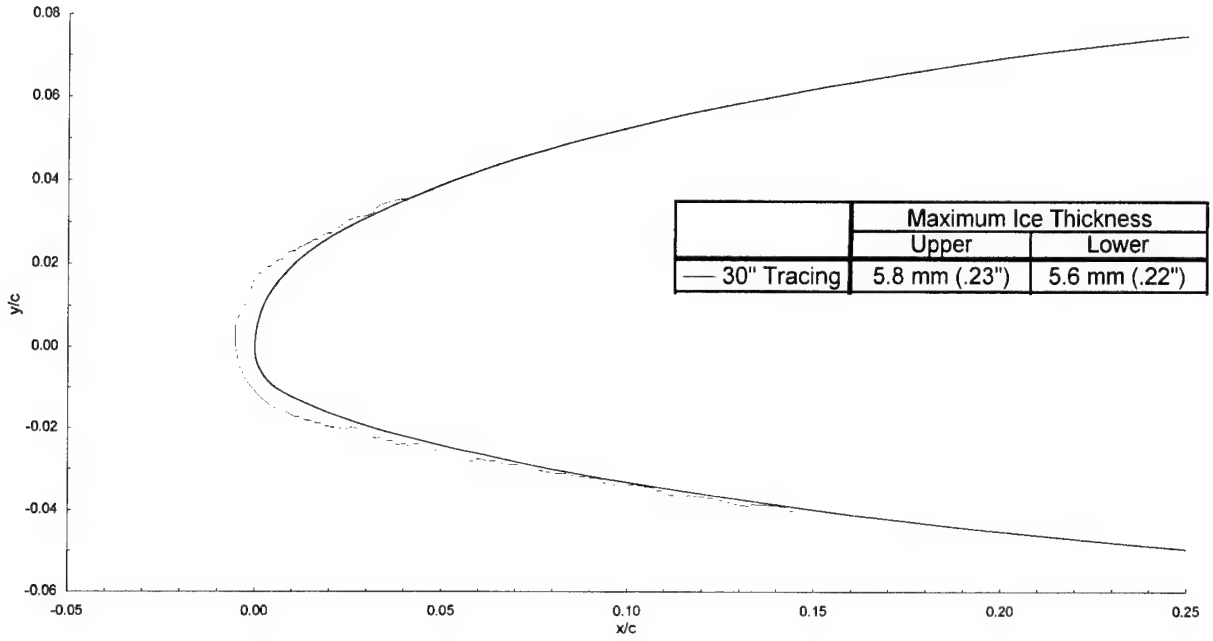

	Maximum Ice Thickness	
	Upper	Lower
— 30" Tracing	5.8 mm (.23")	5.6 mm (.22")

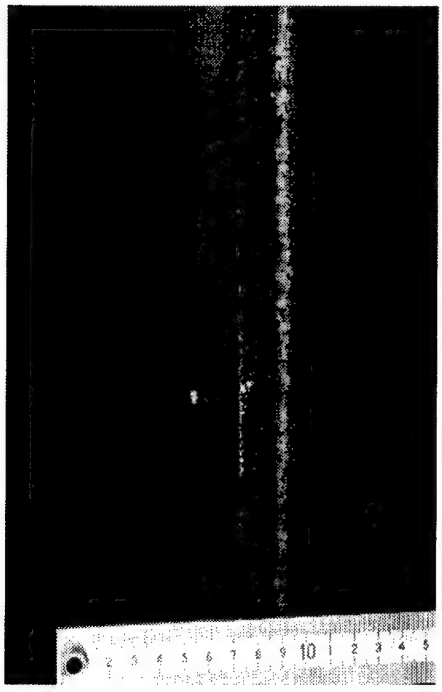

General Aviation - Run 628

T_t = -7.8°C (17.3°F)
T_s = -10.0°C (13.4°F)

V = 66.9 m/s (130 kts)
AOA = 0.3°

LWC = 0.44 g/m^3
MVD = 20 μm
Spray = 22.0 min
chord = 90 cm (36 in)

$C_{d\text{-}clean}$ = 0.0105
$C_{d\text{-}iced}$ = 0.0272

$C_{l\text{-}clean}$ = 0.474
$C_{l\text{-}iced}$ = 0.428

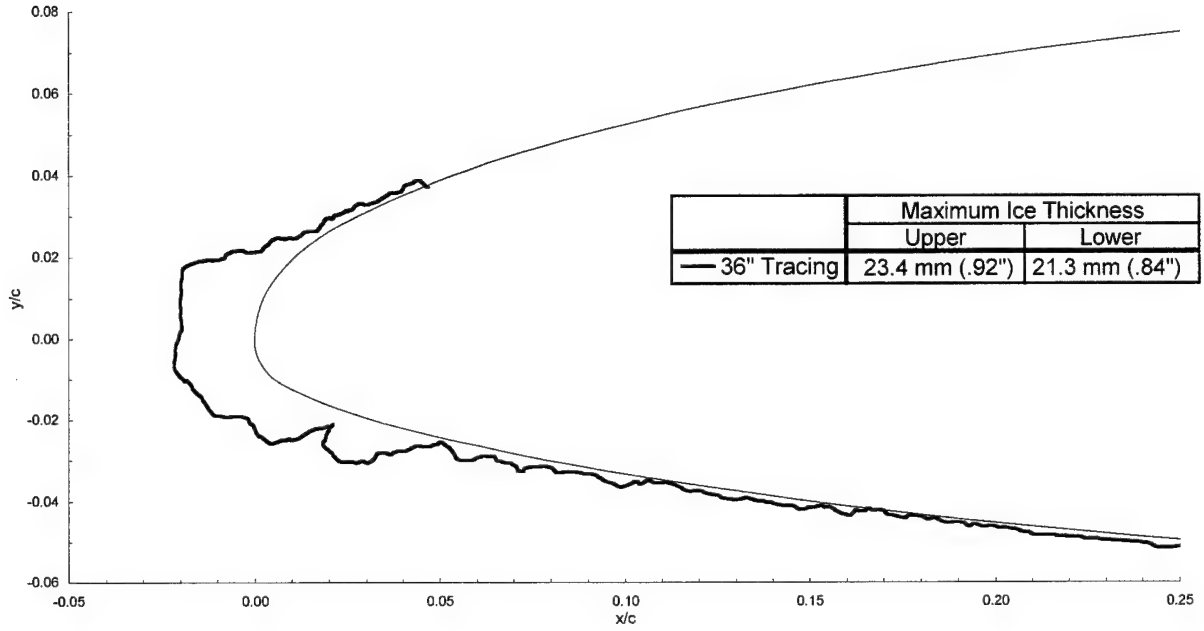

	Maximum Ice Thickness	
	Upper	Lower
36" Tracing	23.4 mm (.92")	21.3 mm (.84")

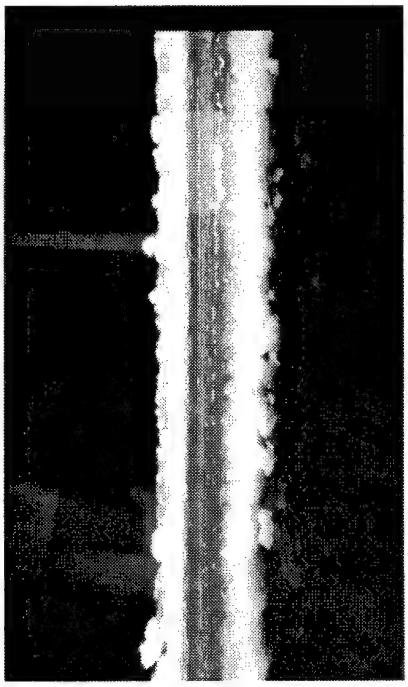

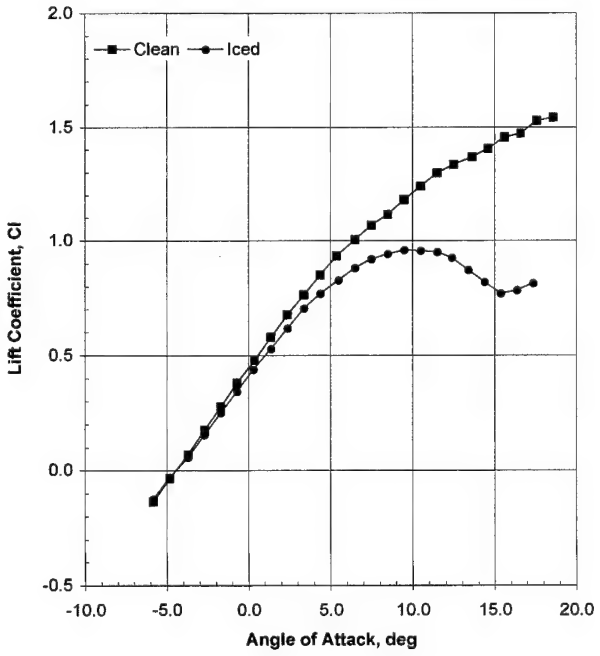

General Aviation - Run 629

T_t = -12.9°C (8.2°F)
T_s = -15°C (4.4°F)

V = 66.9 m/s (130 kts)
AOA = 0.3°

LWC = 0.44 g/m^3
MVD = 20 μm
Spray = 1.4 min
chord = 90 cm (36 in)

$C_{d\text{-clean}}$ = 0.0105
$C_{d\text{-iced}}$ = 0.0131

$C_{l\text{-clean}}$ = 0.470
$C_{l\text{-iced}}$ = 0.447

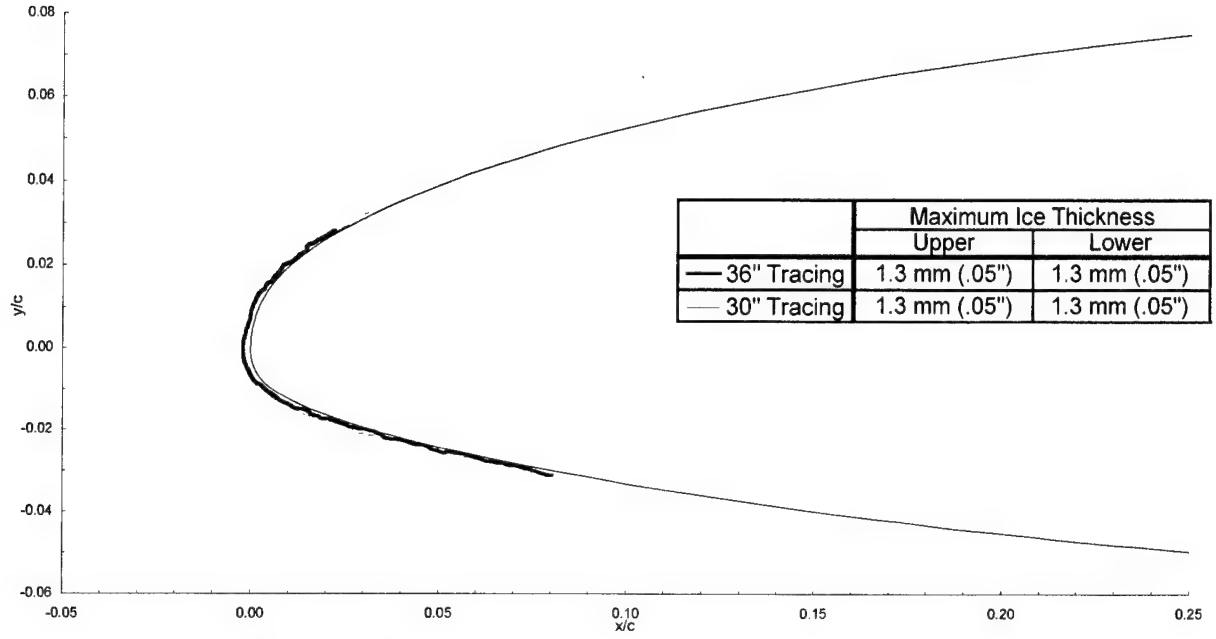

	Maximum Ice Thickness	
	Upper	Lower
—36" Tracing	1.3 mm (.05")	1.3 mm (.05")
—30" Tracing	1.3 mm (.05")	1.3 mm (.05")

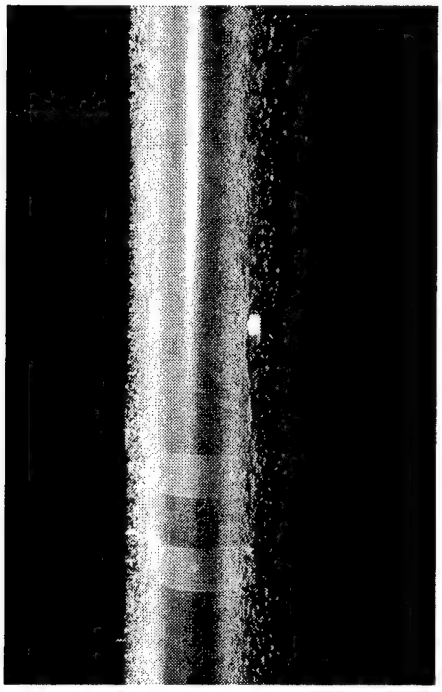

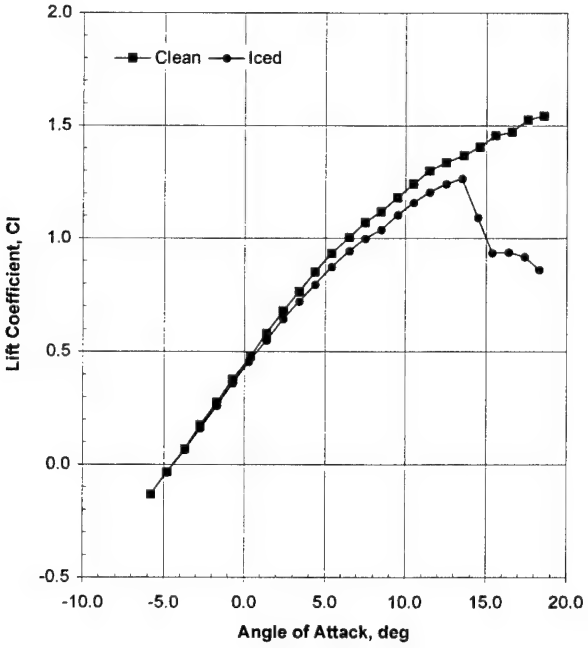

General Aviation - Run 630

T_t = -12.9°C (8.2°F)
T_s = -15.0°C (4.4°F)
V = 66.9 m/s (130 kts)
AOA = 0.3°

LWC = 0.44 g/m^3
MVD = 20 μm
Spray = 4.1 min
chord = 90 cm (36 in)

$C_{d\text{-}clean}$ = 0.0105
$C_{d\text{-}iced}$ = 0.0154
$C_{l\text{-}clean}$ = 0.467
$C_{l\text{-}iced}$ = 0.437

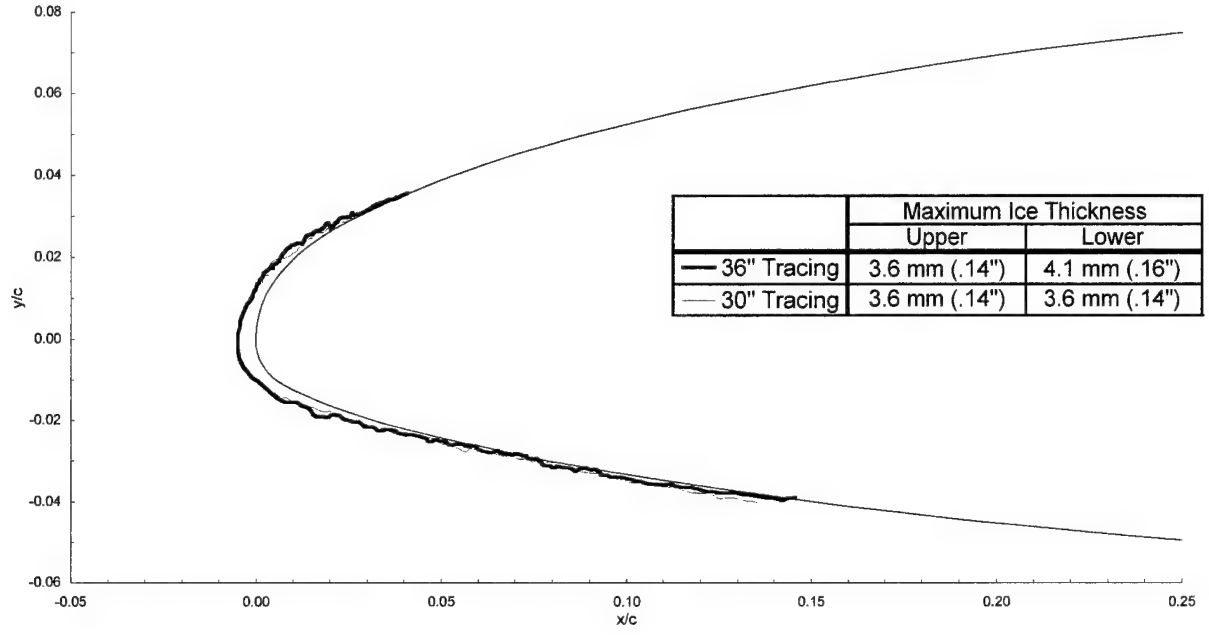

	Maximum Ice Thickness	
	Upper	Lower
36" Tracing	3.6 mm (.14")	4.1 mm (.16")
30" Tracing	3.6 mm (.14")	3.6 mm (.14")

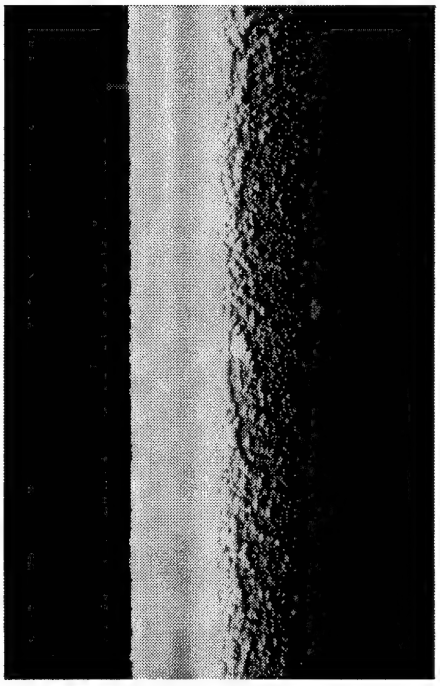

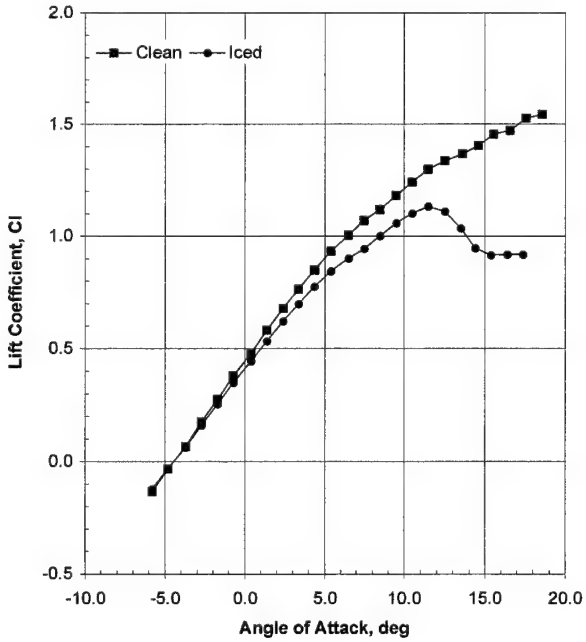

General Aviation - Run 631

T_t = -12.9°C (8.2°F)
T_s = -15.0°C (4.4°F)

V = 66.9 m/s (130 kts)
AOA = 0.3°

LWC = 0.44 g/m^3
MVD = 20 μm
Spray = 15.3 min
chord = 90 cm (36 in)

$C_{d\text{-clean}}$ = 0.0105
$C_{d\text{-iced}}$ = 0.0207

$C_{l\text{-clean}}$ = 0.469
$C_{l\text{-iced}}$ = 0.433

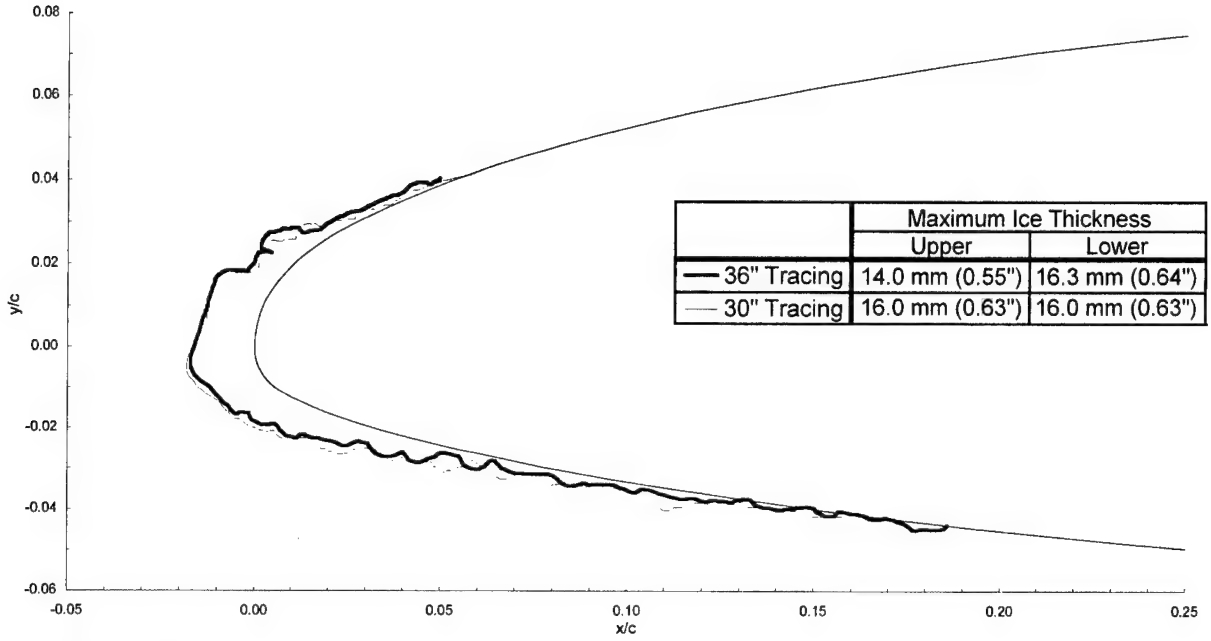

	Maximum Ice Thickness	
	Upper	Lower
36" Tracing	14.0 mm (0.55")	16.3 mm (0.64")
30" Tracing	16.0 mm (0.63")	16.0 mm (0.63")

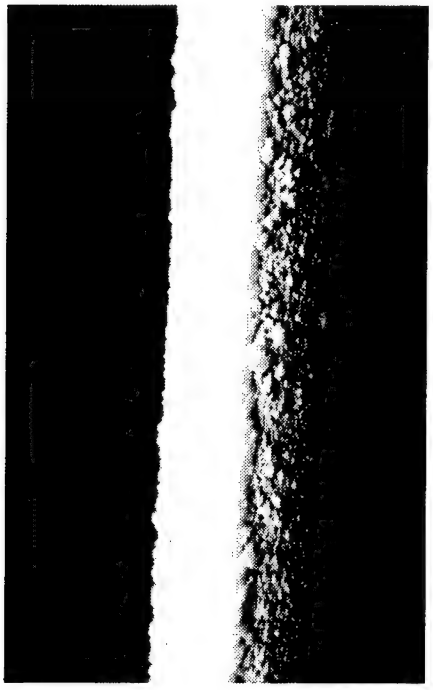

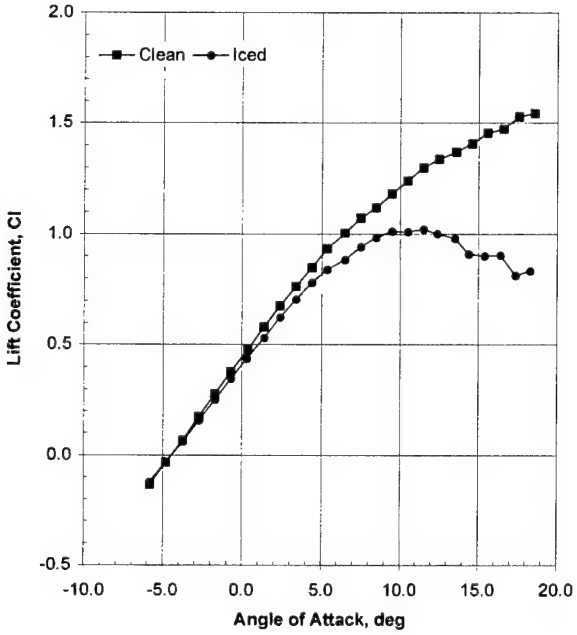

General Aviation - Run 632

T_t = -7.8°C (17.3°F)
T_s = -10.0°C (13.4°F)
V = 66.9 m/s (130 kts)
AOA = 0.3°

LWC = 0.60 g/m^3
MVD = 15 μm
Spray = 2.0 min
chord = 90 cm (36 in)

$C_{d\text{-clean}}$ = 0.0105
$C_{d\text{-iced}}$ = 0.0125
$C_{l\text{-clean}}$ = 0.471
$C_{l\text{-iced}}$ = 0.454

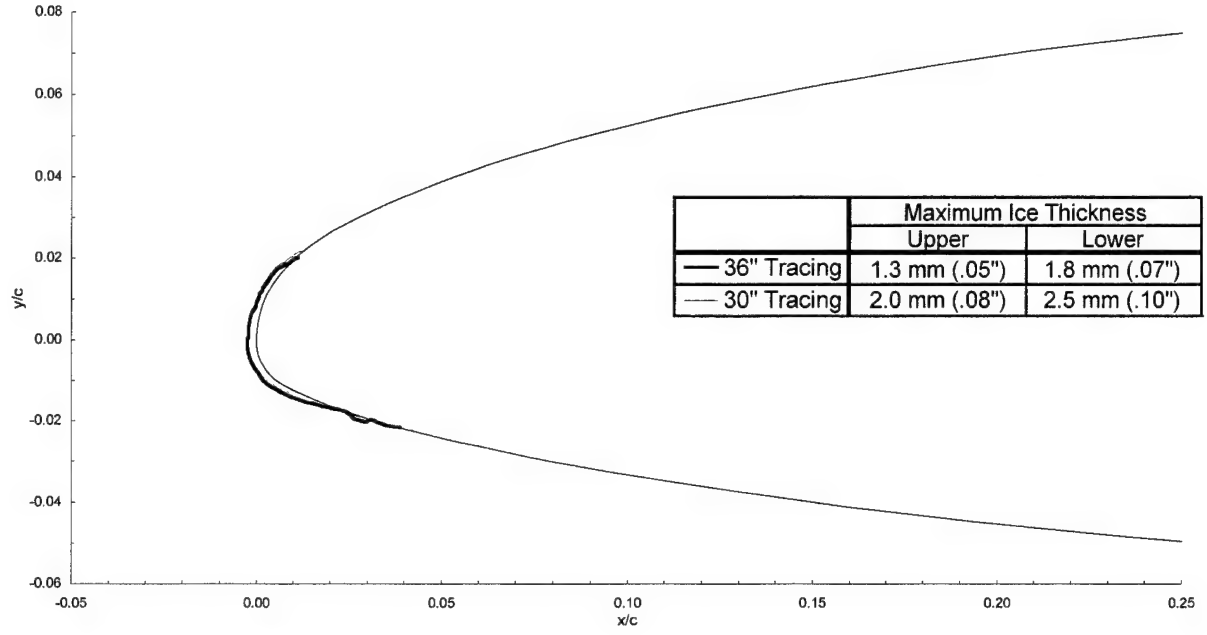

	Maximum Ice Thickness	
	Upper	Lower
—— 36" Tracing	1.3 mm (.05")	1.8 mm (.07")
—— 30" Tracing	2.0 mm (.08")	2.5 mm (.10")

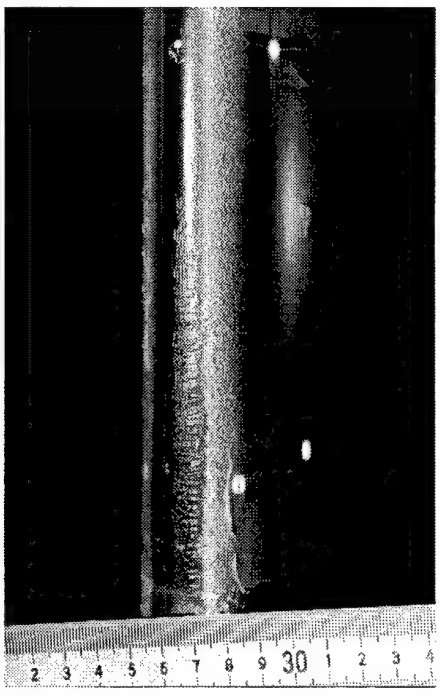

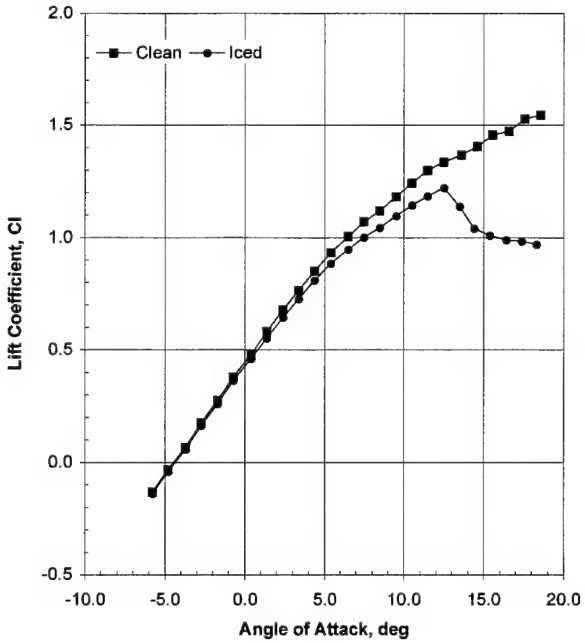

General Aviation - Run 633

T_t = -7.8°C (17.3°F)
T_s = -10.0°C (13.4°F)

V = 66.9 m/s (130 kts)
AOA = 0.3°

LWC = 0.60 g/m^3
MVD = 15 μm
Spray = 6.0 min
chord = 90 cm (36 in)

$C_{d\text{-clean}}$ = 0.0105
$C_{d\text{-iced}}$ = 0.0151

$C_{l\text{-clean}}$ = 0.472
$C_{l\text{-iced}}$ = 0.439

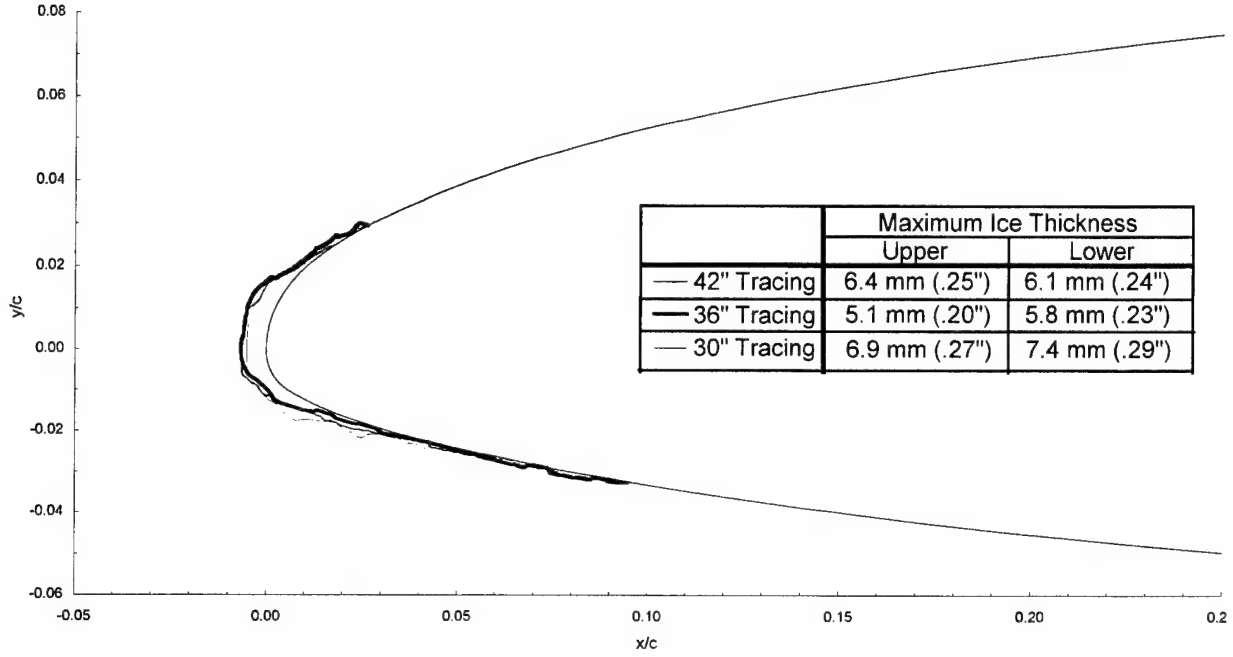

	Maximum Ice Thickness	
	Upper	Lower
— 42" Tracing	6.4 mm (.25")	6.1 mm (.24")
— 36" Tracing	5.1 mm (.20")	5.8 mm (.23")
— 30" Tracing	6.9 mm (.27")	7.4 mm (.29")

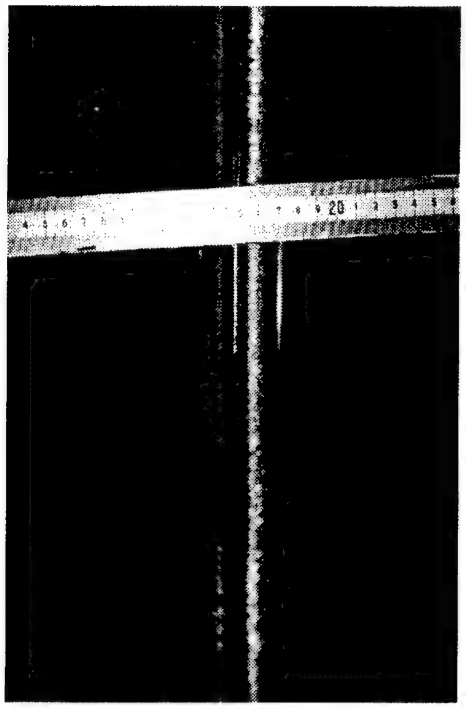

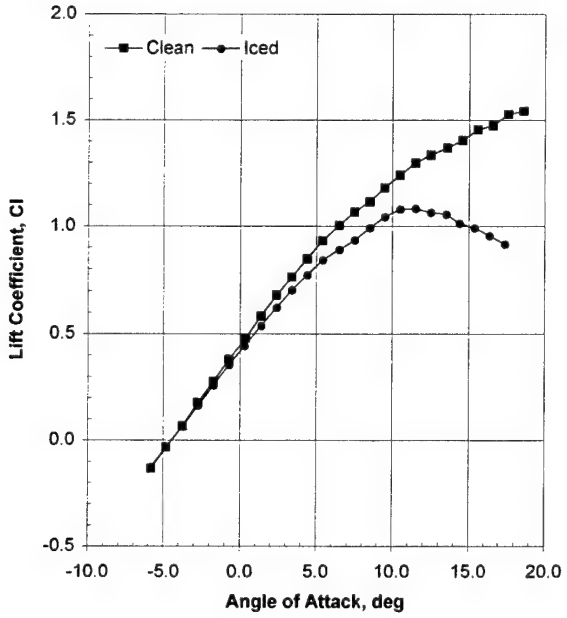

General Aviation - Run 633m

T_t = -7.8°C (17.3°F)
T_s = -10.0°C (13.4°F)
V = 66.9 m/s (130 kts)
AOA = 0.3°

LWC = 0.60 g/m^3
MVD = 15 μm
Spray = 6.0 min
chord = 90 cm (36 in)

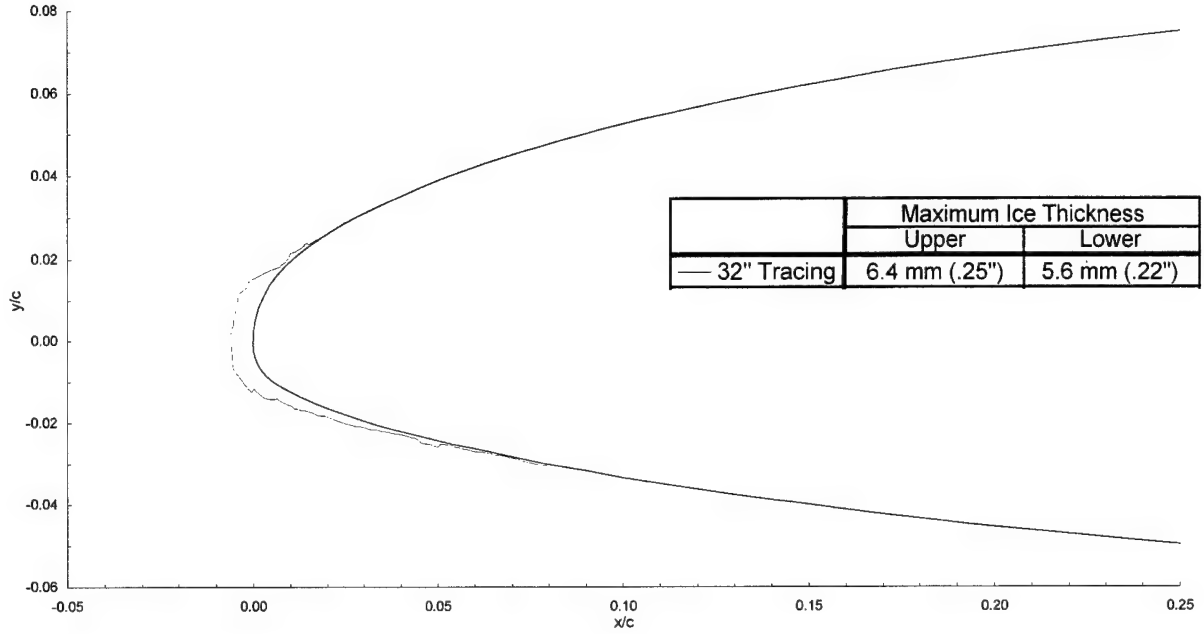

	Maximum Ice Thickness	
	Upper	Lower
— 32" Tracing	6.4 mm (.25")	5.6 mm (.22")

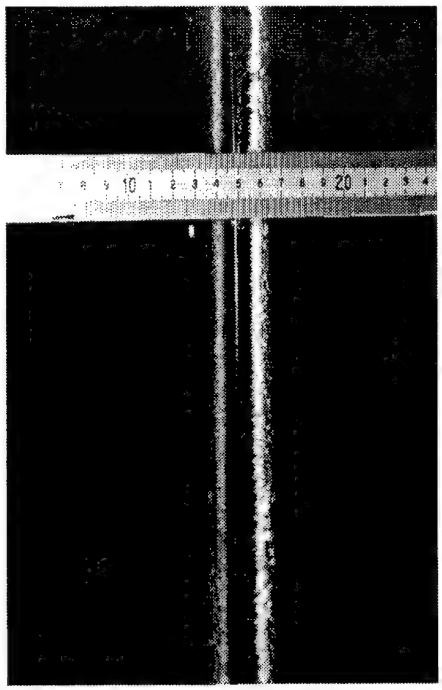

General Aviation - Run 641

T_t = -7.8°C (17.3°F)
T_s = -10.0°C (13.4°F)

V = 66.9 m/s (130 kts)
AOA = -1.7°

LWC = 0.44 g/m^3
MVD = 20 μm
Spray = 2.0 min
chord = 90 cm (36 in)

$C_{d\text{-clean}}$ = 0.0092
$C_{d\text{-iced}}$ = 0.0108

$C_{l\text{-clean}}$ = 0.263
$C_{l\text{-iced}}$ = 0.248

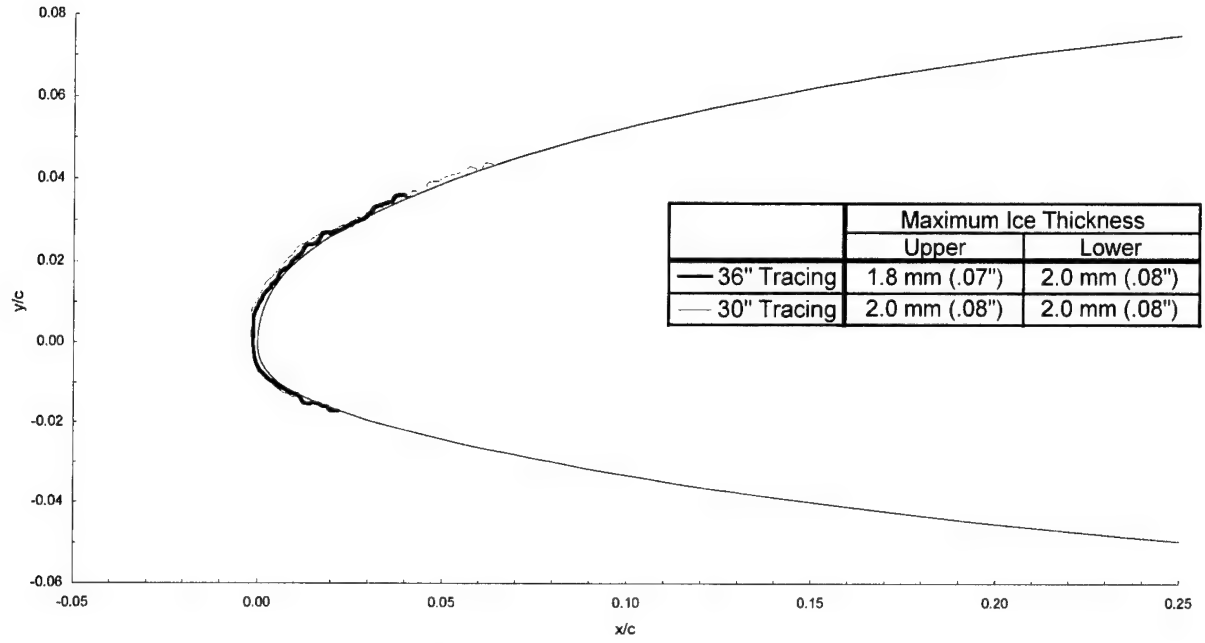

	Maximum Ice Thickness	
	Upper	Lower
—— 36" Tracing	1.8 mm (.07")	2.0 mm (.08")
—— 30" Tracing	2.0 mm (.08")	2.0 mm (.08")

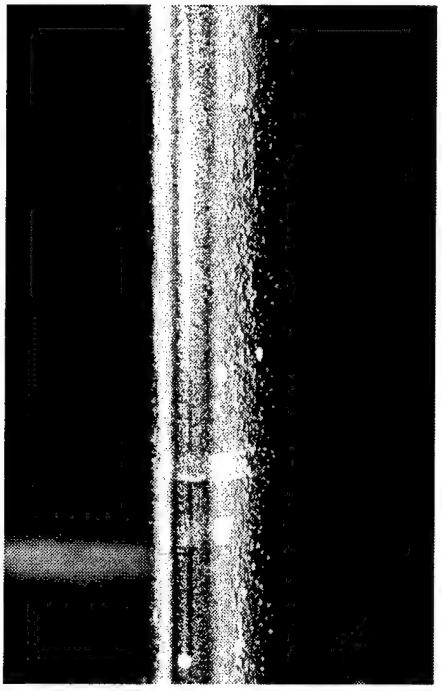

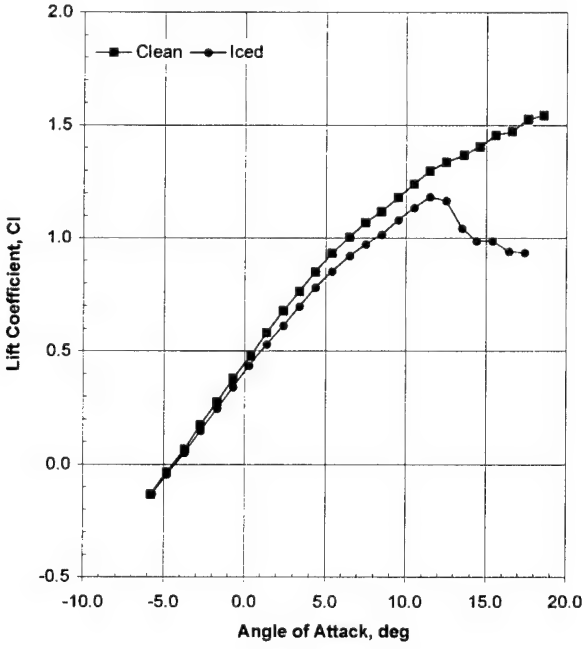

General Aviation - Run 642

T_t = -7.8°C (17.3°F)
T_s = -10.0°C (13.4°F)
V = 66.9 m/s (130 kts)
AOA = -1.7°

LWC = 0.44 g/m^3
MVD = 20 μm
Spray = 5.9 min
chord = 90 cm (36 in)

$C_{d\text{-}clean}$ = 0.0092
$C_{d\text{-}iced}$ = 0.0154
$C_{l\text{-}clean}$ = 0.255
$C_{l\text{-}iced}$ = 0.233

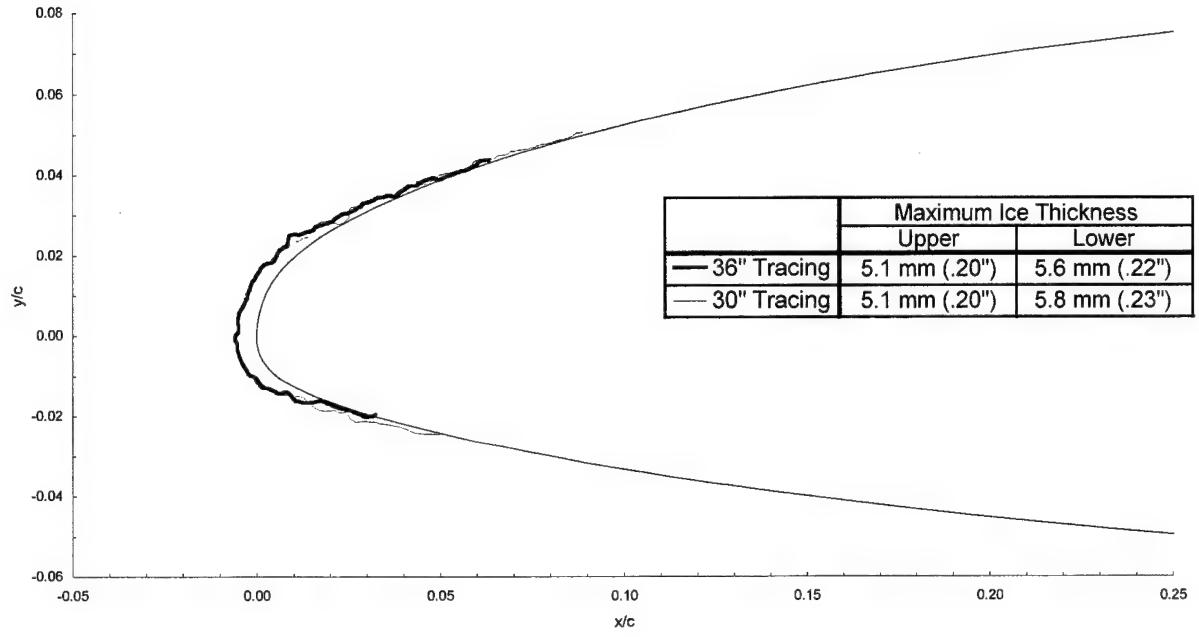

	Maximum Ice Thickness	
	Upper	Lower
—— 36" Tracing	5.1 mm (.20")	5.6 mm (.22")
—— 30" Tracing	5.1 mm (.20")	5.8 mm (.23")

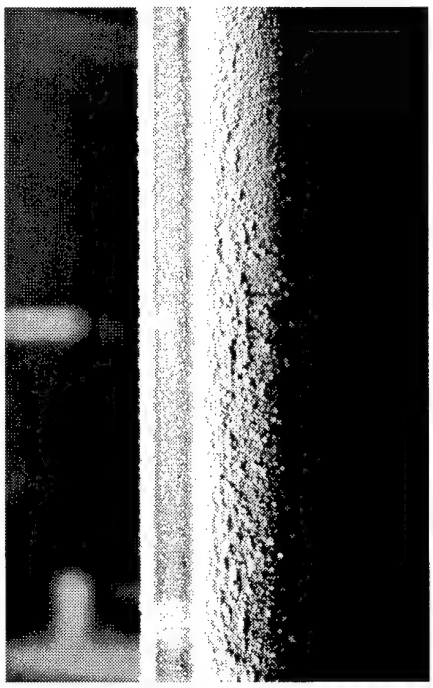

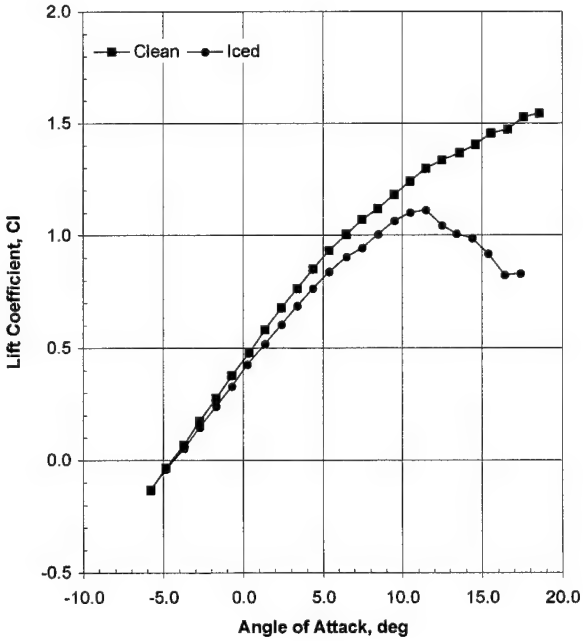

General Aviation - Run 643

T_t = -7.8°C (17.3°F)
T_s = -10.0°C (13.4°F)

V = 66.9 m/s (130 kts)
AOA = -1.7°

LWC = 0.44 g/m^3
MVD = 20 μm
Spray = 22.0 min
chord = 90 cm (36 in)

$C_{d\text{-clean}}$ = 0.0092
$C_{d\text{-iced}}$ = 0.0241

$C_{l\text{-clean}}$ = 0.267
$C_{l\text{-iced}}$ = 0.229

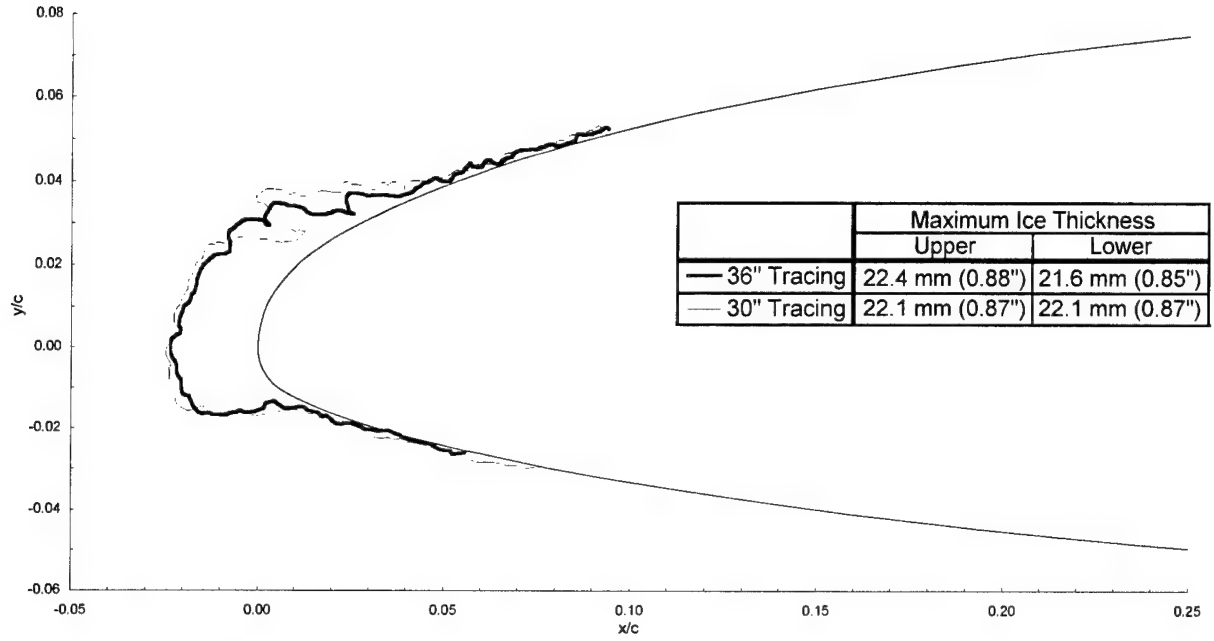

	Maximum Ice Thickness	
	Upper	Lower
—36" Tracing	22.4 mm (0.88")	21.6 mm (0.85")
— 30" Tracing	22.1 mm (0.87")	22.1 mm (0.87")

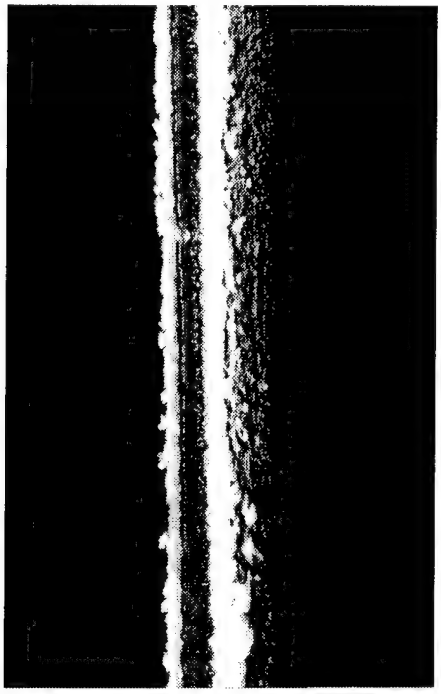

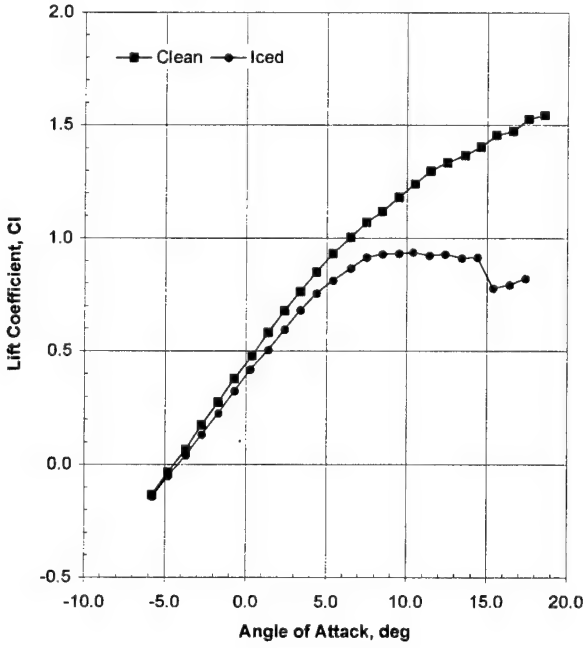

General Aviation - Run 644

T_t = -7.8°C (17.3°F)
T_s = -10.0°C (13.4°F)

V = 66.9 m/s (130 kts)
AOA = 2.4°

LWC = 0.44 g/m^3
MVD = 20 μm
Spray = 2.0 min
chord = 90 cm (36 in)

$C_{d\text{-}clean}$ = 0.0123
$C_{d\text{-}iced}$ = 0.0152

$C_{l\text{-}clean}$ = 0.655
$C_{l\text{-}iced}$ = 0.619

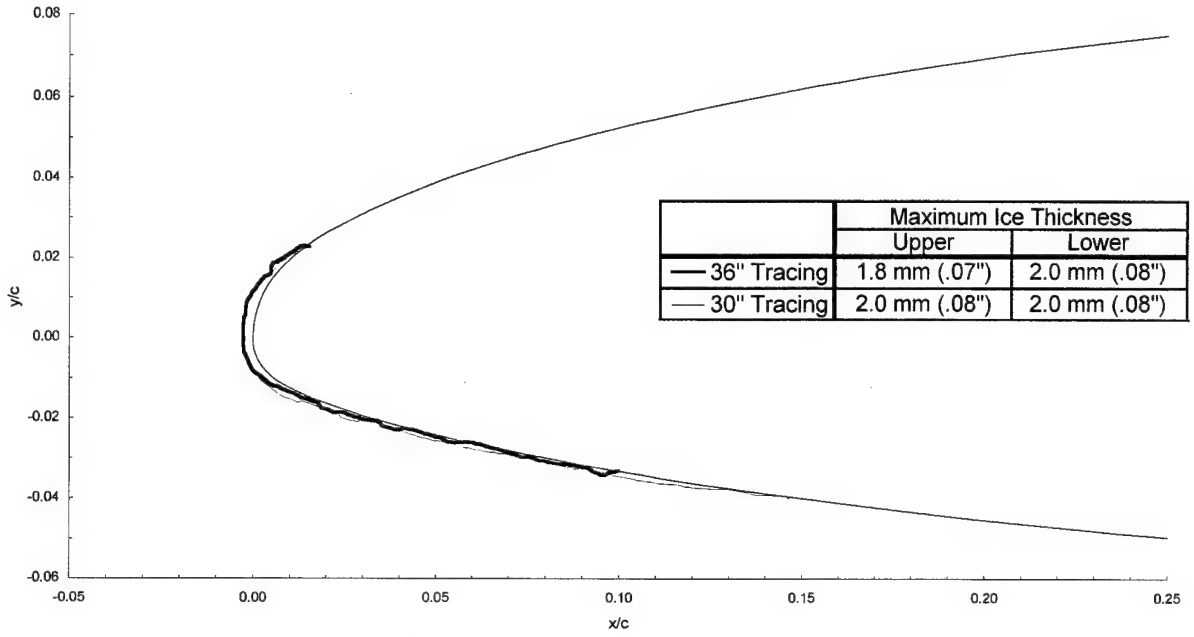

	Maximum Ice Thickness	
	Upper	Lower
—— 36" Tracing	1.8 mm (.07")	2.0 mm (.08")
—— 30" Tracing	2.0 mm (.08")	2.0 mm (.08")

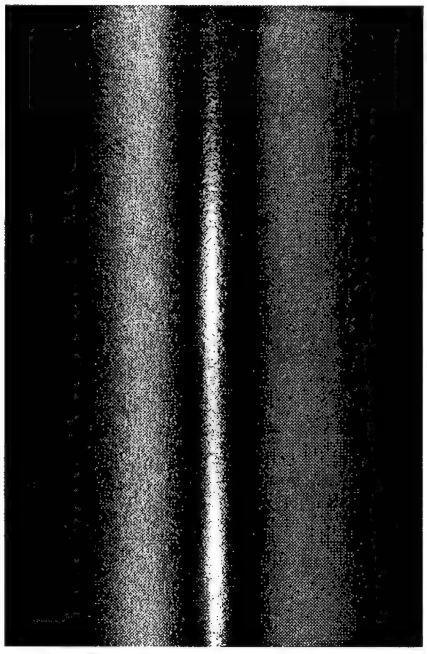

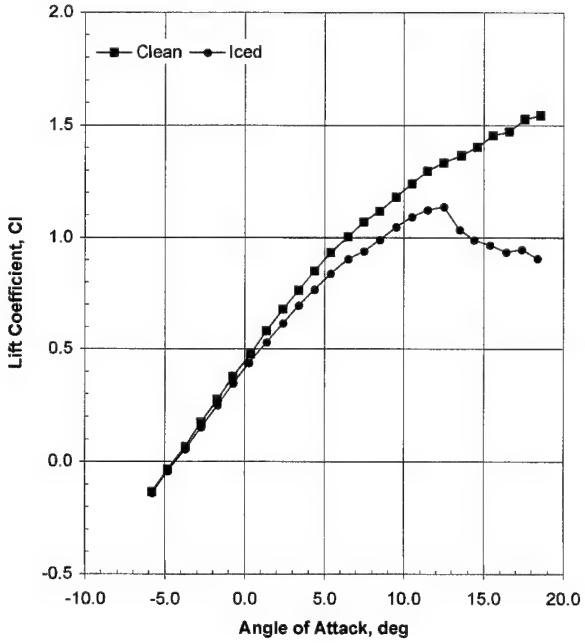

General Aviation - Run 645

T_t = -7.8°C (17.3°F)
T_s = -10.0°C (13.4°F)

V = 66.9 m/s (130 kts)
AOA = 2.4°

LWC = 0.44 g/m^3
MVD = 20 μm
Spray = 5.9 min
chord = 90 cm (36 in)

$C_{d\text{-clean}}$ = 0.0123
$C_{d\text{-iced}}$ = 0.0189

$C_{l\text{-clean}}$ = 0.665
$C_{l\text{-iced}}$ = 0.606

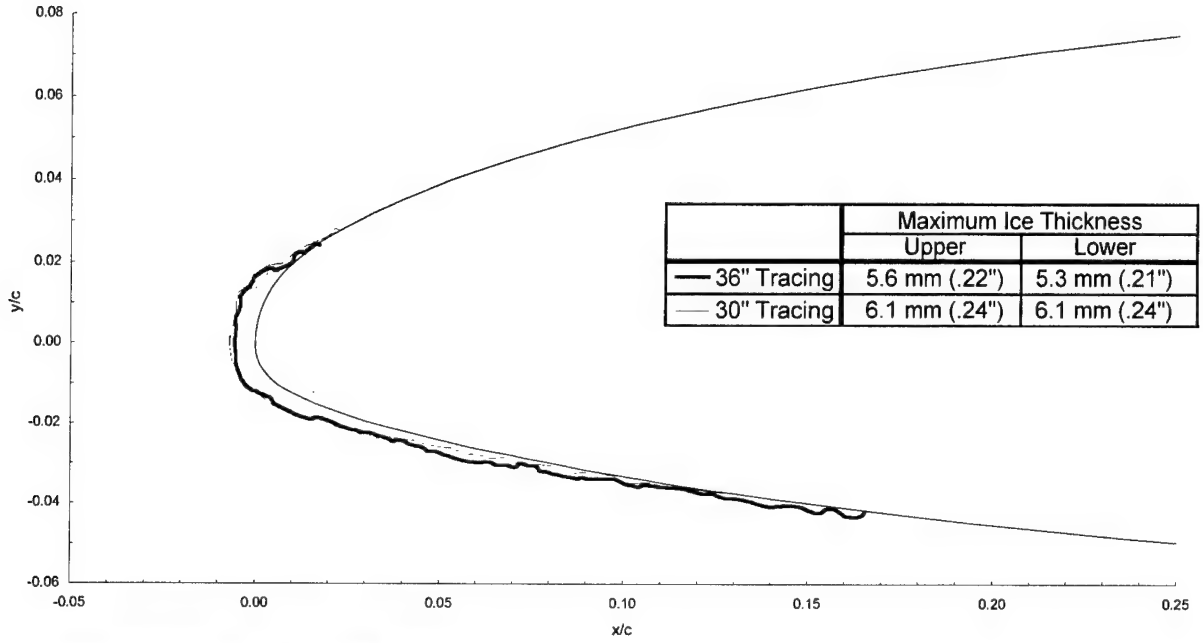

	Maximum Ice Thickness	
	Upper	Lower
36" Tracing	5.6 mm (.22")	5.3 mm (.21")
30" Tracing	6.1 mm (.24")	6.1 mm (.24")

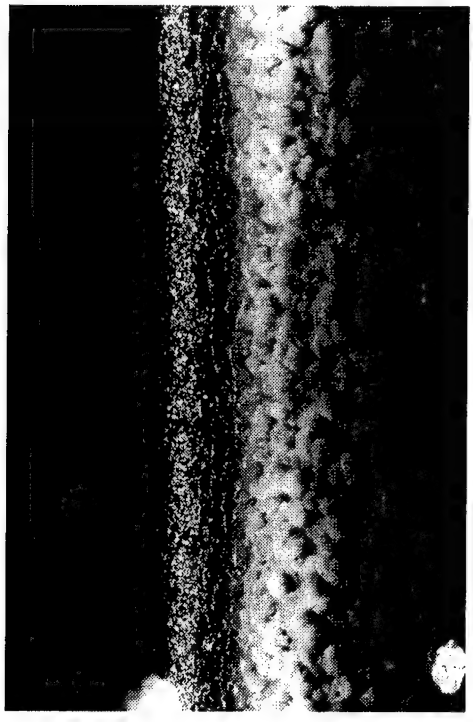

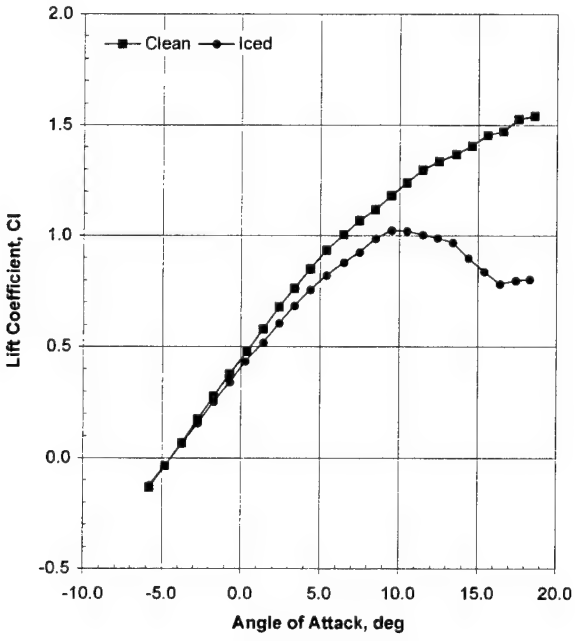

General Aviation - Run 645m

T_t = -7.8°C (17.3°F)
T_s = -10.0°C (13.4°F)
V = 66.9 m/s (130 kts)
AOA = 2.4°

LWC = 0.44 g/m^3
MVD = 20 μm
Spray = 5.9 min
chord = 90 cm (36 in)

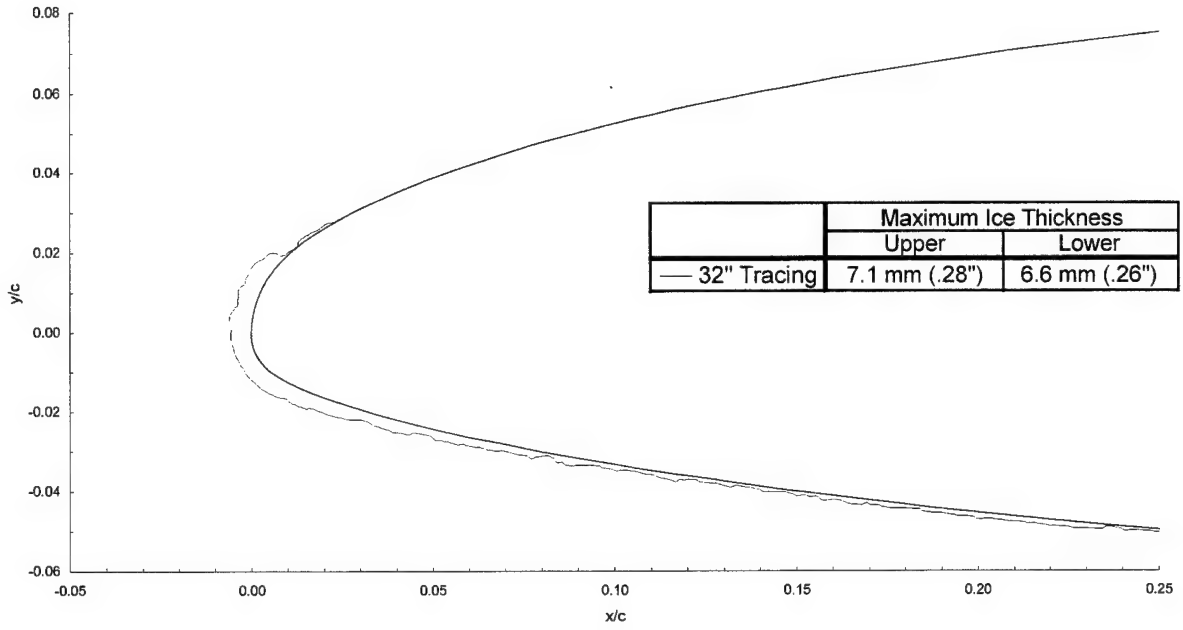

	Maximum Ice Thickness	
	Upper	Lower
— 32" Tracing	7.1 mm (.28")	6.6 mm (.26")

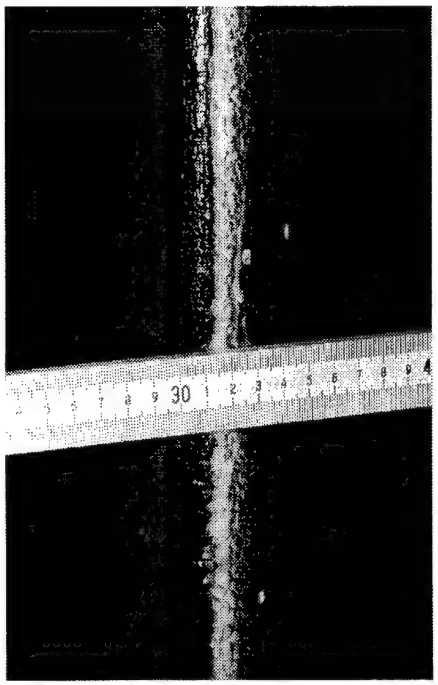

General Aviation - Run 646

T_t = -7.8°C (17.3°F)
T_s = -10.0°C (13.4°F)

V = 66.9 m/s (130 kts)
AOA = 2.4°

LWC = 0.44 g/m^3
MVD = 20 μm
Spray = 22.0 min
chord = 90 cm (36 in)

$C_{d\text{-clean}}$ = 0.0123
$C_{d\text{-iced}}$ = 0.0302

$C_{l\text{-clean}}$ = 0.659
$C_{l\text{-iced}}$ = 0.602

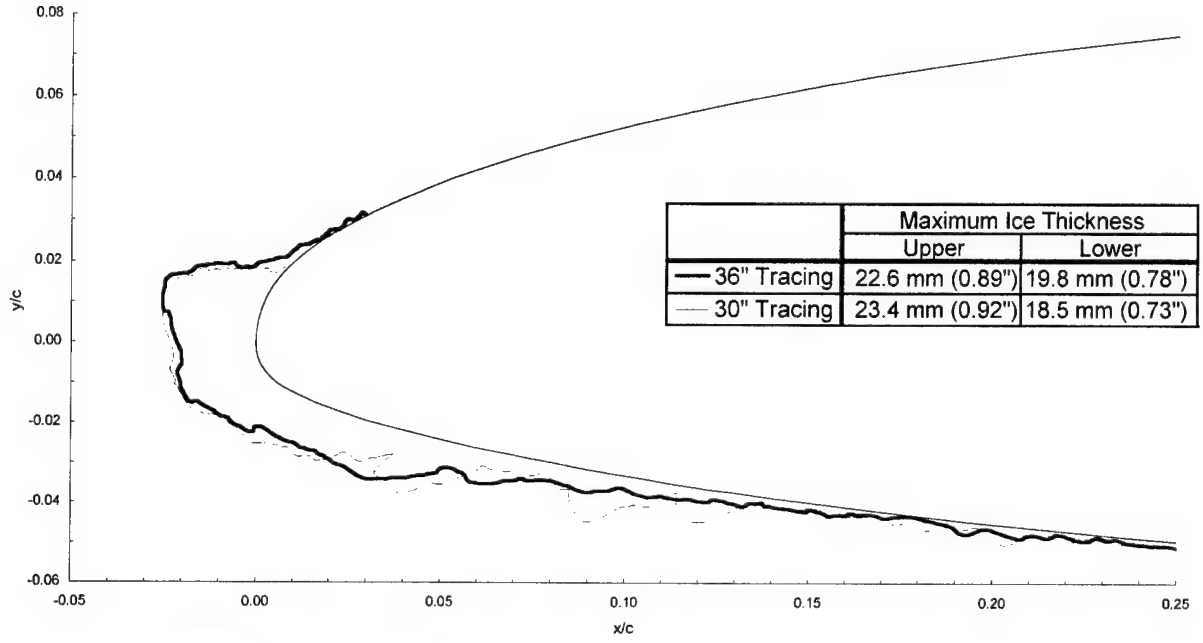

	Maximum Ice Thickness	
	Upper	Lower
36" Tracing	22.6 mm (0.89")	19.8 mm (0.78")
30" Tracing	23.4 mm (0.92")	18.5 mm (0.73")

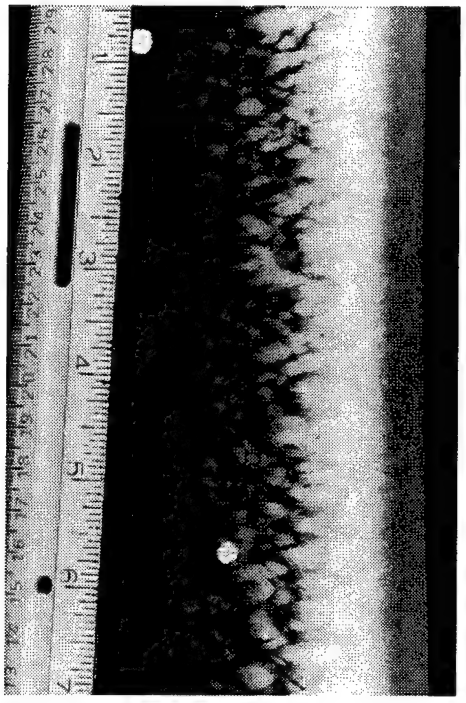

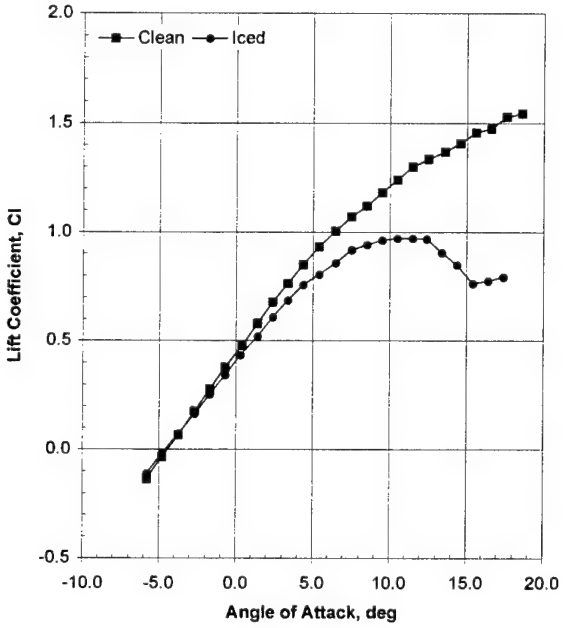

General Aviation - Run 647

T_t = -7.8°C (17.3°F)
T_s = -10.0°C (13.4°F)

V = 66.9 m/s (130 kts)
AOA = 4.4°

LWC = 0.44 g/m^3
MVD = 20 μm
Spray = 2.0 min
chord = 90 cm (36 in)

$C_{d\text{-}clean}$ = 0.0171
$C_{d\text{-}iced}$ = 0.0233

$C_{l\text{-}clean}$ = 0.837
$C_{l\text{-}iced}$ = 0.780

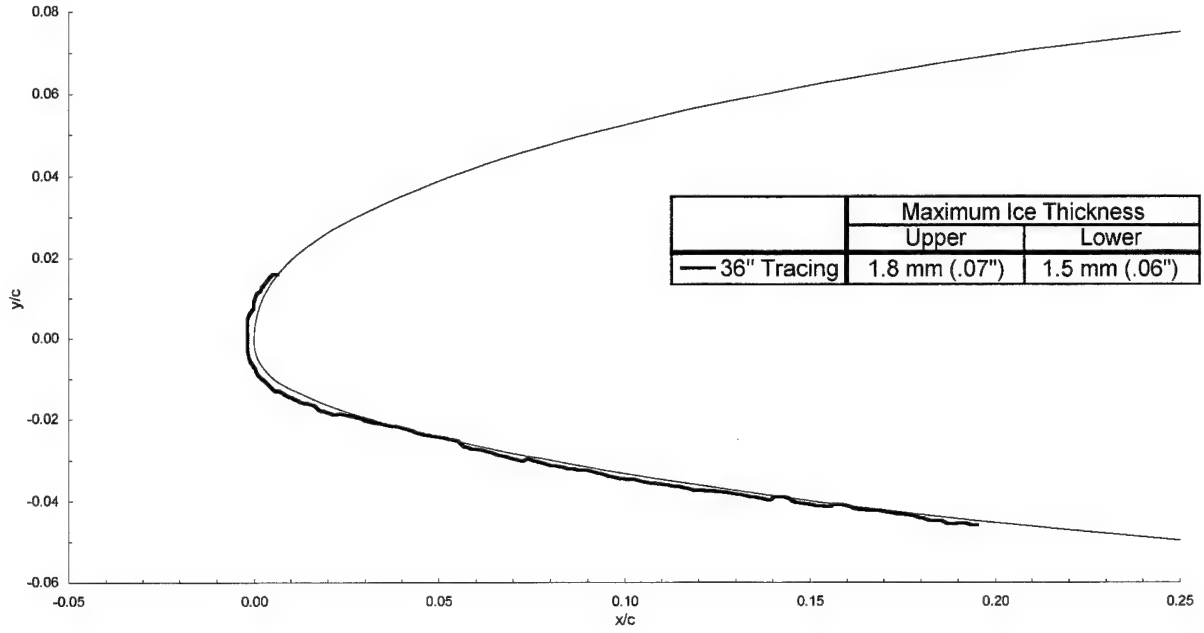

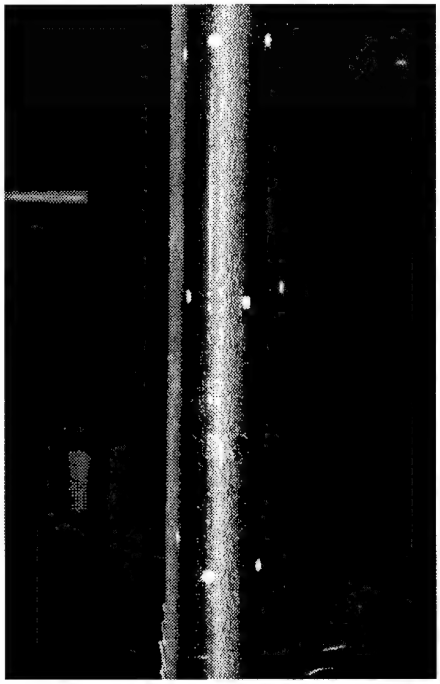

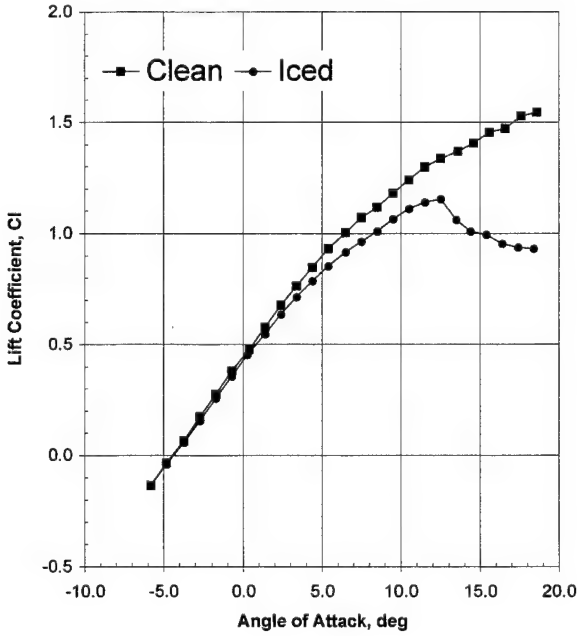

General Aviation - Run 648

T_t = -7.8°C (17.3°F)
T_s = -10.0°C (13.4°F)

V = 66.9 m/s (130 kts)
AOA = 4.4°

LWC = 0.44 g/m^3
MVD = 20 μm
Spray = 5.9 min
chord = 90 cm (36 in)

$C_{d\text{-}clean}$ = 0.0171
$C_{d\text{-}iced}$ = 0.0235

$C_{l\text{-}clean}$ = 0.832
$C_{l\text{-}iced}$ = 0.748

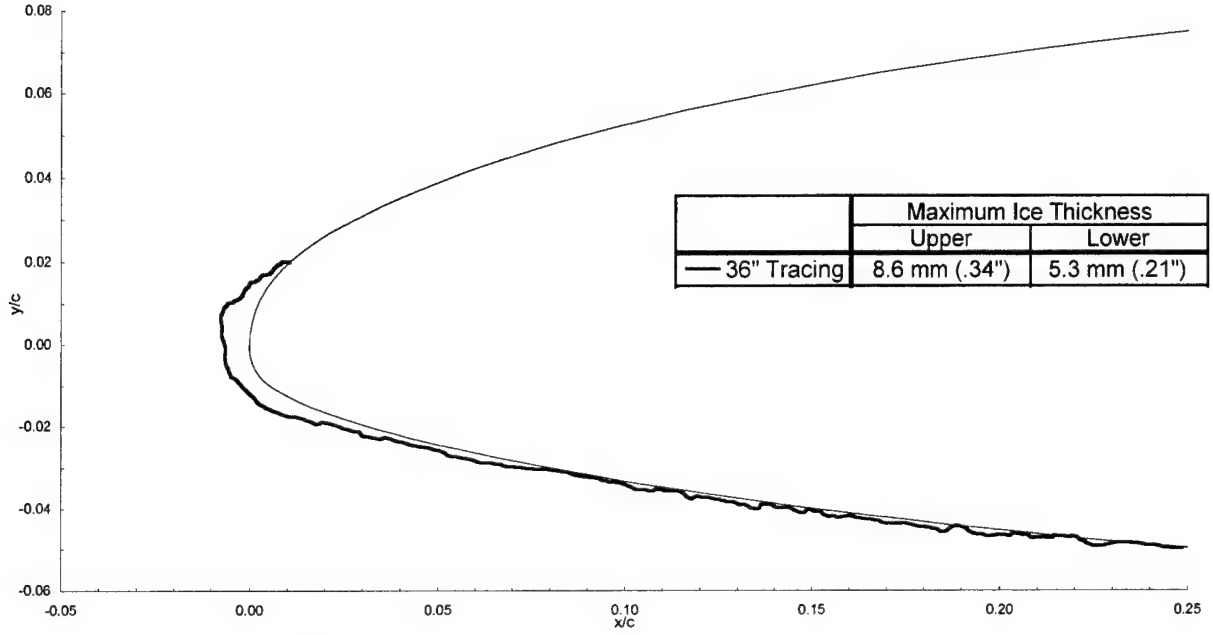

	Maximum Ice Thickness	
	Upper	Lower
— 36" Tracing	8.6 mm (.34")	5.3 mm (.21")

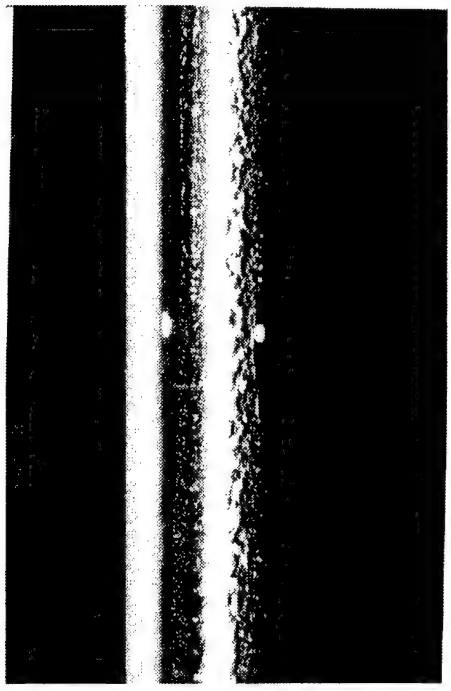

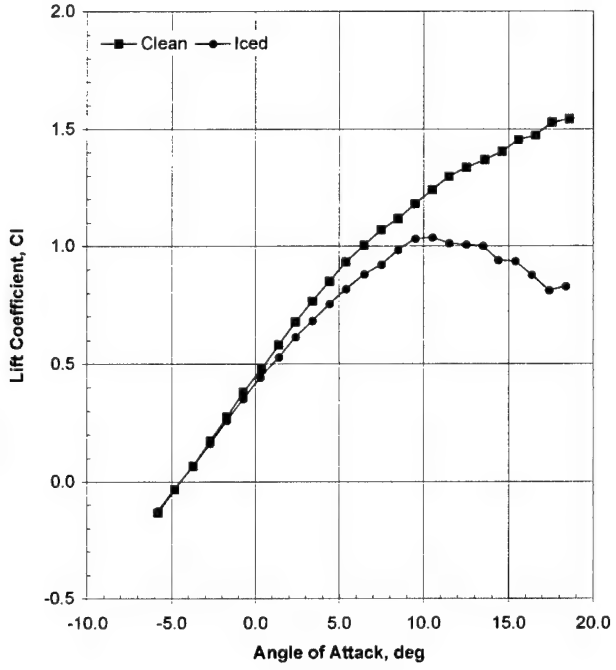

General Aviation - Run 649

T_t = -7.8°C (17.3°F)
T_s = -10.0°C (13.4°F)

V = 66.9 m/s (130 kts)
AOA = 4.4°

LWC = 0.44 g/m^3
MVD = 20 μm

Spray = 22.0 min
chord = 90 cm (36 in)

$C_{d\text{-}clean}$ = 0.0171
$C_{d\text{-}iced}$ = 0.0311

$C_{l\text{-}clean}$ = 0.834
$C_{l\text{-}iced}$ = 0.748

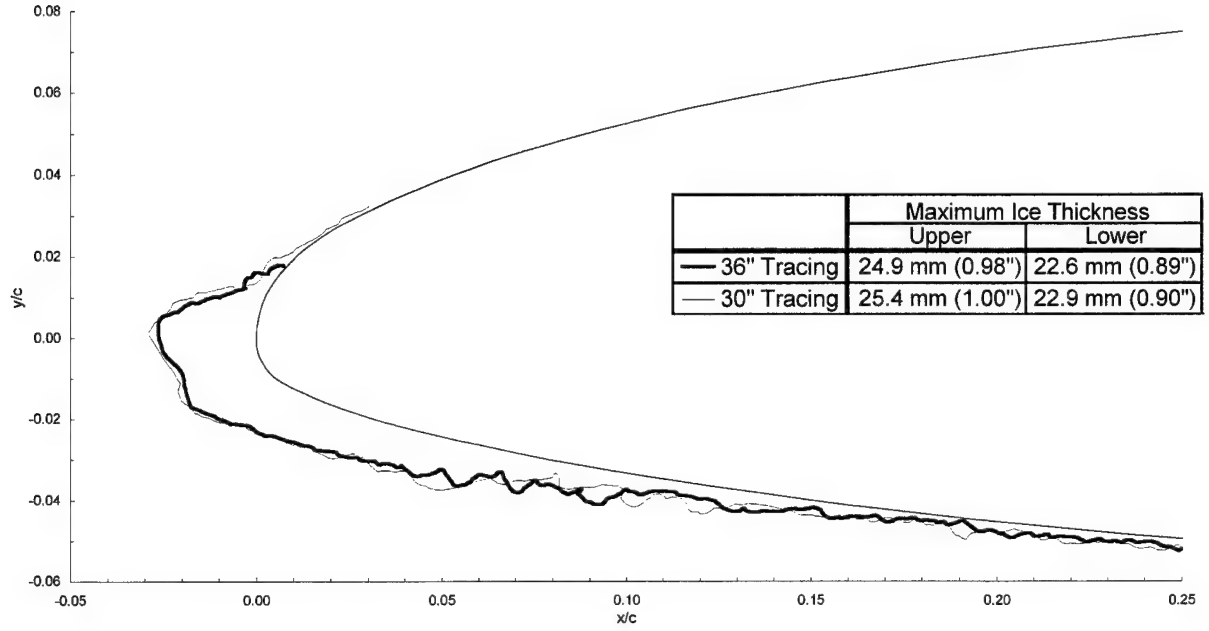

	Maximum Ice Thickness	
	Upper	Lower
36" Tracing	24.9 mm (0.98")	22.6 mm (0.89")
30" Tracing	25.4 mm (1.00")	22.9 mm (0.90")

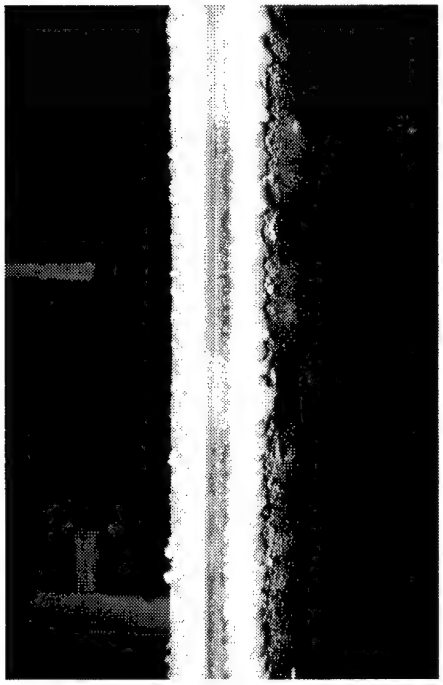

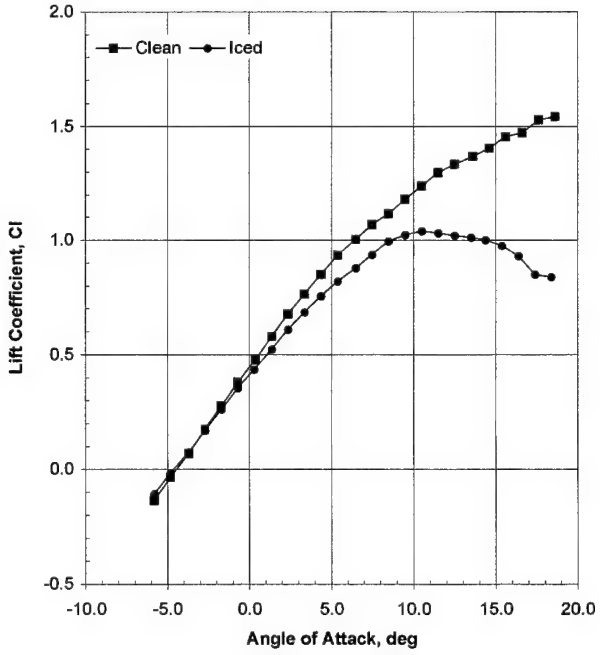

General Aviation - Run 655

T_t = -9.1°C (15.0°F)
T_s = -10.0°C (13.4°F)

V = 42.7 m/s (83 kts)
AOA = 4.4°

LWC = 0.65 g/m^3
MVD = 20 μm
Spray = 2.0 min
chord = 90 cm (36 in)

$C_{d\text{-clean}}$ = 0.0172
$C_{d\text{-iced}}$ = 0.0199

$C_{l\text{-clean}}$ = 0.830
$C_{l\text{-iced}}$ = 0.788

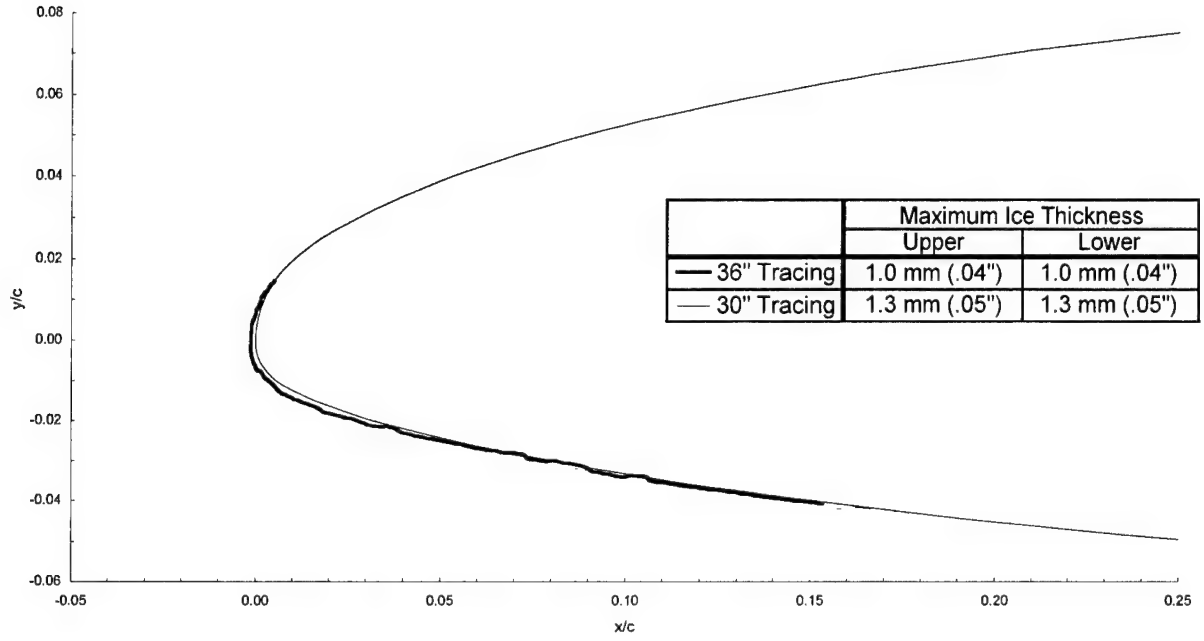

	Maximum Ice Thickness	
	Upper	Lower
36" Tracing	1.0 mm (.04")	1.0 mm (.04")
30" Tracing	1.3 mm (.05")	1.3 mm (.05")

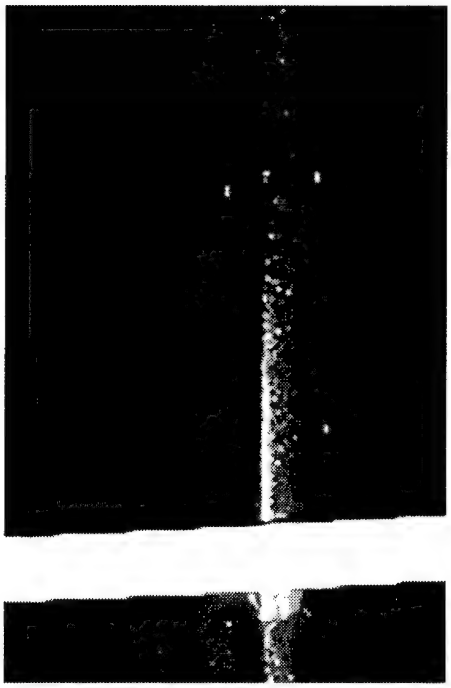

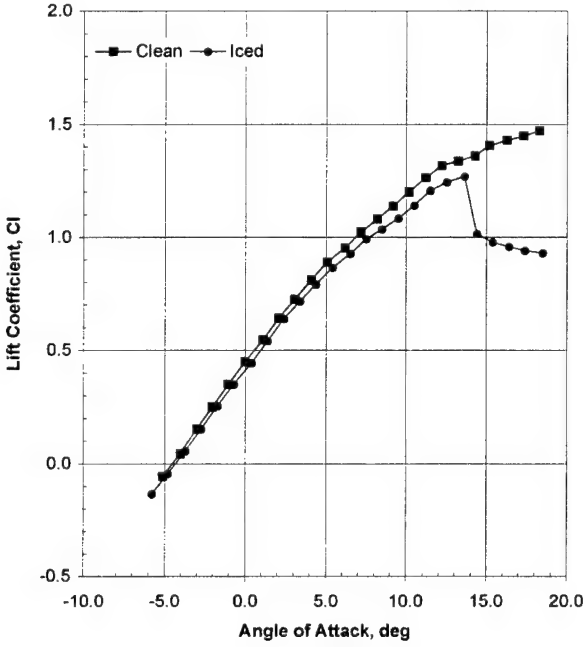

General Aviation - Run 656

T_t = -9.1°C (15.0°F)
T_s = -10.0°C (13.4°F)

V = 42.7 m/s (83 kts)
AOA = 4.4°

LWC = 0.65 g/m^3
MVD = 20 μm
Spray = 6.0 min
chord = 90 cm (36 in)

$C_{d\text{-}clean}$ = 0.0172
$C_{d\text{-}iced}$ = 0.0242

$C_{l\text{-}clean}$ = 0.830
$C_{l\text{-}iced}$ = 0.760

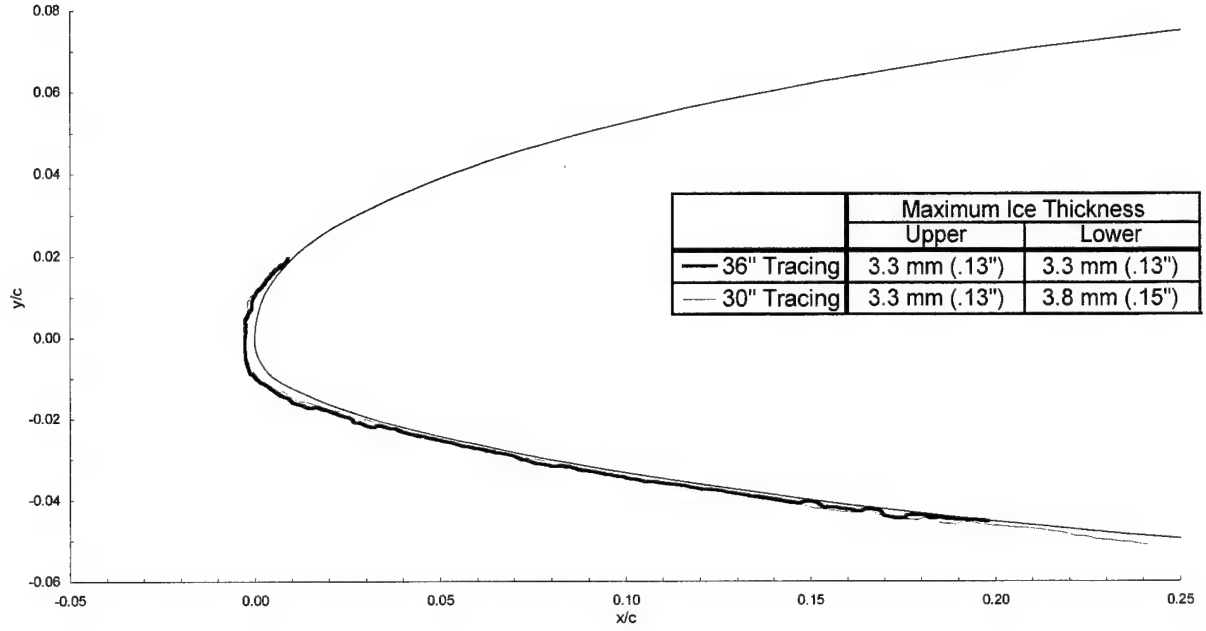

	Maximum Ice Thickness	
	Upper	Lower
36" Tracing	3.3 mm (.13")	3.3 mm (.13")
30" Tracing	3.3 mm (.13")	3.8 mm (.15")

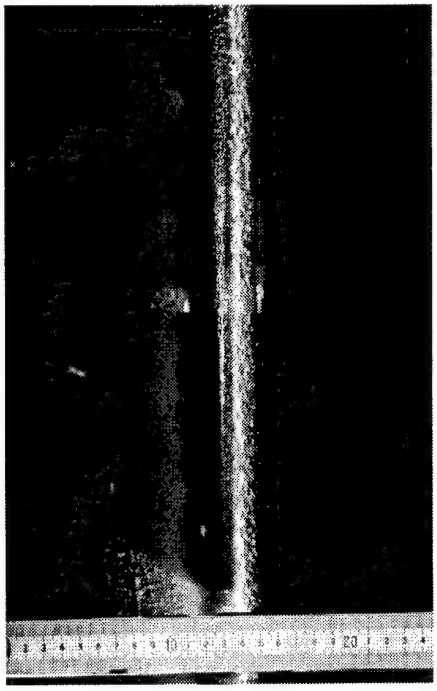

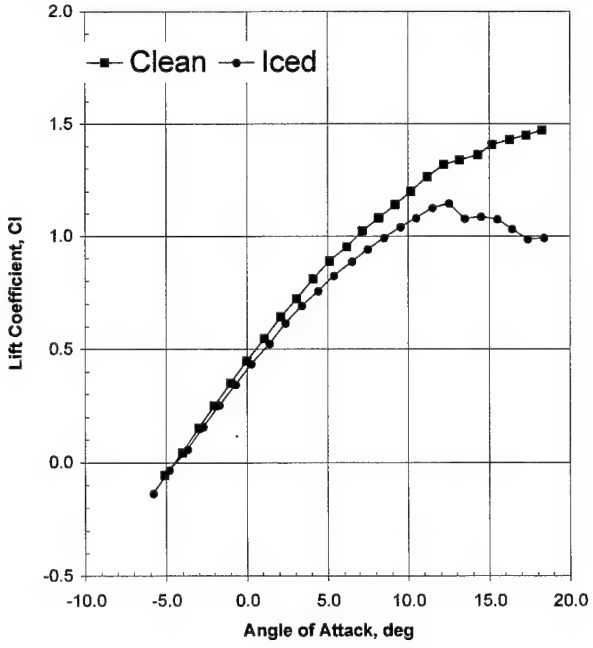

General Aviation - Run 657

T_t = -4.1°C (24.1°F)
T_s = -5.0°C (22.0°F)

V = 42.7 m/s (83 kts)
AOA = 4.4°

LWC = 0.65 g/m^3
MVD = 20 μm
Spray = 5.0 min
chord = 90 cm (36 in)

$C_{d\text{-clean}}$ = 0.0172
$C_{d\text{-iced}}$ = 0.0265

$C_{l\text{-clean}}$ = 0.834
$C_{l\text{-iced}}$ = 0.756

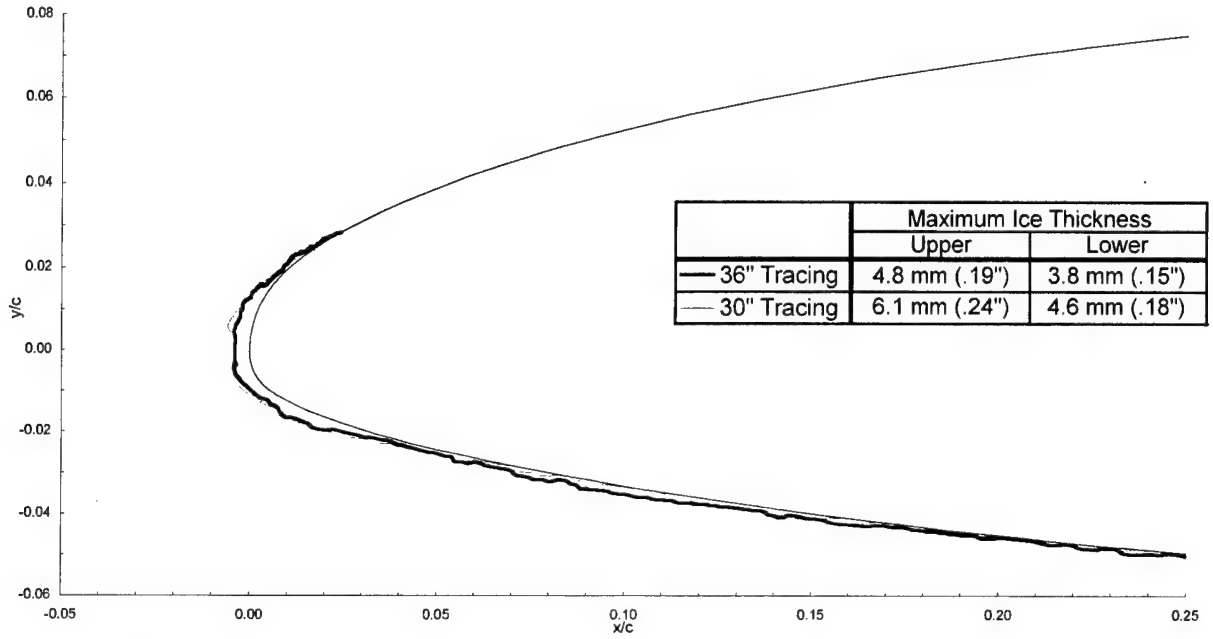

	Maximum Ice Thickness	
	Upper	Lower
36" Tracing	4.8 mm (.19")	3.8 mm (.15")
30" Tracing	6.1 mm (.24")	4.6 mm (.18")

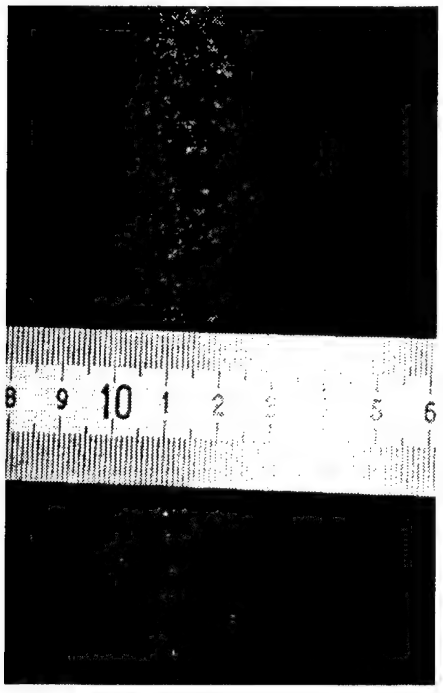

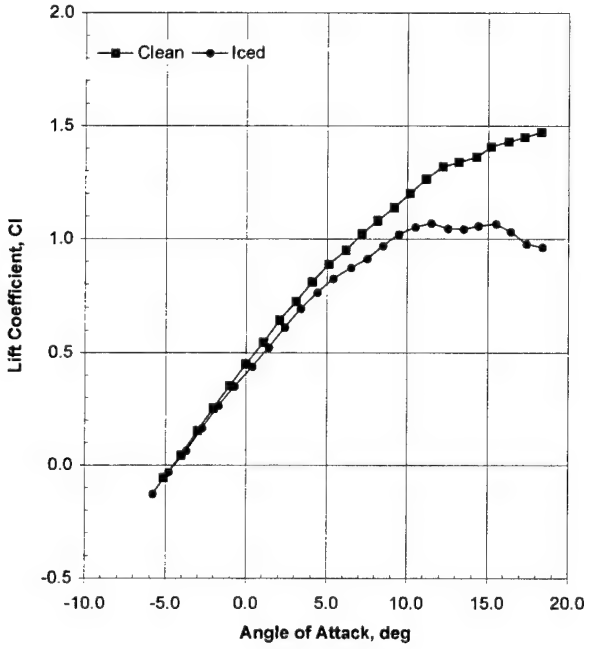

General Aviation - Run 661

T_t = -1.8°C (28.2°F)
T_s = -4.0°C (24.0°F)

V = 66.9 m/s (130 kts)
AOA = -1.7°

LWC = 1.00 g/m^3
MVD = 20.5 μm
Spray = 15.0 min
chord = 90 cm (36 in)

$C_{d\text{-}clean}$ = 0.0092
$C_{d\text{-}iced}$ = 0.0347

$C_{l\text{-}clean}$ = 0.275
$C_{l\text{-}iced}$ = 0.233

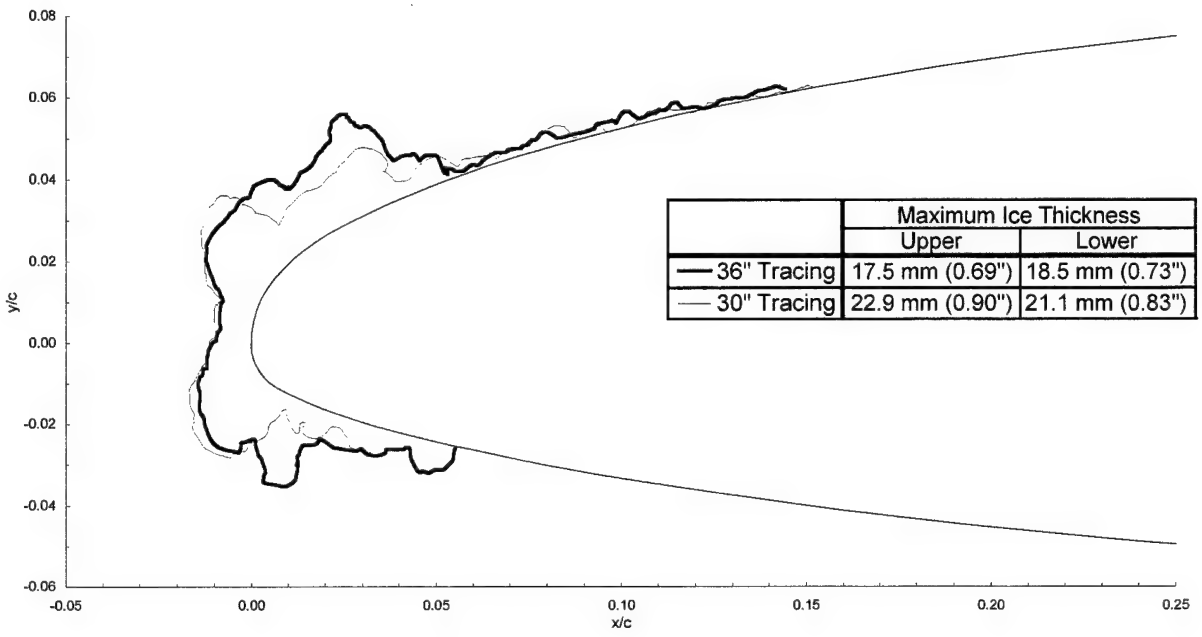

	Maximum Ice Thickness	
	Upper	Lower
—— 36" Tracing	17.5 mm (0.69")	18.5 mm (0.73")
—— 30" Tracing	22.9 mm (0.90")	21.1 mm (0.83")

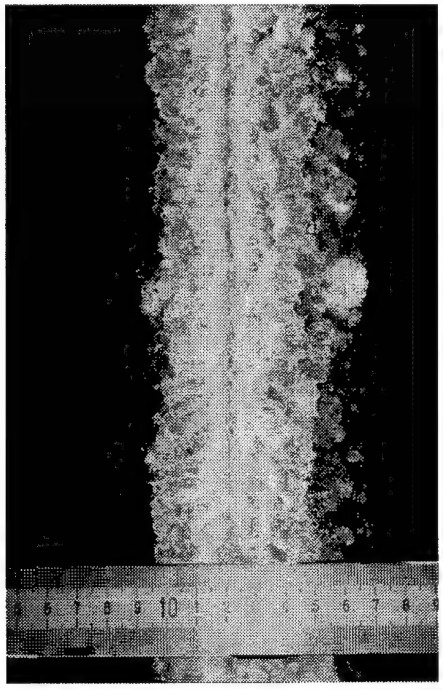

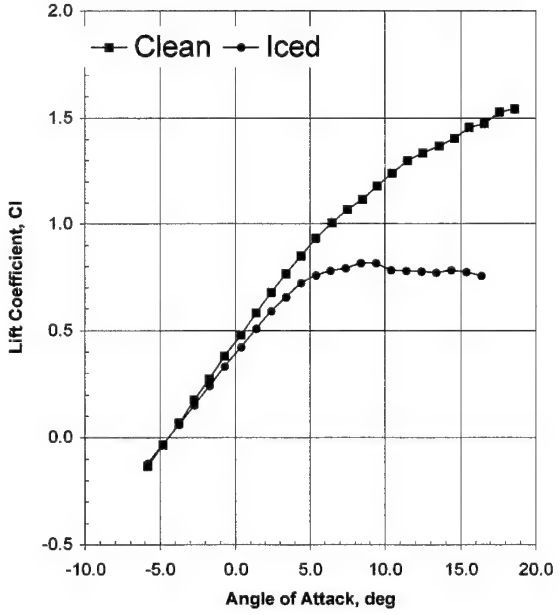

Appendix D4
Test Results, General Aviation—LTPT

LTPT
General Aviation - Clean Model

chord = 90 cm (36 in)

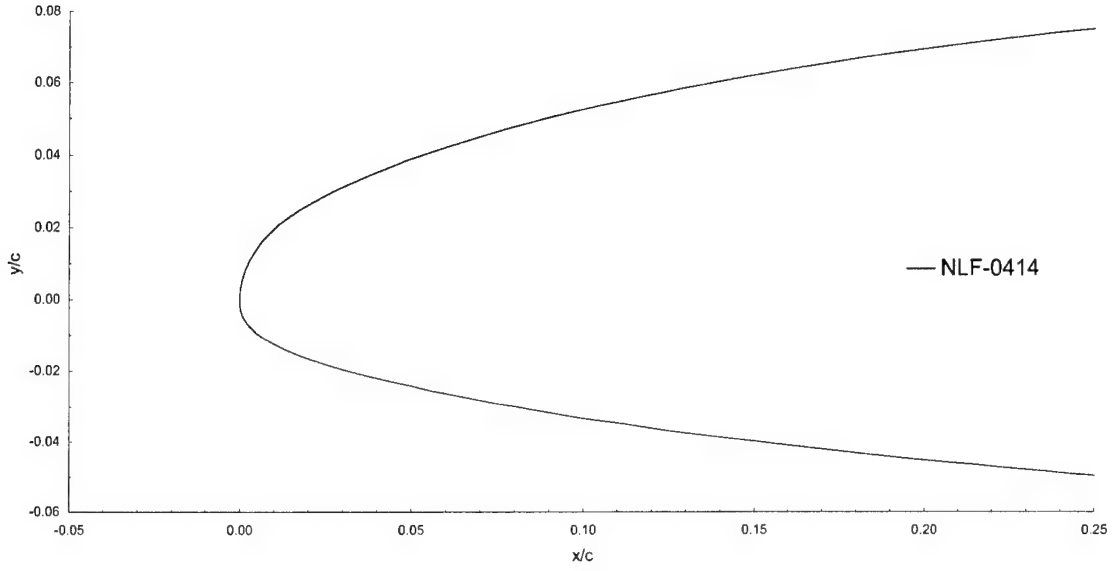

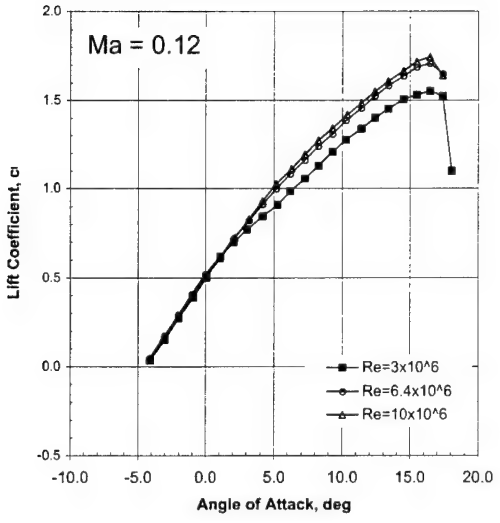

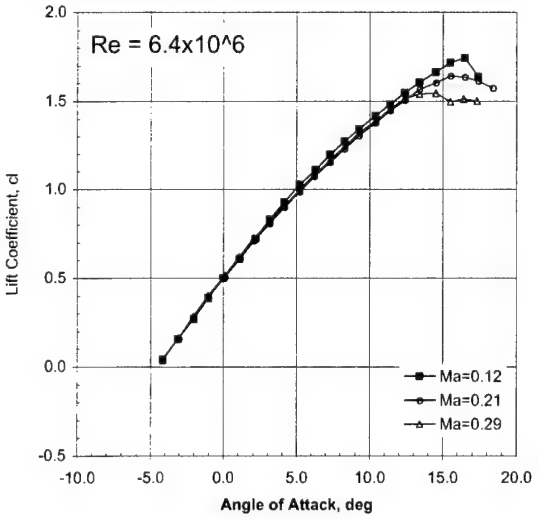

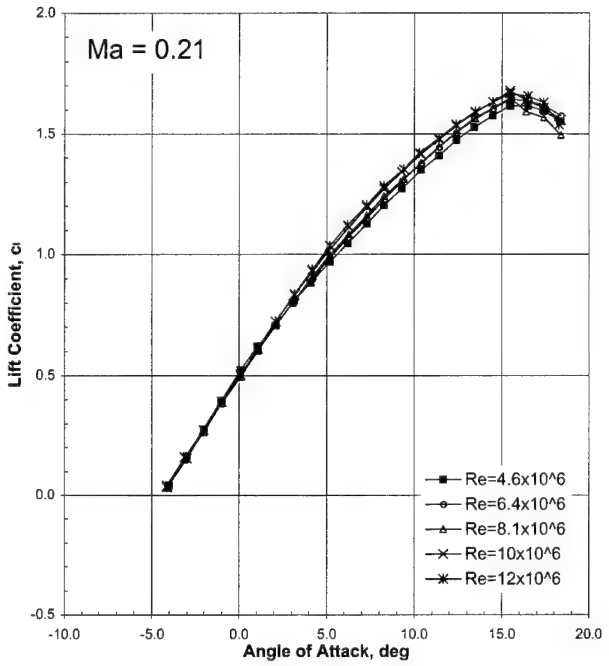

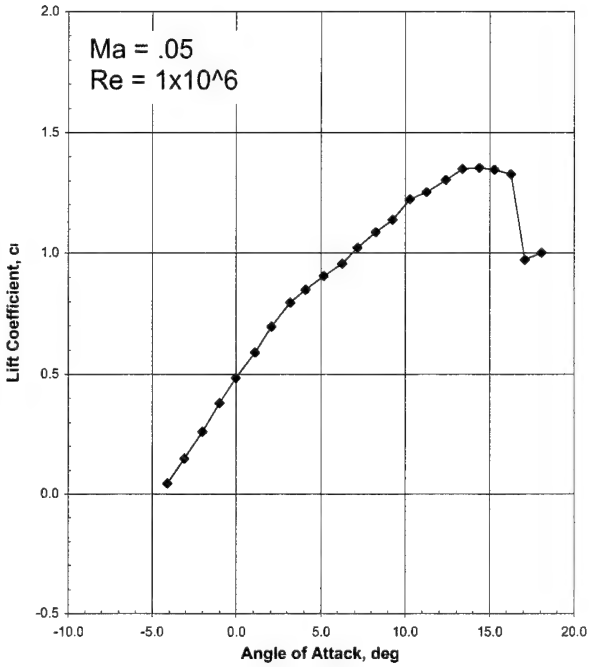

Drag Coefficients, c_d

	α = -2.0	α = 0.0	α = 2.1	α = 4.2	α = 6.2
Run 23, Ma = 0.12, Re = 10x10^6	0.0064	0.0086	0.0114	0.0144	0.0180
Run 24, Ma = 0.12, Re = 6.4x10^6	0.0076	0.0072	0.0082	0.0107	0.0146
Run 25, Ma = 0.12, Re = 3x10^6	*0.0253*	*0.0322*	*0.0299*	*0.0222*	*0.0132*
Run 26, Ma = 0.21, Re = 4.6x10^6	*0.0279*	*0.0287*	*0.0232*	*0.0153*	*0.0087*
Run 27, Ma = 0.29, Re = 6.4x10^6	*0.0418*	*0.0483*	*0.0463*	*0.0407*	*0.0361*
Run 28, Ma = 0.21, Re = 6.4x10^6	*0.0465*	*0.0530*	*0.0501*	*0.0427*	*0.0353*
Run 29, Ma = 0.21, Re = 8.1x10^6	*0.0375*	*0.0439*	*0.0417*	*0.0357*	*0.0303*
Run 30, Ma = 0.21, Re = 10x10^6	*0.0230*	*0.0305*	*0.0282*	*0.0211*	*0.0143*
Run 32, Ma = 0.21, Re = 12x10^6	*0.0261*	*0.0345*	*0.0336*	*0.0282*	*0.0228*
Run 35, Ma = 0.05, Re = 1x10^6	*0.0029*	*0.0044*	*0.0057*	*0.0069*	*0.0078*
Run 701, Ma = 12, Re = 10x10^6	0.0077	0.0067	0.0080	0.0115	0.0174
Run 702, Ma = 21, Re = 4.6x10^6	0.0103	0.0091	0.0106	0.0148	0.0217
Run 703, Ma = 21, Re = 10x10^6	0.0079	0.0068	0.0085	0.0127	0.0196
Run 704, Ma = 29, Re = 6.4x10^6	0.0112	0.0097	0.0112	0.0156	0.0233
Run 705, Ma = 12, Re = 3x10^6	0.0118	0.0102	0.0112	0.1490	0.0215

Italicized font indicates force balance data

Runs 701 - 705, Repeat Runs

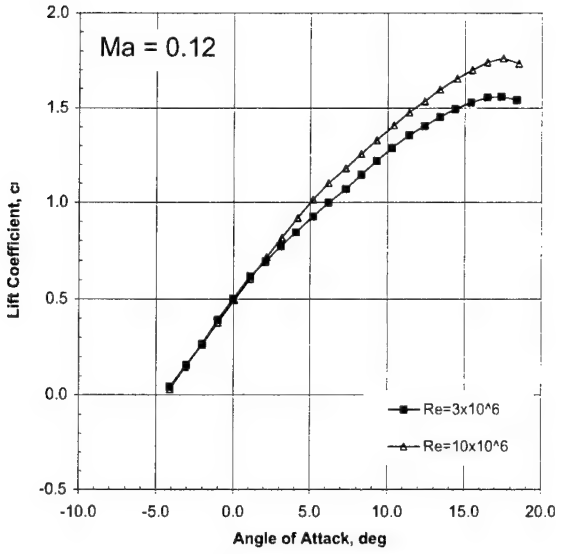

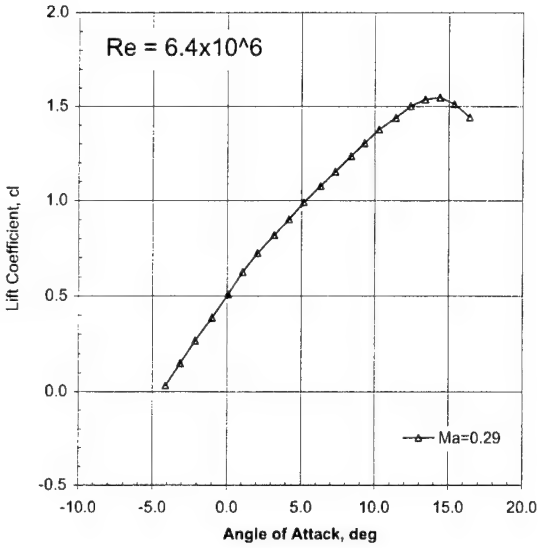

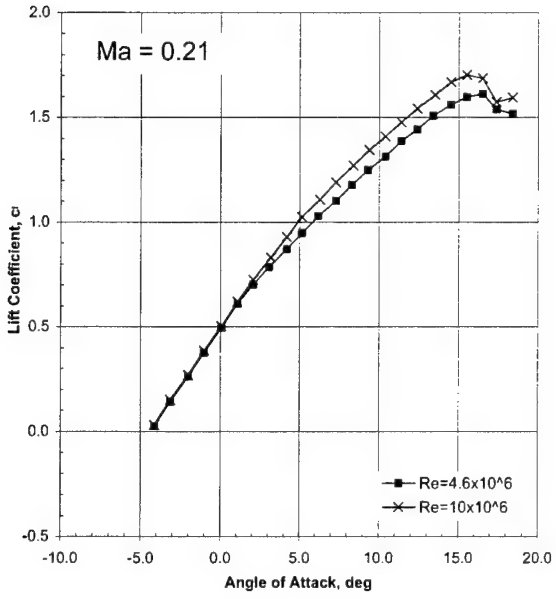

Run 23, Ma = 0.12, Re = 10x10^6

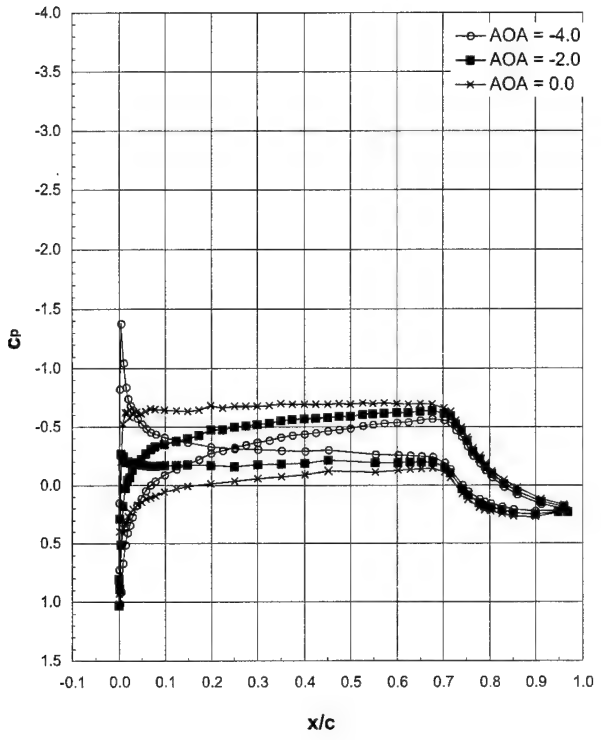

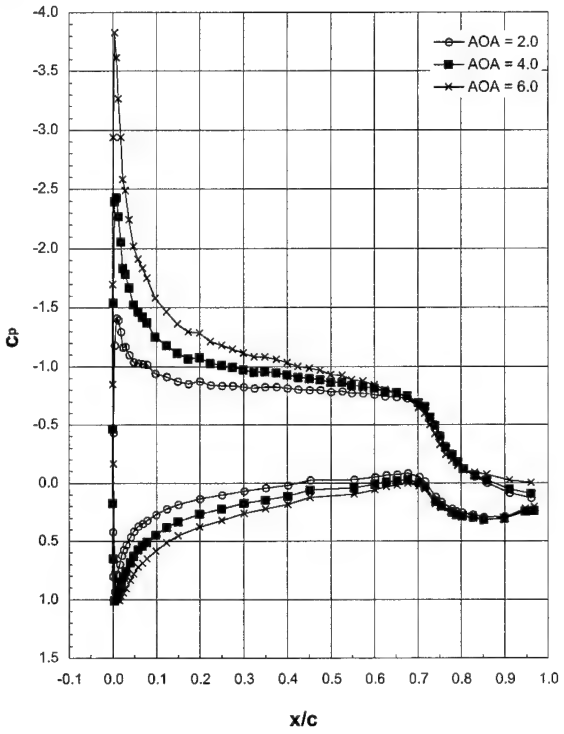

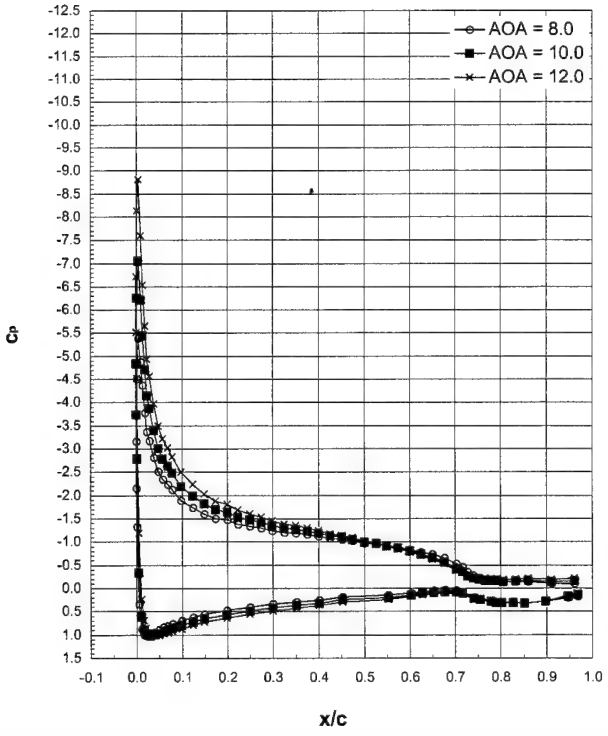

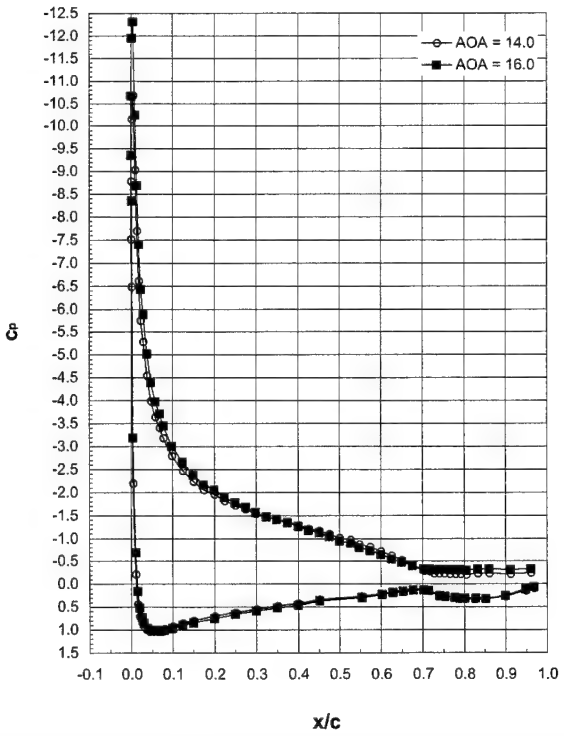

Run 24, Ma = 0.12, Re = 6.4x10^6

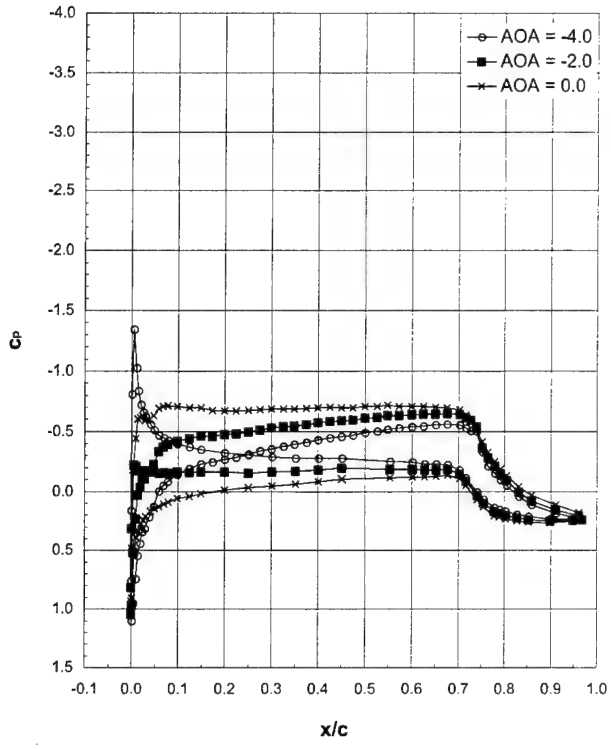

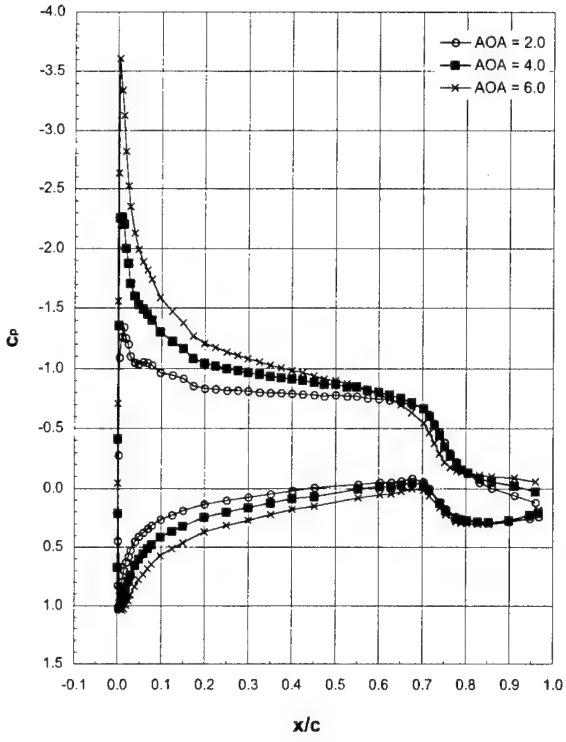

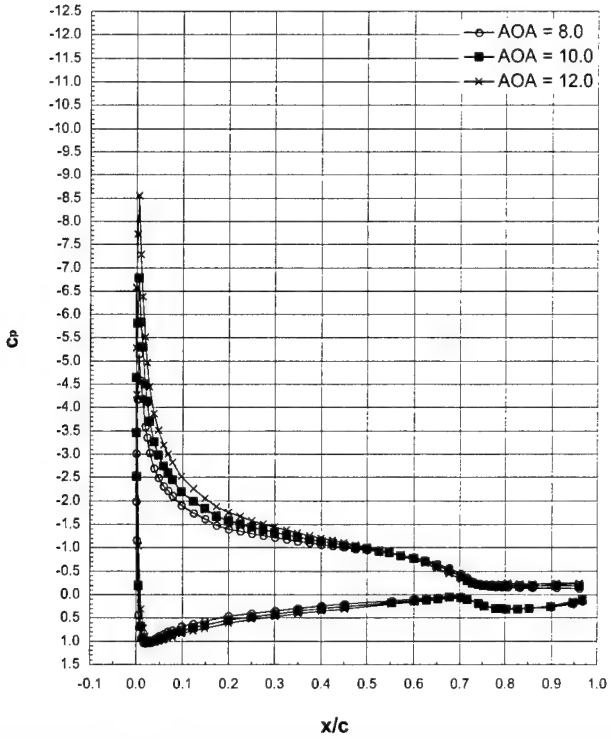

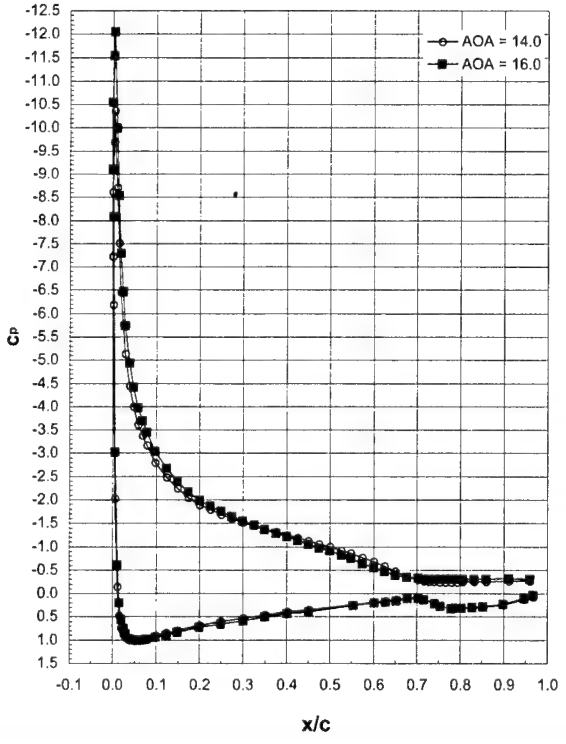

Run 25, Ma = 0.12, Re = 3x10^6

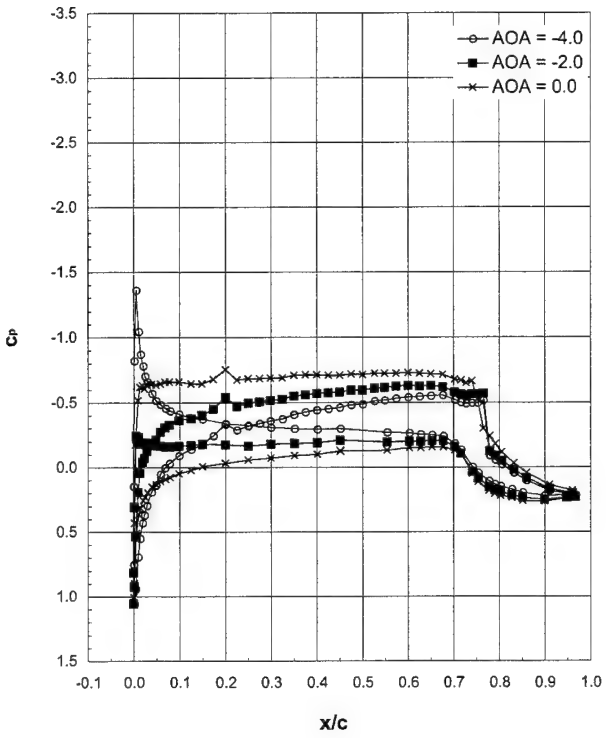

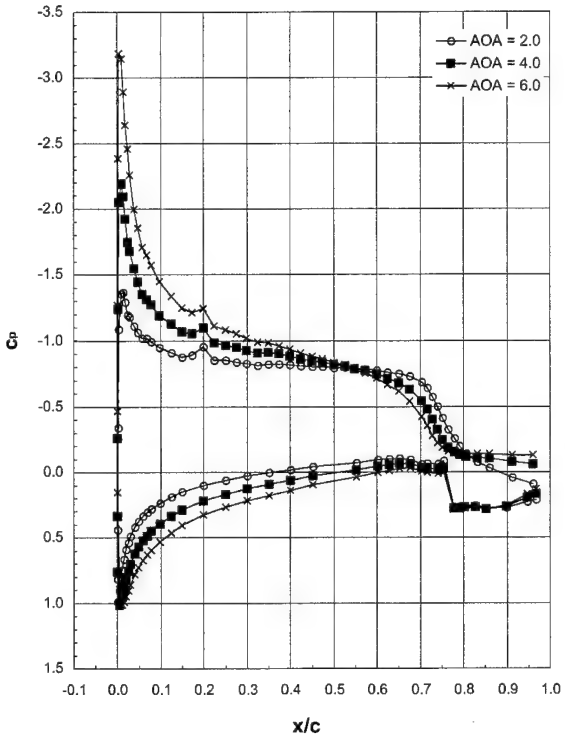

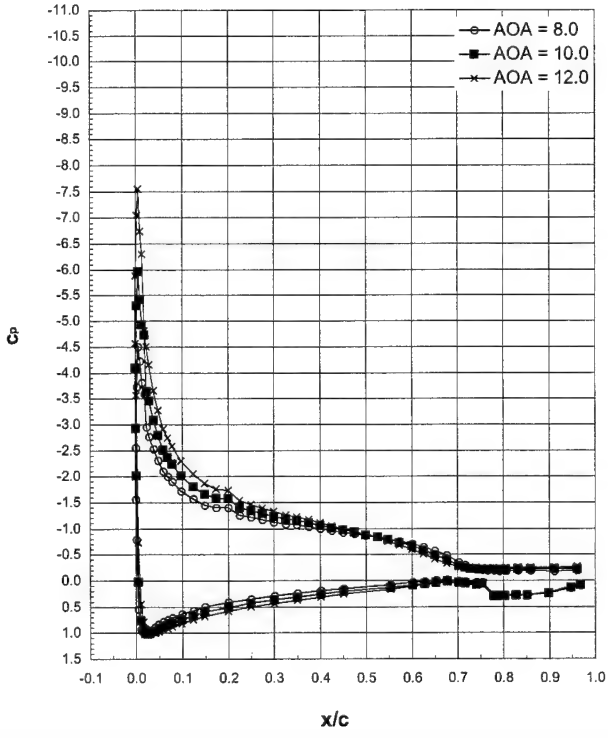

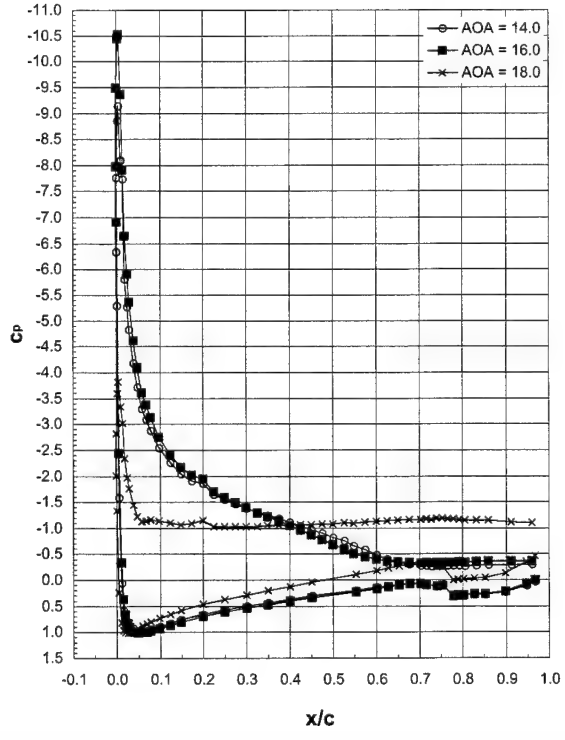

Run 26, Ma = 0.21, Re = 4.6x10^6

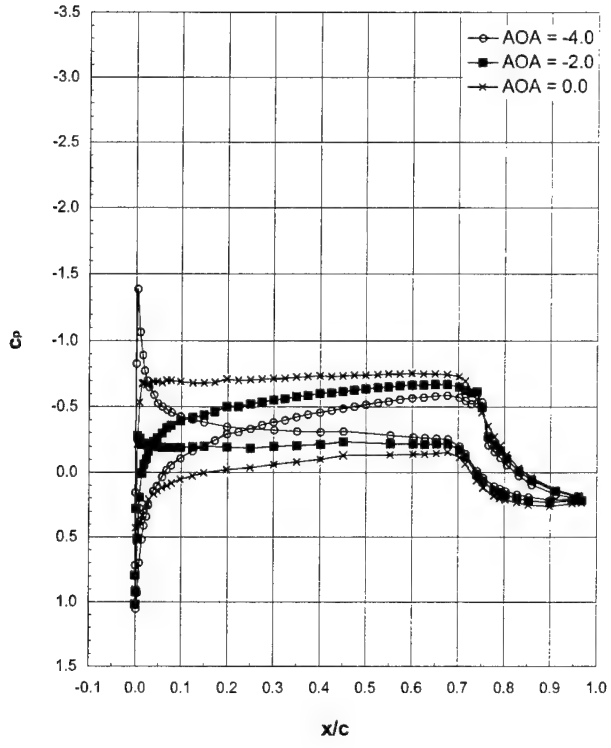

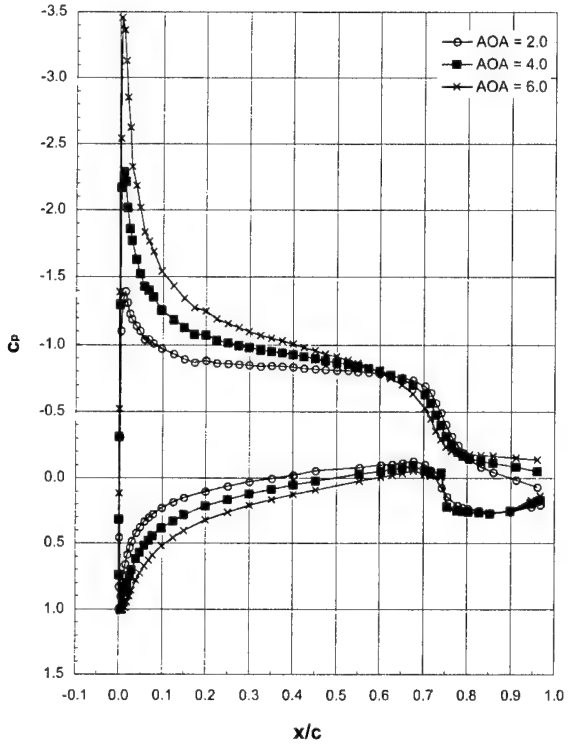

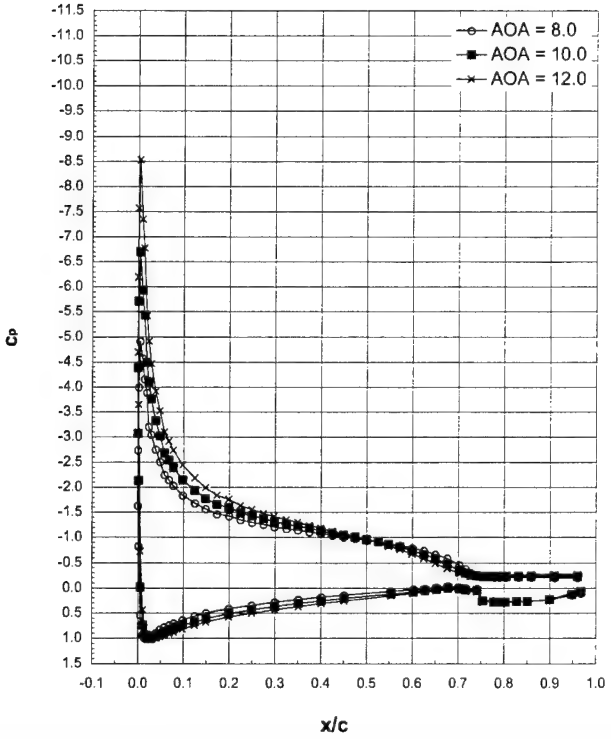

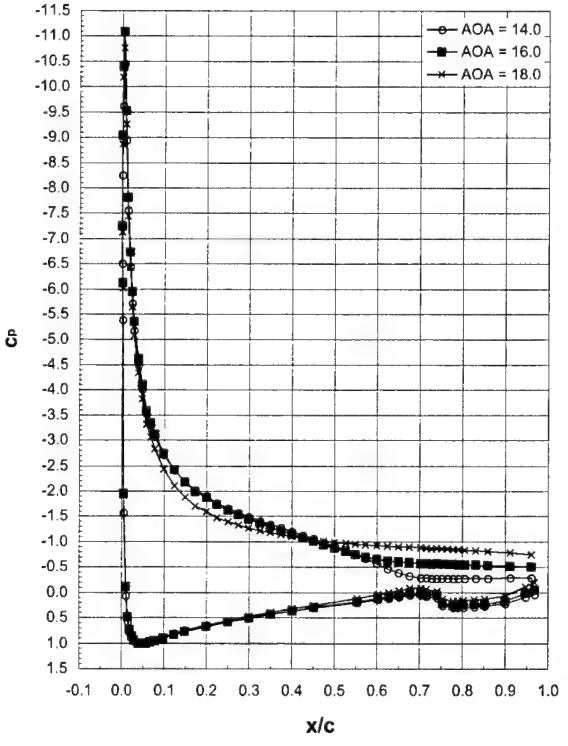

Run 27, Ma = 0.29, Re = 6.4x10^6

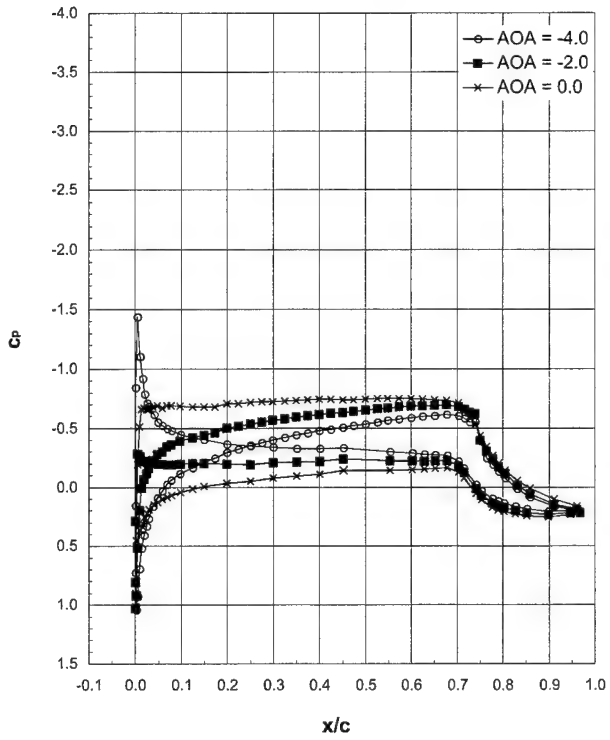

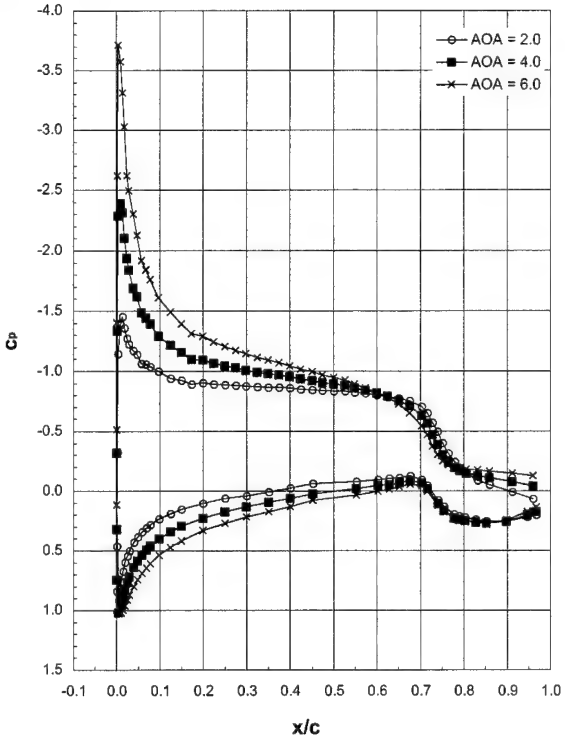

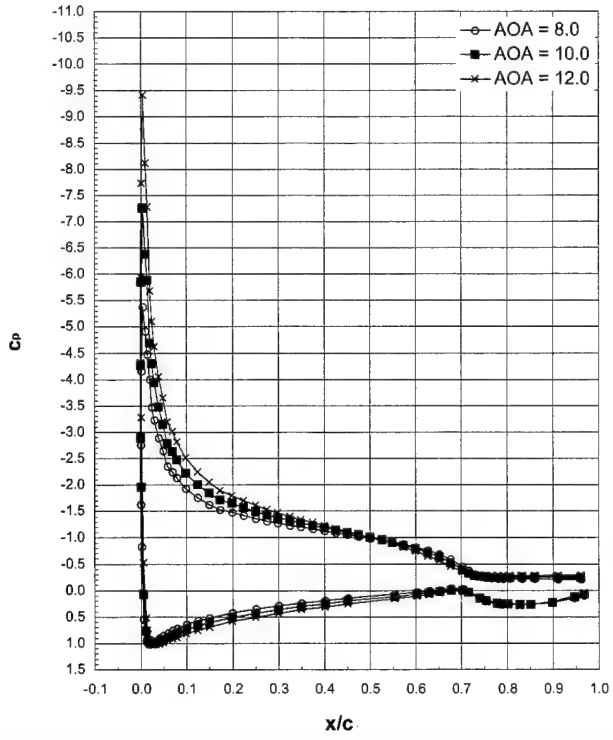

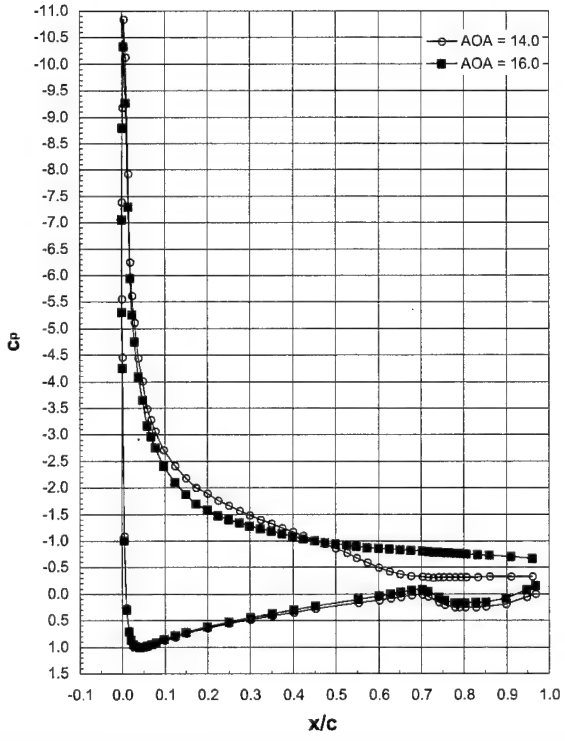

Run 28, Ma = 0.21, Re = 6.4x10^6

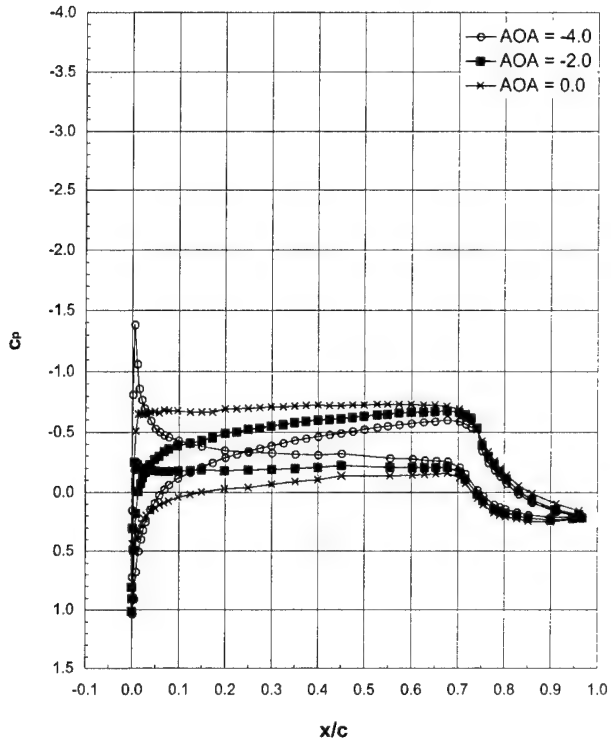

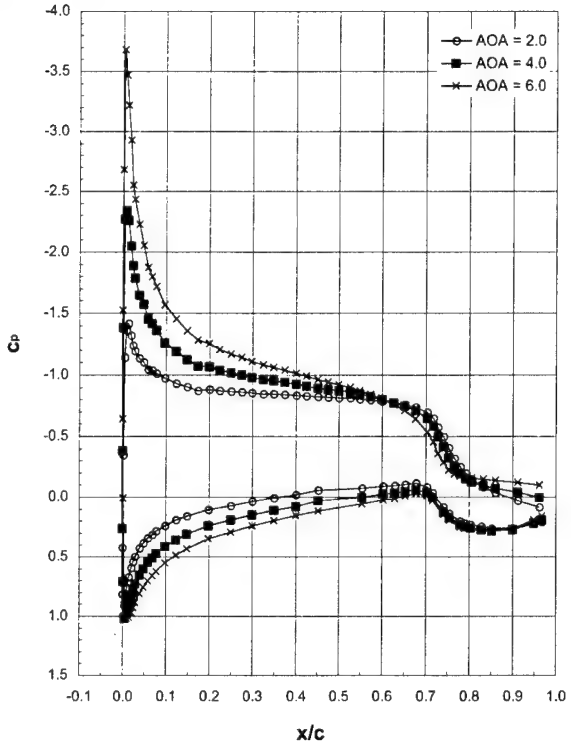

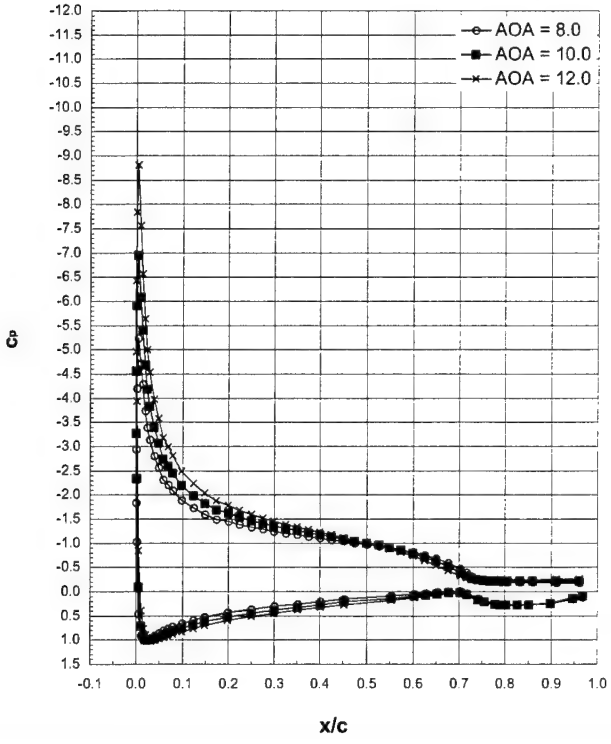

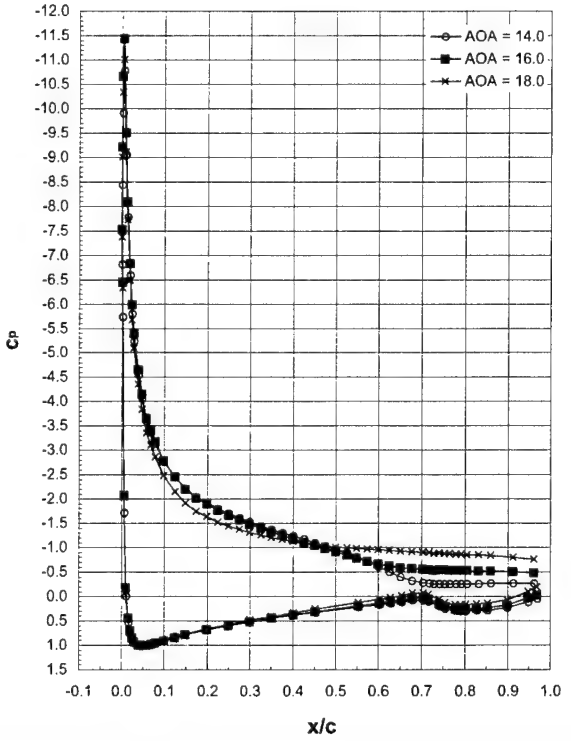

Run 29, Ma = 0.21, Re = 8.1x10^6

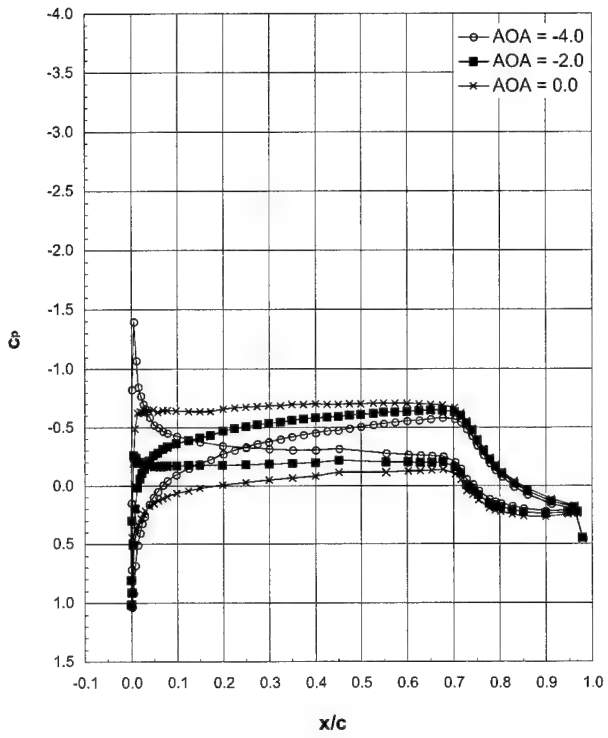

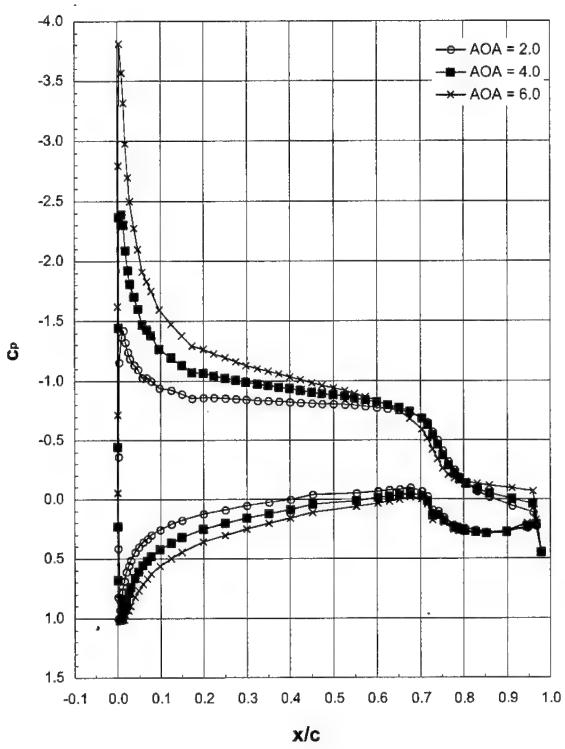

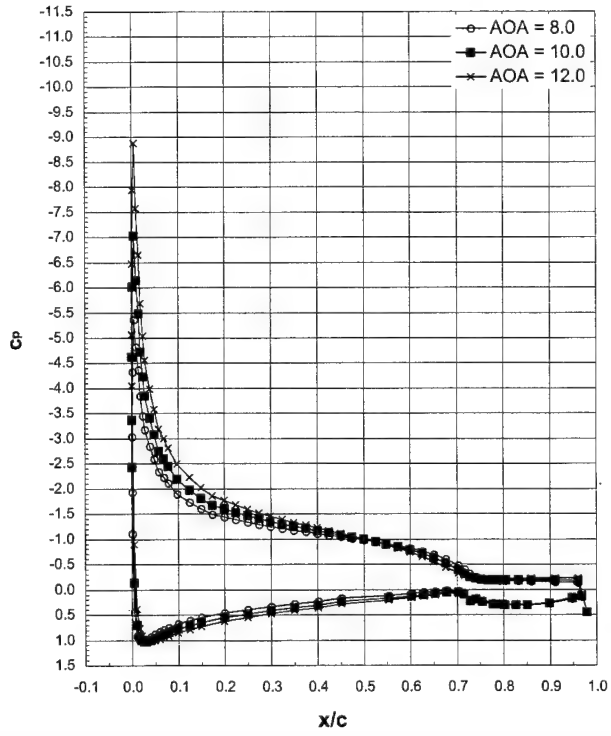

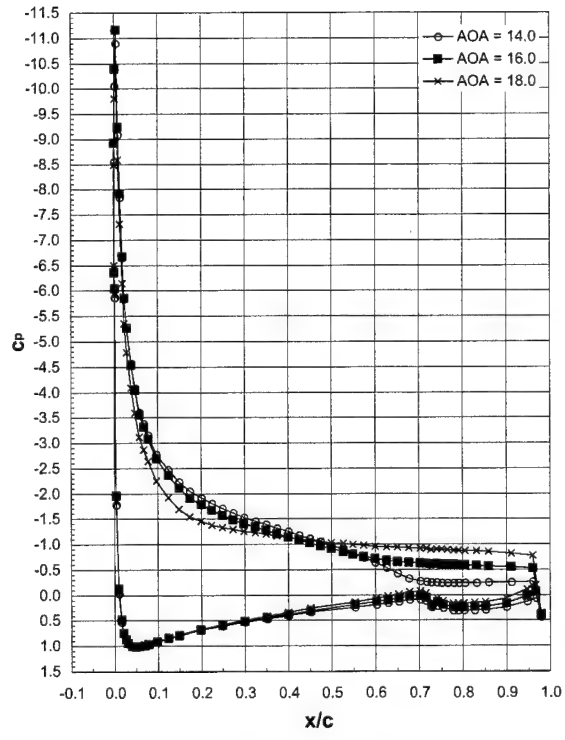

Run 30, Ma = 0.21, Re = 10x10^6

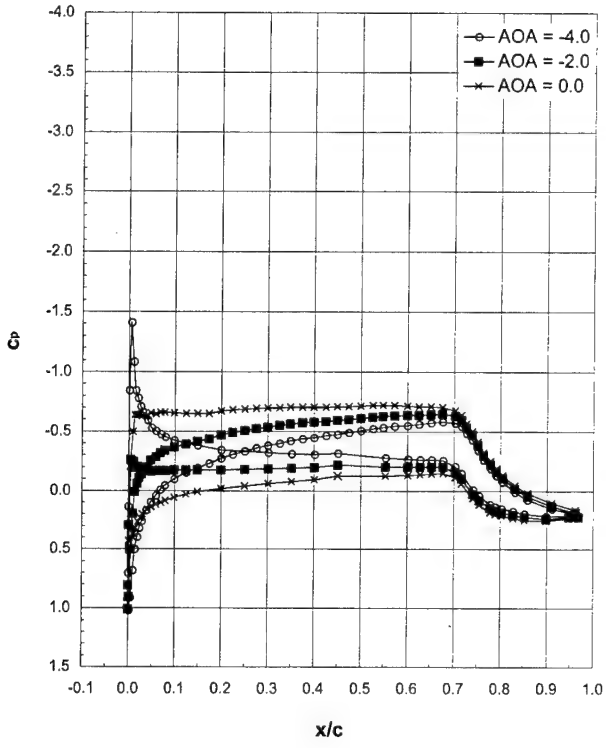

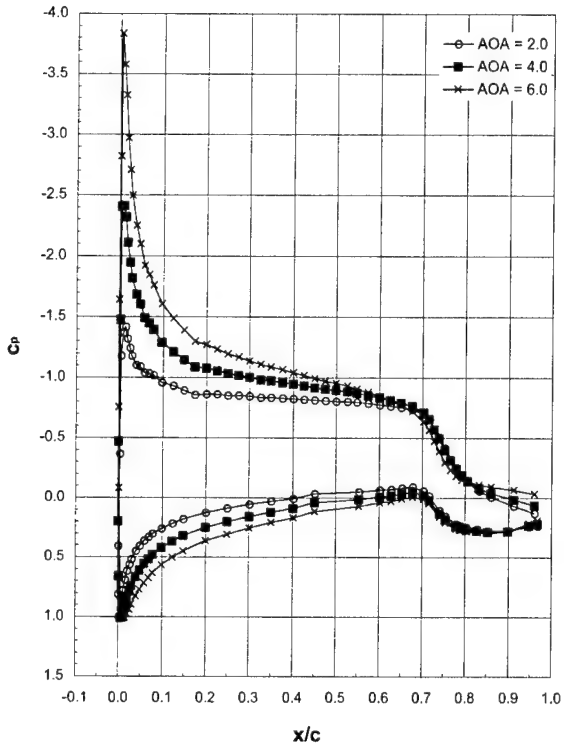

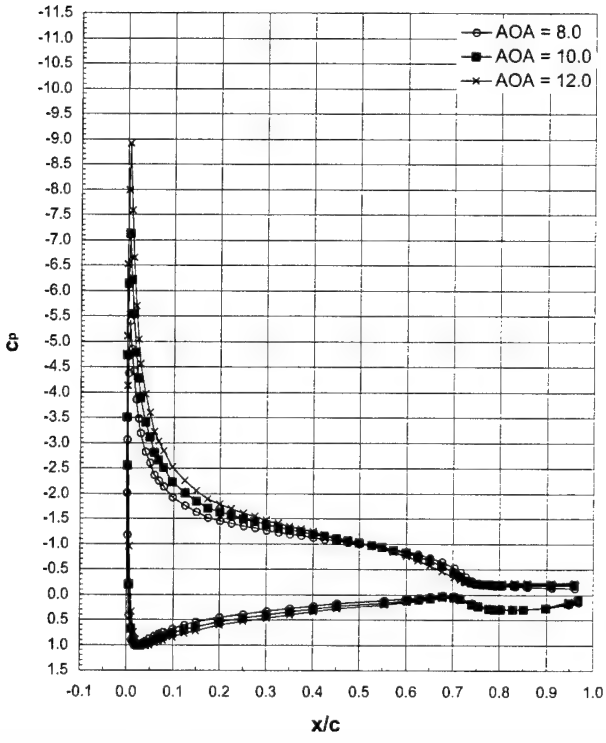

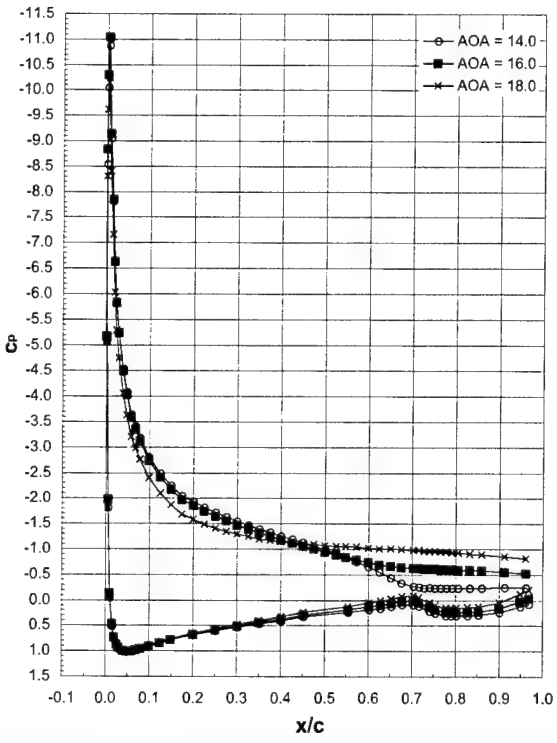

Run 32, Ma = 0.21, Re = 12x10^6

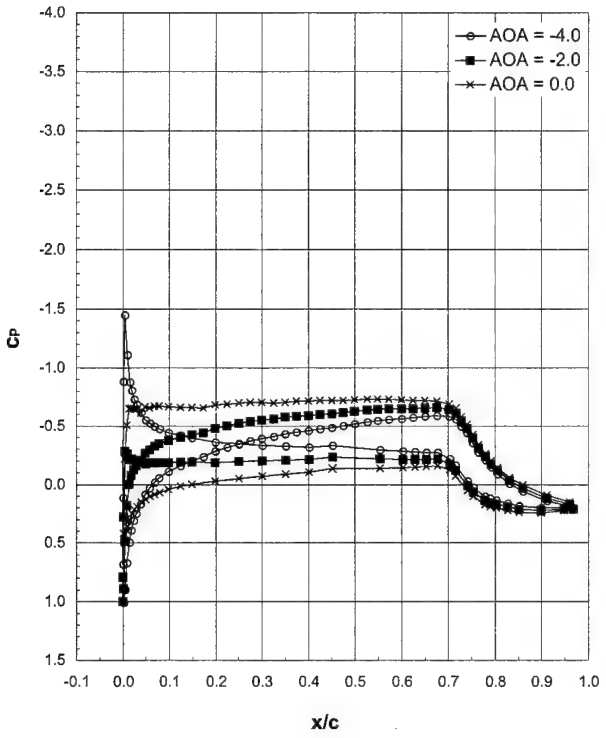

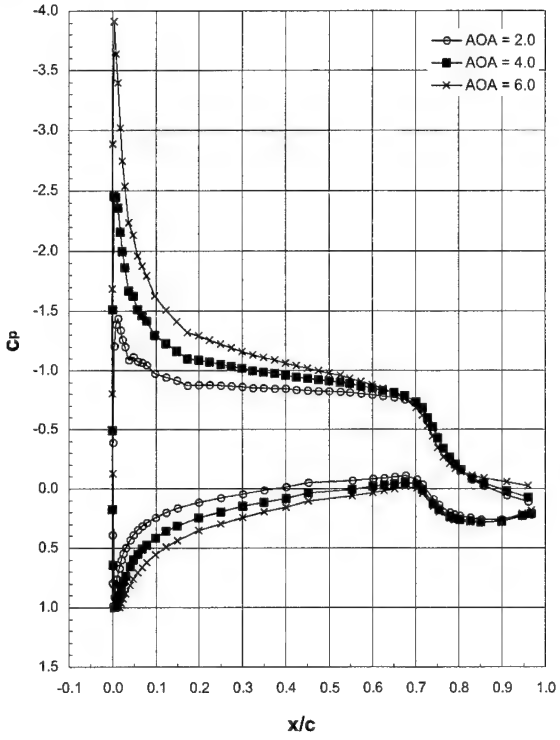

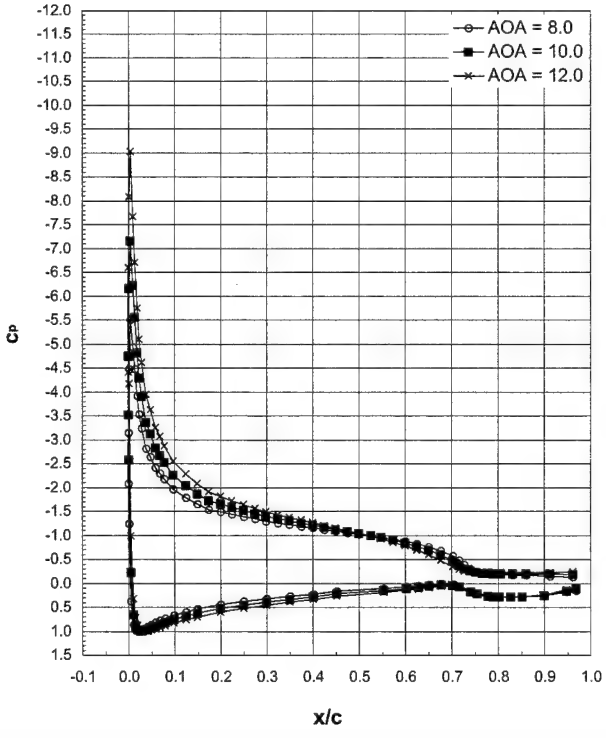

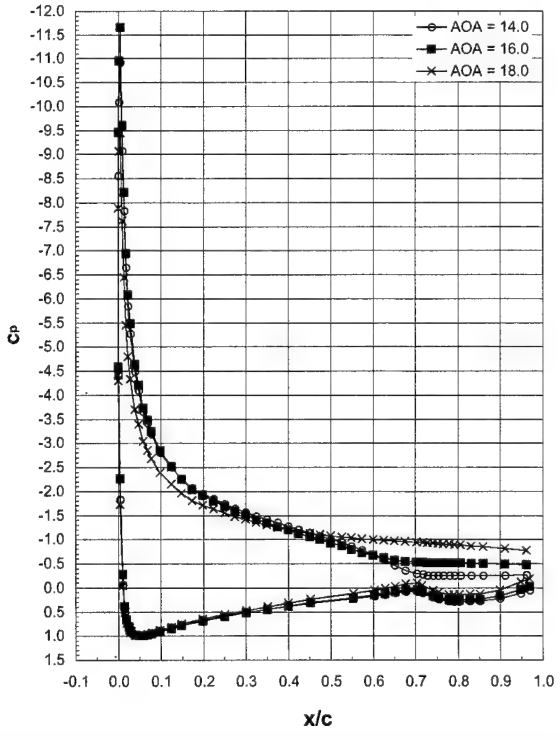

Run 35, Ma = 0.05, Re = 1x10^6

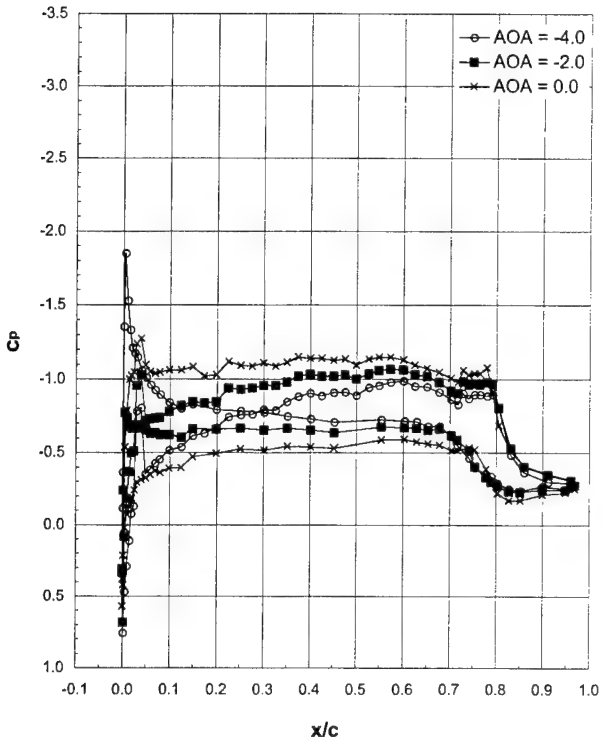

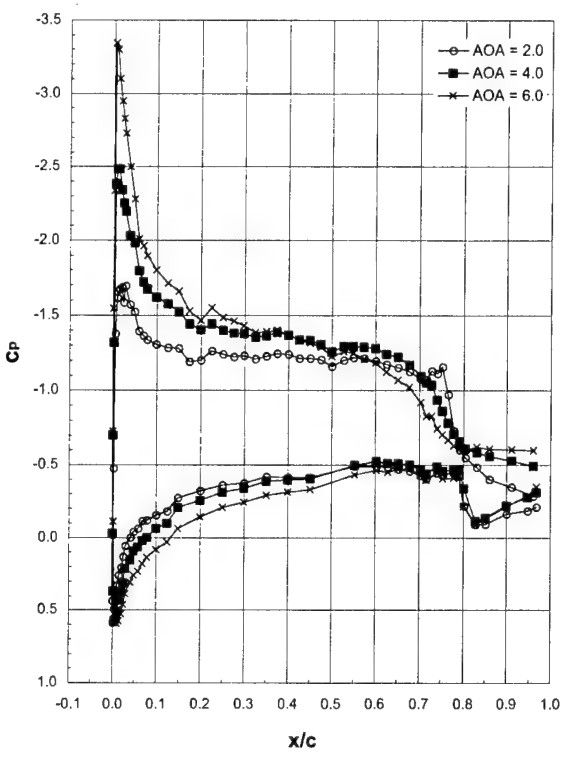

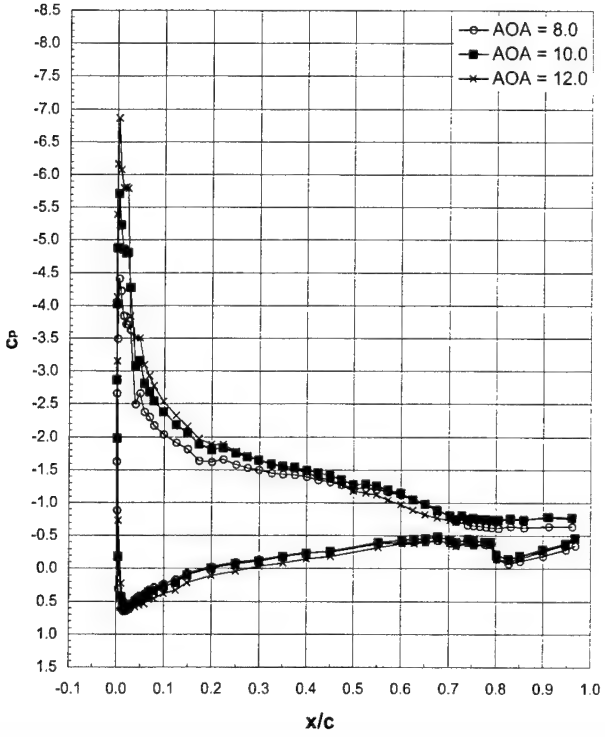

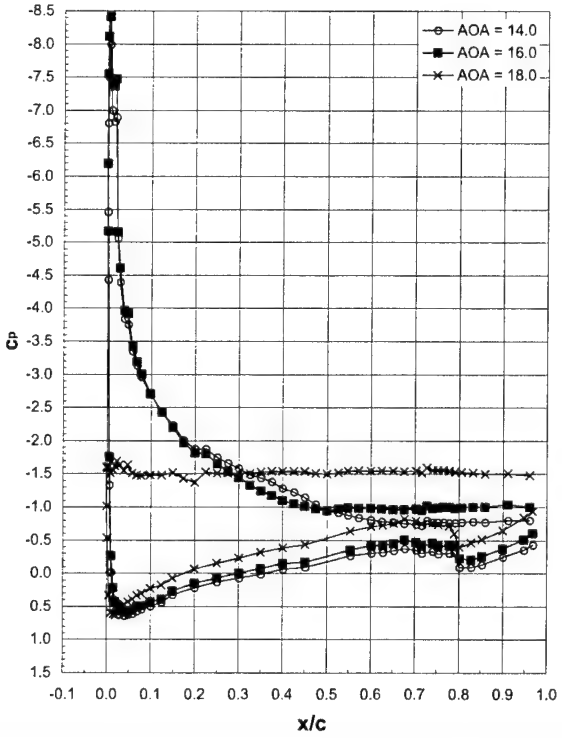

Run 701, Ma = 0.12, Re = 10x10^6

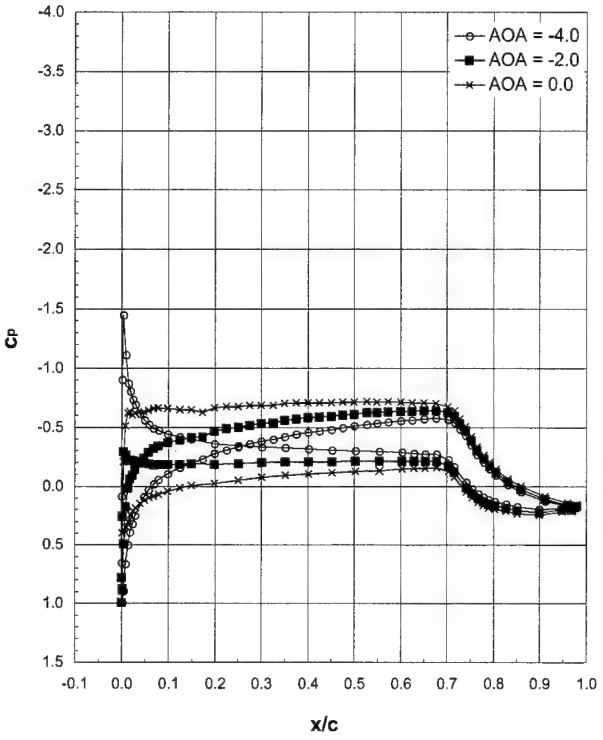

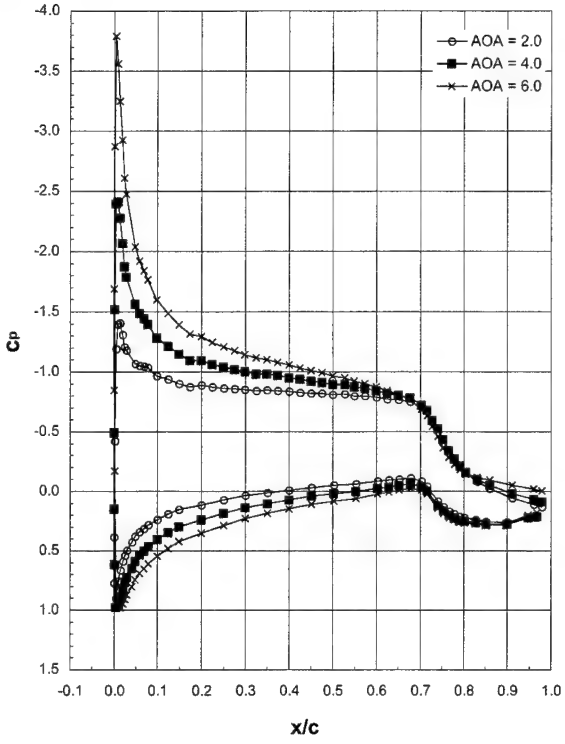

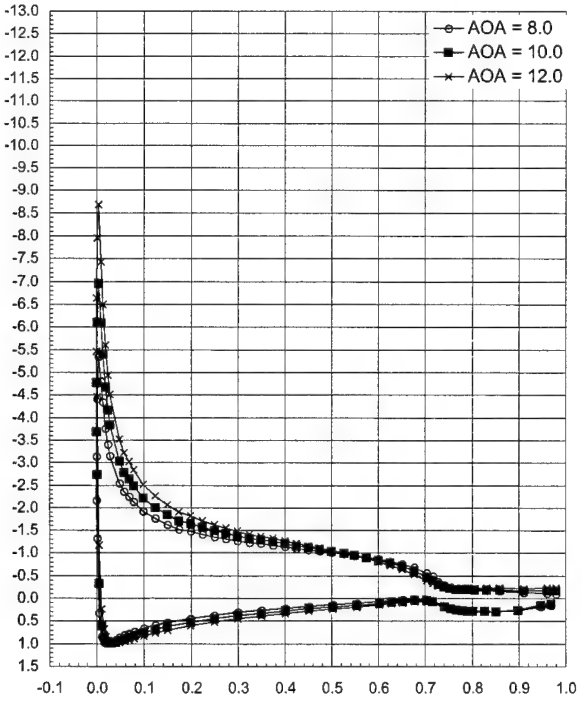

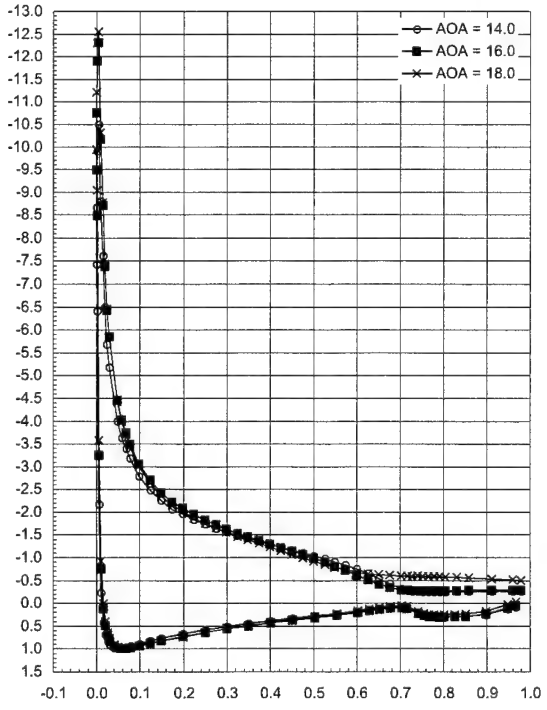

Run 702, Ma = 0.21, Re = 4.6x10^6

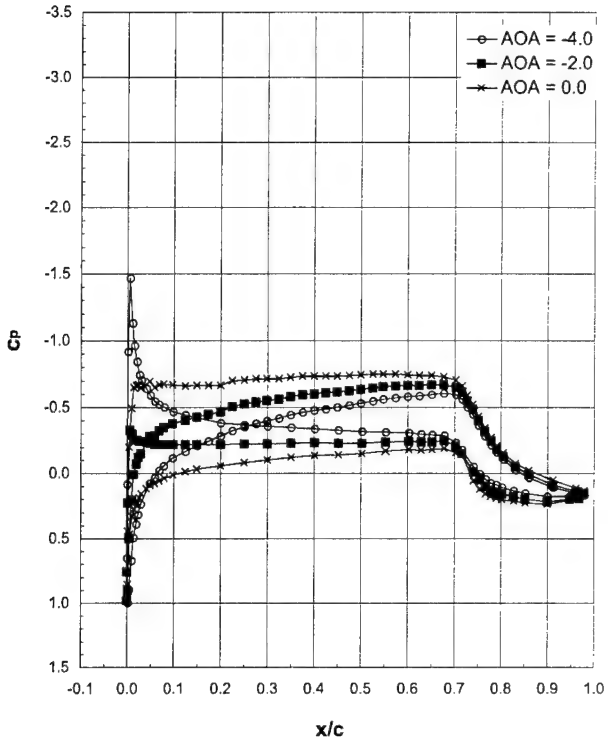

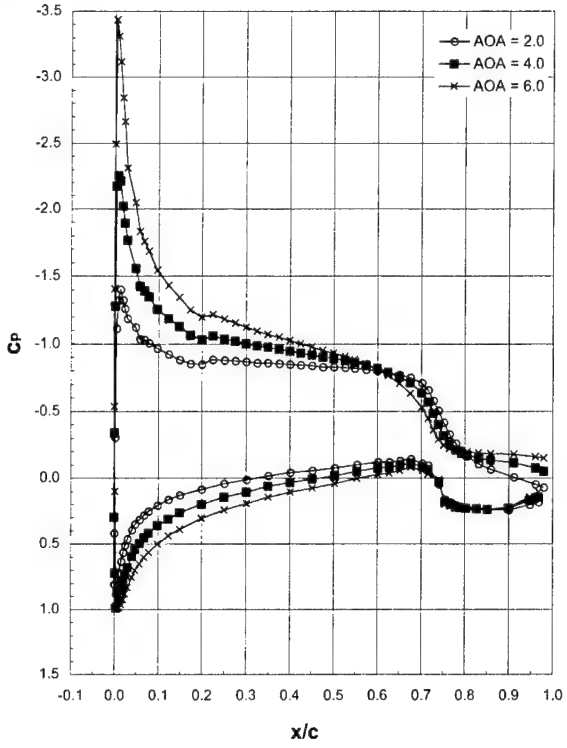

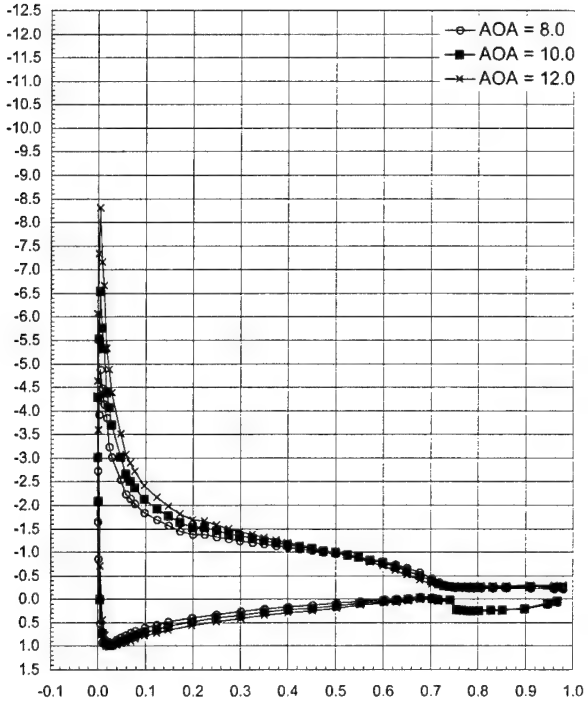

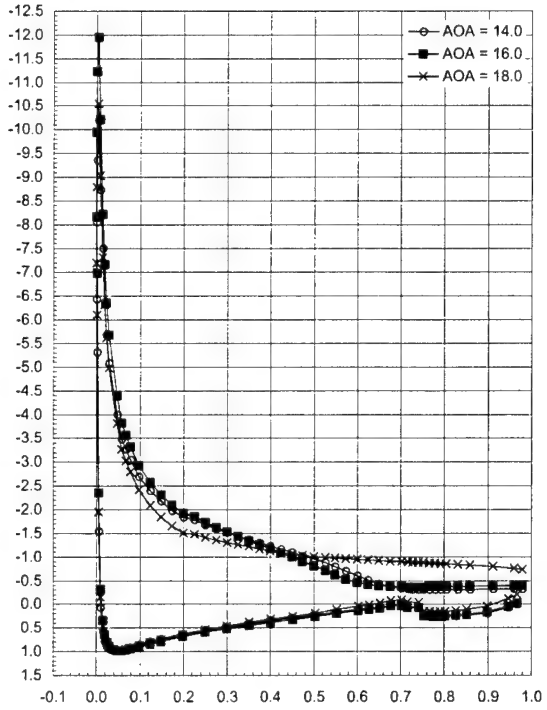

Run 703, Ma = 0.21, Re = 10x10^6

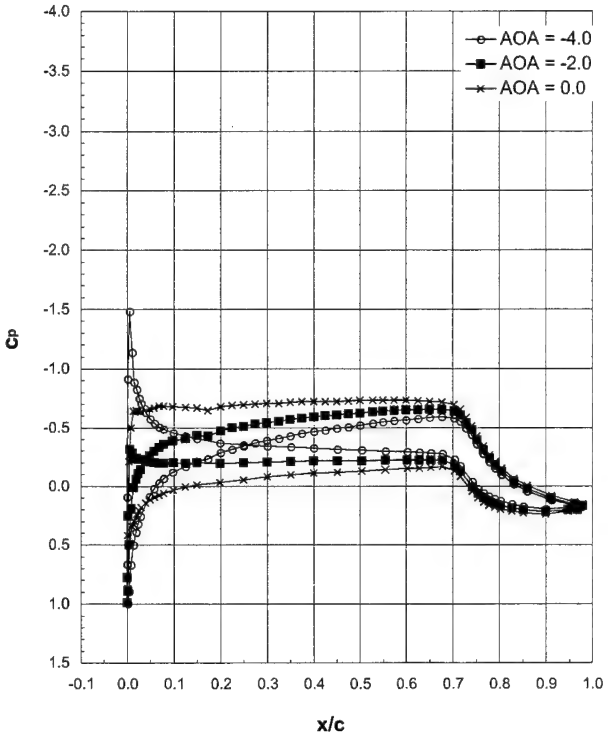

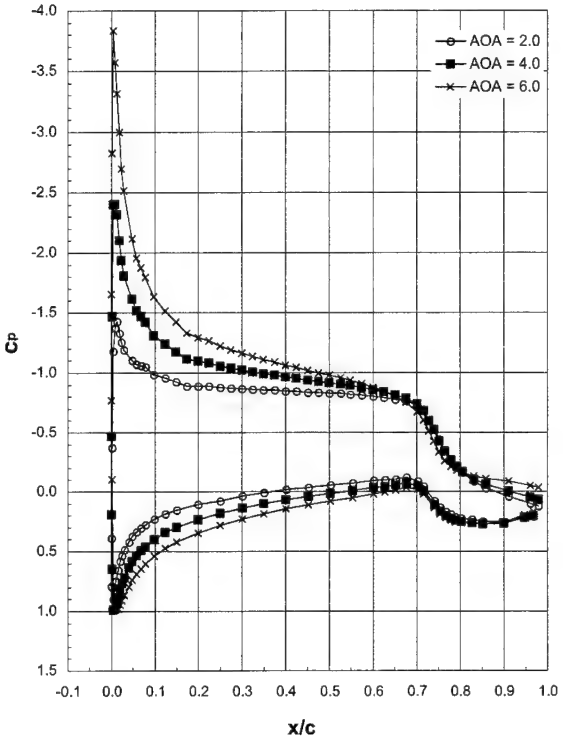

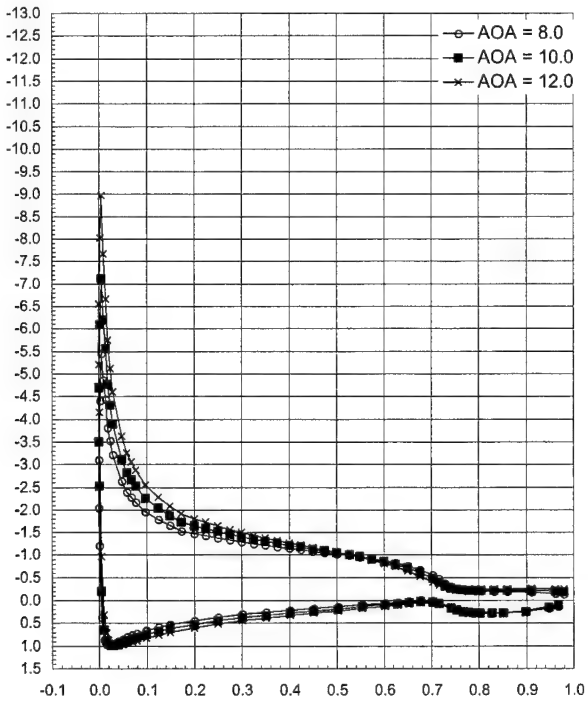

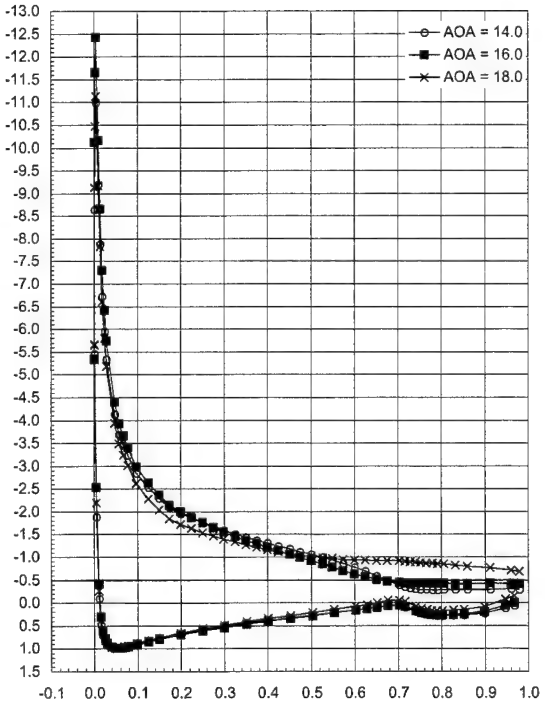

Run 704, Ma = 0.29, Re = 6.4x10^6

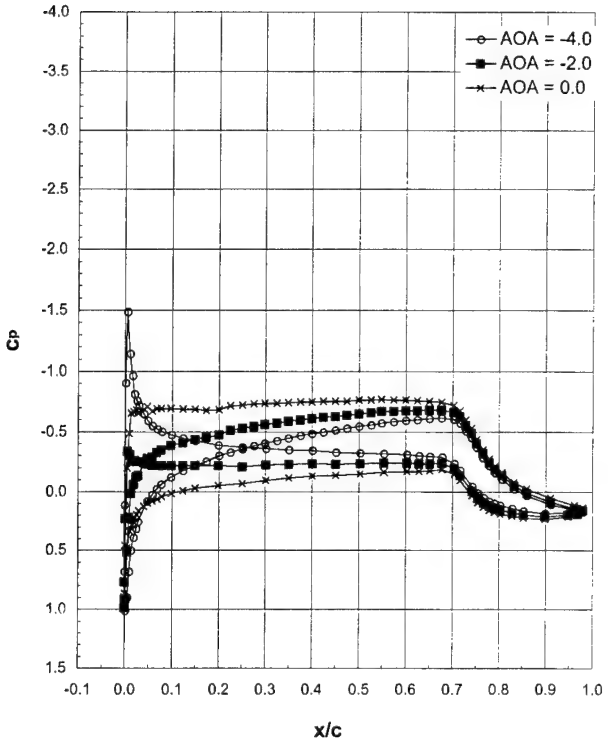

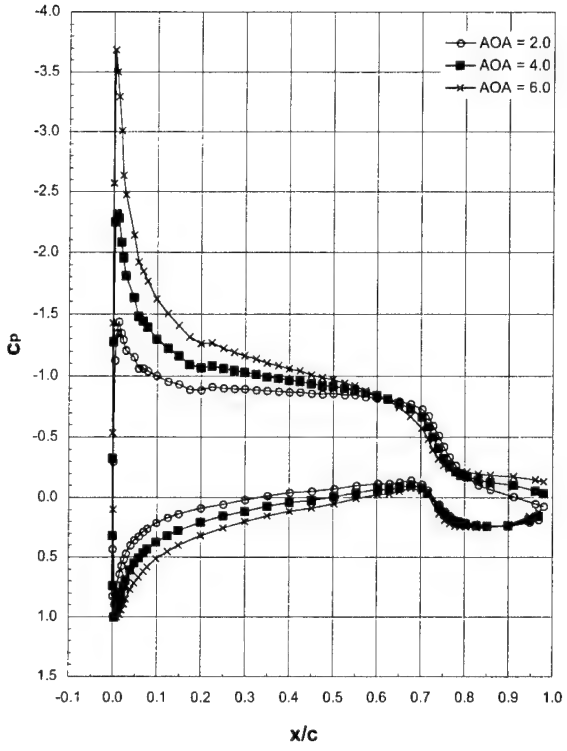

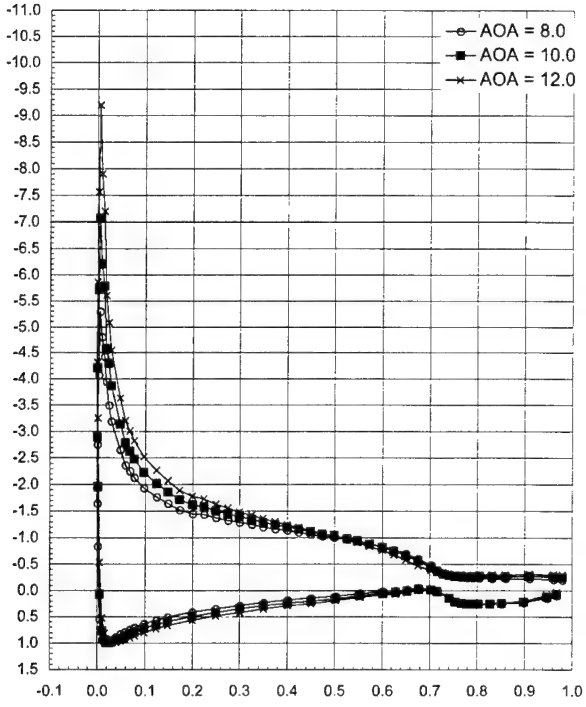

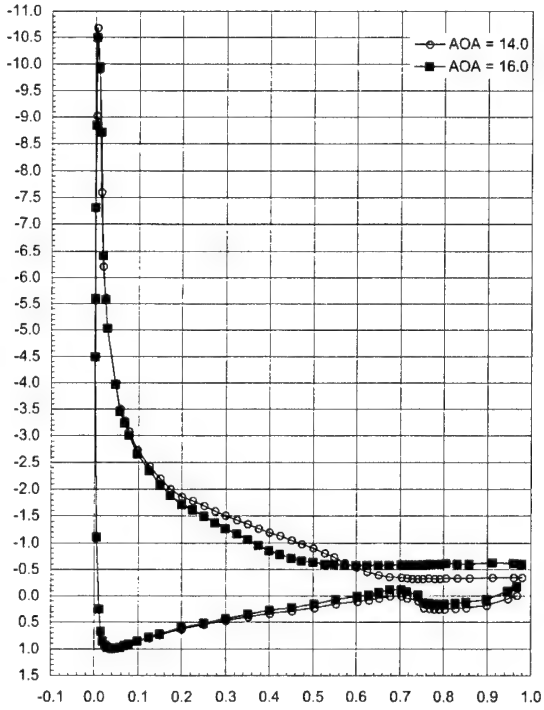

Run 705, Ma = 0.12, Re = 3x10^6

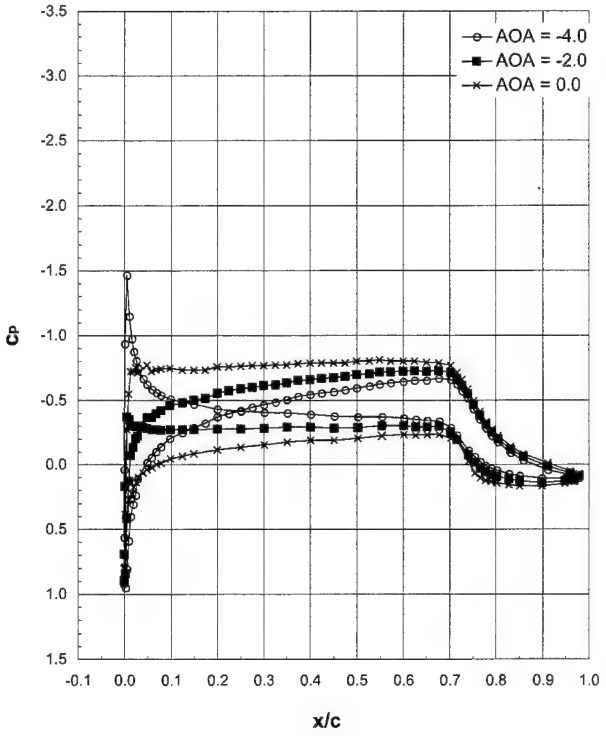

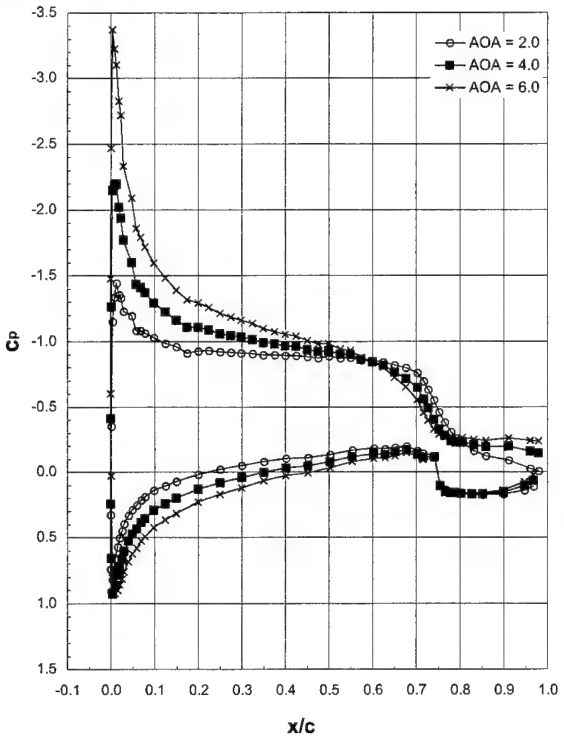

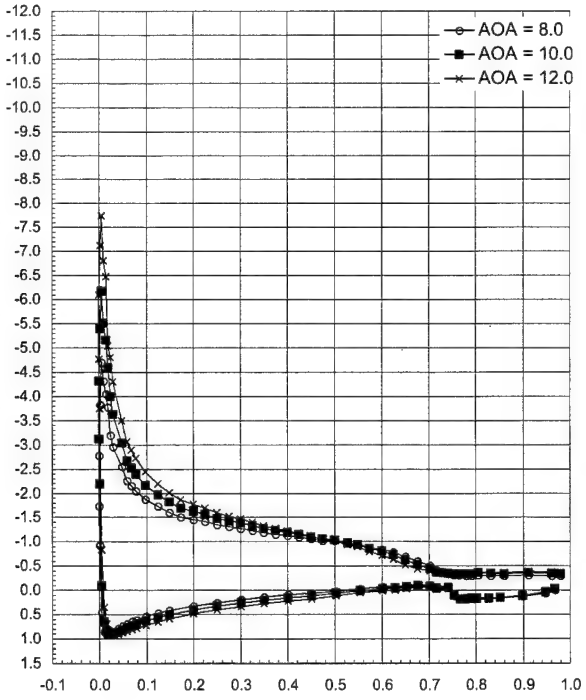

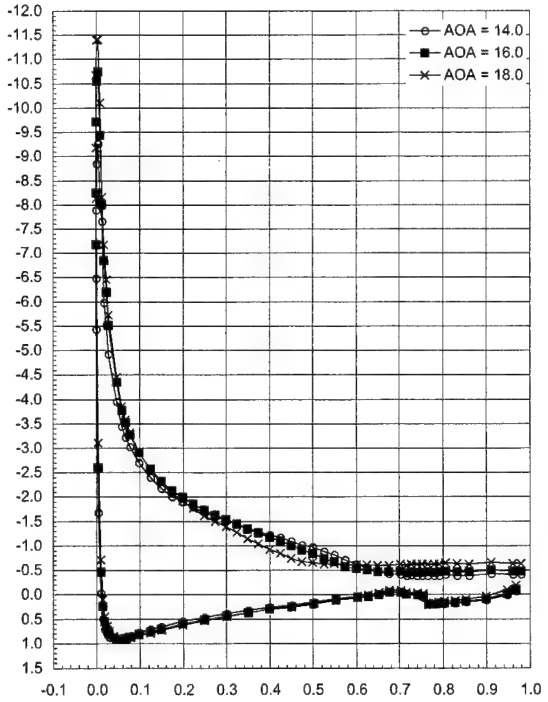

LTPT
General Aviation - Ice Shape 623-2D (SLA)

Ice Shape formed at:

T_t = -2.8°C (26.4°F)	LWC = 0.54 g/m^3
T_s = -5.0°C (22.0°F)	MVD = 20 µm
V = 66.9 m/s (130 kts)	Spray = 22.5 min
AOA = 0.3^O	chord = 90 cm (36 in)

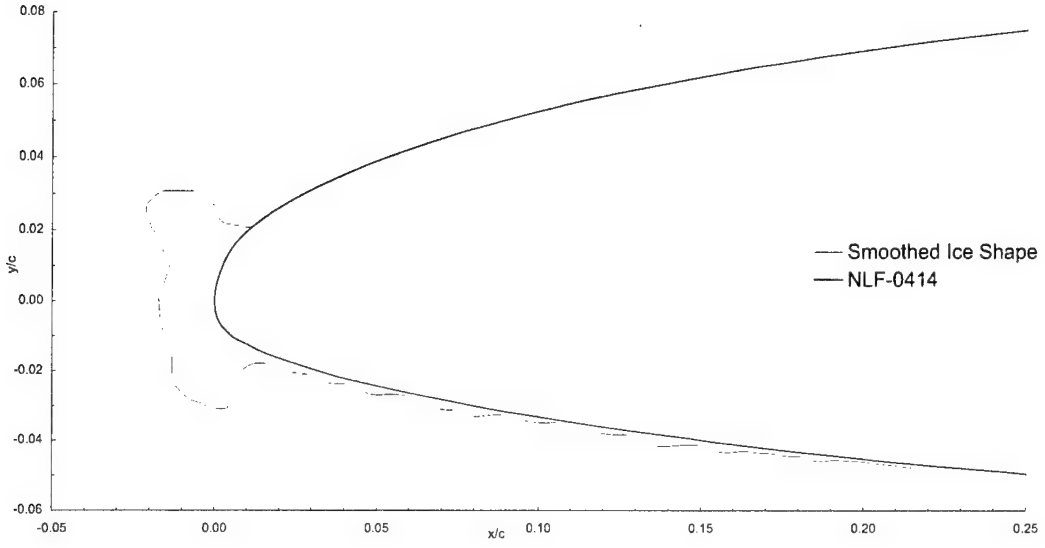

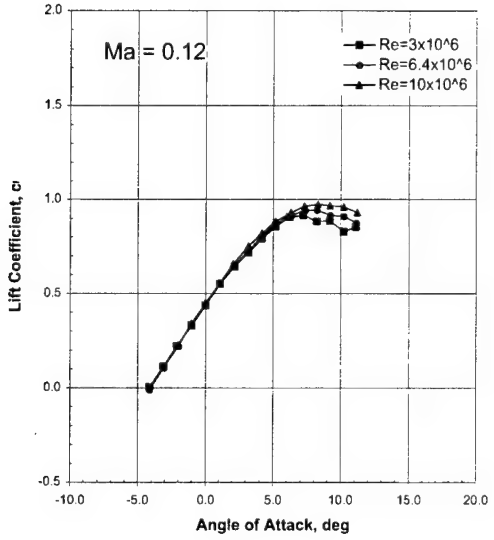

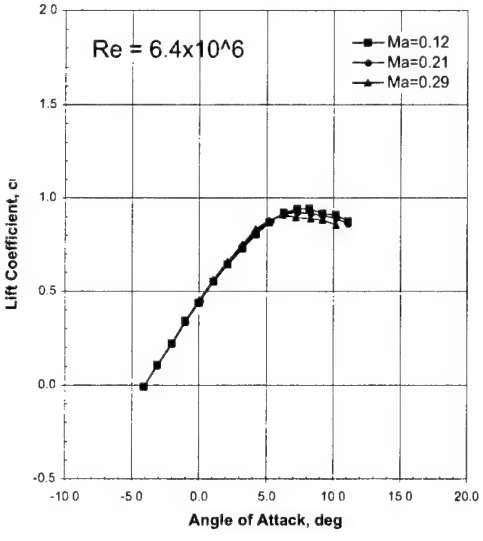

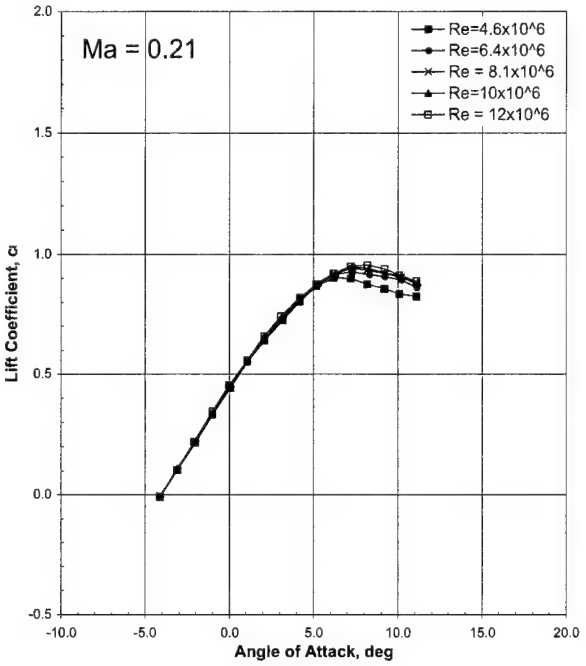

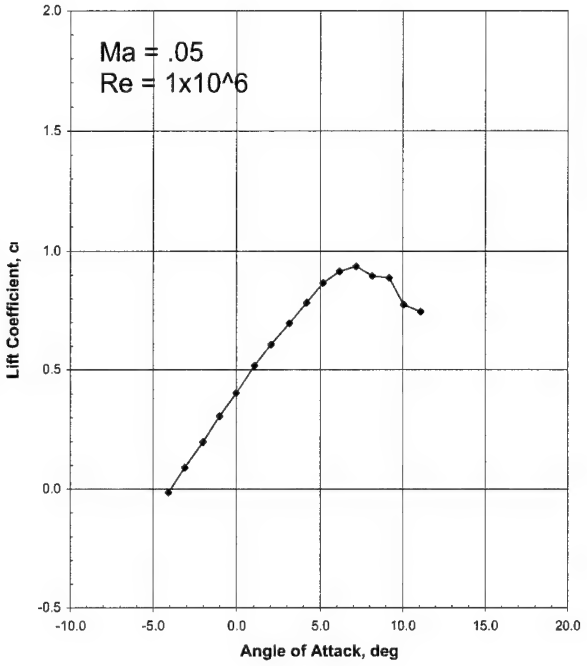

Drag Coefficients, c_d

	α = -2.0	α = 0.0	α = 2.1	α = 4.2	α = 6.2
Run 101, Ma = 0.12, Re = 10x10^6	0.0235	0.0181	0.0234	0.0395	0.0589
Run 102, Ma = 0.21, Re = 10x10^6	*0.0096*	*0.0096*	*0.0249*	*0.0528*	*0.0931*
Run 103, Ma = 0.21, Re = 4.6x10^6	*0.0203*	*0.0215*	*0.0373*	*0.0657*	*0.1039*
Run 105, Ma = 0.21, Re = 12x10^6	*0.0064*	*0.0055*	*0.0204*	*0.0499*	*0.0885*
Run 106, Ma = 0.12, Re = 6.4x10^6	*0.0137*	*0.0137*	*0.0292*	*0.0576*	*0.0969*
Run 107, Ma = 0.21, Re = 8.1x10^6	*0.0127*	*0.0095*	*0.0246*	*0.0543*	*0.0950*
Run 108, Ma = 0.21, Re = 6.4x10^6	*0.0166*	*0.0139*	*0.0289*	*0.0588*	*0.0997*
Run 109, Ma = 0.12, Re = 3x10^6	0.0134	0.0057	0.0168	0.0430	0.0820
Run 111, Ma = 0.29, Re = 6.4x10^6	*0.0292*	*0.0323*	*0.0439*	*0.0663*	*0.1016*
Run 112, Ma = 0.05, Re = 1x10^6	*0.0078*	*0.0069*	*0.0062*	*0.0058*	*0.0058*

Italicized font indicates force balance data

LTPT
General Aviation - Ice Shape 623-2D (SLA) (cont.)

Run 101, Ma = 0.12, Re = 10x10^6

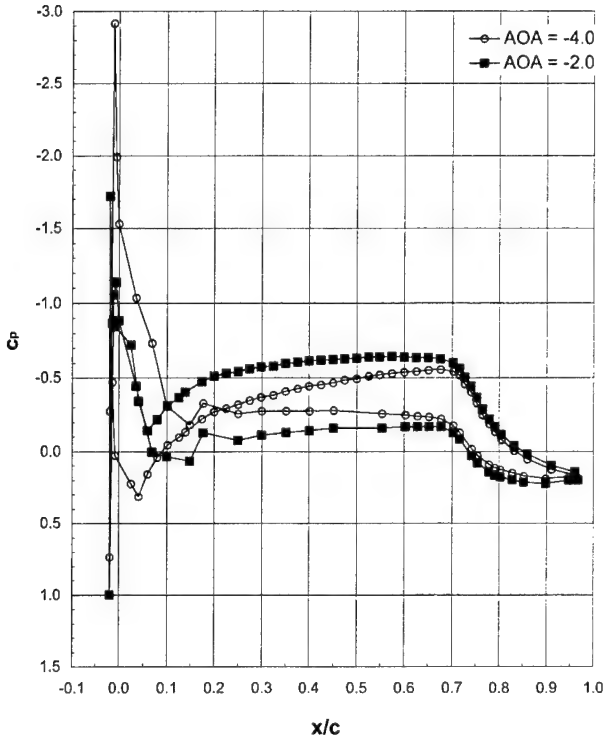

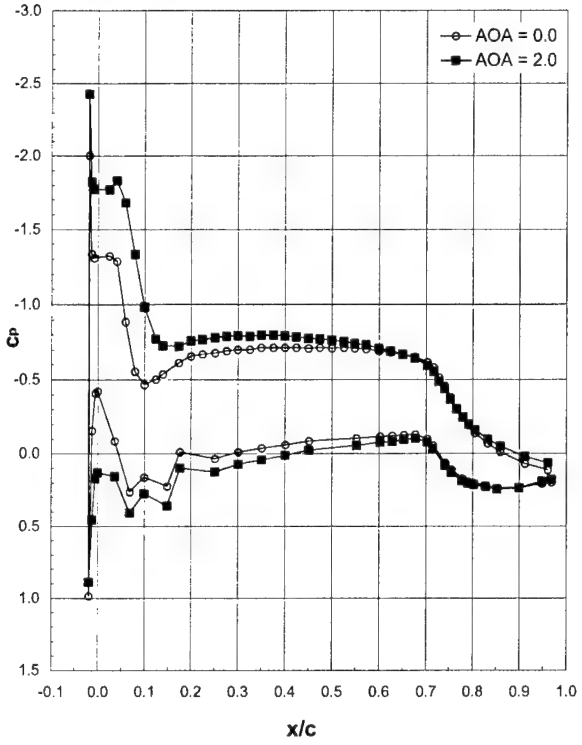

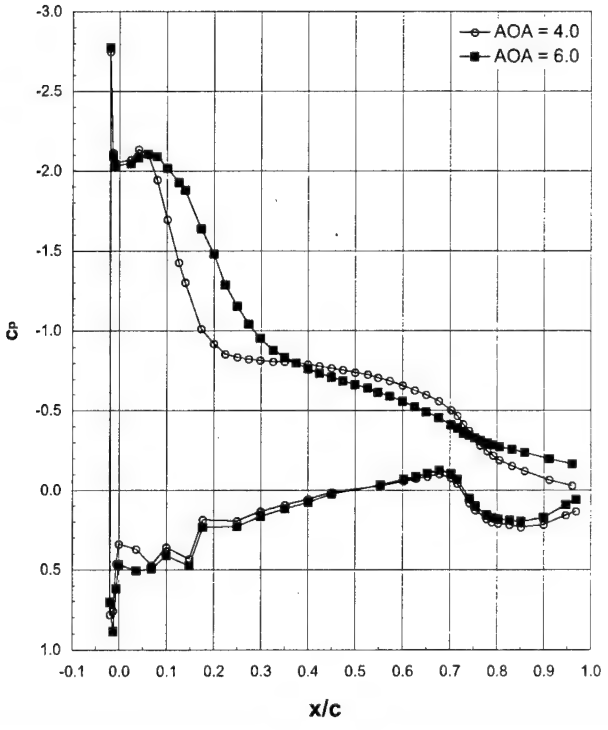

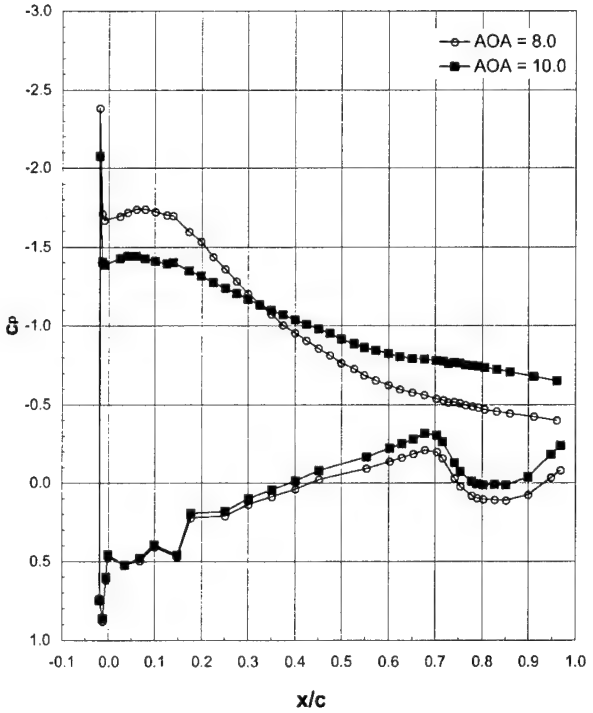

Run 102, Ma = 0.21, Re = 10x10^6

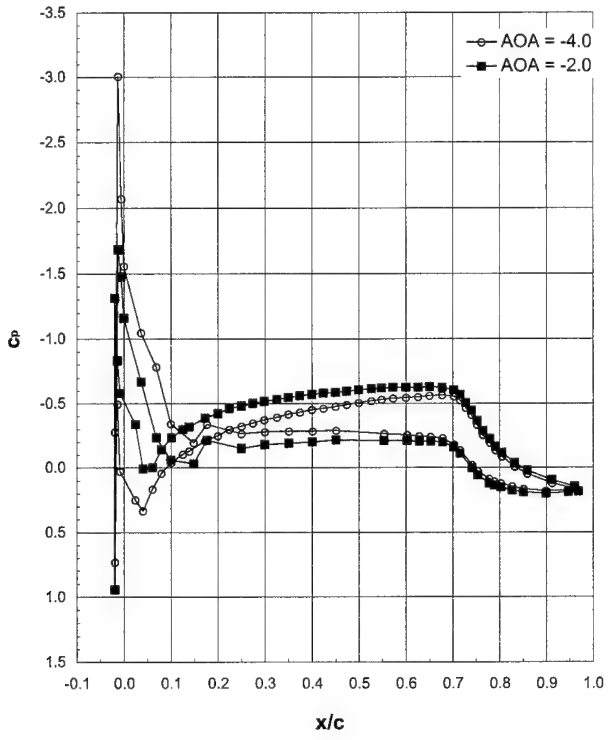

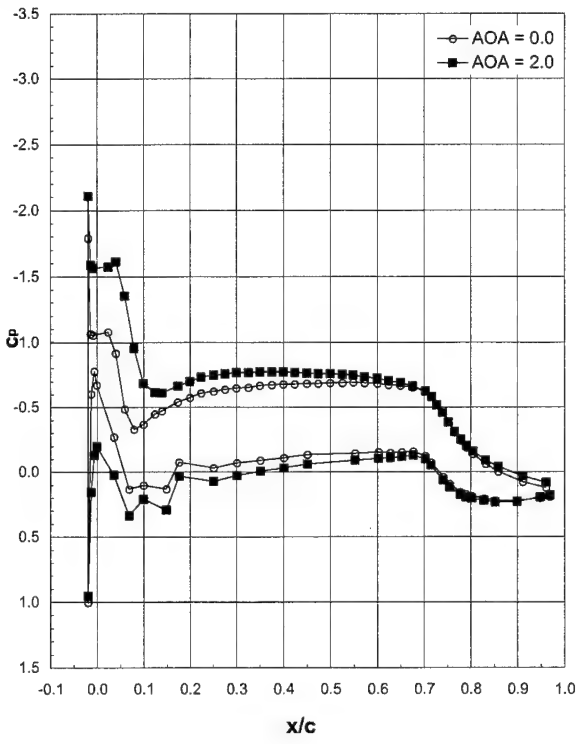

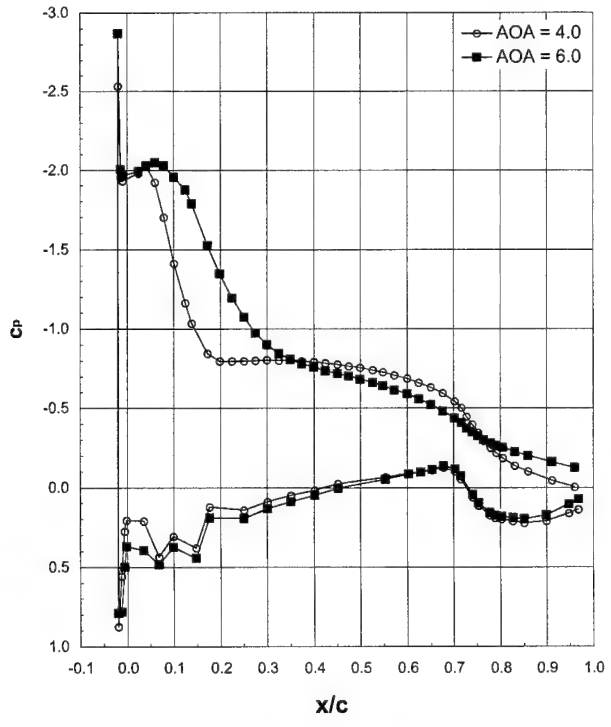

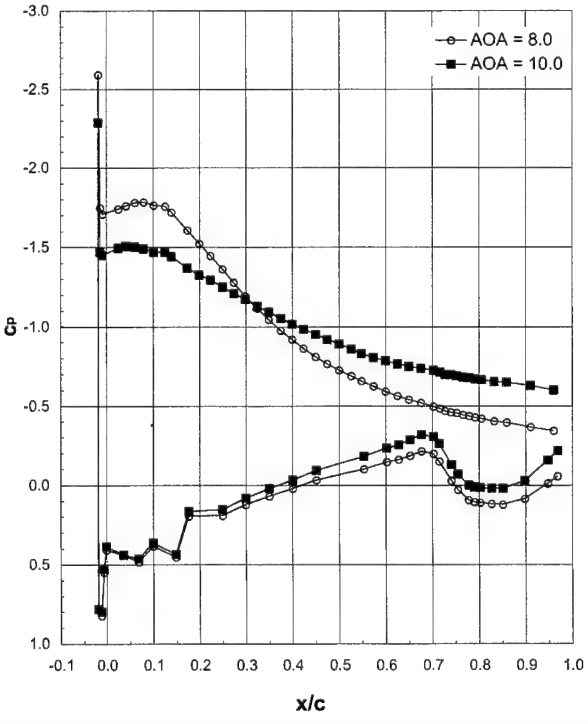

Run 103, Ma = 0.21, Re = 4.6x10^6

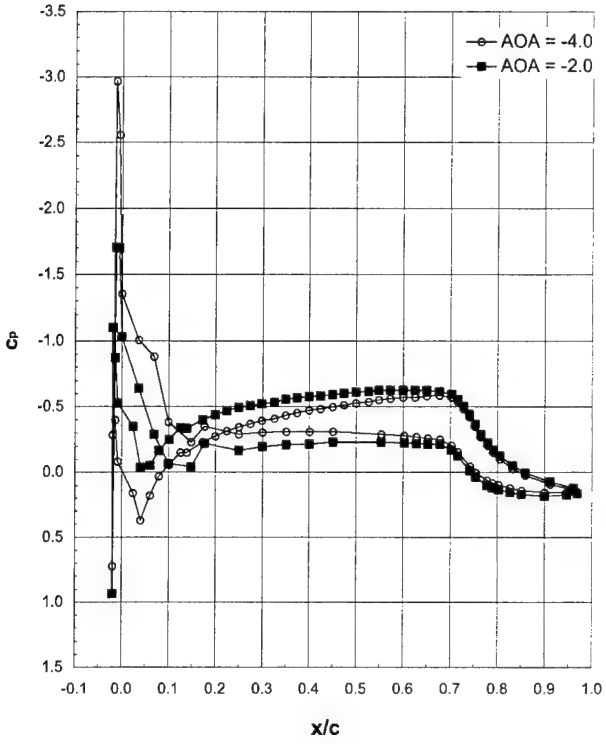

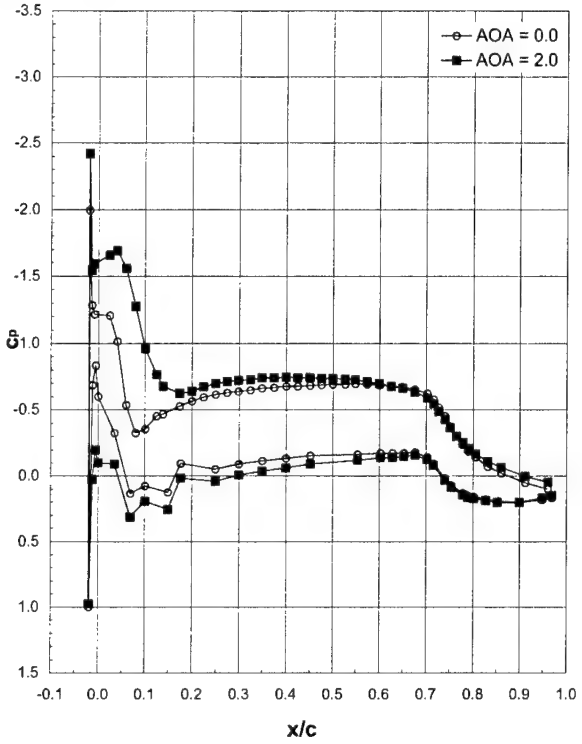

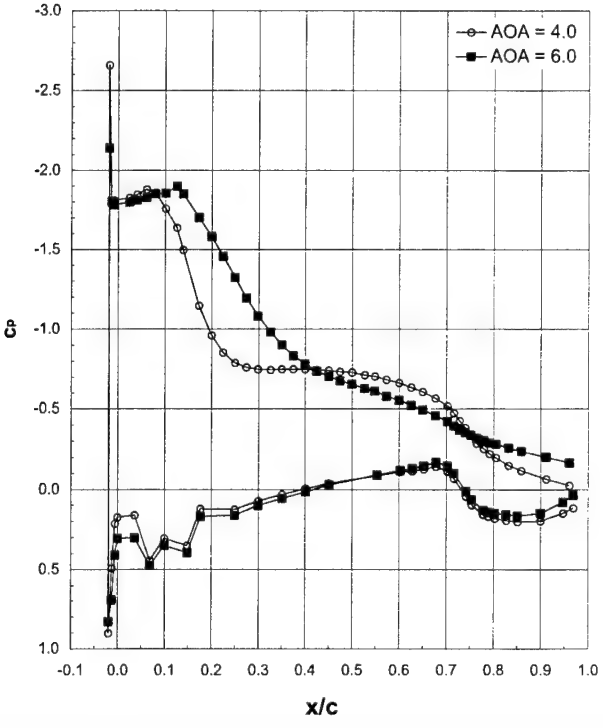

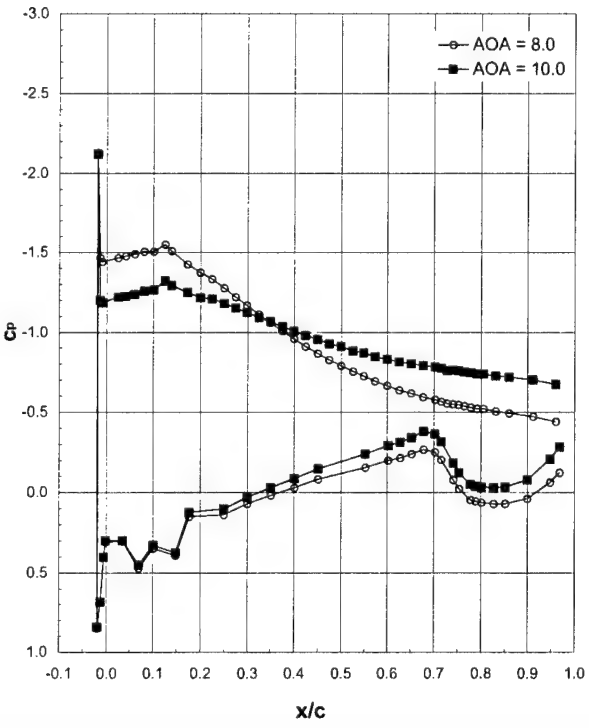

Run 105, Ma = 0.21, Re = 12x10^6

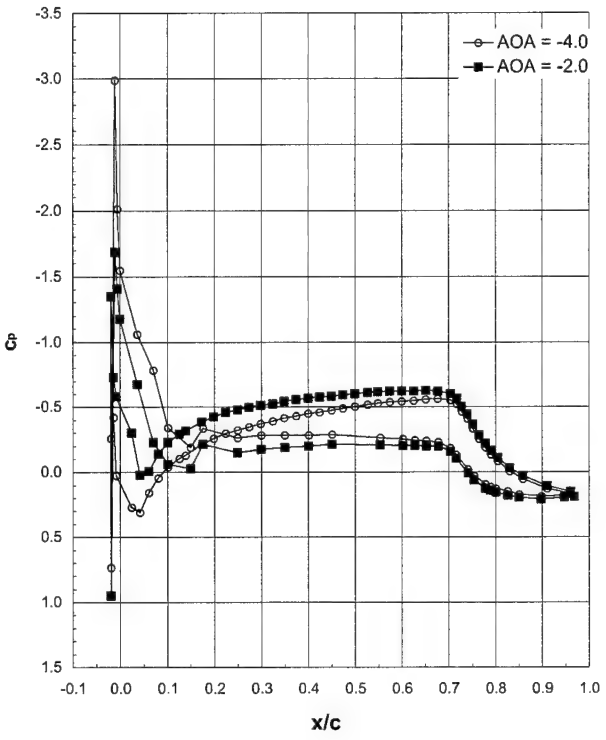

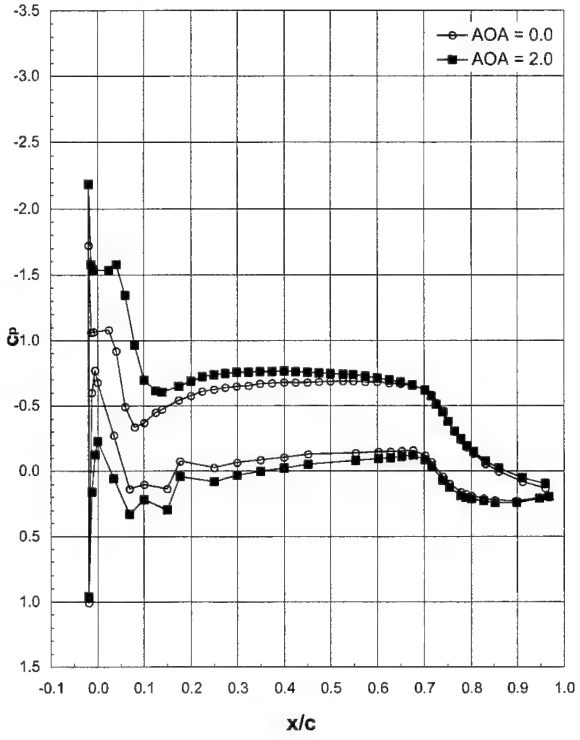

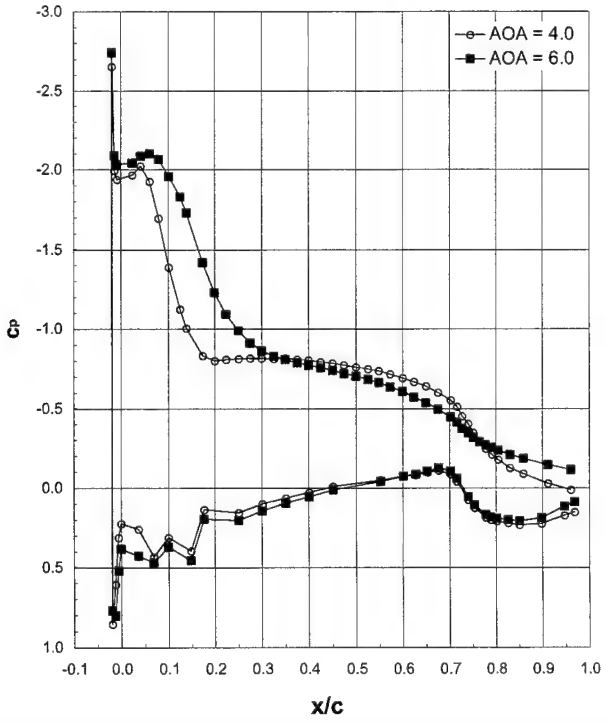

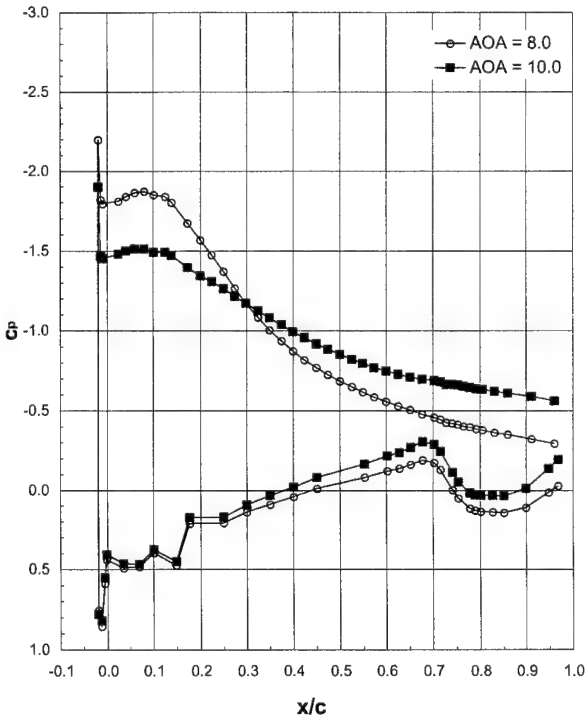

Run 106, Ma = 0.12, Re = 6.4x10^6

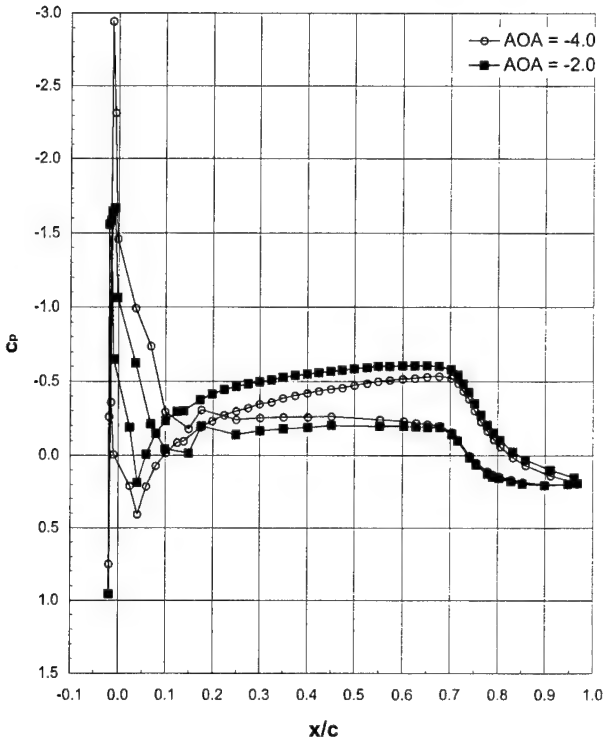

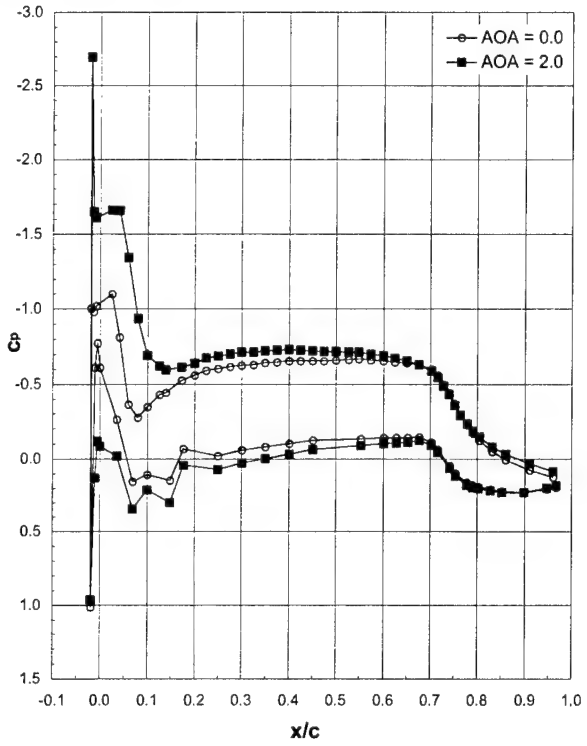

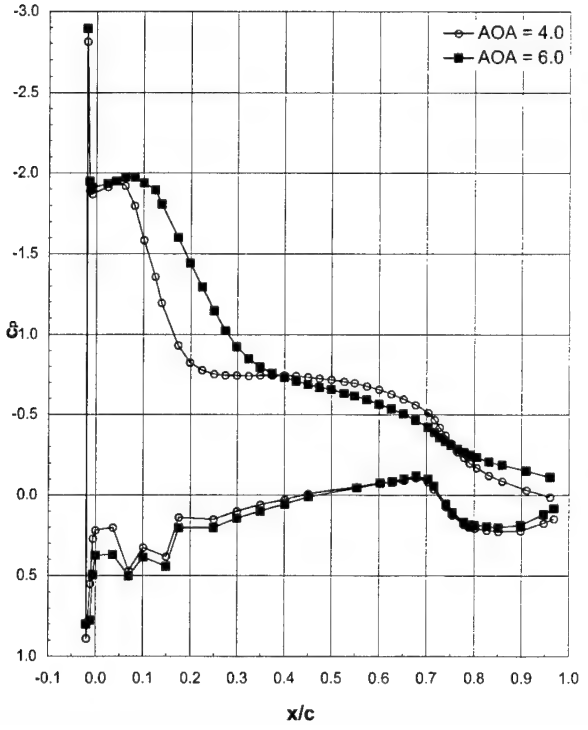

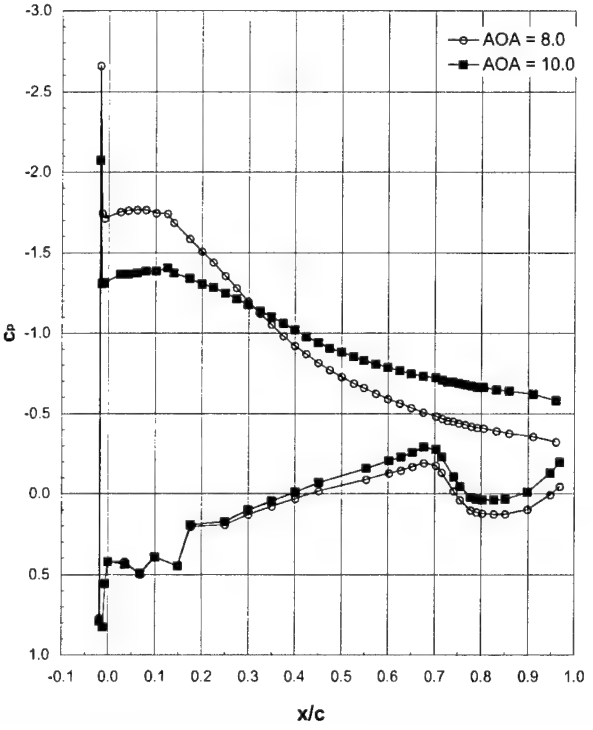

Run 107, Ma = 0.21, Re = 8.1x10^6

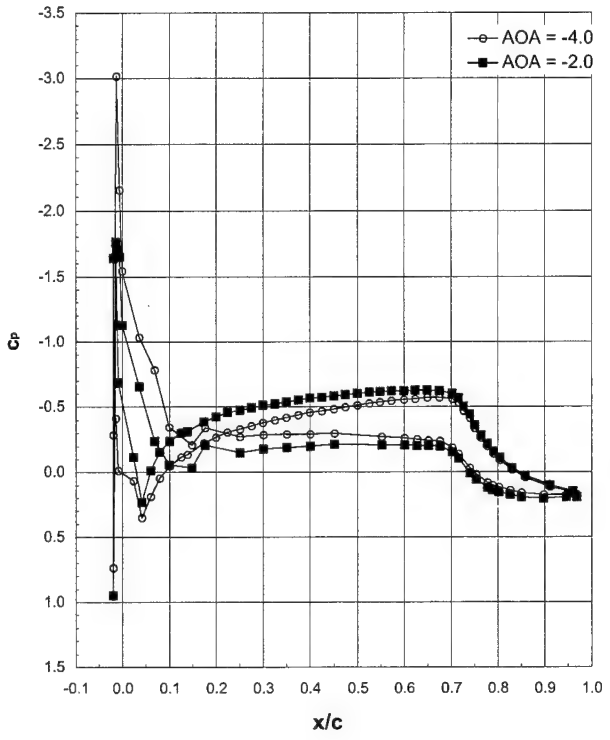

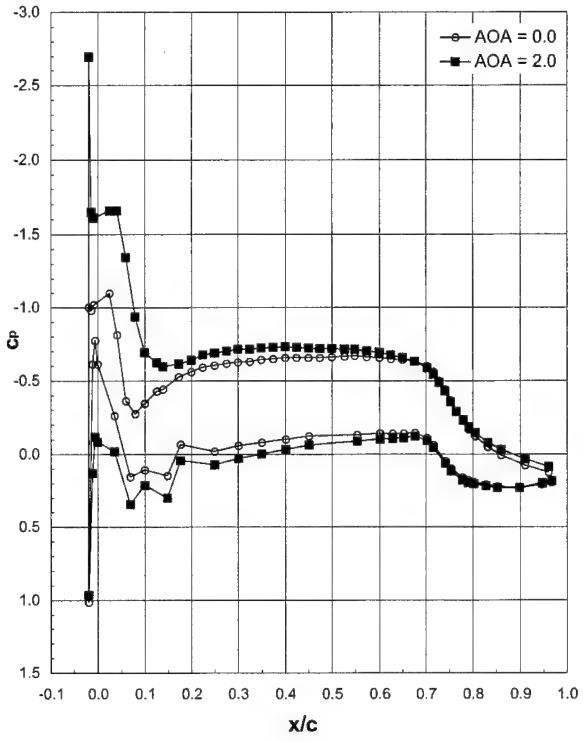

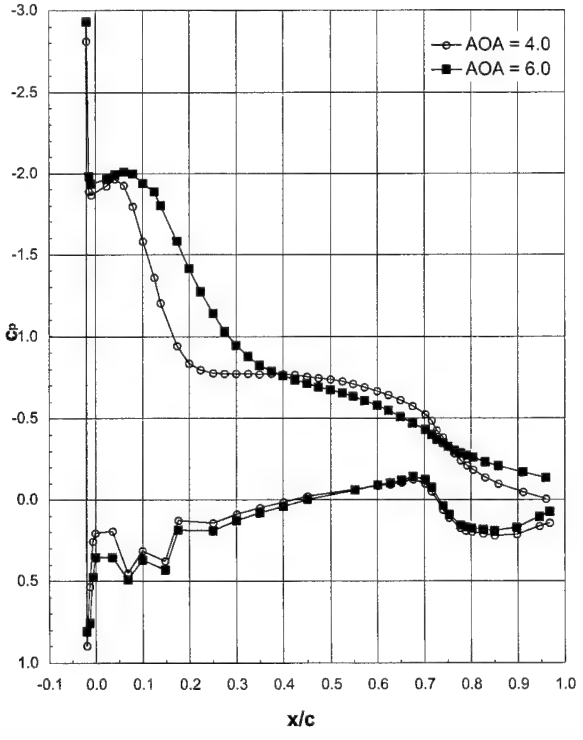

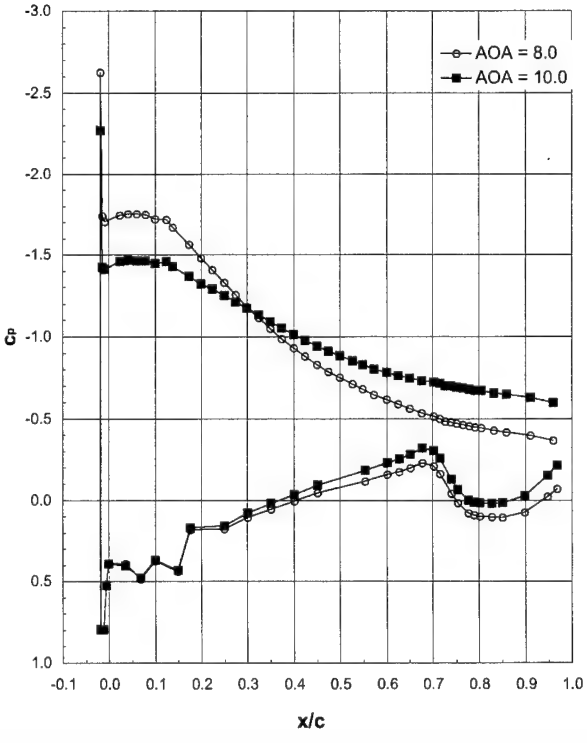

Run 108, Ma = 0.21, Re = 6.4x10^6

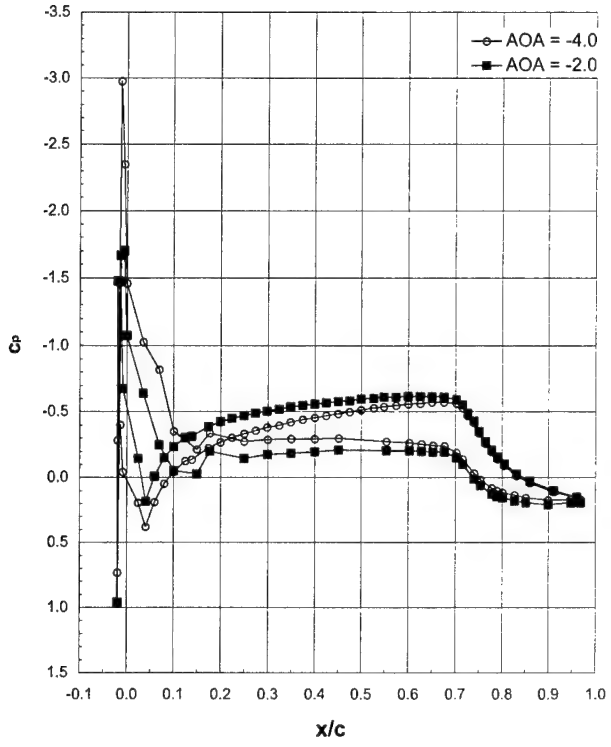

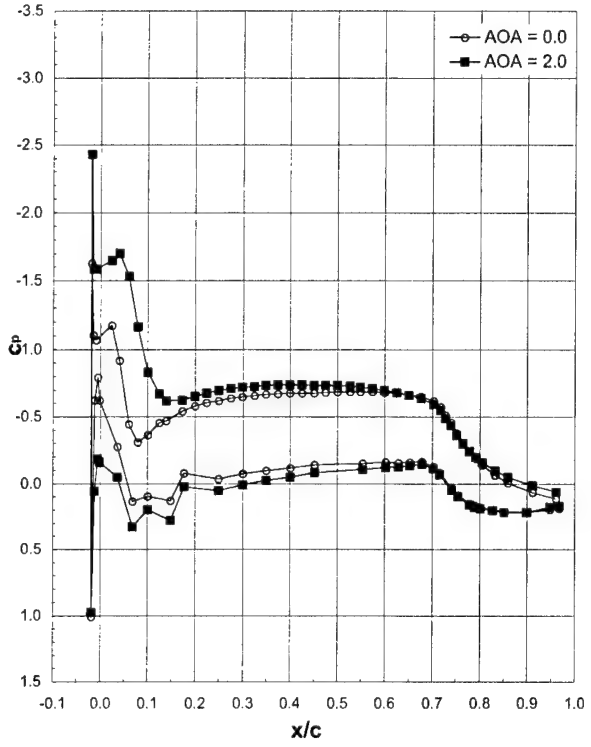

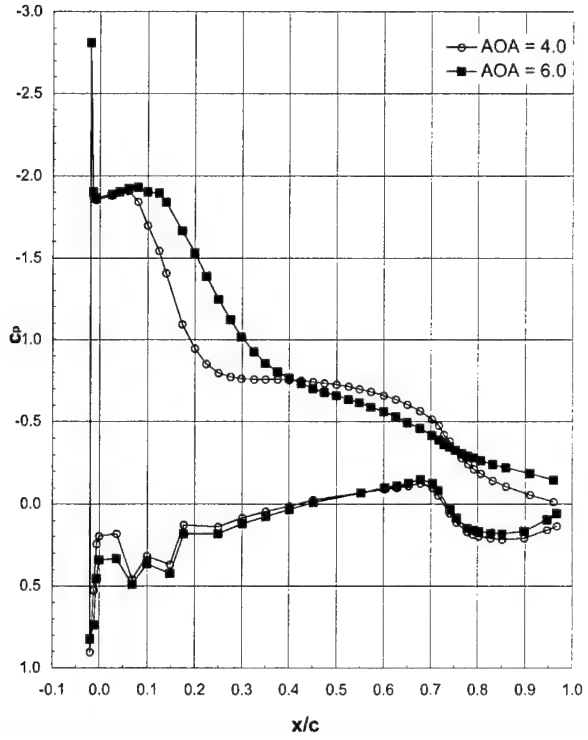

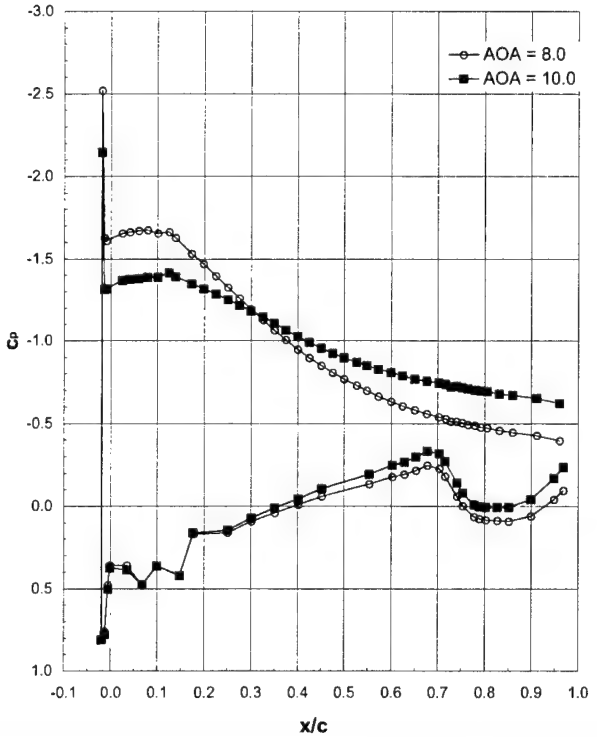

Run 109, Ma = 0.12, Re = 3x10^6

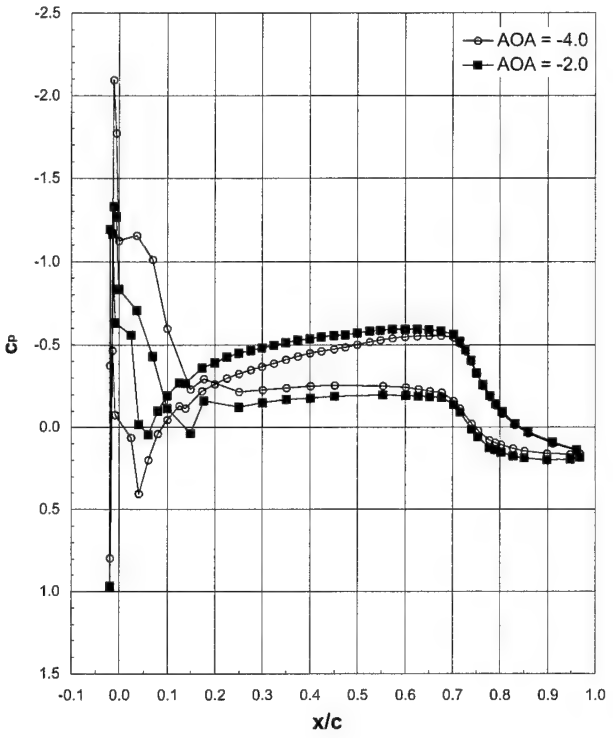

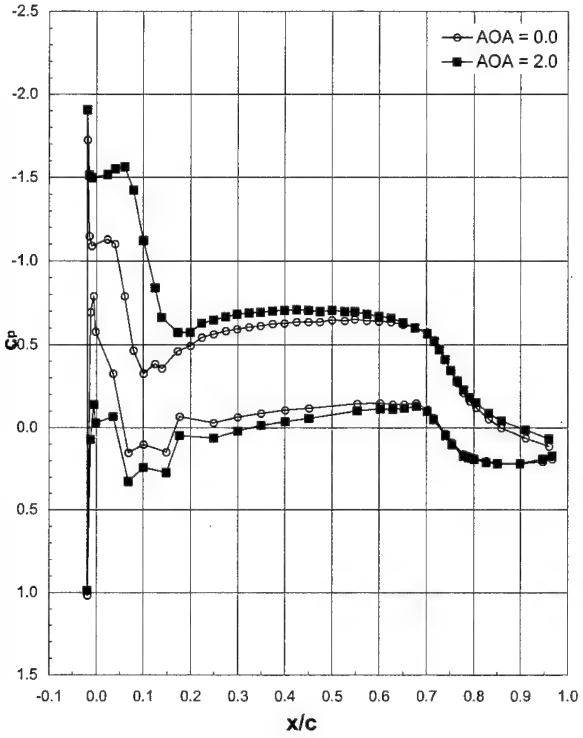

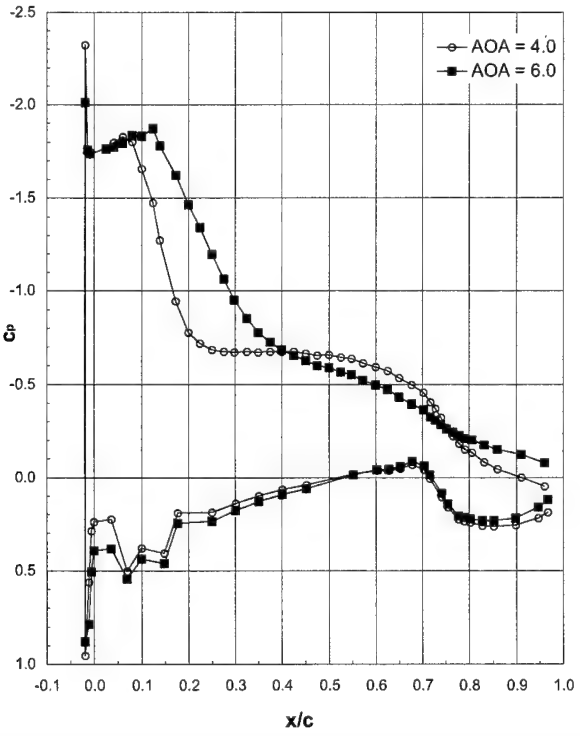

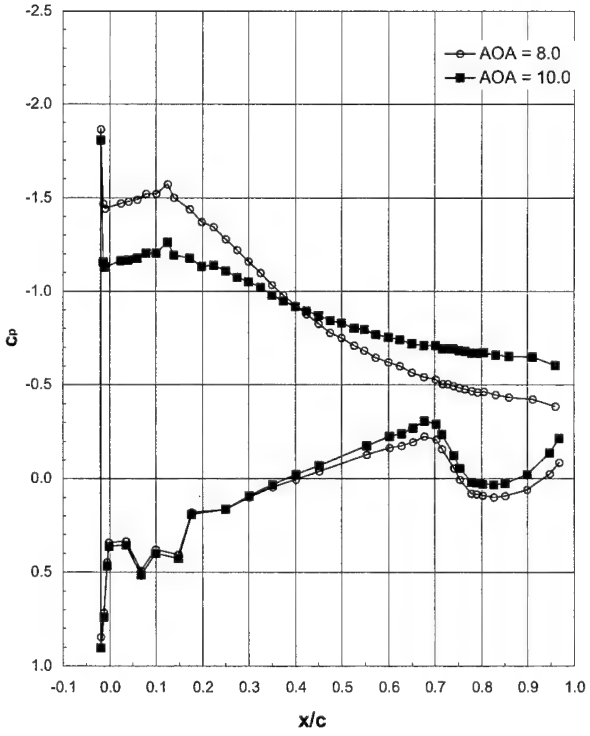

Run 111, Ma = 0.29, Re = 6.4x10^6

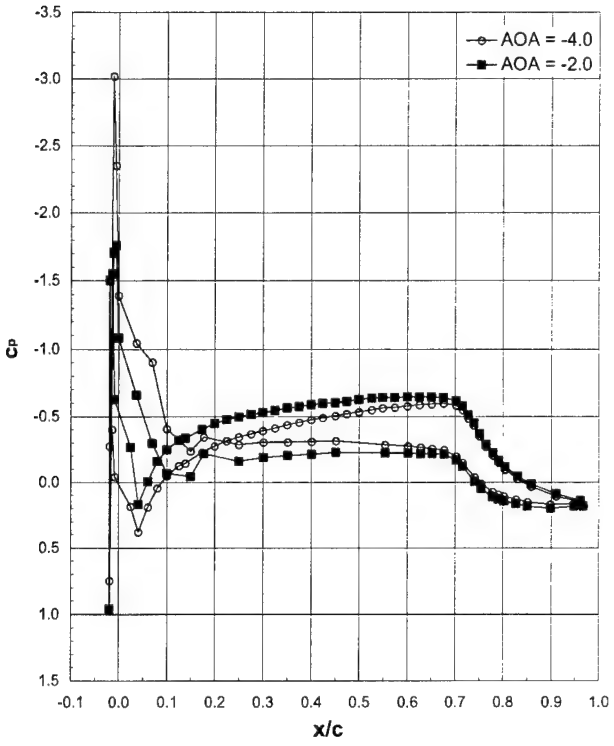

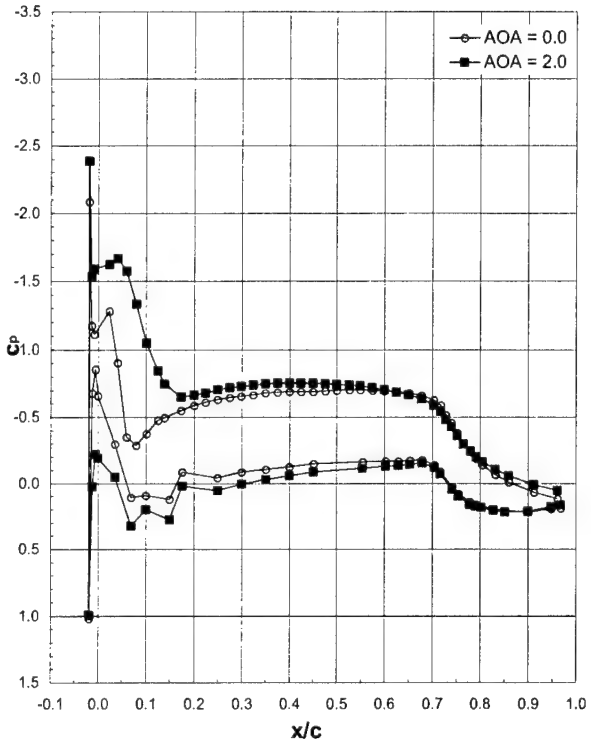

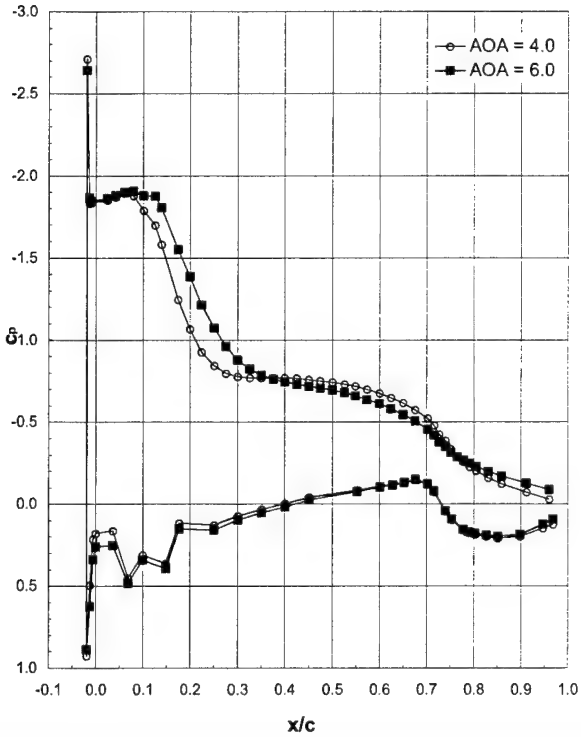

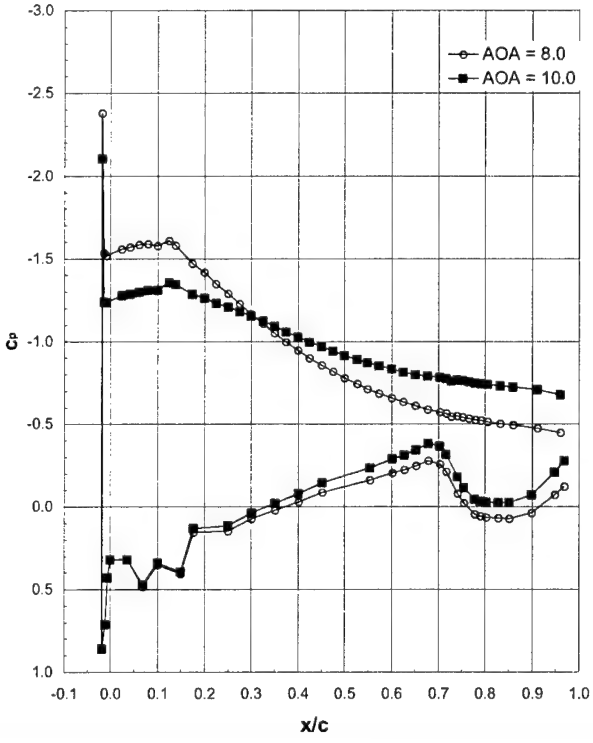

Run 112, Ma = 0.05, Re = 1x10^6

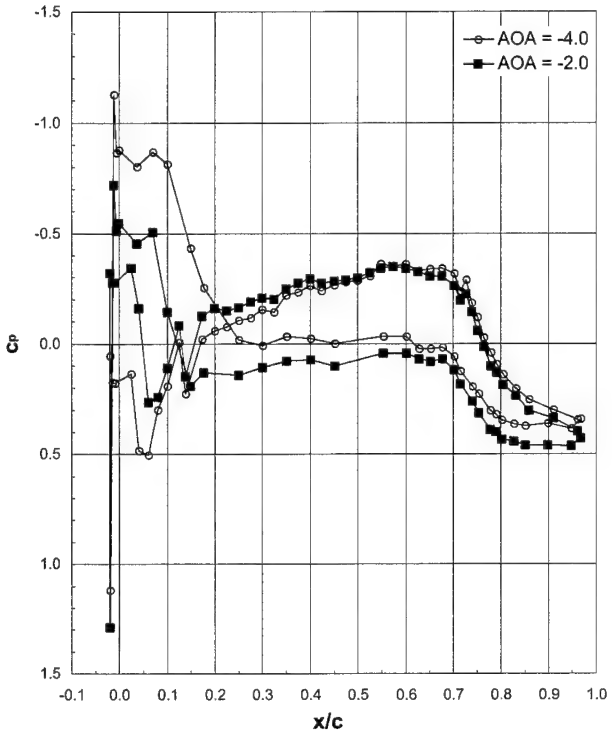

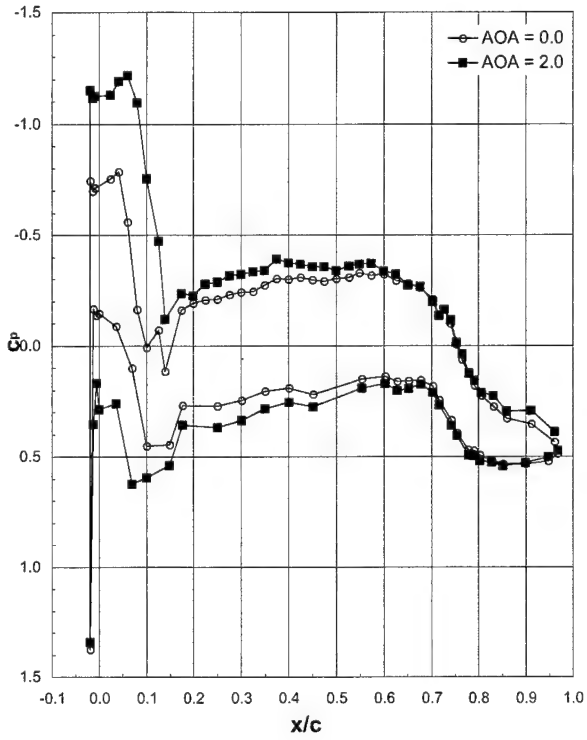

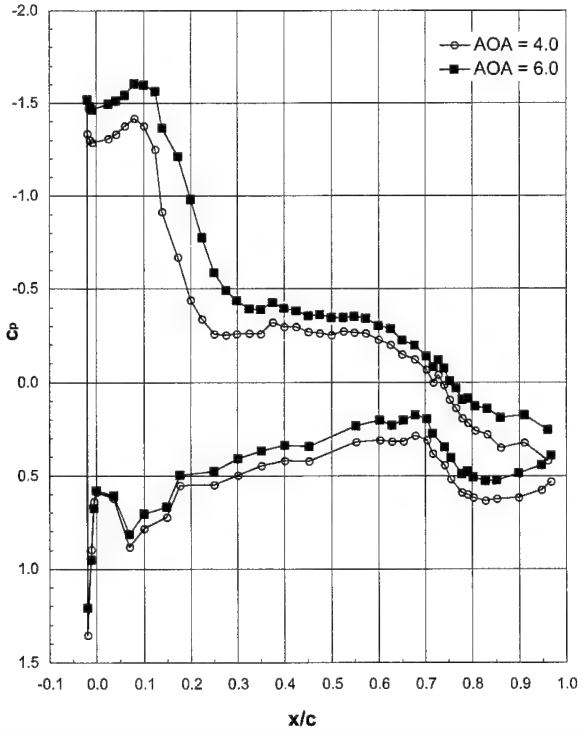

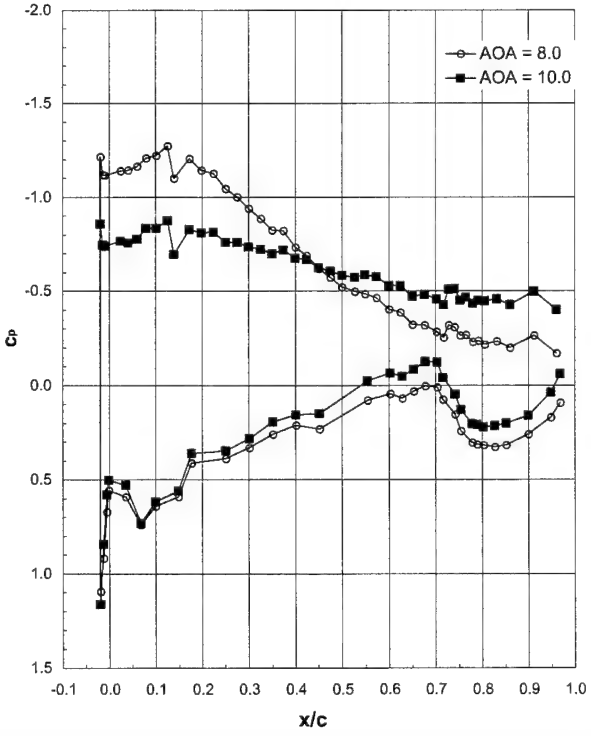

LTPT
General Aviation - Ice Shape 623-3D (Casting)

Ice Shape formed at:

T_t = -2.8°C (26.4°F)	LWC = 0.54 g/m^3
T_s = -5.0°C (22.0°F)	MVD = 20 µm
V = 66.9 m/s (130 kts)	Spray = 22.5 min
AOA = 0.3°	chord = 90 cm (36 in)

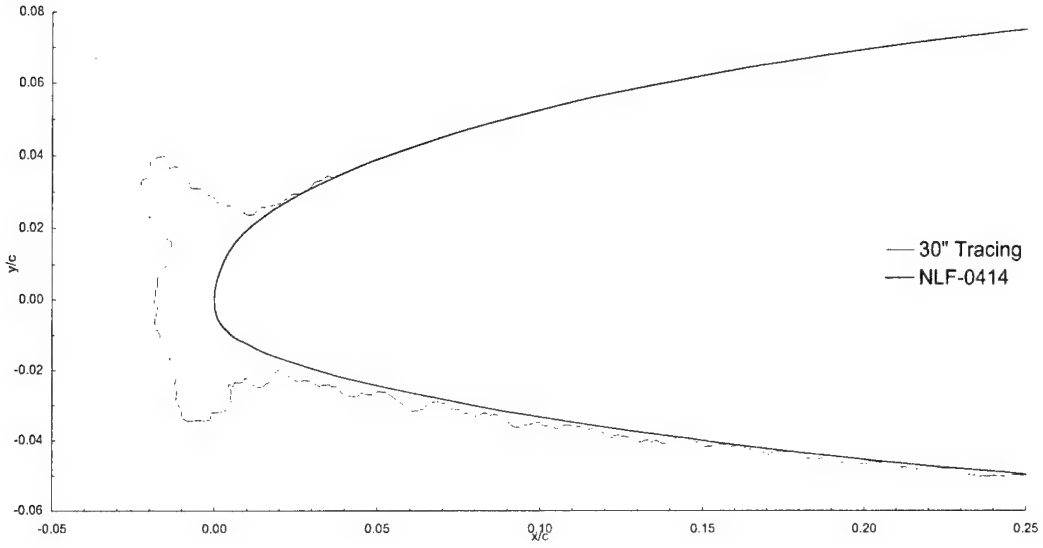

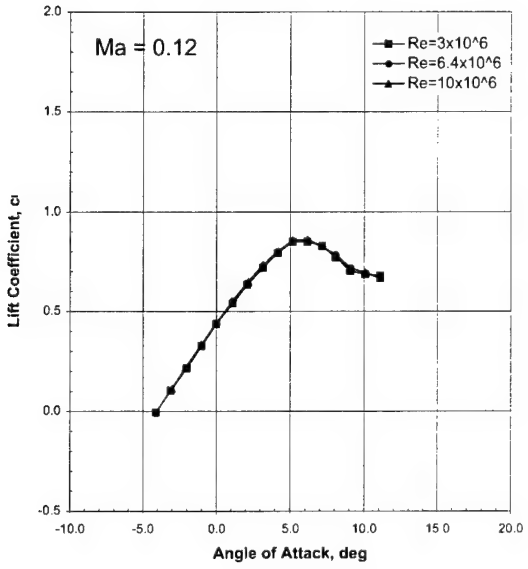

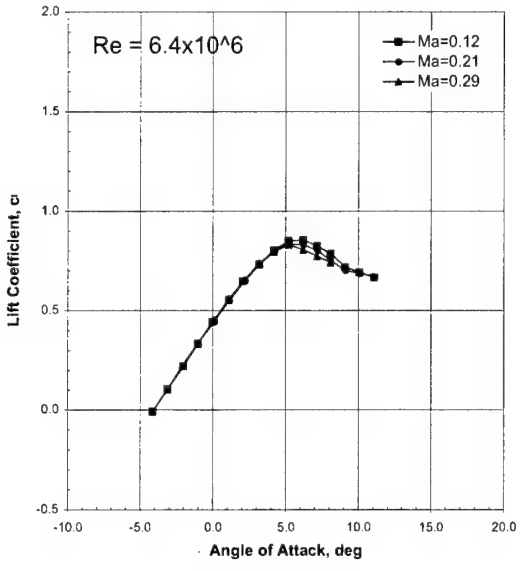

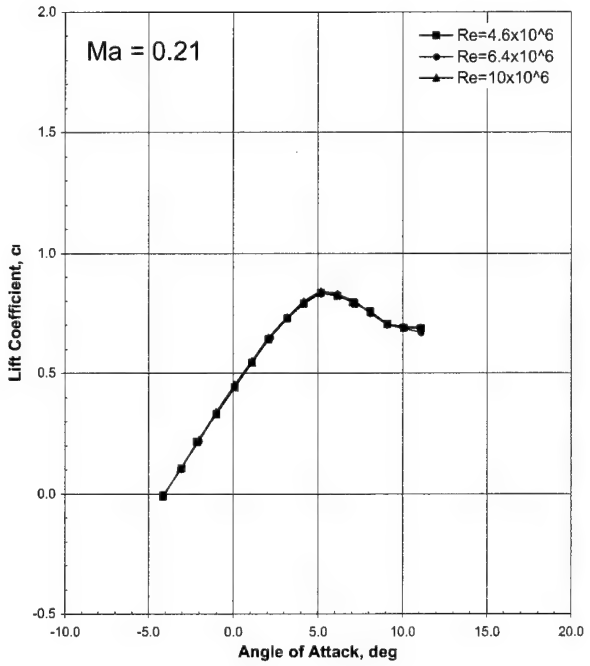

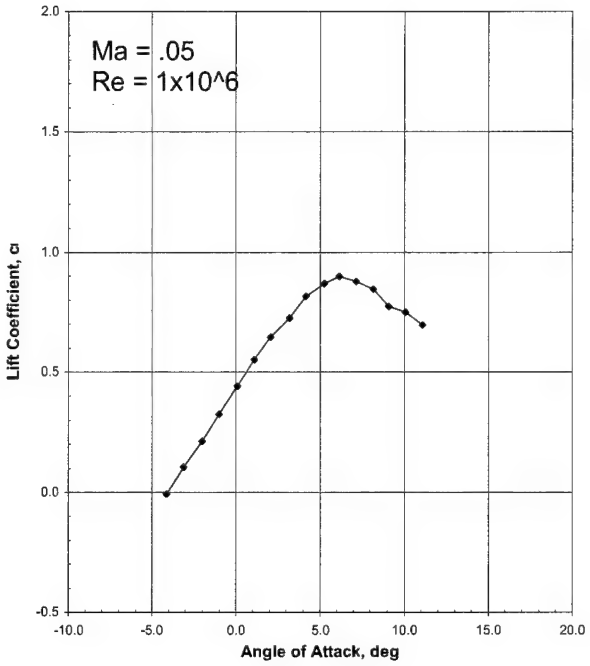

Drag Coefficients, c_d

	α = -2.0	α = 0.0	α = 2.1	α = 4.2	α = 6.2
Run 201, Ma = 0.12, Re = 10x10^6	0.0353	0.0271	0.0351	0.0584	0.1041
Run 202, Ma = 0.12, Re = 6.4x10^6	0.0350	0.0267	0.0349	0.0593	0.1049
Run 203, Ma = 0.21, Re = 10x10^6	0.0349	0.0263	0.0348	0.0605	0.1203
Run 204, Ma = 0.21, Re = 4.6x10^6	*0.0407*	*0.0389*	*0.0559*	*0.0559*	*0.1296*
Run 207, Ma = 0.21, Re = 6.4x10^6	0.0272	0.0164	0.0273	0.0586	0.1222
Run 208, Ma = 0.12, Re = 3x10^6	0.0319	0.0237	0.0317	0.0558	0.0956
Run 210, Ma = 0.29, Re = 6.4x10^6	0.0442	0.0441	0.0553	0.0811	0.1250
Run 211, Ma = 0.05, Re = 1x10^6	*0.0099*	*0.0090*	*0.0082*	*0.0076*	*0.0072*

Italicized font indicates force balance data

LTPT

General Aviation - Ice Shape 623-3D (Casting) (cont.)

Run 201, Ma = 0.12, Re = 10x10^6

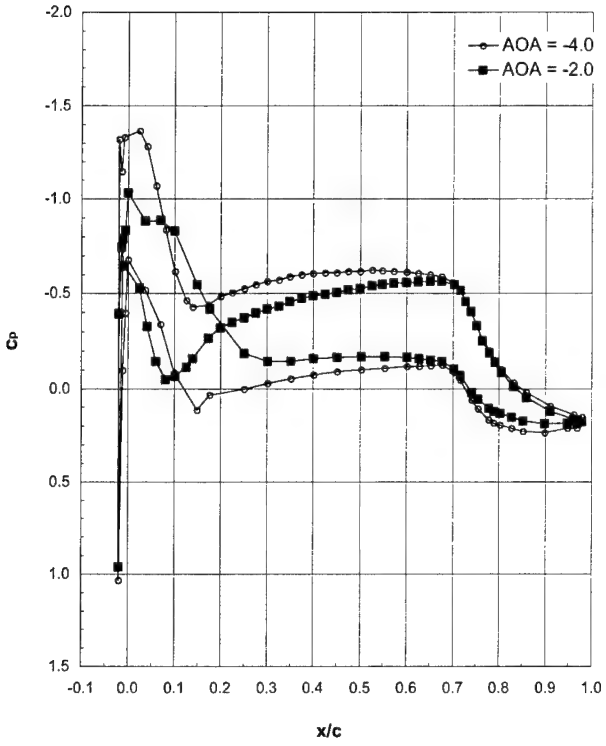

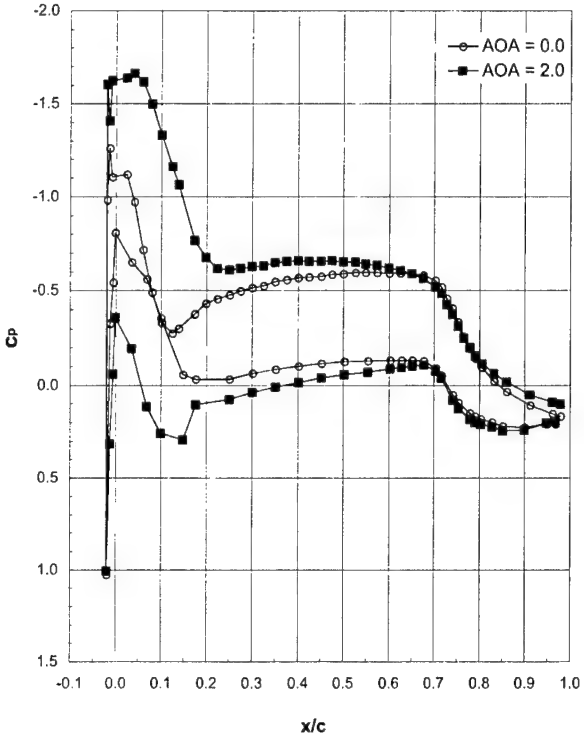

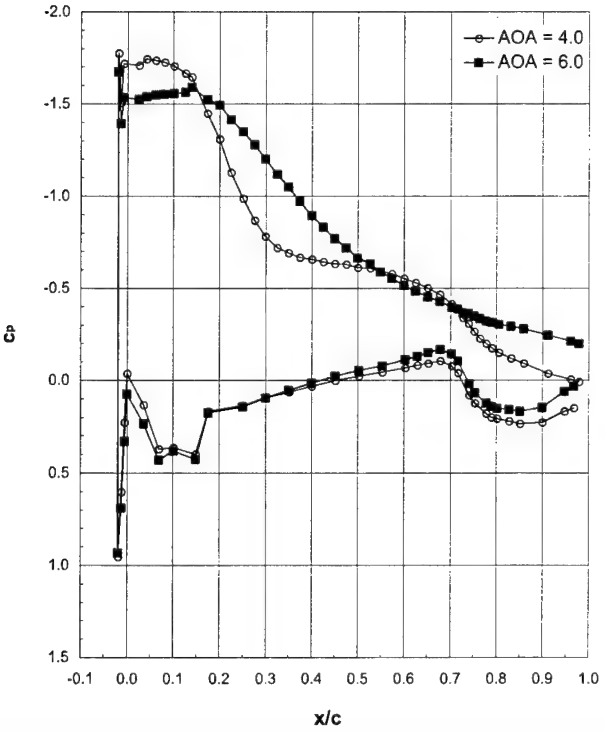

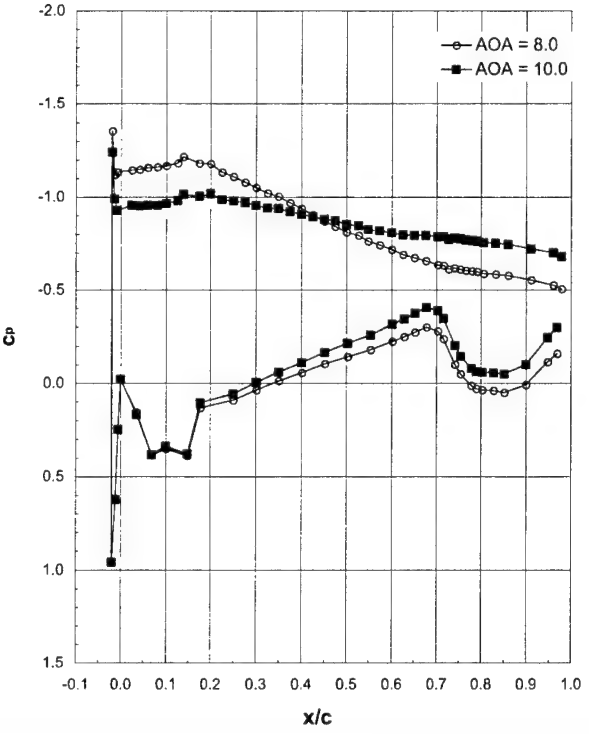

Run 202, Ma = 0.12, Re = 6.4x10^6

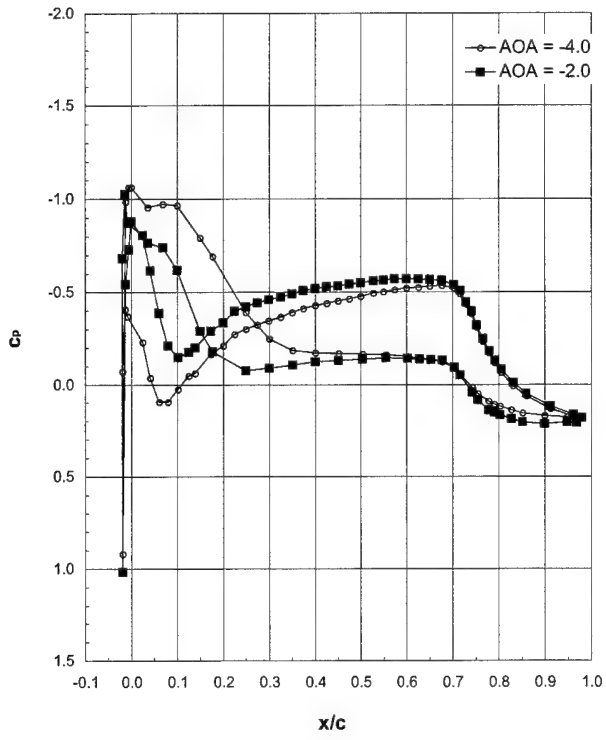

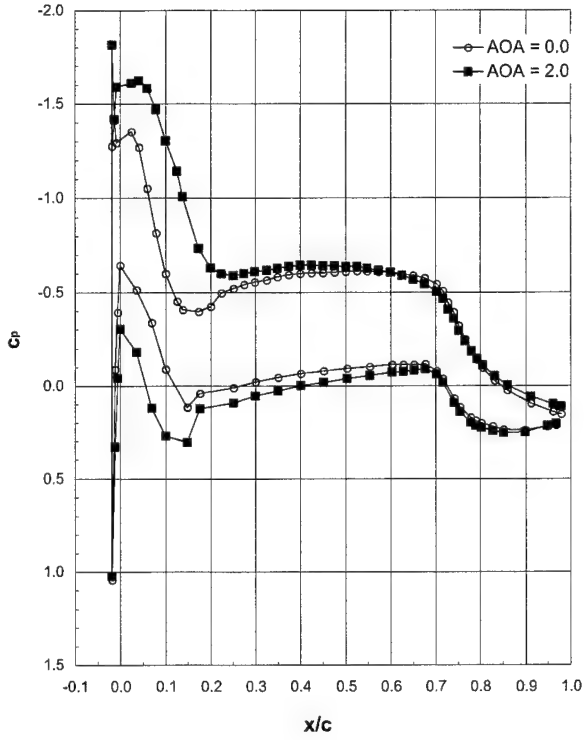

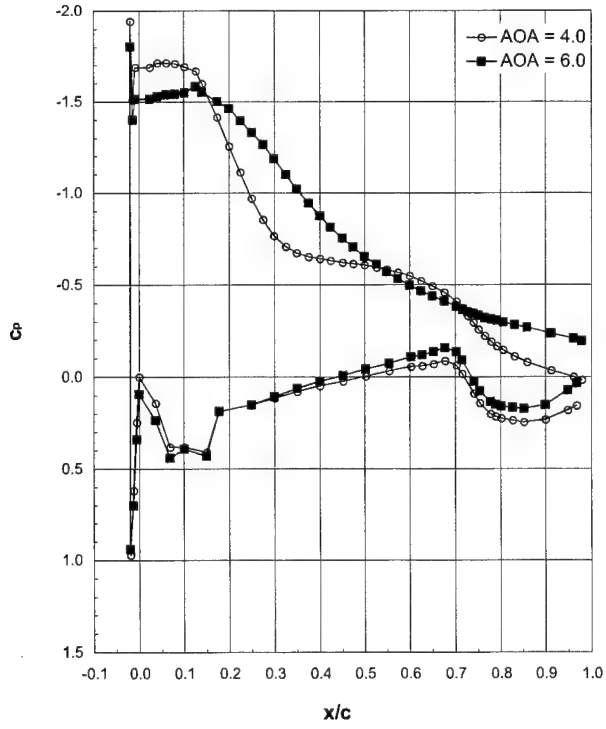

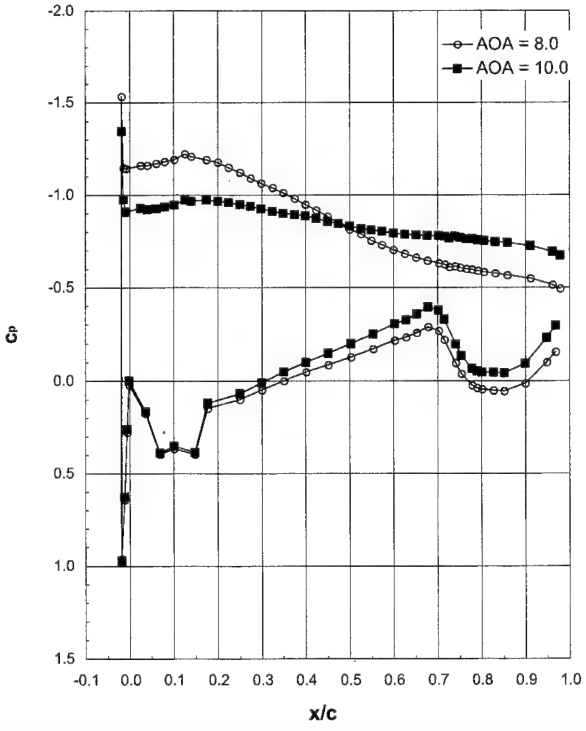

Run 203, Ma = 0.21, Re = 10x10^6

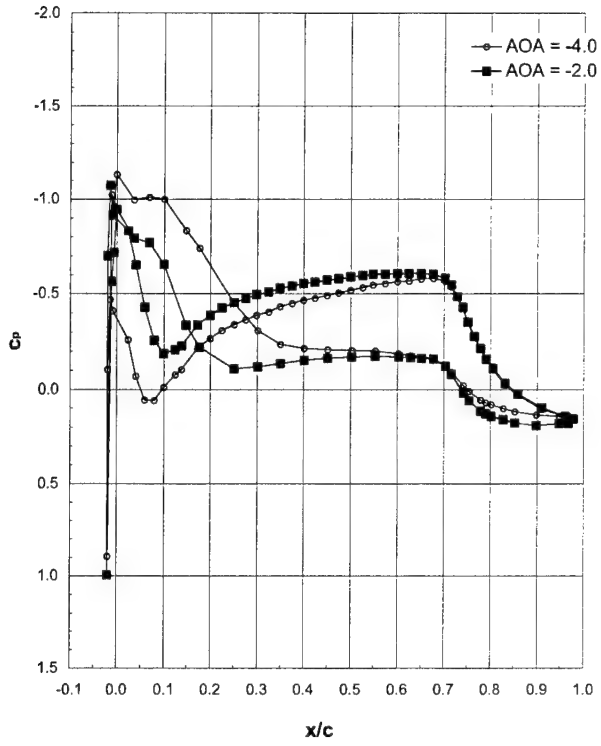

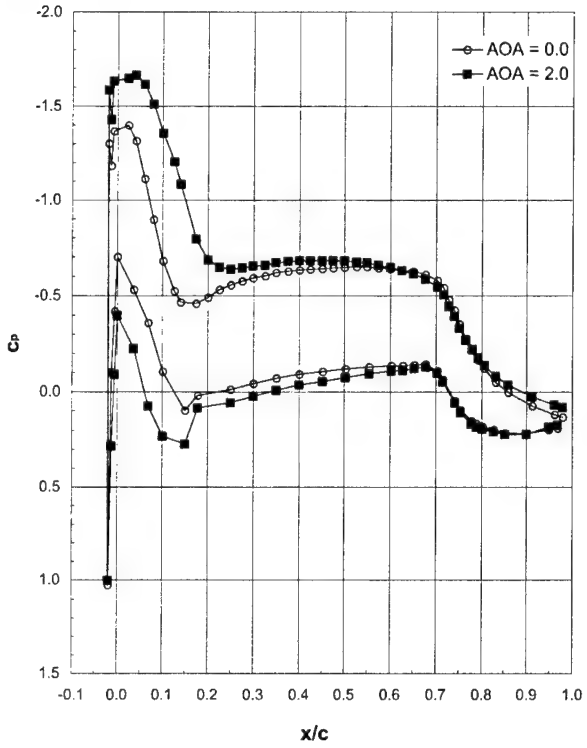

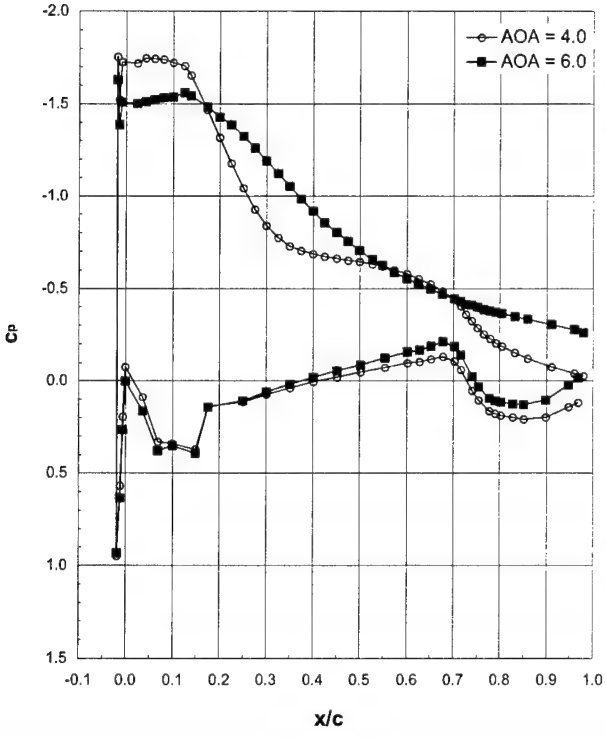

Run 204, Ma = 0.21, Re = 4.6x10^6

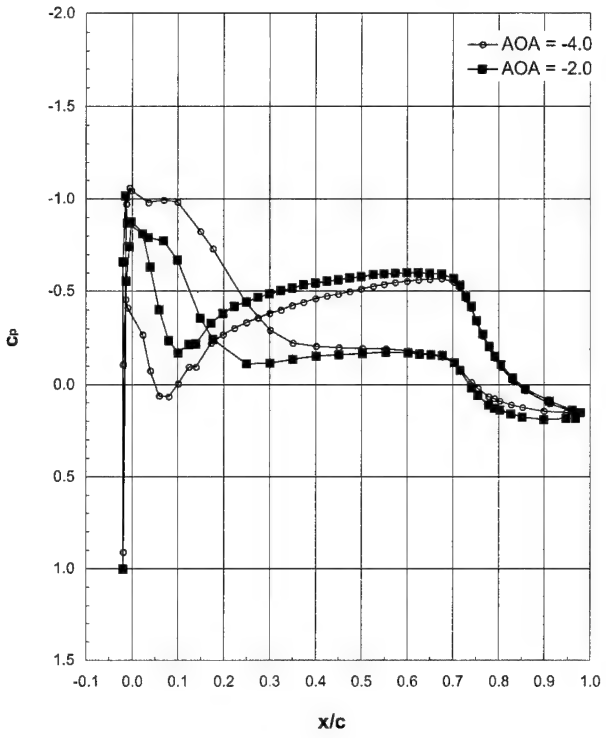

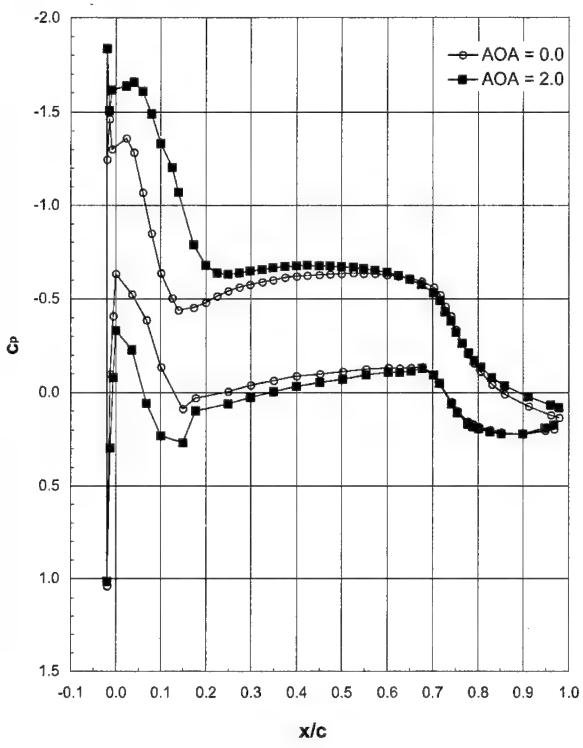

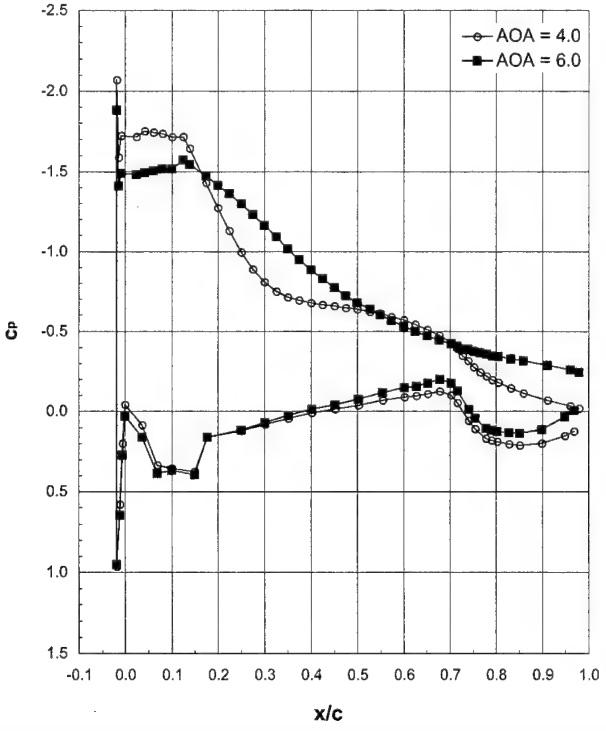

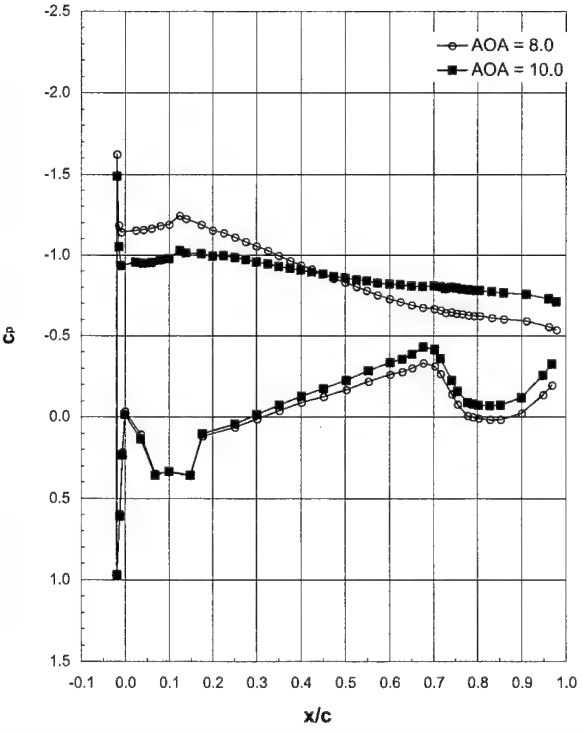

Run 207, Ma = 0.21, Re = 6.4x10^6

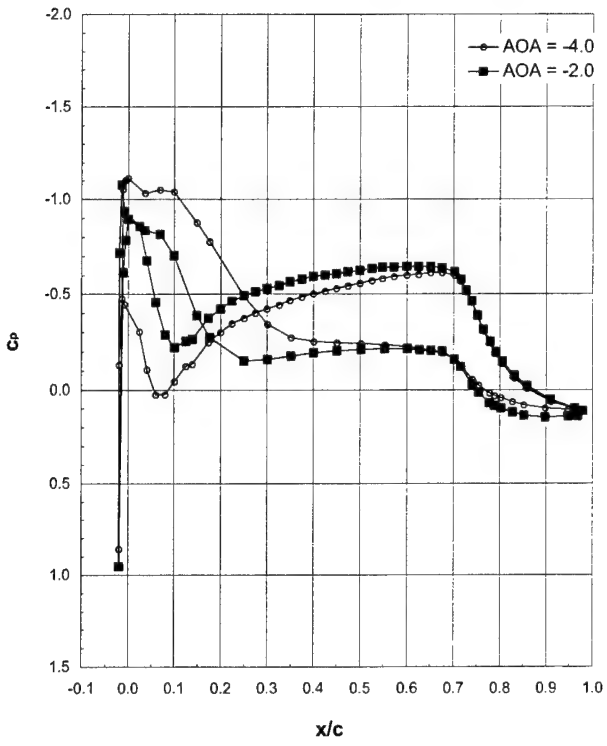

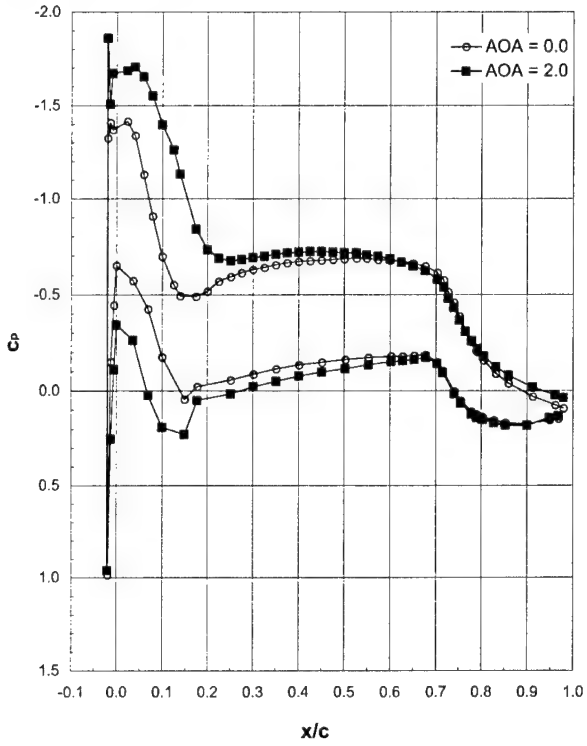

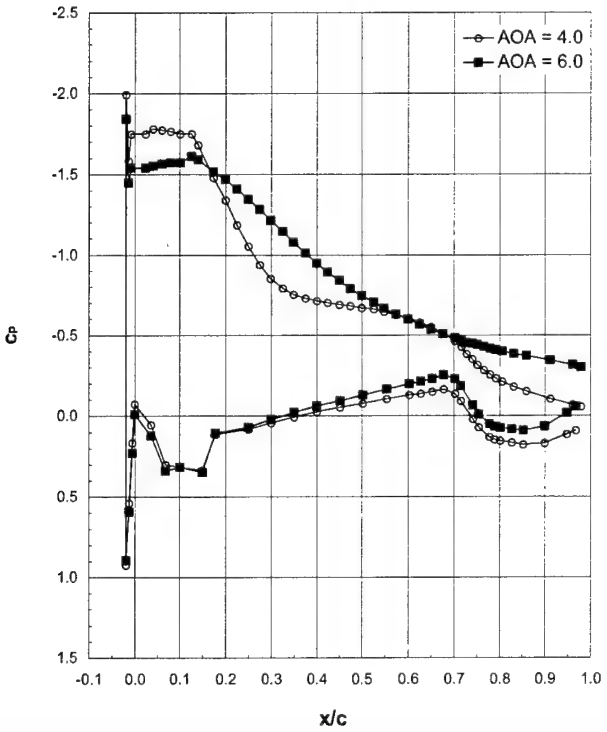

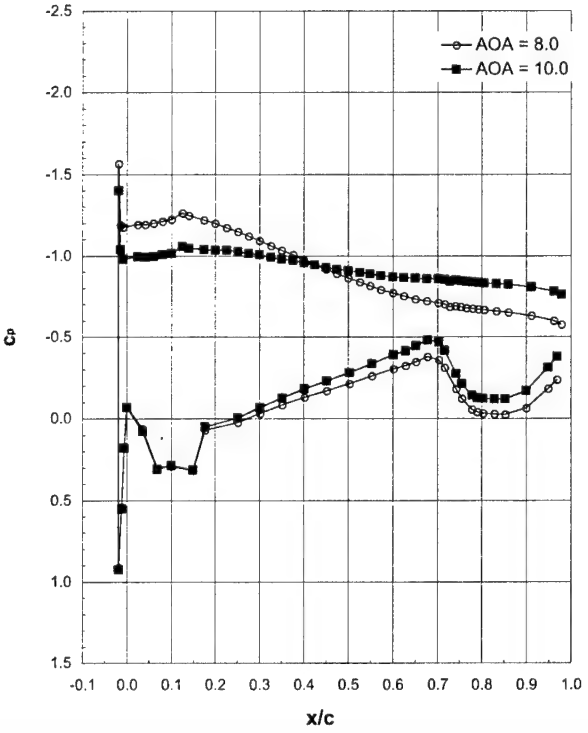

LTPT

General Aviation - Ice Shape 623-3D (Casting) (cont.)

Run 208, Ma = 0.12, Re = 3x10^6

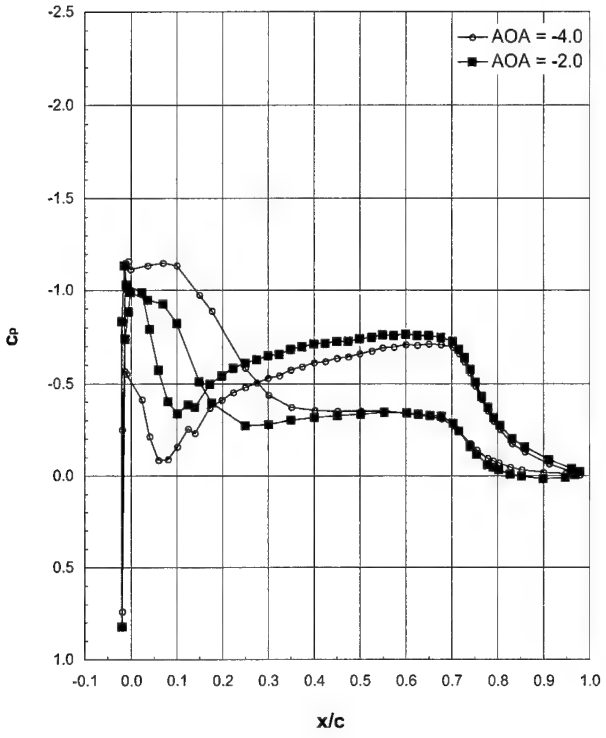

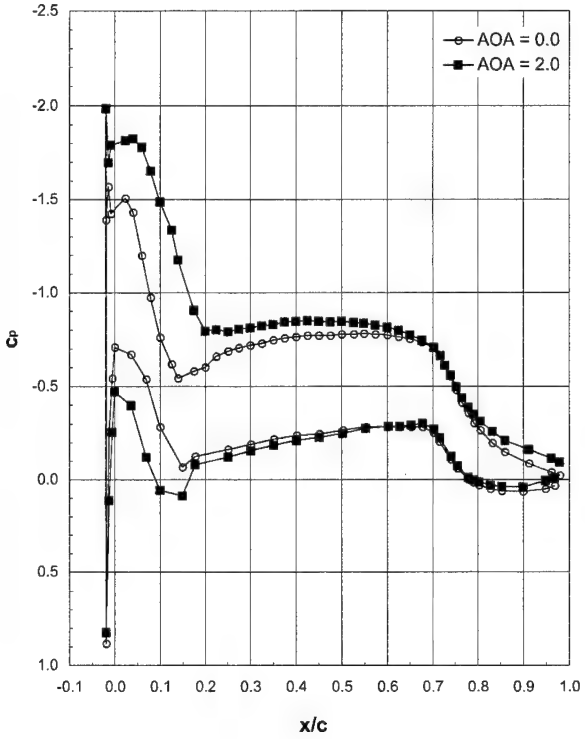

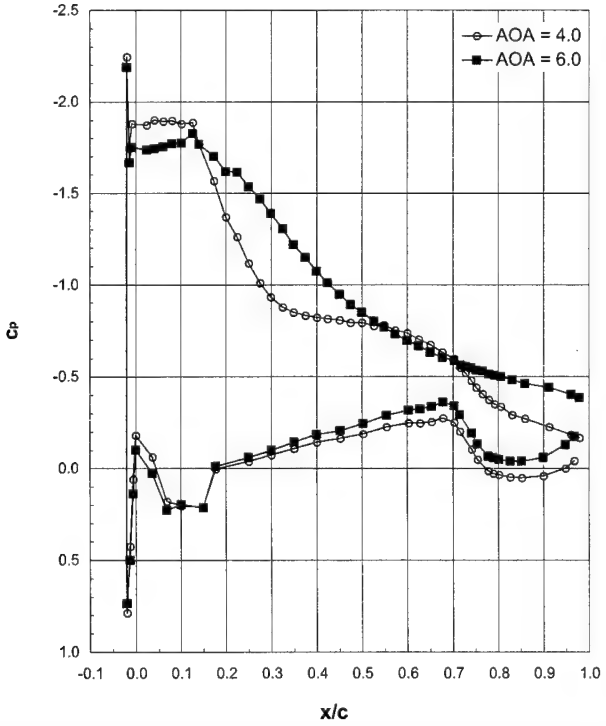

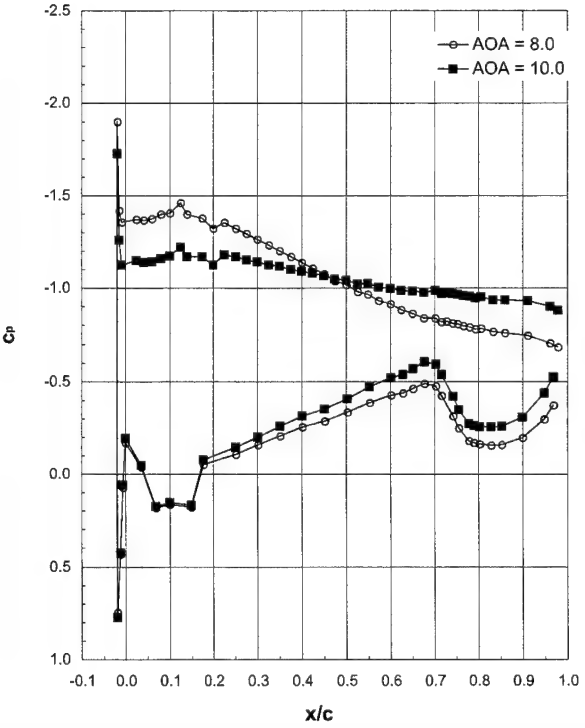

Run 210, Ma = 0.29, Re = 6.4x10^6

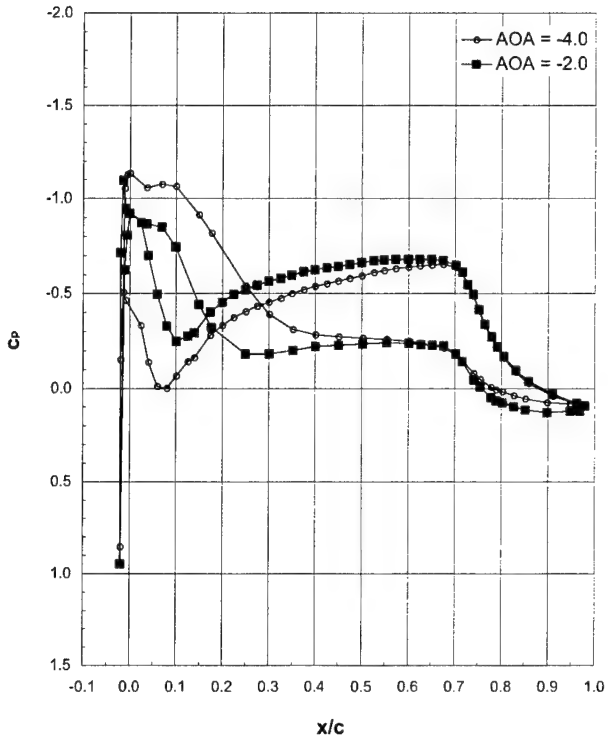

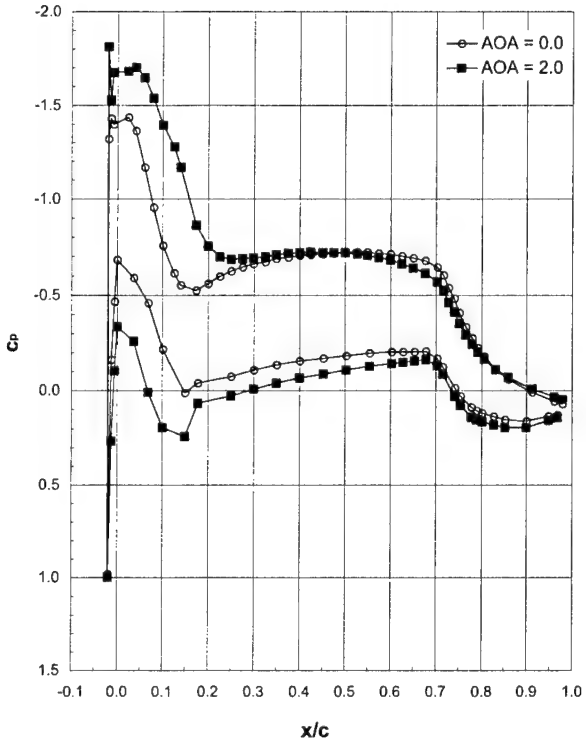

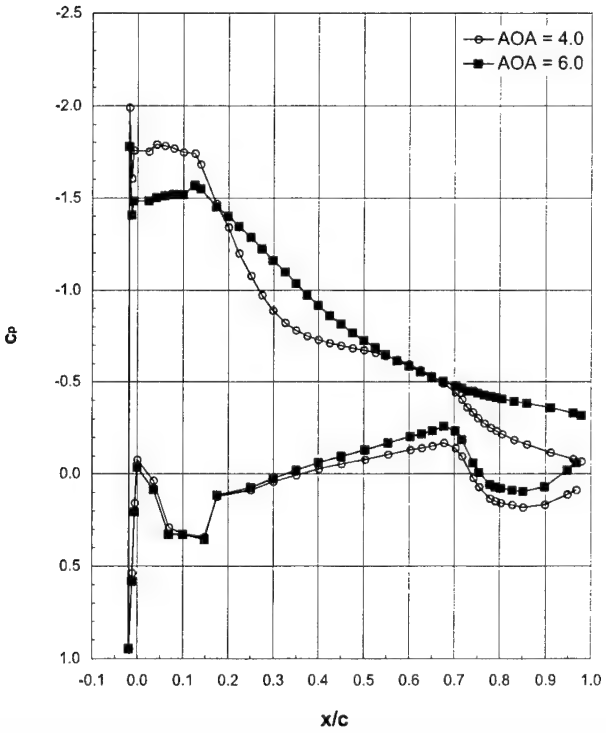

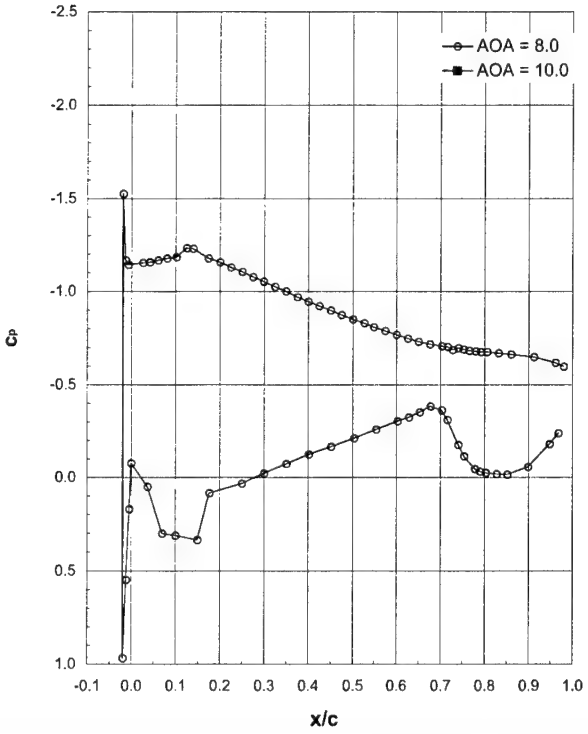

Run 211, Ma = 0.05, Re = 1x10^6

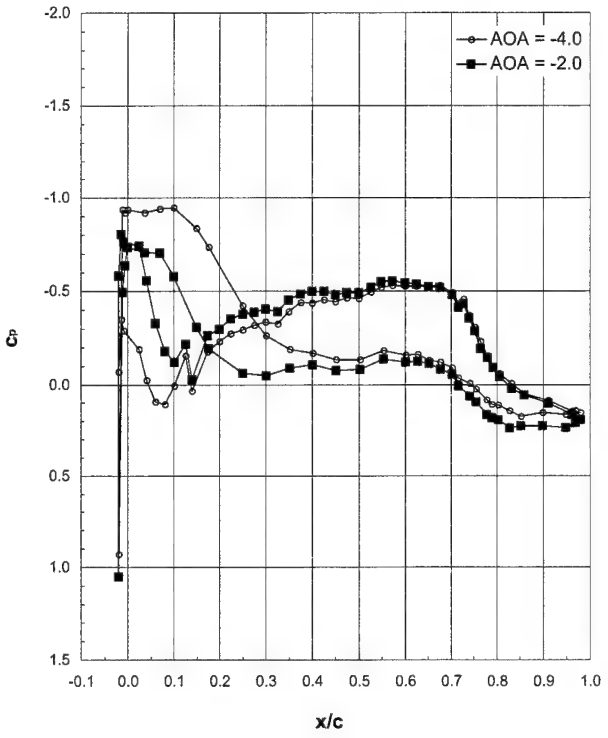

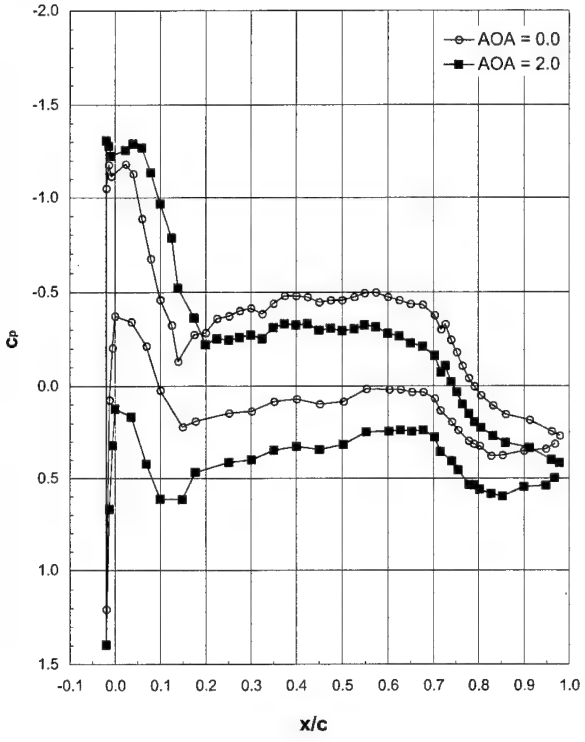

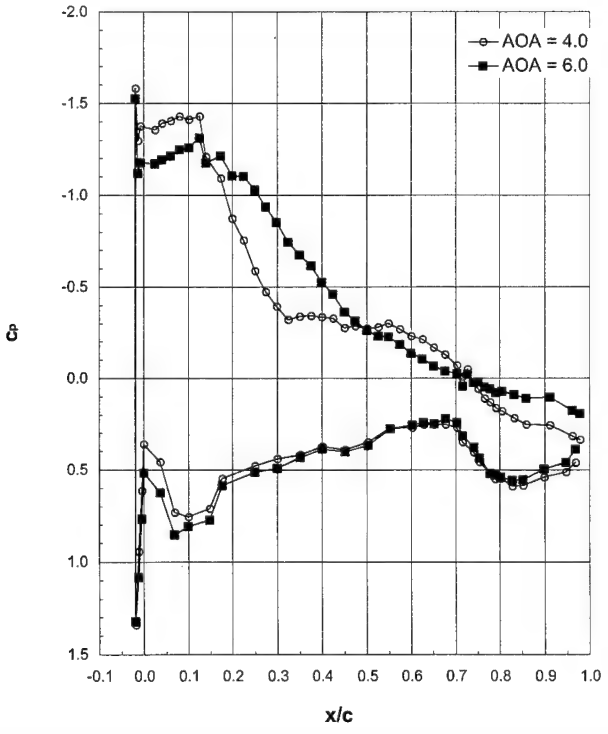

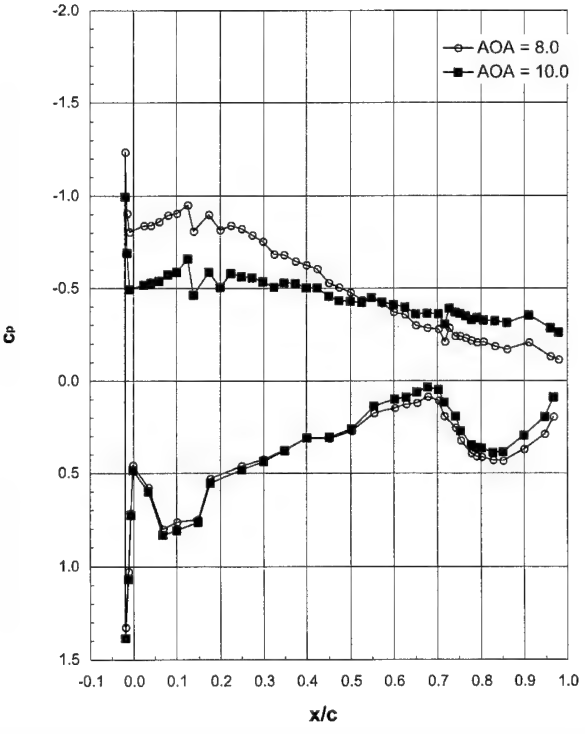

LTPT
General Aviation - Ice Shape 622-2D (SLA)

Ice Shape formed at:

T_t = -2.8°C (26.4°F)	LWC = 0.54 g/m^3
T_s = -5.0°C (22.0°F)	MVD = 20 µm
V = 66.9 m/s (130 kts)	Spray = 22.5 min
AOA = 0.3^o	chord = 90 cm (36 in)

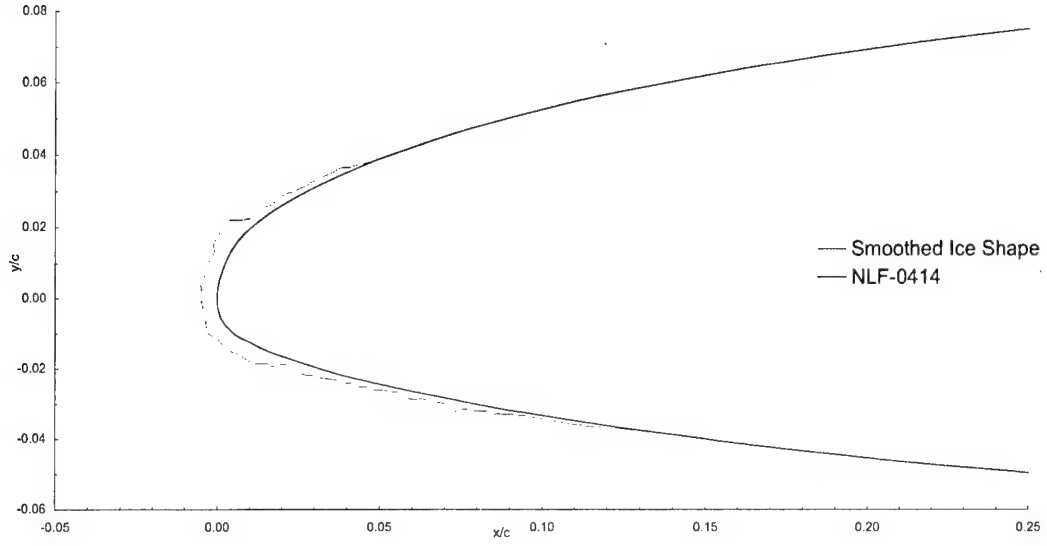

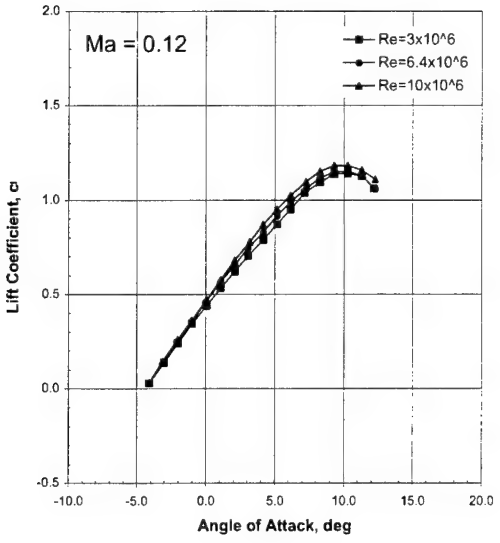

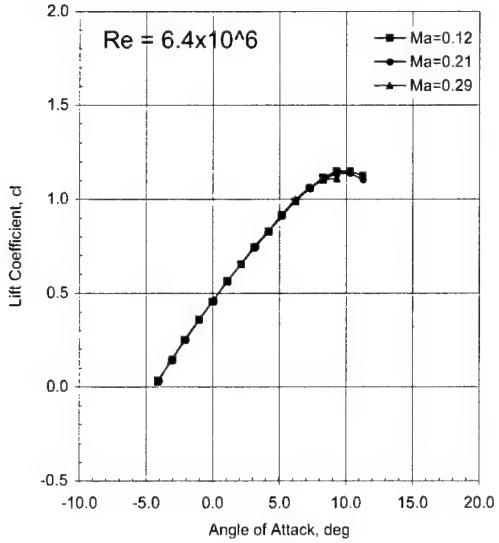

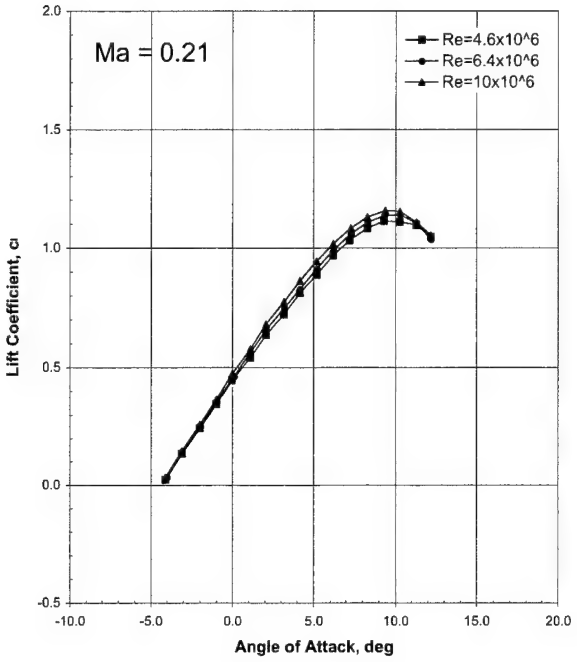

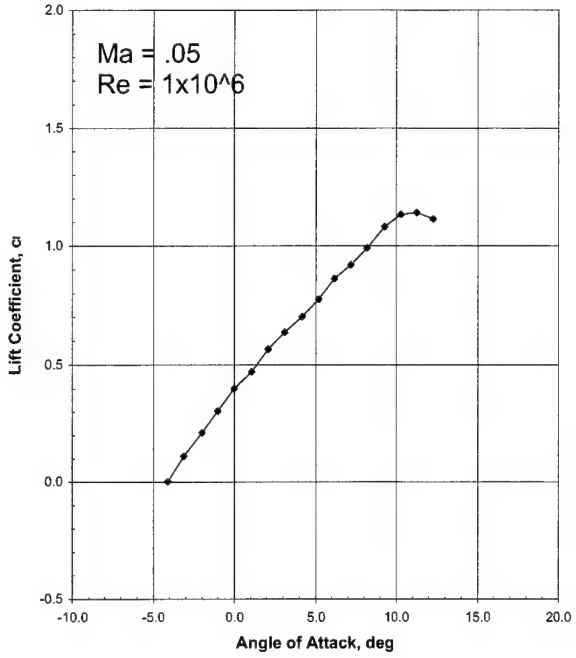

Drag Coefficients, c_d

	α = -2.0	α = 0.0	α = 2.1	α = 4.2	α = 6.2
Run 301, Ma = 0.12, Re = 10x10^6	0.0134	0.0120	0.0134	0.0175	0.0242
Run 302, Ma = 0.12, Re = 6.4x10^6	0.0104	0.0089	0.0104	0.0148	0.0363
Run 304, Ma = 0.29, Re = 6.4x10^6	0.0158	0.0139	0.0157	0.0213	0.0306
Run 306, Ma = 0.21, Re = 10x10^6	0.0129	0.0108	0.0134	0.0205	0.0323
Run 307, Ma = 0.21, Re = 6.4x10^6	0.0137	0.0113	0.0143	0.0226	0.0362
Run 308, Ma = 0.12, Re = 3x10^6	0.0159	0.0135	0.0164	0.0246	0.0379
Run 309, Ma = 0.21, Re = 4.6x10^6	*0.0303*	*0.0170*	*0.0165*	*0.0293*	*0.0528*
Run 310, Ma = 0.05, Re = 1x10^6	0.0062	0.0047	0.0039	0.0038	0.0040

Italicized font indicates force balance data

Run 301, Ma = 0.12, Re = 10x10^6

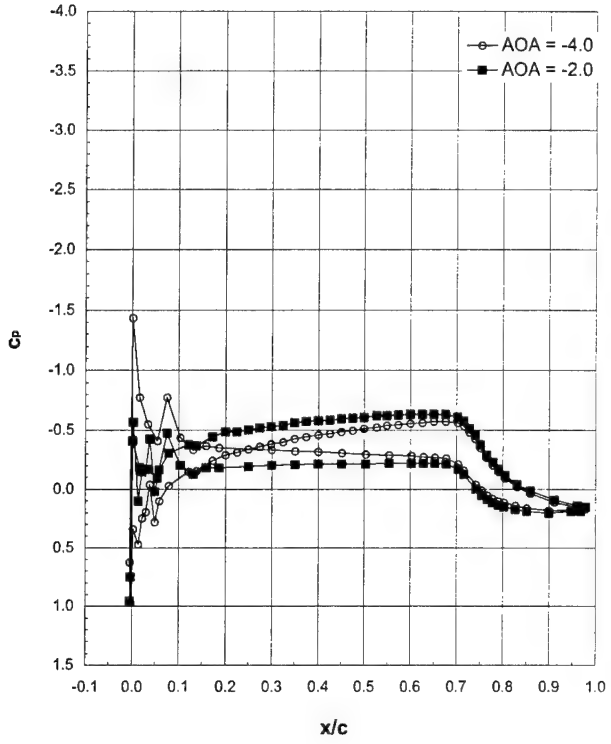

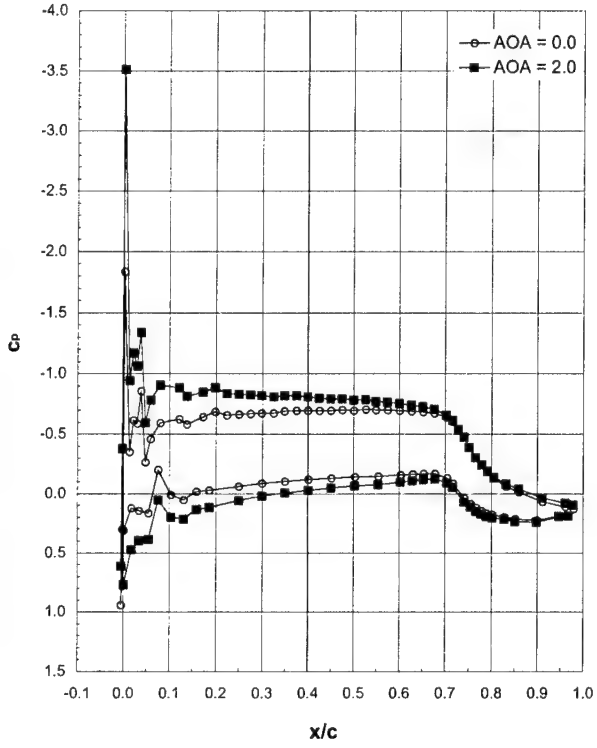

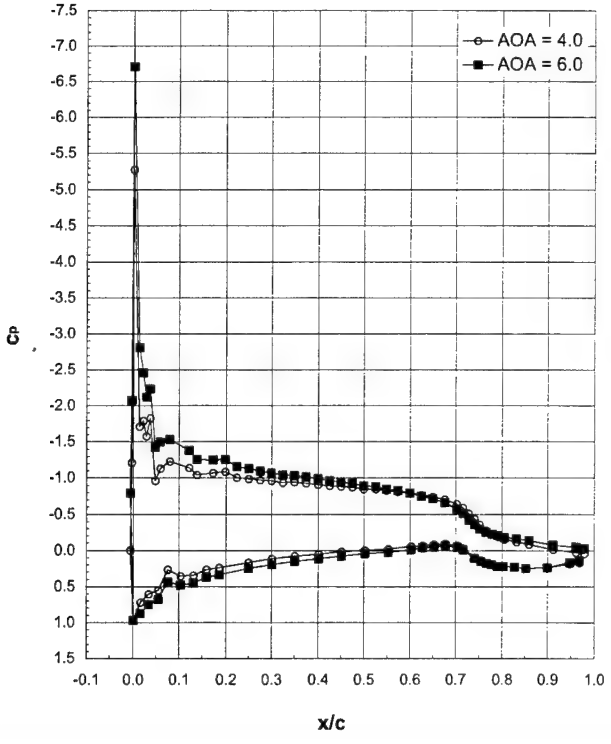

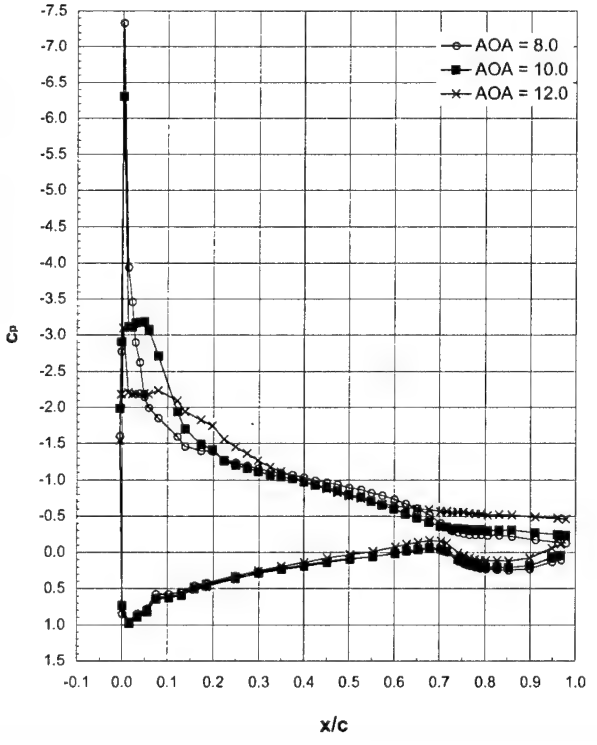

Run 302, Ma = 0.12, Re = 6.4x10^6

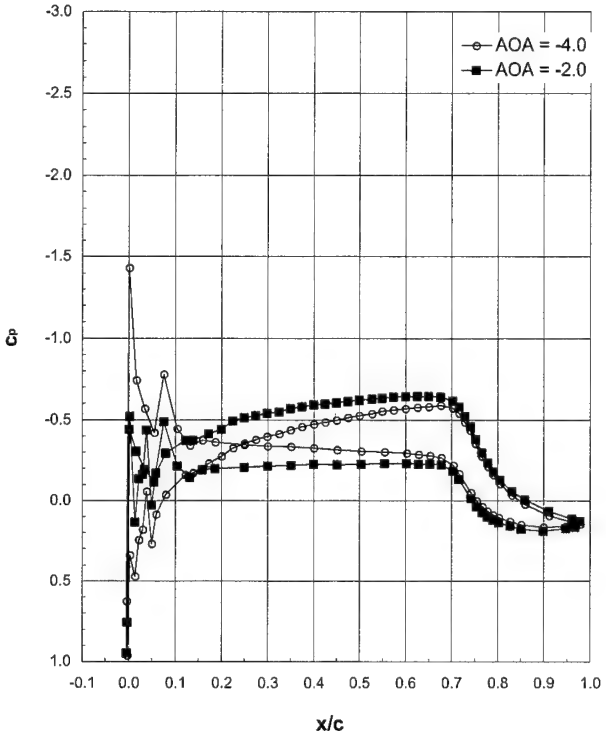

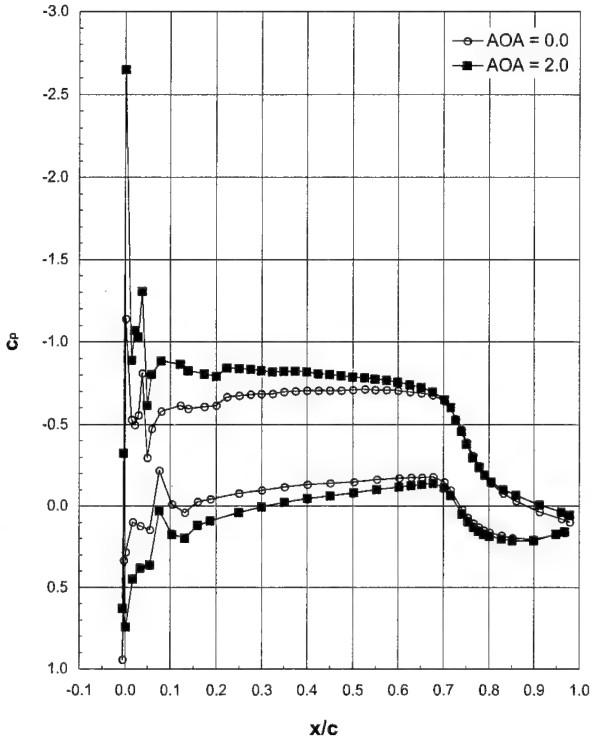

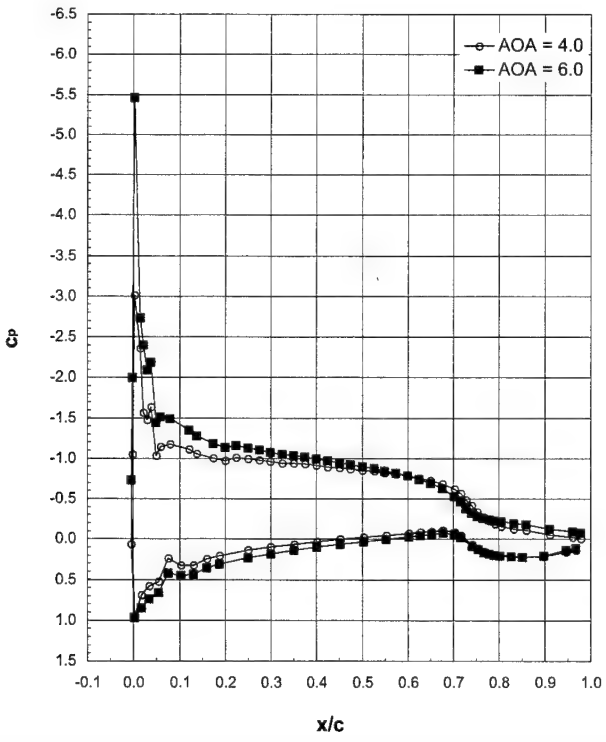

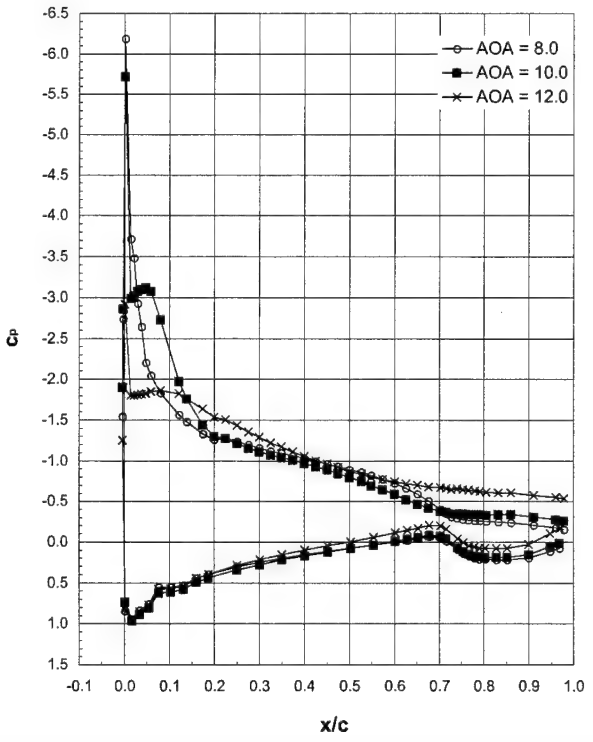

Run 304, Ma = 0.29, Re = 6.4x10^6

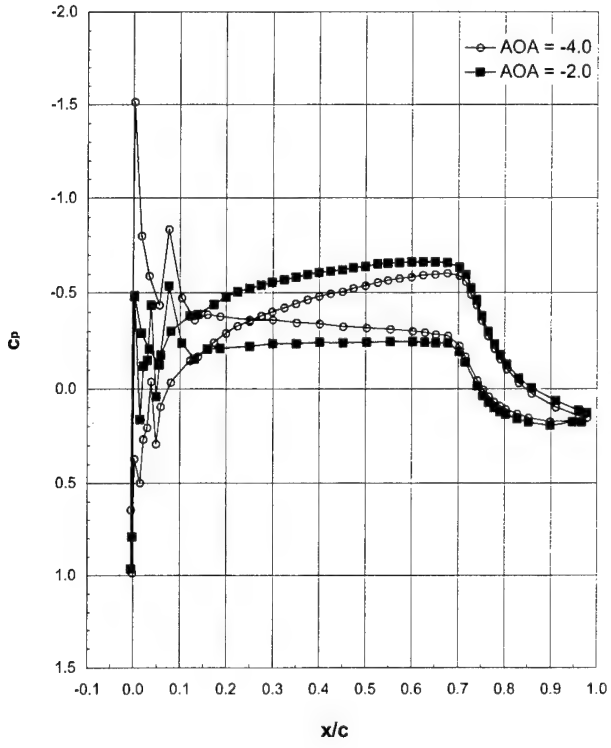

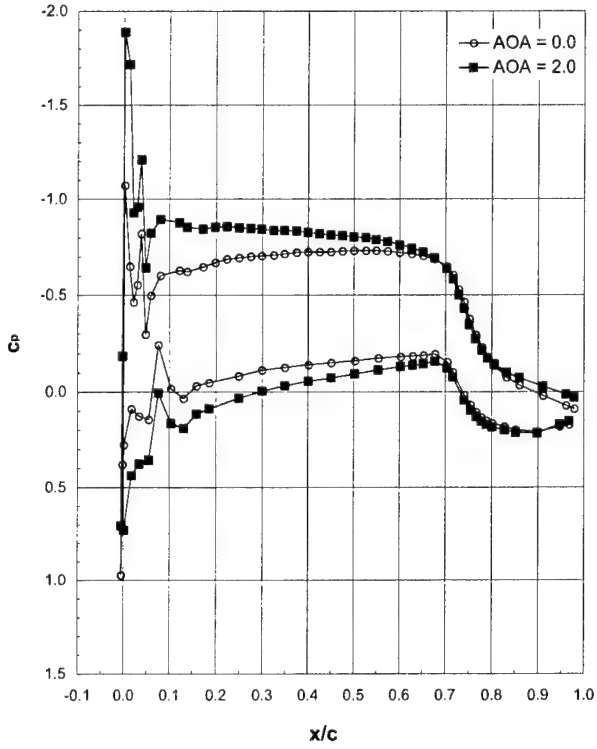

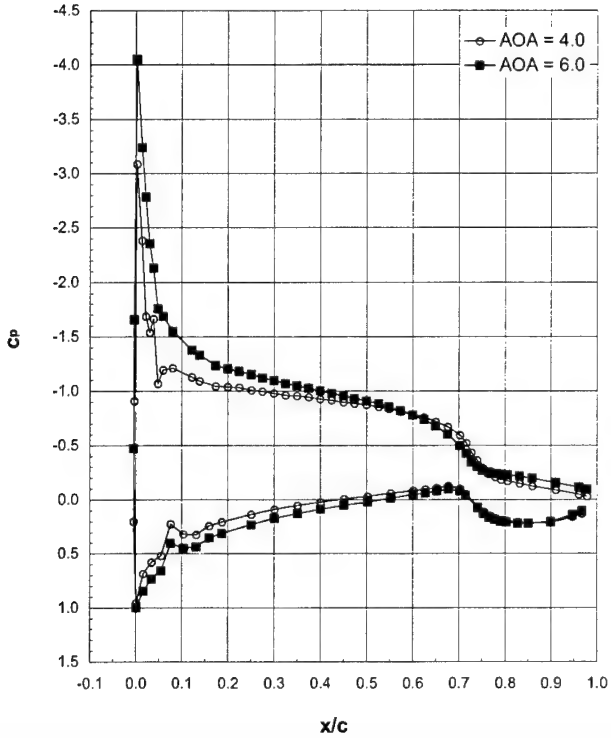

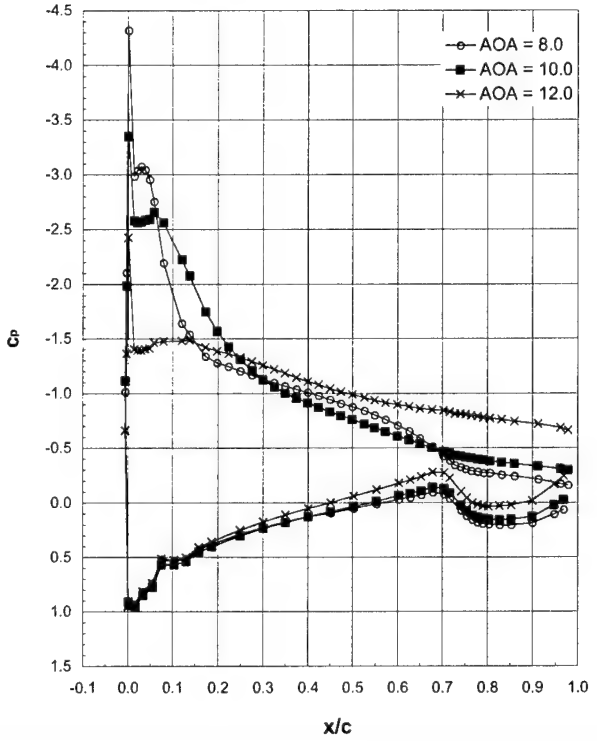

Run 306, Ma = 0.21, Re = 10x10^6

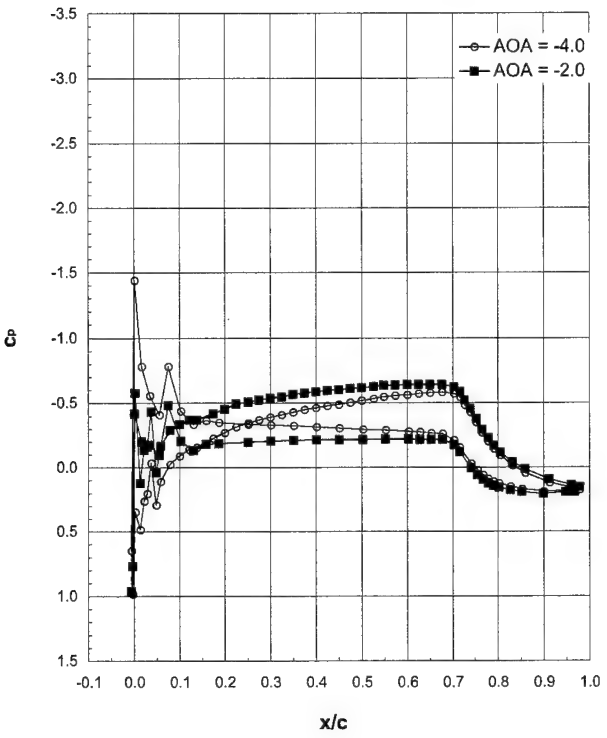

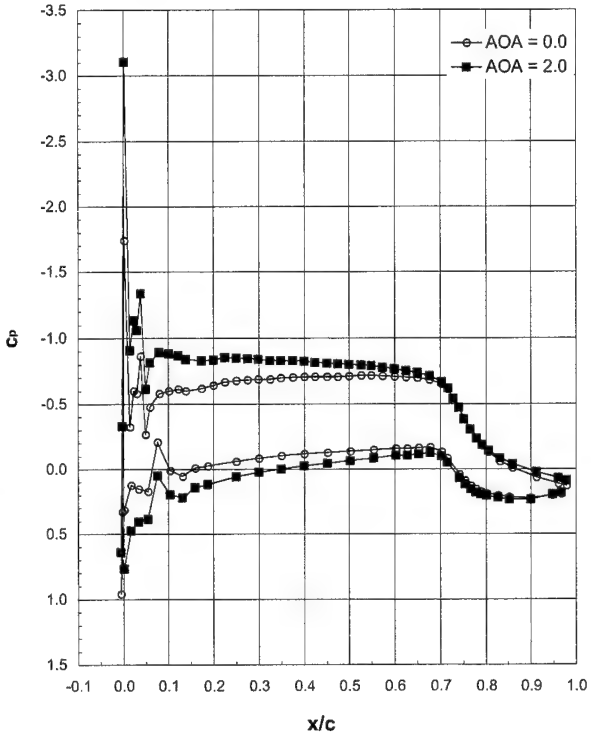

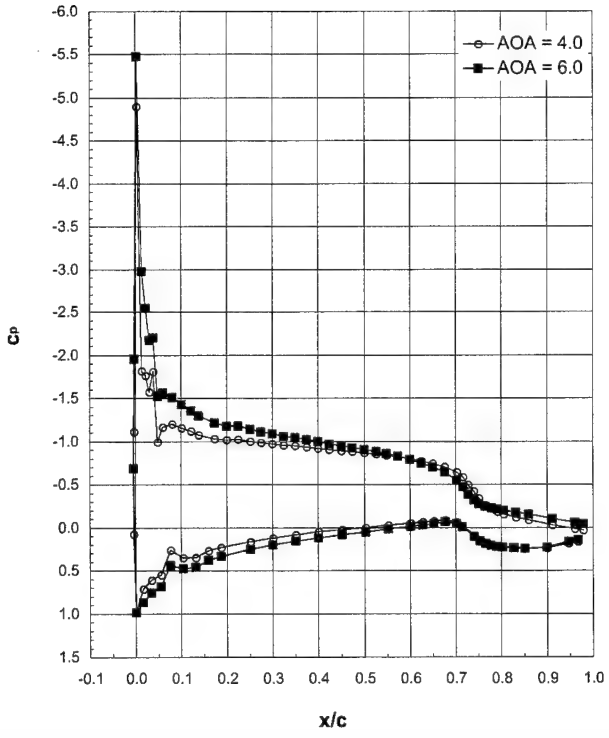

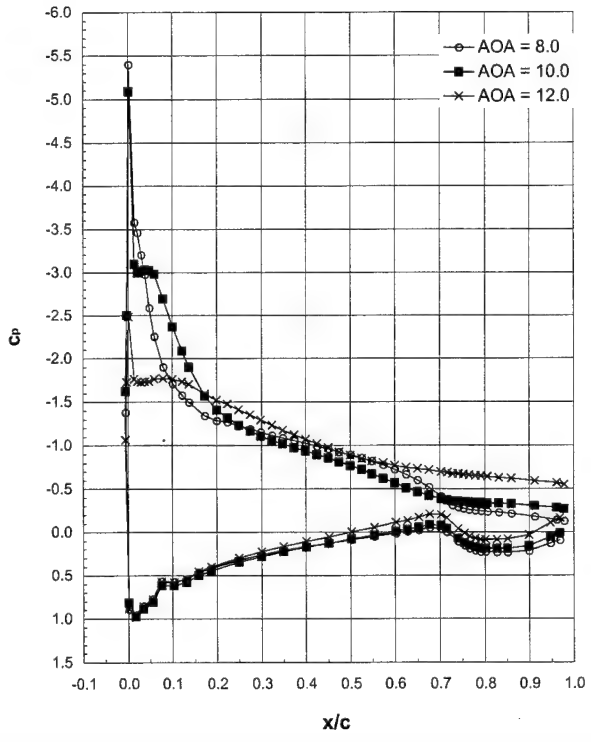

Run 307, Ma = 0.21, Re = 6.4x10^6

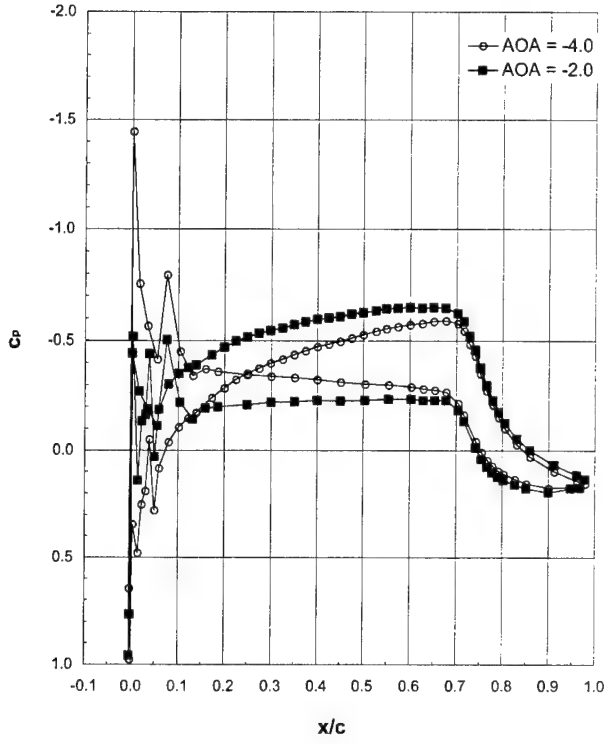

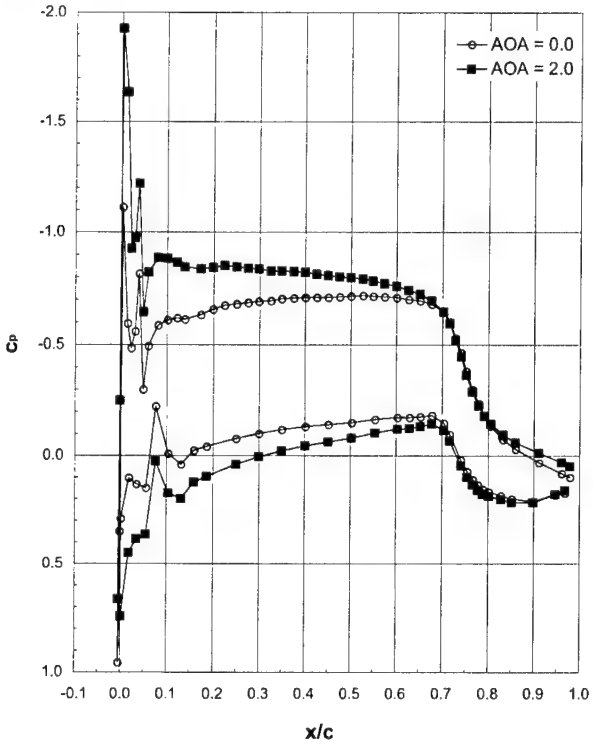

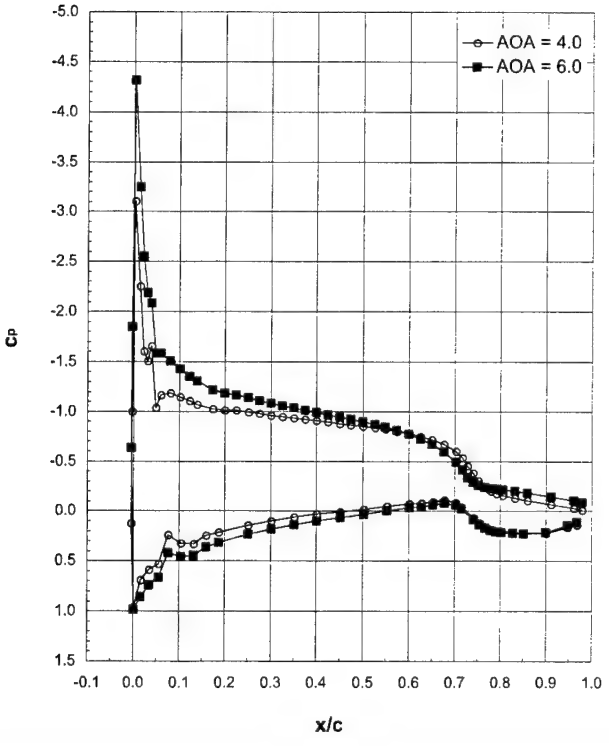

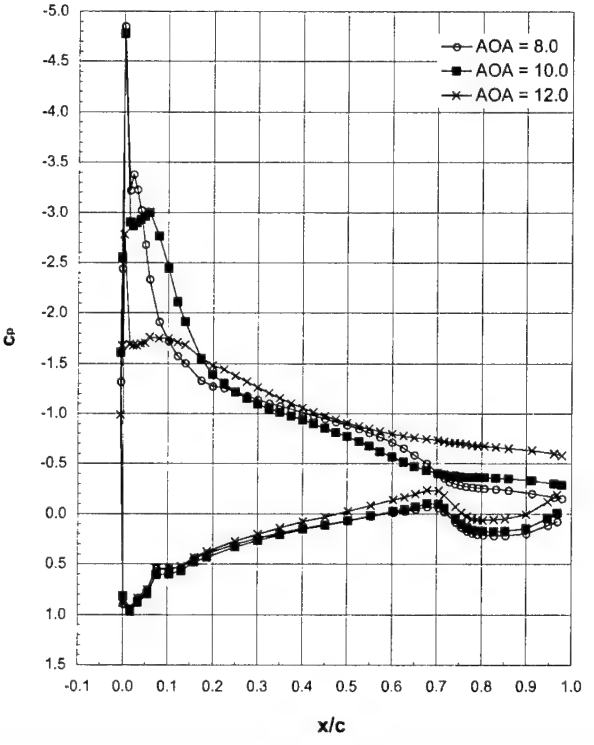

Run 308, Ma = 0.12, Re = 3x10^6

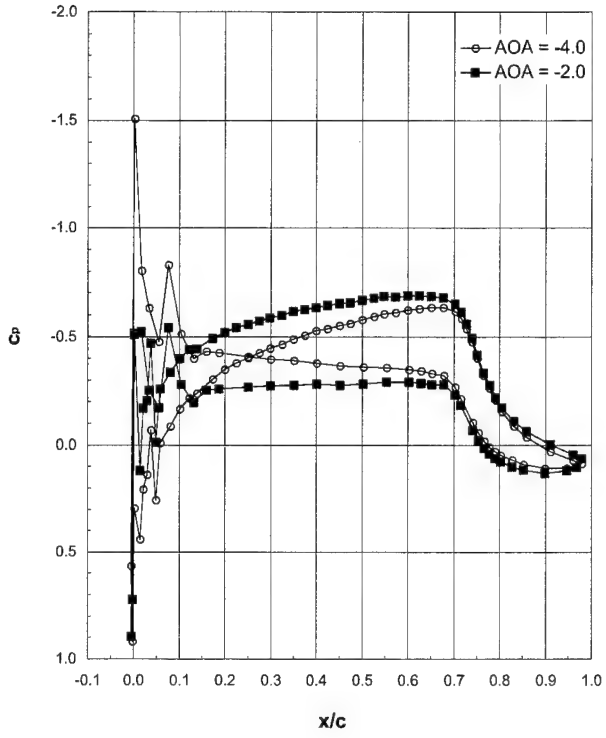

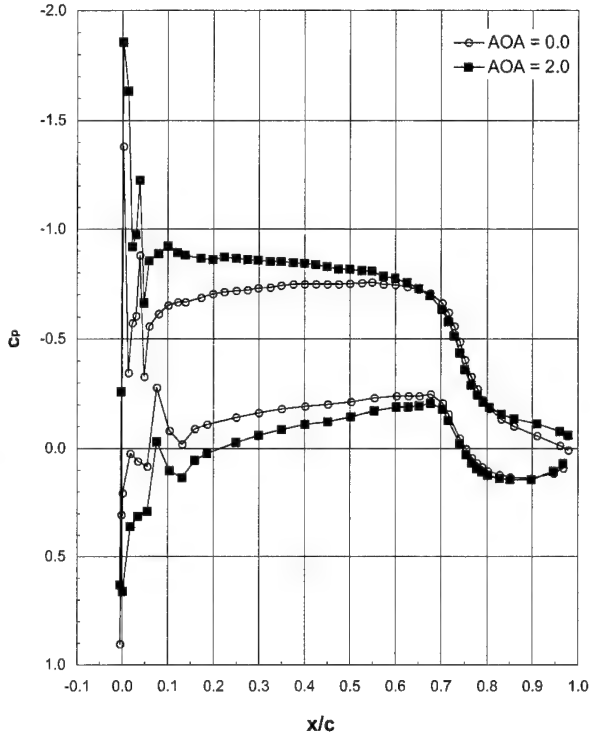

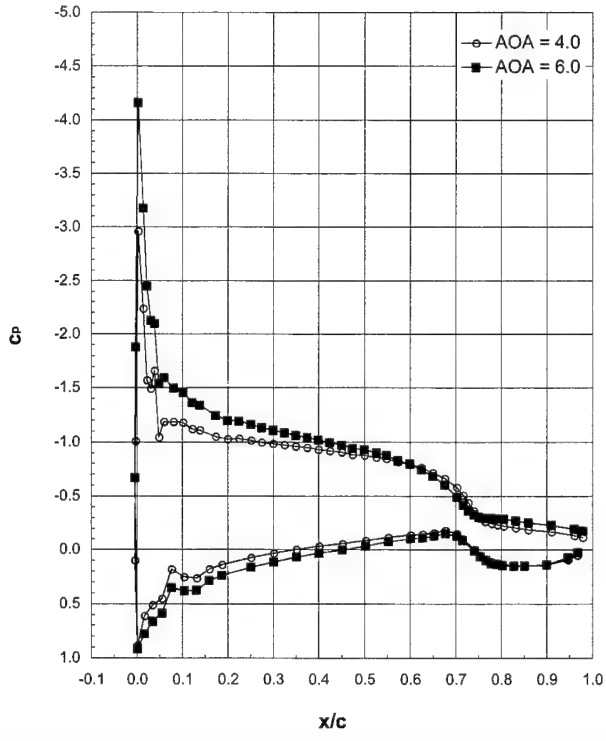

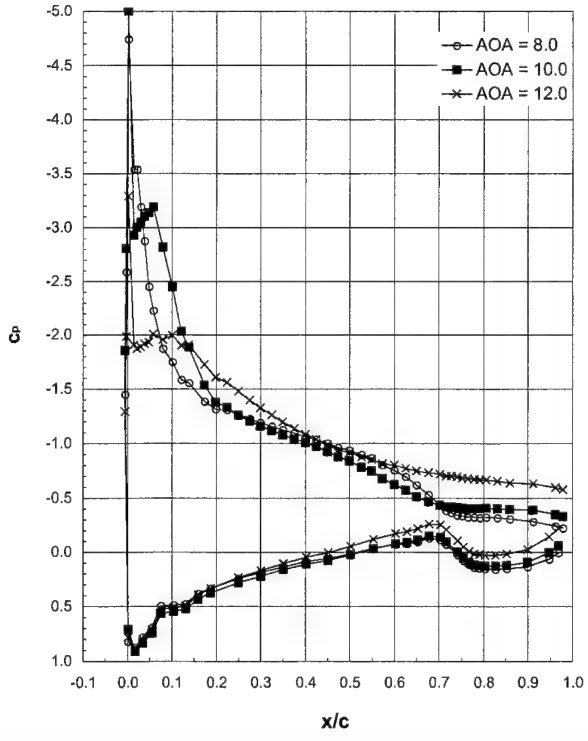

Run 309, Ma = 0.21, Re = 4.6x10^6

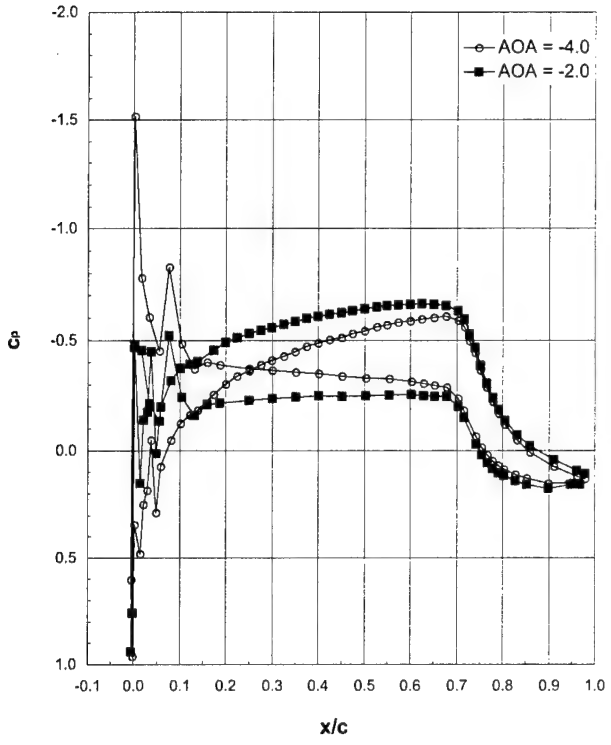

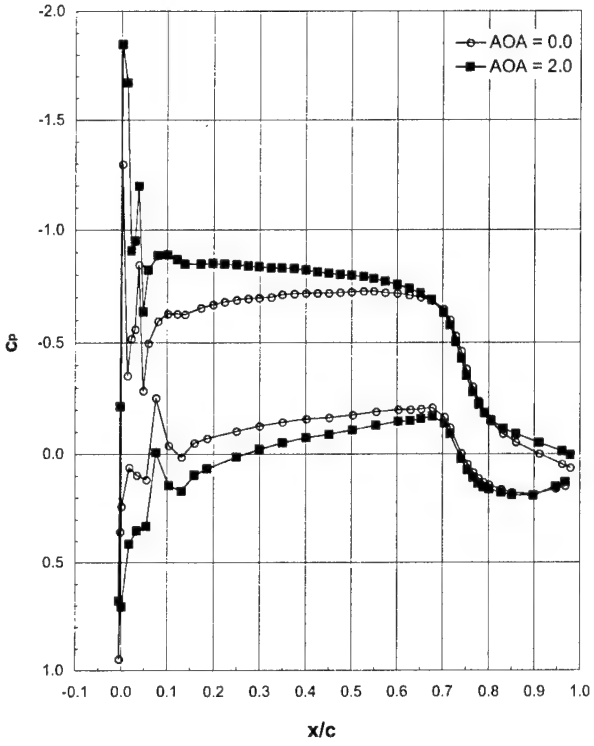

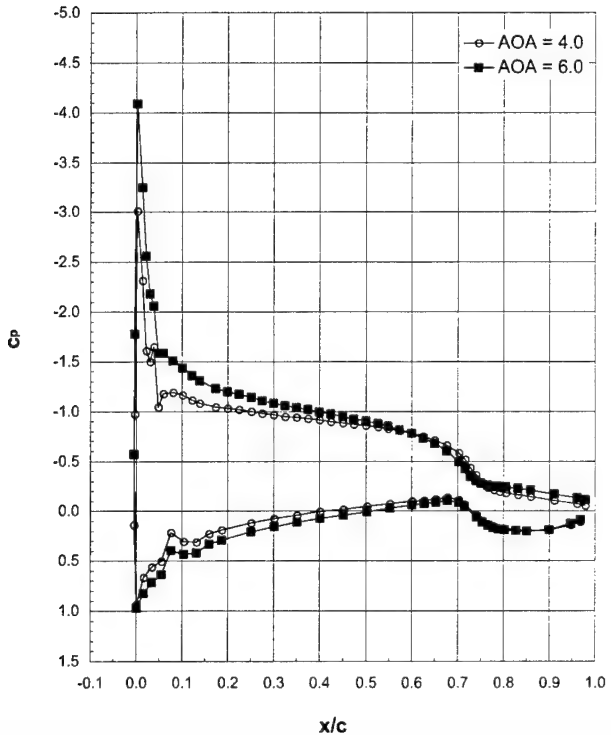

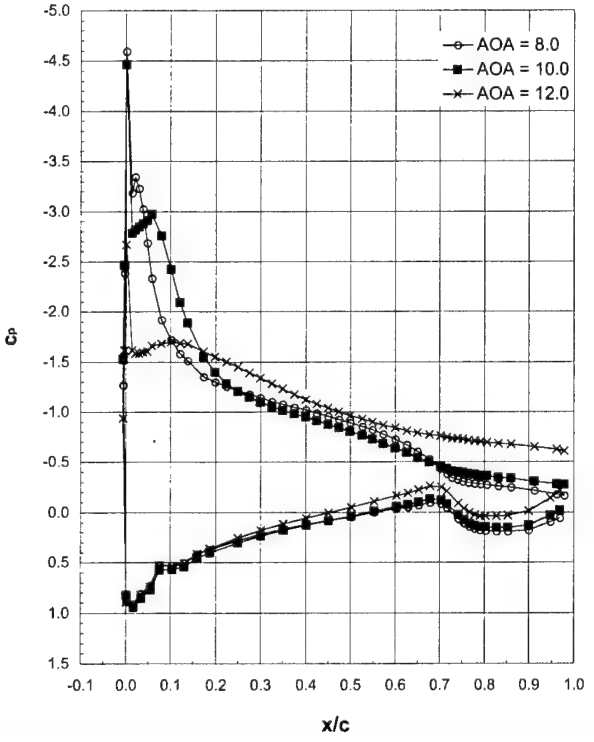

Run 310, Ma = 0.05, Re = 1x10^6

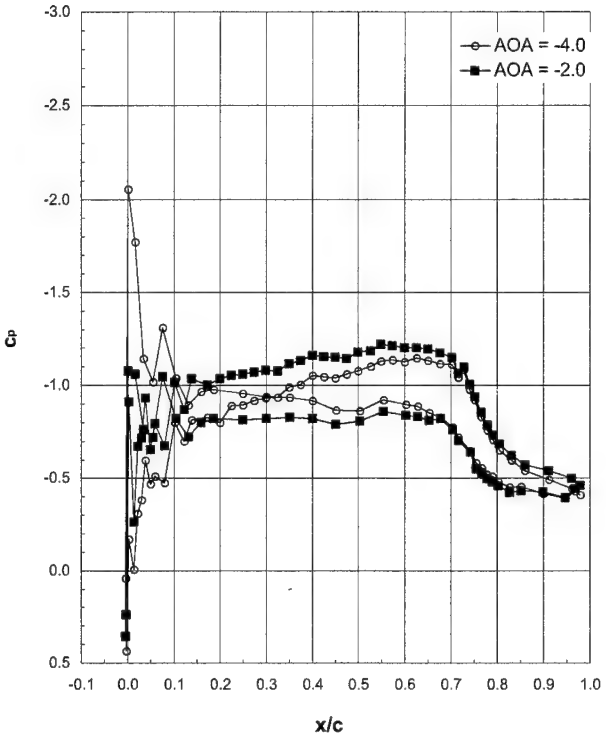

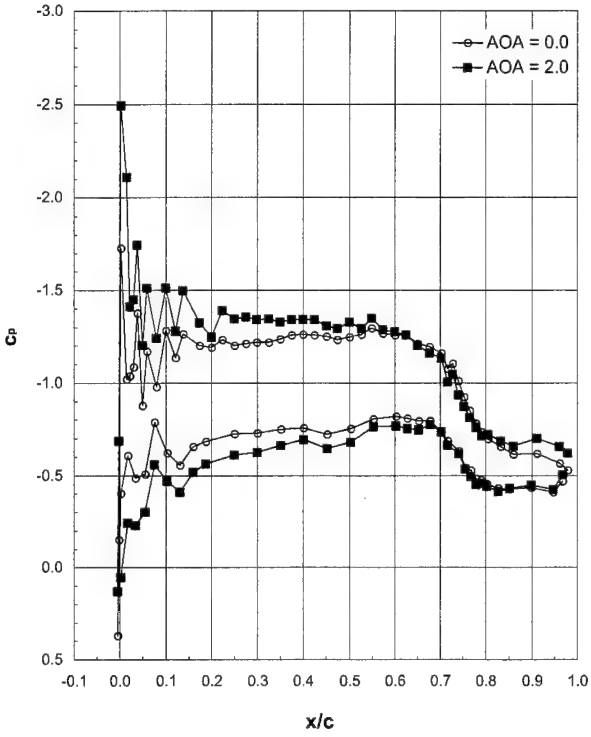

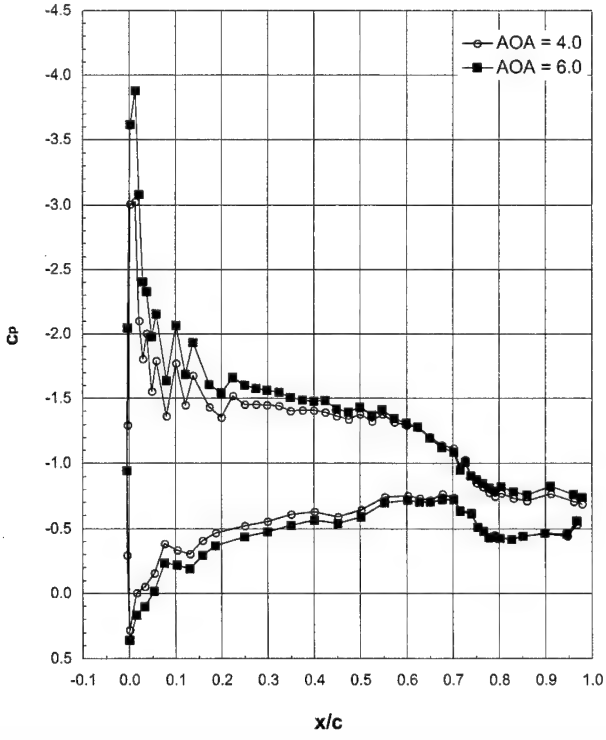

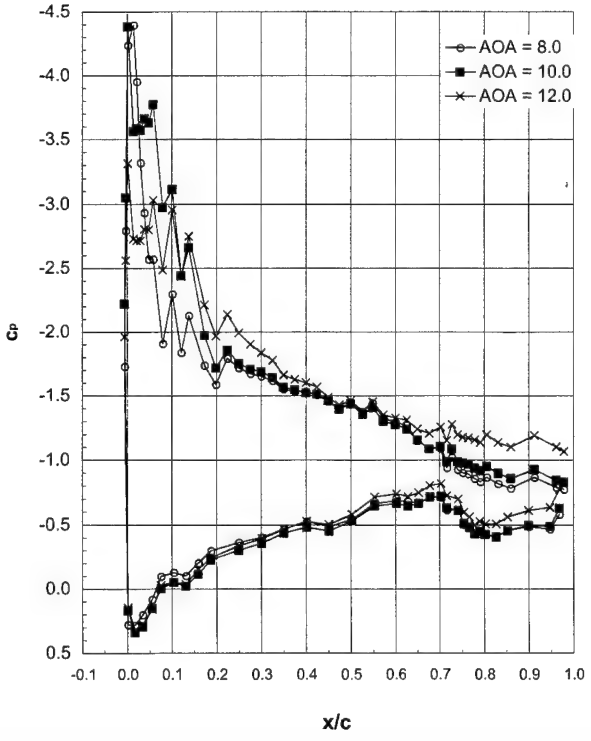

LTPT
General Aviation - Ice Shape 622-3D (Casting)

Ice Shape formed at:

T_t = -2.8°C (26.4°F)
T_s = -5.0°C (22.0°F)
V = 66.9 m/s (130 kts)
AOA = 0.3°

LWC = 0.54 g/m^3
MVD = 20 µm
Spray = 22.5 min
chord = 90 cm (36 in)

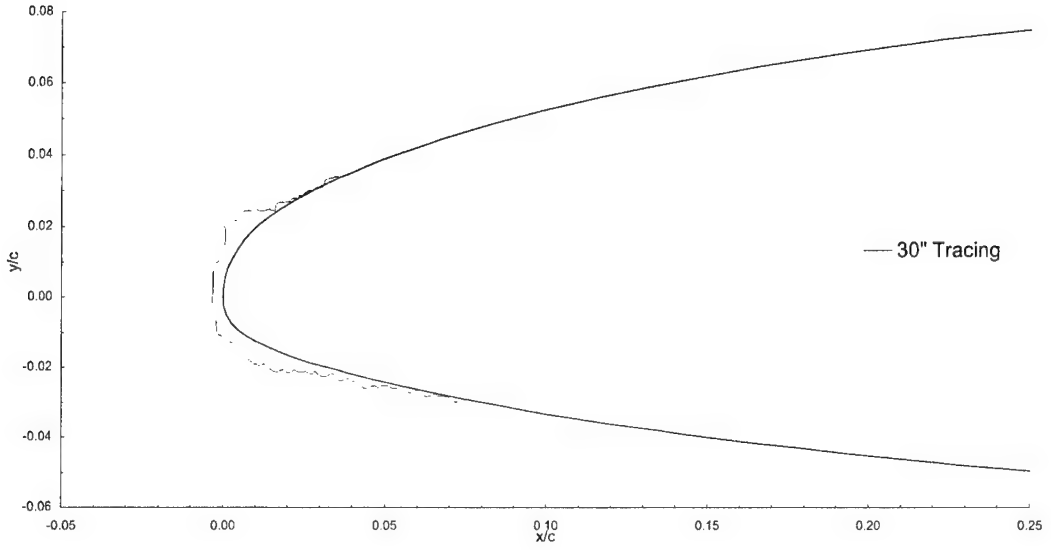

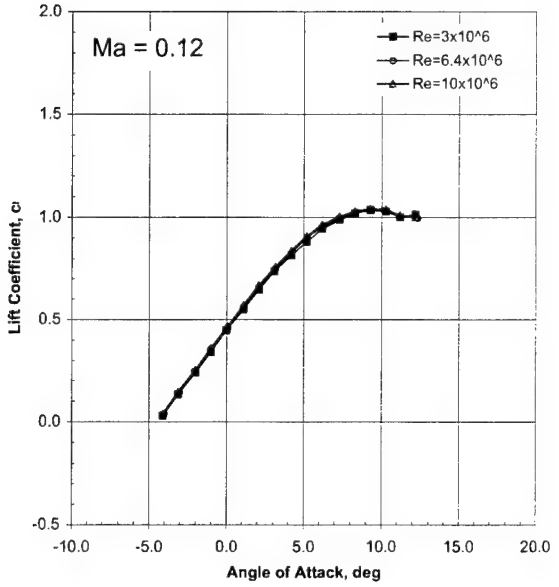

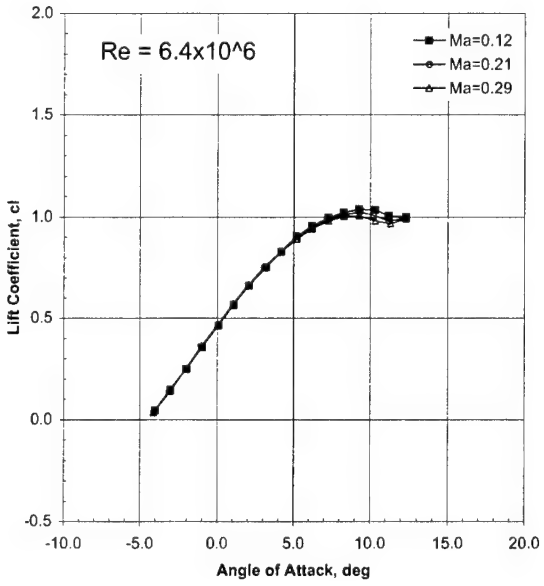

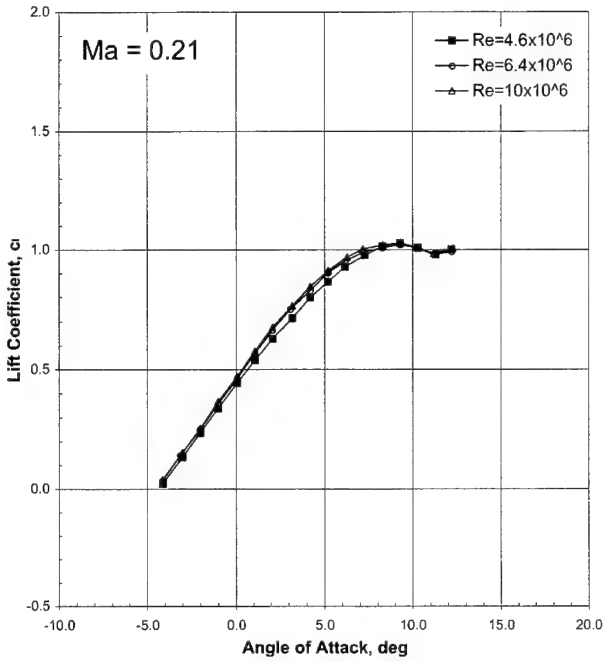

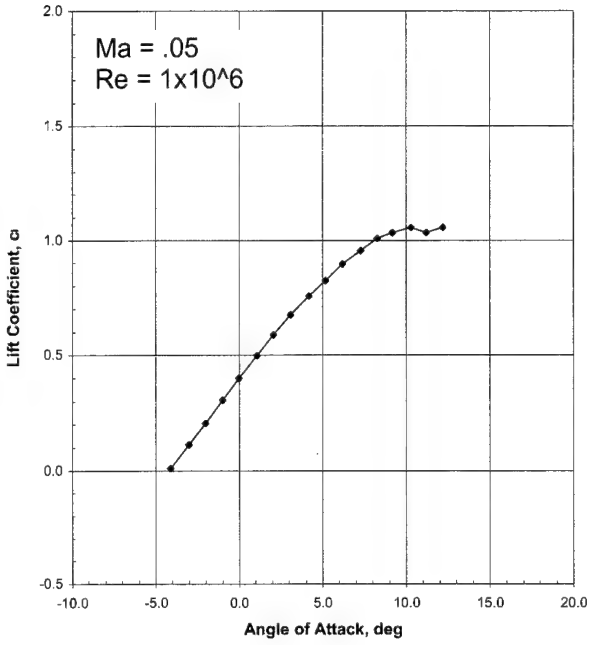

Drag Coefficients, c_d

	α = -2.0	α = 0.0	α = 2.1	α = 4.2	α = 6.2
Run 401, Ma = 0.12, Re = 10x10^6	0.0170	0.0133	0.0178	0.0305	0.0511
Run 402, Ma = 0.12, Re = 6.4x10^6	0.0183	0.0143	0.0188	0.0316	0.0528
Run 403, Ma = 0.21, Re = 4.6x10^6	0.0179	0.0138	0.0185	0.0317	0.0530
Run 404, Ma = 0.29, Re = 6.4x10^6	0.0197	0.0156	0.0200	0.0329	0.0542
Run 406, Ma = 0.21, Re = 10x10^6	0.0173	0.0132	0.0180	0.0316	0.0541
Run 407, Ma = 0.21, Re = 6.4x10^6	0.0184	0.0142	0.0189	0.0321	0.0541
Run 409, Ma = 0.12, Re = 3x10^6	0.0198	0.0158	0.0201	0.0327	0.0532
Run 410, Ma = 0.05, Re = 1x10^6	*0.0033*	*0.0029*	*0.0026*	*0.0026*	*0.0030*

Italicized font indicates force balance data

Run 401, Ma = 0.12, Re = 10x10^6

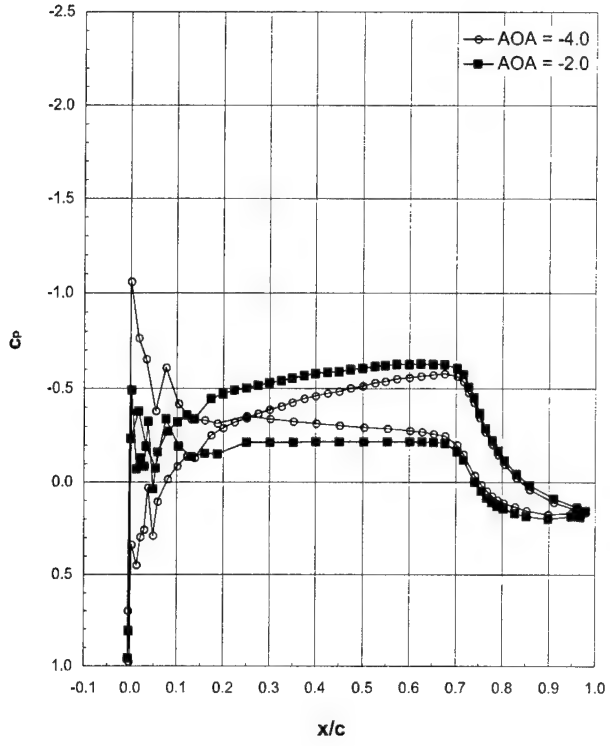

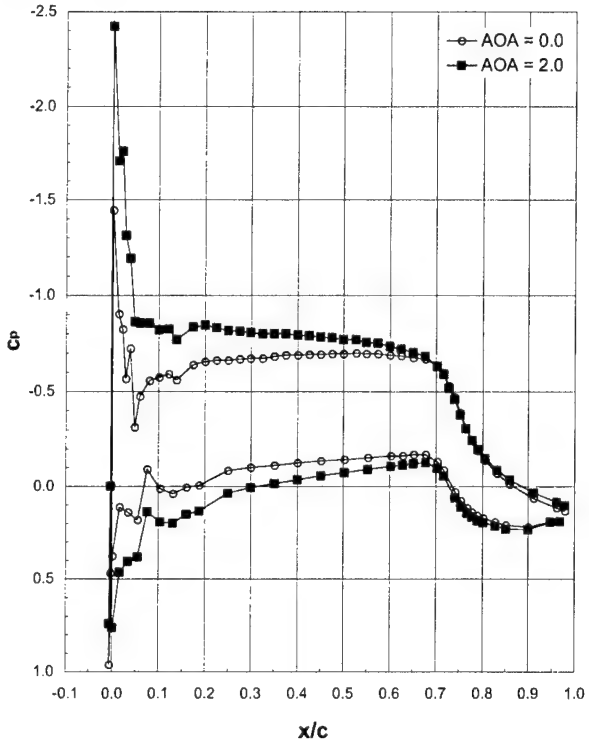

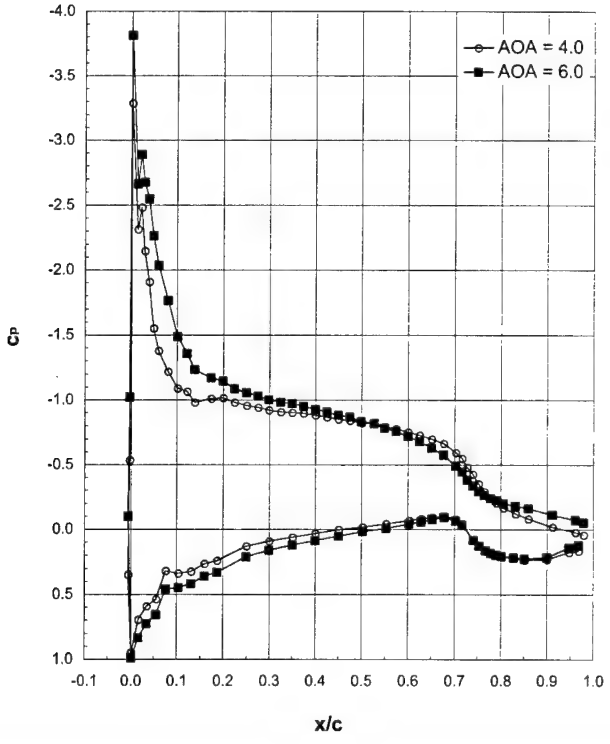

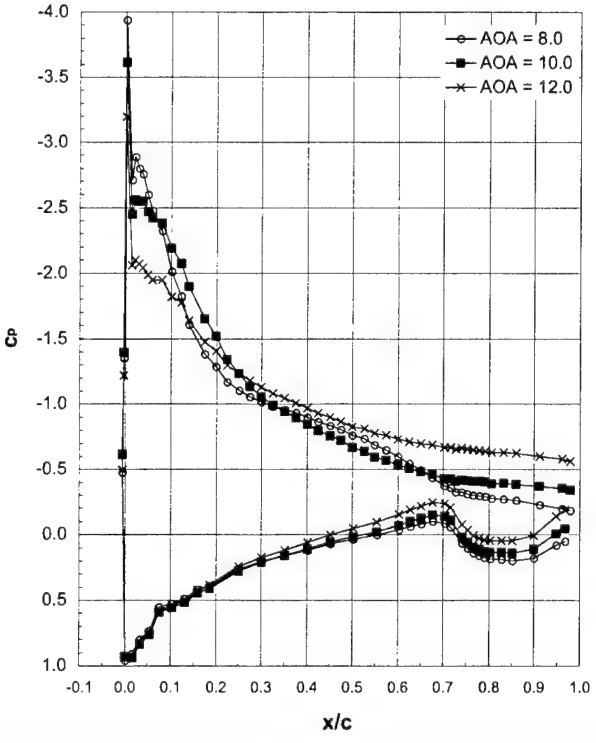

Run 402, Ma = 0.12, Re = 6.4x10^6

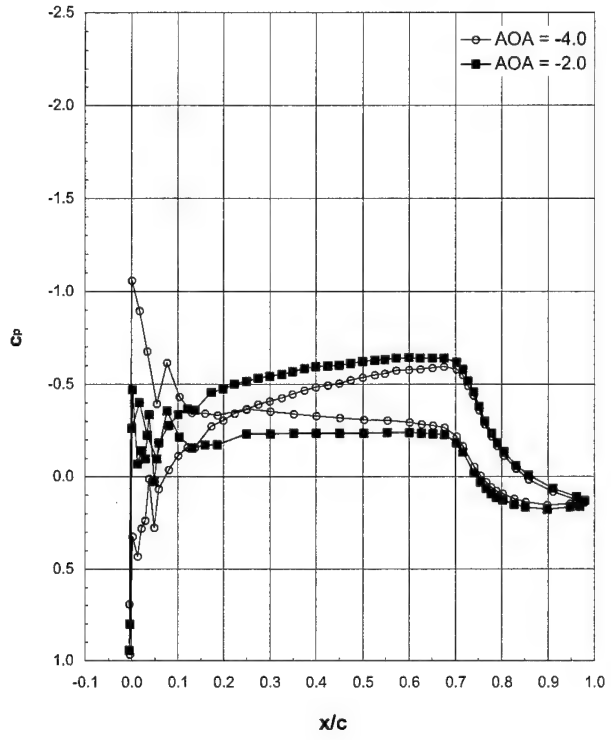

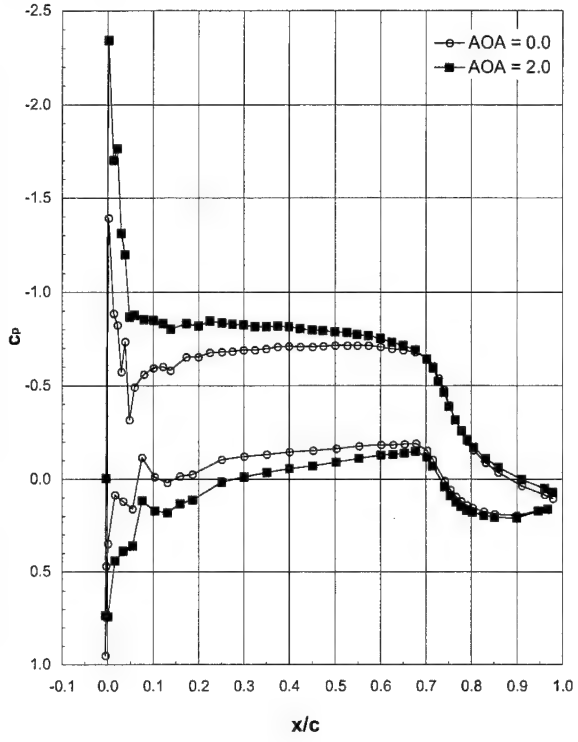

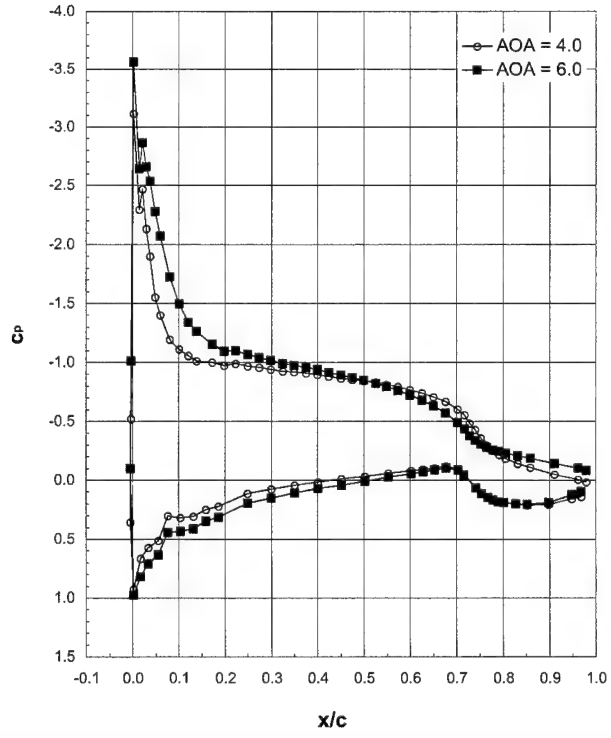

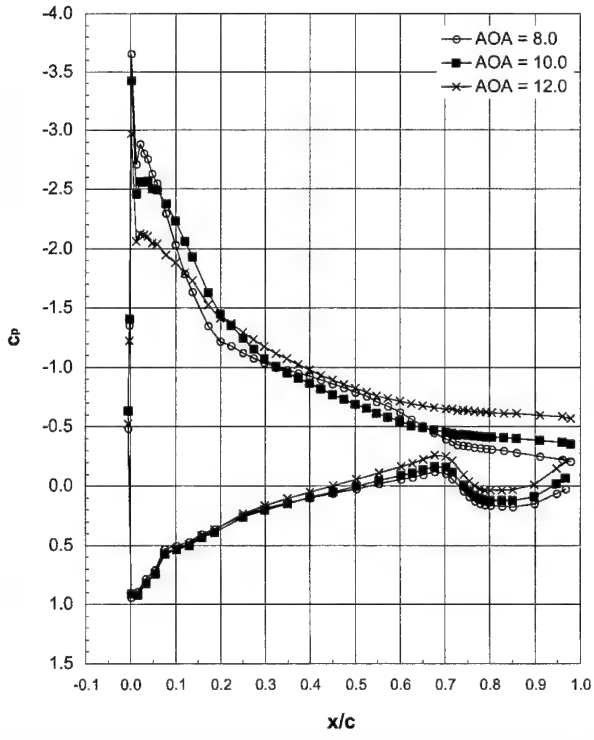

Run 403, Ma = 0.21, Re = 4.6x10^6

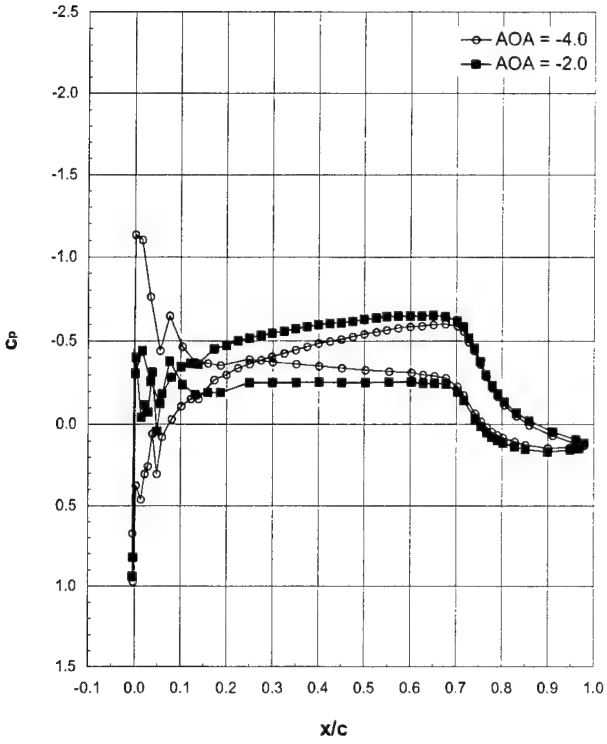

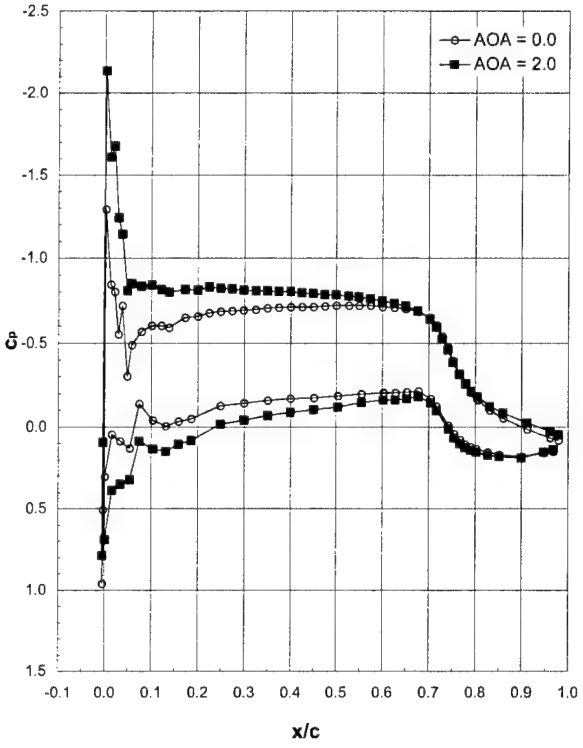

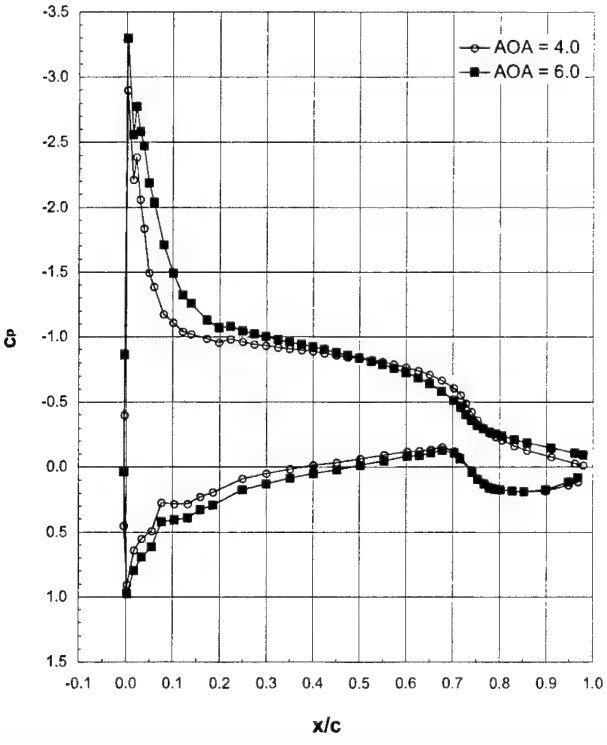

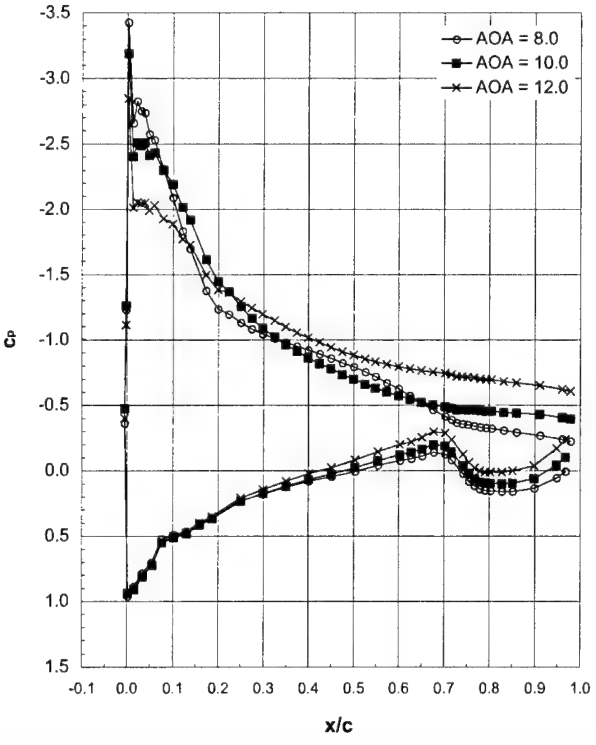

Run 404, Ma = 0.29, Re = 6.4x10^6

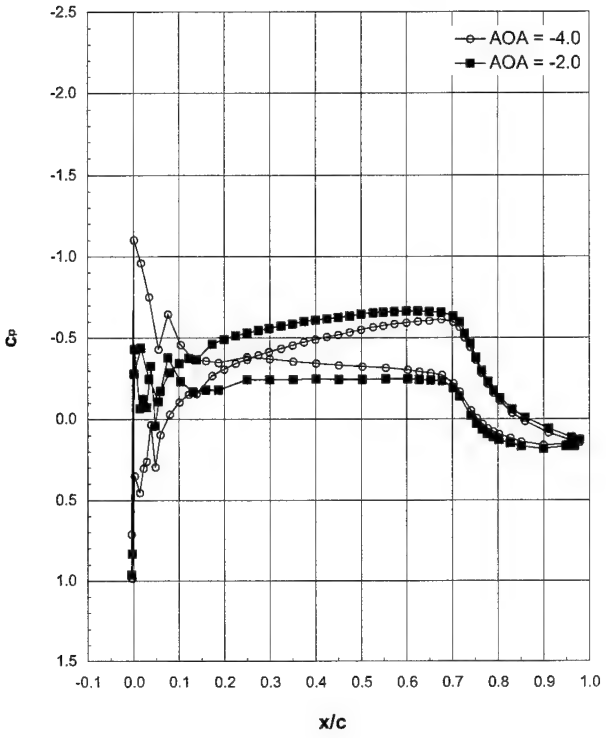

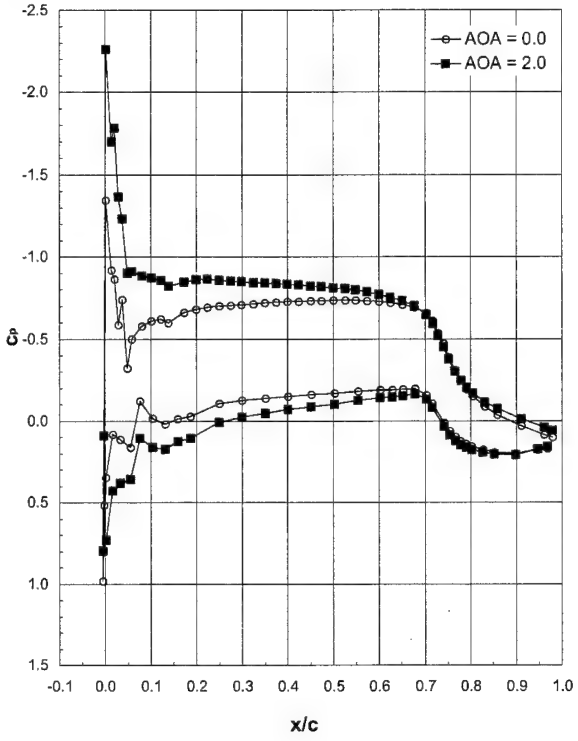

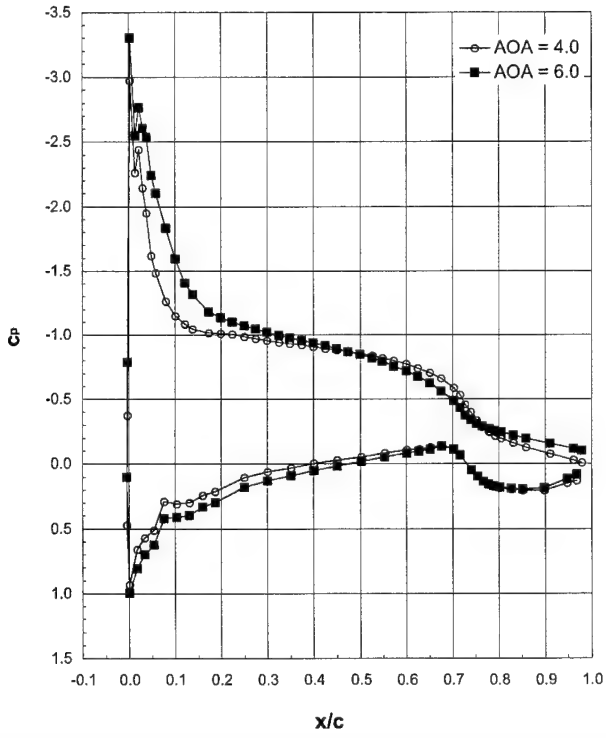

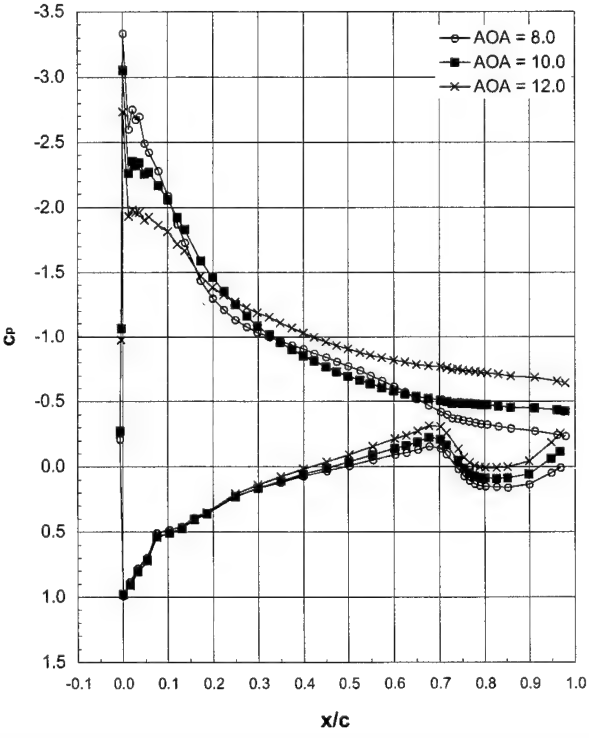

Run 406, Ma = 0.21, Re = 10x10^6

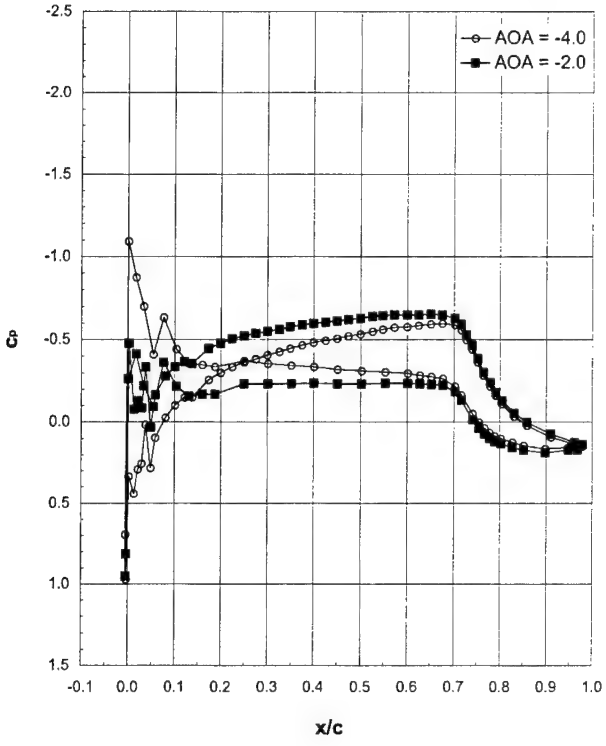

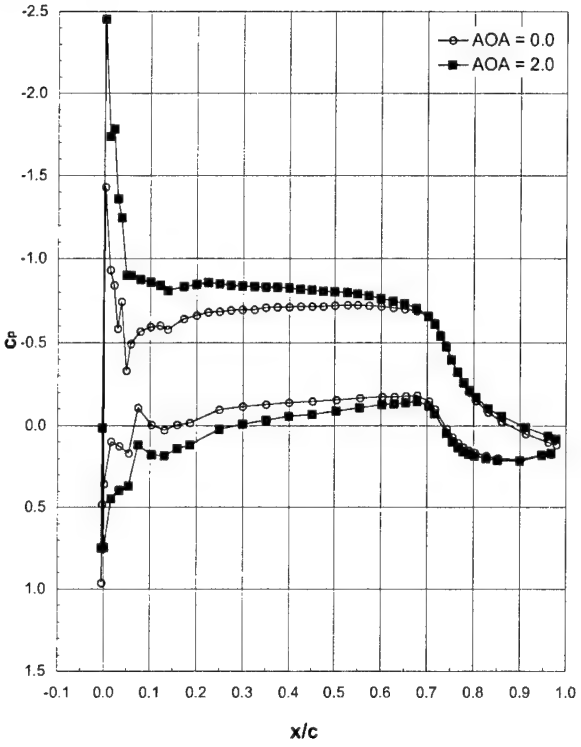

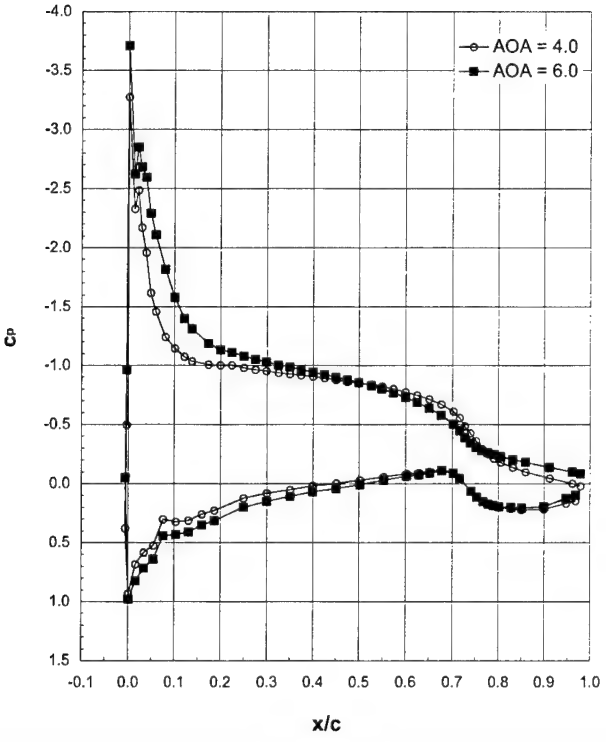

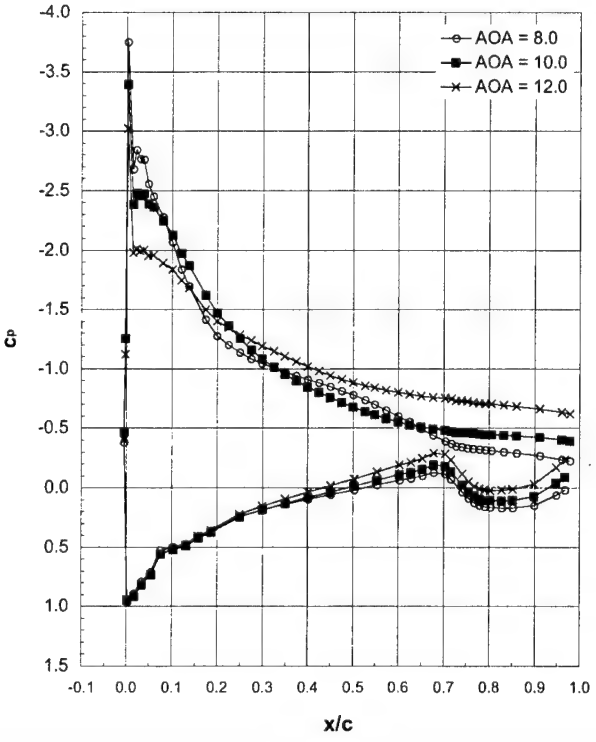

Run 407, Ma = 0.21, Re = 6.4x10^6

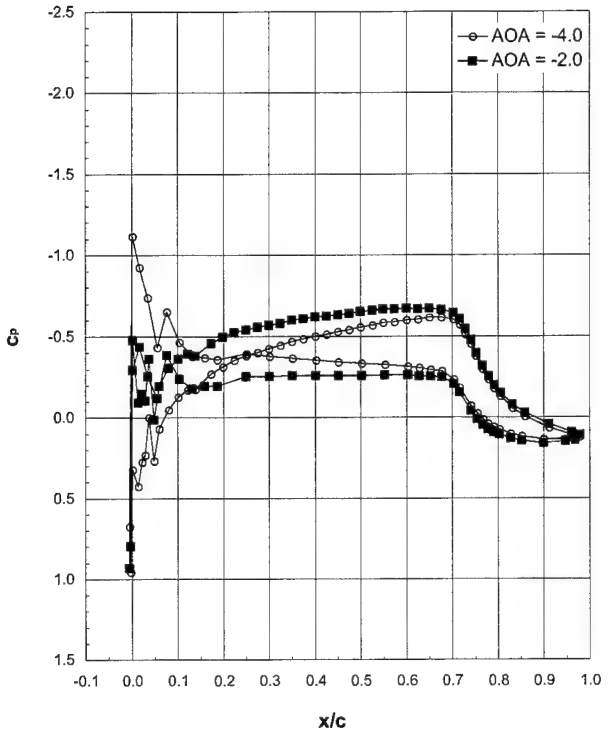

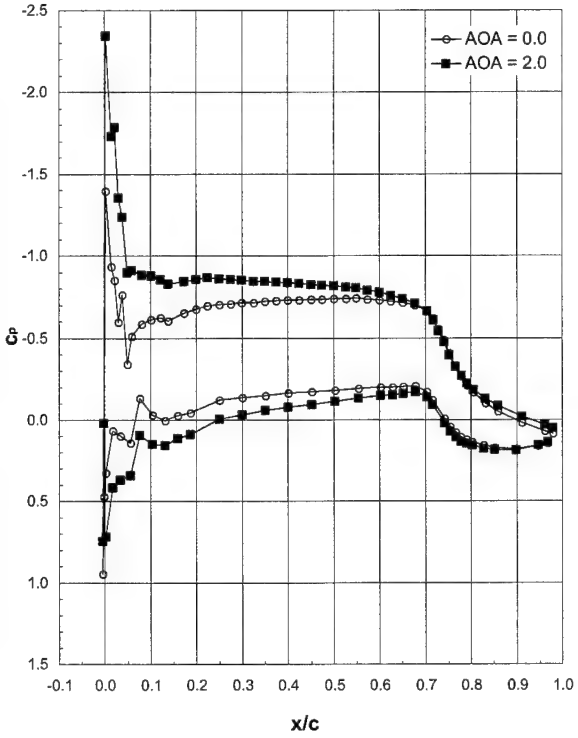

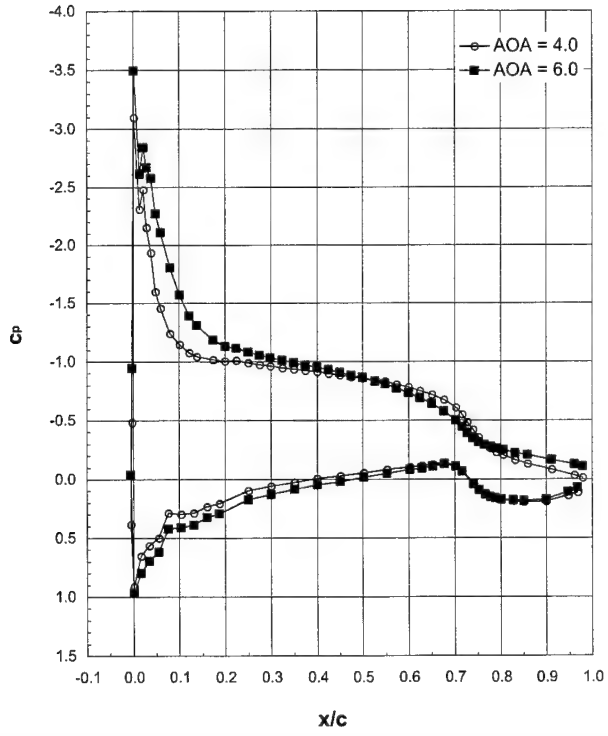

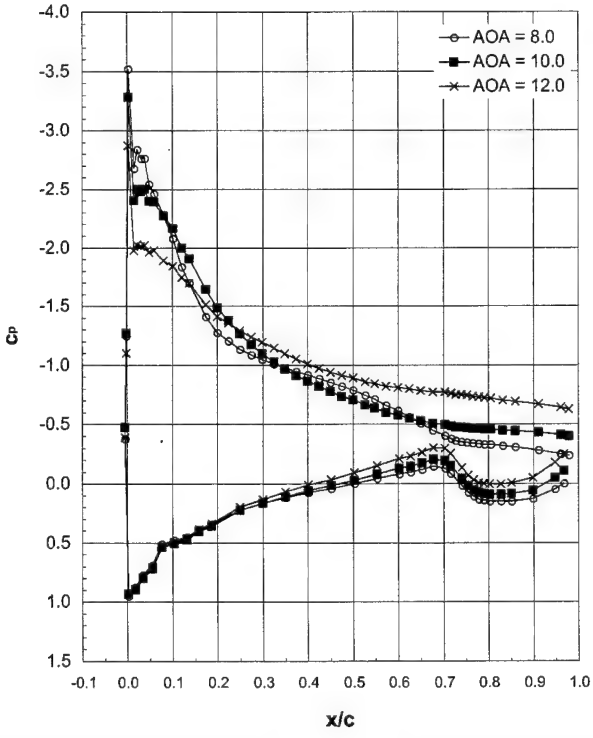

Run 409, Ma = 0.12, Re = 3x10^6

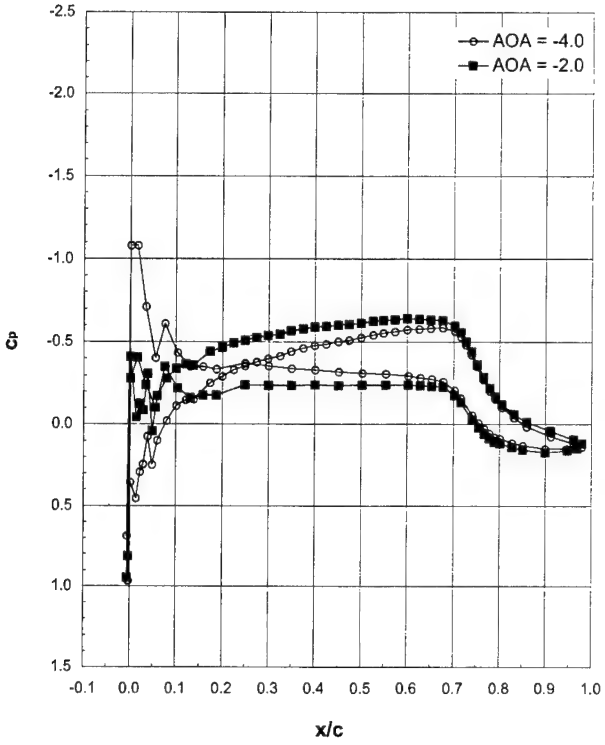

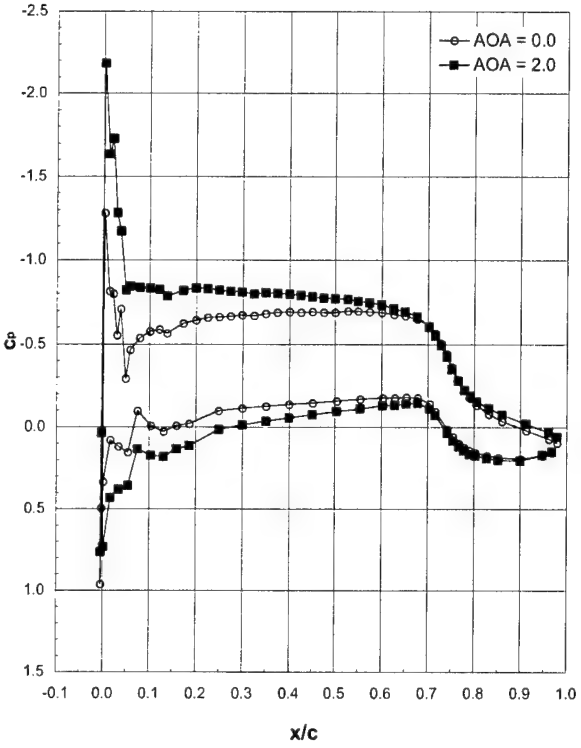

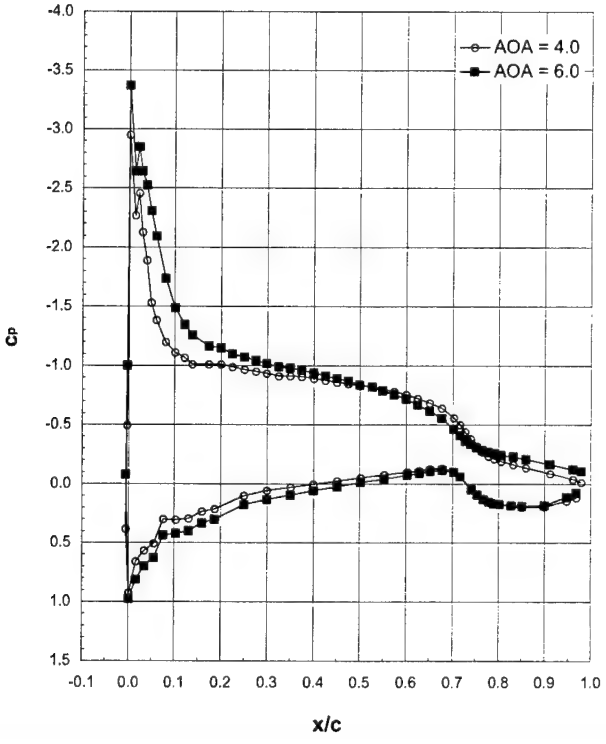

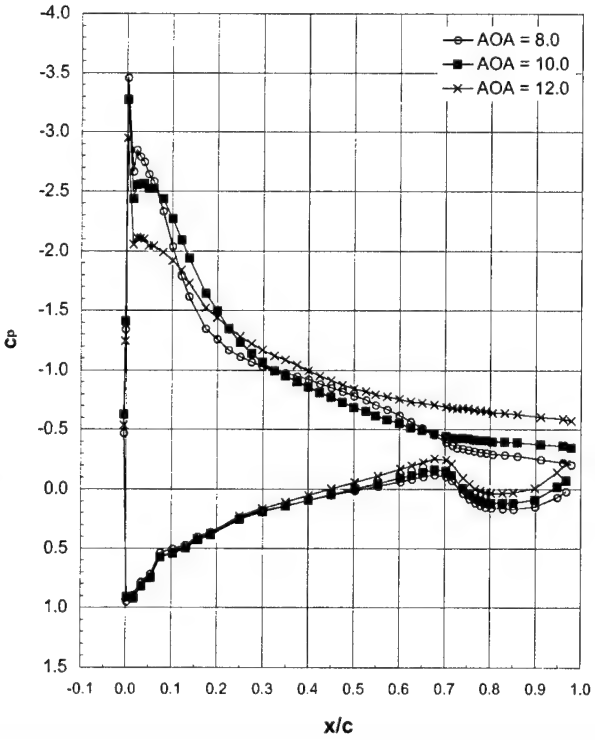

Run 410, Ma = 0.05, Re = 1x10^6

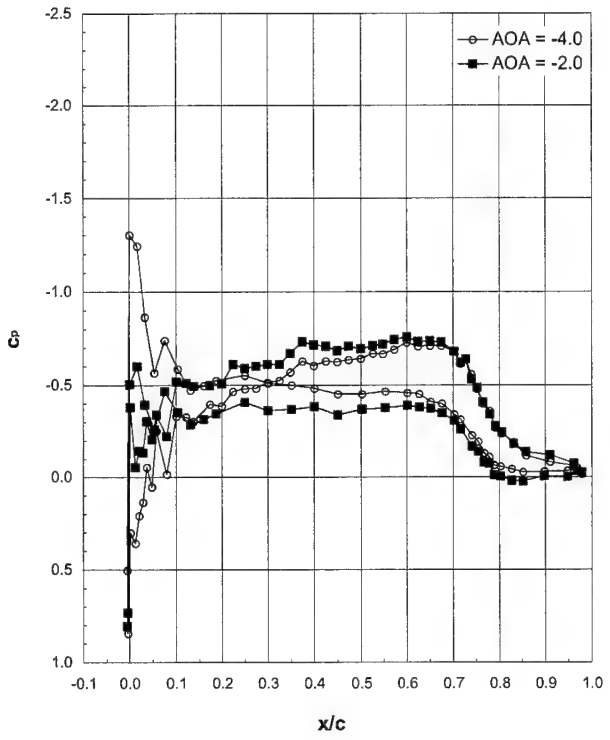

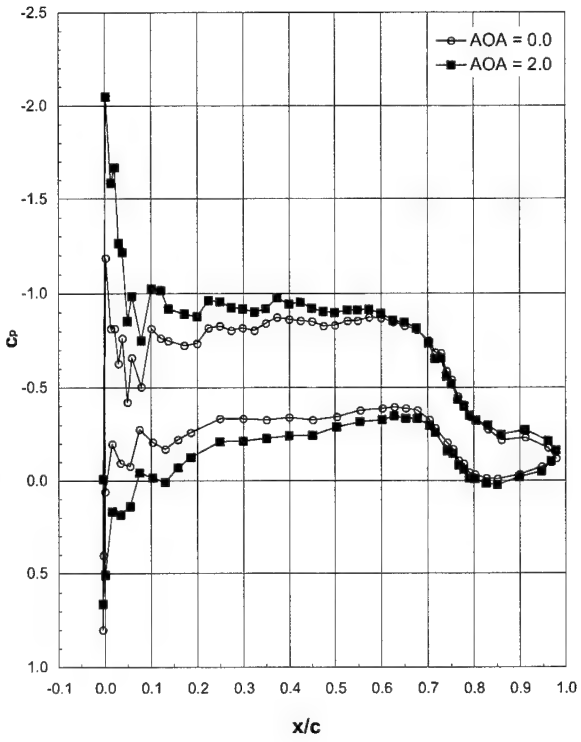

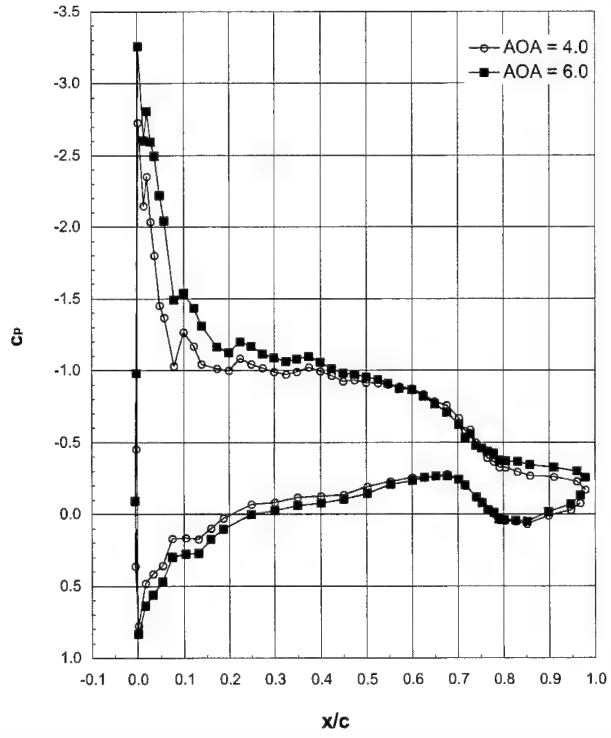

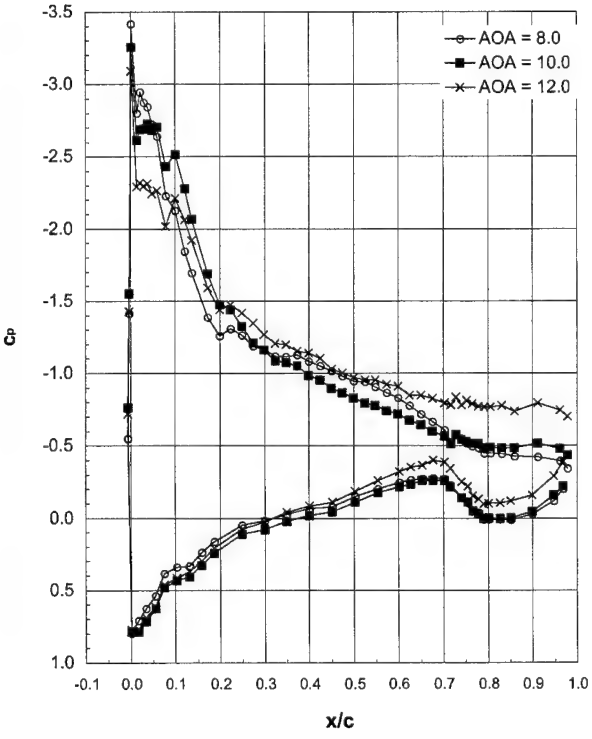

LTPT
General Aviation - Ice Shape 621-2D (SLA)

Ice Shape formed at:

T_t = -2.8°C (26.4°F)
T_s = -5.0°C (22.0°F)
V = 66.9 m/s (130 kts)
AOA = 0.4°

LWC = 0.54 g/m^3
MVD = 20 μm
Spray = 2.0 min
chord = 90 cm (36 in)

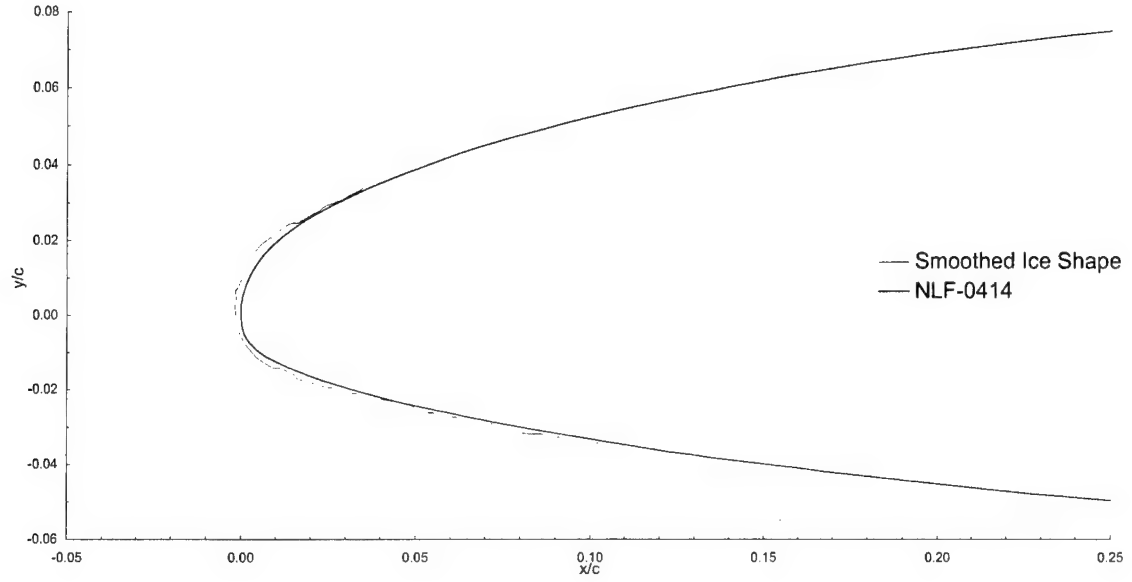

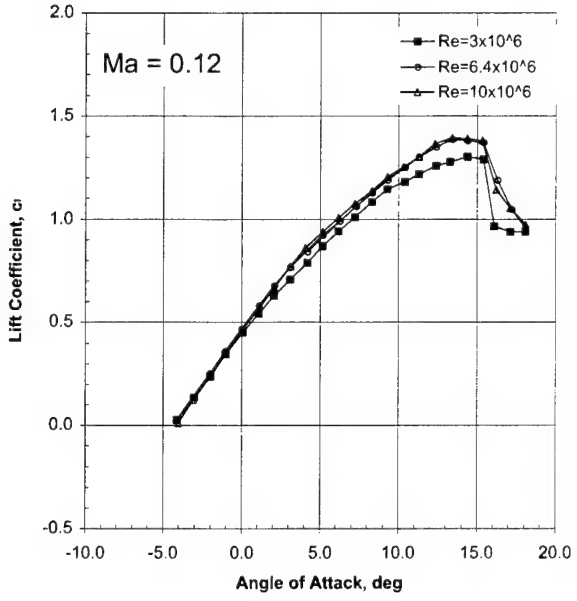

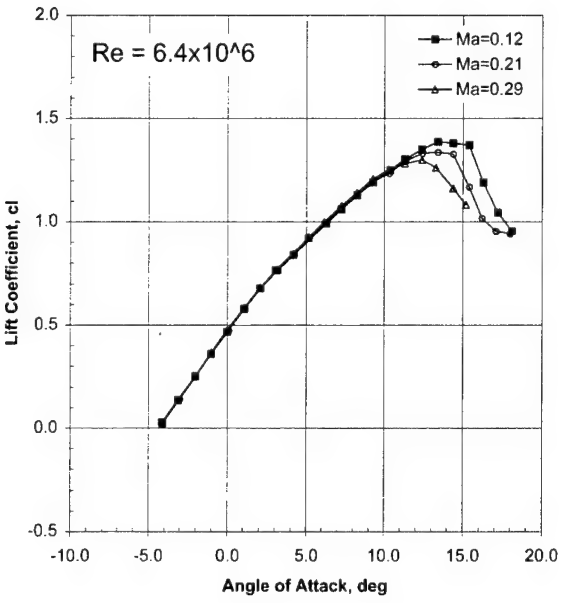

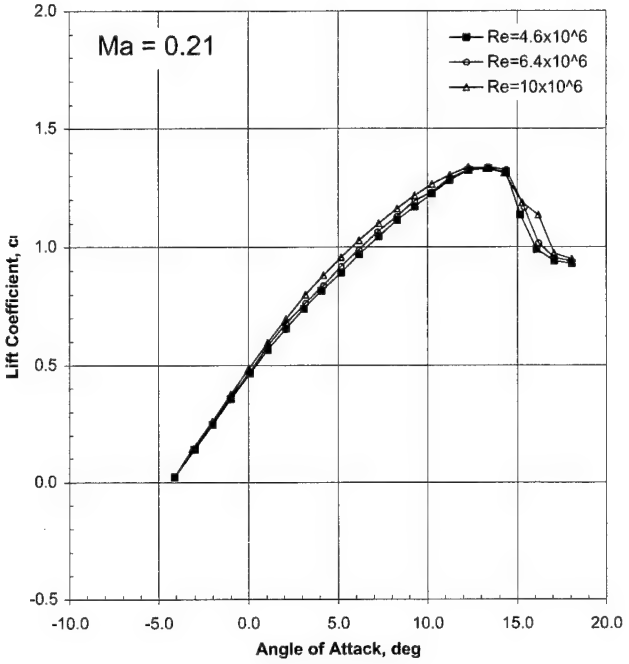

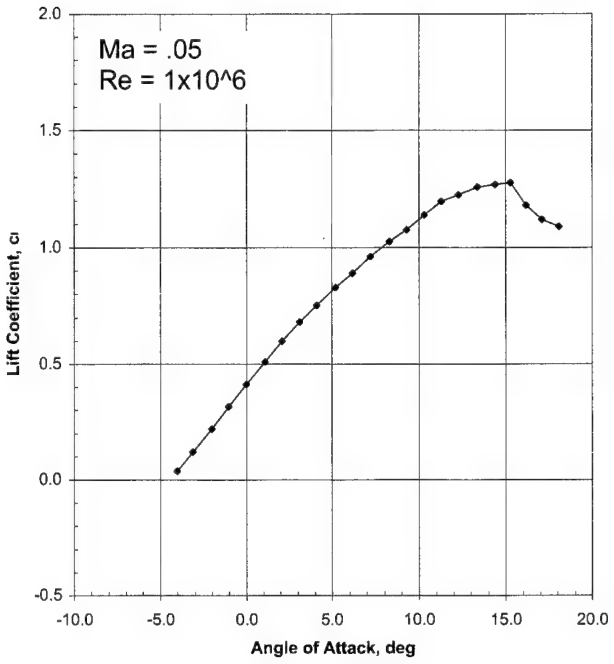

Drag Coefficients, c_d

	α = -2.0	α = 0.0	α = 2.1	α = 4.2	α = 6.2
Run 501, Ma = 0.12, Re = 10x10^6	0.0104	0.0092	0.0104	0.0141	0.0200
Run 502, Ma = 0.12, Re = 6.4x10^6	0.0138	0.0125	0.0135	0.0160	0.0209
Run 503, Ma = 0.21, Re = 10x10^6	0.0114	0.0101	0.0113	0.0151	0.0213
Run 504, Ma = 0.21, Re = 4.6x10^6	0.0181	0.0166	0.0171	0.0198	0.0247
Run 505, Ma = 0.29, Re = 6.4x10^6	0.0172	0.0153	0.0162	0.0197	0.0258
Run 507, Ma = 0.21, Re = 6.4x10^6	0.0154	0.0137	0.0145	0.0176	0.0232
Run 508, Ma = 0.12, Re = 3x10^6	0.0200	0.0183	0.0187	0.0212	0.0259
Run 510, Ma = 0.05, Re = 1x10^6	*0.0452*	*0.0361*	*0.0290*	*0.0241*	*0.0209*

Italicized font indicates force balance data

Run 501, Ma = 0.12, Re = 10x10^6

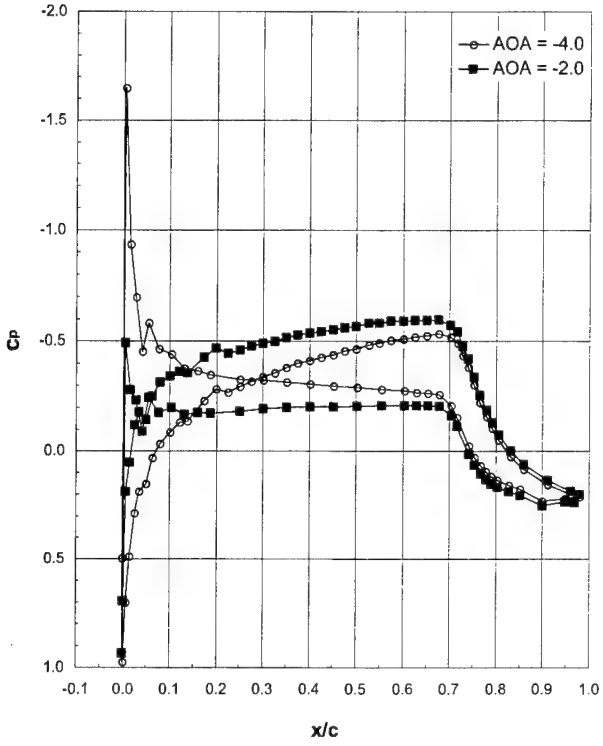

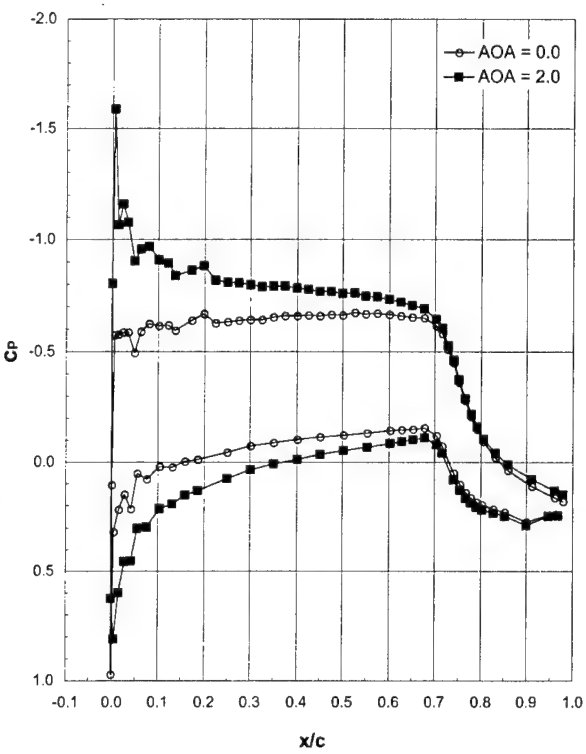

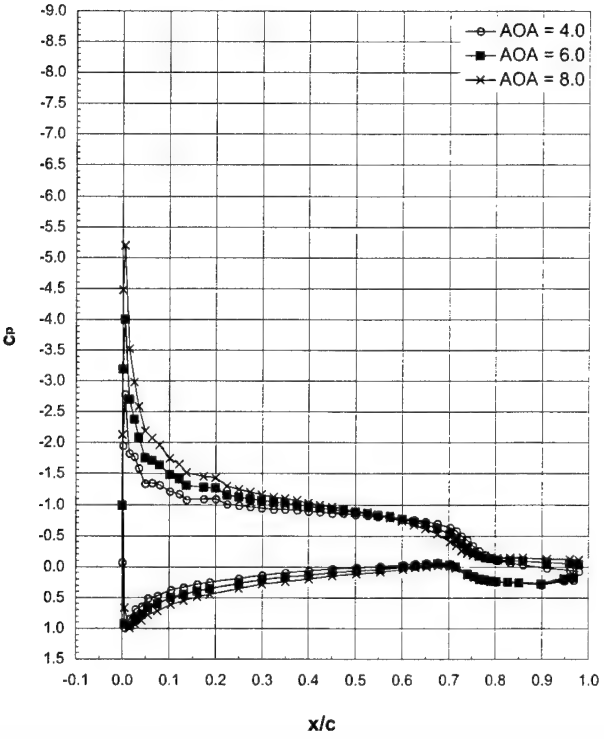

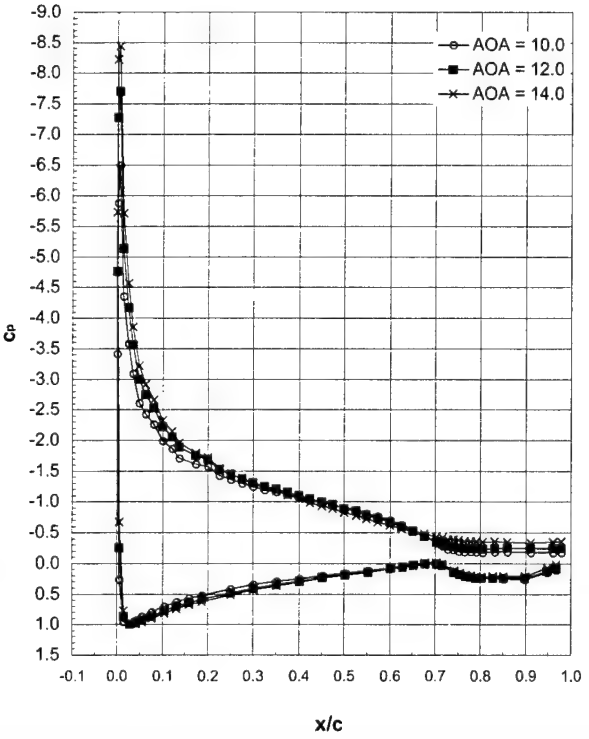

Run 502, Ma = 0.12, Re = 6.4x10^6

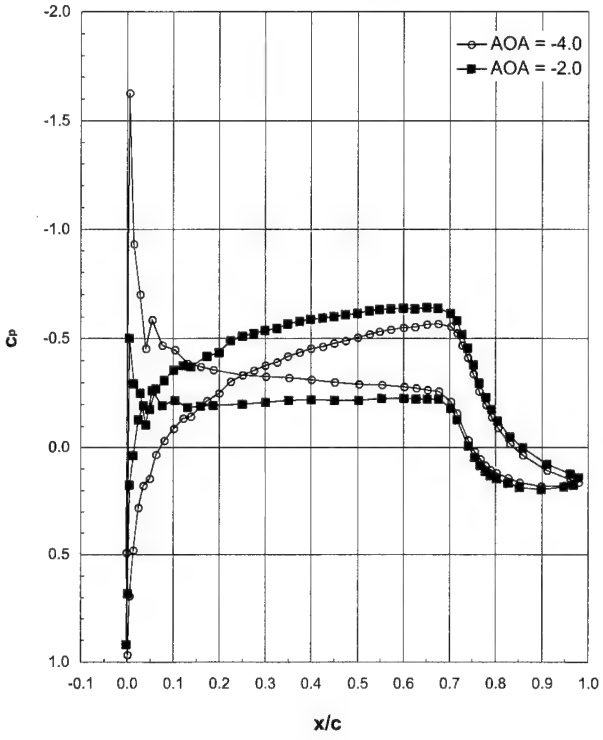

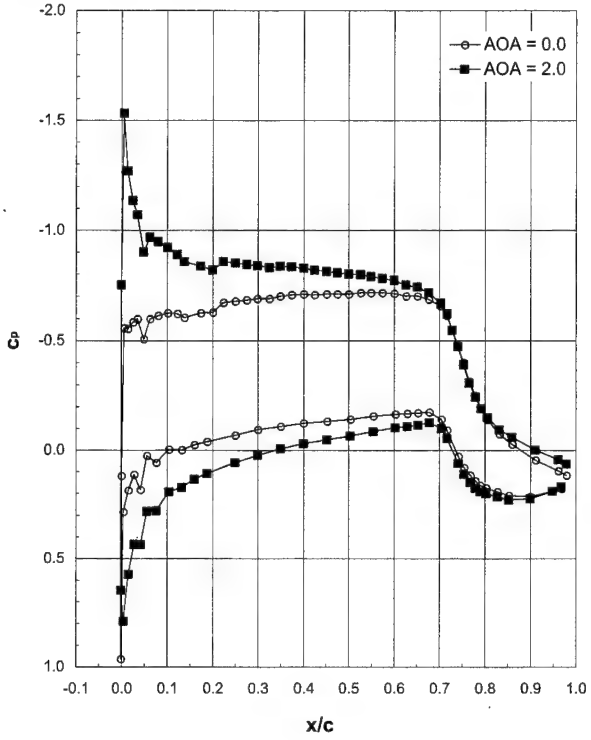

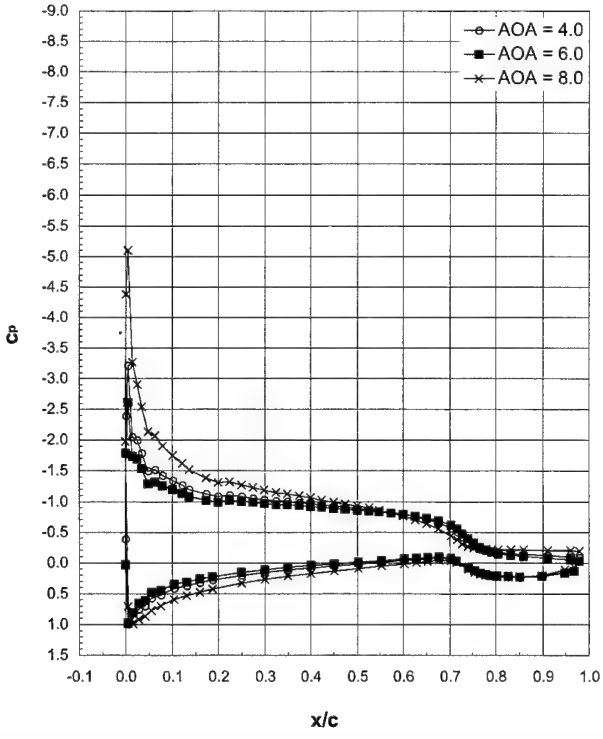

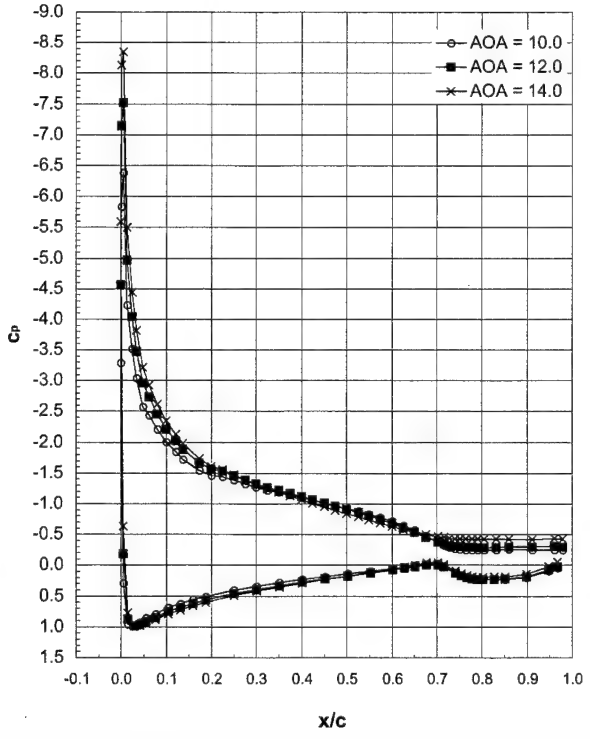

Run 503, Ma = 0.21, Re = 10x10^6

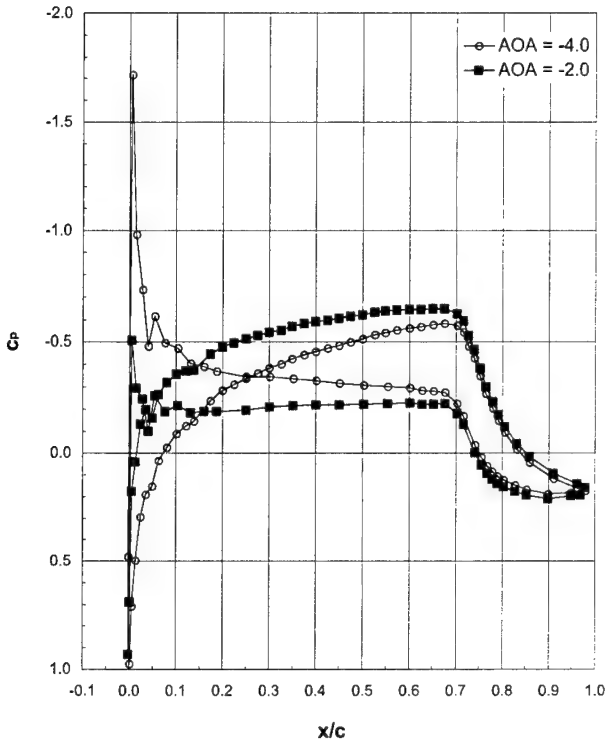

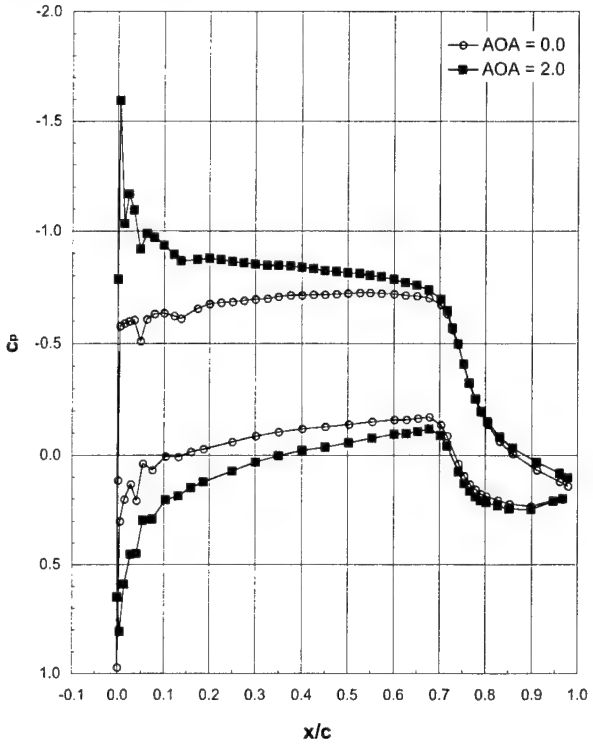

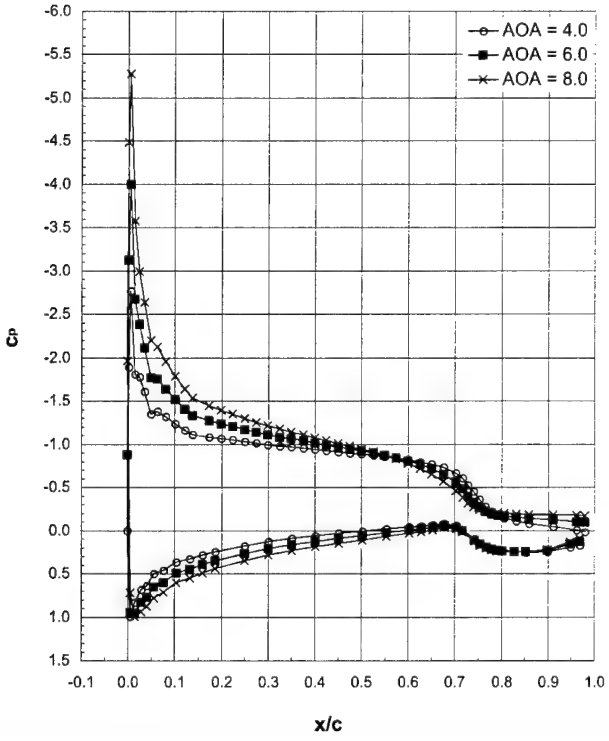

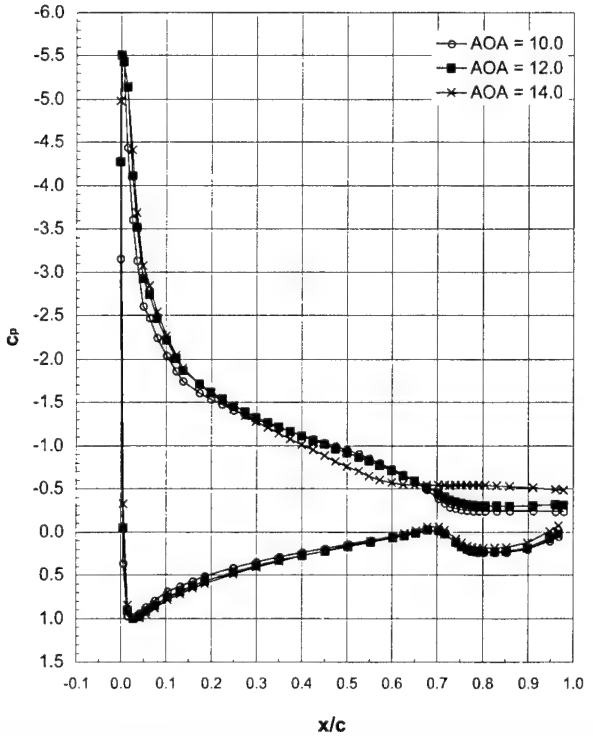

Run 504, Ma = 0.21, Re = 4.6x10^6

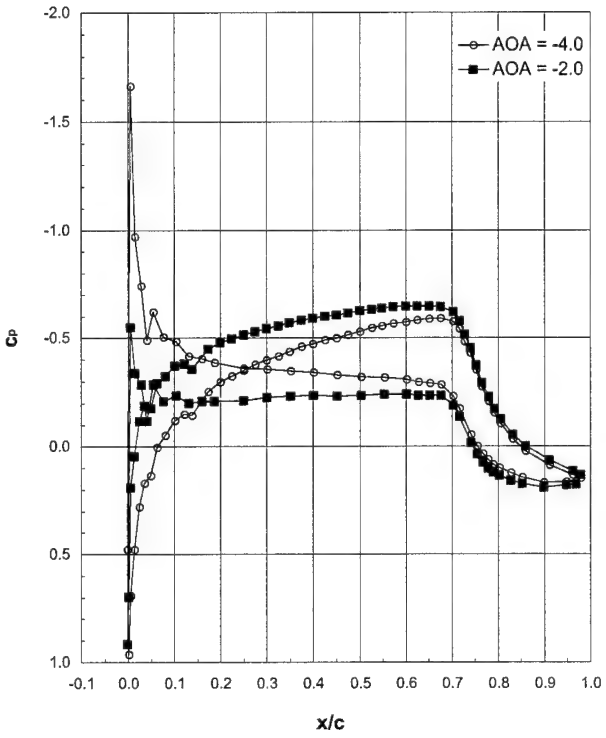

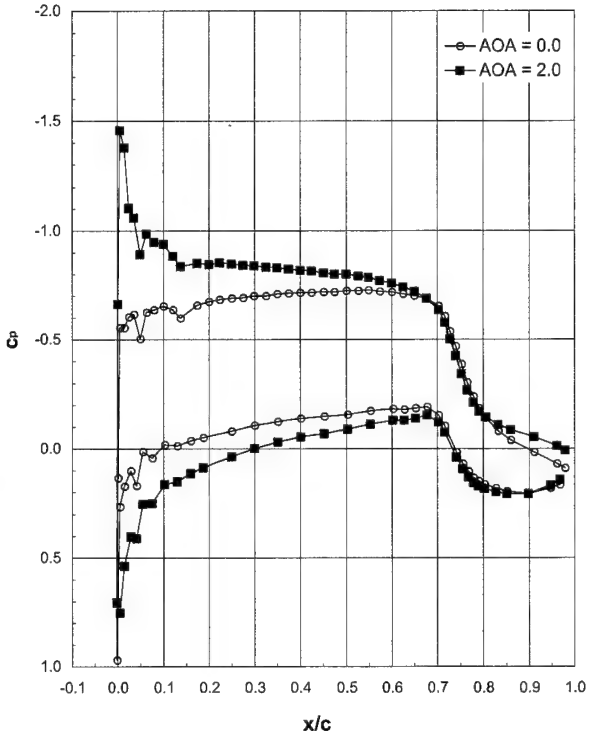

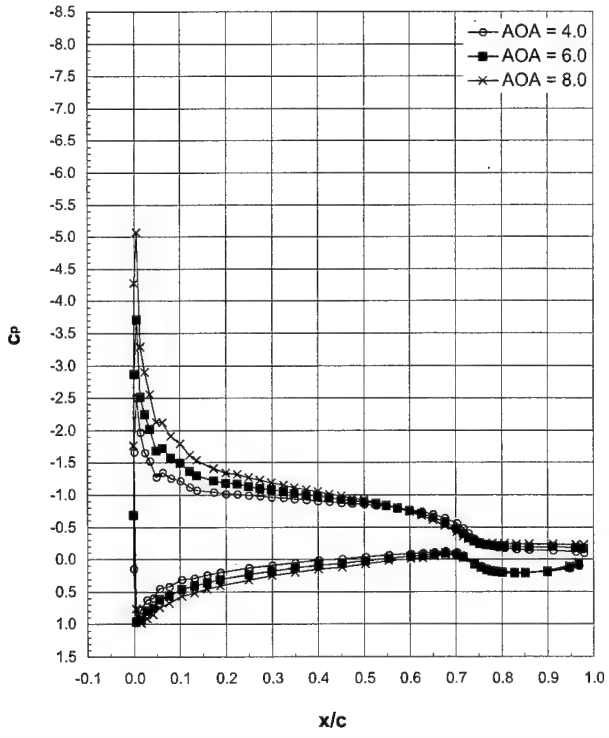

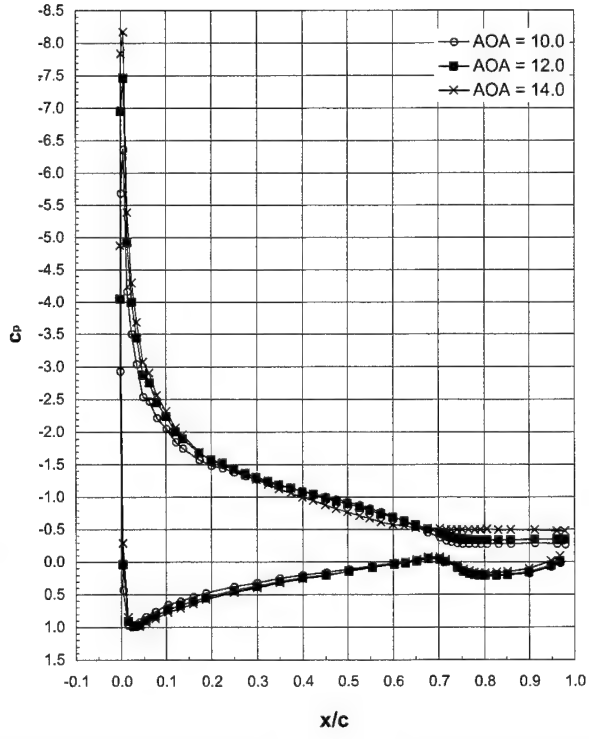

Run 505, Ma = 0.29, Re = 6.4x10^6

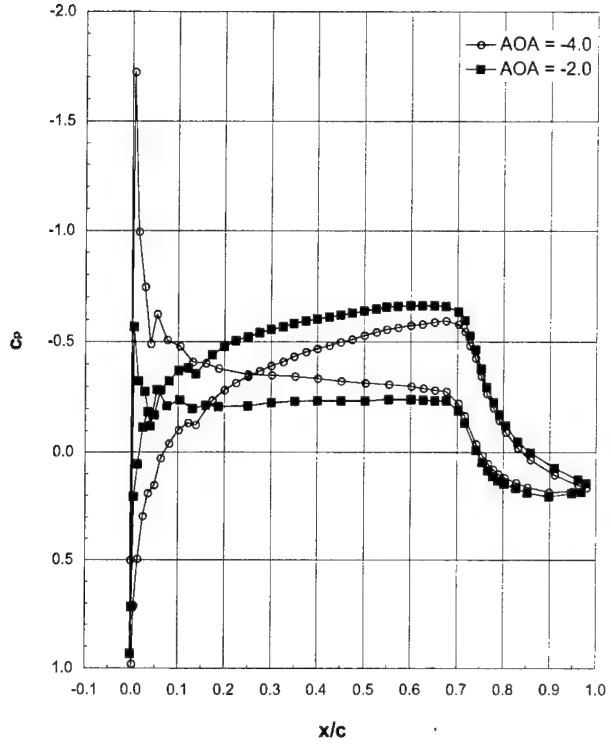

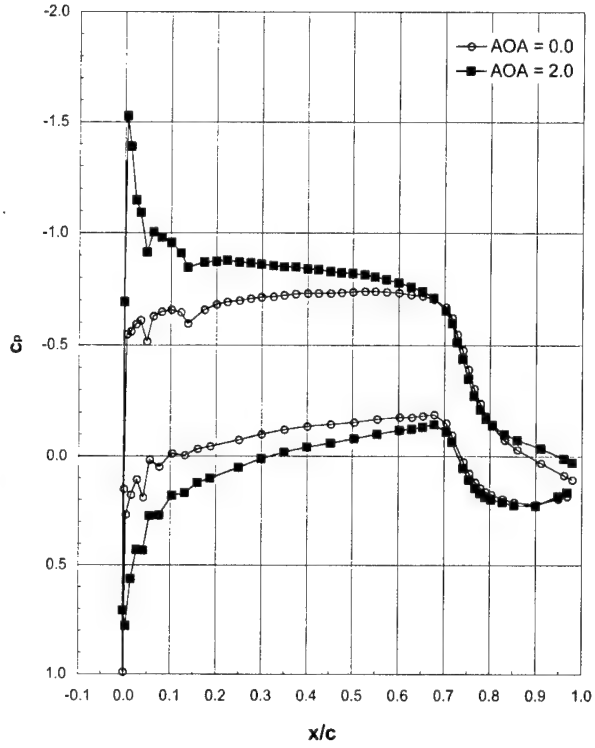

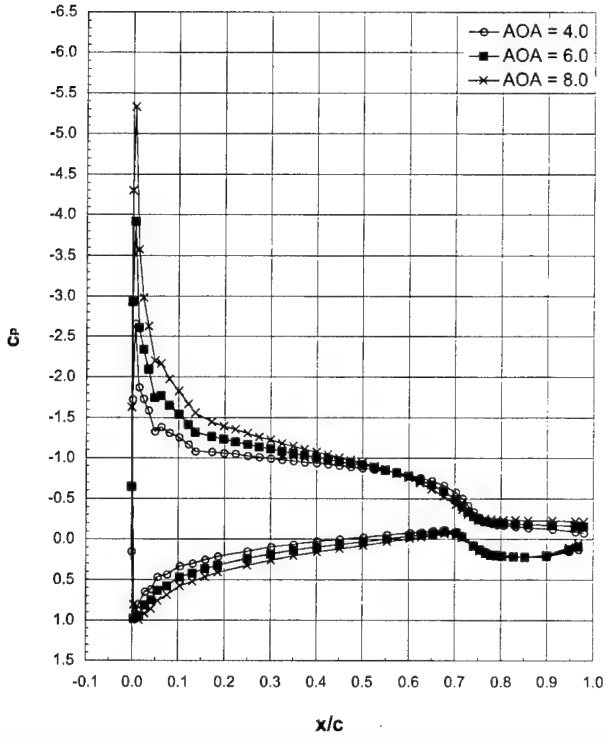

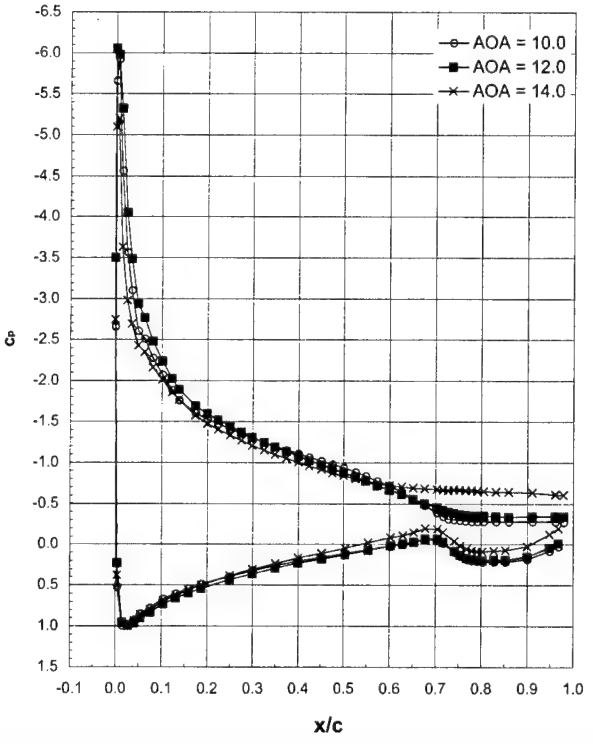

Run 507, Ma = 0.21, Re = 6.4x10^6

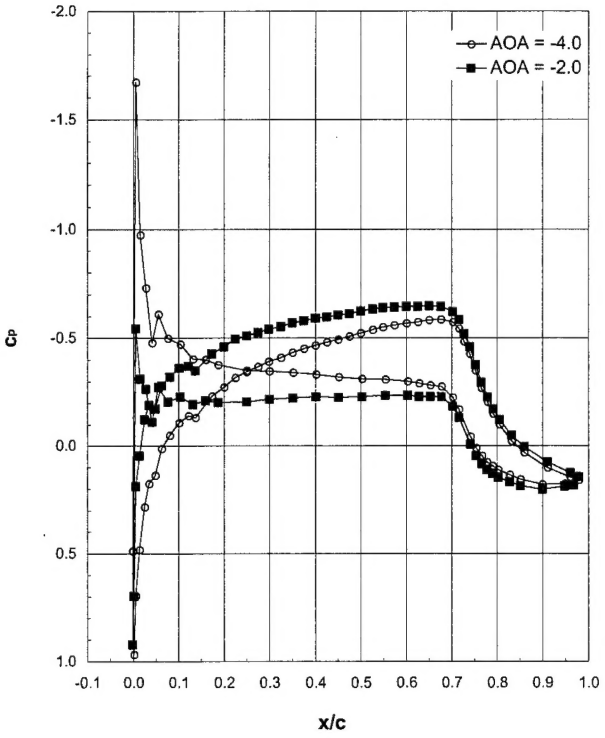

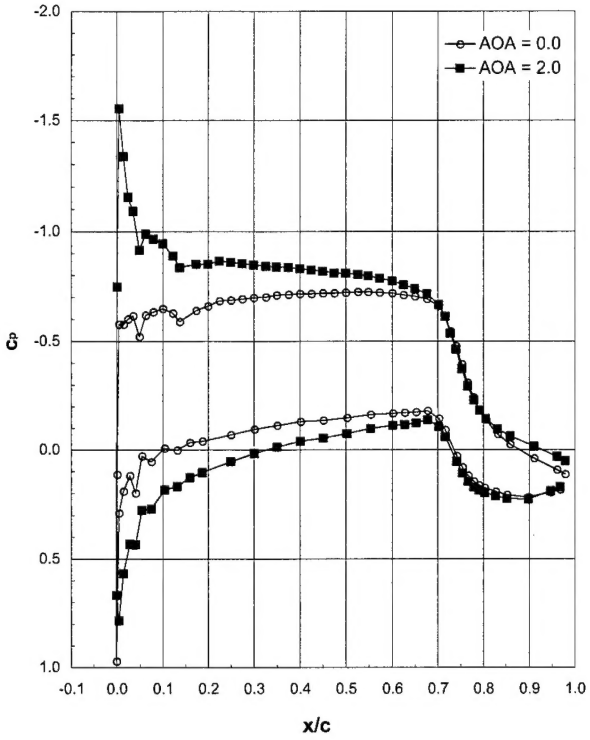

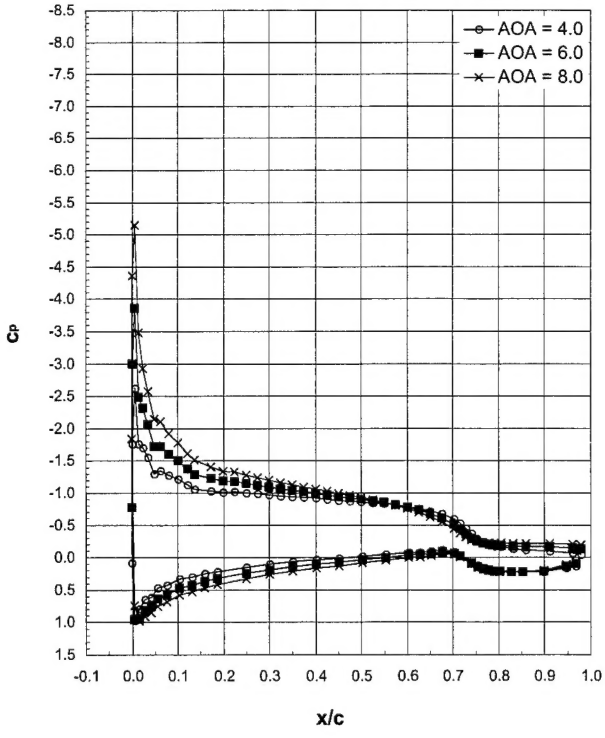

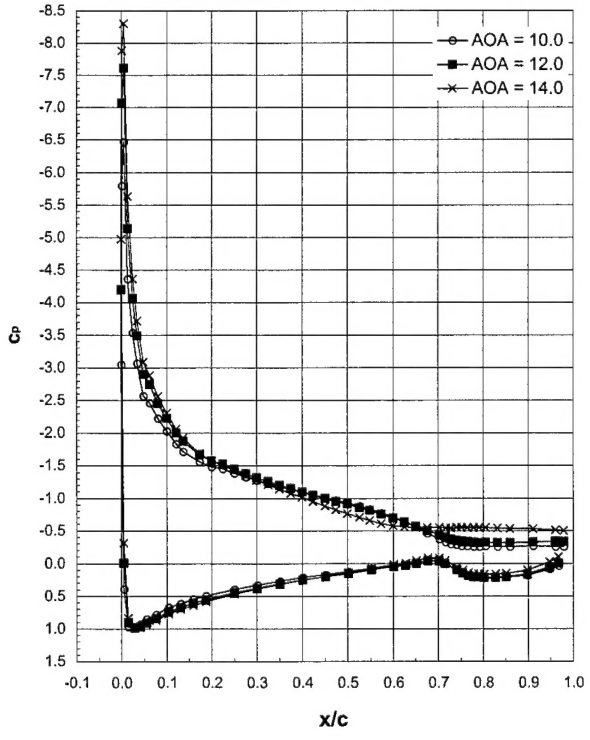

Run 508, Ma = 0.12, Re = 3x10^6

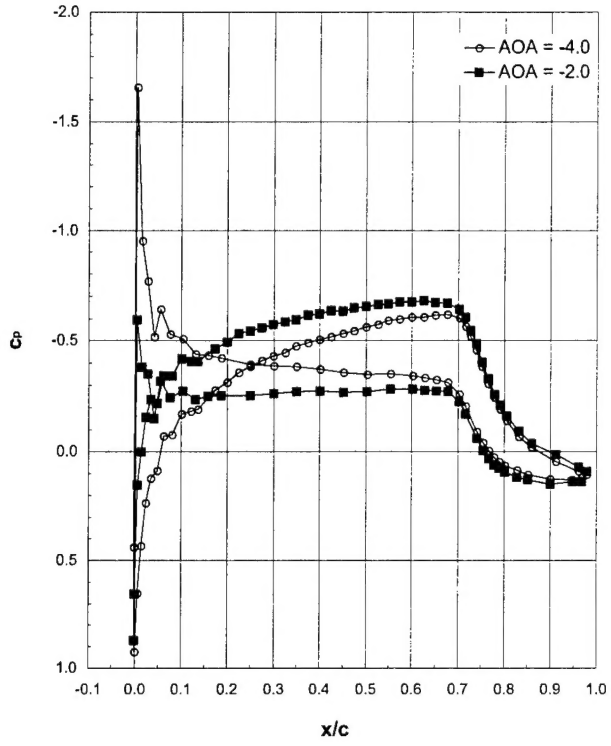

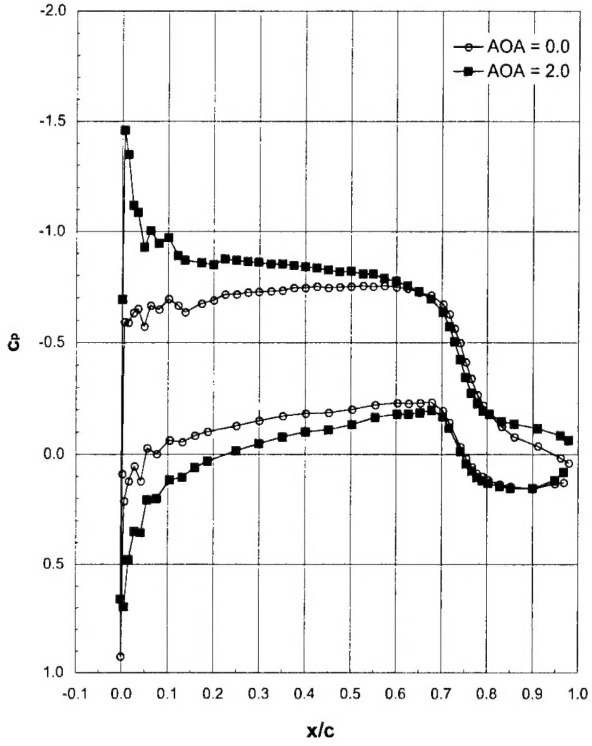

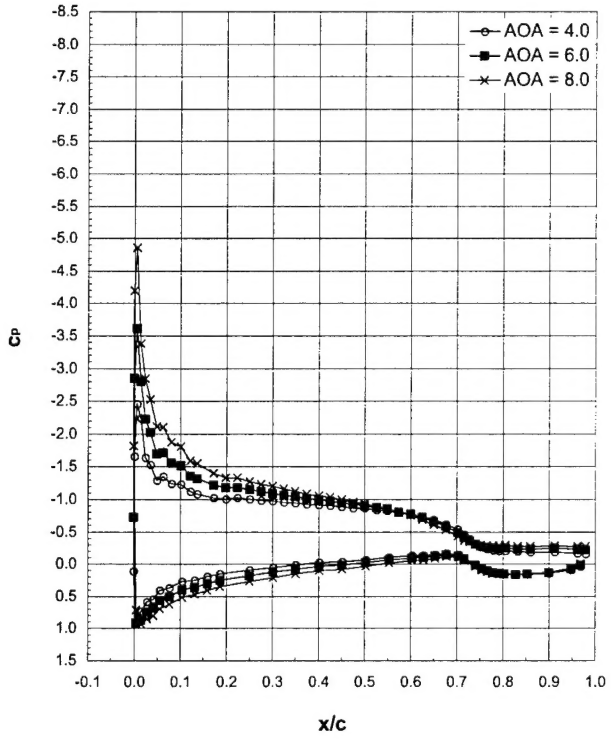

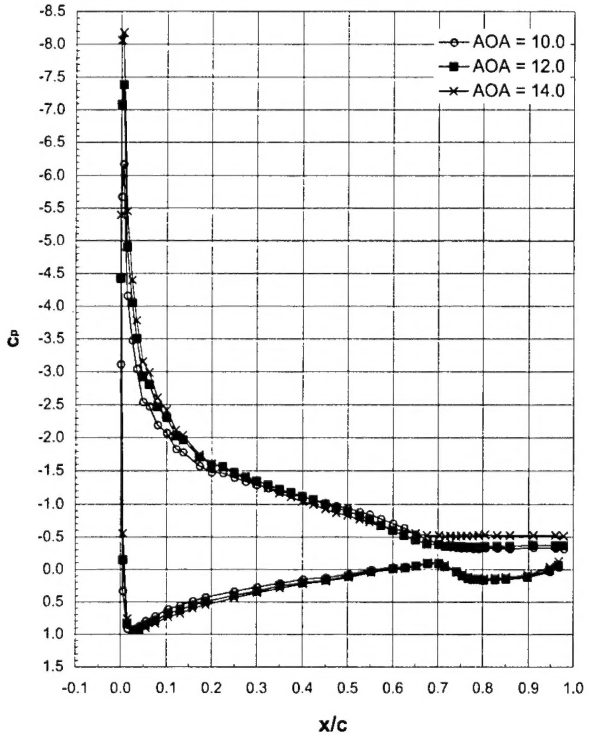

Run 510, Ma = 0.05, Re = 1x10^6

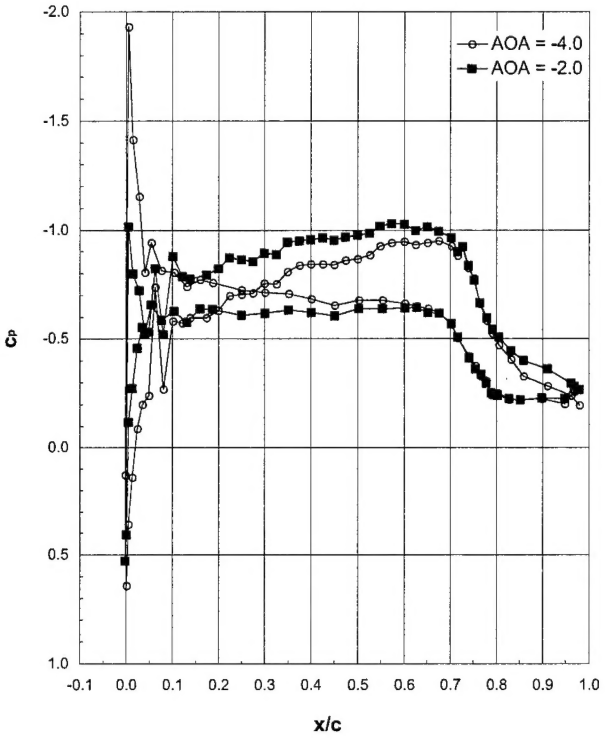

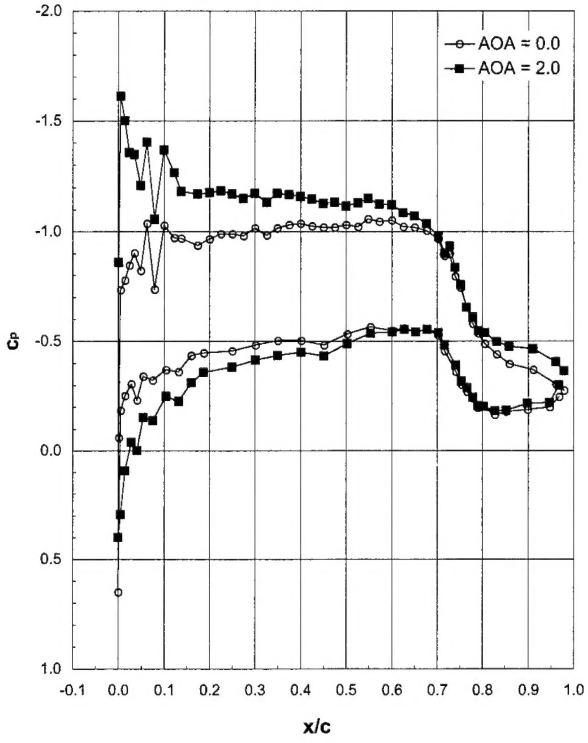

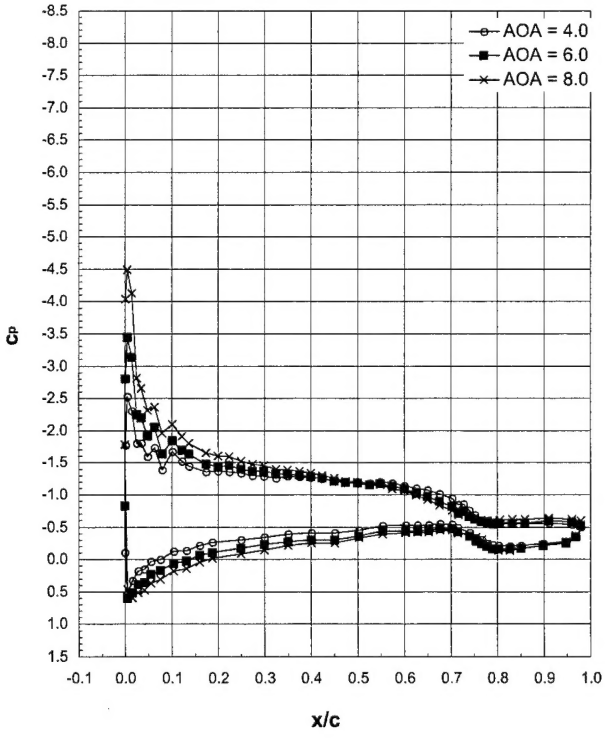

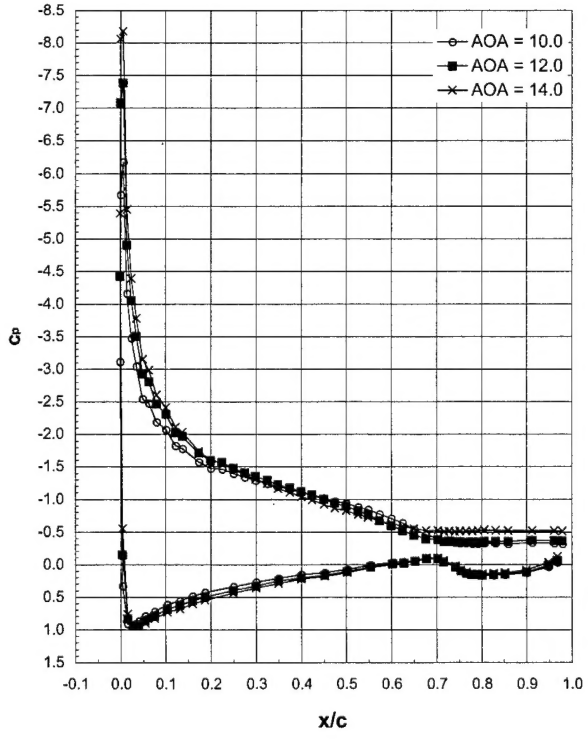

REPORT DOCUMENTATION PAGE

Form Approved
OMB No. 0704-0188

1. AGENCY USE ONLY (*Leave blank*)	2. REPORT DATE	3. REPORT TYPE AND DATES COVERED
	April 2000	Technical Paper

4. TITLE AND SUBTITLE

Ice Accretions and Icing Effects for Modern Airfoils

5. FUNDING NUMBERS

WU–548–21–23–00

6. AUTHOR(S)

Harold E. Addy, Jr.

7. PERFORMING ORGANIZATION NAME(S) AND ADDRESS(ES)

National Aeronautics and Space Administration
John H. Glenn Research Center at Lewis Field
Cleveland, Ohio 44135–3191

8. PERFORMING ORGANIZATION REPORT NUMBER

E–12228

9. SPONSORING/MONITORING AGENCY NAME(S) AND ADDRESS(ES)

National Aeronautics and Space Administration
Washington, DC 20546–0001

10. SPONSORING/MONITORING AGENCY REPORT NUMBER

NASA TP—2000-210031
DOT/FAA/AR–99/89

11. SUPPLEMENTARY NOTES

Responsible person, Harold E. Addy, Jr., organization code 5840, (216) 977–7467.

12a. DISTRIBUTION/AVAILABILITY STATEMENT

Unclassified - Unlimited
Subject Category: 02 Distribution: Standard

This publication is available from the NASA Center for AeroSpace Information, (301) 621–0390.

12b. DISTRIBUTION CODE

13. ABSTRACT ***(Maximum 200 words)***

Icing tests were conducted to document ice shapes formed on three different two-dimensional airfoils and to study the effects of the accreted ice on aerodynamic performance. The models tested were representative of airfoil designs in current use for each of the commercial transport, business jet, and general aviation categories of aircraft. The models were subjected to a range of icing conditions in an icing wind tunnel. The conditions were selected primarily from the Federal Aviation Administration's Federal Aviation Regulations 25 Appendix C atmospheric icing conditions. A few large droplet icing conditions were included. To verify the aerodynamic performance measurements, molds were made of selected ice shapes formed in the icing tunnel. Castings of the ice were made from the molds and placed on a model in a dry, low-turbulence wind tunnel where precision aerodynamic performance measurements were made. Documentation of all the ice shapes and the aerodynamic performance measurements made during the icing tunnel tests is included in this report. Results from the dry, low-turbulence wind tunnel tests are also presented.

14. SUBJECT TERMS

Aircraft icing; Aerodynamic characteristics

15. NUMBER OF PAGES

291

16. PRICE CODE

A13

17. SECURITY CLASSIFICATION OF REPORT	18. SECURITY CLASSIFICATION OF THIS PAGE	19. SECURITY CLASSIFICATION OF ABSTRACT	20. LIMITATION OF ABSTRACT
Unclassified	Unclassified	Unclassified	